CHEMICAL REVIEWS

pubs.acs.org/CR

Review

Technological Innovations in Photochemistry for Organic Synthesis: Flow Chemistry, High-Throughput Experimentation, Scale-up, and Photoelectrochemistry

Laura Buglioni,[§] Fabian Raymenants,[§] Aidan Slattery, Stefan D. A. Zondag, and Timothy Noël*

Cite This: *Chem. Rev.* 2022, 122, 2752−2906

Read Online

ACCESS | Metrics & More | Article Recommendations

ABSTRACT: Photoinduced chemical transformations have received in recent years a tremendous amount of attention, providing a plethora of opportunities to synthetic organic chemists. However, performing a photochemical transformation can be quite a challenge because of various issues related to the delivery of photons. These challenges have barred the widespread adoption of photochemical steps in the chemical industry. However, in the past decade, several technological innovations have led to more reproducible, selective, and scalable photoinduced reactions. Herein, we provide a comprehensive overview of these exciting technological advances, including flow chemistry, high-throughput experimentation, reactor design and scale-up, and the combination of photo- and electro-chemistry.

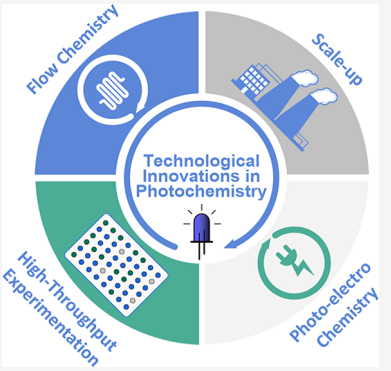

CONTENTS

Special Issue: Photochemical Catalytic Processes

Received: April 21, 2021
Published: August 10, 2021

https://doi.org/10.1021/acs.chemrev.1c00332
Chem. Rev. 2022, 122, 2752−2906

1. INTRODUCTION

In the past decade, photochemistry and especially photocatalysis have been embraced by the organic chemistry community as a transformative synthetic method, allowing to develop new and previously elusive synthetic methods.[1−8] In these methods, light energy can be harnessed by organic molecules and photocatalysts to reach an excited state,[9] leading eventually to new chemical bonds. Many of the recently developed approaches are operative under very mild reaction conditions (i.e., at room temperature, use of visible light, avoidance of toxic and hazardous reagents), thus providing excellent functional group tolerance. Consequently, photochemistry and photocatalysis have seamlessly been merged with other catalytic platforms,[10] such as transition-metal catalysis,[11−16] biocatalysis,[17−19] enantioselective catalysis,[20−27] and even electrocatalysis,[28−31] allowing to construct chemical bonds using a wide variety of unconventional coupling partners.

However, although the use of photons in organic synthesis is as old as the field itself,[32] it was consistently met with skepticism. In one of the earlier reviews on photochemistry,[33] Noyes and Kassel stated already in the first paragraph that "*Unfortunately, while Photochemistry may be said to be much older than its fellows, it is at present in a far more unsatisfactory state.*" Indeed, photochemical transformations are often perceived as very complex with regard to reaction kinetics.[34−36] Also from a scale-up perspective, photochemistry is still regarded as a daunting challenge because of the high cost of photons[37] and the light absorption, which causes a gradual loss of light intensity through the reaction medium.[38] This undermined the confidence of researchers—especially in the fine-chemical industry—to integrate photochemical steps in their synthetic routes toward pharmaceuticals, agrochemicals, and materials. The general perception was to avoid photochemistry altogether as it imposed too many insurmountable issues to bring the molecule to the market. Photochemistry was only considered when there was no alternative available, such as in the production of vitamin D and rose oxide as prime examples.[39]

Nevertheless, this time the moment could be right for a definitive breakthrough of synthetic photochemistry in the industry. The first reason for this statement is the rapid uptake and maturation of photocatalysis in both academia and industry, allowing researchers to completely rethink the assembly of organic molecules.[40] It is remarkable to see how fast companies have established small groups of experts to investigate the potential impact of photocatalysis in their synthetic programs.[41] Second, the tremendous evolution of light-emitting diode (LED) technology has resulted in the development of monochromatic, energy efficient, durable, and high intensity light sources, reducing the effective costs of photons for photochemical applications.[42] And third, various advanced photochemical reactor technologies have been developed in recent years, which show great promise to carry out photochemical processes ranging from laboratory to production scale.[43,44] Several companies have focused on developing and commercializing standardized equipment to carry out photocatalytic transformations on different scales. However, it is important to note that the application of photocatalysis in organic synthesis is not a recent invention.[4] On the contrary, several important contributions were made already decades ago.[45] Therefore, it can be argued that it is actually the combination of these three different technologies (i.e., photocatalysis, light sources and reactor technology), which have developed independently and with their own set of rules, that could ensure that photochemistry is here to stay. In times of increasing environmental awareness, another strong indicator for this statement is that the chemical industry is required to develop more sustainable and energy-efficient processes with reduced waste generation and minimal environmental impact.[46] Photochemistry can play a key role in this transition since light can be regarded as a renewable, traceless reagent,[47−49] and most photochemical processes adhere to the principles of green chemistry.[50]

Herein, we aim to give a detailed perspective on the new technological advances observed within the field of photochemistry and photocatalysis for synthetic organic chemistry. First, the fundamentals of photochemistry are detailed, including the importance of photons for the observed reaction kinetics, the key photochemical laws, and some guidelines for the appropriate light source selection. This introductory section is of importance as it will allow readers to gain a basic understanding into the reasons why technology can make an impact in synthetic photochemistry. Next, we discuss the different photochemical reactor designs along with a vision toward scale-up. In addition, a detailed update on the use of flow technology for synthetic photochemistry and photocatalysis is given from 2016 onward (for examples before 2016, we refer to our previous *Chemical Reviews* contribution[51]). Furthermore, we discuss some new exciting disciplines within the field, including the use of high-throughput experimentation and the combination of photochemistry and electrochemistry.

https://doi.org/10.1021/acs.chemrev.1c00332
Chem. Rev. 2022, 122, 2752−2906

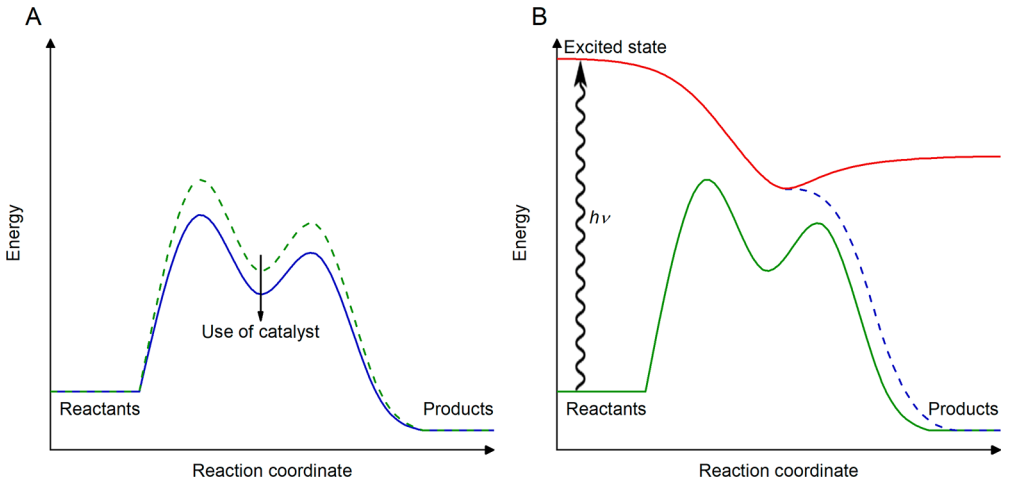

Figure 1. Thermochemical (A) versus photochemical activation (B).

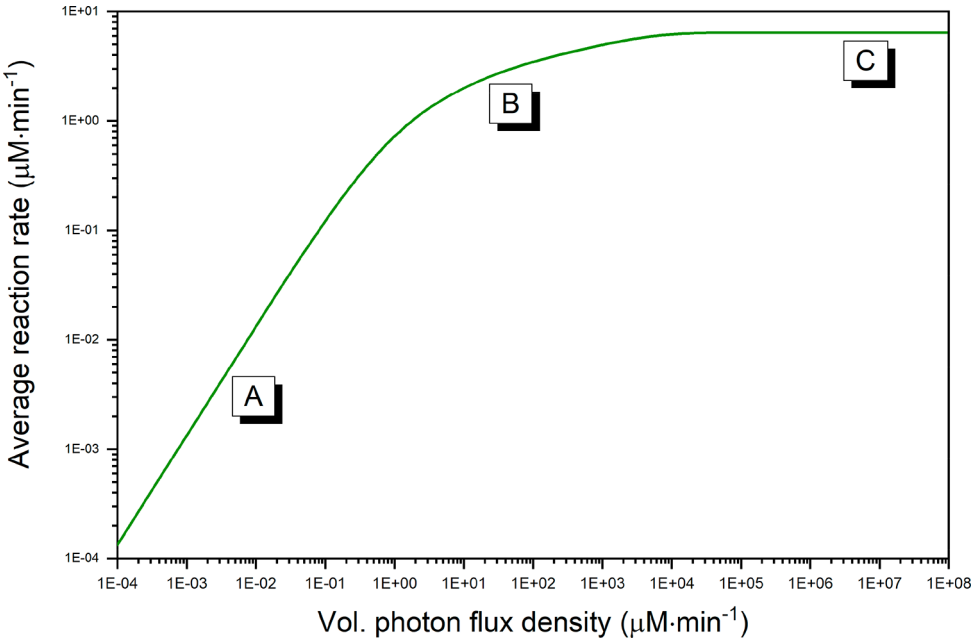

Figure 2. Average reaction rate versus the photon flux. (A) Linear regime where β is 1.0 can be observed at lower light intensities. The reaction is photon limited in the entire reactor. The linear part can be extended by increasing the photocatalyst loading. (B) For intermediate light intensities, β is around 0.5 and kinetic limitations are apparent in some parts of the reactor. (C) For high photon fluxes, β becomes 0, and thus, the reaction rate is independent of the light intensity. Kinetic limitations are observed in the entire reactor.

Throughout the Review, we have mainly focused on the synthesis of small organic molecules. However, where appropriate, we have included examples from other disciplines as well, for example, CO_2 conversion or polymer chemistry.

2. THE FUNDAMENTALS OF PHOTOCHEMISTRY

2.1. Kinetic Rate Dependence on Temperature versus Photons

Increasing the reaction temperature is one of the most utilized strategies to accelerate reactions. An increase in temperature can result in significantly reduced reaction times.[52] Such fast heating can be achieved by carrying out the reaction in microreactors[53] or by subjecting the reaction vessel to microwave energy.[54] As shown in eq 1, the Arrhenius formula provides a direct correlation between the reaction rate and the reaction temperature, which represents one of the fundamental equations in reaction kinetics.[55] This equation can be linearized by taking the natural logarithm of the reaction rate constant and plotting it against the reciprocal temperature ($1/T$). When the rate constant obeys the Arrhenius equation, a straight line is obtained where the slope can be used to determine the activation energy (E_a), which corresponds with the energy required for the molecules to undergo a chemical reaction. Often, the required temperature to undergo reaction is so high that it would result in a premature decomposition of the starting materials prior to reaction. In such cases, chemists have sought strategies to lower the activation energy by adding additional reagents for activation, such as catalysts, acids/bases, reductants/oxidants.

$$k = A \cdot e^{\left(-\frac{E_a}{RT}\right)} \quad (1)$$

https://doi.org/10.1021/acs.chemrev.1c00332
Chem. Rev. 2022, 122, 2752−2906

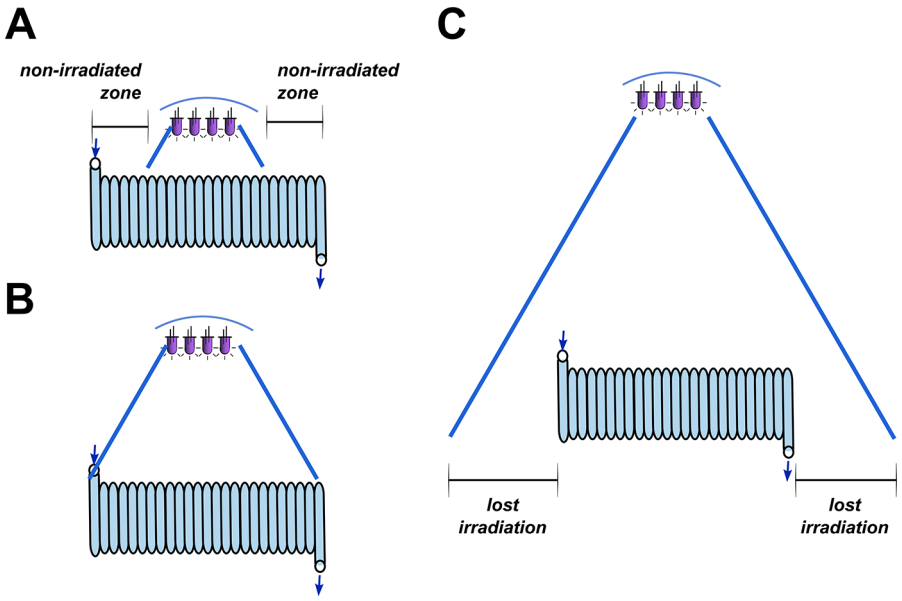

Figure 3. Maximizing the photon capture efficiency by minimizing the lost radiation through optimization of the light source-reactor distance and through use of refractors. (A) Light source is not matched with the reactor dimensions and some regions are not irradiated. This means that the photochemical reactor is effectively smaller than anticipated from its total volume. (B) Optimal positioning of the reactor and the light source. (C) When the light source is positioned too far away from the reactor, the amount of lost irradiation increases following the inverse square law for light.

where k is the rate constant [unit depends on the order of the reaction], T is the absolute temperature [K], A is the pre-exponential factor or frequency factor, which is related to the frequency of collisions between reactant molecules [has the same dimension as the rate constant], E_a is the activation energy for the reaction [J·mol^{-1}], and R is the universal gas constant [8.314 J·K^{-1}·mol^{-1}].

Overcoming these energetic barriers for reaction can also be realized by the selective absorption of photons (Figure 1). Interestingly, the kinetics of photon-driven transformations are strongly dependent on the photon flux, that is, the number of photons observed per unit time (eq 2).

$$k = \alpha \cdot I^{\beta} \tag{2}$$

where k is the rate constant [unit depends on the order of the reaction], α is a constant depending on the type of photochemistry, I is the light intensity [W·m^{-2}], and β is a constant depending on the photon flux.

For low light intensities (<around 200−250 W·m^{-2}), β is equal to 1.0 indicating a linear increase of the reaction rate constant with increasing light intensities (Figure 2).[56] Since there is no thermal component in this equation, photochemical reaction rates can be carried out at room temperature and readily tuned by simply varying the light intensity. From a safety perspective, it is interesting to note that most photochemical reactions can be easily quenched by switching off the light.

At a certain moment, a further increase in light intensity will not result in an enhancement of the reaction rate. The reaction becomes ultimately independent of the photon flux ($\beta = 0$). At that point, the photocatalyst is constantly active and the reaction medium is completely saturated with photons. Additional photons will not be productively absorbed anymore. Notably, it can be easily understood that the linear part of this correlation can be extended by increasing the catalyst loading (or by increasing the concentration of the photon-absorbing species). These important insights have their repercussions on the energy efficiency of the photochemical process, and it is therefore important to carefully balance the catalyst loading with the light intensity.

2.2. Laws of Photochemistry

When a reaction mixture is irradiated, only a fraction of the light will be absorbed as a significant amount of the incoming light will be scattered, transmitted, or reflected.[57] However, it is only the absorbed light that will be able to induce a photochemical transformation. This insight is known as the first law of photochemistry (also called the Grotthüs−Draper law). For example, a reaction mixture can be irradiated with visible light, and no reaction will typically occur as most organic molecules are transparent to such irradiation. However, organic dyes and some transition metal complexes can be added to absorb the light and subsequently transfer that excited state energy via single electron transfer (SET, e.g., photoredox catalysis),[6,58−63] hydrogen atom transfer (HAT),[64,65] proton-coupled electron transfer (PCET)[66] or collision (energy transfer, photosensitization).[10,67−69]

Since photochemistry is chromoselective, it is critical to maximize the overlap between the emission wavelength of the light source and the absorption characteristics of the photon-absorbing molecules. Often the absorption maximum (λ_{max}), that is, the wavelength at which the absorbing species displays maximum absorbance, is selected or, alternatively, a wavelength region where no-competitive photochemical-induced side reactions occur (so-called chromatically orthogonality). As a consequence, light sources with a sufficiently narrow spectrum are preferred (such as LEDs) to avoid excitation of nontargeted functional groups or components in the reaction mixtures, which could lead to undesired side-product formation or solvent heating. It is fair to say that wavelength-selective light sources lead to more selective photochemical reactions.[70] Hence, the light quality of the used light source is a key reaction design factor and can be more important than the total emitted light intensity. A high intensity light source with a broad emission spectrum wastes a

https://doi.org/10.1021/acs.chemrev.1c00332
Chem. Rev. 2022, 122, 2752−2906

lot of energy to wavelengths which are not relevant for the targeted reaction. In addition, because of slight variations during their construction, there are no two light sources which are identical (even LEDs differ slightly in color and intensity).[71] It is, therefore, important that all light sources are carefully calibrated using an integrating sphere, which is a device for measuring and quantifying the intensity and spectral range of optical radiation. Such detailed information on the used light sources should be mentioned in the supporting information of scientific articles.

The positioning of the light source is also a crucial reactor design aspect. According to the inverse-square law of light, the light intensity is inversely proportional to the square of the distance (eq 3) (Figure 3). In other words, the further the light source is positioned from the reactor, the more light is lost and the lower the intensity will be in the reaction medium. Kuhn et al. have shown that for a microfluidic channel an optimal and uniform irradiance (~90%) could be obtained in the reaction mixture when the distance between the microchannel and the LEDs was between 1 and 1.5 cm.[71] The LEDs were positioned along the length of the entire channel with an inter-LED distance between 6.5 and 8 mm. In addition, light can be further focused through use of mirrors or waveguides.

$$I = \frac{S}{4\pi r^2} \tag{3}$$

The inverse-square law for light describes the light intensity passing through a unit area and is inversely proportional to the square of the distance from the light source, which is treated as a point source with a defined source power, where I is the light intensity that passed through a unit area [$W{\cdot}m^{-2}$], S is the source power of the light source [W], and r is the distance between the reactor and the light source [m].

The second law of photochemistry is stated by the Einstein−Stark law of photochemical equivalence. It specifies that one photon can only activate a single molecule, and thus, a photochemical reaction can be regarded as a one-quantum process. It should be noted that the law only applies to primary photochemical processes. Once the photon is absorbed the molecule reaches an excited state, after which it can undergo a chemical change or fall back to its original position through loss of energy via, for example, fluorescence. This means that the quantum yield (Φ) is often less than unity ($\Phi < 1$).[72] When free radicals are generated in the photochemical process, a chain reaction can be initiated leading to apparent Φ values which are much larger than unity.[73] From the perspective of energy cost, such photoinduced radical-chain processes can actually be advantageous as less photons are required to reach full conversion.

$$\Phi = \text{number of molecules formed} / \text{number of photons absorbed} \tag{4}$$

When a beam of light is traveling through a solution, photons will be absorbed leading to a gradual decrease in light intensity. The Bouguer−Lambert−Beer law (eq 5) describes the extent of this light extinction phenomenon, which depends on the molar attenuation coefficient of the absorbing molecules, the concentration of this species and the light path length. As a consequence, photochemical reactions are challenging to scale. Larger-diameter reactors are not suitable as the highest light intensities are observed at the reactor wall while the center of the reactor will see little to no light (Figure 4). Since the reaction rate depends strongly on the local light intensity (eq 2), large variations in local reaction rates can be observed; kinetic rates can easily be 2−3 orders of magnitude different depending on the position in the reactor.[56] Hence, reactors with shallow dimensions provide equal reaction conditions throughout the entire reaction medium and are consequently the preferred vessels to scale photochemical transformations (see section 3).

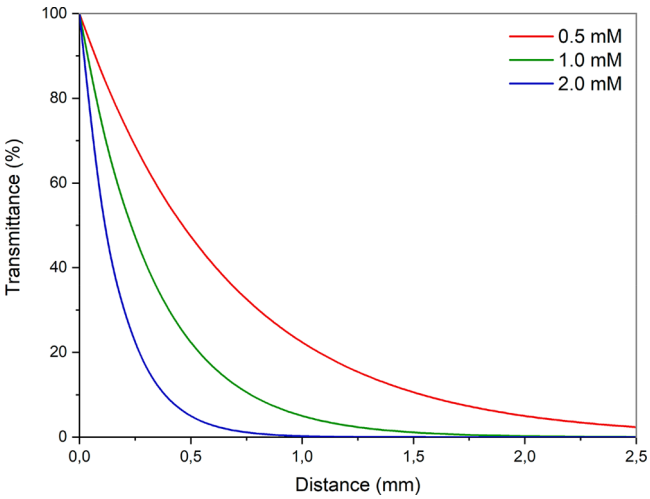

Figure 4. Attenuation of light as a function of distance in a photocatalytic reaction using $Ru(bpy)_3Cl_2$ (c = 0.5, 1, and 2 mM, ε = 13 000 $cm^{-1}{\cdot}M^{-1}$) utilizing the Bouguer−Lambert−Beer correlation (eq 5).

$$A = -\log_{10} T = \log_{10} \frac{I_0}{I} = \varepsilon c l \tag{5}$$

where A is the light absorbance [-], T is the transmittance [-], I_0 is the light intensity received by the light-absorbing medium [$W{\cdot}m^{-2}$], I is the light intensity after passing through the light-absorbing medium [$W{\cdot}m^{-2}$], ε is the molar attenuation coefficient or absorptivity of the light-absorbing species [$L{\cdot}mol^{-1}{\cdot}cm^{-1}$], c is the concentration of the light-absorbing species [$mol{\cdot}L^{-1}$], and l is the optical path length [cm].

If one photon converts one molecule into product, then theoretically 1 mol of photons should be supplied to convert 1 mol of starting material. This insight is expressed by the Bunsen−Roscoe Law of Reciprocity, which stipulates that only the total energy dose (i.e., the total number of incident light quanta) matters to convert a compound. Hence, the intensity of the light multiplied with the exposure time should be kept constant as shown in eq 6

$$I{\cdot}t = \text{constant} \tag{6}$$

where I is the light intensity [$W{\cdot}m^{-2}$] and t is the exposure time [s].

This law has also proven its value in the scaling of photochemical transformations. The required amount of photon equivalents, which are defined as the ratio of absorbed photons to the amount of substrate, needs to be kept equal at each reaction scale. Researchers at Merck-MSD have used this strategy to successfully scale a photocatalytic C−N cross-coupling reaction from milligram scale in batch to multikilogram scale in flow.[74] However, it is important to realize that this law has its limitations and is only valid when there is no follow-up reaction possible. If follow-up reactions are possible (e.g., photochemical oxidation reactions), larger diameter

https://doi.org/10.1021/acs.chemrev.1c00332
Chem. Rev. 2022, 122, 2752−2906

photochemical reactors would result in local regions with high light intensities, typically at the reactor wall. In those regions, it will be more likely that the formed product will be able to absorb another photon and be converted to (undesired) side-products than in regions where the light intensity is lower.

2.3. The Importance of Selecting the Right Light Source

The energy of a photon can be related to the wavelength (or the frequency) of the light, according to the Planck−Einstein law (eq 7). A mole of photons (corresponding to 6.022×10^{23} photons) is called an Einstein.

$$E = h \cdot \nu = h \cdot \frac{c}{\lambda} \tag{7}$$

where E is the energy of a single photon [kcal·mol^{-1}], h is Planck's constant [1.58×10^{-37} kcal·s], ν is the frequency of light [Hz or s^{-1}], λ is the wavelength of light [nm], and c is the speed of light in vacuum [3.0×10^{17} nm·s^{-1}]

Following eq 7, the energy of photons may be calculated from the wavelength associated with the photon (see Table 1).

Table 1. Relationship between the Type of Radiation, Its Wavelength, and the Frequency

type of radiation	wavelength [λ in nm]	energy [E in kcal·mol^{-1}]
UV-C	100−280	286−102
UV-B	280−315	102−90.8
UV-A	315−400	90.8−71.5
blue	∼450	63.6
green	∼500	57.2
red	∼650	44
near-infrared (NIR)	780−2500	37−11

The range of wavelengths which is of interest to organic chemists is limited between 200 and 1000 nm and the limits are determined by practical considerations. In the UV-region, transparent reactor materials are required and the higher the energy of photons, the more it is absorbed by the reactor material itself. The limit in the near-infrared (NIR) region is determined by the ability to induce synthetically relevant electronic excitations of organic molecules.

UV-induced photochemistry has been and remains very useful in synthetic organic chemistry, allowing the direct excitation of organic molecules.[75] Intriguing examples are [2 + 2] cycloadditions yielding strained cyclobutanes in a single step[76] and Norrish-type photoreactions which allow for homolytic cleavage of C−C bonds.[77,78] However, because of the high energy associated with UV irradiation, the likelihood of byproduct formation increases from UV-A to UV-C. This is especially true for densely functionalized organic molecules, such as active pharmaceutical ingredients. Nevertheless, strategies have been developed to combine low and selective UV-induced photochemical conversions in combination with a recycling of the unreacted starting material.[79] In comparison to visible light sources, the options for UV photochemistry are rather limited.[37] Medium- and low-pressure mercury lamps can be used for UV-A and UV-B applications. High-pressure mercury light sources emit a broad range of UV and visible wavelengths along with heat which requires adequate cooling. For such broad wavelength distribution light sources, wavelength-specific optical filters can be used to remove any undesired wavelengths,[80,81] which potentially cause byproduct formation leading to reduced energy efficiencies.[82] These issues can be solved by using light sources which emit light in a narrow spectral range. In this regard, LEDs have received a lot of attention.[42] They are fabricated from layered crystalline semiconductor material, where at the interface of two types of semiconductor a p−n junction is formed. Upon recombination of the electrically generated electrons and holes, light is emitted (i.e., electroluminescence) and the wavelength depends on the material characteristics (and, thus, the energy band gap). A single LED chip has a narrow emission spectrum (10−30 nm), and because of their small size, they can be perfectly aligned with chemical reactor technology (Figure 5A and B). For UV-B and UV-C applications, the emission of LEDs can be tuned over the entire spectral range by alloying GaN with AlN.[83−85] However, these LEDs are often plagued by their low intensity, poor lifetime stability and low wall-plug efficiency (WPE ∼ 1−3%), which is a measure that describes how efficiently the input power is converted into optical light power. Nevertheless, because of their use in the disinfection industry, a lot of research is dedicated to develop higher performance LEDs.[84,86] The 2020 SARS-COV-2 pandemic resulted in an increase of the UV-C market from $144 million in 2019 to $308 million in 2020. This value increase could even have been higher but was limited due to limitations in production capacity. It is predicted that the UV-C industry will further expand to $2.5 billion in 2025.[87] Consequently, it can be anticipated that the quality of these light sources will increase substantially and will make them available for photochemical applications in the near future. In sharp contrast, high quality and high intensity (up to 160 W) UV-A LEDs (>365 nm) are available and are based on well-established GaN and InGaN on sapphire technology (Figure 5C). The UV-A-LEDs are highly advanced as it utilizes essentially the same materials as blue LEDs and due to their widespread use in the UV-induced polymer curing industry.[88,89] As an alternative to LEDs, excimer lamps can be used, where specific excimer molecules emit the UV light as intense and narrow bands (spectral full-width at half-maximum from 2 to 15 nm).[90,91] Depending on the selected excimer, the emission wavelength can be tuned from UV-C (e.g., KrCl for 222 nm) to UV-B (e.g., XeBr for 282 nm) and to UV-A (e.g., XeF for 351 nm).

The energy-content of visible light is often not sufficient to cleave bonds and thus induce chemical reactions. However, this issue can be bypassed by adding another molecule that does absorb the radiation and subsequently exchanges energy (photosensitization), electrons (photoredox catalysis), or hydrogen atoms (hydrogen atom transfer photocatalysis) with other organic molecules. While compact fluorescent light sources are still frequently used for visible-light-induced photocatalytic reactions in academic settings, the use of LEDs is preferred because of their small size, energy efficiency, and narrow emission bands. Interestingly, their intensity can be easily tuned by changing the current.[72] It is also important to keep the operational temperature of LEDs constant due to reduced light intensity and wavelength peak shifting at increasing temperatures.[92,93] High-power LEDs are available in nearly all colors and are of great value for the scale-up of photocatalytic transformations. As an example, high power blue LED chips can deliver a peak irradiance up to 2×10^6 W·m^{-2}·nm^{-1}. In contrast, high power green-yellow LEDs (510−600 nm) are not available; this spectral range, also called the "green gap", suffers from a significant drop in efficiency (<50%).[94,95] This issue can be solved using yellow or green LED-pumped luminescent concentrators, which combine high

https://doi.org/10.1021/acs.chemrev.1c00332
Chem. Rev. 2022, 122, 2752−2906

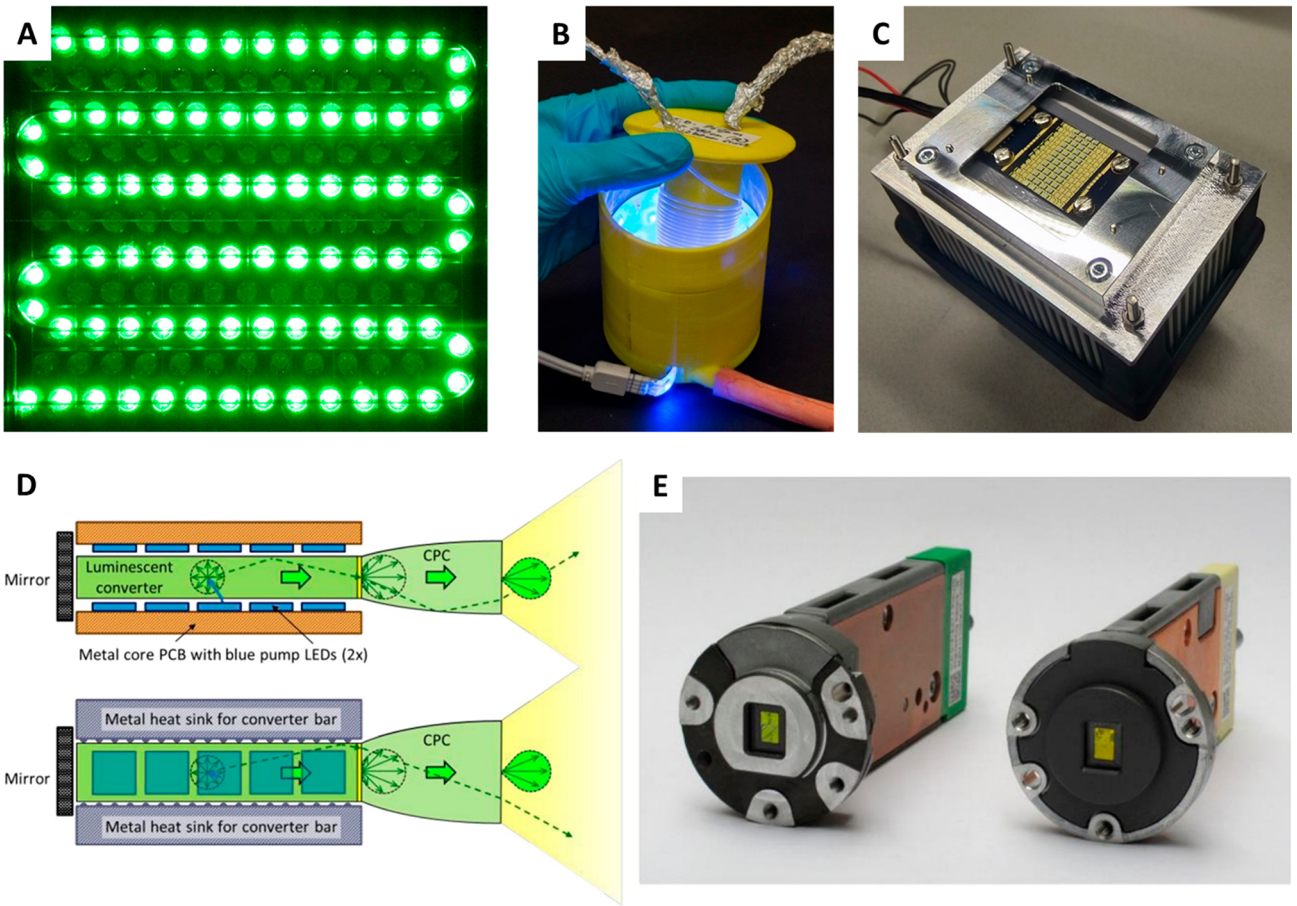

Figure 5. (A) Microreactor with LEDs aligned along the length of the entire microchannel (Courtesy of Kuhn et al.). (B) DIY-assembled photomicroreactor comprising a 3D-printed vessel in which a capillary microreactor is positioned and aligned with a blue LED strip. Reprinted with permission from ref 98. Copyright 2016 American Chemical Society. (C) High-power 365 nm LED light source integrating 48 individual LEDs in a single package, achieving 27.5 W of optical power. To the back of LED module, a heatsink is attached. (D) Schematic representation of the green LED-pumped luminescent concentrators: high power LEDs pump blue photons into the green luminescent concentrator, which after absorption is re-emitted as green light. Via total internal reflection, the light is waveguided to the edge, where it leaves the material as a highly intense light beam. Bottom: Heat sinks are positioned on the other side of the luminescent concentrator to remove generated heat (Courtesy of Signify). (E) Picture of an assembled green LED-pumped luminescent concentrator module (Courtesy of Signify).

power blue LEDs with a green emitting luminescent concentrator (Figure 5D and E).[96,97] Herein, a phosphor rod is illuminated with blue LEDs positioned along its length. The light is absorbed by the phosphor rod and down converted to the desired wavelength. The luminescent light is subsequently waveguided to the edge by total internal reflection where it escapes the luminescent concentrator as a focused light beam.

In general, photons in the NIR region do not contain enough energy to induce any synthetically relevant transformations. Using up-conversion strategies, two or more low-energy photons can be absorbed and converted into a single higher-energy photon (anti-Stokes emission).[99] The main advantage of NIR is the higher penetration depth that can be achieved through various media, including biological tissues. This feature could be advantageous to overcome scale-up limitations associated with the Beer−Lambert law and might be useful for photocatalytic applications in live-cells. NIR light has recently been used to enable photocatalytic reactions using a triplet−triplet annihilation up-conversion strategy.[100,101] However, to become practical and economically viable, certain limitations have to be overcome.[102] As two or more photons need to be absorbed almost simultaneously, high photon fluxes are needed, necessitating the use of NIR lasers. In addition, up-conversion quantum yields are still relatively low ($\Phi_{UC} \sim 5.5\%$ in deaerated organic solvents).[102] Furthermore, oxygen should be removed meticulously to avoid premature quenching of the triplets, which reduces the Φ_{UC} even more.

From a sustainability and economical perspective, the use of the solar energy for photochemical transformations is highly appealing.[103] However, several challenges are associated with the sun as a light source, including the polychromatic nature of solar light, the day/night cycles, the variable light intensity because of the passing clouds and the diffuse nature of solar light caused by light scattering and reflections. Nevertheless, progress has been made in recent years,[104,105] and we refer to section 3.1.1.3 for more information.

3. REACTOR DESIGN AND SCALE-UP

One of the main reasons why there is a clear lack of photochemical transformations in the chemical industry is the challenge associated with its scalability (i.e., mainly caused by the attenuation effect).[106,107] To produce small quantities, most lab-scale flow-based setups suffice for on-demand preparation of the targeted molecules (gram-scale), but the quantities required for industry (kilogram- to ton-scale) ask for a more robust and reliable scale-up process.[108] This not only

https://doi.org/10.1021/acs.chemrev.1c00332
Chem. Rev. 2022, 122, 2752−2906

holds for photochemical applications but is also a highly debated topic in continuous milli- and microflow chemistry in general.[109−111] Simply scaling up a flow reactor design to increase production rate can be the most straightforward approach, especially for tubular or capillary reactors, where reactor volumes can be scaled up by three main strategies: numbering up, sizing up by increasing the length of the channel, and sizing up by increasing the channel diameter (Figure 6).[109]

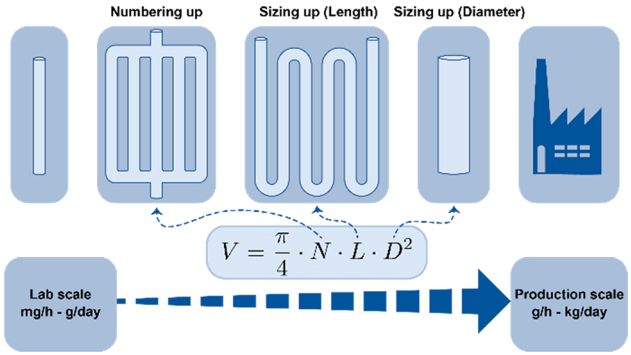

Figure 6. Scale-up strategies for tubular flow reactors: numbering up, sizing up by increasing channel length, and sizing up by increasing the channel diameter. A tubular reactor volume can be calculated using the given equation.

The numbering up strategy can be divided in two conceptually different approaches: external and internal numbering up. External numbering up can achieve an increase in overall setup productivity by multiplying the exact same setup in parallel. This way, additional units can be added until the full system is scaled to produce the desired target amount. A major disadvantage of this approach is the obvious high investment cost when large quantities of a product are desired, where for every setup individual equipment (e.g., pumps, mass flow controllers) is required. Internal numbering up can offer the same principle of scaling up through parallelization, but a significant difference is that in this case some equipment is shared between the instances. In the internal numbering-up strategy, the reactor itself can be multiplied several times, while still using a single feeding, collection, and monitoring section. However, care needs to be taken to ensure equal flow distribution over the different reactors, since slight differences in pressure drop can cause flow maldistribution, which is especially challenging in multiphase reactions, for example, gas−liquid reactions where the gas is a reactant.[112−114]

One of the major drawbacks of scaling flow photochemistry is the effect on the irradiated volume. Homogeneous photon fluxes and controlled irradiation times can be achieved for the irradiated volume for scales in the micro (and to some extent the milli) range. Keeping the diameter as small as possible then maximizes the photon flux over the entire cross section of the reactor.[115] Sizing up by increasing the length of the reactor has the advantage that the surface-to-volume ratio remains constant, but has the drawback of an increased pressure drop along the reactor channel. On the other hand, simply sizing up these reactor designs by increasing a channel or vessel diameter can pose issues due to the Bouguer−Lambert−Beer law. Inhomogeneous irradiation because of the attenuation of light at larger dimensions can cause overirradiation (at the reactor wall), slower overall reaction kinetics, and undesired byproduct formation.[116] This strategy of sizing up also affects the flow characteristics and heat transfer properties of the overall system. For sizing up strategies, a reoptimization of the process might be needed because of the change in flow characteristics and, therefore, in the mass-transfer behavior.

The scale-up of photochemical reactors is, however, not limited to the use of tubular/capillary reactors. In the past decade, a diverse array of reactor designs have been proposed (e.g., falling film reactors, vortex reactors, membrane reactors), which all take advantage of the process intensification concept.[43,52,110,117−129] Process intensification aims to intensify mass, heat and photon transport phenomena with at least 2−3 orders of magnitude, leading to a significant reactor volume reduction.[130] In the next section, attention will be devoted to these novel photochemical reactor designs, differentiating between passive and active reactor designs, and its successive scale-up. These different design considerations and scale-up strategies successfully and reliably increased productivity for custom-made, as well as commercial reactor types.

3.1. Custom Reactors

Novel setups are oftentimes pursued in the laboratory environment to explore new reactor concepts, or, alternatively, to fine-tune a previously reported setup by tweaking the design and operational parameters. This do-it-yourself (DIY) approach can result in particularly interesting designs and with the use of relatively cheap materials and parts flow photochemistry is made easily accessible, partially explaining the increased interest in recent years.

3.1.1. Custom Passive Reactors. The first category of custom reactors discussed in this section is the passive reactor type. In this context, the term passive indicates that no additional mechanical energy is supplied to the process. Fluids are introduced into the system and the flow profile is not altered by moving parts or by any other external forces (e.g., ultrasound, stirring). In essence, this defines that the system only requires a suitable way to introduce the reaction stream, to irradiate and heat/cool the reaction mixture, and finally to collect it.

3.1.1.1. Capillary Reactors. In 2005, Booker-Milburn, Berry, and co-workers introduced a reactor design based on an immersion well batch photochemical reactor, where a light source is placed along the central axis of the immersion well.[131] An issue associated with this type of batch reactor is consistent with the effect of the Bouguer−Lambert−Beer law, where only the volume in proximity of the light source was irradiated effectively. Alternatively, to optimally utilize the irradiation of the central light source, the solvent-resistant fluorinated ethylene propylene (FEP) tubing was coiled around the immersion well (schematically shown in Figure 7A). Different reactor designs were considered, consisting of one or multiple layers (3, 4, or 5) of coiled FEP tubing (either 0.7 mm ID/1.1 mm OD or 2.7 mm ID/3.1 mm OD) wrapped around a commercial or custom-made glass (quartz, Pyrex, or Vycor) immersion well. FEP is commonly used because of its flexibility, good solvent-resistance and, especially important for UV-photochemistry, its high UV-transmittance. The FEP capillaries were irradiated with UV-light by a 400 W medium-pressure mercury lamp and were cooled by directing water through the cooling jacket of the immersion well. The 280 mL custom Vycor immersion well, chosen because of its transmittance in the UV-region, was better suited for the targeted chemistry (Scheme 1) than the custom Pyrex

https://doi.org/10.1021/acs.chemrev.1c00332
Chem. Rev. 2022, 122, 2752−2906

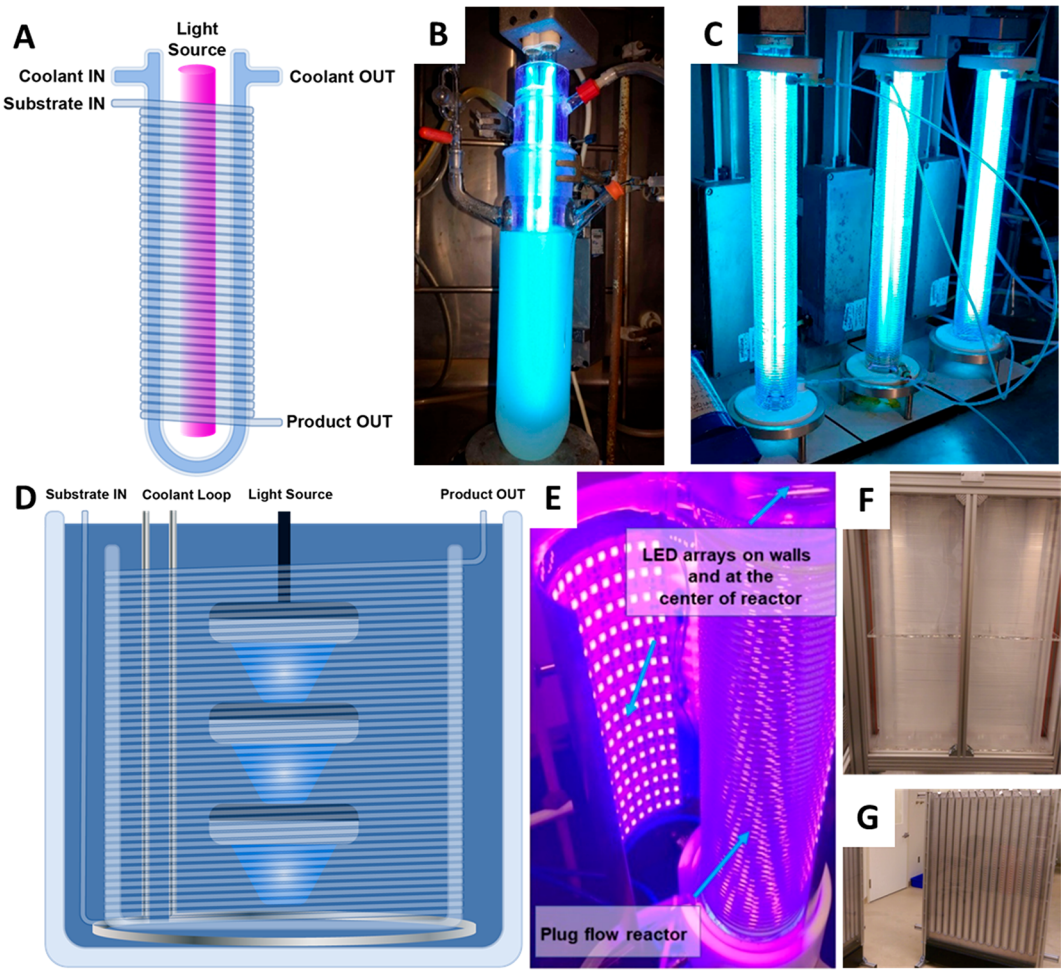

Figure 7. Collection of several different photochemical reactors. (A) Schematic representation of a FEP-wrapped immersion well flow reactor. (B) Immersion well batch reactor. (C) Three coiled FEP flow reactors in series. (B and C) Reprinted with permission from ref 132. Copyright 2018 Royal Society of Chemistry. (D) Schematic representation of the large-scale submerged PFA reactor. Cased cylindrical (E) and plate (F) capillary reactor, with one of the two external LED panels for the plate reactor (G). (E–G) Reprinted with permission from ref 74. Copyright 2020 John Wiley and Sons.

Scheme 1. [2 + 2] Photocycloaddition of Maleimide and 1-Hexyne

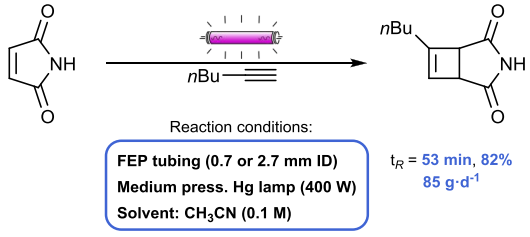

immersion well. This flow setup, equipped with three layers of 2.7 mm ID/3.1 mm OD FEP tubing, was tested on its reliability in a 24 h continuous operation. The FEP tubes showed no apparent coloration or material degradation, and no overheating nor clogging due to byproduct formation was observed. This resulted in a productivity of 85 g·day^{-1} at full conversion of the substrate, and a projected productivity of more than 500 g·day^{-1} using a 600 W lamp, higher substrate concentration and higher flow rate.

Another, more recent, example of scale-up using coiled FEP tubing is presented by Booker-Milburn et al.[132] Results obtained in an immersion well batch reactor (Figure 7B) were used as benchmark information to calculate the optimal flow rates for the upscaled setup (Figure 7C). The flow setup was based on their previous design and consists of a single quartz tube (360 mm length/48 mm OD) wrapped with FEP tubing (2.7 mm ID/3.1 mm OD). A 36 W PL-L UV-C lamp was inserted in the quartz tube, which was capped with polytetrafluoroethylene (PTFE) end-caps.[133] Three of these capillary reactors, each consisting of approximately 90 mL reactor volume and equipped with their own UV-C lamp, were connected in series to produce the scaled setup (~270 mL volume). The predicted optimal flow rate for this system was calculated based on the reaction time and volume used in batch, and the power of the light sources. This calculated value generally differed less than 10% from the experimentally determined optimal flow rate. Larger deviations observed in some cases were hypothesized to be caused by inefficient photon capture in the flow design, due to the shorter path lengths compared to the batch system. The flow setup was used to successfully scale the Norrish–Yang cyclization from 0.7 g·h^{-1} in the batch reactor to 4 g·h^{-1} in flow, and the formation of highly functionalized spirocycles from 0.089 g·h^{-1} in batch to 0.46 g·h^{-1} in flow.

https://doi.org/10.1021/acs.chemrev.1c00332
Chem. Rev. 2022, 122, 2752–2906

FEP-coiled flow reactors were also used by Graham, Noonan et al. to scale a Minisci reaction, used to prepare a dichloropyrimidine intermediate for the cancer drug ceralasertib.[134] The batch reaction was performed in an EvoluChem PhotoRedOx Box (HepatoChem) equipped with a 36 W 450 nm LED light source. This system could produce 105 mg of desired product in 21 h (determined by crude NMR). Moving to a small-scale flow reactor, a 10 mL Vapourtec UV-150 equipped with a 450 nm blue light LED light source (60 W input/24 W radiant power), resulted in a significant increase in productivity, producing a projected 32 g·day^{-1}. Next, larger scale experiments were performed in a custom FEP-wound immersion well flow reactor. Initial testing was done with FEP tubing (4 mm ID/6 mm OD) wrapped around 450 nm blue LEDs (100 W), which was later scaled to even larger diameter tubing (8 mm ID/10 mm OD) to achieve a higher throughput. Using this flow setup, a projected productivity of 65 g·day^{-1} could be achieved.

Wrapping polymeric tubing around light sources is not always done using FEP tubes; also perfluoro alkoxy alkane (PFA) polymers are widely used in flow setups. PFA and FEP are similar in chemical resistance, UV transmittance, and nonsticky behavior (important to avoid, e.g., clogging[135]), which is why both polymers are used almost interchangeably. A large-scale application using PFA tubing was developed by Stephenson et al. to enable the scaling of photochemical trifluoromethylations.[136] The assembled 150 mL flow setup consists of 250 ft (76 m) of PFA tubing (1.6 mm ID/3.2 mm OD), wrapped around a glass beaker. Three AquaDock Blue MegaWatt LED light sources were positioned in the center of a glass beaker and submerged into a stainless-steel housing filled with deionized water, which was cooled by a stainless-steel glycol-loop (schematically shown in Figure 7D). Using this setup, 0.95 kg of trifluoromethylated product was isolated after 48 h operation, which corresponds to 87.2 mmol·h^{-1}, surpassing both their batch (4.2 mmol·h^{-1}) and previous flow (14.2 mmol·h^{-1}) productivities.

Another large-scale setup using PFA tubing was considered by researchers at Merck.[74] Their transformation from batch to large-scale flow was investigated with the help of their newly coined term "photon equivalents". This method is similar to the strategy used by Booker-Milburn et al. to determine the optimal flow rate from batch results.[132] In total, one batch setup and four different flow reactors with increasing dimensions were used to explore this new concept. Initially, the batch C−N cross-coupling benchmark reaction (Scheme 2) was performed in a reaction vial irradiated by a 405 nm 260 mW radiant power laser. This reaction was then translated to their smallest-scale flow reactor, that is, a Vapourtec UV-150 equipped with a 405 nm LED array (60 W input/9 W radiant power). Yields of over 90% were achieved after 15 min residence time, compared to the 88% yield in batch after 120 min reaction time. This large difference between the two systems, caused by different geometry, light source, and volume, was shown to correlate nicely when the yields were compared based on the estimated amount of photon equivalents absorbed by the reaction mixture (Figure 8A). Their developed method for scaling photochemical reactions used the equivalent number of photons absorbed per time-unit to extrapolate yield for other scales. An important remark is the required involvement of photons in the rate-limiting reaction step, since additional photons in an already photon-saturated system will not influence the reaction rate. Subsequent experiments were performed in two custom flow reactors with the same design principle. A 60 mL (1.6 mm ID/3.2 mm OD) or a 150 mL (3.2 mm ID/4.8 mm OD) PFA tube was wrapped around a glycol/water-cooled jacketed glass condenser. An aluminum housing lined with 405 nm LED arrays (158 W) was positioned around the condenser (Figure 7E). As the predicted yield showed nice agreement with the 10 mL flow reactor (Figure 8B), the photon equivalent scaling method was then applied to the largest 3.5 L flow reactor setup. This setup consists of a 48 in. × 48 in. × 12 in. (i.e., 122 × 122 × 30.5 cm^3) acrylic tank filled with water as coolant, in which two posts were located. Around these posts, PFA tubing (3.2 mm ID/4.8 mm OD) was wrapped and two 48 in. × 48 in. aluminum panels lined with 400 nm LEDs (totaling 2300 W input power/644 W radiant power) were placed on either side of the tank (Figure 7F and G). Again, using the concept of absorbed photon equivalents, this scale-up successfully reached high yield (82%, when the method predicted 90%, shown in Figure 8B) and was able to produce 1.43 kg of product in 200 min, which corresponds to 430 g·h^{-1} or 10 kg·day^{-1}.

An updated design of their 3.5 L flow reactor was developed by researchers at Merck and validated in the same photocatalytic C−N cross-coupling reaction (Scheme 2).[137] A limitation of the previous design was the maximum flow rate of 0.6 L·min^{-1} because of the small diameter (3.2 mm ID) of the PFA tube. At larger flow rates an increasingly large pressure drop was observed, associated with the length of the PFA tube amounting to about 0.4 km. Another disadvantage of the previous reactor was its large footprint. For the new design, the objective was to create a flow reactor that would fit within a conventional fume hood. To this end, a 5.5 gallon (i.e., 21 L) aquarium was used. In a similar manner as the previous acrylic tank, two LED-panels of 15 LEDs (440−450 nm, totaling 3000 W input power/790 W output power) were placed on opposite ends of the tank. These plates were cooled by aluminum heatsinks and additionally by water-cooling via copper piping heat exchangers. The PFA tube was replaced by a larger diameter FEP tube (7.9 mm ID/9.5 mm OD), resulting in a reactor volume of 725 mL. The reactor was subsequently submerged into the cooled, water-filled aquarium. The increase in tube diameter in this system caused the transmittance to drop from 59% to 27%, along with an increase in conversion to 67.8% compared to 36.2% in the smaller diameter design. These diameter variation experiments were performed with constant flow rate (212 mL·min^{-1}), to keep the ratio between the molar and photon flow rates constant. However, the irradiated volume and the residence time are larger for the reaction in larger tubing, since the reactor volume for the smaller diameter case is only 195 mL (compared to 725 mL). In the large-scale experiments, the internal reactor volume was increased to 890 mL to make optimal use of the light source,

Scheme 2. Dual-Catalytic C−N Cross-Coupling Reaction

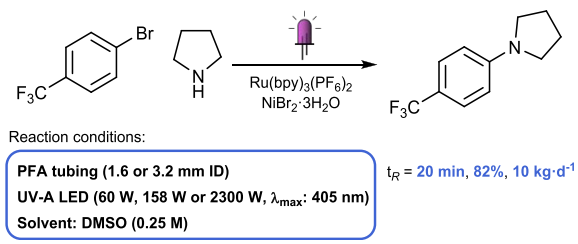

https://doi.org/10.1021/acs.chemrev.1c00332
Chem. Rev. 2022, 122, 2752−2906

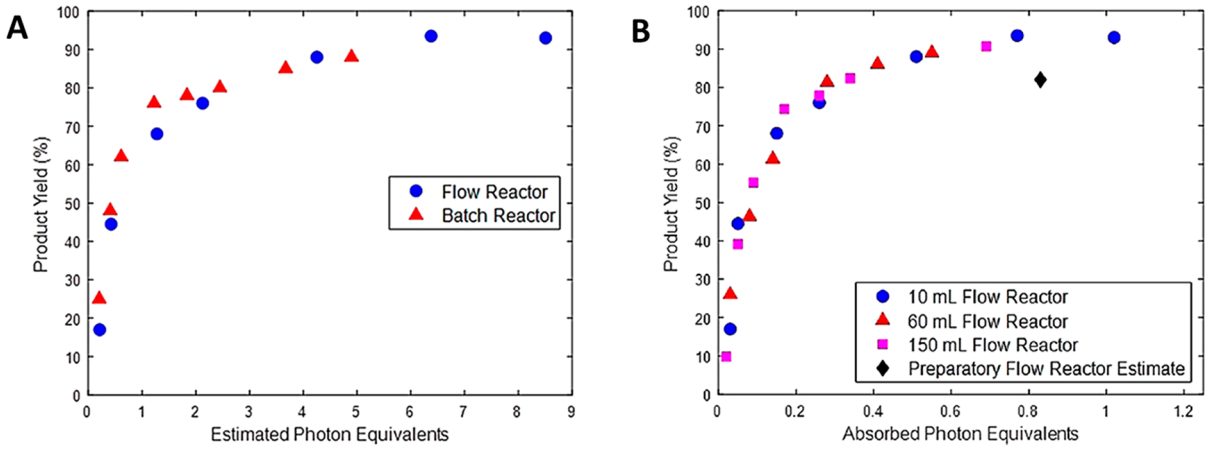

Figure 8. Batch and flow yield for the C−N cross-coupling reaction as a function of estimated (A) and calculated (B) amount of absorbed photon equivalents. Reprinted with permission from ref 74. Copyright 2020 John Wiley and Sons.

and two cases were demonstrated: low- and high-throughput. For the low-throughput, 1.14 kg of product was isolated after 130 min at 90% yield, giving a productivity of 12.6 kg·day^{-1}. For the high-throughput, 1.12 kg of product was isolated after 37.2 min at 41.5% yield, giving a productivity of 43.4 kg·day^{-1}.

Researchers from Amgen and Asymchem performed detailed scale-up investigations toward the multikilogram production of a cyclobutene scaffold using a [2 + 2] photocycloaddition between maleic anhydride and ethylene in a large-scale capillary flow reactor setup (Scheme 3).[138] Three flow reactor

Scheme 3. [2 + 2] Photocycloaddition of Maleic Anhydride and Ethylene Gas

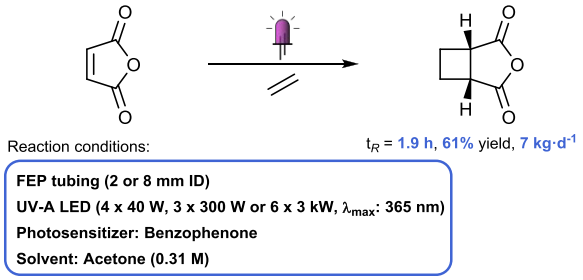

setups were assembled of increasing scale (0.25, 1.56, and 20.76 L reactor volume). Initial experiments to determine the solvent and the reaction dependence on temperature, pressure and photosensitizer concentration were performed in the smallest-scale reactor (2 mm ID/3 mm OD FEP tubing, wrapped around four 40 W 365 nm LED arrays). After selection of the optimized reaction conditions, a setup of intermediate scale was assembled to realize a productivity aim of 500 g·day^{-1}. This setup was able to reach the productivity target using FEP tubing (8 mm ID/10 mm OD) and 365 nm LED panels (3 × 300 W). A 51 h experiment showed to yield continuously 91% ^{1}H-NMR yield, with a productivity of 646 g·day^{-1}. With the desired productivity achieved, a new goal was set to reach a productivity of over 5 kg per day. To this end, a large-scale skid was assembled, consisting of three modules of FEP tubing (8 mm ID/10 mm OD) placed in series, irradiated by 365 nm LED panels (6 × 3 kW). With this setup, engineering runs (24 h), a commissioning run (45 h) and a single uninterrupted 1-week production run were performed. Over 250 kg of cyclobutane was produced over multiple production batches. Notably, a total of 51.8 kg (∼7 kg·day^{-1}) of product was isolated from the 1-week run, which exceeded the 5 kg·day^{-1} productivity objective.

3.1.1.2. Tubular Reactors. It should be noted that in some cases the photochemical flow reactors, the capillaries are wrapped around the light source, whereas in other cases the capillaries are surrounded by the light source. The immersion well-type reactors use outward irradiation, and the inward-irradiating setups are sometimes also called Rayonet-type reactors. Despite this difference in the light source placement, what these designs do have in common is the wrapping or coiling of the capillaries, in which the photochemical transformation takes place. However, another variation of the immersion well-type, introduced by Booker-Milburn, Elliott, and co-workers does not use these wrapped capillaries but instead uses parallel-placed tubes.[139] This parallel tube flow reactor (PTFR), also nick-named the Firefly reactor, was designed to achieve the goal of producing more than 1 kg per day, while simultaneously maintaining a small enough footprint to fit inside a conventional fume hood. Another key design specification was the replacement of the previously used FEP tubes with a more durable and UV transparent materials. To this end, the Firefly reactor was designed to use quartz glass tubes, positioned in parallel around a central medium-pressure mercury lamp. The individual tubes were subsequently connected in series. A 60 mL prototype with a 400 W mercury lamp was built (Figure 9A) and showed similar productivity to their previous three-layered FEP reactor designs[131] (3.41 g·h^{-1} for the PTFR vs 3.62 g·h^{-1} in the FEP reactor) for the same photocycloaddition (Scheme 1) as previously reported but with *N*-methyl maleimide instead of maleimide. The PTFR prototype was used without its metal casing, which would serve as a mirror to reflect the transmitted light back into the reactor. The removal of the metal casing was needed to avoid overheating of the reactor. The Firefly design (Figure 9B) was, then, built to enable the necessary cooling of the setup, where water-cooling was incorporated at the annular space between the inner tube and the outer metal casing. Inside this annular space the quartz tubes with a total internal volume of 120 mL are placed, thereby providing the quartz reactor-tubes with water-cooling. Cooling of the mercury lamp was also foreseen in this design, using a fan to blow air past the light source. With this new design, sufficient heat can be dissipated, and the metal casing could be used to reflect the light back into

https://doi.org/10.1021/acs.chemrev.1c00332
Chem. Rev. 2022, 122, 2752−2906

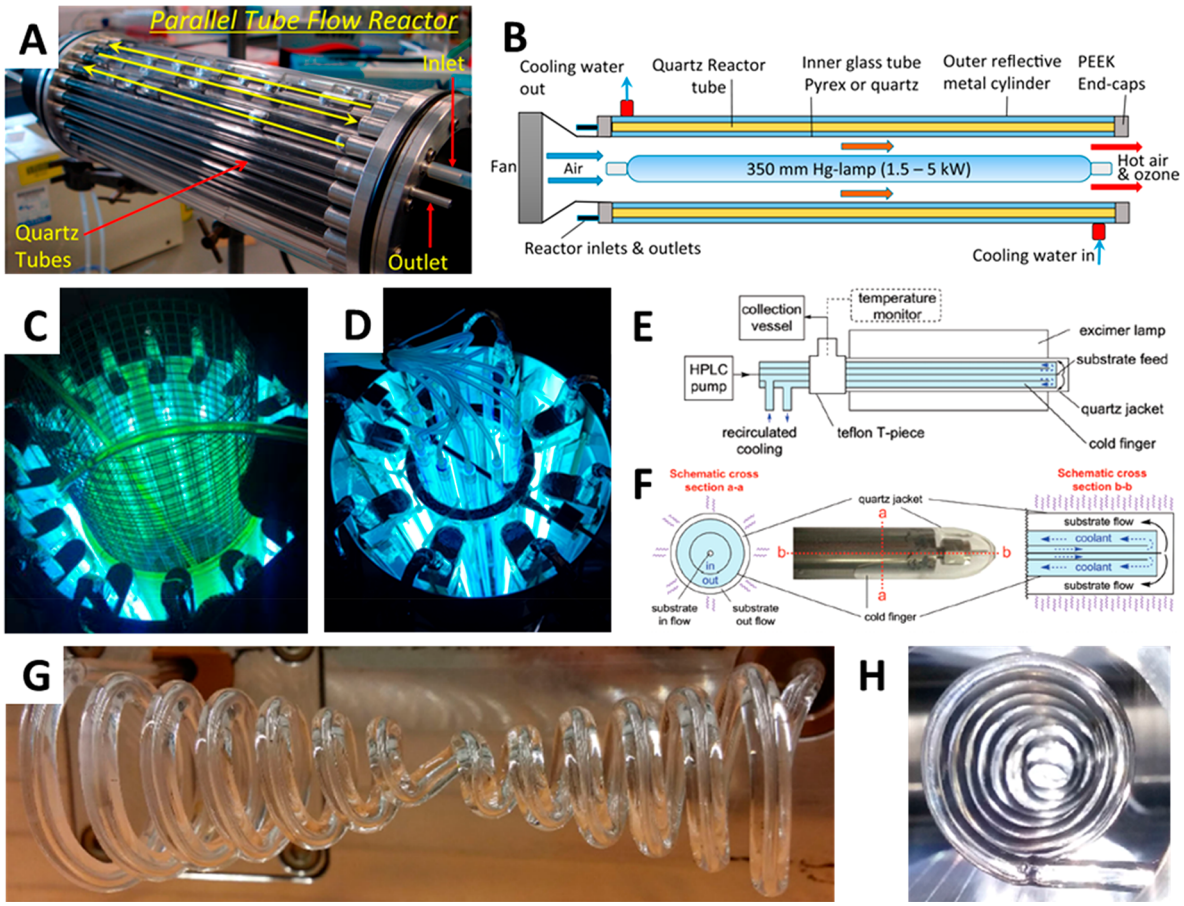

Figure 9. Collection of several different reactor designs. The prototype parallel tube flow reactor without casing (A) and schematic representation of the Firefly reactor (B). (A and B) Reprinted with permission from ref 139. Copyright 2016 American Chemical Society. The FEP4 (C) and PQT6 (D) reactors in the homemade Rayonet-type chambers. (C) Reprinted with permission from ref 140. Copyright 2018 American Chemical Society. (D) Reprinted from ref 141. Published by MDPI. The schematic representation of the excimer lamp setup (E) and close-up of the coldfinger quartz jacket design (F). (E and F) Reprinted with permission from ref 90. Published by Royal Society of Chemistry. Archimedean glass spiral, view from the side (G) and front (H). (G and H) Reprinted with permission from ref 142. Copyright 2018 John Wiley and Sons.

the setup. Hence, UV-light was trapped more effectively inside the cylindrical reactor, which is also advantageous from a safety perspective. Using a 3 kW mercury lamp, instead of the 400 W lamp in the prototype, yielded around a 10-fold increase in productivity. One of the benchmark reactions is shown in Scheme 4, which was performed with a 1.5 and a 3 kW light

Scheme 4. Formation of Cookson's Dione from a Diels–Alder Adduct

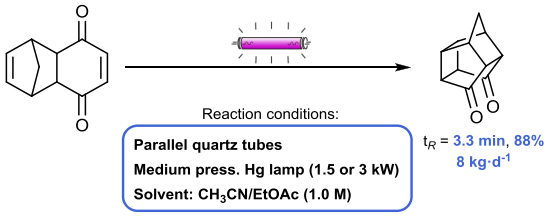

source, resulting in isolated yields of 387 g in 2.31 h and 1165 g in 3.47 h respectively, with projected productivities of 4 and 8 kg·day^{-1}. In total, another 3 different benchmark reactions were performed using the Firefly reactor, showing the scale-up possibilities and applicability with projected productivities ranging from 1.2 to 4 kg·day^{-1}.

Afonso, Siopa, and co-workers developed three scalable reactors using the same design principles as described before: one with coiled FEP tubing and two parallel tube reactors using quartz tubes.[140] All three reactors were placed within a homemade Rayonet chamber, irradiation provided by 254 nm Philips UV-C lamps (16 × 8 W) (Figure 9C). The 302 mL FEP reactor (called FEP4) consists of 23 m of 0.4 cm ID capillary wrapped around a metal grid. The quartz reactors consist of 32 parallel tubes of 0.2 cm ID (PQT2) and 24 parallel tubes of 0.4 cm ID (PQT4), resulting in irradiated volumes of 23 and 68 mL, respectively. After initial batch testing, using the flow reactors in a batch mode operation, the photochemical aziridination of pyridinium salts was done in a flow mode (Scheme 5). Both flow recirculation and single-pass flow experiments were performed. The FEP reactor performed better and provided the possibility of prolonged operation times and larger capacity compared to the quartz tube reactors, providing 2 g·day^{-1} of the *n*-butyl-substituted product. Recirculation was necessary for the quartz reactors since the flexible tubes connecting the parallel quartz tubes in series resulted in nonirradiated dead volume zones. The quartz reactors, when operated in a recirculating flow mode, surpassed the productivity of the FEP reactor, which was 0.3 g·L^{-1}·h^{-1}, with 3.3 g·L^{-1}·h^{-1} for PQT2 and 3.7 g·L^{-1}·h^{-1} for PQT4. Further process intensification of this reaction was later

https://doi.org/10.1021/acs.chemrev.1c00332
Chem. Rev. 2022, 122, 2752–2906

Scheme 5. Photochemical Transformation of Pyridinium Salts to Bicyclic Aziridines

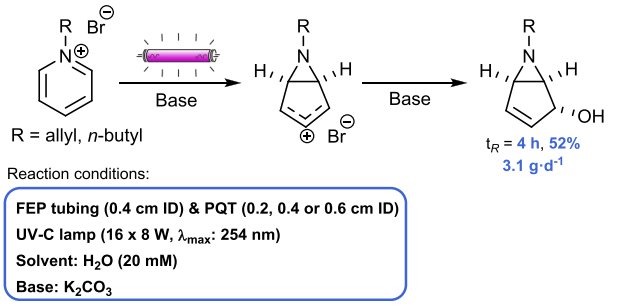

performed by the same group with an updated version of their quartz tube reactor, the PQT6 (Figure 9D), consisting of 12 parallel tubes with 0.6 cm ID, length of 95 cm, and irradiation with 24 lamps (compared to 23 cm length and 16 lamps before).[141] This yielded a productivity of 3.1 g·day^{-1} for the allyl-substituted product.

Another reactor design using externally irradiated quartz was introduced by George, Poliakoff, and co-workers, where instead of using a tube, a quartz jacket was used.[90] This quartz jacket was inserted in the 16 mm bore of the used excimer lamp casing, providing external irradiation by one of the three interchangeable types of excimer lamps (222 nm KrCl, 282 nm XeBr, and 308 nm XeCl, with radiant power of 21, 36, and 49 mW·cm^{-2}, respectively) into the jacket. Inside the quartz jacket a hollow and bored stainless-steel rod was placed (Figure 9E and F). This rod, called the "cold finger", was cooled by internal recirculation of a coolant. The thin bore at the center of the coldfinger is used as an inlet for the substrate solution, and the reaction mixture passes through the narrow annular gap (~120 μm) between the cooling finger and the jacket wall. The total volume of the system is approximately 10 mL, but the irradiated volume is much smaller due to the narrow annular gap (~1.37 mL). An interesting result of the design considerations is that the irradiated light does not pass through the cooling medium, because the coolant is recirculated inside the rod. The performed photochemical transformation (Scheme 6) consists

Scheme 6. Photodecarboxylative Cyclization of a Phthalimide, Followed by an Acid-Catalyzed Dehydration

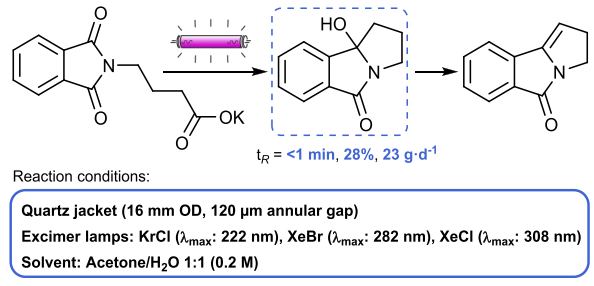

of two steps: the photodecarboxylative cyclization of a phthalimide and its subsequent acid-catalyzed dehydration. The highest space-time yield (STY) found for this system was 3.72 mmol·mL^{-1}·h^{-1} with a yield of 28% using the XeBr lamp, which translates to roughly 0.96 g·h^{-1}. High conversions were reached for the 282 and 308 nm lamps at lower concentrations and flow rates, but those productivities were considerably lower. Neither these high conversions nor higher productivities were achieved for the 222 nm lamp, which is most likely due to the lower spectral irradiance of this lamp compared to the other two lamps. Overall, this system cannot be considered large-scale, but the novelty and practicality of its design specifications show promise for future scale-up possibilities.

Another quartz reactor that cannot be considered large-scale, but where its novelty and unusual design makes it worth noting, was introduced by Hessel, Escribà-Gelonch, and co-workers for the production Vitamin D_3.[142] Especially the irradiation of the reaction mixture is of interest, since, instead of a regular capillary or annular gap configuration, a conical Archimedean quartz spiral is used that is irradiated with a narrow 50 mW 267 nm UV-laser along the spiral. The reason that a tunable UV-laser is used is the need for short pulses required to minimize the formation of undesired secondary byproducts, where the pulses were in the nano- and picosecond range (which was not feasible with the use of LEDs). The Archimedean spiral (0.5 mm ID/3.2 mm OD) enabled comparable irradiation along the spiral, since the first half of the coil is irradiated directly, and scattering/reflection effects ensure low irradiation losses within the system (Figure 9G and H). A conventional UV-lamp was placed to irradiate the spiral from the side, which, in combination with the laser irradiation, is called tandem irradiation. This process intensification strategy achieved similar yields compared to other studies but with significantly shorter irradiation times because of the simultaneous and higher photon flux irradiation,[143] resulting in higher productivity.

3.1.1.3. 3D-Printing of Photochemical Reactors. Apart from the use of reactor capillaries, tubes and vials, advances in 3D-printing have given a boost to the rapid prototyping of lab-scale (micro) flow reactors.[144−148] Not only are reactors fabricated using 3D-printing, but also other general lab equipment, structured catalysts and parts required for a flow setup (e.g., T-mixers, connectors, syringe adapters) can be custom-made.[144,149,150] The low material costs and possibilities for standardization of equipment and rapid prototyping make 3D-printing an attractive option for the lab-environment, and several different additive-based manufacturing techniques can be used.[151,152]

In 2013, Cronin et al. introduced a polypropylene (PP) microfluidic device that was 3D-printed with the commonly used fused deposition modeling (FDM) technique.[153] FDM comprises the extrusion of a molten polymer through a nozzle on a surface, where an object is built layer-by-layer. Since then, the use of additive manufacturing for microfluidic reactor design in organic synthesis has gained traction. For the use of additive manufacturing in photochemistry, additional care needs to be taken in material selection. The used material must not only possess good mechanical stability and chemical resistance, but excellent transparency is also required.[154] Wipf et al. recently developed a microfluidic reactor that was specifically designed for application in photochemistry. The reactor was printed using the FDM-technique, and PP was, again, selected as a material that was suitable for performing photochemical reactions.[155]

Instead of printing the entire reactor structure, Noël et al. recently exemplified a seemingly straightforward scale-up using FDM to print custom molds to allow for fast production and reproducibility of their reactors.[156] The FDM-technique enabled rapid prototyping to experiment with several different design considerations. High-impact polystyrene was 3D-

https://doi.org/10.1021/acs.chemrev.1c00332
Chem. Rev. 2022, 122, 2752−2906

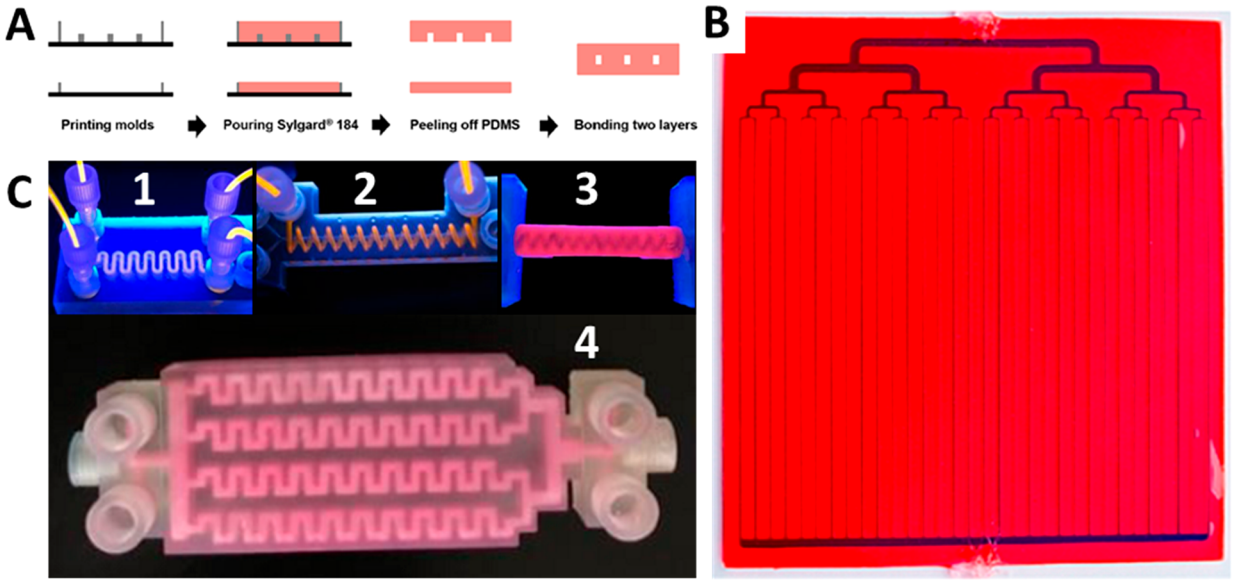

Figure 10. Light-harvesting photoreactor designs. (A) Printing, molding, and bonding of the PDMS layers. (B) 32-Channel LSC-PM with bifurcated flow distributor and flow collection chamber. (A and B) Reprinted with permission from ref 156. Copyright 2017 American Chemical Society. (C) Several different 3D-printed light/reaction channel designs for the FFPM: serpentine/serpentine (C.1), helix/straight (C.2), cylinder/helix (C.3), and the scaled sandwich structure (C.4). (C.1−C.3) Reprinted with permission from ref 163. Copyright 2019 John Wiley and Sons. (C.4) Reprinted with permission from ref 164. Copyright 2020 American Chemical Society.

printed on polystyrene plates to provide two reactor molds (one with a thickness of 1 mm, the other of 2 mm). The reactor channel design was controlled by 3D-printing. The molds were subsequently filled by pouring a polydimethylsiloxane (PDMS) prepolymer mixture into the molds. After degassing, PDMS curing, and peeling off the two separate layers, they were treated with oxygen plasma and subsequently bonded together into one 3 mm slab (Figure 10A). These finalized reactors were based on their previous work on a leaf-inspired luminescent solar concentrator photomicroreactor (LSC-PM), inspired by the light-harvesting phenomena in nature.[157] An LSC-PM uses a luminophore dispersed in a waveguide, a material that is capable of "guiding" light rays by trapping them in the material. The waveguide with the dispersed luminophore can effectively capture light via absorption and re-emit the light for use in the desired photocatalytic transformation.[158] To ensure a high likelihood of the re-emitted photon reaching the reaction mixture, the reactor channels were placed within this waveguide. Careful selection of the used luminophore-catalyst pair ensured optimal overlap in the emission spectrum of the luminophore and the absorption spectrum of the catalyst, thereby increasing the fraction of irradiated light absorbed by the reaction mixture. This down-conversion of light was recently also exemplified by Liu, Du, and co-workers by applying a dip-coated photoluminescent material to enhance light irradiation in the UV-B region.[159]

Using the LSC-PM, the singlet oxygen-mediated cycloaddition of 9,10-diphenylanthracene (DPA) to the corresponding endoperoxide (Scheme 7) was performed as a benchmark reaction. A metal halide solar simulator (1200 W) was used to irradiate the reactor, to emulate the performance of the solar photochemical application of the LSC-PM. Inside the PDMS polymer, the organic dye Lumogen F Red 305 (LR305) was dispersed to match the emission of this dye with the absorption of the photosensitizer methylene blue (MB). The rapid prototyping by 3D-printing enabled the testing of several

Scheme 7. Photocycloaddition of 9,10-Diphenylanthracene to an Endoperoxide

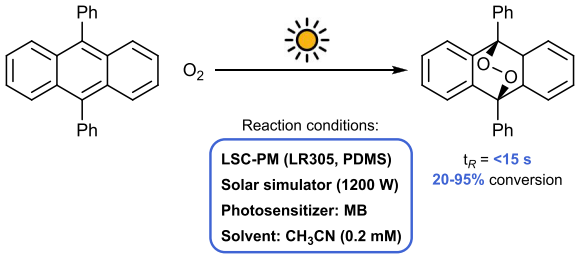

reactor designs, where the interchannel distance, number of channels and flow distribution, and collection sections were optimized. For the flow distribution, a bifurcated flow distributor was found to be most effective for the used internal numbering up strategy. However, also using the bifurcated design for flow collection caused leakages and deformation of the reactor channels because of the large pressure drop in the scaled devices. To prevent this undesired effect and simultaneously decrease the footprint of the reactor, a collection chamber was used. This system (Figure 10B), with 5 mm interchannel spacing and 32 parallel channels was found to partition flow equally within a standard deviation of less than 10%.

Recently, Noël et al. have developed a new LSC-PM design using a combination of commercially available poly(methyl methacrylate) (PMMA) luminescent solar concentrator plates and solvent-resistant PFA capillaries.[160] The new reactors can be made in various colors matching the absorption maxima of a diverse set of visible light-absorbing photocatalysts. Notably, the LSC-PM reactors can be used to harvest solar energy efficiently.[104] Hereto, light fluctuations caused by passing clouds can be addressed effectively using an Arduino-based reaction control system which dynamically changes the

https://doi.org/10.1021/acs.chemrev.1c00332
Chem. Rev. 2022, 122, 2752−2906

residence time depending on the amount of light falling onto the reactor at any given time.[161,162]

Tao et al. introduced another light-harvesting design: the fluorescent fluid photochemical microreactor (FFPM).[163] This design also uses organic dyes to convert incident light to an emission spectrum that is well-suited for the used photosensitizer. However, this dye is not dispersed inside a polymer matrix just as for the LSC-PM, but introduced into the "light channel" as a fluid. A separate channel is used to provide the reactor setup with the reaction mixture, and the placement and structural design of the light channel can control the distribution of the re-emitted light. Several reactor-design prototypes (~6 cm length) were made by curing a 3D-printed transparent photosensitive resin. This 3D-printing technique is called stereolithography (SLA), where a liquid resin bath is selectively polymerized by focused laser irradiation to form a structure layer-by-layer.[151,152] Using SLA, both the shapes of the light channel and the reaction channel were varied (Figure 10C.1−C.3). To optimize the reactor design, a combination of ray-tracing modeling, finite element simulation and the same photocycloaddition of DPA benchmark reaction as for the LSC-PM was used. The light channel was found to function optimally with a cylindrical shape around the reaction channel, providing homogeneous irradiation and the highest photon flux. The reaction channel geometry was optimized as a helix, to allow for fast mixing compared to the straight channel. The scalability of this FFPM reactor concept was then investigated by Zhang, Yu, and co-workers.[164] Instead of consisting of one light- and one reaction channel, it was chosen to provide irradiation to the reaction channel from the top and the bottom, hereby introducing a sandwich structure (top and bottom as a light channel, and a reaction channel in between) and the channel geometry was changed to a serpentine design. The scale-up was performed using the same benchmark reaction as for the small-scale reactor designs, where irradiation was provided by blue LEDs or a solar simulator. The final reactor design (Figure 10C.4) took inspiration from the LSC-PM scale-up[156] by using bifurcated flow distribution and a collection chamber.

3.1.1.4. Photoreactors Based on Nebulizing and Scattering Effects. Drawing inspiration from another phenomenon in nature, Vassilikogiannakis, Pergantis, and co-workers developed a flow reactor that mimics how oxidative photochemistry takes place in clouds.[165] A nebulizer-based photooxygenation system (NebPhotOX) was developed that effectively deals with two issues found with this type of photochemistry: poor oxygen solubility in organic solvents and light attenuation. The proposed solution to these issues was the introduction of the biphasic (gas−liquid) reaction mixture by way of nebulization. Nebulization is the generation of an aerosol that consists of small droplets (estimated ~60 μm droplet diameter) dispersed in a gas, which drastically increases the gas−liquid interface and the gas−liquid mass transfer. A pneumatic nebulizer was used to nebulize the reaction solution with oxygen gas into a cylindrical Pyrex glass chamber (37 cm length, 6.5 cm diameter). Around this glass chamber, a plastic cylinder lined with neutral white LED strips (10 W·m^{-1}, no total power usage was reported) was placed around the chamber to provide irradiation. Two collection vessels were attached in series, where the glass chamber was positioned at a slight downward angle toward the first collection vessel to ensure that all solution was drained. The second vessel was equipped with a condenser to ensure capture of all product (Figure 11A). The

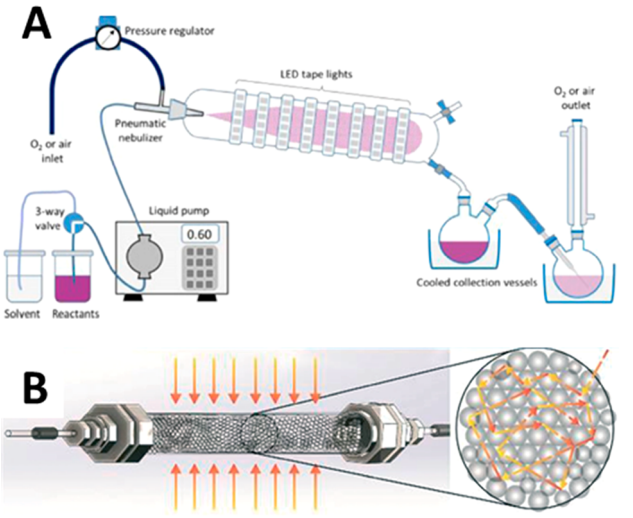

Figure 11. (A) The cloud-inspired nebulizer-based NebPhotOX photoreactor. Reprinted with permission from ref 165. Copyright 2017 John Wiley and Sons. (B) Schematic representation of the cloud-inspired glass bead packed bed reactor. Reprinted from ref 166. Published by Royal Society of Chemistry.

photooxygenation of β-citronellol to the hydroperoxide products A and B with photosensitizer Rose Bengal (RB) (Scheme 8) was performed inside the NebPhotOX reactor by

Scheme 8. Photooxidation of β-Citronellol to Two Hydroperoxide Products A and B

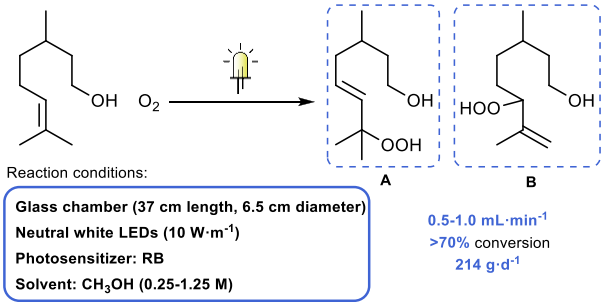

nebulizing the solution flow (0.5−1.0 mL·min^{-1}) with oxygen or air as nebulizing gas. The back pressure of the nebulizing gas was varied between 20 and 60 psi (~1.4−4.1 bar). It is important to note that, because of the nature of the nebulization process, the flow rate can vary between different experiments, so the actual flow rate was calculated based on the measured nebulization time for 5 mL of solution. The highest productivity was found with 1.25 M of citronellol, at a flow rate of 0.80 mL·min^{-1} with 3.4 bar of oxygen backpressure. The combined productivity of products A and B was 0.79 mmol·min^{-1}, which is 214 g·day^{-1} (A:B molar ratio of 1:1.15). The substrate conversions were consistently around 90%, but at higher substrate concentrations, this dropped to ~80%. When oxygen as the nebulizing gas was exchanged for air, comparable results were observed, where the conversion differences at low concentrations were negligible. However, at higher concentrations conversions dropped to ~70%. Nonetheless, using air still provided a maximum productivity of 171 g·day^{-1}. Another set of experiments that was performed in the NebPhotOX, the photooxidation of α-terpinene to ascaridole

https://doi.org/10.1021/acs.chemrev.1c00332
Chem. Rev. 2022, 122, 2752−2906

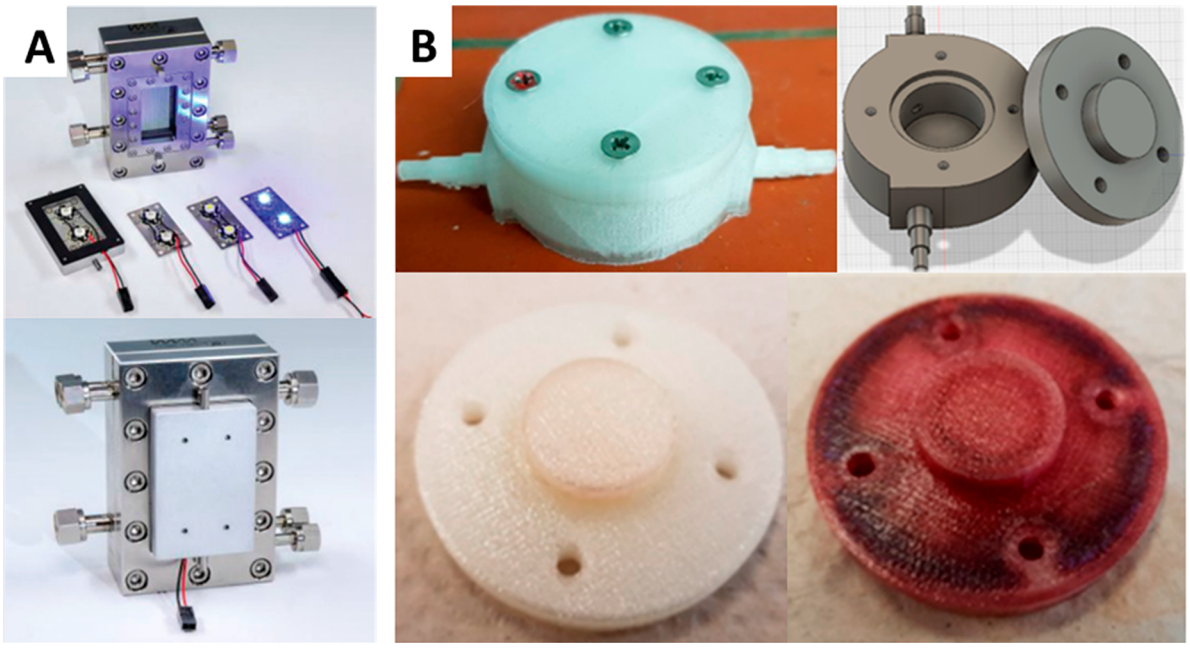

Figure 12. (A) Microstructured falling film reactor with the magnetically attached LED arrays to the inspection window. Reprinted with permission from ref 172. Published by Royal Society of Chemistry (Copyright Fraunhofer IMM). (B) 3D-printed flowmeter reactor, CAD-design, and reactor lid: pre- and postabsorption of TPP. Reprinted with permission from ref 175. Copyright 2020 American Chemical Society.

with RB, almost doubled the maximum productivity to 1.41 mmol·min^{-1} (342 g·day^{-1}) of ascaridole.

The NebPhotOX was recently used for the scale-up of other reactions, such as the photooxygenation of furan substrates to cyclopent-2-enones,[167] the in situ production of reactive *N*-acyl iminium ions,[168] and the photooxygenation of furans.[169] For the latter two cases, the glass chamber was placed vertically, spraying the aerosol downward to minimize droplet-wall interactions encountered with the horizontal or tilted orientations. This effectively prolonged the lifetime of the nebula and simultaneously assisted with collection in the product vessel. Recently, another photoreactor design was reported that also used nebulization to produce aerosols to efficiently harvest the irradiated light.[170] The general concept of this reactor was very similar to the NebPhotOX, but a key difference in reactor operation was the light irradiation. Whereas the NebPhotOX used external irradiation, this design consists of an immersion well-type jacketed glass vessel where a UV-A lamp was placed in the center and the aerosol was passed through the annular hole (the jacket). This way even backscattered light could be absorbed by the aerosol droplets.

Similarly to the development of the NebPhotOX, Khan, Wu, and co-workers drew inspiration for a novel photoreactor design from atmospheric photochemistry inside a cloud's water droplets.[166] Especially of interest was the increased photon path length within clouds, which is caused by multiple scattering, refracting and reflecting events at the gas−liquid interface that effectively trap photons inside the cloud. The goal of their reactor design was to scale a microreactor to the mesoscale without the necessity of a more powerful light source, as is commonly the case for scale-up, but only by optimizing the light-harvesting of a low power light-source. To recreate the desired effect found in clouds, small glass beads (∼75 μm) were introduced into PFA capillaries of increasing diameter (1, 5, and 10 mm ID), to create three packed bed reactor tubes (Figure 11B). These tubes were placed in the center of a glass cylinder (9 cm ID) that was wrapped with a blue LED strip (5 W, 460 nm). The resulting photoreactors were tested with a visible-light-promoted *E*/*Z* isomerization and the production rates, normalized to the same reactor tube lengths, were then evaluated. From the smallest to the largest diameter tubes, the projected production rates increased from 25 to 430 mg·day^{-1} and, finally, 1700 mg·day^{-1}. The reactor with the highest productivity, the 10 mm ID packed bed tube, was then compared to a 5 mm ID single-phase tube (without glass beads) to show the improvement due to the increased path length in the packed bed tube. This single-phase tube was chosen because it holds the same amount of liquid volume per length unit as the larger packed bed tube, where ∼75% of the volume is occupied by the glass beads. In comparison, the single-phase tube was found to produce 1000 mg·day^{-1}, showing that the packed glass beads provide an increase in productivity of 70% for the same irradiated volume.

3.1.1.5. Photoreactors with Immobilized Photocatalysts. In the previous example, a glass bead packed bed design was used to improve light-harvesting by scattering, but another possible application of packed bed reactors in photochemistry is the immobilization of photocatalysts. Continuous-flow designs in photochemistry often use homogeneous catalysts, such as dissolved photosensitizers, instead of heterogeneous catalysts. However, the use of heterogeneous catalysts can generally simplify separation and product workup, thereby reducing production costs. This is especially of importance when production is increased to an industrial scale. There are several ways heterogeneous catalysts can be incorporated, such as by introducing the catalyst as a slurry or by immobilization. To keep the catalyst in suspension often requires external mechanical energy to prevent catalyst deposition or even clogging. Immobilization has the advantage that these external influences are not required and that the separation of the reaction mixture of the catalyst, for example, by filtration, is not necessary, provided there is no leaching.

https://doi.org/10.1021/acs.chemrev.1c00332
Chem. Rev. 2022, 122, 2752−2906

Gupton, Belecki, Ahmad, and co-workers considered the benefits of easy separation and additional reusability of heterogeneous catalysts in the development of a new packed bed photoreactor.[171] The photosensitizer RB was immobilized onto polystyrene and introduced as a preswollen slurry into an Omnifit column (6.6 mm ID, 150 mm length). The resulting functionalized polystyrene packed bed reactor was designed for use in singlet oxygen heterogeneous photocatalysis and could now also be used with RB-insoluble solvents. Furthermore, the immobilized RB was found to be more resistant to photobleaching and agglomeration compared to its homogeneous counterpart, enabling reusability without the need for column repacking. A metal framework was placed around the column reactor, providing LED irradiation (580 and 530 nm, 90 W total input power) around the entire column. Initial optimization was done with the photooxidation of α-terpinene to ascaridole, which maintained a yield of 94% for the continuous 10 h run. The 0.1 mL·min^{-1} solution flow (and 5.0 mL·min^{-1} O_2 flow) with 15 mM substrate concentration yielded a productivity of 0.34 g·day^{-1}. Further investigation in the substrate scope was done with similar operating conditions. Comparable productivities were obtained, showing that this immobilization on a packed bed reactor concept is widely applicable.

Rehm, Rueping, and co-workers also implemented the immobilization of a photocatalyst in another reactor type, a microstructured falling film microreactor (FFMR) (Figure 12A).[172] A previous design of this reactor was already used with an immobilized catalyst coating for nonphotochemical reactions,[173] and another design was used for homogeneous photocatalytic reactions,[174] but the immobilization of a catalyst in the FFMR for use in flow photochemistry was recently developed. The FFMR consists of a stainless-steel reaction plate with 32 microchannels (600 μm width, 200 μm depth, 78 mm length) that was placed inside the reactor casing. This casing has an "inspection window" to which an LED array (455 nm, 2.4 W input power) can be magnetically attached to supply the channels with photons. The surface of these channels is coated with an immobilized layer of titanium dioxide. The liquid flow was introduced at the top of the stainless-steel plate and allowed to flow downward along the channels on the plate by gravity, hereby effectively creating a thin film of reaction solution. This thin film, being concentrated on a catalytically active surface, combined with the irradiation, makes this reactor concept ideal for increasing reaction rates in flow photochemistry. Where falling film reactors are commonly used to promote the gas−liquid interface as well, in this case no gas was required for the chosen chemistry. Nonetheless, an inert gas (N_2) was used to allow for successful draining of the reactor. To investigate the productivity of this reactor, the formation of 2-(4-chlorophenyl)pyridine from 4-chlorobenzenediazonium salt (0.05 M in ethanol) and pyridine was selected. Using a flow rate of 0.5 mL·min^{-1}, the obtained yield after purification was 99%, resulting in a productivity of 36 mmol·day^{-1} or 6.8 g·day^{-1}.

Surface-functionalization with an immobilized photosensitizer was also done by Griesbeck et al.[175] The goal was to develop an experiment for students to incorporate 3D-printing into a flow photochemical reaction. To this end, a flowmeter-like small-scale PP reactor was 3D-printed using the FDM-technique (Figure 12B). Immobilization of the photosensitizer was achieved by immersing the reactor lid in a solution containing the photosensitizer tetraphenylporphyrin (TPP) and drying it overnight. The lid was then screwed on the reactor, resulting in the finalized reactor (external dimensions ∼5 cm diameter, ∼1.5 cm height) that could be irradiated with a white LED (30 W, 590 nm) from the bottom. This was done from the bottom to allow more transmittance into the reaction mixture. The experiments used the photooxygenation of citronellol (Scheme 8) by circulating the reaction mixture, and full conversion (1.4 mmol) was reached after 10 h of circulation.

Griesbeck et al. also reported the use of "4D-printing", where the functionalization of the surface with an immobilized catalyst is part of the printing process.[176] Their previous flowmeter-like reactor design was used, but instead of printing with PP, a hybrid resin is used to print the structure. This is done with SLA- and digital light processing (DLP) techniques. Both are stereolithographic techniques that use a resin bath, but whereas SLA uses a laser that moves across the 2D-plane to polymerize one layer, DLP uses projection of one entire layer at a time to polymerize the structure layer-by-layer. After 3D-printing, there were free isocyanate groups available on the reactor surface, which were readily functionalized with immobilized photosensitizers or even with water to create urea bonds at the surface, allowing for good chemical resistance to solvents while maintaining its transparency. Recently, surface functionalization introduced during the 3D-printing process was also reported by Xuan, Vilela, and co-workers for flow reactor components, exemplified by the incorporation of a photocatalytic monomer in the resin for their SLA-printed monoliths.[177] This novel field in flow photochemistry is still in its infancy but can have a major impact on future scale-up of passive photochemical flow reactors toward industrial scale, where the increased photosensitizer stability, chemical resistance, and ease of separation can make this an attractive option.

3.1.2. Custom Active Reactors. In photochemical reactors, the dimensions affect the reactor performances significantly, owing to the implications of the Bouguer−Lambert−Beer law. Small dimensions enable a homogeneous irradiation of the reaction medium and result in accelerated kinetics, reduced reaction times, and high reaction selectivities. These small dimensions can be reached not only through the use of small, confined spaces, such as capillaries and annular gaps, but also by the generation of thin films. The generation of thin films can be achieved in a number of ways, for instance by gravity in falling film reactors but notably also by the introduction of fluid onto a rotating surface, where centrifugal forces stretch this film across the rotating surface. Academic interest in various reactor designs that utilize this thin film generation is apparent due to the additional advantages of these films, including large surface areas, enhanced heat- and mass transfer, micromixing, and high shearing rates. The high shearing rates and vortices formed with high-speed rotation can also drastically increase the surface areas and mixing by bubble dispersion into the liquid, and therefore, several designs have been published for this type of reactor (e.g., vortex fluidic devices,[178] rotating disk reactors[179]). This section, devoted to custom active reactors, will focus on how reactor designs use agitation of the reaction mixture, the generation of thin films by high-shear rotation, and how they utilize these generated films and supplied mechanical energy for photochemical purposes.

https://doi.org/10.1021/acs.chemrev.1c00332
Chem. Rev. 2022, 122, 2752−2906

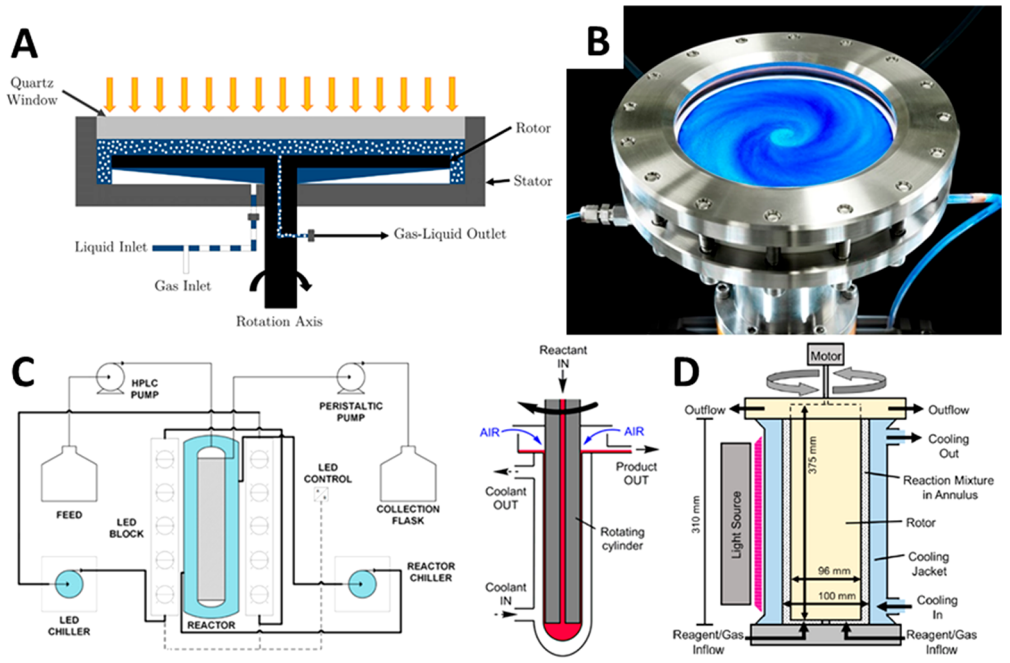

Figure 13. (A) Schematic representation of the pRS-SDR and (B) top-view image of the operational pRS-SDR with photosensitizer MB. Reprinted from ref 180. Published by Elsevier. (C) Flow scheme and schematic representation of the vortex reactor. Reprinted with permission from ref 183. Copyright 2017 American Chemical Society. (D) Schematic representation of the large-scale vortex reactor. Reprinted with permission from ref 184. Copyright 2020 American Chemical Society.

3.1.2.1. Rotor-Stator Reactors. A recent example of a reactor design that used external mechanical energy to increase mixing and throughput is the photo rotor-stator spinning disk reactor (pRS-SDR) developed by Van der Schaaf, Noël, and co-workers.[180] This design combined the advantages of rotor-stator spinning disk reactor technology[181,182] to achieve high mass transfer with a small penetration depth for light irradiation of the reaction mixture. The reactor consists of a rotating disk encased by the stator, leaving an axial and radial gap of 2 mm between the rotor and the stator. The top of the stator is equipped with a quartz window through which the reaction mixture can be irradiated (Figure 13A and B). The reactor has two operation modes where the gas−liquid mixture can be supplied either through the center of the rotor, or from the bottom of the stator. The former operation mode (thin film mode) provides the rotor with a thin liquid film that is stretched outward over the circular plate. The latter mode (dispersed mode) introduces the gas−liquid mixture in such a way that the gas-phase is subsequently dispersed in the liquid as bubbles by the fast rotation. Since the thin film mode only enabled relatively low throughputs, the dispersed mode was preferred for the large-scale experiments. To demonstrate the potential of this reactor setup, the photooxidation of α-terpinene to ascaridole (Scheme 9) was used as a benchmark. The reaction mixture was irradiated through the quartz window by a 120 W white LED light source, which provided the reactor with an irradiated volume of 27 mL (of the 64 mL total volume). The rotational speed was varied between 0 and 3000 rpm (rpm). By increasing the rotational speed, the size of the dispersed droplets decreased, effectively increasing the interfacial surface area. This way, intensification of mixing could be tuned independently of the used flow rates. For a residence time of only 27 s, 1.1 kg·day^{-1} (270 mmol·h^{-1}) productivity was reached (liquid flow rate of 60 mL·min^{-1}, yield of 75%). Both the yield and selectivity toward ascaridole

Scheme 9. Photooxidation of α-Terpinene to Ascaridole (A) and the Common Byproduct *p*-Cymene (B)

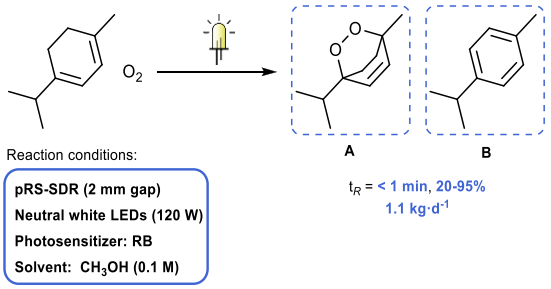

increased with increasing rotational speeds, where increasing this further than 2000 rpm yielded no additional improvement. At this rotational speed, the energy consumption for the rotor was only 15 W, which is approximately 11% of the total energy consumption, showing that the light source remains the most expensive part of continuous production. The reactor performance was compared to a capillary microreactor and, to get the same productivity as the pRS-SDR, 71 microreactors would have to be operated in parallel.

Another reactor design that uses a rotating structure with stationary surroundings is the lab-scale vortex reactor introduced by George, Poliakoff et al.[183] The design of this reactor is similar in style to their previous reactor design,[90] that used a stationary bored rod. This new design consists of a suspended bored stainless-steel rod (18 mm diameter) that functions as the rotor. The rod is placed inside a custom jacketed glass tube (20 mm ID) and the annular space between these (~1 mm) functions as the irradiated volume (8 mL), irradiated by three blocks equipped with 5 white LEDs each (total input power ~ 195 W) (Figure 13C). Liquid was fed into the system through the narrow bore inside the rod, and the required gaseous phase was drawn in by the lower pressure

https://doi.org/10.1021/acs.chemrev.1c00332
Chem. Rev. 2022, 122, 2752−2906

region caused by the rotation of this rod. Therefore, no additional gas-feed was necessary, which was made possible by keeping the top of the reactor open to air. The rotating rod caused high shear-rates and generated Taylor−Couette vortices in the liquid, finely dispersing the gas-phase as bubbles into the liquid and providing rotating-dependent mixing. The production of ascaridole was used as a benchmark gas−liquid photochemical reaction (Scheme 9), where the rotational speed was varied and found to be optimal at 3000 rpm. At higher speeds, the competing oxidation to *p*-cymene was promoted and the yield of ascaridole dropped. A flow rate of 0.5 mL·min^{-1} (0.1 M α-terpinene in ethanol) at 3000 rpm resulted in a productivity of 2.73 mmol·h^{-1} (11.0 g·day^{-1}) with 91% yield of ascaridole.

Starting from the small-scale vortex reactor, George, Poliakoff et al. developed a scale-up version of this reactor concept.[184] Instead of the air being drawn in, a gaseous flow into the reactor was implemented to allow for more precise control of the gas-feed. The rotor was changed from a suspended stainless-steel rod to a polyether ether ketone (PEEK) rod (96 mm diameter) that was attached to both the reactor base and cap, to ensure mechanical stability. This rod was placed inside an open-ended jacketed glass filter tube (100 mm ID) that was closed off by the base and cap (Figure 13D). Both the liquid- and gas-inlets were placed at the base, whereas the outlets are located inside the cap. Irradiation of the annular space (~2 mm, 280 mL) was provided by two curved white LED-blocks for visible-light (totalling 720 W input power), and one or two medium-pressure mercury arc lamps for UV-light (1.4 or 2.0 kW input power). Because tangential velocity (angular velocity multiplied with the radius) of a rotating object increases with an increasing radius, the larger-sized rotor required lower rotational speeds to provide the same Taylor−Couette vortex behavior as the small-scale reactor (1300 vs 4000 rpm). The photooxidation of β-citronellol (previously shown in Scheme 8) was performed in both the small and large-scale vortex reactor. The total productivity of both products for the small-scale reactor (4000 rpm) was <10 g·day^{-1}, whereas the large-scale reactor (660 rpm) was reported to be capable of producing >1.6 kg·day^{-1}. To show the UV-capabilities of both reactors, a previously discussed UV−photochemical reaction was performed (Scheme 4, using ethyl acetate as solvent), where, most importantly, the reactors were operated in single-phase without gas. The small-scale reactor (4000 rpm) reached 0.5 kg·day^{-1} productivity at full conversion and selectivity but could be pushed toward 0.9 kg·day^{-1} by using a quartz vessel instead of a borosilicate glass one. This did provide a wider irradiation spectrum (190 nm vs 280 nm cutoff), but it came at the cost of the selectivity and caused fouling of the reactor. The large-scale reactor (660 rpm), using only borosilicate glass, showed a maximum projected productivity of 7.5 kg·day^{-1} (2 × 2.0 kW).

3.1.2.2. Thin Film Reactors. The pRS-SDR and the vortex reactor design both use a combination of mechanical rotation and a narrow gap cell between the rotor and stator. This narrow gap allows to enhance mixing and dispersion effects and ensures efficient irradiation of the reaction mixture.

A thin film can also be generated solely by rotation. George, Poliakoff, and co-workers developed a photochemical reactor, called the "PhotoVap", based on conventional rotary evaporator technology (Figure 14A).[185] The traditional rotary evaporator was modified for use as a reactor by inserting two PTFE tubes to allow for a reaction solution to be pumped in

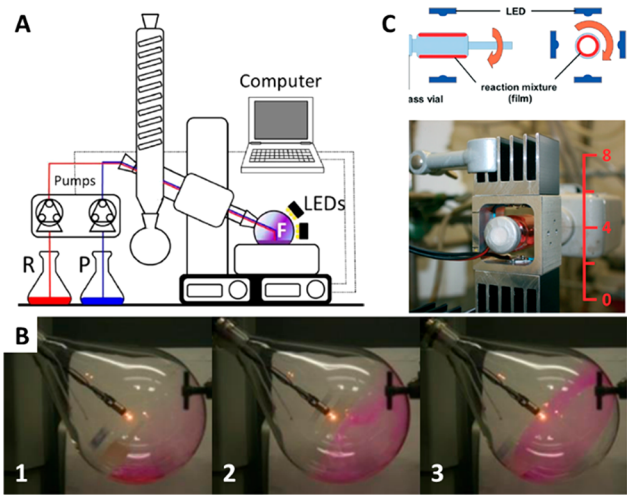

Figure 14. Thin film rotational reactors. (A) Schematic representation of the PhotoVap setup. (B) Film formation for the PhotoVap: (B.1) liquid pool at 50 rpm, (B.2) liquid pool and thin film at 150 rpm, and (B.3) band formation at 200 rpm. (A and B) Reprinted with permission from ref 185. Copyright 2016 American Chemical Society. (C) Schematic representation and photograph of the rotating film reactor setup (ruler indicates cm). Reprinted with permission from ref 187. Copyright 2016 Royal Society of Chemistry..

and out of the flask. The flask was irradiated by two white LED blocks (total power for low intensity ~145 W and for high intensity ~350 W) placed at 2 cm distance from where the thinnest generated films were observed. The reactor was automatically operated semicontinuously by a computer that ran sequential batch cycles. This cycle consisted of filling the flask, irradiating the reaction mixture, and emptying the flask. By bubbling oxygen or air through an additional PTFE tube, the photooxidation of α-terpinene (Scheme 9) yielded productivities ~125 mg·min^{-1} using a 1 L rotating flask (5 mL irradiated volume, 175 rpm) and low intensity light. Using different flask sizes filled with more solution yielded comparable productivities but switching to high light intensity almost tripled the productivity (~370 mg·min^{-1}). The effect of the thin film was demonstrated by an experiment where the flask was kept stationary, which resulted in a productivity of only ~17 mg·min^{-1}. However, the effect of the rotational speed on the film thickness showed that increasing rotational speed was not always beneficial. At low rotational speeds (50−175 rpm), a liquid pool was present at the bottom of the flask that improved mixing and the film thickness was measured between 0.1 and 0.7 mm. For higher speeds (>200 rpm), this pool disappeared and a thicker, less uniform, band was formed, negating the increased mixing and benefits of the thin film (Figure 14B).

The advantage of such PhotoVap reactors is that it can be rapidly assembled from the readily available rotary evaporator equipment. Feringa et al. used such a strategy to scale the selective photooxygenation of furfural.[186] Using a 1 L flask (10 mL irradiated volume, 175 rpm) irradiated by white LEDs (10 × 80 W LEDs), a productivity of 30 mmol·h^{-1} (3.0 g·h^{-1}) was reached, enabling the production of over 1 kg of product.

The PhotoVap applicability was extended by George, Poliakoff, and co-workers to the UV-PhotoVap, by making the setup compatible with UV-light irradiation.[188] The white light LEDs were replaced with medium-pressure mercury lamps (combination of one or two 1.4−2.0 kW lamps). An

https://doi.org/10.1021/acs.chemrev.1c00332
Chem. Rev. 2022, 122, 2752−2906

inert gas (N_2) was delivered into the flask to prevent undesired side-reactions with oxygen. Two cycloadditions (Schemes 1 and 4), both in single and sequential batch mode, were performed in 1 L quartz or borosilicate flasks (150 rpm). Cooling the reaction solutions with the rotary evaporator's water bath was not sufficient to keep the reaction temperature constant during high-power irradiation, but the temperature increase (3.5 °C·min^{-1}) did not seem to affect performance. The productivity of Cookson's dione was ∼55 g·h^{-1} in the quartz flask (30 mL irradiated volume), which dropped to 22 g·h^{-1} in the borosilicate flask due to the lower UV-transmittance. Increasing the irradiated volume to 100 mL yielded productivities >200 g·h^{-1} in the quartz flask. In contrast, the [2 + 2] photocycloaddition of maleimide and 1-hexyne suffered from overirradiation and byproduct formation, resulting in lower yields (∼40%) and more fouling of the used flasks. Again, a change to borosilicate was found to reduce overall yield and increasing the irradiated volume to 100 mL (from 30 mL) improved mixing and reduced fouling/overirradiation. Moderate productivities for this reaction were reported, ranging from ∼5−14 g·h^{-1}.

Another reactor design that incorporates thin film generation is the rotating film reactor, introduced by König et al.[187] This reactor consists of a rotating glass vial irradiated by 4 blue LEDs (455 nm, 28.1 mW·cm^{-2}) placed on an aluminum frame around the vial (Figure 14C). The reactor was operated in batch mode by rotating the vial with a KPG stirrer (1200 rpm), which created a thin film (0.26 mm) of solvent-free reaction mixture. This reactor design was based on a rod mill apparatus that König et al. had previously introduced.[189] In this design, the primary focus was the use of ball milling for the combination of photocatalysis and mechanochemistry.[190−192] The setup used 5 LEDs for irradiation of a glass vial, instead of 4, where the additional fifth LED was placed at the bottom of the vial. A glass rod was rotated (80 rpm) inside the vial containing a heterogeneous (solvent-free) mixture, which created a thin film in the annular space. Another novel batch reactor design that combined mechanochemistry and photocatalysis was introduced by Hernández, which used ball milling in a transparent PMMA milling jar, irradiated by blue and green LEDs.[193] The advantage of using these reactor types, despite currently being reported only in batch operation mode, is the possibility to use neat, heterogeneous reaction mixtures, where side-reactions with the solvent or poor solubility of one of the components can be avoided.[194] Spreading out the reaction mixture in a thin film can also allow for higher concentrations of light-absorbing species, because of the small penetration depth.

3.1.2.3. Solids Handling in Flow. In principle there are two main reactor types for continuous processing: the CSTR (continuous stirred-tank reactor) and the PFR (plug flow reactor), both schematically shown in Figure 15. The majority of the discussed reactor designs that used PFA, FEP, and glass tubes or capillaries are examples of the PFR-type reactors, chosen due to their excellent residence time control and because generally a smaller volume is required to achieve high conversions in comparison to CSTRs. An advantage of CSTRs is that solids handling generally poses less issues as compared to PFRs, where the tubes used are of small dimensions and therefore prone to clogging.[195] Additionally, since the inlet feed in a CSTR is rapidly quenched by the large reaction volume this can provide safety when working with toxic or highly concentrated reactor feeds. In theory the behavior of a PFR can be approximated by placing an infinite amount of CSTRs in series. Selection of a PFR, CSTR, or CSTRs in series for a process depends on a multitude of factors (e.g., heat and mass transfer, residence time control, reaction kinetics).[196]

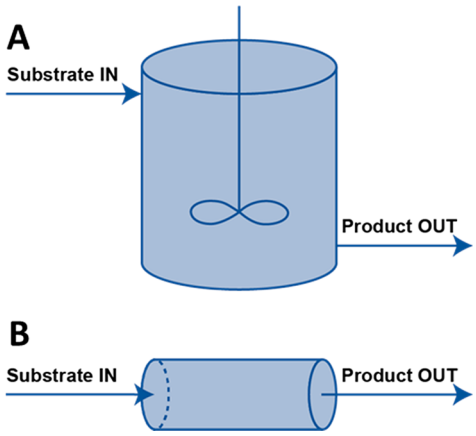

Figure 15. Commonly used schematic representations of a CSTR (A) and a PFR (B).

Researchers from AbbVie developed a photochemical CSTR approach that was capable of managing heterogeneous reaction mixtures in continuous-flow.[197] In this example, a high-power fiber optic laser (25 W, 450 nm) was used to irradiate the entire CSTR vessel. The reaction mixture in the cylindrical 100 mL reactor (5 cm solution depth) was agitated with a magnetic stirring bar and irradiated at the top surface by a laser that passes through a beam expander to ensure irradiation across of the entire cross section and solution depth (Figure 16A). The inlet was placed close to the bottom of the vessel, and the outlet was placed as far away as possible: on the opposite side and near the surface of the reactor volume. With this setup in place, an almost ideal CSTR residence time distribution was observed as shown by the performed tracer-experiments. The reactor was benchmarked in a C−N cross-coupling reaction, previously shown in Scheme 2 (an iridium-based photocatalyst is used instead). With a 20 min residence time, excellent productivity was achieved after 32 h of continuous production, resulting in 1.85 kg of isolated aryl bromide product. This translates to a productivity of 1.16 kg·day^{-1}. The energy efficiency of the CSTR is a big advantage (∼46 g·W^{1-}·day^{-1}). Furthermore, it was proposed that two CSTR modules in series (100 and 38 mL respectively), with a combined residence time of 8 min, can even achieve a 3-fold increase of productivity to 3.9 kg·day^{-1} at 90% predicted conversion (using 2 × 25 W lasers, ∼78 g·W^{1-}·day^{-1}). This prediction was done using a Levenspiel analysis that accurately described their CSTR module. Some solids deposition on the reactor walls was observed, however, the large vessel encountered no flow-related problems, indicating an advantage of the CSTR design compared to narrow tubular/capillary reactors, and the top-surface irradiation was not influenced (e.g., by scattering) by this deposition.

Jensen et al. developed a CSTR cascade reactor that benefits from the solids-handling capabilities of CSTRs.[198] This cascade is a connection of 5 small CSTRs in series (13 mm diameter, 9 mm depth, 5.3 mL total volume) to emulate reactor performance of a PFR. The reactor consists of a PTFE block, enclosed by aluminum housing and a glass window (Figure 16B and C). The separate CSTR chambers are

https://doi.org/10.1021/acs.chemrev.1c00332
Chem. Rev. 2022, 122, 2752−2906

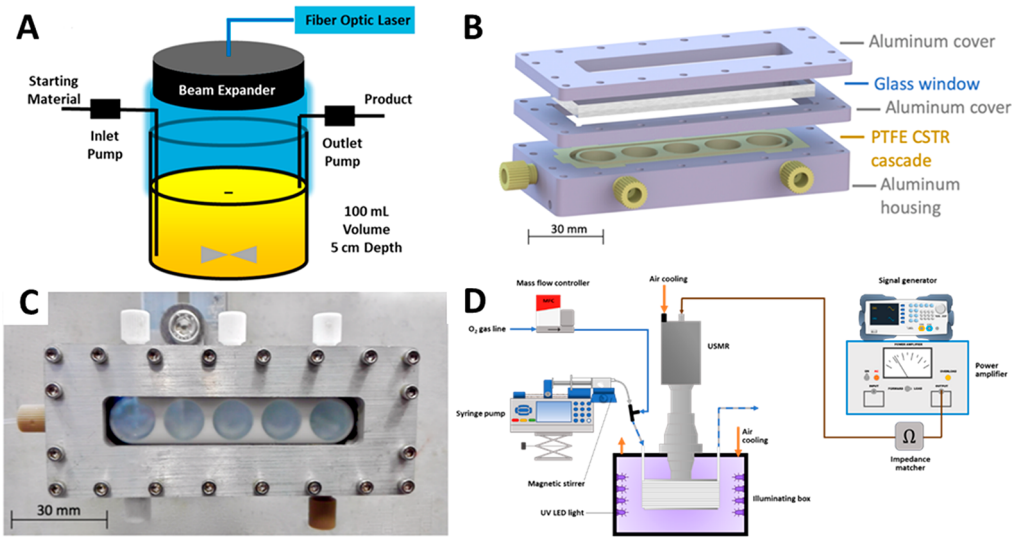

Figure 16. (A) Schematic representation of the high-intensity laser CSTR. Reprinted with permission from ref 197. Copyright 2019 American Chemical Society. (B) Schematic representation and (C) assembled version of the CSTR cascade reactor. Reprinted with permission of ref 198. Copyright 2019 American Chemical Society. (D) Schematic setup of the ultrasonic milli-reactor. Reprinted from ref 199. Published by Elsevier.

connected by holes drilled into the PTFE (CSTR1: 2.5 mm ID, or CSTR2: 0.7 mm ID) and in each chamber a magnetic stirring bar is placed. The CSTRs were irradiated by blue LEDs (440 nm, 3 × 40 W), focused onto the glass surface with condenser lenses. A custom slurry pump was used to supply the reactor with the heterogeneous reaction mixture. The CSTR cascade CSTR1 was at lower risk of clogging, but some back-mixing between the individual chambers was observed. The risk of clogging was higher for CSTR2, but this did reduce back-mixing. The residence time distribution was extensively studied and CSTR1 showed larger deviation from ideal (CSTRs in series) behavior than CSTR2, due to the extensive back-mixing, making it more difficult to achieve full conversion with CSTR1. Therefore, a 13 h production run (cross-coupling of 4-bromotetrahydropyran and methyl-4-bromobenzoate) was demonstrated using CSTR2, which resulted in a productivity of 80 mg·h^{-1} (58% yield, 99% conversion). The CSTR2 setup was operated continuously without observation of any clogging events.

Another approach to solids handling is the use of ultrasonic irradiation (sonication). Submersion of flow reactors in conventional ultrasonic baths has previously been used to prevent the bridging and constriction mechanisms that cause clogging of capillaries.[200,201] Horie et al. reported a photochemical reactor setup for the dimerization of maleic anhydride, where FEP tubing was wrapped around the external surface of a beaker that was submerged in an ultrasonic bath.[202] A medium-pressure mercury lamp was placed in the center of beaker to provide light irradiation of the capillary, while ultrasonic irradiation successfully kept the reaction mixture in suspension. A more direct way to provide acoustic irradiation to a reactor, where sound did not have to travel through a medium (e.g., water in an ultrasonic bath), was developed by Jensen et al.[203] Their microreactor, not suited for photochemistry due to absence of transparent windows, consists of stacked layers of PTFE with an integrated piezoelectric actuator. This actuator, operated at sufficient load power, provided the microchannel with ultrasonic irradiation and generated cavitation bubbles capable of breaking up particle agglomerates. These cavitation bubbles are formed by locally concentrated low pressure regions, created by the traveling soundwave.

Recently, Noël et al. introduced an ultrasonic milli-reactor that applied direct ultrasonic irradiation for photochemical purposes (Figure 16D).[199] This reactor consists of an ultrasonic transducer that generates the ultrasonic soundwave, a sonotrode, and an irradiating cylinder. The generated soundwave forms standing waves in the longitudinal direction of the sonotrode and radial direction of the cylinder. A glass capillary (2.2 mm ID/3.9 mm OD) was coiled around this cylinder, where the soundwave is efficiently transported into the capillary. The resulting reactor structure (working frequency of 22.6 kHz, ultrasound load power 60 W, irradiated volume of 12.88 mL) was irradiated by a Rayonet-type chamber, lined with an LED strip (365 nm, 65 W) and cooled with compressed air. The effects of ultrasound on the three-phase flow (oxygen, acetonitrile, titanium dioxide) were extensively investigated, where oscillations of the gas slug and cavitation bubbles were observed. Continuous sonication resulted in a substantial temperature increase (∼+11 °C), so pulsed sonication was applied, significantly reducing this temperature increase (∼+3 °C). The reactor was benchmarked with the photooxidation of 4-(trifluoromethyl)benzyl alcohol to the corresponding aldehyde using titanium dioxide as photocatalyst. An increase in conversion by a factor of ∼3−4 was found when comparing sonication to nonsonicated operation of the reactor, which could be attributed to an increase in mixing due to the formation of the cavitation bubbles.

3.2. Commercial Reactors—Driven by the Need for Standardization

With the wide variety in custom photoreactors, researchers can select a reactor that suits their specific needs. Custom reactors are often cheap to assemble compared to the investment costs associated with commercially available reactors, which can be a strong incentive to go for custom ones. This is especially true for academic laboratories where funding can be a bottleneck. However, when custom reactor designs are adopted and copied in other laboratories, this can lead to unforeseen complications. Slight differences (e.g., used light sources and

https://doi.org/10.1021/acs.chemrev.1c00332
Chem. Rev. 2022, 122, 2752−2906

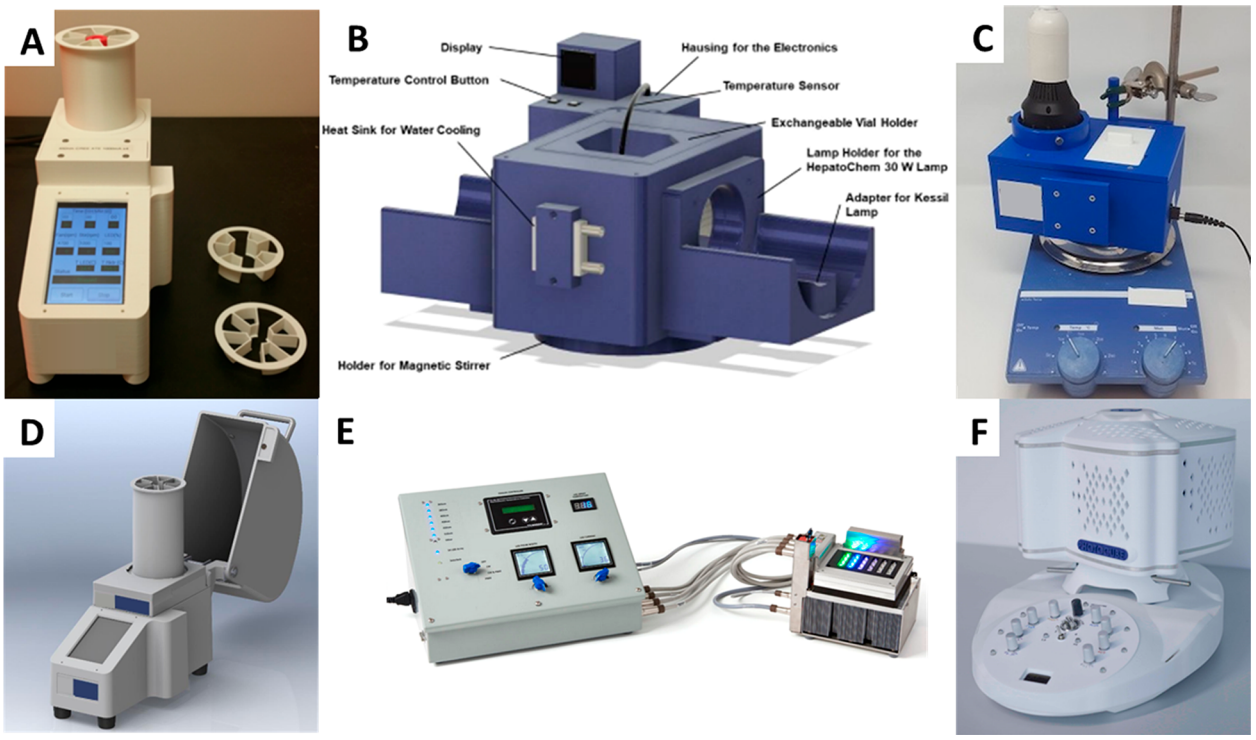

Figure 17. (A) Integrated photoreactor by Merck. Reprinted with permission from ref 204. Copyright 2017 American Chemical Society. (B) Open-access photoreactor. Reprinted with permission from ref 205. Copyright 2021 John Wiley and Sons. (C) EvoluChem PhotoRedOx Box by HepatoChem.[206] (D) Photoreactor M2 by Penn PHD.[207] (E) Photochemistry LED Illuminator (PHIL) by Pacer.[208] (F) The PhotoCube[210] (Courtesy of ThalesNano).

materials, light-reactor distance, reactor cooling) in the reactor design can cause significant deviations from the reported results. Consequently, standardization of the reactor design can offer consistency of reactor operation and interlaboratory reproducibility of obtained results; this is a feature, which is valued highly in the industry. Successful implementation of standardization requires ease of use, robust design, and a wide applicability range. Realizing this in practice calls for clear documentation and user-friendly interfaces to facilitate ease of operation and parameter control. Modular and interchangeable reactor parts, combined with a robust design, allow for a wide range of applications and universal practicality of a reactor design. A collection of commercially available batch and flow photoreactors is presented here and provides an overview of what is currently available in this field.

3.2.1. Commercial Batch Reactors. Researchers at Merck introduced an integrated photoreactor that allows for reproducible and fast photochemical batch reactions to be performed (Figure 17A).[204] The reactor contains of an integrated cooling system, LED irradiation, a reflector chamber, a user-interface and a modular vial holder (2−40 mL). A collection of 8 photochemical reactions was carried out using this setup and validated across multiple Merck sites to show the achieved standardization. Another integrated photoreactor system that was 3D-printed was developed by researchers from Boehringer Ingelheim.[205] This reactor setup was built from commercially available parts, and the 3D designs have been made available as open-access (Figure 17B). The reactor offers exchangeability of light sources, variable light intensities, exchangeable holders for vials, flasks and capillary flow units, temperature control and a user-interface. There are several companies that offer different types of photoreactors, all with their own specifications. HepatoChem offers the EvoluChem PhotoRedOx Box, a batch photochemical reactor (for 0.3−20 mL vials), equipped with a cooling fan, possibility to run 32 reactions simultaneously and compatible with a common magnetic stirring plate and several light sources (Figure 17C).[206] Additionally, versions with double capacity, a temperature control unit and a flow module are available as well. The Photoreactor M2, offered by Penn PHD, supports vials of multiple sizes (2−40 mL) and use of different light sources (365, 420, and 450 nm) because of its modular design (Figure 17D).[207] The M2 is a newer version of the M1 model, made in collaboration with Merck. The reactor can be controlled with the user-interface, that can be used to vary temperature, light intensity and stirring speed. The light shield prevents users from exposure to the irradiation. Pacer developed the Photochemistry LED Illuminator (nicknamed PHIL)[208] for high-throughput screening, demonstrated by researchers at GlaxoSmithKline (Figure 17E).[209] This reactor uses LED cassettes that allow for interchangeable monochromatic LEDs (365, 385, 405, 420, 450, and 525 nm) and the LED driver module allows for variable output power and operation modes (continuous and pulsed). The well plate that is irradiated can hold up to 48 vials to be irradiated simultaneously and is cooled by a plate cooler. The PhotoCube, available at ThalesNano, can be applied for batch, but also offers flow, stop-flow and CSTR configurations (Figure 17F).[210] The module can hold glass batch vials (8 × 4 and 4 × 30 mL) and capillaries (2−20 mL) of both FEP and PFA. LEDs of 7 different wavelength are available (365, 395, 457, 500, 523, 595, and 623 nm), as well as white LEDs, which can be applied simultaneously and will be turned off automatically when the reactor chamber is opened. Further-

https://doi.org/10.1021/acs.chemrev.1c00332
Chem. Rev. 2022, 122, 2752−2906

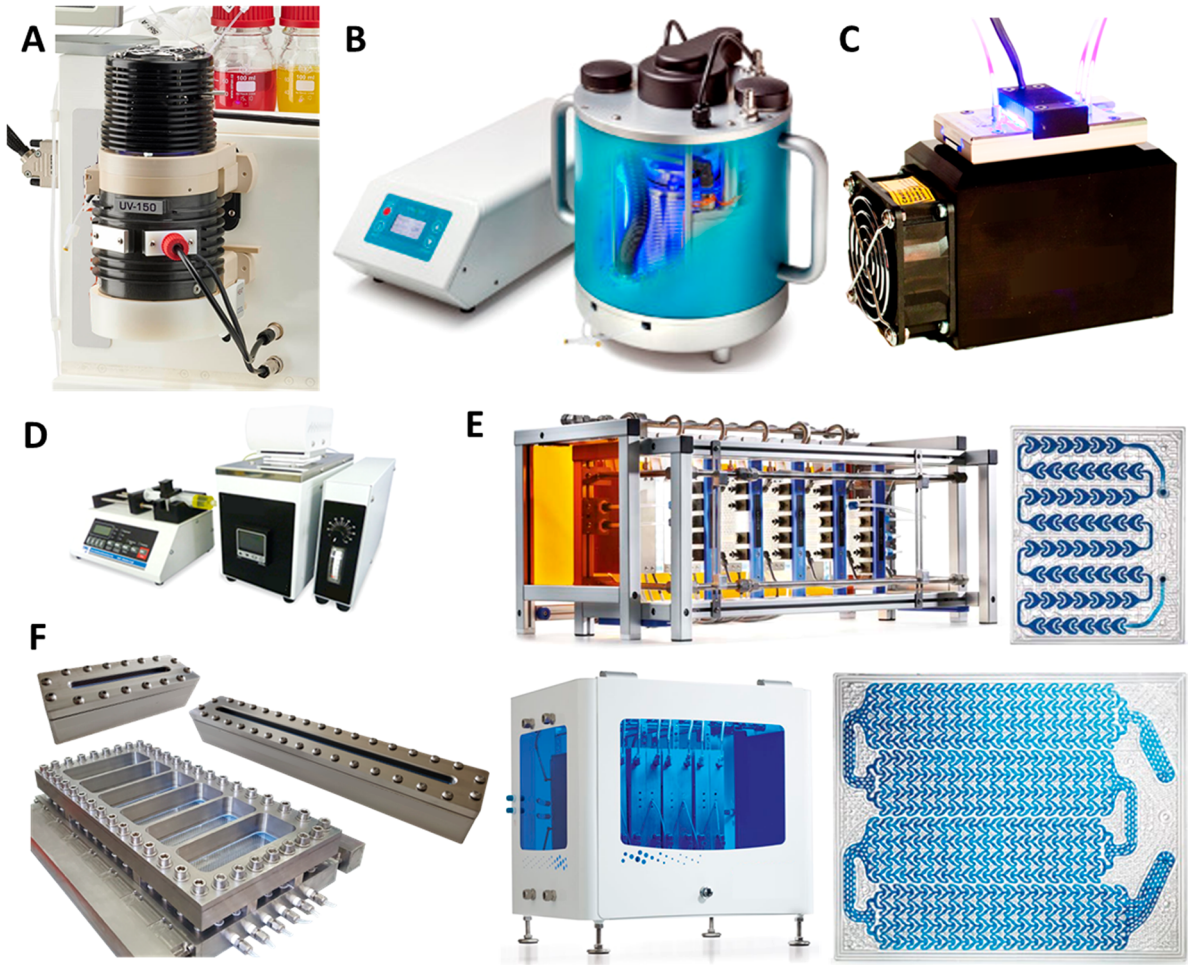

Figure 18. (A) UV-150 module by Vapourtec.[211] (B) PhotoSyn by Uniqsis.[213] (C) Photochemistry Module for FlowStart Evo by FutureChemistry.[216] (D) KeyChem-Lumino by YMC.[217] (E) Two of the Corning AFR reactors: G1 Photo Reactor (top) and G3 Photo Reactor (bottom) designs, with the heart-shaped fluidic modules.[219] (F) HANU 2X 5 (lab-scale), HANU 2X 15 (process development) and HANU HX 150 flow reactor (pilot/production-scale)[220] (Courtesy of Creaflow).

more, light intensity, stirring speed, and fan-cooling can be user-controlled.

3.2.2. Commercial Dedicated Flow Reactors. Apart from the photoreactors for both batch and flow applications, there are also dedicated flow photoreactors commercially available. One such reactor is the Vapourtec UV-150 (Figure 18A).[211] This flow reactor is compatible with their R-Series and E-Series modular flow systems. The setup can be equipped with differently sized coiled reactors (2, 5, and 10 mL) and be irradiated by several different light sources. These include monochromatic LEDs (13 types between 365 and 535 nm, standard 60 W, some high power 150 W available), low-pressure mercury lamps (254, 310, and 370 nm) and a broad range medium-pressure mercury lamps (75−150 W), which can be combined with modular wavelength filters. There is no light leakage during operation and the LEDs automatically shut off when the reactor is opened. The Vapourtec UV-150 reactor was one of the first commercially available systems and is therefore one of the most used flow-based photoreactors in the flow chemistry literature.[212] Another photoreactor module is the PhotoSyn by Uniqsis Ltd. (Figure 18B).[213] This high-power LED module (tunable up to 700 W) can be operated with multiple light sources (e.g., UV-A, blue, green and custom), is fan-cooled and is compatible with the other available FlowSyn systems. The closed design ensures no light leakage and autoshutdown occurs when the casing is opened during operation. This module was used by Ley et al. with reactor several different PFA coil volumes (5, 20, and 50 mL).[214,215] Two photochemistry modules are available for the FlowStart Evo system by FutureChemistry: the standard and Deep UV Photochemistry Module (Figure 18C).[216] Both modules are compatible with the FlowStart Evo system, where the standard module is intended for wavelengths >365 nm and uses LEDs, and the Deep UV module uses a mercury−xenon lamp (possible to use in combination with available filters). Users can vary light-intensity and further parameters (e.g., reactor volume, material, temperature) are determined by the FlowStart Evo system specifications. Another available system is the KeyChem-Lumino by YMC (Figure 18D).[217] This system offers customization of microchannel materials (e.g., quartz glass, PTFE) and adjustable light sources (365 nm LED, medium-pressure mercury lamp) to meet specific needs of the customer. Commercial photoreactors that are tuned to meet specific desires of the customer are also offered by Snapdragon Chemistry.[218] Additionally, they offer a multiwavelength photoreactor (365, 385, 405, and 457 nm) with adjustable light intensity and the ability for precise temperature control through the use of external circulators.

Photoreactors ranging from lab-scale, to process development and large-scale are offered by Corning.[219] Their reactors

https://doi.org/10.1021/acs.chemrev.1c00332
Chem. Rev. 2022, 122, 2752−2906

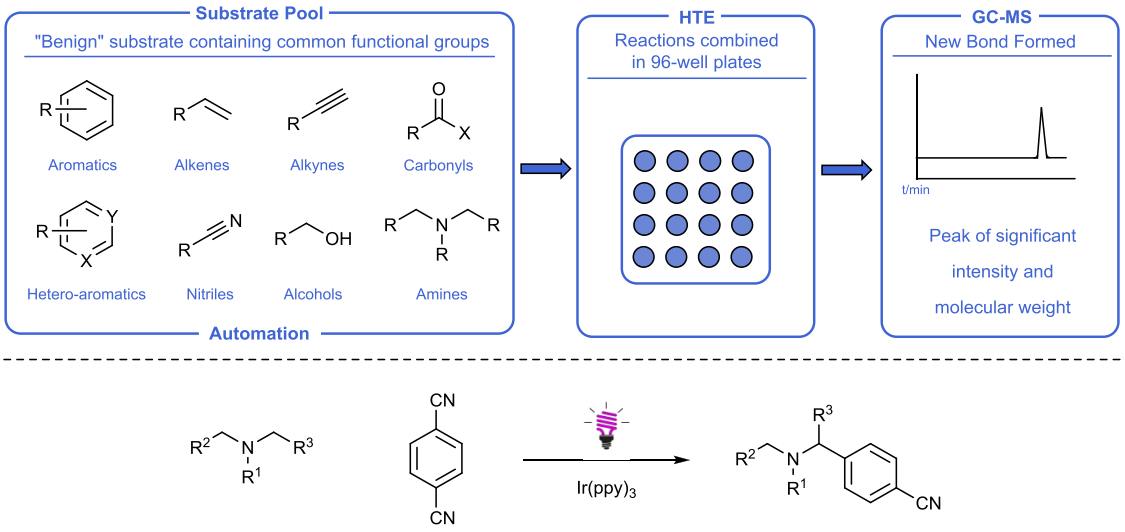

Figure 19. Approach for the automated accelerated discovery of new photoredox reactions and subsequent discovery of an α-amino C−H arylation reaction.

consist of typical fluidic modules (e.g., Lab Reactor ∼2.7 mL, G1 Photo Reactor ∼9 mL, and G3 Photo Reactor ∼60 mL), with the patented heart-shaped designs (Figure 18E). This shape is used in the reactors available of their Advanced-Flow Reactor (AFR) products because it enhances heat- and mass transfer (e.g., for scaling gas−liquid reactions[221]). The modules can be irradiated by the available (monochromatic) LEDs from both sides, and multiple modules can be connected to scale up total reactor volume and throughput.[222−224] Creaflow also offers scalable flow reactors and the oscillatory flow HANU reactors (5−150 mL) is especially designed for photochemistry (Figure 18F).[220] Oscillatory flow reactors superimpose a symmetrical oscillation on the net flow, enhancing mixing and heat transfer, additionally improving the PFR behavior.[225] The HANU flow reactors benefit from the three features, including: continuous processing in a linear plate flow reactor, the superimposed oscillatory flow (generated by a pulsator) and the static mixing elements in the process channel.[226] This allows for both homogeneous[227] and heterogeneous[228−230] (e.g., slurry, solids-handling) photochemical applications, with enhanced mixing independent of the net flow rate, enabling the continuous single-pass operation of slower photochemical reactions (i.e., without the need for recirculation). Furthermore, the reactors (with a temperature/pressure window of 150 °C and 25 bar) are equipped with heat exchangers and are available with dedicated water-cooled high-power LED arrays (9 exchangeable strips in the 365−625 nm range) but can also be used with low-pressure and excimer lamps enabling operation with both UV (254−351 nm) and visible light. Complete PLC-controlled turnkey systems (e.g., the MPDSE-VO developed together with Peschl Ultraviolet[231]) with integrated HANU reactors are also available for process development.

4. HIGH-THROUGHPUT EXPERIMENTATION

High-throughput experimentation (HTE) is a crucial tool for modern pharmaceutical development and synthetic methodology work-flow.[232−236] As the hunt for novel drugs becomes more difficult every year, new methods for the screening of growing libraries of molecules has become of vital importance to both hit to lead discovery and lead optimization.[237−239] While HTE has traditionally remained in the purview of industry, increasingly, it is being implemented in an academic setting.[240] HTE work-flows range from advanced robotized systems screening thousands of reactions a day at nanomole scale to simple parallelization techniques.[241−244] Increasingly, this technique is being coupled with machine learning and artificial intelligence to extract huge amounts of data on broad chemical spaces.[245−247] Laboratory automation has long been a goal in the chemical industry to increase productivity, reproducibility and safety.[248−250]

Enabling technologies like flow photochemistry are being used to screen reactions in an efficient manner.[116,251] These enabling technologies have allowed the coupling of closed-loop chemical platforms to algorithms to produce self-optimizing reaction platforms.[252] These methods have been applied to many areas of chemistry, materials development,[253] polymers,[254] and catalysis.[255] Here we aim to give an overview of how these technologies have been used to advance the known photochemical space.

4.1. Batch-Based High-Throughput Experimentation Work-Flows

High-throughput experimentation in chemistry is synonymous with the parallelization in batch via well-plates. Here, reactions take place on a small scale in parallel wells. This method has been used to accelerate reaction discovery, increase the speed of reaction optimization, for functional group tolerance screening, mechanistic studies, and robustness screening.

In 2011, Macmillan et al. applied an automated high-throughput experimental work-flow to rapidly identify photoredox transformations to accelerate the discovery of new reactions by forced serendipity (Figure 19).[256] A robotic system (Chemspeed) was used to pair substrates from a substrate pool with common, nonreactive functional groups in 96-well plates together with an inorganic photoredox catalyst. To perform the reactions, the wells were irradiated by a 26 W fluorescent lamp, followed by GC-MS analysis. This revealed a hit combination for the reaction *N,N*-dimethylaniline and 1,4-dicyanobenzene with the photocatalyst $Ir(ppy)_2(dtbbpy)PF_6$ to form the α-amino cyanobenzene product in 11% yield. Optimizations on solvent, base and photocatalyst were further carried out and yields of 85% were achieved. An extensive

https://doi.org/10.1021/acs.chemrev.1c00332
Chem. Rev. 2022, 122, 2752−2906

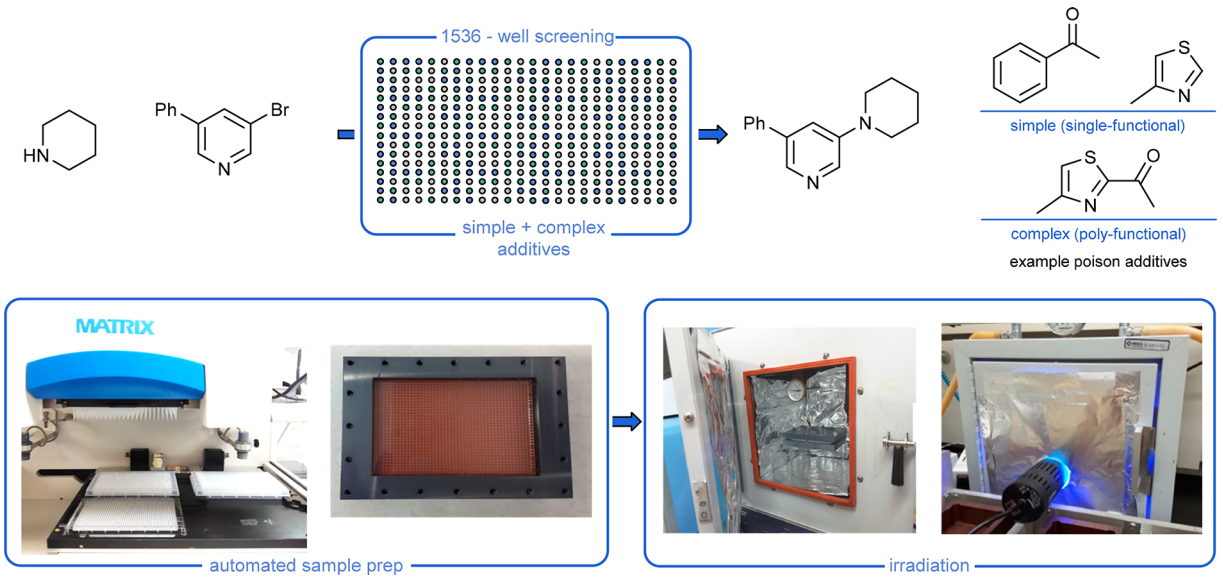

Figure 20. High-throughput screening by Merck in conjunction with MALDI-TOF MS for the screening of nanomole scale reprinted with permission from ref 257. Copyright 2018 American Association for the Advancement of Science.

scope was then performed. For the amine part, the reaction could tolerate pyrrolidine, piperidine, morpholine *N*-Boc piperazine, and azepane rings, as well as an acyclic amine. The reaction also performed well with electron-deficient arenes (ester, amide, phosphonate esters of benzonitriles) and heteroaromatics (cyano pyridines, triazole, and azaindoles). Finally, direct derivatization of linezolid was achieved using the optimized conditions to afford the heteroarylated product in 58% yield.

A nanomole-scale HTE screening platform combined with the use of matrix-assisted laser desorption/ionization-time-of-flight mass spectrometry (MALDI-TOF MS) was reported by researchers at Merck.[257] Photoredox C−N cross-coupling reactions were carried out using either iridium- or ruthenium-based photocatalysts and a nickel cocatalyst. Both simple and complex additives, which represent functional groups commonly found in drug-like molecules, were added to reactions so a full reaction/substrate suitability profile could be developed for a wide range of molecules (Figure 20). Robotic liquid handling (Mosquito HTS) was utilized to make up reaction conditions in 1536-well plates, which could then be directly analyzed from the well-plates using MALDI-TOF. This quick analysis method yielded whole 1536-well plate readout in under 10 min.

To evaluate a range of photocatalysts and oxidants for the photoredox catalyzed hydroxymethylation of heteroaromatic bases, researchers at Merck used a high-throughput screening method.[258] Experiments took place in a 96-well plate, where each well was charged with a photocatalyst and an oxidant. The 96-well plate was sealed and illuminated with blue light (13 mA on array of 96 LEDs) for 16 h at room temperature. Highest photocatalytic activity for this reaction was observed for $[Ir(dF(CF_3)ppy)_2]PF_6$. Concerning the oxidants, *tert*-butyl peracetate (TBPA) and *tert*-butylperoxy 2-ethylhexyl carbonate (TBEC) both gave mixtures of hydroxymethylated product (A) and methylated product (B). In contrast, high selectivity was observed with ammonium persulfate or benzoyl peroxide (BPO) as oxidant, resulting in excellent yields of hydroxymethylated product (A) (up to 99%) (Figure 21).

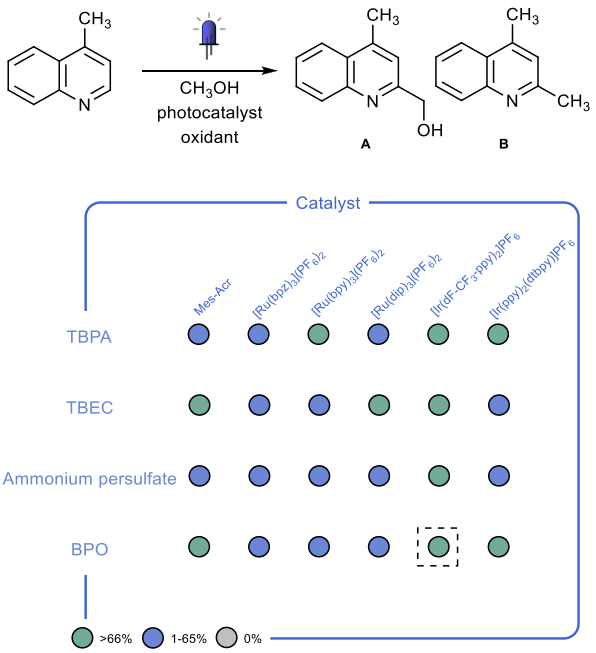

Figure 21. Heat map for the high-throughput screening of the photoredox catalyzed hydroxymethylation of heteroaromatic bases.

A well-plate based high-throughput experimentation optimization was also performed by Rovis, Lehnherr, and coworkers during the discovery of a photocatalyzed concurrent tandem reaction to synthesize hindered primary amines.[259] Figure 22 showcases the 5 × 9 assay which was carried out with a range of photocatalysts, solvents, and either diisopropylamine (DIPA) or diisopropylethylamine (DIPEA) as reductants. The well-plate was irradiated for 20 h and each reaction analyzed by UPLC with yields quantified using a calibrated method. Results indicate that the highest yields were obtained with DMSO as solvent and DIPA as reductant and either $[Ir(dF(Me)ppy)_2(dtbbpy)]PF_6$ (71% yield) or $[Ir(dF(H)ppy)_2(dtbbpy)]PF_6$(68% yield) as catalyst. Notably, even though DIPEA is easier to oxidize than DIPA, a secondary

https://doi.org/10.1021/acs.chemrev.1c00332
Chem. Rev. 2022, 122, 2752−2906

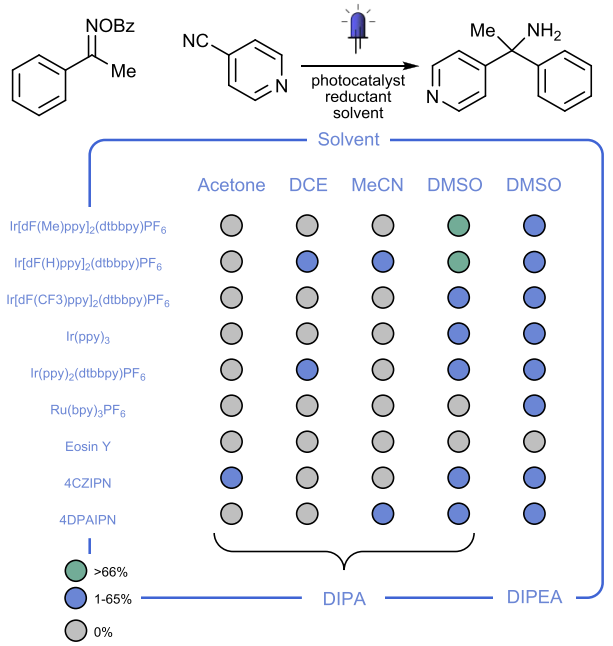

Figure 22. Heat map for the high-throughput screening of the optimal conditions for the concurrent tandem synthesis of primary amines.

α-amino radical was generated when DIPEA was used as a reductant. The α-amino radical itself was able to couple with 4-cyanopyridine, resulting in reduced yields.

To perform the late-stage methylation of biologically active heterocycles, researchers at Merck employed a HTE assay with a custom 96-well reactor.[260] Each well was irradiated with an independent LED, which improved the consistency of irradiation across conditions and reaction locations. Reactions were carried out at 10 μmol scale with 8 solvent and 12 photocatalyst combinations (Figure 23) and irradiated with

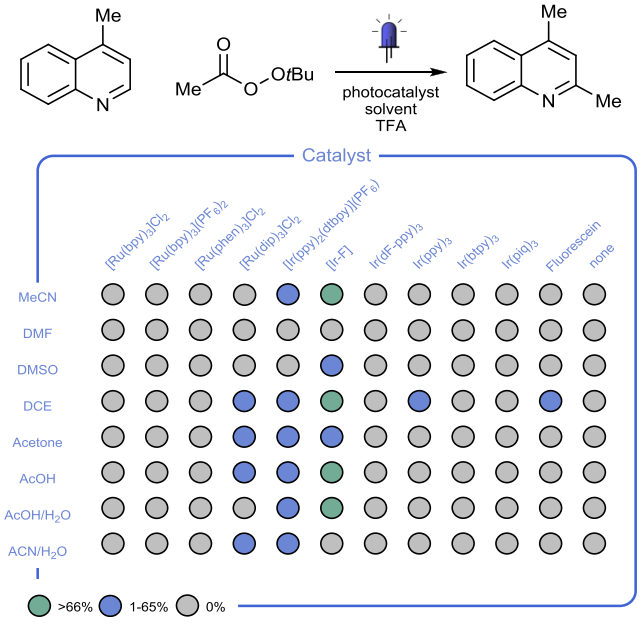

Figure 23. Heat map for the 96-well plate high-throughput screening toward the photoredox catalysis enabled late-stage methylation of lepidine.

blue LEDs. Reactions were analyzed for conversion based on UPLC-MS using an internal standard. Results showed that $[Ir(dF(CF_3)ppy)_2(dtbbpy)]PF_6$ was the best catalyst for the transformation of lepidine and *tert*-butyl peracetate (TBPA) with trifluoroacetic acid as an additive (10 equiv). Moreover, it was the most robust catalyst, showing conversion in all but two of the solvent systems and achieving high yields in acetonitrile (72%), dichloroethane (71%), acetic acid (75%), and acetic acid/water (74%). No product was formed in the control wells containing no photocatalyst. When other peroxides were used (di-*tert*-butyl peroxide and *tert*-butyl hydroperoxide), no product was found, indicating that the carbonyl motif on TBPA was necessary for the targeted reactivity.

A high-throughput screening approach was employed by Knowles, DiRocco, and co-workers for the optimization of a photoredox-mediated dehydrogenation of indoline toward the synthesis of elbasvir.[261] A 96-well plate was used and the reactions at 2.5 μmol scale were irradiated for 24 h with blue LEDs (465 nm). Reactions were screened for oxidant, solvent and catalyst (Figure 24) and yields were obtained by HPLC

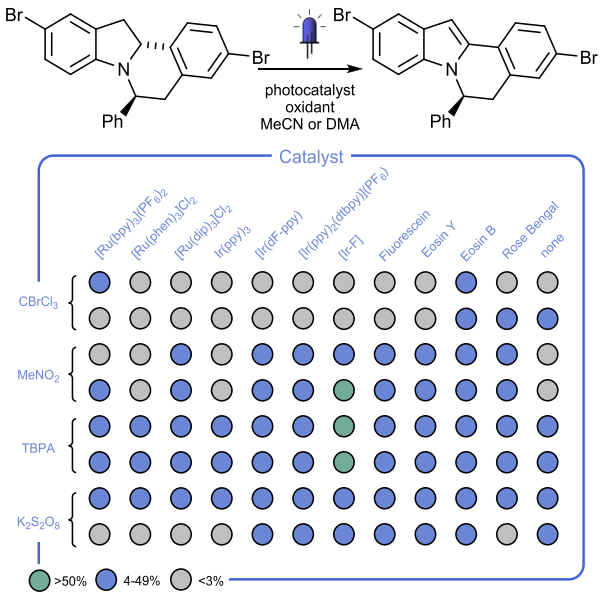

Figure 24. Heat map for the 96-well plate high-throughput screening toward the photoredox-mediated dehydrogenation of indoline.

analysis with respect to an internal standard. Results indicated that nitromethane and *tert*-butyl peracetate were good stoichiometric oxidants and the most active catalyst was $[Ir(dF(CF_3)ppy)_2(dtbbpy)]PF_6$ ([Ir−F]) with yields of up to 62%. The modest yields can be attributed to product decomposition due to overirradiation and can be avoided with shorter irradiation times. For scale-up, a flow-based approach was chosen. The flow reaction was optimized for catalyst loading, use of one of two peracetate oxidants (TBPA or *tert*-butyl perbenzoate (TBPB)), residence time, and temperature. With optimal conditions, a scale-up was completed in a flow reactor (3.2 mm or 1/8 in. ID, 150 mL, t_R = 60 min, −10 °C, 0.04 mol·h^{-1}) with TBPB as oxidant. After 5 h, 100 g of product was processed with 88% isolated yield and 99.8% ee.

Similarly, a high-throughput experimentation was performed by researchers at Merck in their profiling of the photoredox

https://doi.org/10.1021/acs.chemrev.1c00332
Chem. Rev. 2022, 122, 2752−2906

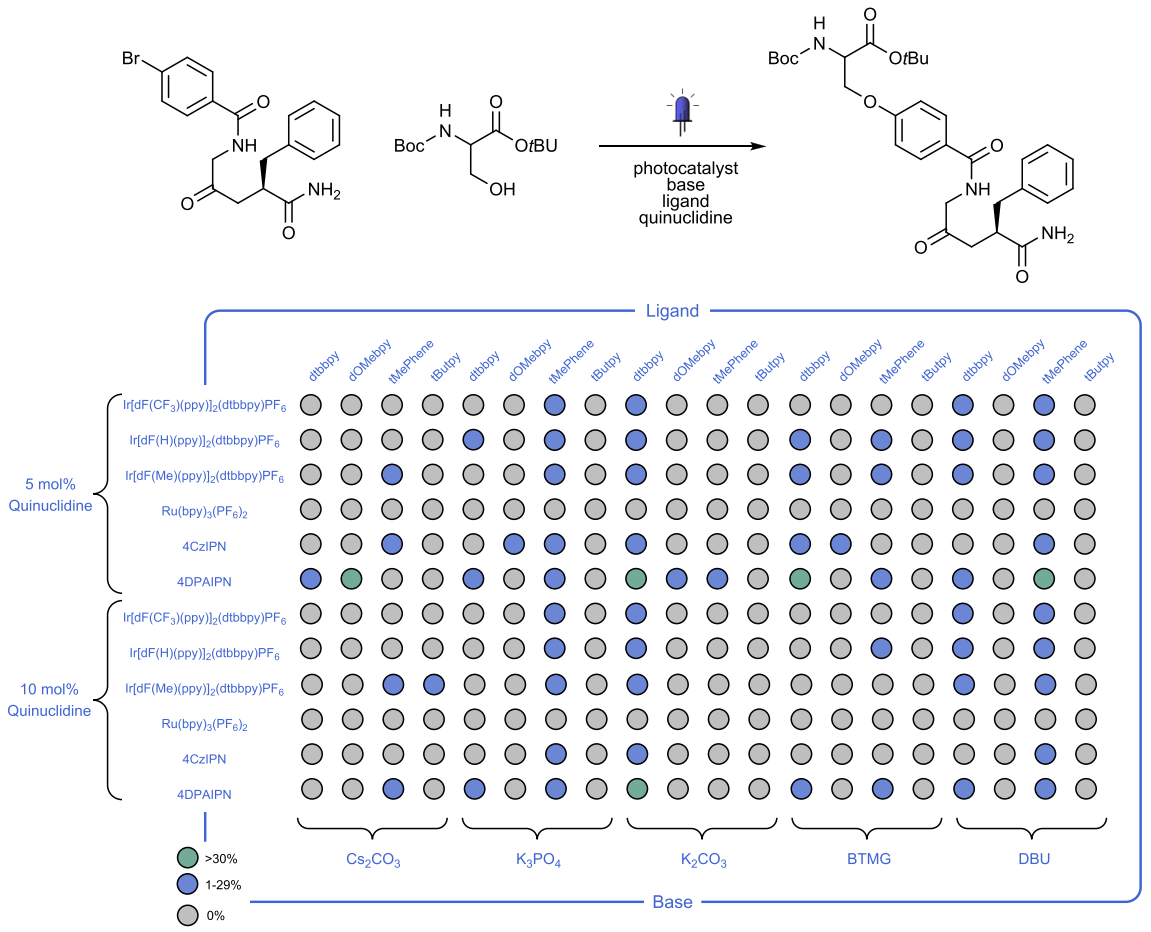

Figure 25. 240 nanomole scale reaction for the photoredox/nickel catalyzed peptide C(sp^2)-oxygen cross-coupling.

nickel-catalyzed peptide C(sp^2)-oxygen cross-coupling.[262] 240 nanomole scale reactions were carried out in well-plates in an automated manner and analyzed by UPLC-MS, similar to the groups previous work on high-throughput experimentation.[244] The reaction wells were irradiated for 24 h with blue LEDs (450 nm) and optimal conditions were investigated for photocatalyst, quinuclidine loading, ligand, solvent, and base (Figure 25). The best results were obtained with the organic dye 4DPAIPN, with $NiBr_2$·glyme, the ligand dtbbpy, K_2CO_3, 5 mol % quinuclidine, and *N*-methyl-2-pyrrolidone (NMP) as solvent, which was found to afford the product in 66% yield.

A high-throughput work-flow was used by Britton, researchers at Merck et al. for the investigation of a new synthetic step en route to Odanacatib, mediated by the direct photocatalytic C−H fluorination of leucine methyl ester (Figure 26).[263] Reactions took place in a 96-well plate photochemical screening platform at a 10 μmol scale, parameters, such as amino acid salt, catalyst, catalyst loading, solvent composition, and concentration, were investigated. In general sodium decatungstate was superior to TBADT in catalyzing the reaction. HCl salts performed the poorest due to a competitive chlorination reaction, especially at lower concentrations of water. These competitive chlorination reactions were avoided with the use of mesylate (MSA) and bisulfate salts. The optimized conditions indicated in the figure gave the highest response factor by UPLC-MS and were reproduced on a 20 mg scale to provide 97% assay yield after 18 h of irradiation. Next, a scale-up was performed in flow

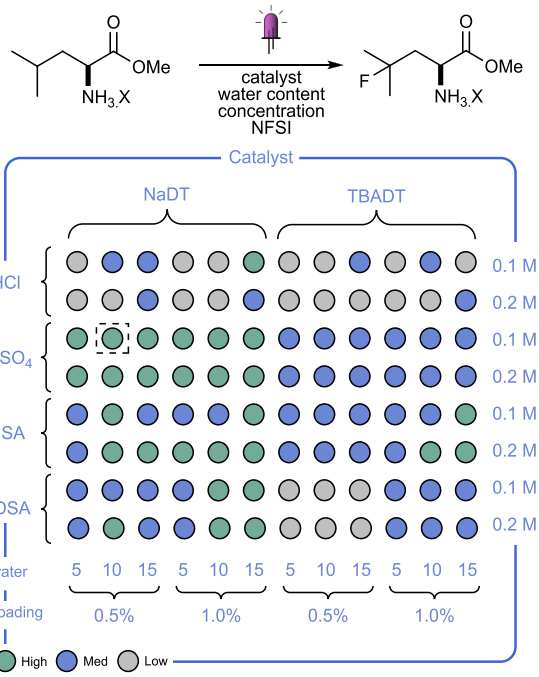

Figure 26. High-throughput screening of the direct C−H fluorination of leucine methyl ester on the route to Odanacatib.

using the same conditions and 44.7 g (90%) of the product was isolated by precipitation from 2-MeTHF.

https://doi.org/10.1021/acs.chemrev.1c00332
Chem. Rev. 2022, 122, 2752−2906

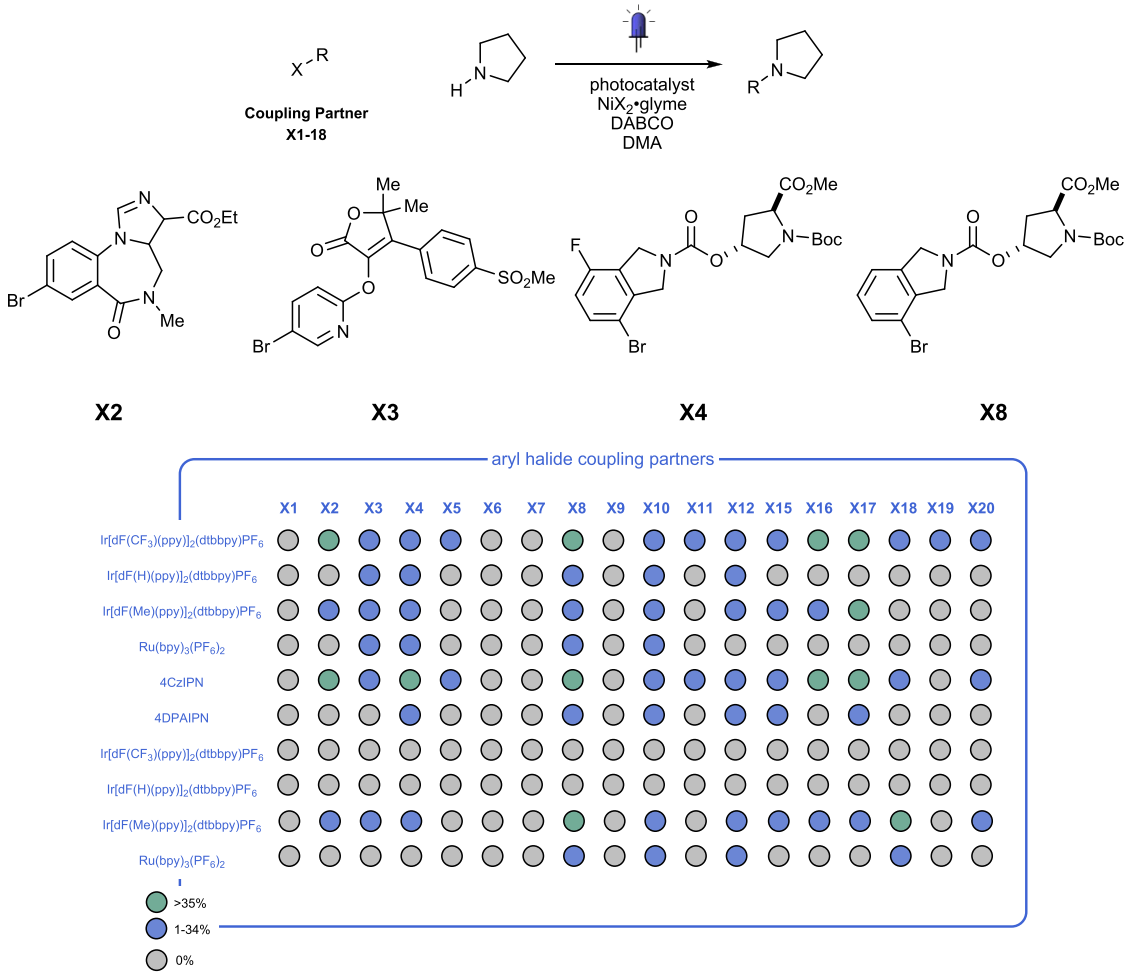

Figure 27. High-throughput screening of aryl amination of drug scaffolds using ligand free nickel(II) salts and a selection of photoredox catalysts.

Macmillan, Buchwald, and co-workers also utilized a high-throughput experimentation work-flow in their pioneering work on the discovery of photoredox mediated C−N cross-coupling protocol using ligand-free nickel(II) salts.[264] Coupling reactions with piperidine were carried out on a 2.5 μmol scale in 96-well plates, which were irradiated for 16 h. A screening was performed for a selection of organic and inorganic photocatalysts and 18 drug-like coupling partners (Figure 27). Yields were determined by UPLC-MS. Notably, 78% of the scaffolds underwent photocatalytic cross-coupling with a single photocatalyst $[Ir(dF(CF_3)ppy)_2(dtbbpy)]PF_6$. According to the authors, this represented one of the most successful catalysis platforms that had been evaluated by Merck.

Macmillan et al. developed a microscale flow simulation (FLOSIM) high-throughput experimentation platform for the translation of photochemical batch HTE to commercially available photo flow chemistry systems (Figure 28).[265] First, extensive testing was performed to prove the homogeneous irradiation of the platform's wells. Next, four model photochemical reactions (decarboxylative arylation, decarboxylative alkylation of N-nucleophiles, cross-electrophile coupling, C−O coupling) were investigated in the platform with a total of >2000 reaction conditions over the four reactions. The FLOSIM device was designed to replicate the internal diameter of a flow device for easy translation to flow. Flow reactions were then run in commercial photoflow reactors (UV-150 Vapourtec E-Series and PhotoSyn flow photoreactor by Uniqsis) to compare with the results obtained in the FLOSIM device. Interestingly, the FLOSIM device was found to give accurate HTE yield and reaction time predictions for all conditions (low yield, moderate yielding, and high yielding), enabling the quick identification of ideal flow reaction conditions through HTE in batch.

Researchers at Bristol Meyers Squibb and Princeton used a high-throughput experimentation approach in the discovery of a photocatalytic decarboxylative intramolecular arene alkylation of *N*-(acyloxy)phthalimides.[266] Reactions took place in 1 mL glass vials (0.01 mmol scale) within a 96-well photoredox block. The vials were irradiated by a Lumidox 96-well LED array for 15−19 h, and parameters, such as photocatalyst, acid additive, LED wavelength, and solvent, were varied (Scheme 10). First, a screening of iridium, ruthenium, and organic photocatalysts was undertaken under blue light irradiation. Ruthenium and most organocatalysts proved to be ineffective for the reaction, as low conversions were observed. In contrast, the organocatalyst 4CzIPN, as well as iridium-based photocatalysts, proved to be effective catalyst and both were used for further screening. Next, a screening of LED wavelength indicated that both green and white light gave sluggish reactivity, but that purple light (415 nm) gave comparable yields to blue LEDs (465 nm) with a notably increased rate. Therefore, purple light was chosen for the proceeding experiments. Additionally, acid additives were crucial for high

https://doi.org/10.1021/acs.chemrev.1c00332
Chem. Rev. 2022, 122, 2752−2906

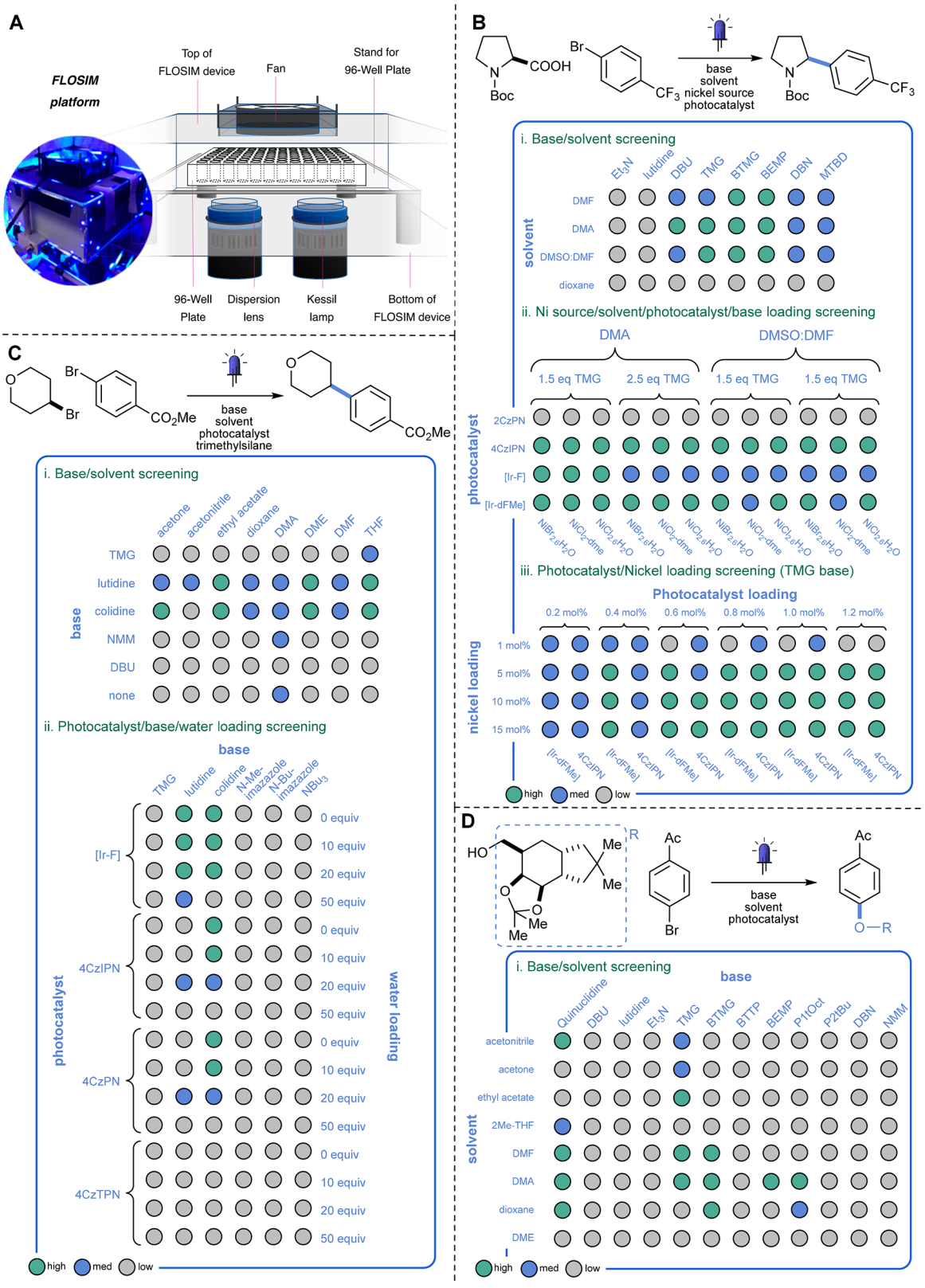

Figure 28. (A) FLOSIM device. (B) Selected HTE results from decarboxylative arylation. (C) Selected HTE results from the cross-electrophile coupling. (D) Selected HTE results from C−O coupling adapted with permission from ref 265. Copyright 2021 American Chemical Society.

yields and a number of acids were shown to be effective. Best results were obtained with 10 equiv of TFA when using the organo-photocatalyst and with 1 equiv of TFA when using the iridium-based photocatalytic system. A solvent screen was then performed with other polar solvents, which indicated that DMSO was indeed the most effective. The best reaction system contained the 4CzIPN catalyst with TFA (10 equiv) and purple LEDs, resulting in 81% yield of the intramolecularly

https://doi.org/10.1021/acs.chemrev.1c00332
Chem. Rev. 2022, 122, 2752−2906

Scheme 10. Selected Results from High-Throughput Screening of the Photocatalyst Mediated Decarboxylative Intramolecular Arene Alkylation Using *N*-(Acyloxy)phthalimides

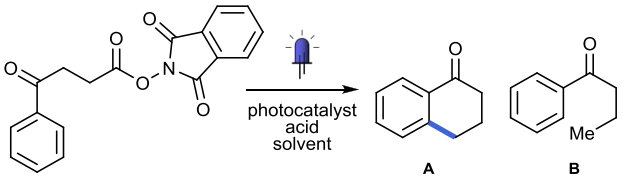

Photocatalyst	acid	light (nm)	A (%)	A:B
$[Ir(dF(CF_3)ppy)_2(dtbbpy)]PF_6$	TFA	470	74	88:12
4CzIPN	TFA	470	74	88:12
4CzIPN	TFA	470	73	87:13
4CzIPN	TFA	527	15	86:14
4CzIPN	TFA	white	64	88:12
4CzIPN	TFA	415	73	87:13
4CzIPN	$BF_3{\cdot}OEt_2$	470	59	87:13
4CzIPN	$BF_3{\cdot}OEt_2$	415	72	86:14
4CzIPN	TFA	415	67	85:15
4CzIPN	TFA	415	61	93:7
4CzIPN	TFA	415	81	94:6
$[Ir(dF(Me)ppy)_2(dtbbpy)]PF_6$	TFA	415	80	91:9
4CzIPN	none	415	23	77:23
none	TFA	415	<5	n/a
none	none	415	<5	n/a

cyclized product and a product ratio of 94:6 (A:B). Scale-up to 0.5 and 2.0 mmol using the optimal conditions from the high-throughput screening was completed in a flow reactor (10 mL, t_R = 70 min, 34 °C, 60 W) with corresponding yields of 72% and 65%, respectively.

A high-throughput experimentation work-flow was used by Collins et al. for the discovery and optimization of heteroleptic copper(I)-based complexes for photocatalysis with single electron transfer (SET), energy transfer (ET) and proton-coupled electron transfer (PCET)-based transformations.[267] A library of 50 copper catalysts with a broad range of bisphosphine and diamine ligands (Figure 29) were prepared and the visible-light decarboxylative fragmentation of *N*-(acyloxy)phthalimides was first evaluated. Results indicate that the 2,2′-biquinoline ligand (dq) was most effective for the coupling reaction with Cu(dq)(BINAP)BF_4, (BINAP = 2,2′-bis(diphenylphosphino)-1,1′-binaphthyl) providing the highest yield (87%). Second, the homolytic activation of ketones was investigated. The ligands 1,10-phenanthroline (phen) and trimethoxy-2−2′-bipyridine (tmp) performed well for this reaction and again Cu(dq)(BINAP)BF_4 was found to be one of the most effective catalysts for the reaction providing a yield of 71%. Triazole-based ligands also proved effective with Cu(quintri)(Xantphos)BF_4(quintri = 2-(1-(*p*-tolyl)-1*H*-1,2,3-triazol-4-yl)quinoline, Xantphos = 4,5-Bis-(diphenylphosphino)-9,9-dimethylxanthene) resulting in 79% yield. Finally, the visible light sensitization of vinyl azides was investigated. All dual ligand-copper catalysts provided product, and six catalysts provided excellent yields of >95%.

Scheidt et al. used a high-throughput screening work-flow for the photoredox mediated reductive arylation of arylidene malonates (Figure 30).[268] Reactions were carried out at 5 μmol scale in a Lumidox 96-well plate under blue LED irradiation (456 nm) for 18 h. The choice of photocatalyst, solvent and reductant, as well as presence of a Lewis acid (LA)

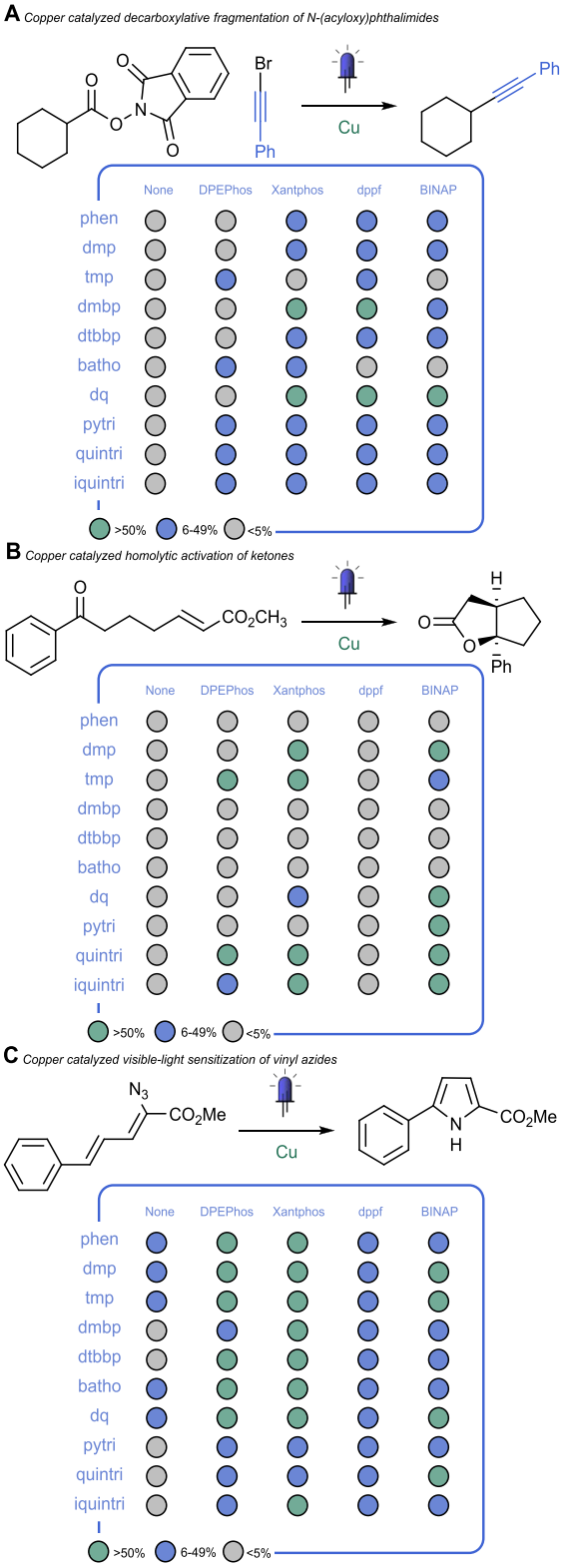

Figure 29. High-throughput experimentation work-flow for the discovery and optimization of heteroleptic copper(I)-based complexes for photocatalysis with single electron transfer (SET), energy transfer (ET), and proton-coupled electron transfer (PCET)-based transformations.

were investigated. The photocatalyst loading and reaction concentration were held constant at 3 mol % and 0.1 M respectively. The optimized conditions called for 4DPAIPN

https://doi.org/10.1021/acs.chemrev.1c00332
Chem. Rev. 2022, 122, 2752−2906

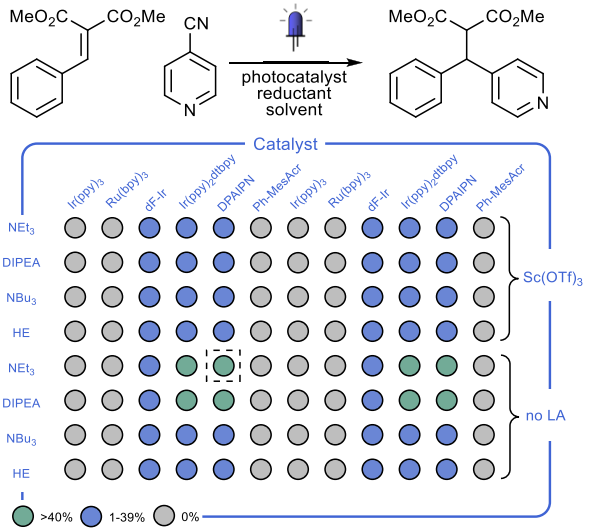

Figure 30. High-throughput workflow for the photoredox mediated reductive arylation of arylidene malonates.

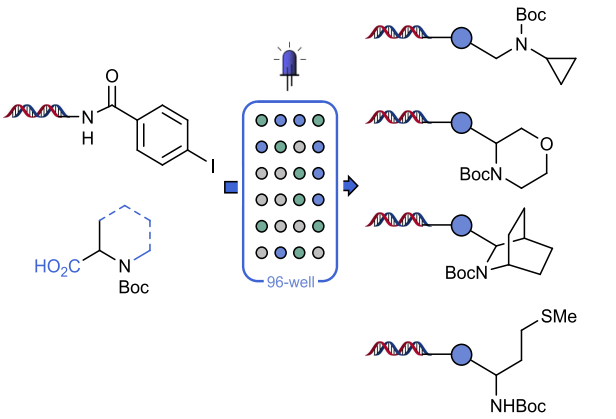

Figure 31. Parallel synthesis for the direct decarboxylative arylation of DNA by dual photoredox/nickel catalysis.

and 2.5 equiv of NEt_3 in CH_3CN, which afforded the product in 85% yield. A trend in the results indicated that photocatalysts which were both strong oxidants and reductants were most efficient (4DPAIPN, $Ir(ppy)_2$ dtbpy), whereas strong oxidants and mild reductants (Ph-MesAcr) afforded no product and strong reductants/mild oxidants ($Ir(ppy)_3$) lead to the dimerization of the starting arylidene malonate. Tertiary amines were shown to be superior terminal reductants in comparison to Hantzsch ester (HE), which only afforded the product in trace amounts even with the strongest catalyst system. Tertiary amines form 2-center/3-electron systems upon single-electron reduction, which results in the amine first serving as the reductant, and after it has been oxidized the amine acts as a Lewis acid necessary for the reaction to occur. This explains why the reactions that contain no Lewis acid but do contain a tertiary amine show increased efficiency compared to reactions where an exogenous Lewis acid additive is used. The tertiary amine acts as the necessary Lewis acid once oxidized during the reaction and exhibits a much simpler reaction profile leading to comparatively higher yields. Further scope exploration for the reaction was performed using the optimized conditions with electron-rich and electron-poor variations of arylidene malonate and a number of variations of cyanoarene (pyridines, pyrmidines, pyrroles, and indoles) resulting in yields of 62−88%.

A dual photoredox/nickel catalysis method was developed by researchers at Pfizer for the decarboxylative coupling of α-amino acids with DNA-tagged aryl halides in aqueous medium.[269] The great potential of the method for the generation of DNA encoded libraries was further exemplified by performing the reactions in a 96-well plate reactor. The reaction wells were irradiated with a blue LED array and were degassed and sealed by an inflatable enclosure under inert atmosphere. Reactions were carried out at 20 μmol scale, were irradiated for 3 h for a range of 26 carboxylic acids (Figure 31), and were, subsequently, analyzed by UPLC. Reactions that were carried out in 96-well plates were found to produce yields between 5 and 10% lower than reactions carried out in glass vials in batch.

Researchers at Astex Pharmaceuticals developed a high-throughput experimentation platform using 1536-well microtiter plates (MTPs).[270] The HTE protocol employed liquid handling robots to screen suitable reaction conditions for the direct cross-dehydrogenative coupling between 5-bromoisoquinoline and *N*-Boc morpholine on a 768 nmol-scale, using a selection of iridium, ruthenium, copper and organo-photocatalysts. Two sets of 192 discrete reaction conditions were performed, with one set subjected to white light and the duplicate subjected to blue light. The heat map (Figure 32) indicated that 3 of the reactions gave significant conversions and yields as shown by HPLC analysis using an internal standard method. With the optimal reaction conditions from the high-throughput screening, a scale-up was carried out in a continuous-flow photoreactor (1/16 in. OD, 0.05 in. ID, 10 mL volume, 420 nm, 17 W, t_R = 10 min). Using the flow strategy, the target compound could be isolated in 58% yield (1.3 g).

An example of how high-throughput experimentation can aid drug discovery programs in the development of a versatile and broad method, is given by Leonori et al., who employed a HTE work-flow for the late-stage amination of dextromethorphan (Robitussin) with a range of alkyl amines.[271] Reactions were carried out in a commercial 24-plate photoreactor at 25 μmol scale and irradiated at 0 °C for 2−4 h to achieve yields of up to 99% (Figure 33).

Over the past few years, Glorius et al. have reported a number of "mechanism-based", additive-based and functional group tolerance screening approaches.[272] In Figure 34, an overview of a mechanism-based approach is shown, which attempts to directly gain a better understanding of a mechanistic step common to a class of reactions in three stages. In the first stage, a library of 100 potential quenchers was tested on the ability to quench the widely used photocatalyst $[Ir(dF(CF_3)ppy)_2(dtbbpy)]PF_6$ ([Ir−F]). Of the 100 potential quenchers studied a total of 7 produced fluorescence quenching of >25%, among which 2 were known quenchers that were planted to validate the screening method. Another 2 were widely known to act as quenchers in other reported visible-light-mediated reactions; and 1 other quencher was shown to have a strong absorbance at the wavelength of interest. These were removed from further evaluation, leaving a benzotriazole and a phenol, which were identified as the lead compounds for further quenching evaluation. Next, *fac*-Ir(ppy) was selected as the lead catalyst to design two new photocatalytic transformations involving the new quenchers:

https://doi.org/10.1021/acs.chemrev.1c00332
Chem. Rev. 2022, 122, 2752−2906

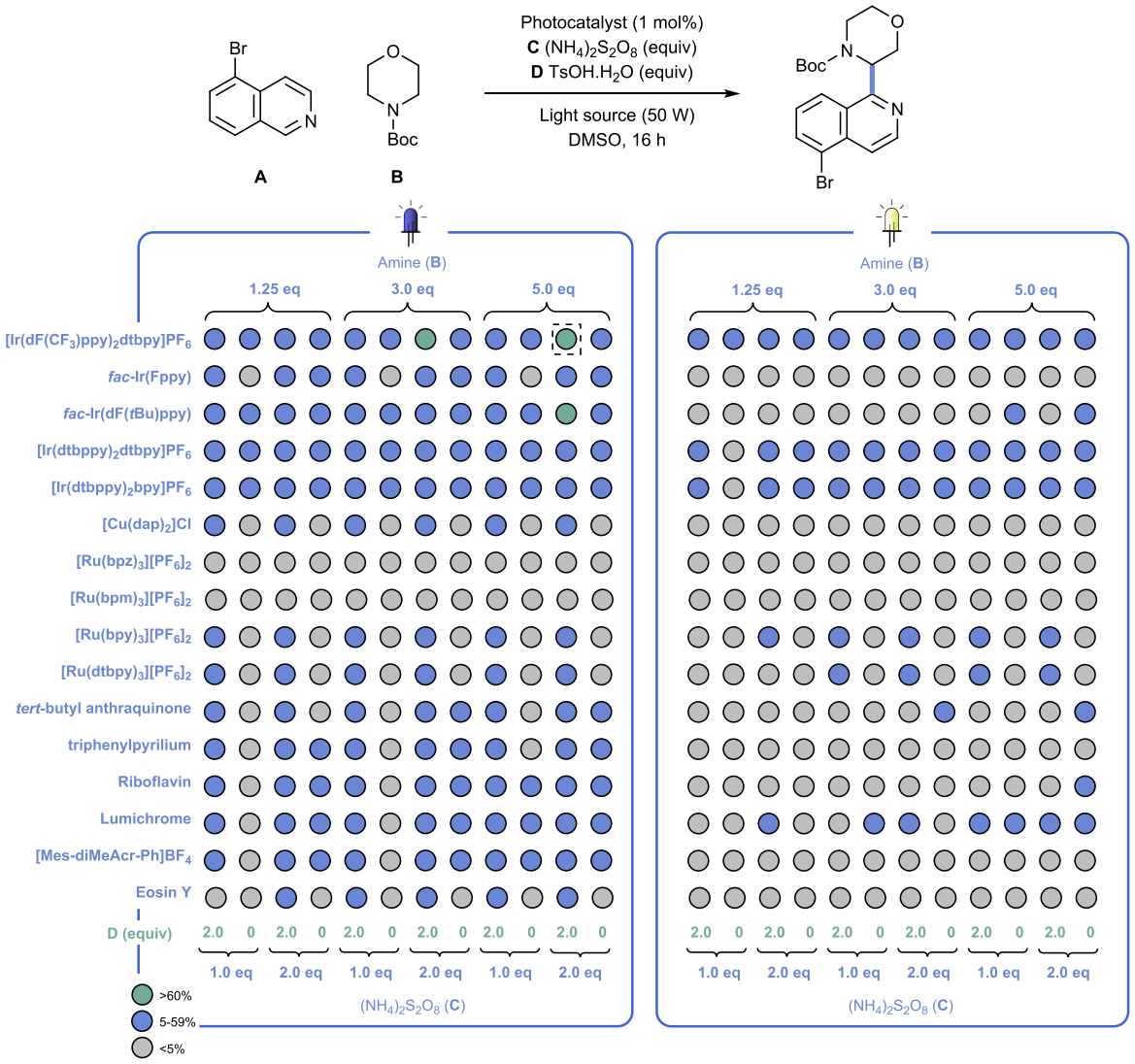

Figure 32. High-throughput screening using a liquid handling robot for the photoredox-mediated cross-dehydrogenative heteroarylation of cyclic amines.

namely the visible-light catalyzed denitrogenation of benzotriazoles by phenyl anhydrides and bromination of phenols.

When further investigating the denitrogenation of benzotriazoles with alkynes to synthesize 2-substituted indoles, Glorius et al. further utilized an additive-based robustness screening.[273] This screening evaluates the ability of a given reaction to tolerate a series of exogenous additives which gives a sense of the robustness of the reaction, as well as the functional group preservation of the molecules in the reaction. Reactions were carried out in Schlenk tubes in a custom-made photoreactor and results indicate that a high number of additives were well tolerated (Figure 35). All but two reactions proceeded with comparable yields for the product to control reactions containing no additive, in most cases the additives were recovered with an average yield of 80%. The reaction was then scaled to 3.0 mmol and a yield of 61% was obtained. Notably, when the solvent was changed from DMSO to CH_3CN a chemodivergent switch was observed, with the *(Z)*-stilbene derivative being obtained in preference to the 2-substituted indole.

Next, Glorius et al. utilized the same approach to indicate the robustness and functional group tolerance of a previously reported photocatalytic decarboxylative trifluoromethylthiolation (Figure 36).[274,275] Reactions were again carried out in Schlenk tubes and irradiated for 4 h with 365 or 455 nm LEDs; yields were calculated by ^{19}F-NMR. In total, 41 additives were screened, covering a wide breadth of functional groups and reactivities (i.e., basic, acidic, nucleophilic, and electrophilic). Reactions show a similar robustness under both conditions, giving nearly identical yields (63% and 65%). However, the functional group preservation was markedly better for condition B (455 nm) than those of condition A (365 nm), which is showcased by the lower recovery of additives. This lower functional group preservation was suggested to be due to decomposition with the higher energy light, which was confirmed with an additive stability investigation under 365 nm light.

Moreover, Glorius et al. also explored a mechanism based approach to discover visible light promoted functionalization of benzotriazoles by *o*-thiolation, *o*-borylation, and alkylation to afford aniline derivatives (Scheme 11).[276] Together with a scope investigation, an additive-based robustness screening was performed as previously described. The results indicated that the transformation tolerated any kind of additives, with aniline

https://doi.org/10.1021/acs.chemrev.1c00332
Chem. Rev. 2022, 122, 2752−2906

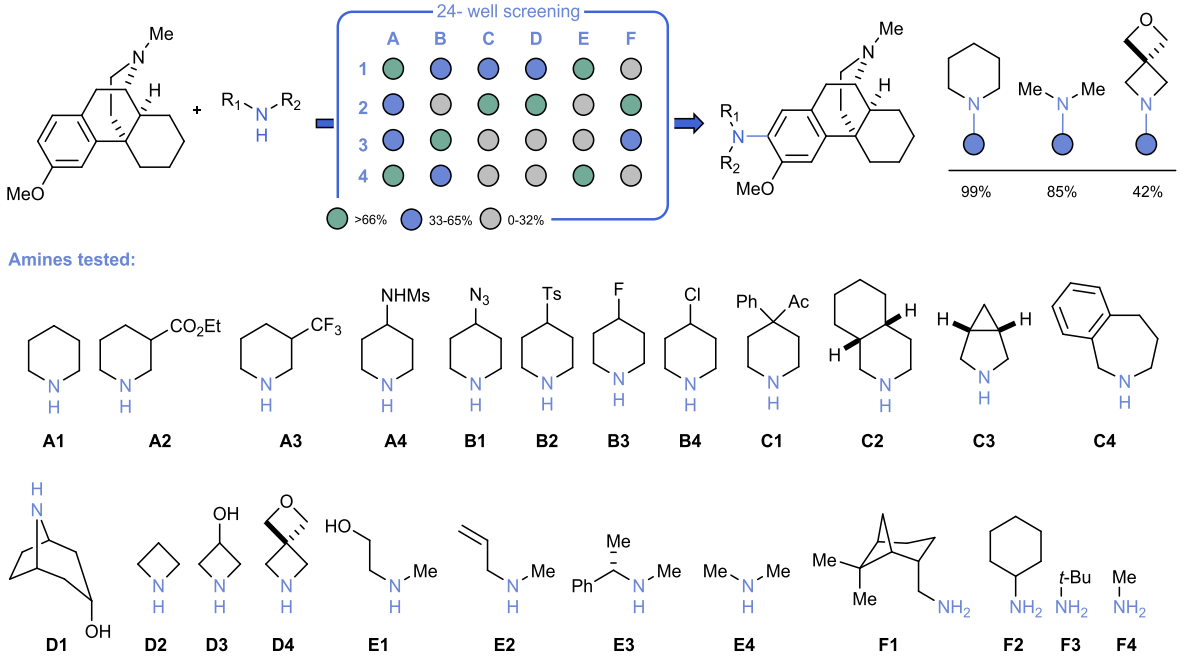

Figure 33. High-throughput screening for the late-stage amination of dextromethorphan.

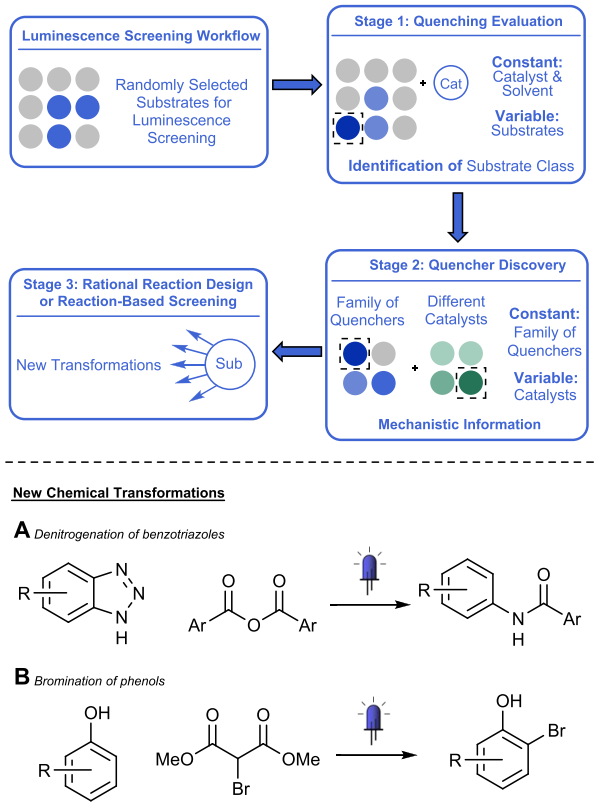

Figure 34. Mechanism-based screening approach for the discovery of new quencher classes and subsequent discovery of new reactivity of benzotriazole and phenol derivatives.

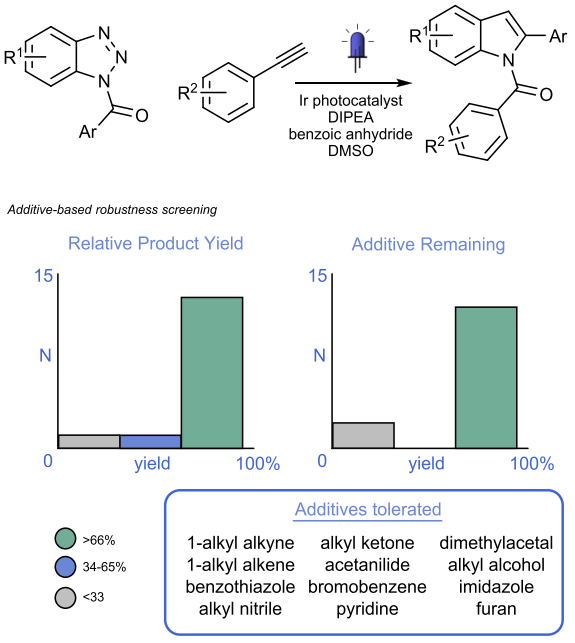

Figure 35. Synthesis of 2-substituted indoles from benzotriazoles and alkynes by photoinitiated denitrogenation and robustness and functional group tolerance screening.

being the only exception. The same process was also employed to assess the generality of the photocatalyzed denitrogenation of benzotriazoles followed by the radical addition of alkynes yielding 2-substituted indoles. Finally, by Stern–Volmer analysis, the three functionalizations were proven to proceed via single electron transfer.

In another example, Glorius, Guldi, and co-workers used a the mechanism-based approach in the investigation of an energy-transfer-enabled biocompatible disulfide–ene reaction (Scheme 12).[277] The ability of dimethyl disulfide to quench a series of iridium or ruthenium based photocatalysts with different triplet excited state energies was investigated. [Ir–F] was found to be the most efficient quencher with a quenching fraction of 42%, which corresponds to a yield of 58%. The efficiency of luminescence quenching was directly correlated to the excited state energy of the catalyst, with [Ir–F] having the highest triplet excited state energy of the catalysts investigated.

https://doi.org/10.1021/acs.chemrev.1c00332
Chem. Rev. 2022, 122, 2752–2906

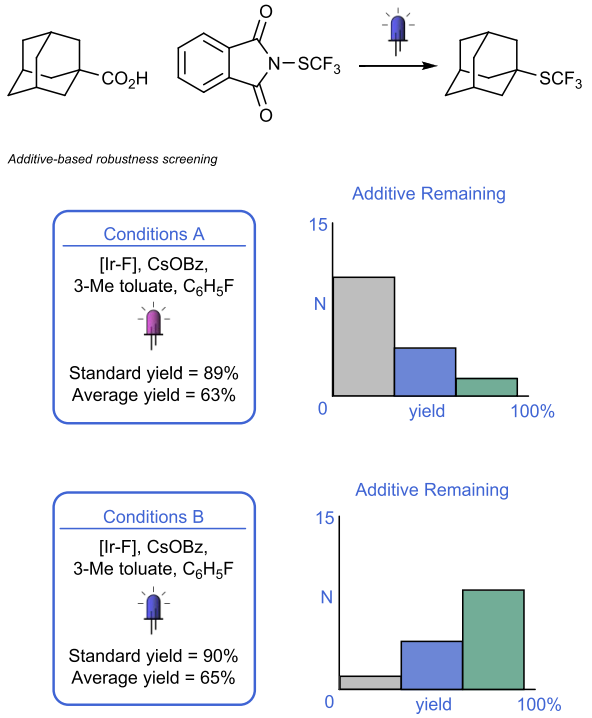

Figure 36. Photocatalyzed decarboxylative trifluoromethylthiolation with robustness and functional group tolerance screening.

Scheme 11. Exploration of *o*-Thiolated, Borylated, and Alkylated *N*-Arylbenzamide Aniline Derivatives by Visible Light-Mediated Functionalization

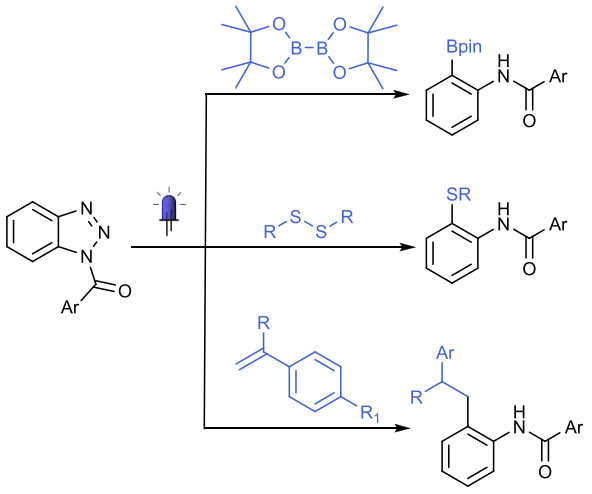

Glorius et al. later improved on this approach by combining the mechanism−based screening[272] with a previously reported reaction-based screening approach,[273] which allowed to reduce the drawbacks associated with each approach (Figure 37).[278] First, a mechanism-based luminescence screen was carried out on 25 randomly selected potential quenchers using [Ir−F] as photocatalyst. A high quenching fraction was achieved with 6 of the potential quenchers. Phenylsydnone was found to have the highest quenching fraction (91%) was carried through to the reaction-based screening. A phosphorus-based MS tag was installed covalently on phenylsydnone, and this quencher was added to a 96-well plate along with [Ir−F] and a diverse range of chemical reagents. The reactions were subsequently

Scheme 12. Results for the Mechanism Based Photocatalyst Screening of a Disulfide−ene Reaction

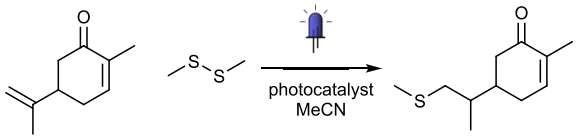

Photocatalyst	E_T (kcal mol^{-1})	Quenching Fraction	Yield
[Ir-F]	60.8	42	58
fac-{Ir(dF(ppy))3	59.1	24	53
[Ir(ppy)2(NHC-F2))]	57.8	31	47
fac-[Ir(ppy)3]	57.8	19	46
Ir(ppy)2(ftbbpy)](PF6)	49.2	<5	0
[Ru(bpz)3](PF6)2	48.4	<5	0
[Ru(phen)3](PF6)2	46.8	<5	0
[Ru(bpy)3](PF6)2	46.5	<5	0

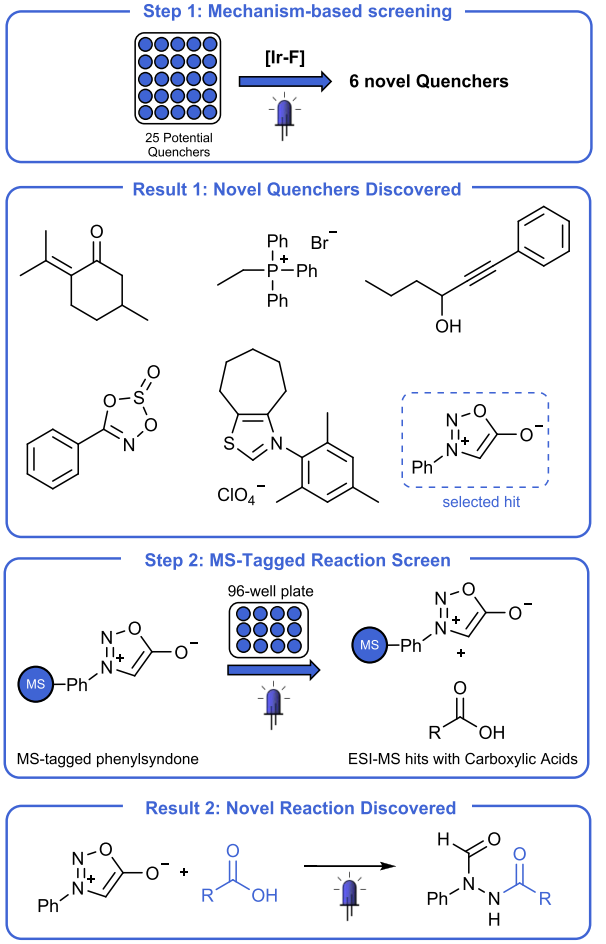

Figure 37. Combined mechanism-based and reaction-based using mass spectrometry toward the discovery of diacylhadrazides from phenylsydnones and carboxylic acids.

analyzed by electrospray ionization mass spectrometry (ESI-MS). The presence of additional peaks after irradiation were indicated as a "hit". Using this strategy, it was observed that reaction conditions containing carboxylic acid motifs reacted readily and produced new ESI-MS signals. To test this observation, the reaction of untagged phenylsydnone and cyclohexanecarboxylic acid was scaled to 0.3 mmol and after

https://doi.org/10.1021/acs.chemrev.1c00332
Chem. Rev. 2022, 122, 2752−2906

irradiation and purification, the formation of diacylhydrazide was identified as a previously unknown transformation.

Similarly, an additive-based robustness screening was performed by Gouverneur et al. to evaluate tolerance toward various functional groups during their discovery of an organophotoredox mediated hydrodefluorination of trifluoromethylarenes (Figure 38).[279] Experiments were carried out

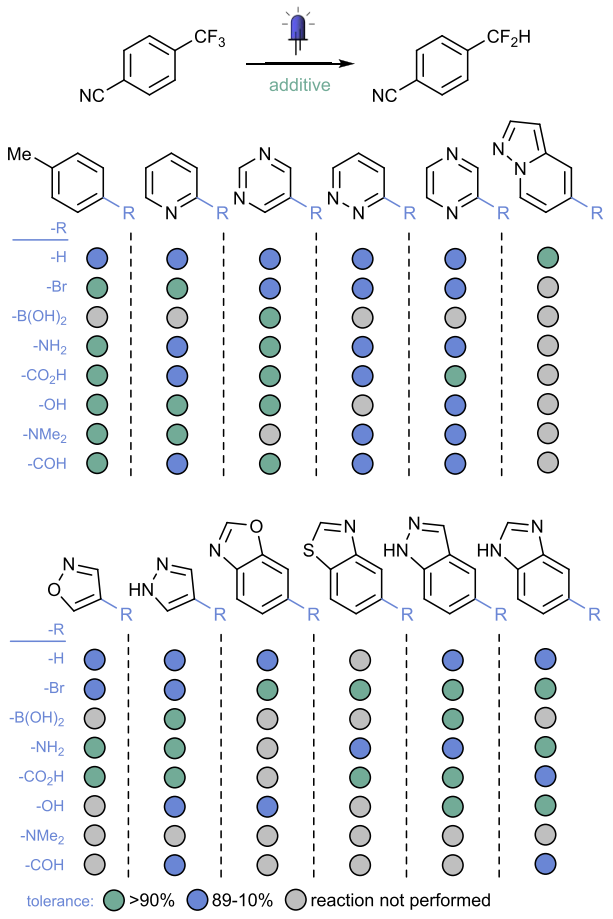

Figure 38. Additive based robustness screening for a photocatalyzed hydrodefluorination of trifluoromethylarenes.

on 2.5 μmol scale in 96-well plates. Common pharmacophoric functional groups were investigated, such as para-substituted toluenes, 2-pyridines, 5-pyrimidines, 3-pyridazines, 2-pyrazines, isoxazoles, pyrazoles, pyrazolopyridines, benzooxazoles, benzothiazoles, indazoles, and benzimidazoles. Reactions containing para-substituted toluenes proved to be the most robust with 6 of the derivatives obtaining yields >90%. In contrast, 3-pyridazines and 2-pyrazines were poorly tolerated.

Lin, Lehnherr, Kalyani, and co-workers developed the HTe-Chem, a high-throughput microscale electrochemical reactor to accelerate the discovery of electrochemical reactions.[280] In particular, they were able to use the platform for the high-throughput screening of the photoelectrochemically mediated oxidative C−H amination of mesitylene with pyrazole. Three voltages, three electrolytes and two reaction times were screened, as well as a number of nonstandard reaction conditions in a 24-well plate configuration (Figure 39). Yields of up to 78% were obtained in 24 h using $LiClO_4$ as an electrolyte and 1.75 V on a 0.4 mmol scale. To prove the reproducibility of the system across each reaction chamber, the

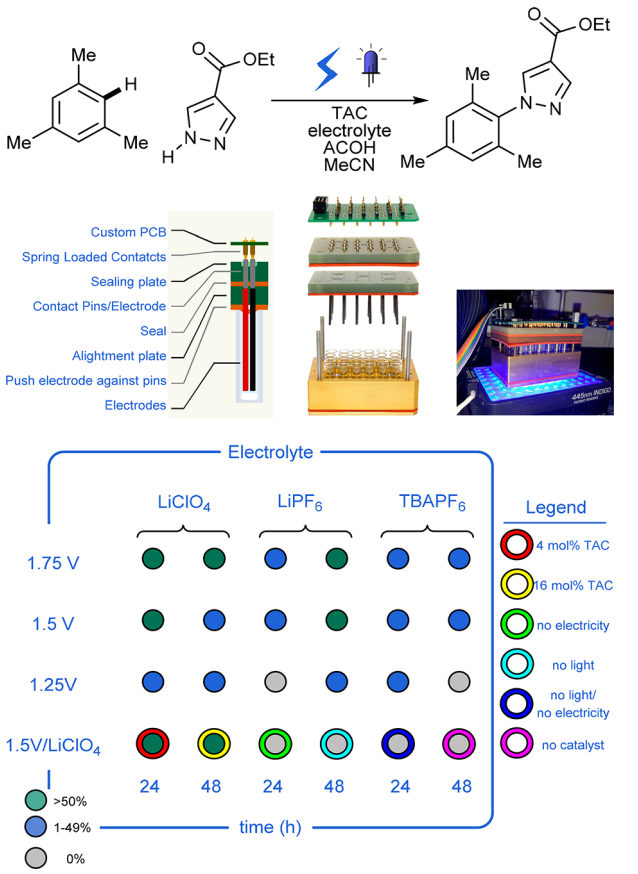

Figure 39. High-throughput microscale electrochemical reactor to accelerate the discovery of photoelectrochemical reactions. Reprinted from ref 280. Copyright 2021 The Authors (CC BY NC ND 4.0 License).

optimized conditions were used in each of the 24 wells and gave an average yield of 75% with a standard deviation of 5.2%.

Bernhard et al. performed a high-throughput screening of dual catalytic Eosin Y with cobalt complexes for the reduction of water and production of hydrogen gas using visible light (Figure 40).[281] Parallelized experimentation allowed for a large amount of cobalt catalysts containing two dimethylglyoxime-type ligands (GL1) and an axial monodentate ligand (L) ($Co(GL1)_2(L)Cl$). First, the reaction condition optimization reactions were performed using eosin Y and $Co(dmg\text{-}BF_2)_2$ pyCl in water and 2-ethoxyethanol, triethanolamine was used as a sacrificial reductant. Optimized reaction conditions were screened using HTE with ranges of photocatalyst concentration (0−1.5 mM) cobalt catalyst loading (0−5 mM), pH (7.5−14), and water volume fraction (0.09−0.5). A custom photoreactor was used and colorimetric tape sensitive to hydrogen was placed above the reaction vials. Reactions were irradiated for 16 h using blue LEDs and progress was monitored by photography. A picture was taken every 10 min while the experiment was running, and hydrogen evolution could be tracked by the color change of the colorimetric tape. Mathematica was used to digitize the color of the tape at each time-interval and this was plotted vs reaction time and the optimal conditions found from the resulting graph. Results indicated that the optimal catalyst/water molar ratio was 1:7000. A further screening using the same HTE of 46 ligands revealed that alkyl-substituted glyoximes were needed for the reaction to proceed. A further

https://doi.org/10.1021/acs.chemrev.1c00332
Chem. Rev. 2022, 122, 2752−2906

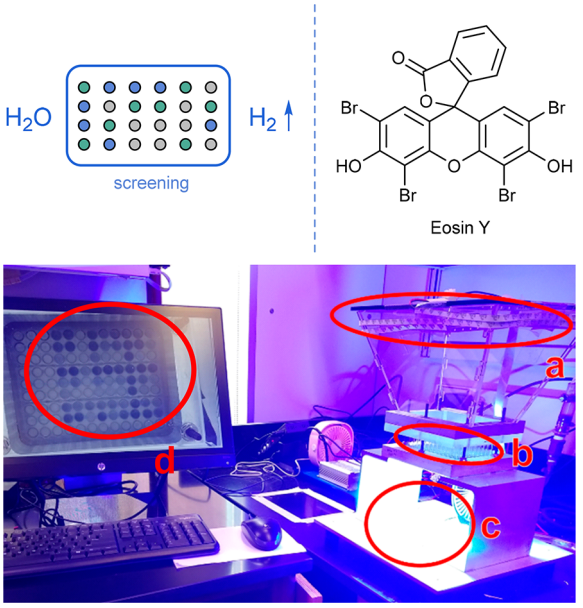

Figure 40. High-throughput screening of hydrogen evolution from the reduction of water by dual eosin Y and cobaloxime catalysis adapted with permission from ref 281. Copyright 2021 American Chemical Society. (a) LED strips and camera, (b) 108 reaction vial assay, (c) 2 × 100 W blue LED chips and (d) HTE experiment results unprocessed.

screening of 616 cobaloxime catalysts gave promising hits for two potential catalysts, namely, the hydroxyquinoline derivative Co(GL1)-(HQ2)pyCl and pyridine/pyrazole-containing derivative Co(GL1)-(NH4)pyCl.

Furthermore, Bernhard et al. developed a parallelized screening platform for the colorimetric detection of hydrogen evolution from water splitting by bimetallic cocatalysts.[282] The platform was capable of screening up to 96 reactions in parallel. Reactions took place in vials with chemosensory colorimetric H_2-sensitive tape on top and irradiation by LEDs through the bottom of the vials. First, the system was calibrated using known amounts of atmospheric pressure H_2. Pictures were taken of the tape from the top down view before and after (Figure 41) and the green and red values were extracted. When

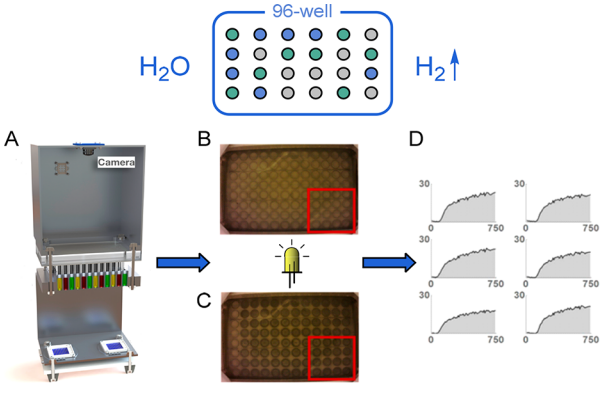

Figure 41. Parallelized screening platform for the colorimetric detection of hydrogen evolution from water splitting by bimetallic cocatalysts: (A) experimental platform, (B) experiment preirradiation, (C) experiment postexperimentation, and (D) data visualization. Adapted with permission from ref 282. Copyright 2021 American Chemical Society.

plotted, the change in color of the colorimetric tape was directly correlated to H_2 concentration added. With this knowledge in hand, the catalytic activities of over 700 bimetallic water-reducing catalysts were investigated.

Rohrer et al. developed a high-throughput experimentation system for the measurement of hydrogen evolution for an investigation of the influence of pH when using $BaTiO_3/TiO_2$ core/shell photocatalysts (Figure 42).[283] Similarly to the work

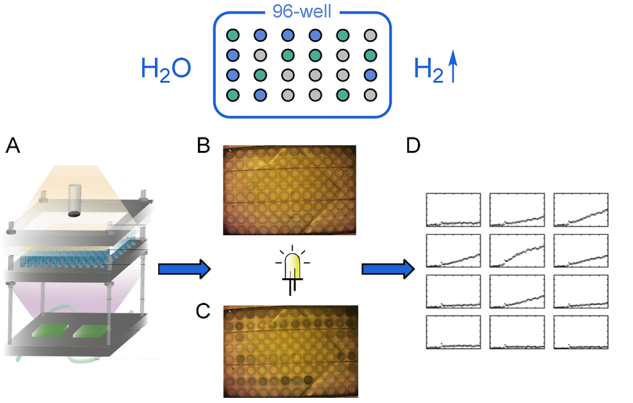

Figure 42. High-throughput experimentation platform for the measurement of hydrogen evolution for an investigation of the influence of pH when using $BaTiO_3/TiO_2$ core/shell photocatalysts: (A) experimental platform, (B) experiment preirradiation, (C) experiment postexperimentation, and (D) data visualization. Adapted from ref 283. Published by Elsevier.

of Bernhard et al.,[281,282] the system used chemosensory colorimetric H_2-sensitive tape, and a camera was used to visualize the evolution of hydrogen over time. Reactions took place in parallel in sets of 96. At lower pH values (3−9) changes in the rate of hydrogen evolution are directly proportional to the pH of the system because of the effect of pH on surface potential. At pH > 9, the rate of hydrogen evolution decreases to its minimum.

König et al. developed a colorimetric indicator method for the detection and quantification of byproducts in 96 parallel photocatalytic reactions.[284] These byproducts correlate strongly with both yield and conversion and thus a quantification can be ascertained. The photooxidation of benzyl alcohols and benzylamines to benzaldehyde by riboflavin tetraacetate (RFTA) was investigated. Potassium iodide and starch were used to indicate the presence and evolution of hydrogen peroxide indicating a successful reaction. Three benzyl alcohols and all the amines were successfully oxidized, and yields could be estimated by the color change (Figure 43).

Cooper, Sprick, Zwijnenburg, and co-workers developed a high-throughput robotic platform for the screening of 170 organic copolymers for the photocatalytic hydrogen generation from water.[285] A diverse selection of dibromoarene building blocks were coupled with either diboronic arene acids or esters, resulting in a library of 706 candidate dibromoarenes and 9 diboronic acids/esters (6354 combinations in total). These were first screened computationally and a subsection of 127 dibromides were synthesized by microwave-assisted Suzuki−Miyaura polycondensation using a robotic formulation platform (Figure 44) and brought forward for automated screening, leading to the discovery of new polymers with hydrogen evolution rates (HERs) of more than 6 mmol·g^{-1}.

https://doi.org/10.1021/acs.chemrev.1c00332
Chem. Rev. 2022, 122, 2752−2906

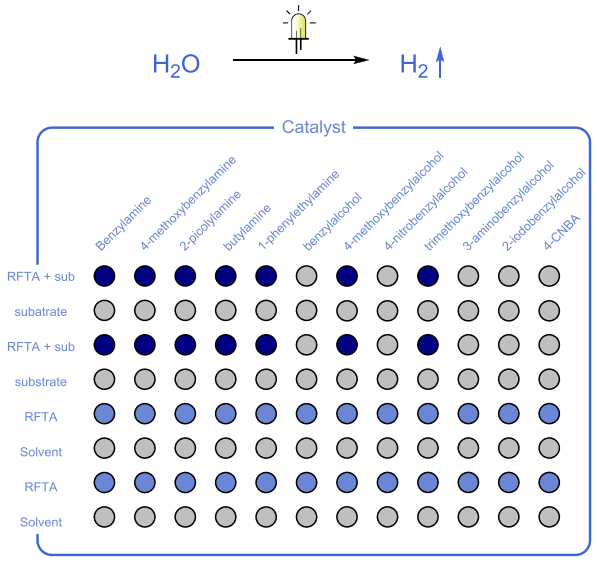

Figure 43. High-throughput experimentation platform for the colorimetric indicated quantification of the photooxidation of benzyl alcohols and benzylamines to benzaldehyde by RFTA.

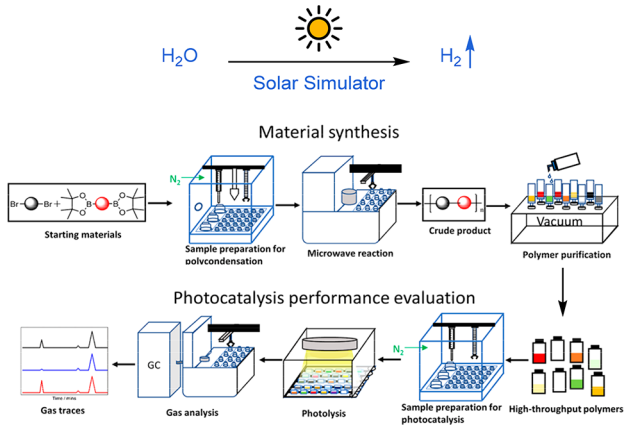

Figure 44. High-throughput robotic platform for the screening of organic copolymers for the photocatalytic hydrogen generation from water adapted with permission from ref 285. Copyright 2019 American Chemical Society.

h^{-1}. Machine learning was applied to the resulting data sets and four variables (electron affinity, ionization potential (predicted), optical gap, and dispersibility of polymer particles in solution) could successfully describe up to 68% of the polymer-to-polymer variation in the HER data.

The same authors developed a high-throughput work-flow to screen a structurally diverse family of 39 covalent triazine-based framework materials (CTFs) for photocatalytic water splitting.[286] The Chemspeed SWING robotic platform was utilized for the automation of the screening section. Degassed solvents (triethylamine and methanol) and a stock solution of H_2PtCl_6 were loaded onto the platform (Figure 45). Crimp top vials were charged with 5 mg of polymer powder and transferred to the platform. Under inert conditions, 1.7 mL of degassed water, aqueous H_2PtCl_6 solution, triethylamine, or methanol was added; vials were crimped and shaken for 5 s and irradiated by a solar simulator with an output of 1.0 sun equivalent. This screening led to the discovery of two high-performing CTFs based on benzonitriles and dibenzo[*b*,*d*]-thiophene sulfone linkers with catalytic activity that is among

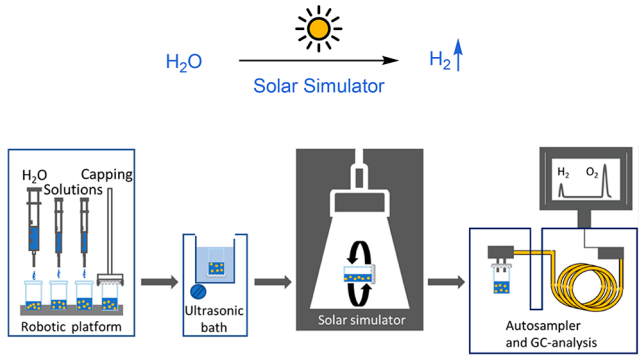

Figure 45. High-throughput work-flow for the development of structurally diverse family of covalent triazine-based framework materials for photocatalytic water splitting for the evolution of hydrogen. Adapted with permission from ref 286. Copyright 2019 American Chemical Society.

the highest in their material class. Two variables (electron affinity and dispersibility) were found to be the best predictors of ability to evolve hydrogen from the splitting of water.

4.2. Flow-Based Automated Platforms

A versatile, modular photoreactor platform was developed by Edwards et al. capable of high-throughput experimentation, batch reactions, and continuous processing called the Photochemistry LED Illuminator (PHIL) (Figure 46).[209] With the ability to tune for wavelength, light intensity, and very precise temperature control, the platform can deal with a broad range of photochemical transformations. The HTE module has the ability to screen up to 48 reactions simultaneously over a range of 6 wavelengths (365−525 nm). First, photochemical actinometry was carried out in the HTE platform using rhodamine-6G as a photocatalyst for the coupling of a pyrrole with a bromothiophene. Surprisingly, the reaction outcome was independent from both the applied wavelength and the presence of the photocatalyst, indicating that a homolytic cleavage of the C−Br bond is occurring. Next, the intramolecular [2 + 2] cycloaddition of maleimide with an alkyne was analyzed. The reaction proved to be sluggish at all wavelengths tested so benzophenone (10 mol %) was added leading to a large increase in the rate observed with reactions going to completion in 10 min. Further to this, a number of other reactions were investigated including and intramolecular [2 + 2] cycloaddition, a Norrish type 1 reaction with [1.1.1]-propellane, the biocatalyzed hydroxylation of ethylbenzene, and a cross-coupling of aryl iodides.

A photochemical cascade CSTR platform (Freactor) was developed by Bourne et al. for the auto-optimization of multiphasic and mass transfer limited photochemical reactions (Figure 47).[287] Because of the constant agitation, the reactor is resistant to clogging and fouling. First, to get a greater understanding of the Freactor, chemical actinometry was carried out by the photochemical transformation of *o*-nitrobenzaldehyde (NBA) to *o*-nitrobenzoic acid using 365 nm light. The photon flux obtained was found to be ∼10× higher than batch systems in the literature.[288] Next, automated reaction optimization was carried out on the aerobic oxidation of tetralin with benzophenone as a catalyst using a hybrid algorithm. The hybrid algorithm consisted of the coupling of three distinct algorithms (global optimization by SNOBFIT, surrogate Gaussian process modeling, and a central composite face-centered (CCF) designed screening). The reactor was run

https://doi.org/10.1021/acs.chemrev.1c00332
Chem. Rev. 2022, 122, 2752−2906

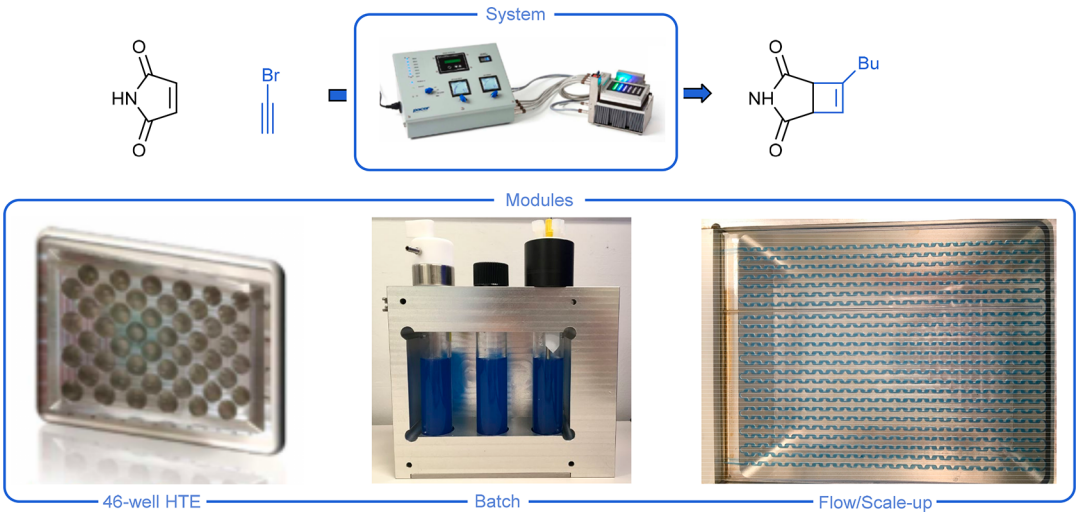

Figure 46. Photochemistry LED Illuminator (PHIL) with modules for high-throughput experimentation and batch and flow chemistry for the screening and scale-up of a diverse range of photochemical reactions. Reprinted with permission from ref 209. Copyright 2019 John Wiley and Sons.

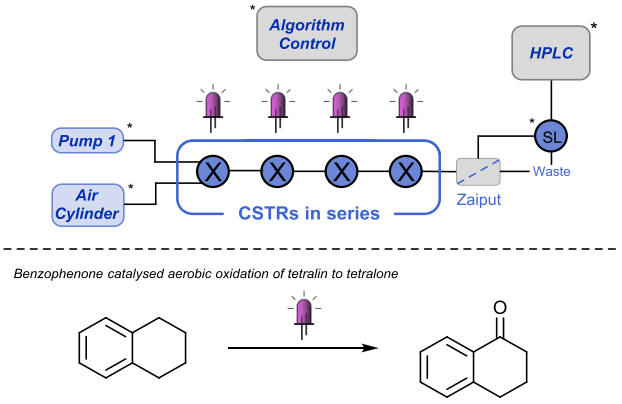

Figure 47. Photochemical cascade CSTR platform (Freactor) for the auto-optimization of multiphasic and mass transfer limited photochemical reactions.

for a total of 36 h and 61 experiments were performed (38 SNOBFIT, 12 Gaussian screenings, and 11 CCF experiments). A total yield of 65% was obtained for tetralone, with a residence time of 18.3 min and 4.69 oxygen equivalents.

A fully autonomous continuous-flow platform for fluorescence quenching studies and Stern−Volmer analysis was developed by Noël et al. using Python-based code and inline UV−vis spectroscopy (Figure 48).[289] The use of automation and flow has a number of defined benefits, such as improved consistency, accuracy and reproducibility. The repetitive tasks of performing this reaction manually can lead to reproducibility issues which are mainly associated with oxygen interference and human error. The system utilizes small sample volumes, which is especially useful when screening expensive catalysts. Two benchmark reactions were carried out in order to test the system: the photocatalytic decarboxylation of α,β-unsaturated carboxylic acids and the photocatalytic decarboxylative alkylation of N-containing heteroarenes with *N*-(Acyloxy)phthalimides. Overall, the system leads to better, more reproducible results in comparison to manual and produced data within 15 min for analysis.

A self-optimizing, segmented flow reactor was reported by Jensen, Robinson, and co-workers for the optimization of

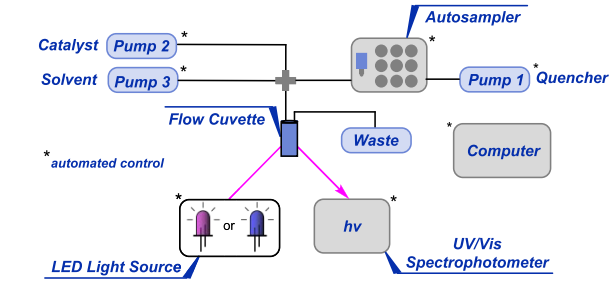

A *Photocatalytic decarboxylation of α,β-unsaturated carboxylic acids*

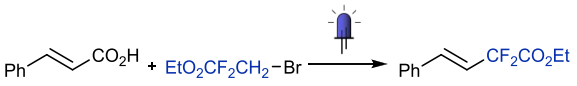

Photocatalyst	Quencher	R^2	Rate Constant ($M^{-1}\cdot s^{-1}$)
fac-Ir(ppy)$_3$	$BrCF_2CO_2Et$	0.992	1.84×10^8
fac-Ir(ppy)$_3$	Cinnamic Acid	0.995	3.37×10^8
fac-Ir(ppy)$_3$	*trans*-cinnamate	0.999	1.24×10^8

B *Decarboxylative alkylation of N-containing heteroarenes with N-(Acyloxy)phthalimides*

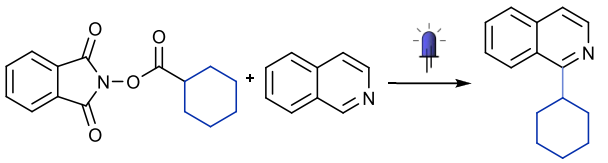

	A	B	C
Photocatalyst	A	B	B + TFA	TFA
Ir(ppy)$_3$	>50	<25	>50	<25
Ru(bpy)$_3^{2+}$	<25	<25	>50	<25
Mes-Acr$^+$	<25	<25	<25	<25
2CzPN	<25	<25	>50	<25
4CzIPN	<25	<25	>50	<25

Figure 48. Fluorescence quenching studies and Stern−Volmer analysis using a fully automated platform showcased by the photocatalytic decarboxylation of α,β-unsaturated carboxylic acids and the decarboxylative alkylation of N-containing heteroarenes.

https://doi.org/10.1021/acs.chemrev.1c00332
Chem. Rev. 2022, 122, 2752−2906

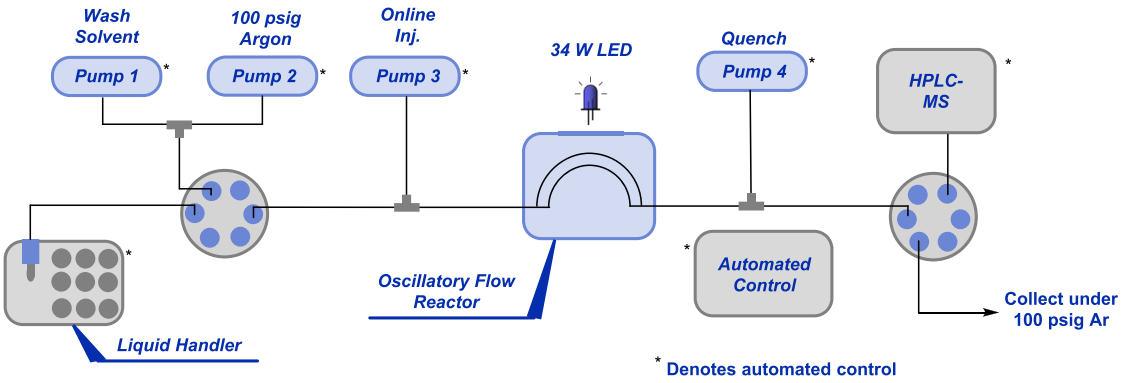

Figure 49. Platform for the auto-optimization of photocatalytic decarboxylative coupling.

iridium−nickel photoredox decarboxylative arylation cross-coupling (Figure 49).[290] A liquid handling robot was used to make each experimental condition automatically from a set of stock solutions. The system utilized an oscillatory flow reactor integrated with a photochemistry module, equipped with a 34 W blue LED that had the ability to operate at a range of temperatures between 20 and 70 °C. The selected optimization algorithm could handle both discrete parameters (bases, photocatalysts, and nickel catalysts) and continuous parameters (reaction temperature and reaction stoichiometry). The system used online-HPLC for analysis, the results of which could be interpreted by the algorithm in order for it to decide a new set of reaction parameters to subsequently try. Each microslug (~15 μL) acts as a discrete experimental condition and could be determined by the auto-optimization algorithm.

Utilizing a similar system attached to an LC-MS, Jensen et al. also devised a comparable microfluidic platform for exploratory studies of visible light photoredox catalysis.[291] Three distinct photocatalyzed reactions were studied. The oxidation of 9,10-diphenylathracene (DPA) served as a chemical actinometer to better understand the irradiation characteristics of the flow platform. By measuring the consumption of DPA throughout the reaction with online UV−vis spectroscopy, photon fluxes for the platform across a range of light intensities could be measured. Second, visible light catalyzed oxidative hydroxylation of arylboronic acids to phenols were carried out to demonstrate the versatility of platform. Third, the dimerization of thiophenol to diphenyldisulfide was investigated. Reactions could be screened for continuous variables (residence time, reaction temperature and light intensity) and discrete variables (e.g., substrates). Over 150 reaction conditions were explored using a total volume of 4.5 mL, with the results being directly transferable to flow systems.

An autonomous self-optimizing reactor platform was reported by Junkers et al. for the photoiniferter polymerization of methacrylates (Figure 50).[292] The program LabVIEW was chosen to interact with the setup. The algorithm selected the reaction parameters, which were then implemented by the LabVIEW program to optimize chemical process in a closed-loop feedback system. Size exclusion chromatography (SEC) was utilized as the online PAT for the system, as it allows to measure and optimize critical polymer parameters, such as weight-average (M_w), number-average (M_n), and peak molecular weight (M_p). The system was tested by completing a sequence of three number-averaged molecular weights of

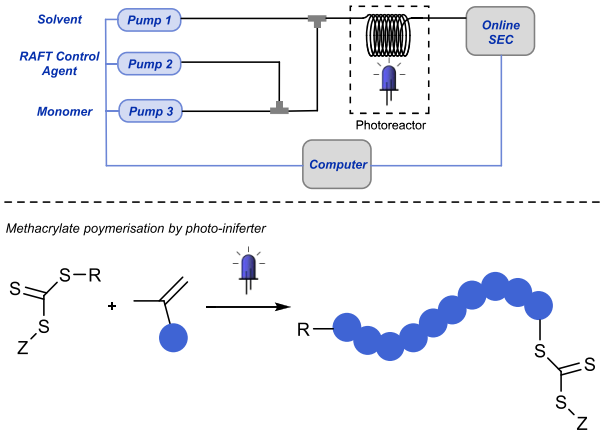

Figure 50. Self-optimizing reactor using online SEC for the auto-optimization of the photoiniferter polymerization of methacrylates.

5000, 7500, and 10000 g·mol^{-1}. Accuracies achieved were within a 1% deviation of average molecular weight at 80% conversion.

A HTE platform to optimize photocatalytic transformations on the picomole scale was reported by Stephenson et al. using flow photochemistry (Figure 51).[293] The pump system was used in an oscillatory manner with a constant forward flow-rate to sustain the beneficial flow properties (e.g., increased heat/mass transfer) along with the ability to use extended residence times (1 h). They tested and validated the HTE system on radical trifluoromethylation reactions using four small molecule drug candidates. Reaction droplets of 4 nL were interspersed with 8 nL of perfluorodecalin as the carrier phase. By looking at the ESI-MS data, they could validate the capability of the platform to perform rapid analysis and categorize a reaction into a "hit" or "nonhit". Results were consistent and relative standard deviations between 1% and 19% were obtained. The authors then moved on to investigate photoredox reactions, specifically visible-light driven alkene aminoarylations. Hereto, 10 sulfonylacetamides and 10 alkenes were selected for the screen. Of the 100 possible combinations, 37 were identified as possible hit conditions. Of these hits, 9 were scaled up to the 0.01 and 0.1 mmol scale using continuous-flow processing. Finally, 7 of these potential hits were isolated and strong correlating yields were observed between the HTE results and the large scale conditions.

Lemaire, Luxen, Genicot, and co-workers developed an automated flow photoredox ^{18}F-radiolabeled difluoromethylation of acyclovir using a commercially available AllinOne

https://doi.org/10.1021/acs.chemrev.1c00332
Chem. Rev. 2022, 122, 2752−2906

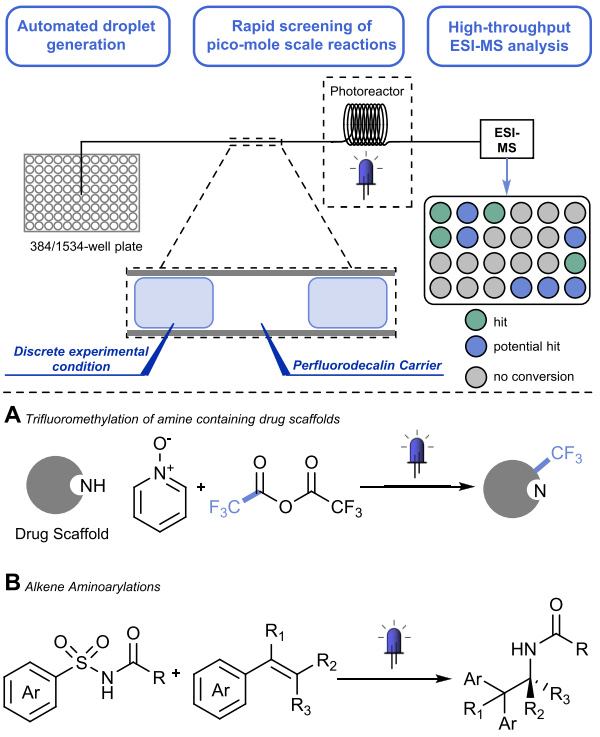

Figure 51. HTE system for the rapid screening of pico-mole scale reactions using ESI-MS showcased by the trifluoromethylation of amine containing drug scaffolds and alkene aminoarylations.

synthesizer (Trasis) (Figure 52).[294] Automation of the process is important to minimize the amount of exposure to radiation and for better reducibility. The process was automated in two stages, the two-step synthesis of the ^{18}F-difluoromethylation agent, followed by the direct ^{18}F-difluoromethyl incorporation to acyclovir. Both stages required an automated isolation using preparative HPLC. After optimization of stage one, the highest radiochemical yields (RCY) (11.9%) were obtained using [^{18}F]KF, aminopolyether (K_{222}), K_2CO_3 in acetonitrile at 85 °C, followed by oxidation using $NaIO_4$ and $RuCl_3$. Next the conditions for the flow photoredox ^{18}F-difluoromethylation of acyclovir were optimized, giving photocatalyst 4CzIPN, 1.2 mL total volume, blue LEDs (Kessil, 32 W), t_R = 1 min as the optimal conditions. Finally, both stages were combined in series with a high activity batch of [^{18}F]fluoride using the optimized conditions with the radiolabeled acyclovir being obtained with 1.4 ± 0.1% RCY.

A machine-assisted self-optimizing reaction system for continuous-flow photochemical reactions was developed by Rueping et al. by utilizing flow-react-IR for the optimization of the Paternò–Büchi reaction of benzophenone (Figure 53).[295]

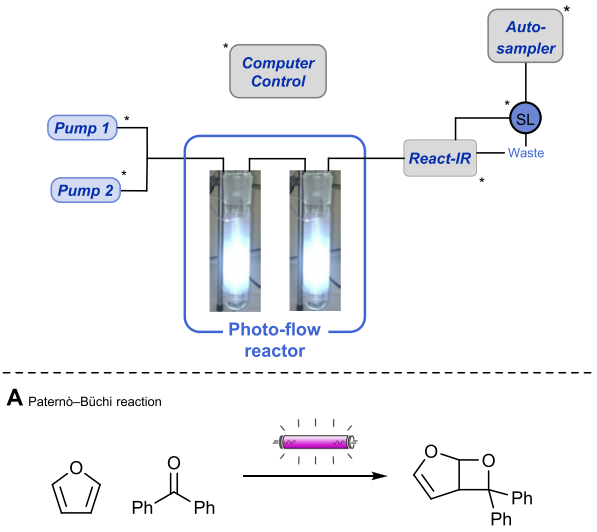

Figure 53. Auto-optimization platform using react-IR for the optimization of the photocatalyzed Paternò–Büchi reaction of benzophenone and furan. Reprinted with permission from ref 295. Copyright 2018 Elsevier.

The modified simplex algorithm (MSIM) was used and the HPLC pumps were controlled by LabView. To investigate the influence of concentration, both benzophenone dissolved in furan and neat furan were pumped individually into the photomicroreactor, while the algorithm incrementally changed the flow rates of both solutions. The intensity of the carbonyl peak at 1662 cm^{-1} was optimized, as it gives an indication of consumption of starting materials, whereas the yields were calculated later using GC. The system self-optimized over the course of 25 experiments, bringing the conversion from 16% in the initial conditions up to 90%.

A flow radial synthesizer was developed by Gilmore et al. with inline monitoring by flow NMR spectroscopy (Figure 54).[296] The system can run both linear and convergent strategies for the development of single or multistep reactions. A 16-way valve at the center of the radial synthesizer directs reactions toward storage, reactors (including a photoreactor) and in-line analytics. In order to expand the scope of the system, dual nickel/photoredox C–C and C–N cross-coupling were investigated. A full optimization of the coupling of pyrrolidine and 4-bromobenzonitrile was performed as a two-step process using a 420 nm photoreactor module.

Jensen, Jamison, and co-workers described a reconfigurable platform for the development of diverse chemical reactions.[297] The system consisted of 5 distinct bays in which standardized reconfigurable modules could be added and removed quickly. The modules consist of units to perform synthetic steps (e.g.,

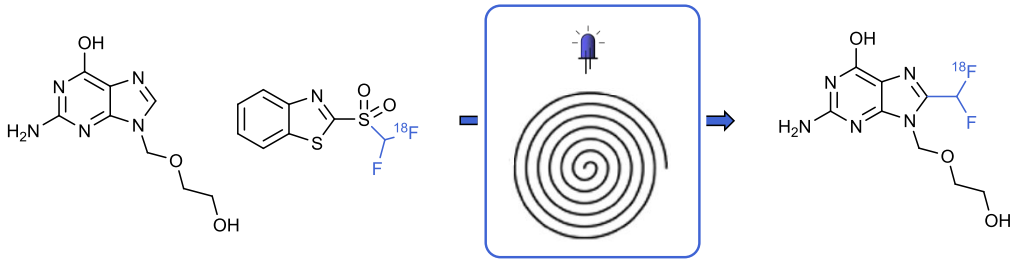

Figure 52. AllinOne synthesis platform for the photocatalyzed incorporation of ^{18}F-difluoromethyl onto acyclovir.

https://doi.org/10.1021/acs.chemrev.1c00332
Chem. Rev. 2022, 122, 2752–2906

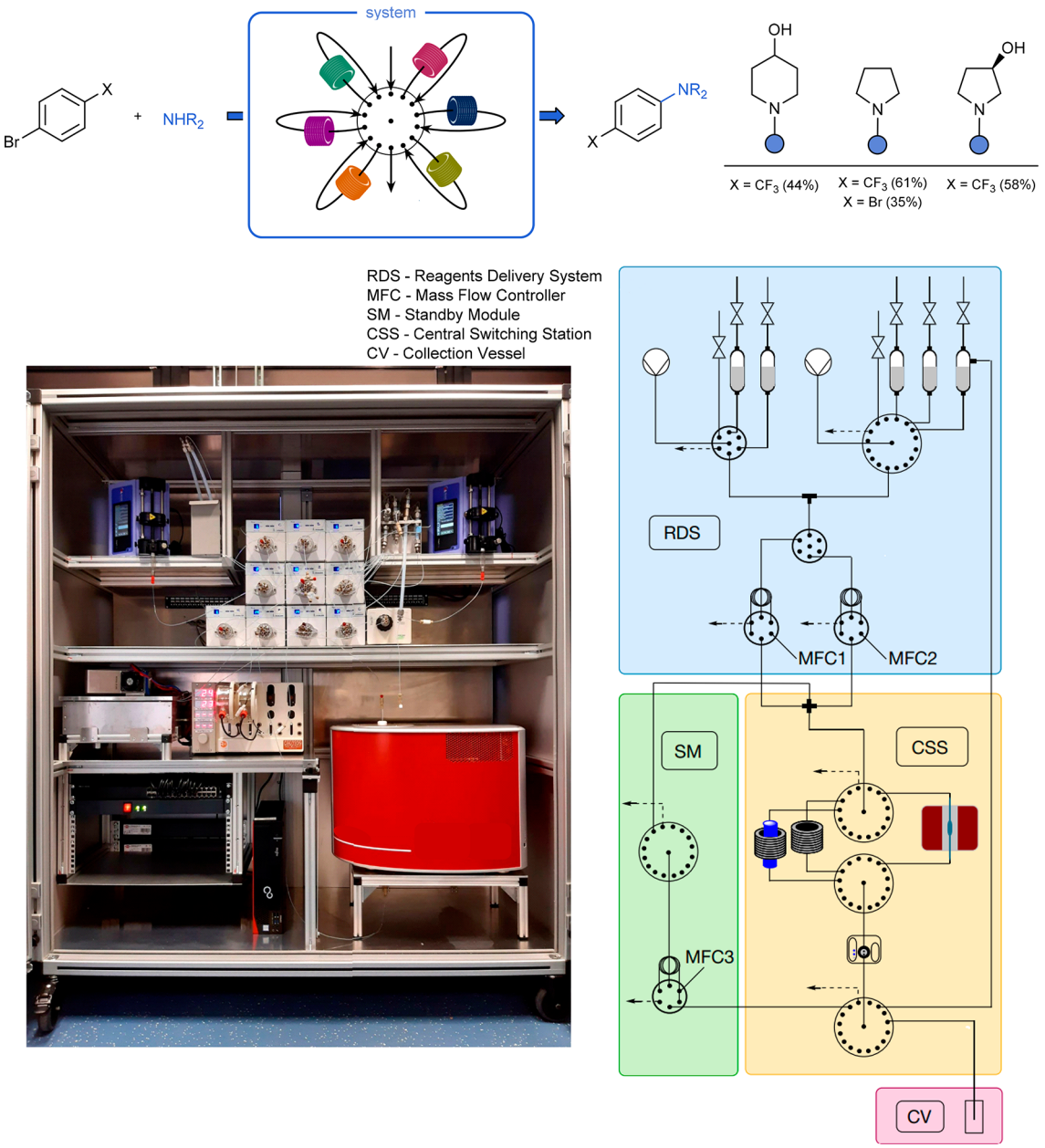

Figure 54. Radial synthesizer platform developed by Gilmore et al. for the automation of photoredox enabled C−N cross-coupling adapted with permission from ref 296. Copyright 2020 Springer Nature.

photochemical, thermal control) or separations (e.g., in-line membrane separators). Autonomous optimization was performed by utilizing in-line HPLC for quantification coupled with a black-box algorithm. The SNOBFIT algorithm was chosen for its ability to reach the global minima of a search space and its lowered probability of encountering local minima with algorithms like Simplex.[298] The algorithm iteratively performed local optimizations around the best conditions while also searching other areas far removed in order to ensure the global optimum is found. The bounds for the reaction parameters were hardcoded into the experiment by a chemist with knowledge of the system being optimized. To test the ability for the platform, the previously reported trapping of 1,2,3,4-tetrahydroquinoline with an iminium ion under photocatalysis was investigated.[299] Two modules were installed in the system, the photoreactor followed by a temperature control module. Four stock solutions were prepared (tetrahydroquinoline, the internal standard, $Ru(bpy)_3PF_6$, and sodium cyanide). The objective function of the algorithm was set to maximize the conversion of the tetrahydroquinoline vs the internal standard, optimizing three flow rate variables. The system reached the optimized conditions in a total of 7 h, which called for a total residence time of 4.28 min, catalyst loading of 1.89 mol % and 4 equiv of sodium cyanide and afforded an optimized yield of 91% and a throughput of 223 $mg \cdot h^{-1}$ (Figure 55).

Further advances in transient flow-based systems have been put forward by Tellarek et al. by utilizing online HLPC.[300] When using process analytical tools (PAT), it is generally accepted that one makes a trade-off between analytical measurement time and the complexity of the analysis undertaken. They attempted to decouple the time-scale of the reaction and the time-scale of the analytical method, by utilizing a system where they "park" (i.e., hold them stationary

https://doi.org/10.1021/acs.chemrev.1c00332
Chem. Rev. 2022, 122, 2752−2906

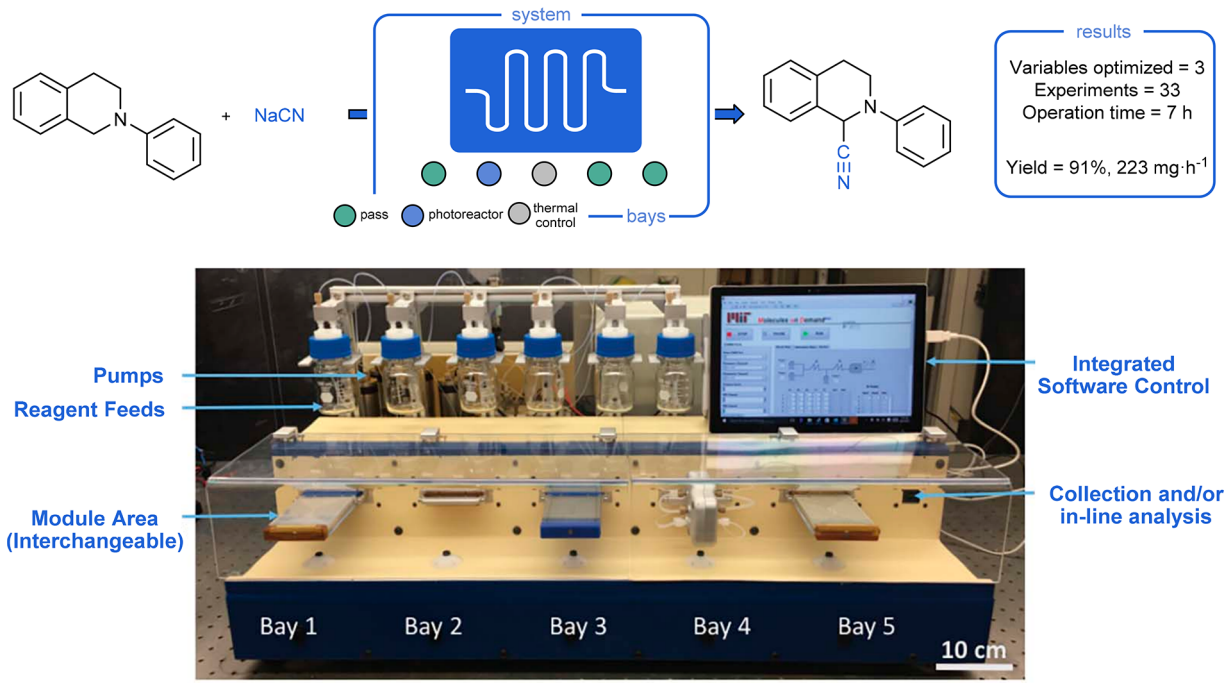

Figure 55. Modular, reconfigurable system for automated optimization of chemical reactions for the optimization of the trapping of iminium ion with 1,2,3,4-tetrahydroquinoline under photocatalysis. Reprinted with permission from ref 297. Copyright 2018 American Association for the Advancement of Science.

in capillary tubing) reaction samples prior to analysis by using a novel multiple heart-cutting (MHC) interface (enables platform to take reaction samples, to park these samples, and to subsequently inject the samples into an online-coupled HPLC/MS system) (Figure 56). The benefits of this approach

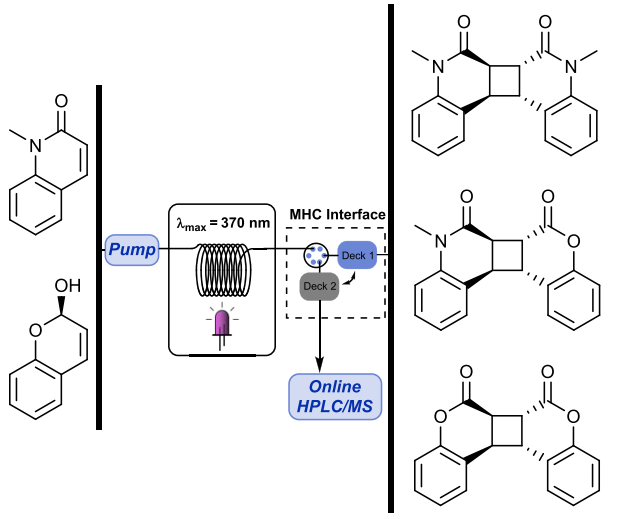

Figure 56. HTE combined with a multiheart cutting interface to decouple reaction time from analysis time showcased for the optimization of the [2 + 2] cycloaddition between 1-methyl-2-quinolinone and coumarin.

were the minimized reagent consumption associated with transient flow systems while simultaneously resolving analytical complexity in the form of HPLC analysis. As a model reaction, the optimization of the reaction conditions for the [2 + 2] cycloaddition between 1-methyl-2-quinolinone and coumarin was used. Using the screening method, they were able to generate 400 individual data points in 75 h. However, because of the use of the MHC interface, the reactor was only utilized for 17 h. This example serves to highlight the ability to decouple reaction time from analysis time. Automated data processing was used in order to plot conversion against reaction time and reaction concentration to give a DoE-type model of the reaction space.

4.3. Alternative Methods

Researchers at Abbvie developed a method of parallelization via catalyst encapsulation and applied it to the screening of metallophotoredox mediated C−N cross-couplings.[301] By using the encapsulation method, broad substrate libraries could be built up, easily stored for long periods, and screened en masse in a parallelized fashion. Capsules containing an iridium catalyst, $NiBr_2$·glyme, and 1,4-diazabicyclo[2.2.2]-octane (DABCO) were formed by first weighing and mixing in a glovebox then simultaneously filling 100 hydroxypropyl methylcellulose (HPMC) capsules (Figure 57). Capsules are

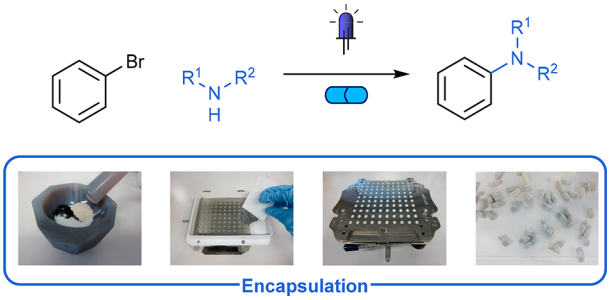

Figure 57. Parallelization of experiments through an encapsulation work-flow for the screening of metallophotoredox mediated C−N cross-couplings. Adapted with permission from ref 301. Copyright 2020 American Chemical Society.

https://doi.org/10.1021/acs.chemrev.1c00332
Chem. Rev. 2022, 122, 2752−2906

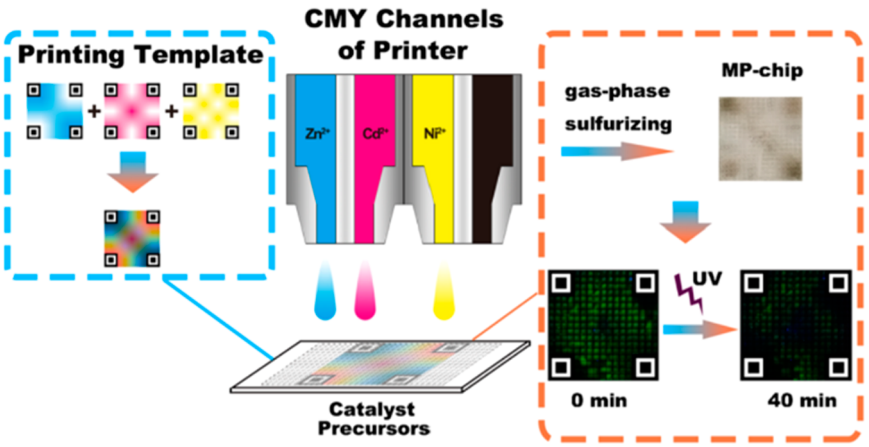

Figure 58. Chemical inkjet printing technology for the parallelization of experimentation for the discovery of $M_3S/g\text{-}C_3N_4$ multicomponent photocatalysts. Reprinted with permission from ref 301. Copyright 2015 John Wiley & Sons.

oxygen and water transmission resistant and possess a 2-year shelf life. Ten reactions were set up in parallel by adding an aryl bromide amine and capsule, followed by dimethylacetamide and sparging with argon, saving time on the creation of stock solutions. Reactions were irradiated overnight (16 h) with blue LEDs and isolated by preparative HPLC. Good yields of 51−85% were obtained, indicating that the HPMC capsule did not interfere with the reaction.

Lee et al. utilized a high-throughput experimentation/UV lithography technique to prepare a small footprint platform to screen the photocatalytic decomposition of organic pollutants using fluorescence imaging.[302] Each chip contained 1262 independent experimental conditions. The library of catalysts, which consisted of polymetallic sulfides (M_6S/MoS_2, where M = Cd, Zn, Ni, Sr, Ce, and Y) with $nanoMoS_2$ chosen as a constant main catalyst pairing. To build up a material library, inkjet printing (IJP) was utilized. The catalyst precursors were applied and linked to cyan−magenta−yellow (CMY) values on the IJP. The efficiency of the printed catalysts was tested by calculating the degradation of sodium fluorescein (NaFl) by 365 nm light through its decrease of fluorescence over the course of 40 min from each printed cell like structure, with the darkest zones representing the zones of highest catalytic activity. By creating a grayscale image subtracting the image at 0 min from the image at 40 min, an optical density measurement could be evaluated for each cell on the chip. The greater the optical density measurement, the greater fluorescence quenching had been achieved in that cell. Four metals, Ni, Ce, Y, and Cd, showed the most activity when compared to the other two metals.

Lee et al. further iterated on this idea to test the photocatalytic ability of (Zn, Cd, and Ni) sulfide modified graphitic carbon nitride ($g\text{-}C_3N_4$) for the screening of a chip containing $M_3S/g\text{-}C_3N_4$ multicomponent photocatalysts (Figure 58).[303] Fluorescence imaging technology and chemical IJP technology were combined to perform 225 parallel independent microreaction experiments. Optical density measurements were again utilized to evaluate the cells for the photocatalytic ability of that reaction condition.

5. FLOW PHOTOCHEMISTRY

Flow chemistry takes advantage of microreactors to carry out (organic) reactions in continuously flowing streams.[304] Microreactors consist of coil and chip reactors with volumes ranging from micro- to mesoliter scale.[43,305,306] Flow chemistry represents an important tool to overcome some typical limitations of batch synthesis, such as slow heat and mass transfer,[307] and offers the ability to work at high pressures and high temperature in a tightly controlled environment, as well as to shorten reaction times and in some cases to increase selectivities. Moreover, it facilitates scale-up and process intensification.[308] For these reasons, flow chemistry has become an essential enabling technology for industry, especially for drug development,[196,309−313] but also for material and catalyst manufacturing.[314] Continuous-flow photochemistry refers to the synergistic combination of photochemistry with flow techniques to ensure uniform light irradiation[104,315] and thus better performances, with the previously outlined advantages of continuous processing. This field has witnessed a tremendous expansion in research in recent years,[116,316−319] as was previously described in our review from 2016.[51] The next sections will try to cover in the most comprehensive way the developments of photochemistry in flow.

5.1. Photocycloaddition

The photocycloaddition reaction is one of the oldest photochemical transformations. However, even to this day, it remains among the most popular ones, as is evident by the increasing amount of publications appearing on the subject.[320−324] One of the reasons for its popularity is that photocycloadditions give rapid access to complex carbo- and heterocycles, such as cyclobutanes and oxetanes, in an atom-efficient way, which is difficult to realize using traditional synthetic methods.[76,325] In medicinal chemistry, for example, the often one-step increase of three-dimensional character of organic molecules is especially valued for the generation of new drug candidates.[326]

The intramolecular [2 + 2] photocycloaddition of unsaturated enones to either straight or bridged polycyclic cyclobutanes was performed in a commercially available flow reactor with high power UV-A LEDs (365 nm), resulting in a higher reaction efficiency compared to batch (Scheme 13A).[327] The ability to precisely control the reaction conditions in the flow setup enabled the determination of highly accurate kinetic data, indicating that straight polycyclic butanes were generated faster than crossed ones. The reaction was second order in enone and photocatalyst. Furthermore, the shorter path length in the microflow reactor led to higher yields and shorter

https://doi.org/10.1021/acs.chemrev.1c00332
Chem. Rev. 2022, 122, 2752−2906

Scheme 13. Intramolecular [2 + 2] Photocycloaddition of (A) Enones and (B) Enaminones

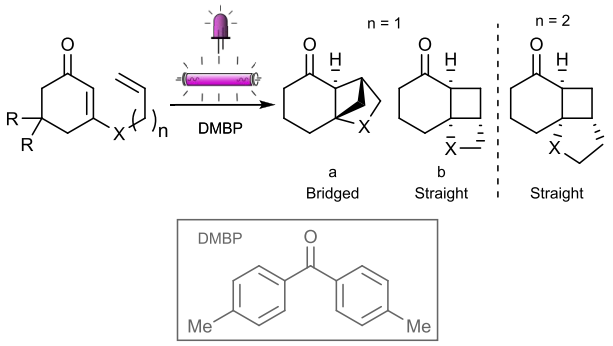

	Substrate		Yield	t_R	Ratio a:b
(A)	X = O	n = 1	50-85%	180 min	1:0
		n = 2	95-98%	60 min	1:0
(B)	X = N-Boc	n = 1	96%	30 min	4:1
		n = 2	95%	40 min	1:0

Microflow conditions (A):
- Glass microreactor (0.5 x 2.0 mm)
- UV-A LED (230 mW cm^{-2}, λ_{max}: 365 nm)
- Solvent: CH_3OH (37 mM)

Microflow conditions (B):
- FEP tubing (2.7 mm ID, 105 mL)
- UV-C lamp (55 W , λ_{max}: 254 nm)
- Solvent: CH_3CN (40 mM)

reaction times in flow (96% yield after 2 h) compared to batch (45% yield after 4 h).

A similar intramolecular photocycloaddition was performed by Rutjes et al., starting from enaminones instead of enones (Scheme 13B).[328] In contrast to the previous case, the bridged product was preferentially formed over the straight product in a 4:1 ratio for allyl substituted enaminones. Initial reaction optimization was performed in a Rayonet RMR-600 photochemical reactor (95−96% yield), followed by scale-up in a self-fabricated reactor system. In this system, the reaction mixture was pumped by HPLC through FEP tubing (2.7 mm ID, 105 mL volume) coiled around a Philips PL-L 55 W UV-C lamp (254 nm). The tubing and lamp were surrounded by a metal jacket, containing cooling water to dissipate heat generated by the light source. The self-fabricated flow system was capable of converting >100 g of enaminones per day and was successfully applied to the target compounds in high isolated yields.

A different complex ring system that can be formed through intramolecular [2 + 2] photocycloaddition is the bicyclo[3.2.1]octane ring system (Scheme 14).[329] This ring system is an important scaffold in medicinal chemistry as molecules with this scaffold can inhibit dopamine and serotonine transporters and could thus serve as central nervous system (CNS) drugs.[330] The photocycloaddition was performed both in batch and in flow. In the flow scenario, the desired photocycloaddition products were obtained in short residence time and in moderate to high yields (6−12 min, 48−95% yield), outperforming the results obtained in batch (5−15 h reaction time, 12−90% yield). The higher productivity obtained in flow is attributed to the enhanced heat and mass transfer, more efficient irradiation, and higher substrate concentrations than those applied in the batch reaction.

Monosubstituted 2,4-methanopyrrolidines were synthesized on a kilogram scale using the parallel tube flow "Firefly" reactor,[139] and these photochemically generated scaffolds were used for library generation.[331] Also disubstituted 2,4-

Scheme 14. Intramolecular [2 + 2] Photocycloaddition, Formation of Bicyclo[3.2.1]octadienes

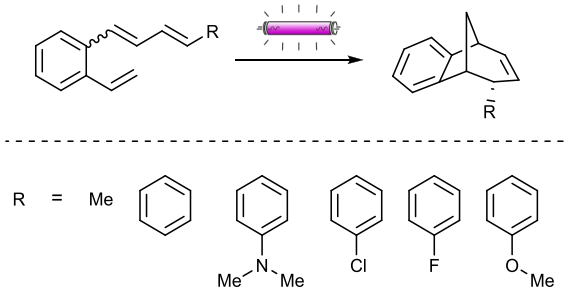

Microflow conditions:
- FEP tubing (0.76 mm ID, 8.6 mL)
- UV lamp (16 x 8 W, λ_{max}: 300 or 350 nm)
- Solvent: Toluene (93 mM)

Flow: t_R = 6-12 min, 24-95%
Batch: t_R = 5-15 h, 12-90%

methanopyrrolidines could be synthesized through intramolecular [2 + 2] photocycloaddition in flow (Scheme 15).[332] These pyrrolidine analogues are more soluble in

Scheme 15. Photochemical Synthesis of 2,4-Methanopyrrolidines through Intramolecular [2 + 2] Photocycloaddition

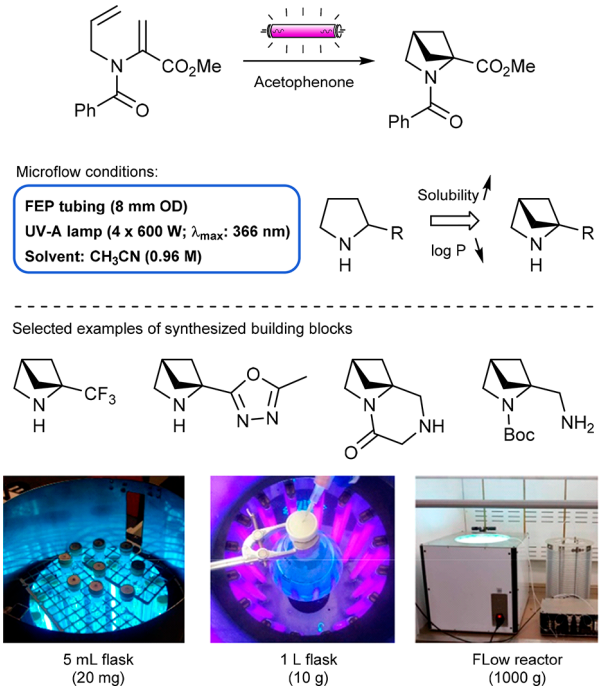

Reprinted with permission from ref 332. Copyright 2018 American Chemical Society.

water and have a lower lipophilicity than pyrrolidines and could, therefore, serve as more water-soluble structural analogues of pyrrolidines. Initial optimization of the photochemical reaction was performed in a 5 mL glass flask irradiated by a UV-A light source (366 nm), followed by reaction in flow on a kilogram scale. The easy scale-up in flow generated sufficient 2,4-methanopyrrolidine material to form a multitude of novel building blocks for medicinal chemistry purposes.

https://doi.org/10.1021/acs.chemrev.1c00332
Chem. Rev. 2022, 122, 2752−2906

Photocycloadditions have the capability to significantly reduce the number of steps required to form complex structures, as compared to traditional chemistry methods. This is shown in the total synthesis of solanoeclepin A (Scheme 16). More specifically, 15 steps were required in the literature method to obtain the tricyclo[5.2.1.0^{1,6}]decane core,[333] whereas only six steps were needed when using a photocycloaddition method in flow as a key step.[334] This crucial photocycloaddition step, starting from the α,β-unsaturated ester, was performed in a flow reactor with FEP tubing (0.5 mm ID, 6.28 mL volume) wrapped around two 365 nm UV-lamps (1.5 h residence time). Once more, the continuous-flow method enabled the generation of sufficient material to support further functionalization studies.

Scheme 16. Intramolecular [2 + 2] Photocycloaddition of a α,β-Unsaturated Ester to Form a Tricyclic Key Intermediate in the Total Synthesis of Solanoeclepin A

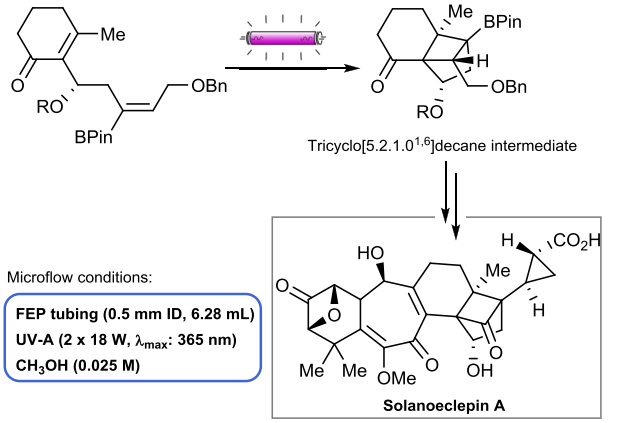

The synthesis of the highly strained dimethyl 1,4-cubanedicarboxylate was achieved using an intramolecular [2 + 2] photocycloaddition in flow as the key synthetic step (Scheme 17).[335,336] The diagonal of the cubane scaffold (2.72 Å) is close to that of benzene (2.79 Å), making cubane an interesting three-dimensional phenyl bioisostere. Additionally, the ester groups on either side of dimethyl 1,4-cubanedicarboxylate allow for convenient functionalization or incorporation into complex molecules. The synthetic pathway toward dimethyl 1,4-cubanedicarboxylate relies on an intramolecular photocycloaddition step. This photocycloaddition was performed by Tsanaktsidis et al. in a pilot-scale glass flow cell (6.4 L volume) equipped with a 2000 W medium-pressure mercury lamp.[336] The solution was recirculated for 7 days to perform the cycloaddition at a 2.7 kg scale and generated the cubane scaffold in 23% overall yield. Later, the photocycloaddition was also applied and scaled up using a diverse set of custom-built flow reactors by Linclau et al.[335] Scale-up was performed by increasing the length of the FEP capillary reactor (0.8 mm ID, 2−18 mL volume), by numbering-up from one to three capillary coils (0.8 mm ID, 54 mL volume) and by increasing the light intensity and wavelength of the UV-B light source (1 × 9 W broadband to 3 × 36 W, λ_{max} = 311 nm). With the improved system a productivity of 3.4 g·h^{-1} was reached for the photocycloaddition and the desired dimethyl 1,4-cubanedicarboxylate was obtained in 54% overall yield (12.8 g).

Scheme 17. Synthesis of Dimethyl 1,4-Cubanedicarboxylate via Intramolecular [2 + 2] Photocycloaddition as Key Step (A) in Glass Flow Cell and (B) in FEP Capillary Reactor

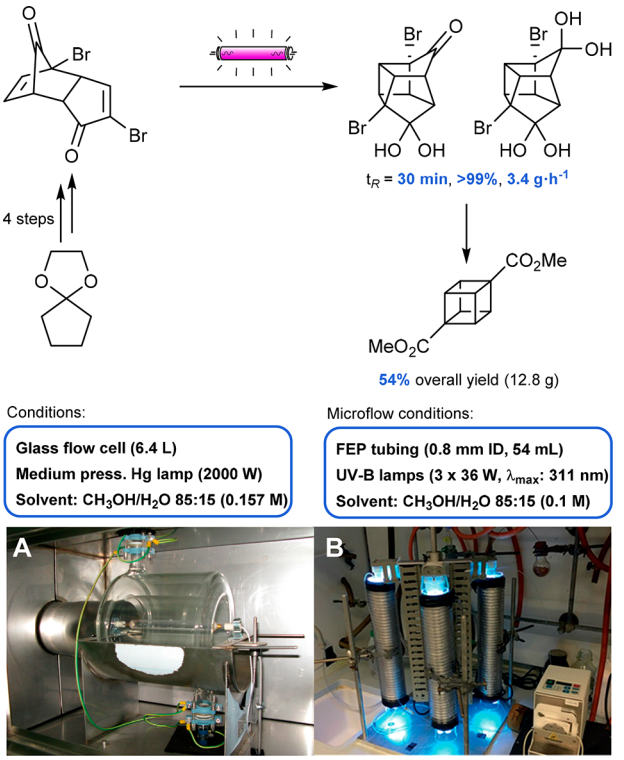

Reprinted with permission from ref 335. Copyright 2021 Georg Thieme Verlag KG.

The photochemical synthesis of 1-aminonorbornanes from aminocyclopropanes was performed via a formal intramolecular [3 + 2] cycloaddition, initiated by homolytic fragmentation of amine radical cation intermediates (Scheme 18).[337] Reactions were initially optimized in a batch, and subsequently, the methodology was straightforwardly translated into a flow protocol with similar yields and significantly shorter reaction time (79% over 12 h in batch and 78% over 6.2 min in flow). Importantly, in the flow reactor the formation of 1-aminonorbornanes could also be performed on a gram scale.

Besides excellent irradiation of the reaction mixture, intermolecular photocycloadditions can also benefit from flow technology due to the associated short diffusion distances resulting in an excellent contacting between the reaction partners. This is especially the case for gas−liquid reactions, such as the intermolecular [2 + 2] photocycloaddition using gaseous reactants, like ethylene gas, to form functionalized cyclobutanes (Scheme 19).[138,222,338]

This transformation was initially carried out in batch by researchers at Merck,[338] but the ineffective irradiation and the biphasic nature of the reaction mixture led to very low productivity. In contrast, switching to a continuous-flow reactor provided the advantage of enhanced gas−liquid mass transfer and more efficient irradiation. An additional advantage of the flow reaction was the higher ethylene concentration that could be obtained in solution by increasing the pressure. Moreover, to improve the reaction outcome, benzophenone was selected as photosensitizer, harnessing photons from the 365 nm LED source and transferring energy to the maleic

https://doi.org/10.1021/acs.chemrev.1c00332
Chem. Rev. 2022, 122, 2752−2906

Scheme 18. Formal [3 + 2] Cycloaddition Toward 1-Aminonorbornanes

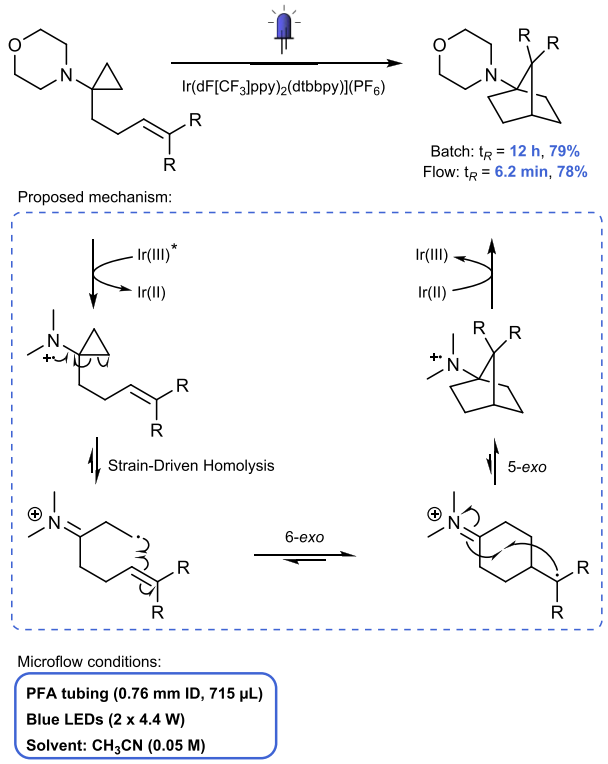

Scheme 19. Biphasic [2 + 2] Photocycloaddition of Ethylene and Maleic Anhydride Analogues

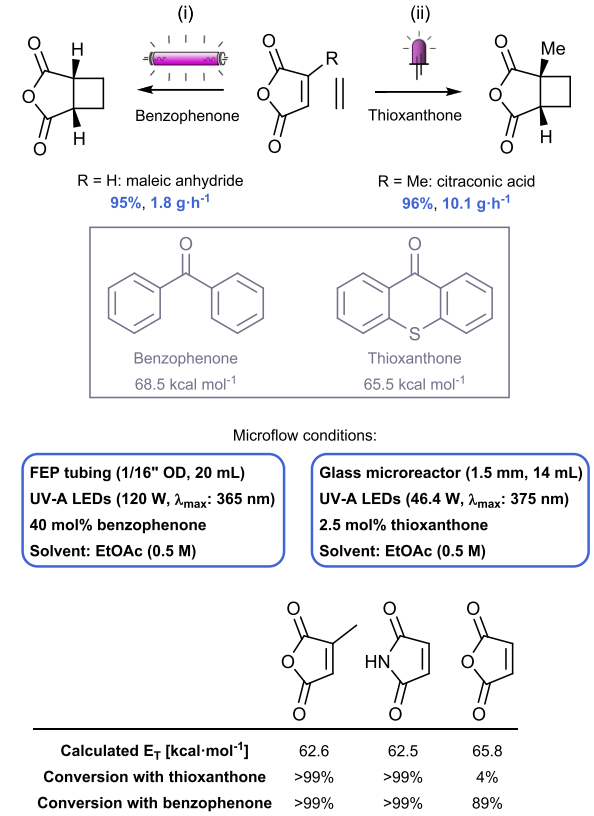

Calculated E_T [kcal·mol^{-1}]	62.6	62.5	65.8
Conversion with thioxanthone	>99%	>99%	4%
Conversion with benzophenone	>99%	>99%	89%

anhydride substrate. This resulted in 95% conversion and a productivity of 1.8 g·h^{-1}.

To further improve this biphasic photochemical reaction, Kappe, Monbaliu, Mateos, and co-workers combined experimental results with computational studies.[222] For the experimental part, a screening of different LED wavelengths and light power in a plate-based photoreactor was performed, while the triplet energy levels (E_T) of various sensitizers and anhydride substrates were calculated using density functional theory (DFT). The results show that matching the triplet energies of substrate and sensitizer, together with the light source emission wavelength, is crucial for achieving high conversions. This example shows that light *quality* is in fact more important than light *quantity*. One example of ineffective matching was given by the photocycloaddition of maleic anhydride (E_T = 65.8 kcal·mol^{-1}) and ethylene with thioxanthone (E_T = 65.5 kcal·mol^{-1}) as photosensitizer (Scheme 19). Instead, a positive example is represented by the reaction between ethylene and the methyl-substituted citraconic acid (E_T = 62.6 kcal·mol^{-1}, space-time-yield of 759 g·L^{-1}·h^{-1}). The cycloaddition of citraconic acid and ethylene with thioxanthone was seamlessly scaled up in a Corning G1 reactor and showed high productivity of >100 g over 10 h reaction time, without the need for reoptimization at larger scale.

Apart from the bimolecular photocycloaddition with ethylene, the photodimerization of maleic anhydride was performed in continuous-flow as well.[339] An additional challenge of this transformation is the risk of reactor clogging due to the insolubility of the cyclobutanetetracarboxylic dianhydride product. This challenge was previously addressed in a quartz glass photoflow reactor by the combination of ultrasonic waves and the addition of a N_2 stream to create a segmented Taylor flow.[202] Using this approach, a further investigation into the influence of various reaction parameters was executed, such as internal diameter of the microcapillary tubing, power input of the light source, gas−liquid ratio and flow rate. Best results were obtained with a 0.5 mm ID capillary, 30 min residence time and 500 W power input of the mercury lamp, resulting in 66% yield of photodimerized product.

The synthesis of truxinic and truxillic acid derivatives via [2 + 2] photodimerization is another transformation that has received considerable attention in recent years.[340−342] For the stereoselective synthesis of ε-diaminotruxillic acid derivatives, Urriolabeitia et al. developed a three-step approach,[340,343] including an ortho-palladation, a [2 + 2] photodimerization, and a hydrogenation step. The photodimerization was performed in a continuous-flow photomicroreactor subjected to low-energy LED irradiation, with a residence time of 5−20 min. This flow method resulted in a much broader substrate scope than previously reported,[344−347] tolerating complete stereoselectivity for the ε-isomer and efficient photocycloaddition (10 examples, 34−41% overall yield).

A one-pot, metal-free method to access 1,3-diaminotruxillic acids was developed by the same group.[341] The flow reactor was irradiated with low power blue LEDs (1 W, 465 nm) and in-line NMR spectroscopy was used to enable quick reaction optimization. A reaction mechanism was proposed, with stepwise formation of two new C−C bonds through a transient diradical singlet intermediate. The ε-isomer was preferentially formed as it has the lowest activation barrier and is thus kinetically favored during the rate limiting C−C bond formation step (Scheme 20). Altogether, the new approach

https://doi.org/10.1021/acs.chemrev.1c00332
Chem. Rev. 2022, 122, 2752−2906

offers more operational convenience and higher overall yield under mild conditions (9 examples, 75−100% yield, 30 min residence time).

Scheme 20. Stereoselective Synthesis of ε-Diaminotruxillic Acid Derivatives by [2 + 2] Photodimerization

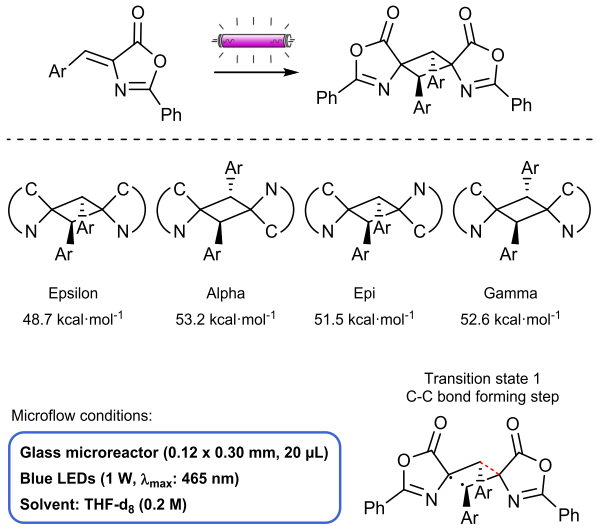

Another example of a [2 + 2] photodimerization toward cyclobutanes in continuous-flow is given by Wang et al., who used a packed-bed reactor filled with heterogeneous carbon nitride photocatalysts (Scheme 21).[348] The catalysts were

Scheme 21. [2 + 2] Photocycloaddition in Packed Bed Reactor with Carbon Nitride Immobilized on Glass Beads

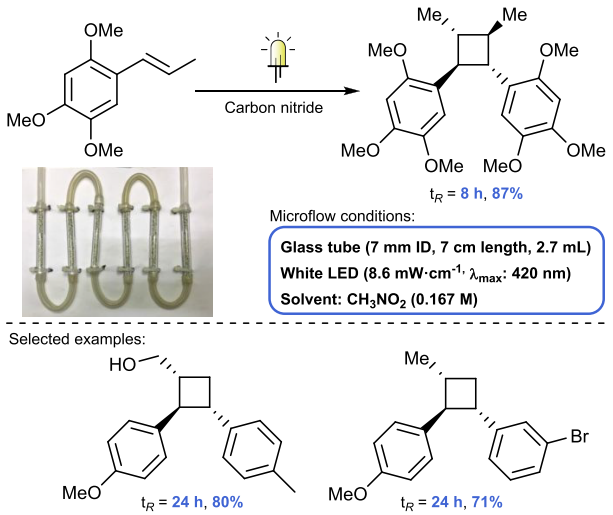

Reprinted from ref 348. Published by Springer Nature.

immobilized on either glass fibers or glass beads to reach a catalyst content of 1−1.2 wt %. The immobilized catalysts were subsequently packed in a glass tube (7 mm ID, 7 cm length, 2.7 mL volume). In these reactors, a solution of α-asarone in CH_3NO_2 (0.167 M, 60 mL) was recirculated over the packed bed for 48 h and irradiated with a white LED light source (8.6 $mW·cm^{-1}$ output power, 420 nm band-pass filter) to reach 81% isolated yield of the photodimerized cyclobutane. By using an alternative photoreactor with six parallel glass tubes, the reaction time could be reduced from 48 to 8 h with slightly improved yield for the desired magnosalin product (87%). Interestingly, with a glass fiber support a decrease in activity was observed over repeated runs, whereas yields remained constant and high over five consecutive runs with carbon nitride immobilized on glass beads. To further test the utility of the developed system, the intermolecular [2 + 2] photocycloaddition of anethole and various styrene derivatives was performed resulting in 49−80% yield for 13 examples.

Booker-Milburn et al. have developed a continuous-flow synthesis of tricyclic aziridines through [2 + 2] photocycloaddition of substituted pyrroles. Notable reactions performed with these aziridines are (i) a mild Tsuji−Trost type ring-opening using carbon-nucleophiles, (ii) a new Pd-catalyzed [3 + 2] cycloaddition of aldehydes and imines, and (iii) a novel method toward tricyclic fused β-lactams.[349] Furthermore, a short, 5-step total synthesis of (±)-3-demethoxyerythratidinone was performed with the formation of the tricyclic aziridines as key step (Scheme 22).[350] The use of flow enabled easy access to sufficient material of these strained photochemical products, which in turn enabled the exploration of their reactivity.

Scheme 22. Functionalization of Photochemically Generated Bicyclic Aziridines

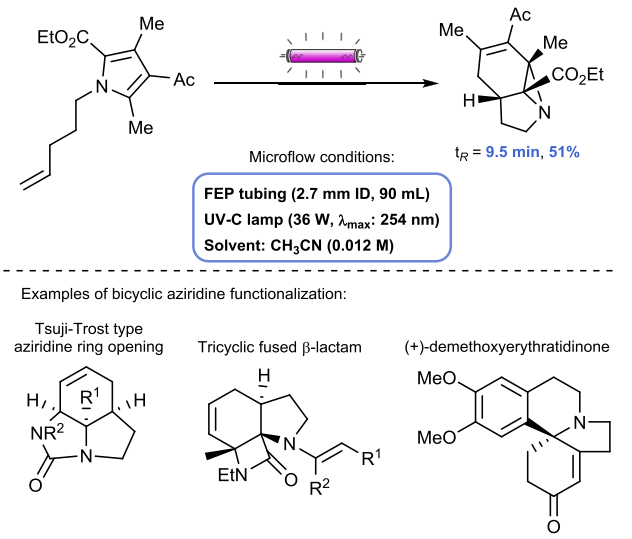

Photocycloadditions were also applied to the synthesis of even more strained compounds than cyclobutanes, such as cyclopropanes and cyclopropenes.[351−353] Substituted cyclopropanes were synthesized from diiodomethylpinacol boronate and styrene derivatives in a continuous-flow reactor (Scheme 23).[351] The photolabile C−I bond is cleaved under UV-A irradiation and the resulting carbene is added to the styrene derivatives. The residence time inside the photoreactor could be decreased from 3 to 1 h through the addition of 5 mol % of xanthone as photosensitizer, while achieving similar yields (76% and 78% yield respectively). When compared to a batch system, unsurprisingly shorter irradiation times and higher yield were observed in flow than in batch (78% after 1 h in flow vs 58% yield after 18 h in batch). For a larger scale flow reaction, two reactors were placed in series and the flow rate was increased to maintain a 1 h residence time. This resulted in a 19% increase in productivity, converting 4 mmol of starting material in 1 h 25 min.

https://doi.org/10.1021/acs.chemrev.1c00332
Chem. Rev. 2022, 122, 2752−2906

Scheme 23. Synthesis of Substituted Cyclopropanes by [2 + 1] Photocycloaddition of Diiodomethylpinacol Borate and Styrene Derivatives

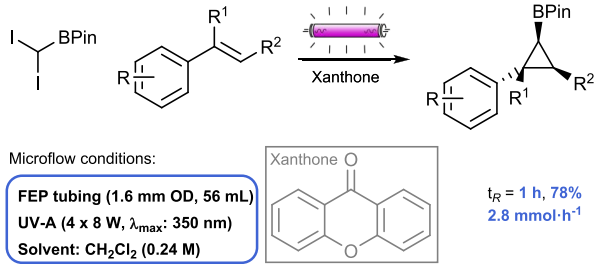

Cyclopropanes and cyclopropenes were also generated by photolysis of aryl diazoacetates and subsequent coupling to alkenes and alkynes, respectively (Scheme 24).[352,353] The

Scheme 24. Cyclopropanes and Cyclopropenes from Diazoacetates by Photolysis and [2 + 1] Photocycloaddition to Alkenes and Alkynes

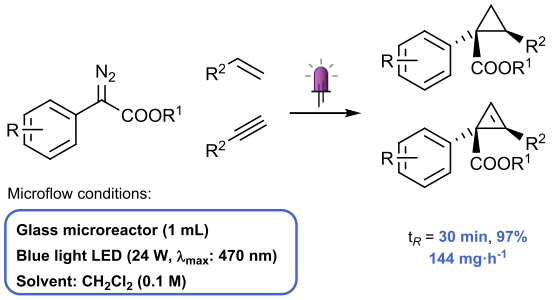

reaction was first performed in a conventional batch reactor, reaching full conversion after 16 h irradiation with blue light LEDs (3 W). Then, the reaction was performed in flow in a glass microreactor and a similar productivity was observed when using the same light source (5 mg·h^{-1} in flow versus 4 mg·h^{-1} in batch). Eventually, to achieve higher productivity, two microreactors were placed in series and were irradiated with 8 LEDs (24 W), which had the desired effect of higher productivity, as now 144 mg of cyclopropene was generated per hour.

An example of how overirradiation issues can be circumvented by the use of continuous-flow technology is provided by the synthesis of rocaglates through intermolecular [3 + 2] photocycloaddition between hydroxyflavones and cinnamates (Scheme 25). Rocaglates are a structural class of molecules found in Aglaia plants that possess a cyclopenta[b]benzofuran core structure. The synthesis goes via an excited-state intramolecular proton transfer (ESIPT)-mediated [3 + 2] photocycloaddition between 3-hydroxyflavones and cinnamate derivatives. When expanding the scope to N-containing rocaglate analogues,[354] the batch method proved to be ineffective, as long reaction times (48 h) were needed and overirradiation resulted in degradation of product. Productivity could be significantly enhanced for the synthesis of both *N*-alkyl and N−H substituted aza-rocaglates by switching to a continuous-flow reactor, with reaction completion after 9 h (46% yield, 89% yield based on recovered starting material).

For scale-up and library building purposes, a higher productivity of a wide range of rocaglates was required. For

Scheme 25. Synthesis of Rocaglates through [3 + 2] Photocycloaddition between Hydroxyflavones and Cinnamates

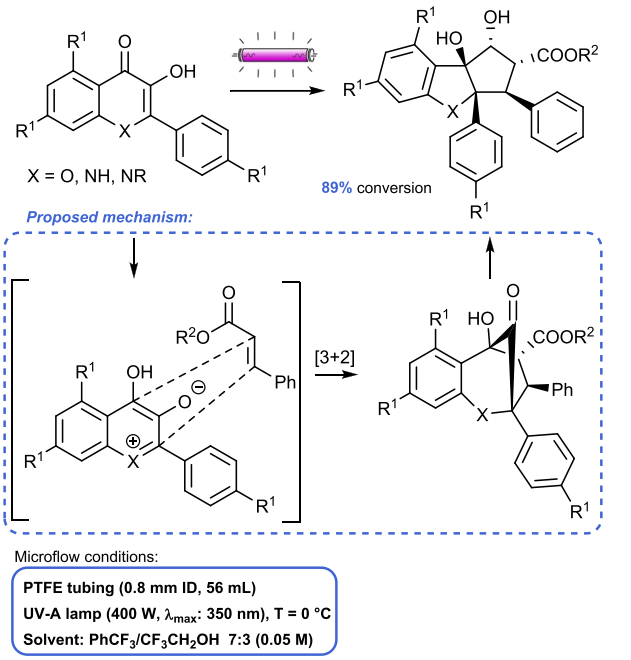

this reason, Porco, Beeler, and co-workers performed the synthesis of these compounds in a numbered-up photoflow reactor setup.[355] Three photoreactors, with metal-halide lamp (λ > 330 nm), glycol cooling chamber, and total internal volume of 37.5 mL, were placed in series. With a total residence time of 35 min, flow rate of 1.07 mL·min^{-1} and 36% isolated yield, this resulted in a throughput of 1.16 g·h^{-1}. Performing the photocycloaddition reaction with a wide range of substituted cinnamate analogues validated the usefulness of the flow system for multigram scale synthesis of various rocaglates. Additionally, the total synthesis of a number of aglain natural products was achieved by performing the photocycloaddition of hydroxyflavones with substituted unsymmetric diphenyl butadienes.[356]

A similar flow reactor was designed to scale up a photoinitiated dehydro-Diels−Alder reactions (PDDA) toward macrocyclic naphthalenophanes (Scheme 26).[357] Batch scale-up required high dilutions of the reaction mixture and under

Scheme 26. Photoinitiated Dehydro-Diels−Alder Reaction Towards Macrocyclic Naphthalenophanes

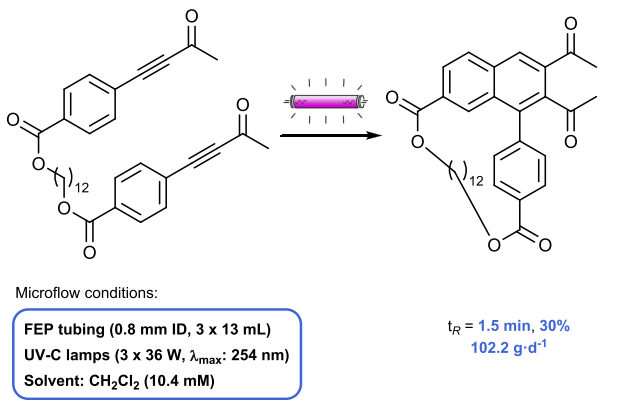

https://doi.org/10.1021/acs.chemrev.1c00332
Chem. Rev. 2022, 122, 2752−2906

these conditions, long irradiation times resulted in substantial photodegradation of the product. To overcome this scale-up limitation, a flow reactor was fabricated with (i) a metal casing, (ii) a reaction and cooling zone, and (iii) an HPLC pump. The reaction zone contains three 36 W UV-lamps (UV-A = 254 nm, UV-B = 310 nm, UV-C = 350 nm), with FEP tubing (0.8 mm ID, 3 × 13 mL volume) coiled around them. Additionally, the tubing is wrapped with aluminum foil to reflect irradiation and coiled with a water-cooling tube to cool the reaction mixture. Different substrate concentrations, flow rates and light sources (UV-A, UV-B, UV-C) were evaluated and a productivity of 102.2 g·day^{-1} was reached. The photoinitiated intramolecular Diels–Alder reaction was also applied by Li and co-workers in the continuous-flow synthesis of naturally occurring arylnaphtalene lignans and their analogs.[358]

Bridged lactones can be synthesized by a formal cycloaddition of cycloalkanols and electron-deficient alkenes (Scheme 27).[359] The protocol benefits from the synergistic

Scheme 27. Bridged Lactones by Formal Cycloaddition of Cycloalkanols and Electron-Deficient Alkenes

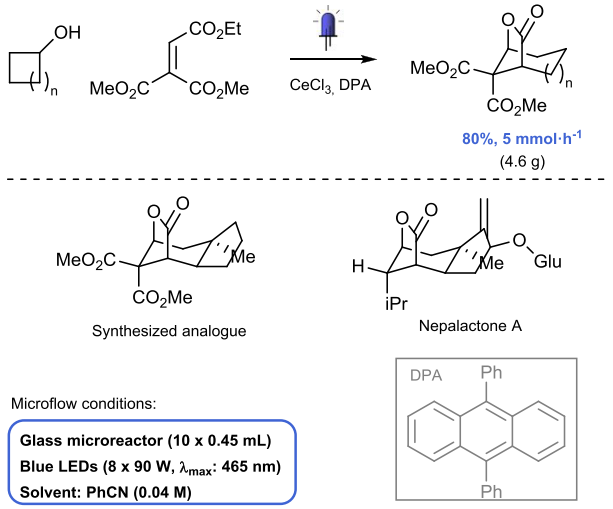

photocatalytic effect of $CeCl_3$ and 9,10-diphenylanthracene (DPA) to harvest low energy blue light and is applicable to a wide range of substrates. One example led to the polycyclic core structure of the natural product nepalactone A, which highlights the synthetic usefulness of the method. The practical aspect of the method was highlighted by performing a 100-fold scale-up of the batch reactions in ten glass microreactors (Corning Low Flow) placed in series. The reaction mixture was pumped through the total internal volume of 4.5 mL and was illuminated with eight 90 W blue LED lamps. At a flow rate of 3 mL·min^{-1}, this resulted in a productivity of 5 mmol·h^{-1}.

A diastereoselective [4 + 2] photocycloaddition was performed in continuous-flow between 2-methylbenzophenone and coumarin or chromone, forming valuable tetracyclic molecules benzoxanthene and naphthochromenone under complete diastereoselective control (Scheme 28).[360−362] The microfluidic photoreactor consisted of PFA tubing (0.75 mm ID, 1.0 mL volume) irradiated by a 365 nm light bulb. With a residence time of 35 min, quantitative yield and complete diastereocontrol was achieved. Interestingly, the photochemical reactions were unsuccessful under batch conditions, as low conversions were observed at short reaction times and high

Scheme 28. Diastereoselective [4 + 2] Photocycloaddition Towards Benzoxanthene and Naphthochromenone

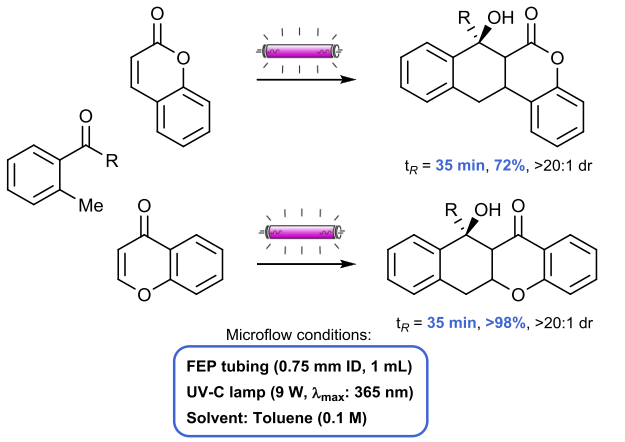

amounts of unidentifiable side products were formed at longer reaction times. Altogether, these results indicate how the use of microflow technology was indispensable for the successful execution of these transformations.

Heterocycles play a central role in organic synthesis and are used in medicinal chemistry to tune pharmacokinetic and pharmacodynamic properties of drug candidates.[363] An efficient method for the synthesis of heterocycles is thus highly valuable. The high atom economy and one-step heterocycle generation of the Paterno–Büchi reaction makes this photocycloaddition an ideal strategy for this purpose. The Paterno–Büchi reaction has also been used to study the effect of a segmented Taylor flow in continuous-flow reactors.[364,365]

The Paterno–Büchi [2 + 2] photocycloaddition between an enol ether and benzaldehyde delivered an oxetane precursor of the cytotoxic lactone (+)-Goniofufurone (Scheme 29).[366] The

Scheme 29. Paterno–Büchi [2 + 2] Photocycloaddition in the Total Synthesis of (+)-Goniofufurone

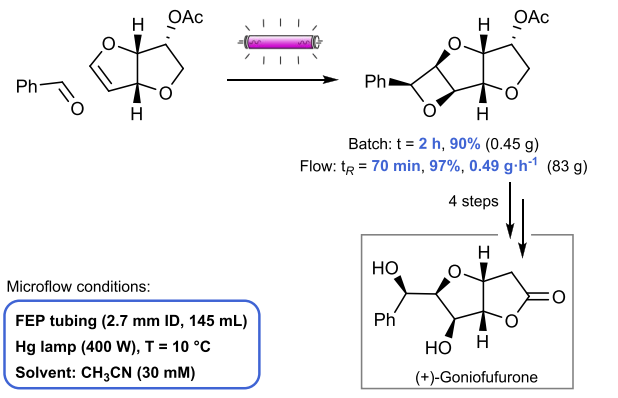

initial batch protocol delivered a high yield (93%); however, in batch, extended irradiation times and high dilutions were required, complicating its scale-up. Therefore, for larger scale, the Paterno–Büchi reaction was performed in a three-layer FEP flow reactor irradiated with a 400 W lamp, generating 41 g of the photocyclized product in a single 83 h run (97% yield).

The synthesis of 1,3,4-oxadiazoles was performed with a photochemical Huisgen reaction in continuous-flow (Scheme 30).[367] To perform the reaction 5-phenyl-1*H*-tetrazole and a

https://doi.org/10.1021/acs.chemrev.1c00332
Chem. Rev. 2022, 122, 2752−2906

Scheme 30. Photochemical Synthesis of 1,3,4-Oxadiazoles from 5-Substituted Tetrazoles and Carboxylic Acids in Continuous Flow

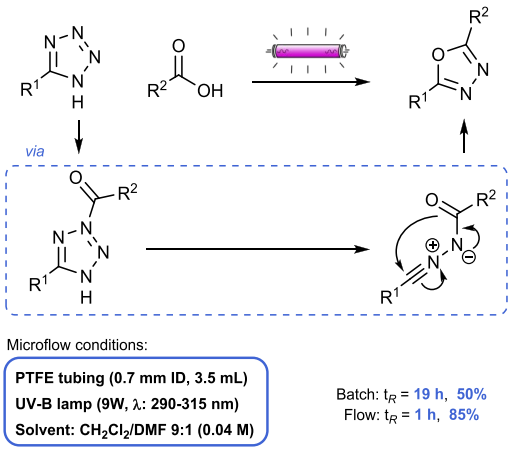

carboxylic acid were combined in a PTFE reactor (0.7 mm ID, 3.5 mL volume), and the resulting *N*-acyl tetrazole is activated under irradiation with a UV-B lamp (9 W, 290−315 nm) to form the nitrile imine intermediate. This intermediate subsequently collapses via 1,5-dipolar electrocyclization to the desired 1,3,4-oxadiazole with 85% yield in 1 h residence time. A wide substrate scope was performed for both reaction partners, exemplifying the robustness of the developed process.

Benzo-fused seven-membered ring sultam is another example of a heterocyclic ring system that was photochemically synthesized in batch and in flow (Scheme 31).[368] In contrast to the multistep methods found in literature to access these

Scheme 31. Seven-Membered Ring Benzosultams through Photocycloaddition

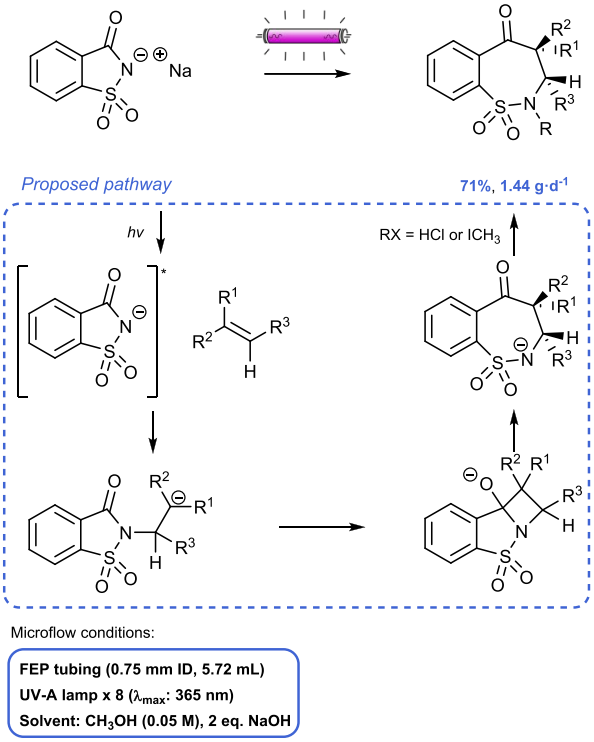

scaffolds, either via a radical cyclization using tributyltin hydride[369] or via a Pd(0)-catalyzed Heck cyclization followed by ozonolysis,[370] photochemistry allows to reduce the synthesis to one step. In flow, the reaction mixture with saccharin sodium salt and 2 equiv of alkene was continuously irradiated (300 nm), resulting in an isolated yield of 71% and a productivity of 1.44 g·day^{-1}. In comparison to batch, the versatility of the flow transformation is broader as light-absorbing olefins with aromatic substituents were well tolerated, with faster reaction times and improved scalability. A computational study revealed that upon irradiation the saccharin anion is promoted to its singlet excited state, after which the nitrogen atom performs a regioselective nucleophilic attack on the terminal carbon of the alkene. It is suggested that an anionic intermediate is generated, that collapses to the azetidine [2 + 2] cycloaddition product and subsequently undergoes ring expansion to form the targeted benzosultam.

Finally, 1,3-diazabicyclo[3.1.0]hexanes were synthesized through a visible-light driven photocascade reaction, involving photosensitization, photoredox catalysis, and [3 + 2] photocycloaddition steps (Scheme 32).[371,372] Through this photo-

Scheme 32. Photocascade with [3 + 2] Cycloaddition to Form 1,3-Diazabicyclo[3.1.0]hexanes: (A) Fused *β*-carbolines and (B) Bicyclic Aziridines

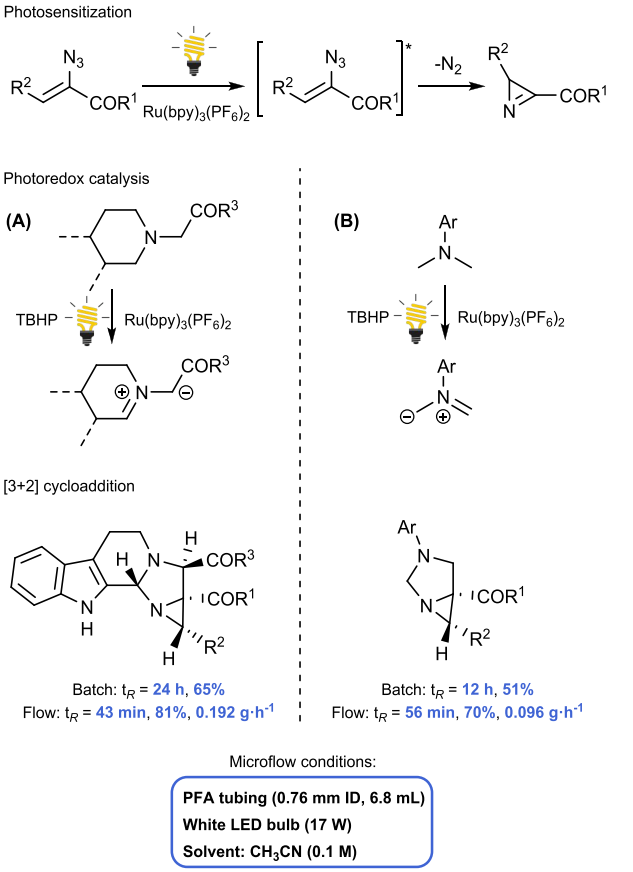

cascade, various *β*-carbolines and *α*-keto vinyl azides could be coupled (18 examples), in which one new C−C bond and two new C−N bonds were formed to generate fused *β*-carbolines (Scheme 32A).[371] Similarly, bicyclic aziridines (20 examples) were formed by coupling *N*,*N*-dimethylanilines and *α*-azidochalcones through the same photocascade sequence

https://doi.org/10.1021/acs.chemrev.1c00332
Chem. Rev. 2022, 122, 2752−2906

Scheme 33. *E*−*Z* Isomerization to Yield *trans*-Cyclooctenes and In-Line Complexation with Ag^+

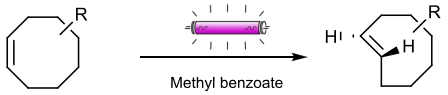

Conditions	Fox *et al.* (2008)	Bormans, Hessel, Noël *et al.* (2016)	Rutjes *et al.* (2018)	Mikula *et al.* (2016)
Reactor	Round bottom flask	FEP tubing	FEP tubing	Quartz glass tube
Dimensions		0.5 mm ID, 1 mL	2.7 mm ID, 105 mL	16 mm ID, 0.79 m length, 159 mL
Light source	Low press. Hg lamp	Low press. UV lamp	UV-C LED	Low press. Hg lamp
Light output	8 x 35 W, λ_{max}: 254 nm	10 W, λ_{max}: 254 nm	55 W, λ_{max}: 254 nm	2 x 55 W, λ_{max}: 254 nm
Solvent	1:1 Et_2O / n-hexane (15 mM)	3:7 Et_2O / n-hexane (20 mM)	n-heptane (150 mM)	1:1 Et_2O / n-hexane (5-20 mM)
	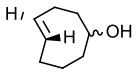	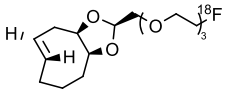	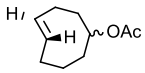	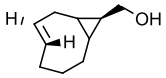
	71% 3.9 g	76% 46 mg	79% 1.9 g	79% 1.19 g

(Scheme 32B).[372] In both cases, increased yields and shortened reaction times were reported in flow compared to batch.

5.2. Photoisomerizations

The absorption of light can provide the energy required for organic substrates to isomerize.[373,374] This can be applied in organic synthesis to transform a compound into its geometrical or structural isomer. Because of the simple mass balance of photoisomerizations, these reactions are often used to validate novel microreactor designs,[375] or to perform reactor characterization experiments, such as visible light actinometry.[376,377]

5.2.1. *E*−*Z* Isomerization. The *E*−*Z* isomerization to form *trans*-cyclooctenes (TCOs) has received increased attention in recent years. The reason for this is the ability of TCOs to undergo quick inverse electron-demand Diels−Alder (IEDDA) type cycloadditions with tetrazines under highly diluted reaction conditions, making them interesting targets for biorthogonal chemistry studies.[378] The most common method for accessing TCOs is by performing a sensitized *E*-to-*Z* photoisomerization under UV light irradiation (Scheme 33).[379] At equilibrium, the trans isomer is the minor product (10−23%), necessitating an efficient setup for achieving high yields.[380]

Such an efficient setup was proposed by Fox et al. (Figure 59).[381,382] In a closed-loop photoreactor, the reaction mixture was recirculated and in-flow separation was achieved through the selective complexation of the desired trans isomer with Ag^+ in packed beds containing $AgNO_3$-impregnated silica gel. The cis isomer was not retained and could be recycled to the photoreactor until all substrate was converted to *trans*-cyclooctene. After reaction, the *trans*-isomer was eluted from the bed by directing a NH_4OH solution over it. The *trans*-isomer could be isolated in 52% to 77% yield.

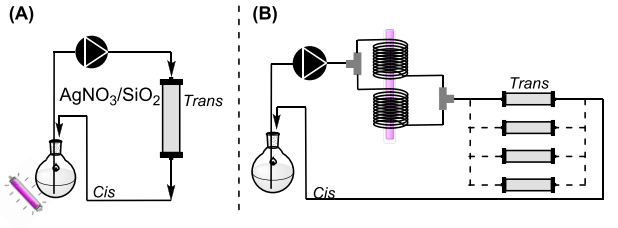

Figure 59. Photoreactor setup for the isomerization toward trans-cyclooctenes with in-line complexation on a Ag^+ packed bed: (A) with a round-bottom flask and (B) with FEP capillary coils and multiple packed beds to enable continuous operation.

The reactor setup was further improved by Bormans, Hessel, Noël et al. to not only benefit from in-flow separation but also from the more efficient irradiation under microflow conditions.[383] The trans-for-cis photoisomerization step was performed in two microflow reactors placed in parallel and saturation of the packed beds was avoided by switching between beds (after 30−90 min), allowing the process to be run continuously. The two-step photoisomerization and adsorption process was later optimized through a combined experimental and theoretical effort,[384] resulting in 90% trans-for-cis conversion after 3 h recirculation time. Using this method, new TCO derivatives with ^{18}F-labeled polyethylene glycol chains were synthesized for pretargeting PET imaging studies.

Other continuous-flow setups for the trans-for-cis photoisomerization of cyclooctenes consisted of a long quartz glass tube (16 mm ID, 790 mm length, 165 mL internal volume) irradiated by two 55 W low-pressure mercury lamps[385] or contained a L−L extraction unit instead of a packed bed for retention of the *trans*-cyclooctene product.[386] Also, Fox et al. expanded their scope to form $AgNO_3$ complexes of the much more labile *trans*-cycloheptenes and *sila-trans*-cycloheptenes in a low-temperature flow photoreactor.[387]

The *E*−*Z* photoisomerization of 2-aminophenyl-enones was performed in a continuous-flow reactor.[388] With subsequent cyclocondensation between the *Z*-enone and the free amine group, the formation of substituted quinolines was achieved (Scheme 34). When comparing light sources, the UV-C LED (365 nm, 75 W) allowed for higher yields and productivity than the medium-pressure mercury lamp (110 W). Importantly, the productivity in flow (9.5 mmol·h^{-1}) was a 100-fold increase compared to a reported batch method (0.09 mmol·h^{-1}).[389] Additionally, the tandem isomerization-cyclocondensation reaction was combined with a continuous-flow hydrogenation step to form substituted tetrahydroquinolines in a telescoped flow process. This way, the synthesis of the antimalarial galipinine was performed in 72% overall yield.

The *E*−*Z* isomerization of 3-benzylidene-2-ones was performed in a microfluidic photoreactor, both with an

https://doi.org/10.1021/acs.chemrev.1c00332
Chem. Rev. 2022, 122, 2752−2906

Scheme 34. Synthesis of Quinolines through *E*−*Z* Isomerization of 2-Aminophenyl-enones and Subsequent Cyclocondensation

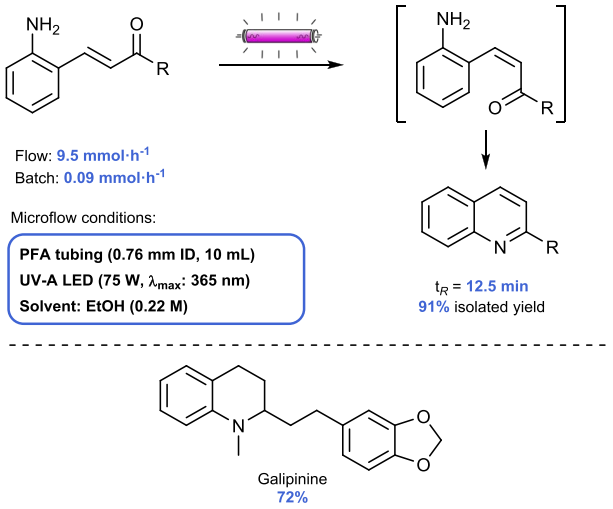

artificial light source and with solar irradiation (Scheme 35).[390] For optimization, the influence of solvent, residence time, light

Scheme 35. Solar Sensitized *E*−*Z* Isomerization of 3-Benzylidene-2-ones with Inline Extraction

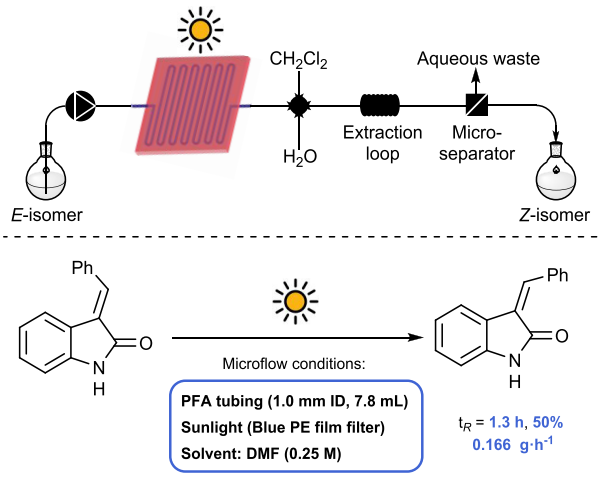

source and temperature were investigated on a milligram scale. DMF was chosen as solvent and best results (76% LC-MS yield, 71% isolated yield) were obtained when irradiating the reaction mixture for 15.7 min with a medium-pressure mercury lamp (250 W) at 10 °C. Longer residence times did not result in higher yield (76% in 157 min). To facilitate workup, an in-line extraction was performed by dropwise adding CH_2Cl_2 and water into the product stream, which was then efficiently separated with a L−L microseparator. Finally, after completing the optimization and validating the methodology for a number of 3-benzylidene-2-one derivatives, the reaction was performed under solar irradiation with a self-fabricated solar panel microreactor. In this solar reactor, an isolated yield of 50% was achieved, with a productivity of 0.166 $g \cdot h^{-1}$.

A photochemical microchip reactor was used in combination with an ion mobility spectrometer for the quick catalyst screening of a photocatalyzed *E*−*Z* isomerization.[391] The microchip with a total internal volume of 560 nL (20 μm depth, 100 μm width) was irradiated by a 404 nm LED light for the photocatalyzed *E*−*Z* isomerization of an ethyl-cinnamate derivative (Scheme 36). The applied flow photo-

Scheme 36. Rapid Catalyst Screening for the *E*−*Z* Isomerization of Ethyl Cinnamate Derivatives with an Ion Mobility Spectrometer

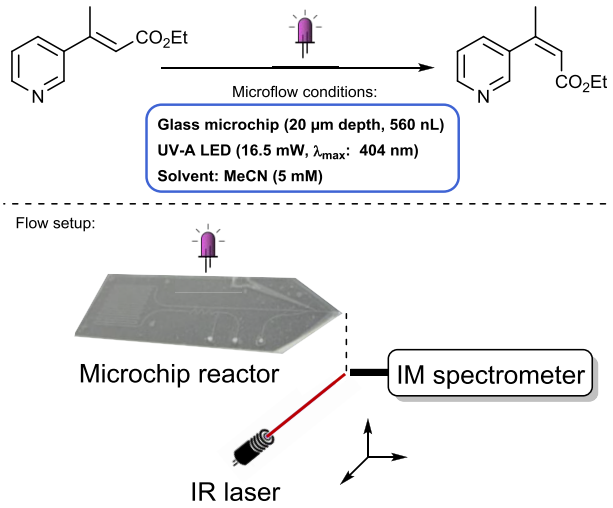

chemical setup allowed for two major advantages compared to standard batch setups: first, the real-time analysis and short irradiation times needed for the reaction allowed for the identification of the best catalysts in only minutes. Second, because of the extremely small dimensions of the reactor, only very small amounts of catalyst (2 nmol) were required per test, significantly reducing costs.

5.2.2. Rearrangements. Apart from geometrical isomerizations (i.e., converting cis to trans isomers or vice versa), several photochemical rearrangements have recently been performed in flow leading to the formation of structural isomers.

One example is given by the radical Smiles rearrangement of 2-aryl-oxybenzoic acids to aryl salicates (Scheme 37).[392] The reaction was performed in batch and in flow with Mes-Acr$^+$ as photocatalyst. To increase the scale of the reaction, a continuous-flow reactor was employed resulting in similar yields as in batch, but with improved productivities (0.010 $mmol \cdot h^{-1}$ in batch, versus 0.172 $mmol \cdot h^{-1}$ in flow). This increase in productivity from batch to flow was attributed to

Scheme 37. Photochemical Smiles Rearrangement of Aryl-oxybenzoic Acids to Aryl Salicates

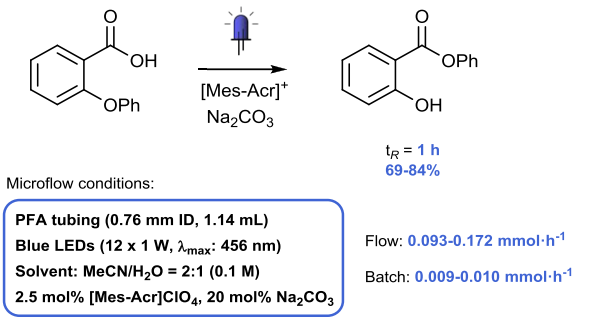

https://doi.org/10.1021/acs.chemrev.1c00332
Chem. Rev. 2022, 122, 2752−2906

the more efficient light irradiation in the microcapillary compared to batch.

Also the photo-Fries rearrangement of aryl benzoates was performed in batch and in continuous-flow.[393,394] The mechanism of the photo-Fries rearrangement involves the generation of a singlet radical pair by homolytic cleavage of the ArO−COR ester bond after photoexcitation. Depending on the mobility of the singlet radicals, these can either rearrange to form *ortho*- or *para*-hydroxyaryl phenone, or the phenoxy radical can escape from the solvent cage to form phenol (Scheme 38). Thus, the selectivity of the photorearrangement can be tuned by limiting the mobility of the singlet radical pair.

Scheme 38. Photo-Fries Rearrangement of Aryl Benzoates to Hydroxybenzophenone

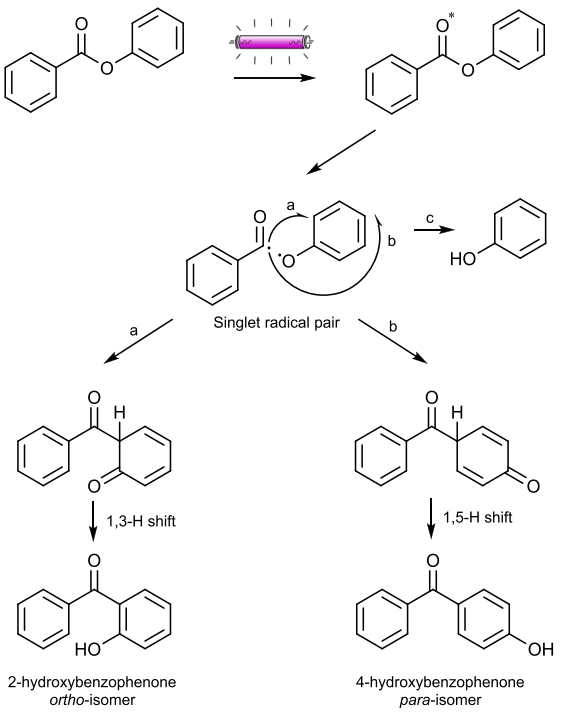

Solvent	Viscosity (Pa·s)	Mode	t_R (min)	Ratio *o*-/*p*-	Conversion
Methanol	5.9 x 10^{-4}	Batch	40	2.2	92%
		Flow	5	1.68	100%
		Flow	11.13	1.51	100%
Ethylene glycol	1.6 x 10^{-2}	Batch	180	6.28	100%
		Flow	10	2.72	100%
		Flow	42.6	12.4	100%

Microflow conditions Kalkurni:
Quartz coil (3 mm ID, 2.5 m, 50 mL)
Medium press. Hg (450 W)
Solvent: Ethylene glycol (10 mM)

Microflow conditions Wu:
FEP tubing (1.0 mm ID, 4.71 mL)
UV-C light (8 W)
Solvent: CH_3CN (5 mM), 0.1 M CTAB

One method for limiting the radical mobility is the use of a viscous solvent, as the radical pair is restrained in its position by a solvent cage.[393] In batch, a 4-fold increase in ortho/para isomer ratio was achieved when moving from methanol to the more viscous ethylene glycol as solvent. Additionally, in flow the isomeric ratio was further increased to 12.4:1 ortho/para ratio by increasing the irradiation time. Apart from the improved ortho-selectivity, the flow reactor offered the advantage of better temperature control, more homogeneous irradiation and shorter reaction times compared to batch (5 min in flow vs 40 min in batch).

Another method for reducing the radical pair mobility is the application of aqueous micellar reaction conditions.[394] Different surfactants were compared, and best results were obtained with CTAB (cetyl trimethylammonium bromide). Interestingly, in this study the addition of surfactant had a more significant effect on the amount of phenol formed than changing the solvent viscosity.

The photo-Fries rearrangement of dihydropyrido[1,2a]-indolone was also combined with the capture of the resulting imine in continuous-flow for the preparation of several monoterpene indole alkaloids.[395] The synthetic utility of the protocol was shown by the first total synthesis of (+)-alsmaphorazine C and formal synthesis of (+)-strictamine.

Cyclobutene lactones are interesting building blocks in synthetic chemistry as they offer access to differently functionalized cyclobutanes and cyclobutenes. The batch photochemical rearrangement to these cyclobutene lactones starting from 2-pyrone[396] was translated into a photo flow method by Kappe, Maulide, and co-workers (Scheme 39A).[397]

Scheme 39. Photorearrangement of 2-Pyrone Analogues to Bicyclic Cyclobutene Lactones

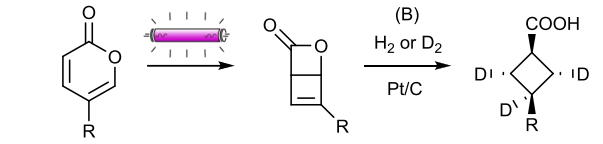

(A) R = H — 95% conversion, 0.114 g·h^{-1}
(B) R = CO_2Me, CO_2t-Bu — 86% conversion, 0.36 g·h^{-1}

Microflow conditions:
FEP tubing (0.75 mm ID, 10 mL)
High press. Hg lamp (400 or 450 W)
Solvent: CH_3CN (0.05-0.1 M)

Compared to batch, the flow reaction resulted in reduced reaction times (from 24 h to 10 min) and a significantly higher throughput (from 14 to 21 to 144 mg·h^{-1}). Reactor fouling on the PFA tubing resulted in a decrease in productivity over time. However, this loss in productivity could be minimized by performing the reaction at 10 °C instead of 50 °C and to some extent by decreasing the concentration from 50 mM to 25 mM.

Similarly, for the synthesis of 1,3-cyclobutanedicarboxylates, alkyl coumalates were subjected to photoisomerization and subsequent hydrogenation in a photo flow system (Scheme 39B).[398] For the photoisomerization, a Pyrex immersion-well with a high-pressure mercury lamp (400 or 450 W) was used to irradiate a FEP capillary. While in batch high dilutions and long irradiation times were typically needed, resulting in low productivity;[399] instead, scale-up of the reaction in flow could be performed with minimal byproduct formation and significant productivity (360 mg·h^{-1} with 10 min residence time). By performing the hydrogenation step with deuterium gas, a high degree of deuteration could be achieved, making the method useful for the preparation of internal standards for drug candidate molecules in pharmacokinetic studies.[400]

Using the same photoisomerization reaction, 1,2-azaborines were converted into their Dewar isomers, which were then

https://doi.org/10.1021/acs.chemrev.1c00332
Chem. Rev. 2022, 122, 2752−2906

further used as 4C + 1N + 1B synthons for organic synthesis.[401,402] More specifically, the 1,2-azaborine isomer was converted into 1,2-disubstituted cyclobutanes with vicinal boron and nitrogen containing substituents. By manipulating the boron unit, differently functionalized *cis*-aminocyclobutanes could then be prepared (Scheme 40). It was reasoned

Scheme 40. Photoisomerization of 1,2-Azaborines to Form B,N-Substituted Cyclobutanes

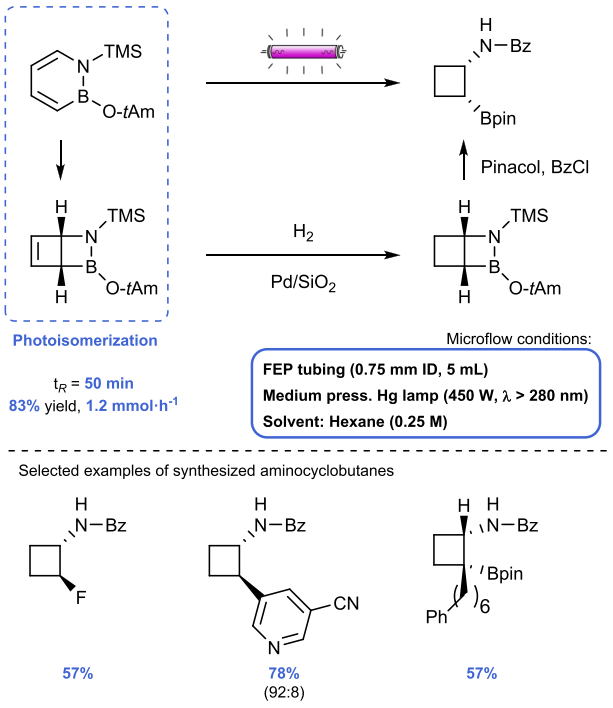

that a continuous-flow protocol was better suited for scale-up of the photoisomerization, as the product was known to undergo photodegradation after prolonged irradiation.[401] Therefore, a continuous-flow reactor was fabricated consisting of an FEP capillary coiled around a medium-pressure mercury lamp. The residence time inside the photoreactor and the substrate concentration were balanced to achieve both high productivity (1.2 mmol·h^{-1}) and high yield (83% isolated yield). The product of this regio- and diastereoselective photoisomerization was successfully derivatized to produce functionalized aminocyclobutanes.

A photoinduced Beckmann rearrangement to convert ketoximes to secondary amides was performed in a two-step sequential flow process, with a Vilsmeier–Haack reagent being formed by photoredox catalysis in a first reactor and a thermal Beckmann rearrangement taking place in the second reactor (Scheme 41).[403] By separating the photoredox and the thermal process, optimal reaction conditions can be selected for each, maximizing the overall reaction outcome. In the first reactor, a solution of CBr_4 and photocatalyst in DMF were irradiated with blue or green light at 0 °C to produce the Vilsmeier–Haack reagent. The reaction mixture was subsequently merged in a T-mixer with a solution of the oxime substrate and was allowed to react to the amide product at 40 °C in the second reactor, affording 95% HPLC yield after 110 min total residence time. A one-pot photochemical Beckmann rearrangement was performed as well, in which the effect of varying temperature was investigated. At low temperatures, the

Scheme 41. Two-Step Beckmann Rearrangement of Ketoximes to Secondary Amides in a Photochemical and Thermal Flow Reactor

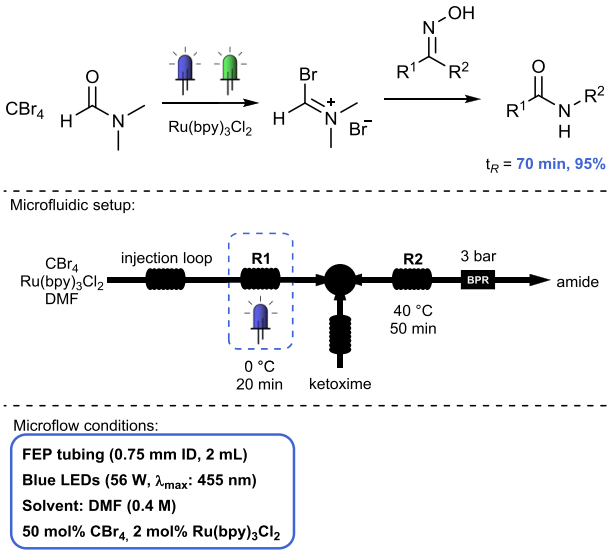

reaction rate of the Beckmann rearrangement was significantly reduced. When the reaction was performed at 40 °C under light irradiation, significant side-product formation was observed. These results indicate the beneficial effect of separating the photochemical and the thermal step, which is easily achieved in flow.

The Schmidt or Beckmann rearrangements are useful methods for generating ring-expanded lactams from cyclic ketones. To induce chirality, however, these methods offer insufficient directional control. A two-step enantioselective variant to produce chiral lactams from prochiral ketones was developed by Lattes and Aubé,[404,405] in which a prochiral ketone is first converted into a chiral oxaziridine and subsequently photochemically converted to a chiral lactam (Scheme 42A). This photochemical Lattes–Aubé reaction of chiral oxaziridines to chiral lactams was performed in continuous-flow by irradiating an oxaziridine solution with a medium-pressure mercury lamp as light source.[406] Significantly higher reaction rates were observed when using the full UV spectrum of the lamp, than when a Vycor filter was used (~220 nm UV cutoff). Compared to the batch method,[405] the reaction time could be significantly reduced from several hours to 30 min in flow. Furthermore, the practical use of the flow method was demonstrated by performing the reaction on a 20 g scale, achieving >80% yield for the desired lactam, and by expanding the scope of the reaction to a bicyclic ring system.

The oxaziridine rearrangement to chiral lactams was later also used to generate chiral bicyclic homopiperazines (Scheme 42B).[407] In a first attempt, a nonphotochemical method involving a Schmidt rearrangement to the chiral lactams was employed, but productivity and enantioselectivity to the desired lactam were limited. Instead, more successful was the photochemical Lattes–Aubé reaction in a parallel tube reactor. This flow reactor was constructed by threading PFA tubing through the batch photochemical reactor, containing a 4 W UV-C light bulb. During the flow reaction precipitation issues were encountered, but these were solved by lowering the reactant concentration and increasing the flow rate. Next, the reactor was run for 42 h without interruption. Additionally, the

https://doi.org/10.1021/acs.chemrev.1c00332
Chem. Rev. 2022, 122, 2752–2906

Scheme 42. Lattes–Aubé Reaction of Chiral Oxaziridines to Chiral Lactams and Further Derivatization

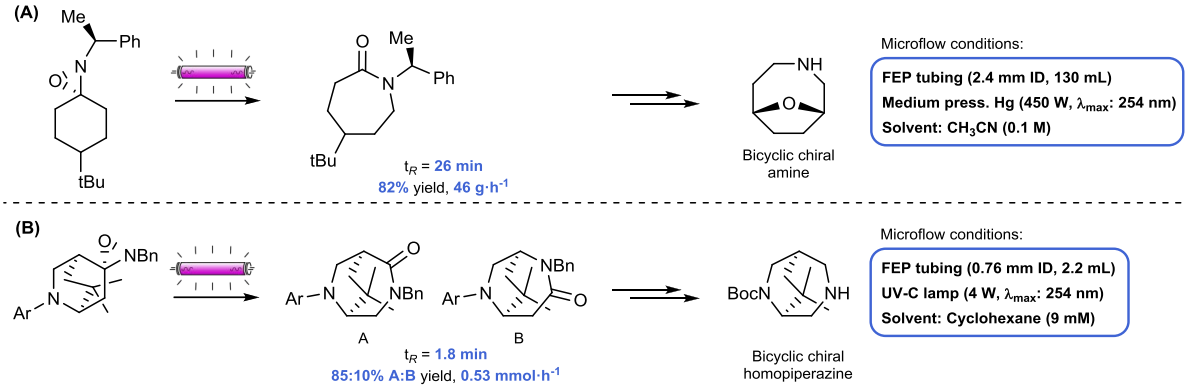

productivity was increased to 0.53 mmol·h^{-1} by doubling the length of the exposed tubing (32 tubes in parallel, V = 2178 μL, 4.80 m irradiation length) and further increasing the flow rate to 1.20 mL·min^{-1}.

Isoxazoles can be directly converted into oxazoles, either by a thermal pathway[408] or by a photochemical one.[409,410] The general applicability of these methods is limited, as the thermal process requires a phenolic moiety and the reported photochemical processes in batch require long reaction times and suffer from photodegradation.

Bracken and Baumann performed the photoisomerization of various isoxazoles to their oxazole structural isomer in a microflow reactor (Scheme 43).[411] This way, the reaction rate

Scheme 43. Isoxazole to Oxazole Rearrangement in Continuous Flow

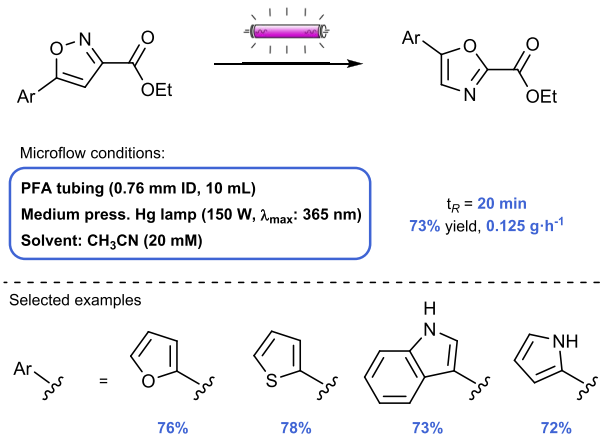

was significantly enhanced, as only 20 min residence time was required to achieve conversions of 90% and higher, compared to 4–8 h for reported batch methods. For the aryl-substituted isoxazoles, higher yields were generally obtained with electron-rich substrates than with electron-poor ones under the same conditions. This was explained by the better overlap of absorption maximum of the electron-rich substrates (λ_{max} > 300 nm) with the emission spectrum of the medium-pressure mercury lamp. Additionally, heteroaryl-substituted isoxazoles, like furans, thiophenes, indoles, and pyrroles, were well tolerated, and no N atom protecting groups were required. The system proved to be robust and scalable as 1.5 g of oxazole product was generated in 12 h operation time.

Apart from the interconversion of isoxazoles to oxazoles, other N,O-containing heterocycles were also generated in an efficient photoisomerization method. More specifically, quinoline scaffolds were converted into their ring-expanded benzo[1,3] oxazepines, with first batch oxidation and C–H functionalization to 2-aryl quinoline *N*-oxide, followed by flow photoisomerization (Scheme 44).[412] The flow reactor

Scheme 44. Ring-Expansion of Quinoline Scaffolds to Benzo[1,3]oxazepanes

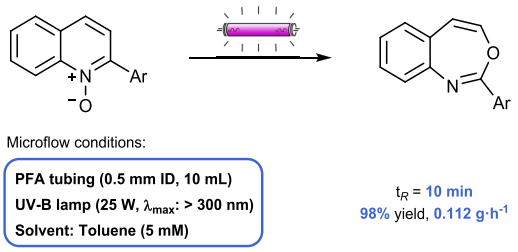

consisted of FEP tubing irradiated by a 25 W Exo Terra UVB200 lamp. The use of this light source was found particularly suitable for the transformation, as the quinoline *N*-oxide absorption spectrum (λ_{max} = 346 nm) showed good overlap with the broad emission band of the lamp (λ_{max} = 335 nm). In the flow reactor this resulted in near quantitative yield (98%) of the benzo[1,3]oxazepane product in just 10 min residence time, which is a significant improvement compared to the batch method in terms of reaction time and side product formation (73% yield, 18 h).

Similarly, a dearomative ring-expansion of *N*-ylides under blue LED irradiation led to the formation of 7-membered ring azepines (Scheme 45).[413] In the presence of a base, the aromatic *N*-ylide is generated from its quaternary aromatic salt, which upon irradiation rearranges to the azepine. The flow reactions were performed in a self-assembled reactor, consisting of an FEP capillary (1/16 in. or 1.59 mm OD, 4.75 mL volume) coiled around a glass beaker (7.6 cm OD), which was placed over a hexagonal bar with 24 × 5 W blue LEDs. Optimal results were obtained with 5 equiv of base and 2 h residence time, leading to 91% ^{1}H NMR yield for the model substrate. Under similar conditions in batch, only 46% ^{1}H NMR yield was obtained. With the optimized conditions, a range of pyridinium salts were successfully photorearranged in the flow reactor, including pyridines, isoquinolines, quinoline and phenanthridinine (23 examples). A combined thermal and

https://doi.org/10.1021/acs.chemrev.1c00332
Chem. Rev. 2022, 122, 2752–2906

Scheme 45. Photorearrangement of *N*-Ylides to Their Ring-Expanded Azepines

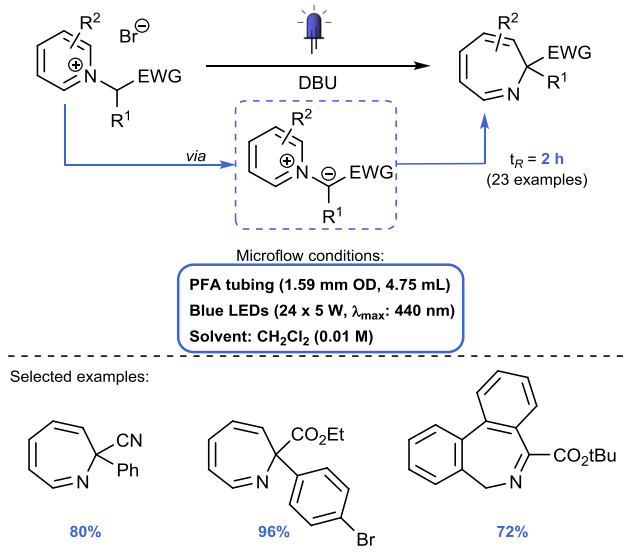

photochemical ring expansion method of 6- to 8-membered nitrogen heterocycles was also developed by Harrowven et al. through [1,3]-sigmatropic rearrangement in continuous-flow.[414]

The classical photorearrangement of dienones involve 1,2-addition, 1,4-addition, and dipolar cycloaddition. A nonclassical rearrangement of dienones and the natural product Santonin, mediated by amines, was performed in a photochemical flow reactor (Scheme 46).[415] This compact flow reactor consisted of 0.8 mL of PFA tubing coiled in a concentric circle, which was irradiated by an array of 365 nm LEDs. The efficient irradiation of the reaction mixture (30 W over 20 cm^2) allowed for short reaction times (8 min) for the nonclassical dienone rearrangements.

Interestingly, a different reaction outcome was observed, depending on the solvent used. When irradiating a dichloromethane solution of the dienone substrate in the presence of benzylamine, the main product was a ring-opened product (72% ^{1}H NMR yield), with complete cis-selectivity (Scheme 46A). On the other hand, with the same protocol but dimethoxyethane as solvent, the main product was a cyclobutene-containing amide (Scheme 46B). Both reactions could be performed with dienone and a range of amines in similar yields (52−82% ^{1}H NMR yield). Additionally, Santonin was photorearranged in the presence of methylamine to form two previously unknown structures.

[6,6]-Phenyl-C61-butyric acid methyl ester (PCBM) is used as an organic semiconductor material for organic photovoltaic applications and can be synthesized via a [2 + 1] cycloaddition of C_{60} fullerene with diazoalkane and subsequent thermal or photoisomerization. Both the thermal[416] and photoisomerization[417] toward PCBM have been performed under continuous-flow conditions. However, the photochemical approach suffered from limited productivity (up to 6 mg·h^{-1}).[417]

Ryu et al. combined the cycloaddition and photoisomerization step in a telescoped flow process and achieved a higher productivity in the photoisomerization step than the literature method by a judicious choice of light source (Scheme 47).[418] For the photoisomerization, a sodium lamp (589 nm, 360 W) was selected as light source and full conversion of the fulleroid

Scheme 46. Nonclassical Photorearrangement of Dienones and Santonin with Different Reaction Outcomes for Different Solvents

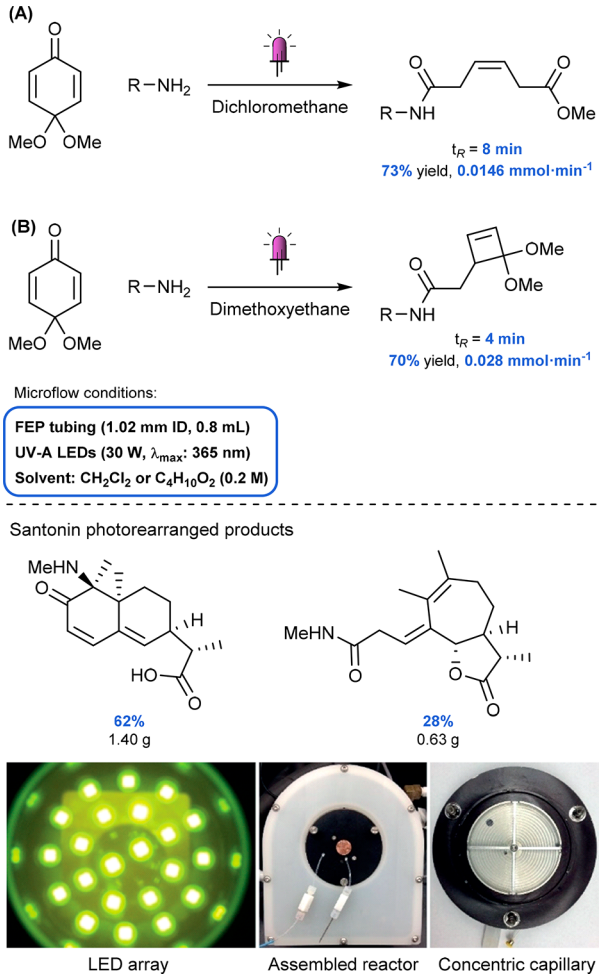

Reprinted with permission from ref 415. Copyright 2017 John Wiley and Sons.

Scheme 47. Telescoped Thermal Cycloaddition and Photoisomerization of Fullerene and Diazoalkane to PCBM

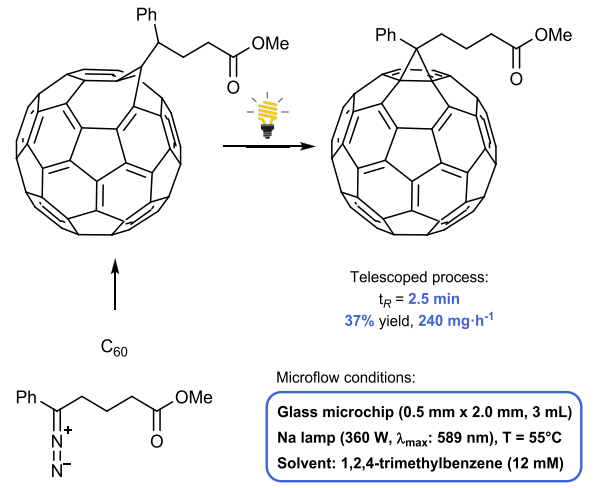

substrate was achieved after just 45 s residence time in the presence of 1 equiv of C_{60}, which was assumed to act as a photosensitizer for this reaction. After optimization of each

https://doi.org/10.1021/acs.chemrev.1c00332
Chem. Rev. 2022, 122, 2752−2906

step separately, the two steps were efficiently combined in a continuous-flow setup to produce 0.79 g of PCBM over 3.3 h (total residence time <2.5 min).

5.3. Photocyclizations

Photocyclizations offer quick access to complex carbo- and heterocycles from often simple starting materials. A feature that has recently proven its utility in the total synthesis of several natural products with complex ring structures.[77,419−423]

An example of the ability of continuous-flow photocyclizations to convert relatively simple starting materials into highly complex heterocycles was shown by Tranmer et al.[424] A two-step flow process was developed, including an amidation and photocyclization step, to convert 2-chlorobenzoyl chlorides and anilines into tricyclic phenanthridinones (Scheme 48). In the flow setup, the starting materials were

Scheme 48. Synthesis of Tricyclic Phenanthridinones from Simple Starting Materials

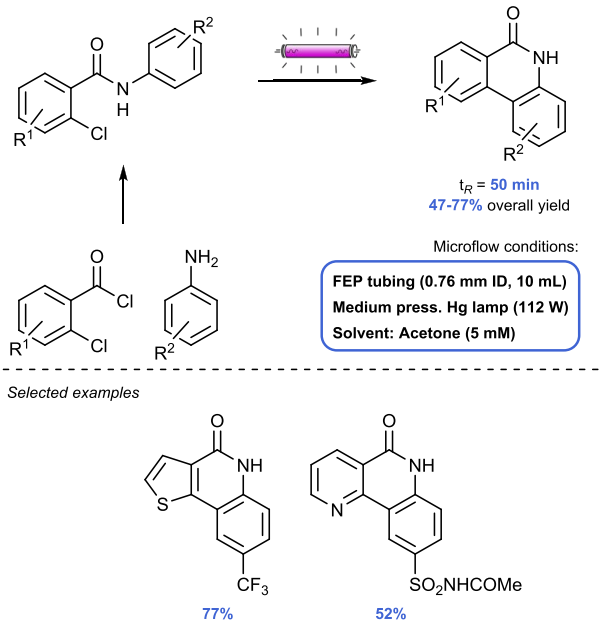

combined in a T-mixer and injected into a reactor loop. After allowing the thermal condensation reaction toward 2-chlorobenzamide to occur at 60 °C, the reaction mixture was introduced into the photoreactor (FEP tubing, 10 mL) and irradiated with a medium-pressure mercury lamp (112 W). High conversions were achieved in the photocyclization step (up to 99%) for a wide range of substrates (16 examples). Interestingly, no intermediate purification between the two reactions was required, allowing to simply connect the two reactors in series. By exchanging the benzoyl chloride for thiophenyl or pyridinyl chloride, the scope of the reaction was later expanded to include different bioisosteres.[425] The simple two-step method outperformed literature examples in terms of substrate scope, atom efficiency, and yield.[426−429]

Complex carbo- and heterocycles with an exomethylene group were also produced in a continuous-flow reactor through a Cossy-type photocyclization of various alkynyl halides (Scheme 49).[430] The glass microreactor chip (0.2 mm channel depth, 0.11 mL volume) was irradiated with a low-pressure mercury lamp (1.2 W, 254 nm), affording the photocyclized products in medium to high isolated yields (45−93%) in short

Scheme 49. Cossy Photocyclization of Alkynyl Halides

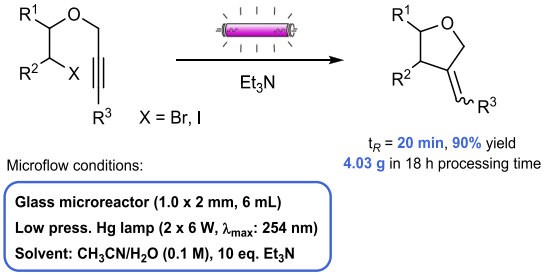

residence times (5−8 min). To elucidate the reaction mechanism, a deuterium labeling study was performed, supporting the SET reaction mechanism proposed by Cossy et al.,[431] in which a triethylamine (TEA) cation serves as sacrificial electron donor. The reaction was also performed in a 6 mL glass microreactor (t_R = 20 min), generating 4 g of product in 18 h processing time.

The synthesis of polycyclic heterocycles, including unprotected carbazoles, indoles and pyrroles, through photochemical azide activation and cyclization was performed by Collins et al. under continuous-flow reaction conditions (Scheme 50).[432] Although the reaction proceeded well with

Scheme 50. Two-Step Photochemical Flow Process to Substituted Carbazoles

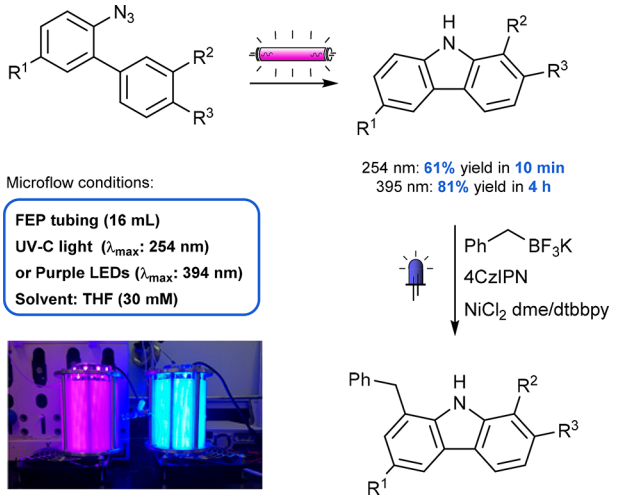

Reprinted with permission from ref 434. Copyright 2018 John Wiley and Sons.

a UV-C lamp (254 nm) in just 10 min residence time, increased yields and improved functional group tolerance were observed when using purple LEDs (394 nm) instead. This can be attributed to the lower energy light source which minimized product degradation. However, because of the reduced spectral overlap, longer residence times (2−4 h) were required to reach full conversion. As a concrete example, higher isolated yields were observed for a chlorinated carbazole with purple LEDs (81% after 4 h reaction) than with UV-C light (61% after 10 min). Furthermore, the utility of the azide activation reaction was further showcased in the synthesis of the carbazole-based drug carprofen and compared with an existing photochemical route using a copper-based sensitizer.[433] Interestingly, whereas the copper-sensitized method resulted in a complex mixture of

https://doi.org/10.1021/acs.chemrev.1c00332
Chem. Rev. 2022, 122, 2752−2906

products, with different regioisomers and dechlorination byproducts, the photochemical azide activation method proceeded regioselectively without the need for transition metal catalyst and without any dechlorination.

The method was also applied to a two-step photochemical flow sequence toward the biologically active carbazole clausine C.[434] The photocyclization to carbazole under purple LED irradiation was coupled with a photocatalytic/Ni-catalyzed cross-coupling reaction with potassium trifluoroborate salts in flow under blue LED irradiation (Scheme 50). Since no additives, catalysts or reagents were required in the photocyclization reaction, the outlet stream could directly be introduced into the second photochemical reactor without intermediate purification. This two-step process serves as an interesting example on how photochemical processes, each requiring their own specific set of reaction conditions, can be promoted sequentially by light of different wavelengths.

The Norrish−Yang photocyclization is an efficient method for the preparation of cyclobutanes from simple acyclic ketones. This reaction has been carried out in flow for the transformation of 2-amino ketones to 3-hydroxyazetidines (Scheme 51A).[435] As is often the case for photochemical transformations, the reported batch methods require prolonged irradiation times and dilute substrate concentrations, leading to the formation of photodegradation products and low productivity.[436] These problems were circumvented by performing the reaction in a flow reactor (FEP tubing, 10 mL) irradiated by a medium-pressure mercury lamp (150 W, 365 nm). In the flow setup, a broad substrate scope was carried out, revealing that electron-poor aryl groups were well tolerated. In contrast, lower yields were observed for substrates bearing electron-donating substituents. It should be noted though that higher yields could be attained for the latter compounds by carrying out a reoptimization of the reaction conditions. It was proposed that this loss in reactivity for electron-rich substrates was caused by a shift in light absorption, causing a mismatch between absorption and the peak emission of the light source. After defining the scope and limitations of the photocyclization, a scale-up was performed, converting 100 mmol of amino ketone in 11.5 h (60% isolated yield).

Scheme 51. Norrish−Yang Photocyclization Towards (A) Hydroxyazetidines, (B) Hydroxycyclobutanones, and (C) as a Key Step in the Total Synthesis of Zaragozic Acid C

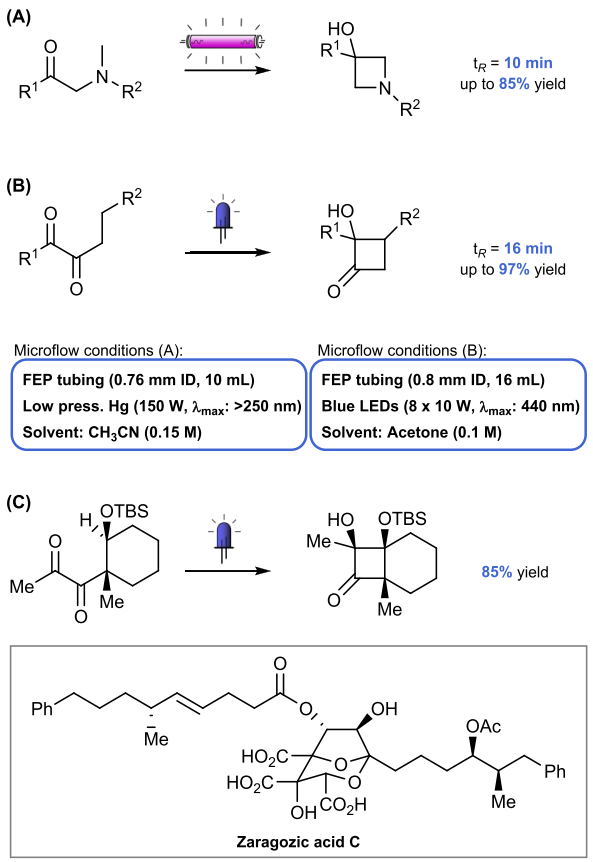

Similarly, the Norrish−Yang photocyclization of 1,2-diketones to 2-hydroxycyclobutanones was also done in flow (Scheme 51B).[437] A first exploration of the reaction in batch afforded the desired product; however, long irradiation times were required (16−24 h), and a number of side products were formed, which were difficult to separate from the product. The flow reactions were performed in a three-layered FEP capillary reactor (32 m, 0.8 mm ID, 1.6 mm OD, 16 mL volume) irradiated by 440 nm LEDs (8 × 10 W). In this flow setup, 4.35 g of 2-hydroxy-2-methylcyclobutanone was obtained in 8 h. Importantly, unreacted diketone was removed by evaporation and the cyclobutanone product could be obtained without further purification.

A flow Norrish−Yang photocyclization was also used in the total synthesis of Zaragozic acid C (Scheme 51C).[438] Crucial for achieving high yields in this transformation was the use of a light source that matched the substrates' absorption spectrum (λ_{max} = 405−413 nm). With violet LED (λ_{max} = 405 nm), 85% ^{1}H NMR yield of the *cis*-fused bicycle was obtained, whereas only 26% ^{1}H NMR yield was achieved with blue LED (λ_{max} = 465 nm).

Tin amine protocol (SnAP) and silicon amine protocol (SLAP) reagents, as a tin-free alternative, were carried out in a continuous-flow photoreactor for the synthesis of substituted saturated N-heterocycles (Scheme 52).[439,440] The photocyclization reactions were performed in a glass chip microreactor (1 mm channel depth, 1.7 mL volume) subjected to blue LED irradiation. For the reactions with SnAP reagents, the stoichiometric copper promoter could be replaced by an iridium photocatalyst, leading to a significantly easier workup.[439] The reactions with SLAP reagents were also performed photocatalytically; inexpensive 2,4,6-triphenylpyrylium tetrafluoroborate ($TPPBF_4$)[441] was used as a photocatalyst resulting in a ^{1}H NMR yield of 90% for the model reaction in 17 min residence time.[440] After reaction optimization, the method was successfully applied to other substrates leading to the formation of various substituted morpholines, benzomorpholines, oxazepanes, thiomorpholines, and thiazepanes. Additionally, a 30 mmol scale-up experiment was performed using the optimized conditions, generating 5.5 g of product in 2 days, which exemplifies the greater convenience and better scalability of the photo flow method compared to the previously reported batch method.[442]

Several recent publications reported on the synthesis of spirocyclic compounds through photocyclization reactions in flow.[419,420,443] For example, the photocyclization of aryl enamines to spiroindolines was performed by researchers at Vertex Pharmaceuticals under batch and flow conditions (Scheme 53).[419] The batch reactions suffered from extended

https://doi.org/10.1021/acs.chemrev.1c00332
Chem. Rev. 2022, 122, 2752−2906

Scheme 52. Application of SnAP and SLAP Reagents in the Synthesis of Saturated Heterocycles

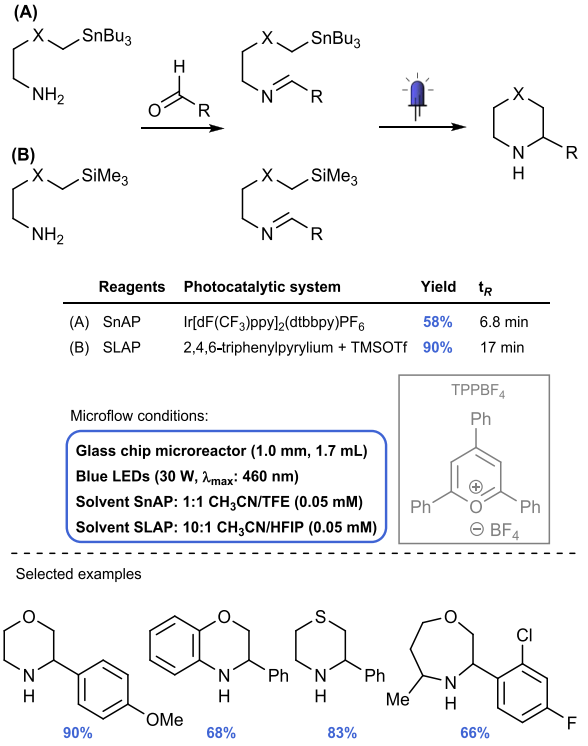

Scheme 53. Photocyclization of Aryl Enamines to Spiroindolines Enables the Short Total Synthesis of (±)-Horsfiline

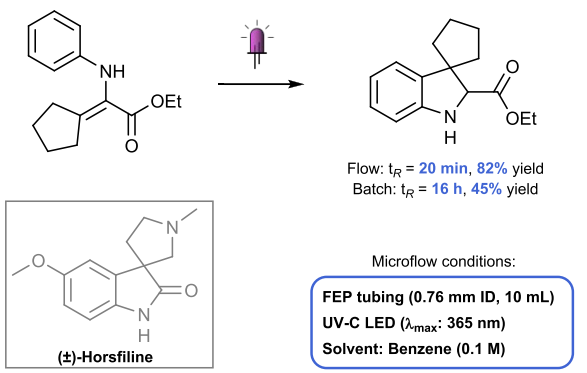

irradiation times, modest yields and batch-to-batch variability due to poor control over the reaction conditions. The best results in batch were obtained by irradiation with UV-A light in benzene, resulting in 45% spiroindoline after 16 h. In contrast, the flow reactions proceeded smoothly, resulting in 82% yield in 20 min residence time. Additionally, some aryl enamines were completely unreactive in batch but converted in flow quantitatively into the corresponding spiroindoline. The synthetic utility of the protocol was further exemplified by a shortened total synthesis of the natural product (±)-horsfiline, compared to a previously reported method.[444]

Spiro derivatives were also obtained in a biomass valorization strategy to synthesize γ-butyrolactone scaffolds through radical addition of alcohols to fumaric and itaconic acids and subsequent cyclization (Scheme 54).[443] A commercially available mesofluidic reactor was used to perform the reaction. In-line analysis with NMR spectroscopy allowed for a rapid

Scheme 54. Biomass Valorization Strategy to γ-Butyrolactones

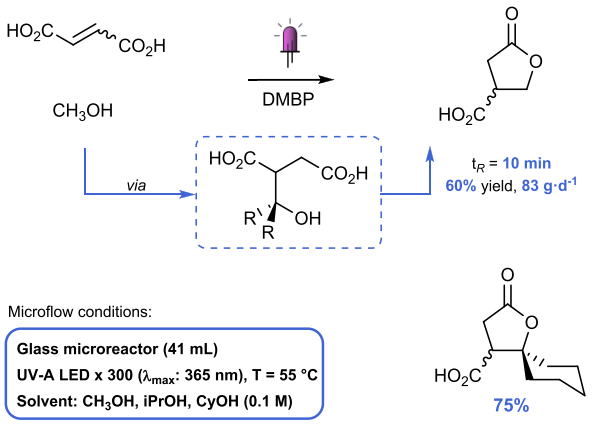

parameter optimization. It was found that both an elevated temperature (T = 55 °C) and an increase of the photosensitizer loading from 5 to 40 mol % had a positive impact on the reaction. The model reaction between fumaric acid and isopropanol was scaled out to a pilot-scale mesofluidic reactor (41 mL volume), affording 83 g of product per day with a residence time of 10 min.

A diastereoselective ipso-cyclization toward a 6,6-spirocyclic core structure was performed under blue LED irradiation in continuous-flow. This reaction constitutes the key step in the total synthesis of zephycarinatines (Scheme 55).[420] The crucial

Scheme 55. Diastereoselective ipso-Cyclization Towards the 6,6-Spirocyclic Core Structure of Zephycarinatine

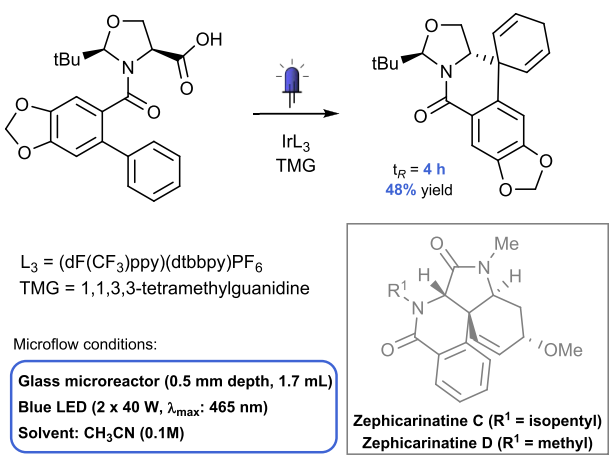

photocyclization step was first performed in batch with a 40 W blue LED bulb in the presence of an iridium catalyst and base, generating 58% of the desired isomer after 24 h. Switching to a glass microreactor required the solubilization of the base to avoid reactor clogging. After reoptimization of the reaction conditions, 48% product could be isolated after 4 h reaction time. The flow conditions were applied to a 0.5 mmol scale reaction, allowing the investigation of further steps in the total synthesis of zephycarinatines C and D.

Another example where a flow photocyclization enabled a shorter or even a new total synthesis of a natural product is provided by Porco et al.[421] A regiodivergent photocyclization strategy of dearomatized acylphloroglucinols was applied to prepare (−)-nemorosone in 7 steps. This represents the

https://doi.org/10.1021/acs.chemrev.1c00332
Chem. Rev. 2022, 122, 2752−2906

shortest total synthesis reported to date, and the protocol also allowed for the first total synthesis of (−)-6-*epi*-garcimultiflorone A (Scheme 56). The photocyclization reactions were

Scheme 56. Short Total Synthesis of Dearomatized Acylphloroglucinols with Photocyclization as a Key Step

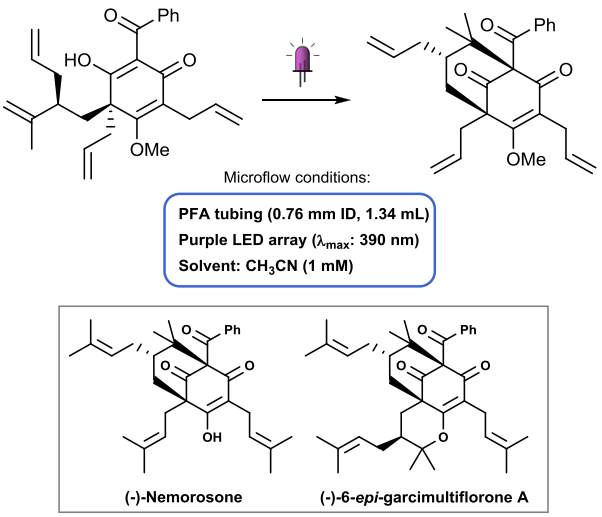

performed in a microcapillary (0.76 mm ID, 1.34 mL volume) irradiated with purple LEDs (390 nm). With a residence time of 4 h, this resulted in 29% yield of the photocyclized nemerosone core (67% based on recovered starting material). A similar procedure allowed to obtain the garcimultiflorone core in 54% yield.

Czarnocki et al. applied their continuous-flow photocyclization methodology, previously used in the formal total synthesis of podophyllotoxin,[422] to similar chiral bisbenzylidene succinates forming various cyclolignan analogues (Scheme 57).[423,445,446] For the photocyclization, a different

Scheme 57. Photocyclization of Chiral Bisbenzylidene Succinates in the Total Synthesis of Cyclolignan Analogues

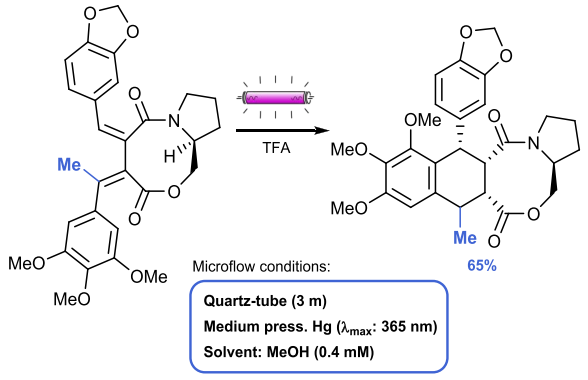

stereochemistry was found depending on the chiral auxiliary used and a different regioselectivity was observed depending on the substitution pattern of the benzylidene moiety adjacent to the ester group. Additionally, the total synthesis of (+)-epigalcatin was achieved with the flow photocyclization of a chiral atropisomeric 1,2-bisbenzylidene succinate amide ester as a key step.

An update of a Mallory photocyclization protocol was described by Yamaji et al. to produce phenacenes in a combined batch and flow process (Scheme 58).[447,448] First, a batch Wittig reaction was performed between the phospho-

Scheme 58. Mallory Photocyclization to Phenacenes

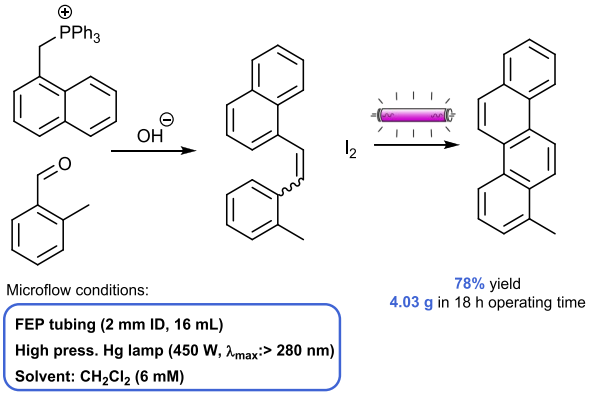

nium salt and an arylaldehyde to yield the diarylethene. Without purification, the mixture was then pumped through a silica-gel column to trap excess base and Ph_3PO formed in the Wittig reaction. An iodine solution in toluene was added in flow using a T-mixer and the reaction mixture was irradiated with a 450 W high-pressure mercury lamp to induce the photocyclization. Optimal yields were obtained within 6 min residence time (78%). Longer residence times led to substantial oxidative photodegradation. The two-step protocol was performed for a wide range of substrates resulting in the generation of (un)substituted 4-, 5-, and 6-ring phenacenes in good overall yields (18 examples, up to 92% isolated yield).

A photoinduced multicomponent cyclization reaction of 2-vinylphenols, *N*-alkoxypyridinium salts, and sulfur ylide was performed in batch and flow to synthesize substituted dihydrobenzofurans.[449] In general, higher yields were obtained during the scope investigation when using the flow conditions (46−58% in flow, versus 33−49% in batch).

5.4. Singlet Oxygen-Mediated Oxidations

Oxidations are among the most common reactions encountered in biological systems, as well as in academic and industrial laboratories. From all potential oxidants, oxygen can be considered the greenest.[450] However, ground state triplet oxygen often necessitates high pressure and/or metal complexes to induce oxidative transformations. In contrast, singlet oxygen ($^1O_2$) is known to be more reactive.[451] $^1O_2$ can be generated in situ with an energy transfer from a photosensitizer to triplet oxygen,[452] although other possibilities in the absence of light have been described as well.[453,454] Despite the low cost and the high atom economy, the use of singlet oxygen is not widespread in industry, mainly because of the associated safety concerns and its short lifetime.[455] These specific issues can be overcome by using flow technology.[456−459] Considering the technological challenges associated with the safe handling of gaseous oxygen, many studies have been reported on the development of efficient biphasic[459] or even triphasic flow regimes.[460−464] The photocatalyst concentration is an important variable to be considered as well, not only because it has relevant consequences in an industrial flow setup, not only for economic reasons but also because it could affect downstream purification processes. On this regard, researchers at Corning highlighted the importance

https://doi.org/10.1021/acs.chemrev.1c00332
Chem. Rev. 2022, 122, 2752−2906

of the physical characteristics of the photoreactor and the nature of the light source.[465]

Up to 2016, several reports about singlet oxygen oxidations in continuous flow were described.[466−469] In particular, various studies reported on the oxidation of sulfides in batch[470] and in flow,[471] reflecting the importance of sulfoxides especially in medicinal chemistry.[472] The Rose Bengal (RB)-photocatalytic methionine oxidation serves as a good benchmark study to compare the performance of a continuous-flow microreactor with a batch setup.[473] Although it is possible to reach full conversion in both reactors, microreactor technology proved to be superior in terms of irradiation efficiency, kinetics, and space-time yield (STY). In fact, whereas 120 min were necessary to reach full conversion in batch, this time was reduced to 5 min in flow. This is mainly due to a higher light intensity across the entire cross section of the microcapillary and to a higher oxygen availability deriving from improved gas−liquid mass transfer.

The photocatalytic oxidation of methionine was also studied by Dreesen, Heinrichs, Monbaliu, and co-workers, who developed a scalable flow protocol (Scheme 59).[474] The

Scheme 59. Photooxidation of Methionine Mediated by RB in Flow

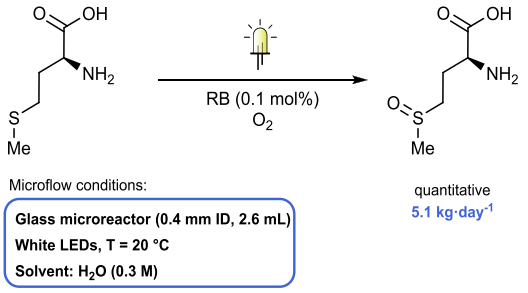

photochemical reactor consisted of a commercially available glass module (Corning Lab Reactor: 0.4 mm ID, 2.6 mL internal volume) equipped with two high-capacity heat exchanger (22 mL, 1 $W \cdot mL^{-1} \cdot K^{-1}$) and surrounded by two LED panels. The reaction outcome was determined by in- and off-line NMR analysis. The best results were obtained with RB as the photocatalyst (0.1 mol %) with white LEDs at room temperature and a residence time of 1.4 min. Importantly, only 1.1 equiv of oxygen were necessary. Theoretically, the scale-up of this process would lead to a sulfoxide production of 31.1 $mol \cdot day^{-1}$, corresponding to 5.1 $kg \cdot day^{-1}$.

To further improve the efficiency of the photosensitizer, Mendoza et al. reported the positive interaction between Au nanobipyramids@$mSiO_2$ (AuBPs@$mSiO_2$) nanoparticles with RB to successfully oxidize methionine in flow.[475] This positive interaction is attributed to AuBP plasmon resonance, which magnifies the photophysical properties of RB, resulting in improved production of singlet oxygen and thus results in a faster formation of the sulfoxide product. Reactions were performed in a PFA capillary reactor (0.8 mm ID, 2.6 mL) surrounded by three high power green LEDs (540 nm). In this system, 92% methionine conversion was reached in 69 s residence time with RB in the presence of AuBPs@$mSiO_2$, whereas 77% conversion was observed in absence of nanoparticles.

The $^1O_2$ oxidation of sulfides in flow is also a very relevant reaction to neutralize dangerous chemicals, as in the case of bis(2-chloroethyl)sulfide (mustard gas), which is infamously known for its use as a chemical warfare agent (Scheme 60).[476]

Scheme 60. (A) Neutralization of a Mustard Gas Simulant through Singlet Oxygen Oxidation in Flow and (B) Reactor Design with Glass Fluid Modules and in-Line Analysis

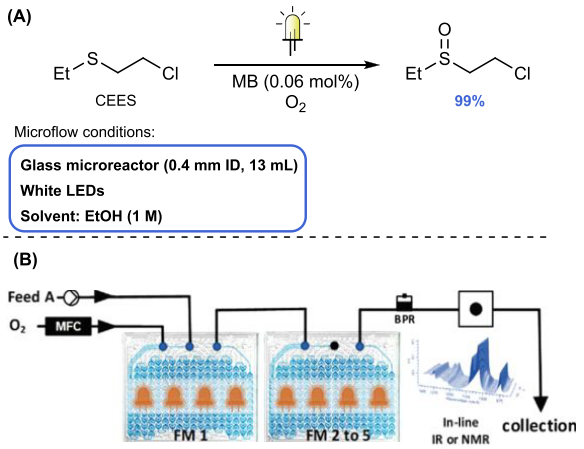

Reprinted with modifications from ref 476. Copyright 2020 Royal Society of Chemistry.

Singlet oxygenoxidation is very selective toward sulfoxides, thus avoiding the formation of mustard gas sulfone, which is comparably toxic to the sulfide itself. 2-Chloroethyl ethyl sulfide (CEES) was selected as a simulant of mustard gas and its oxidation was performed in five commercially available microreactors connected in series (Corning AFR: 0.4 mm ID, 5 × 2.6 mL volume). The glass microreactors contain static mixing elements, which improve the mass transfer efficiency between oxygen and the alcoholic solution. The temperature inside the reactor is maintained with a double layer heat exchanger. This way, the selective oxidation of mustard gas to its nontoxic sulfoxide is performed under irradiation with 300 white LEDs (99% yield) in 4 min residence time, with minimal formation of other toxic byproducts.

Apart from sulfide oxidations, a classic model reaction to study the efficiency of new photocatalysts, as well as different reactor designs, is the conversion of α-terpinene into ascaridole via a [4 + 2] cycloaddition between singlet oxygen and the diene (Scheme 61). A common byproduct of this trans-

Scheme 61. Photooxidation of α-Terpinene into Ascaridole as Benchmark Reaction

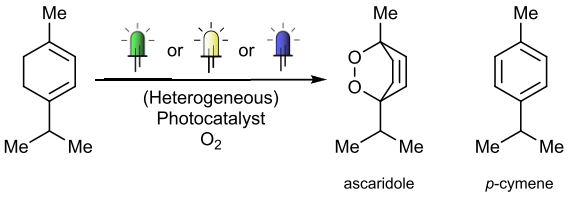

formation is *p*-cymene. In one example, the photooxidation of α-terpinene was used as a benchmark reaction to analyze the effect of various operating conditions (concentration, flow rate) in a commercial reactor (Vapourtec UV-150: FEP capillary 1.15 mm ID, 2−10 mL volume) on the reaction outcome, taking into account the kinetics and photobleaching of the photosensitizer.[477]

https://doi.org/10.1021/acs.chemrev.1c00332
Chem. Rev. 2022, 122, 2752−2906

In another example, Oelgemöller et al. investigated the productivity of the α-terpinene photooxidation in a falling film microreactor (FFMR) using RB as photocatalyst.[478] The FFMR is characterized by a liquid flowing down a plate in a thin film, with a thickness in the order of micrometers, to increase the gas−liquid interfacial area. The main components of this reactor are a heat exchange unit, an inlet, an outlet, the reaction plate with microchannels and a window in borosilicate glass or in quartz to be irradiated with an external light source (Figure 60).[479] A solution of α-terpinene (50 mM) and RB

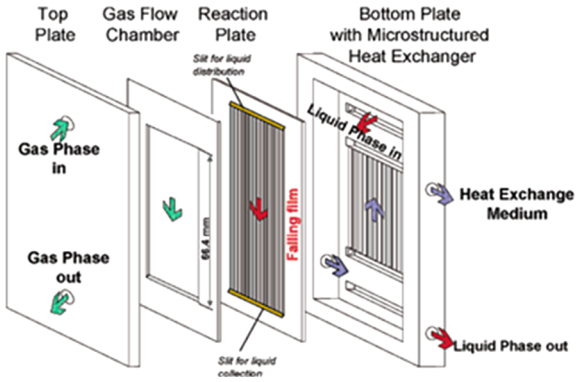

Figure 60. Schematic representation of a FFMR and its main components. Reprinted with permission from ref 479. Copyright 2005 American Chemical Society.

(0.49 mM, 1 mol %) in isopropanol was injected in the FFMR, containing 32 parallel microchannels (0.2 × 0.6 mm, 78 mm length, 0.3 mL volume) and was irradiated by a compact fluorescence lamp (CFL, 18 W). This way, 89% selectivity toward ascaridole was achieved with a STY of 2.1 mol·L^{-1}·h^{-1}. Higher STY values up to 3.6 mol·L^{-1}·h^{-1} could be obtained by increasing the substrate concentration (from 50 to 75 mM with 6 s of residence time or 100 mM with 13 s of residence time), and by increasing the sensitizer concentration (0.49 mM to 0.98 mM). However, in this case the selectivity dropped to 74%. In terms of STY, the FFMR outperforms the batch setup, where the best STY (1.2 mol·L^{-1}·h^{-1}) was obtained with 15 min irradiation.

In another case, a new series of five bimetallic Ti(IV) complexes was prepared and their efficiency as homogeneous photosensitizer was proven with the same α-terpinene photooxidation.[480] In contrast to TiO_2, these new Ti−O−Ti bridged amine bis(phenolate) complexes are soluble in organic solvents and absorb light in the visible region of the spectrum. A capillary reactor (10 mL) irradiated with 420 nm LEDs (61 W) was used to investigate the efficiency of the new complexes. Every member of this new set of Ti-complexes afforded ascaridole in 2 to 4 h residence time, with excellent selectivity. On the contrary, when TiO_2 was used, *p*-cymene was obtained instead.

Heterogeneous photocatalysis in flow offers interesting possibilities in terms of facile purification and reusability.[481−484] The efficiency of different kinds of immobilized photocatalytic systems has also been tested with the α-terpinene photooxidation as benchmark reaction (Scheme 2). In one case, Rose Bengal (RB) was grafted in a polymer microgel with swelling ability in ethanol (Figure 61).[485] The photoactive colloids were prepared through a copolymerization of vinyl acetate, *N*-vinylcaprolactam, divinyl adipate (DVA) cross-linker, and vinylbenzyl Rose Bengal (VBRB). The

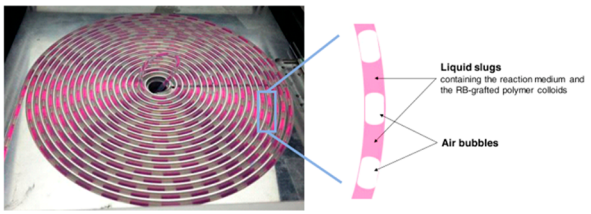

Figure 61. Picture of the slurry Taylor flow established between the solution of VBRB@MG in ethanol and O_2 in the Archimedean spiral reactor. Reprinted with permission from ref 485. Copyright 2020 American Chemical Society.

resulting microgels (MGs) VBRB@MG-8 or VBRB@MG-14 contain either 8 mol % or 14 mol % of DVA cross-linker. The photosensitizer loading is estimated around 215 ± 30 μmol RB per gram of dried MG. The homemade microreactor (FEP capillary: 1 mm ID, ∼4 mL volume) was shaped into an Archimedean spiral irradiated with a LED array with emission from 400 to 700 nm. Slurry Taylor flow conditions were established to allow efficient mixing. The system allowed for conversions above 80% in only 4 min residence time. The grafted photosensitizer was stored for 8 months without a drop in efficiency and was reused several cycles with almost constant activity. Interestingly, its performance is comparable to the homogeneous RB, but the covalent anchoring seems to prevent RB photodegradation.

In another case, mesoporous silica nanoparticles (MSNs) were used as a support to covalently incorporate RB.[486] To perform the photooxidation, a solution of α-terpinene (0.1 M) in methanol was pumped into the PFA capillary reactor (0.8 mm ID) under LED irradiation (540 nm), resulting in 90% conversion in 72 s residence time. To assess recyclability, the RB@MSN catalyst was recovered and reused for four consecutive cycles. The conversion remained constant for two cycles but dropped to 62% in the third run with 77% catalyst degradation. In the fourth cycle, there was even no ascaridole production observed. The developed RB@MSNs successfully catalyzed the photooxidation of other substrates, such as methionine, triphenylphosphine, and cyclopentadiene with conversions of 47%, 55%, and >99%, respectively.

RB was also immobilized on a number of vinylimidazolium functionalized supports, consisting of a Merrifield resin with alkyl- or vinyl-substituted imidazoles (PS-alkylimidazolium).[487] RB@PS-vinylimidazolium (Figure 62) showed superior

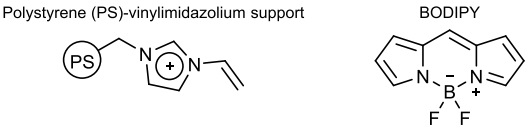

Figure 62. Structure of polystyrene-immobilized vinylimidazolium and BODIPY structure.

stability compared to the other supports, both in flow and in batch (up to 11 days). The oxidation of α-terpinene in dichloroethane was performed at 0 °C in a PTFE tube (2 mm ID, 10 cm length, 0.3 mL volume) filled with 220 mg of RB@PS-vinylimidazolium catalyst and irradiated with white LEDs. With a total flow rate of 0.52 mL·min^{-1}, complete conversion of α-terpinene was achieved and 80% GC-yield of ascaridole was observed. Moreover, the catalyst also worked efficiently for the oxidation of triphenylphosphine and a sulfide.

https://doi.org/10.1021/acs.chemrev.1c00332
Chem. Rev. 2022, 122, 2752−2906

A packed bed photoreactor with RB immobilized onto polystyrene was employed for the α-terpinene photooxidation.[171] The photoreactor consisted of an Omnifit column (6.6 mm × 150 mm) irradiated with green LEDs (90 W, 530 and 580 nm). The reaction temperature was between −15 and 0 °C. When oxygen had a 50-times higher flow rate than the liquid solution, ascaridole was obtained in 94% yield. The system worked efficiently also in the oxidation of various substrates, such as α-pinene, alkenes, a sulfide, and triphenylphosphine (60−98% yields). The volume-time output (VTO), which is the productivity of a chemical step in relation to its reactor space and has to be <1 for industrial processes, accounts for 0.622337 $m^3 \cdot h \cdot kg^{-1}$ in average. Finally, the antimalaria drug artemisinin was also prepared through singlet oxygen oxidation.[488]

Similarly, BODIPY (4,4-difluoro-4-bora-3a,4a-diaza-s-indacene, Figure 62) was immobilized on microporous polymers by Xu, Vilela, and co-workers to prepare a heterogeneous photocatalyst.[489] BODIPY is known for its excellent spectroscopic properties and chemical robustness, while conjugated microporous polymers (CMP) are characterized by their microporous structure and high surface area. New BODIPY-based conjugated microporous polymers (BDP_CMP and PHTT_BDP) were prepared to take advantage of the characteristics of both materials. In BDP_CMP, modified BODIPY is one of the building blocks of the copolymer, whereas in PHTT_BDP, BODIPY is grafted into the polymer. The prepared materials were tested in the α-terpinene oxidation in a capillary reactor (Vapourtec: 10 mL) irradiated with 530 nm LEDs. A chloroform suspension with sensitizer and α-terpinene was combined with an air flow (1 $mL \cdot min^{-1}$ flow rate each) and pumped into the reactor. After 1 h recirculation, both BDP_CMP and PHTT_BDP converted α-terpinene quantitatively into ascaridole. To test the catalyst stability, a solution containing just BDP_CMP was recirculated and irradiated for 6 h. After that, α-terpinene was added and completely oxidized to ascaridole in one additional hour of recirculation. With PHTT_BDP, 90% conversion was achieved, thus proving an enhanced photostability of BDP_CMP, probably because of the different incorporation of BODIPY in the two polymers.

Inspired by these results, commercially available Merrifield-type resins were derivatized with BODIPY via aryl ester linking in flow.[490] The obtained functionalized polymers PS-Est-BDP (200 mg, equivalent to ∼5 mol %) were placed in a borosilicate glass photoreactor (6.6 mm ID, 150 mm length, 5.1 mL volume) to form a fixed bed, which was irradiated with 500 nm LEDs (7.44 W). The α-terpinene (0.67 M) in chloroform, through which air was bubbled, was recirculated through the reactor at 1 $mL \cdot min^{-1}$ flow rate and was analyzed by an in-line benchtop NMR spectrometer. The best conversion was obtained with the heterogeneous polymer PS-Est-BDP, achieving 58% in 24 h reaction time and 3 cycles, for a total of 72 h irradiation. The resin was proven to be stable for 96 h. However, the homogeneous photocatalysts used in a PTFE reactor coil (1 mm ID, 10 mL volume) proved much more efficient than the heterogeneous one (99% conversion in 3 h). For this reason, PS-Est-BDP was modified with *N*-chloro succinimide to improve its performance (Scheme 62). With PS-Est-BDP-Cl_2, complete conversion of α-terpinene was achieved in ∼1 h when sufficiently high pressure was applied to increase the solubility of oxygen (5.5 bar). Moreover, PS-Est-BDP-Cl_2 was recycled 5 times, for a total of 12.5 h of irradiation. Although conversion was not stable over time, the catalyst activity was improved compared to the parent material.

Scheme 62. Preparation of the Heterogenous Chlorinated BODIPY Photosensitizer Linked to a Merrifield-Type Resin

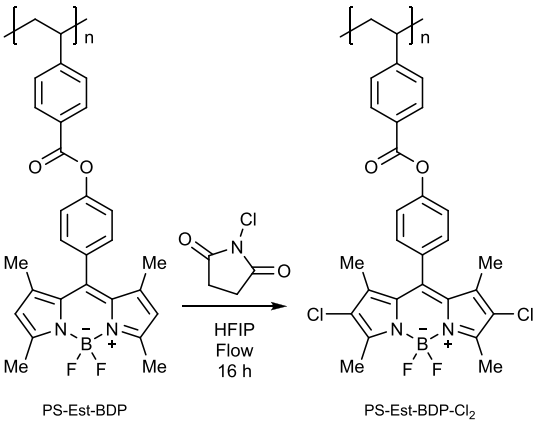

A new heterogeneous photosensitizer was prepared starting from 2,1,3-benzothiadiazole (BTZ)-based vinyl cross-linker, which was copolymerized with styrene (St-BTZ, Scheme 63).[491] Through a precipitation polymerization with a free radical initiator (AIBN) in the presence of divinylbenzene (DVB) as a nonphotoactive cross-linker, particles were formed as micrometer-sized beads (Bead-BTZ). When the free radical polymerization took place in the presence of a high internal phase emulsion (Span 80), a monolith was formed instead (pHIPE-BTZ). The two polymer-supported BTZs were designed for continuous-flow applications, as an alternative to polymeric gels, which can cause clogging. Instead, the beads were dispersed in the solvent mixture, whereas p-HIPE-BTZ was prepared and swelled in a glass column (7 mm ID). In the photoreactor, the reaction mixture was combined with an air flow and was irradiated with 420 nm LEDs. With Bead-BTZ, the solution of α-terpinene was completely converted into ascaridole within 1 h of recirculation, with an ascaridole productivity of 136 $mg \cdot h^{-1}$. With the monolith, the combined flow rate was reduced from 2 $mL \cdot min^{-1}$ to 1 $mL \cdot min^{-1}$, to increase the contact time between the substrate and catalyst,

Scheme 63. Bead-BTZ or pHIPE-BTZ Catalyst Preparation through Copolymerization of St-BTZ with Styrene and Divinylbenzene

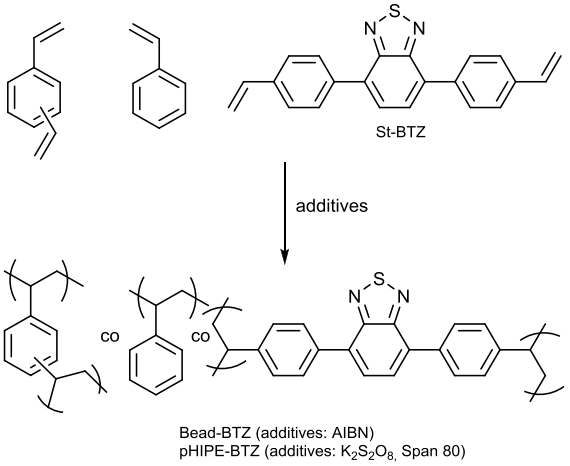

https://doi.org/10.1021/acs.chemrev.1c00332
Chem. Rev. 2022, 122, 2752−2906

and oxygen was used instead of air. In this case, full conversion of the starting material was obtained after one pass of the 10 mL solution, with a productivity of 192 mg·h^{-1}. The pHIPE was very stable, even after more than 80 h reaction time. For comparison, when the homogeneous St-BTZ was used in the photooxidation of α-terpinene in batch, 90 min were required to reach full conversion and after 45 min the photosensitizer started to degrade in such strong oxidative conditions.

The oxidation of 2-furoic acid is another benchmark reaction, which was selected to test the activity of RB supported on an ionic liquid (IL)-like phase (Scheme 64).[492]

Scheme 64. RB-SILLP Catalyzed Furoic Acid Photooxidation in Flow

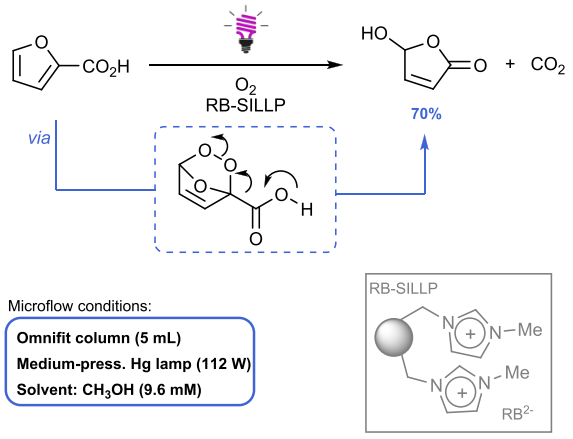

Supported IL-like phases (SILLPs) consist of a polymeric backbone and ionic-liquid like fragments. There are two ways to prepare the supported ionic liquids: (i) direct copolymerization of the IL monomers and (ii) grafting the IL-like units onto the preformed polystyrene-divinylbenzene polymer (PS-DVB). A grafted IL-like polymer was tested as a photosensitizer in a flow setup. The RB-SILLP with an RB loading of 0.89 μmolRB per g of polymer, was swelled in a fluid-bed reactor (5 mL Omnifit column) and irradiated with a medium-pressure Hg lamp (112.5 W) equipped with a glass light filter. The developed polymer outperformed a commercial heterogeneous photocatalyst (RB@PS-DVB), which provided a maximum yield of 25% and was deactivated after 200 min. Instead, the RB-SILLP was stable for at least 8 h, providing the product in 45% yield. This result could be increased to 70% by doubling the residence time.

Another important class of photosensitizers are porphyrin derivatives, which under light irradiation pass from an excited singlet state to triplet state via ISC (intersystem crossing) to then perform an energy (or electron) transfer.[493] As such, they have proven their efficiency especially in singlet oxygen generation in a number of flow and batch organic transformations.[494] In a report from 2016 concerning the photooxidation of activated naphthol derivatives, de Oliveira and McQuade screened the efficiency of 4 porphyrinoids and a phthalocyanine (Scheme 65A).[495] The homemade photoreactor consists of a PFA capillary (1.65 mm ID, 25 mL) coiled around a 24 W white LED lamp. Tetraphenylporphyrin (TPP) outperformed the other derivatives (82% juglone yield, 1.54 g·day^{-1} productivity) with a short residence time (less than 17 min). The scope of the photooxygenation was then evaluated, affording higher yields in flow than in batch for each substrate.

Scheme 65. (A) TPP-Photocatalyzed Photooxidation of Naphthol Derivatives in Flow and (B) TcPP-Photocatalyzed DHN Oxidation through Formation of Singlet Oxygen in the FFMR

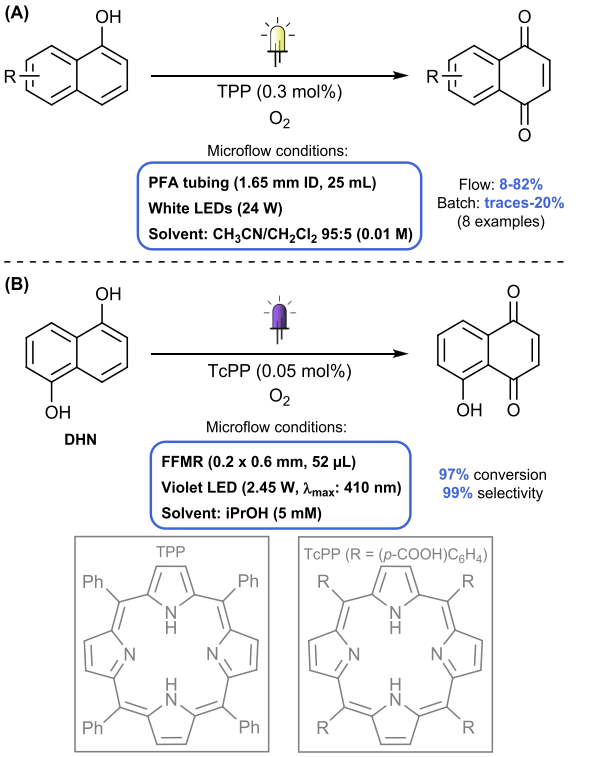

Similarly, the photooxidation of dihydroxynaphthalene (DHN) to juglone through in situ formation of singlet oxygen was also studied by Rehm et al. in a falling film microreactor (FFMR) (Scheme 65B).[174] Various parameters were screened, such as reactor architecture, light source, sensitizer, and oxygen partial pressure. The conversion was higher in a reactor with smaller channel architecture (0.2 × 0.6 mm vs 0.4 × 1.2 mm) as this corresponds to a greater film thickness (50 μm). Rose Bengal gave the best results with green LEDs as expected due to the spectral overlap, while *meso*-tetracarboxyphenylporphyrin (TcPP) gave the best results with violet LEDs (410 nm). However, a higher selectivity was achieved with TcPP, which is also more photostable than RB. Analyzing the applied LED power proved that 1.1 W was not sufficient to reach complete conversion, but 3.6 W proved to be detrimental for the selectivity. For this reason, 2.45 W was considered the most appropriate LED power to apply. Additionally, the use of pure oxygen was beneficial for the transformation, particularly in terms of selectivity. After this optimization, conversion and selectivity reached 97% and 99% respectively, in 19.4 s residence time and an irradiated volume of 52 μL.

The same DHN oxidation reaction was used to test the activity of two silica-supported photocatalysts, namely, [Ru(bpy)$_3$Cl$_2$,] and TMPyP^{4+}(5,10,15,20-tetrakis(*N*-methylpyridinium-4-yl)porphyrin).[496] The functionalized materials contained 2.5 mg PC per gram for [Ru(bpy)$_3$]@SiO$_2$ and 4.5 mgPC per gram for TMPyP@SiO$_2$. The solution was pumped into a 6.4 mm PTFE tube (1.5 mL volume) containing the silica-supported photosensitizer (1.3 g) and was irradiated with white LEDs. Both immobilized photocatalysts performed better in flow than in batch. In flow, higher yields were

https://doi.org/10.1021/acs.chemrev.1c00332
Chem. Rev. 2022, 122, 2752−2906

obtained by pumping pure oxygen in the solution instead of air. The desired juglone was afforded in GC quantitative yield with TMPyP@SiO_2, reaching up to 5.35 $g{\cdot}L^{-1}{\cdot}h^{-1}$ STY with a residence time of 30 min.

The photocatalytic activity of TPP and methylene blue (MB) was also compared in the citronellol photooxidation.[497] Both TPP and MB were efficient catalysts, with a strong dependence on the selected solvent for the observed productivity of the reaction. For example, in 2 min full conversion was achieved for TPP (0.1 mol %) in dichloromethane and MB (0.1 mol %) in deuterated methanol, whereas 9 min were required for MB (0.1 mol %) in methanol. This difference in productivity can be attributed to the difference in lifetime of singlet oxygen in each solvent: 10 μs in methanol, 100 μs dichloromethane, and 230 μs in deuterated methanol. Better results were obtained by switching to a more appropriate light source for MB, from 6500 K white LED to 3000 K white LED. When using higher citronellol concentrations (2 vs 0.1 M, or even in neat citronellol), the authors highlighted the importance of a good mass transfer efficiency to reach high conversions in shorter times. This can be improved with thinner PFA capillary (0.25 mm vs 0.75 mm ID). Finally, with the optimal O_2/citronellol molar ratio of 1.2, the calculated productivity was 0.360 $mmol{\cdot}min^{-1}$.

The limited lifetime of singlet oxygen in various solvents is a problem addressed also by Von Wangelin et al. (Scheme 66).[498] To circumvent the problem, a solvent-free system was

Scheme 66. Alkene Photooxidation in Flow in Solvent-Free Conditions

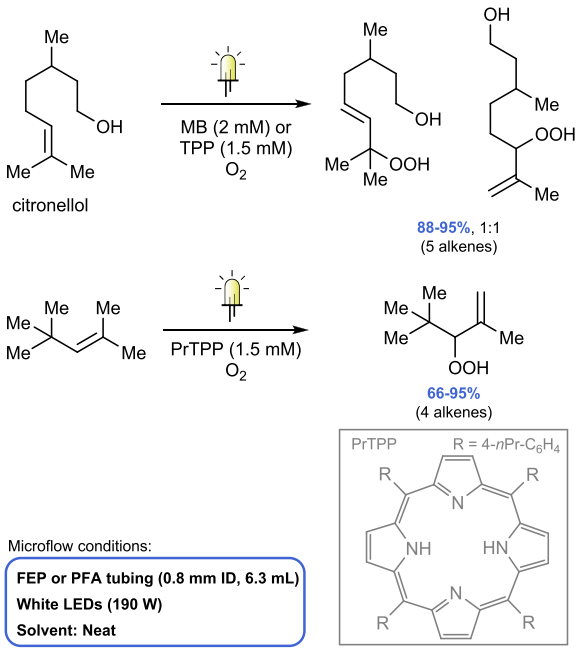

reported for the photooxidation of alkenes, which undergo $^1O_2$-ene reactions to form peroxides. The reactor design, a FEP or PFA coil (0.8 mm ID, 6.3 mL volume) irradiated with 190 W white LEDs, was based on a previous report.[460] Once more, the photosensitizers of choice were either MB or TPP, and when evaluated with a set of alkenes both gave high STY values (950−4600 $g{\cdot}L^{-1}{\cdot}h^{-1}$). Because of the poor solubility of commercially available organic dyes, especially in apolar substrates, a propyl-TPP (PrTPP) photocatalyst was developed and successfully employed, with STY between 300 and 850 $g{\cdot}L^{-1}{\cdot}h^{-1}$.

Another problem when performing oxidations mediated by singlet oxygen is its poor solubility in other organic solvents, which is generally overcome in flow due the increased mass transfer due to Taylor recirculation patterns. Another option is to use supercritical CO_2 ($scCO_2$) and liquid CO_2 ($liqCO_2$), which not only have the advantages to be nonflammable and nontoxic, but also offer better oxygen solubility. Moreover, singlet oxygen even has a longer lifetime in $scCO_2$ (5.1 ms at 147 bar and 41 °C), compared to organic solvents (230 μs in CD_3OD).[499] For these reasons, George, Poliakoff, and coworkers reported the photooxidation of cyclopentadiene in $scCO_2$/$liqCO_2$ in continuous-flow (Scheme 67A).[500] Once

Scheme 67. (A) Photooxidation of Cyclopentadiene in Flow Using liqCO2 and scCO2 as Solvents in Flow and (B) Photooxidation of Fulvene in the Same Reactor Setup

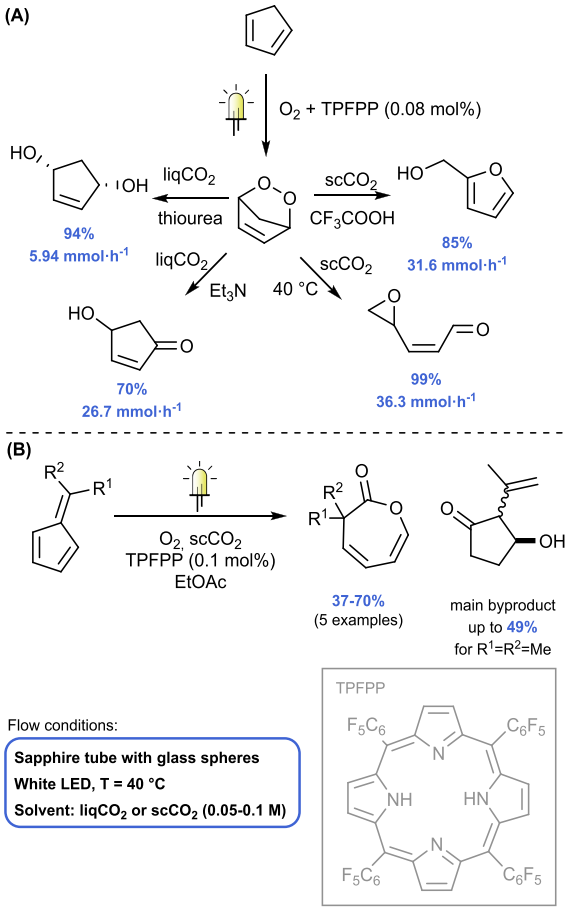

more, the photosensitizer was a porphyrin derivative, that is, 5,10,15,20-tetrakis(pentafluorophenyl)porphyrin (TPFPP). The endoperoxide intermediate, undergoes other thermal transformations in flow, being selectively transformed into various oxygenated products (Scheme 67A). The reactor designinvolves two static mixers placed in series, followed by the photoreactor and a thermal reactor. Oxygen and CO_2 are pumped through the first static mixer, consisting of a stainless-steel tube filled with sand, before being combined and mixed with cyclopentadiene in the second one. The photoreactor itself is a high-pressure sapphire tube (8 mm ID, 12 cm length) filled with 6 mm glass spheres and irradiated by LEDs. After

https://doi.org/10.1021/acs.chemrev.1c00332
Chem. Rev. 2022, 122, 2752−2906

the photoreactor, the flow was directed to a thermal flow reactor for further derivatization of the endoperoxide. With this reactor design, a number of derivatives were prepared in good to excellent yields (70−99%) and appreciable productivities (5.94−36.3 mmol·h^{-1}). The same reactor design system was also employed in the continuous-flow photooxidation of fulvenes in $scCO_2$ (Scheme 67B).[501] In this case, the selectivity to the desired lactone was improved by adding ethyl acetate as a cosolvent.

Considering the increasing applications of flow techniques to access bioactive molecules,[118] it is not surprising that the cyclopentadiene photooxidation was explored also by researchers at Pfizer and Syncom.[502] The photooxidation was used as the first step in the synthesis toward (1*R*,4*S*)-4-hydroxycyclopent-2-en-1-yl acetate, an important building block for prostaglandin synthesis.[503] The flow reactor consisted of a PFA capillary (1.6 mm ID, 9 mL volume) coiled around a Drechsel bottle and was irradiated with green LEDs (530 nm). The endoperoxide intermediate was directly quenched in batch with thiourea to the corresponding diol. Using half the amount of the solvent used in batch and with only 3 min residence time, up to 8.6 g of diol per hour were obtained. The productivity was further increased to 1 kg·day^{-1} with a five times longer coil and extra lamp power. After acetylation of the diol, the enzymatic desymmetrization was performed, affording the final chiral product in good yield and excellent enantioselectivity (Scheme 68).

Scheme 68. Multistep Synthesis of (1*R*,4*S*)-4-Hydroxycyclopent-2-en-1-yl Acetate Starting from the Photooxidation of Cyclopentadiene in Continuous Flow

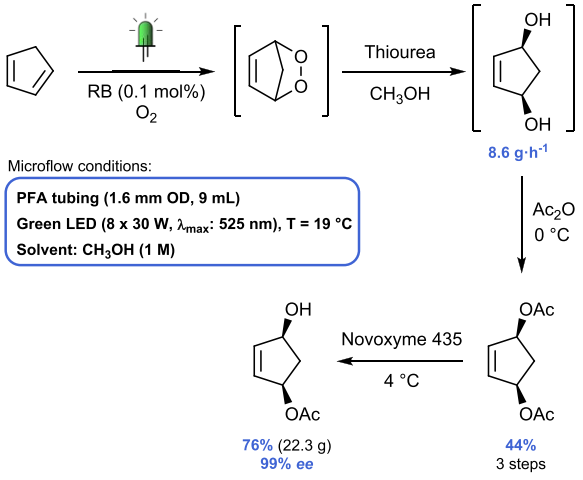

A TPP photosensitizer was also used in combination with cinchona alkaloids as a phase transfer catalyst (PTC) to catalyze the enantioselective photooxidation of dicarbonyl compounds (Scheme 69).[504] This example showcases the feasibility of merging enantioselective synthesis and flow techniques.[505] Because of the biphasic nature of the medium (water/toluene), the two solvents were premixed in a first reactor and then pumped together with oxygen through the photoreactor (a commercially available Corning AFR), irradiated by 20 W white LEDs. Reaction conditions were adapted when moving from batch to flow. For instance, the low temperatures (−15 °C) and the concentrated base (50% K_2HOP_4) used in batch led to clogging issues and could damage the microflow reactor. For this reason, the basic

Scheme 69. Enantioselective Photooxidation of β-Dicarbonylic Compounds in Flow with TPP and a Cinchona Alkaloid As Phase-Transfer Catalyst

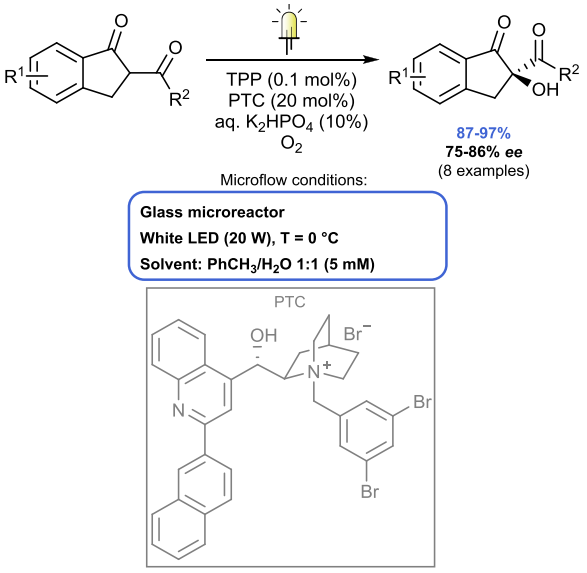

solution was diluted to 10%, and the temperature was raised to 0 °C to obtain homogeneous reaction conditions, without major decrease of the enantioselectivity of the transformation. Moreover, the reaction time was reduced, from 8 h in batch to 54 s in flow. Almost simultaneously, similar results were obtained in another report on the enantioselective photooxidation of carbonyl compounds. In this case, reactions were performed without TPP and under blue LED irradiation.[506] The authors claim that the blue LEDs directly excite the triplet oxygen, without the need of a photosensitizer. However, longer residence times were required (∼1 h).

"Tube-in-tube" reactors contain a gas-permeable membrane to supply gas to the reaction mixture.[507,508] These type of reactors have also been used to supply O_2 for photooxidation reactions.

Researchers at EcoSynth NV described the oxidation of 3-(2-furyl)propanoate in a homogeneous flow regime (Scheme 70).[509] After some positive preliminary results in microcapillary membrane reactors,[51,510,511] a larger-scale setup was tested. To supply oxygen, a reverse tube-in-tube reactor was chosen.[512] This means that the liquid phase is recirculated in the outer tube, enabling better temperature control of the

Scheme 70. Methylene Blue Photocatalyzed Oxidation of Ethyl 3-(2-Furyl)propanoate in a Microflow Reactor in a Gas−Liquid Membrane Reactor

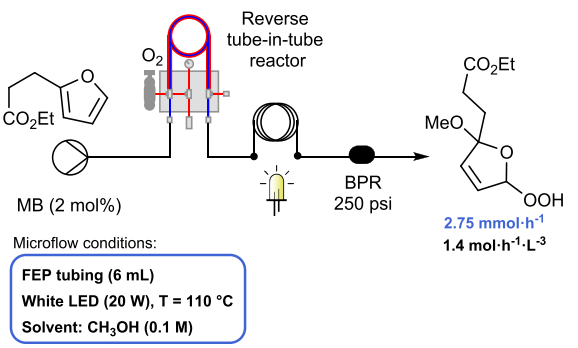

https://doi.org/10.1021/acs.chemrev.1c00332
Chem. Rev. 2022, 122, 2752−2906

reaction mixture, and the gas is supplied via the inner tube. The so-formed homogeneous solution is then irradiated with white 20 W LEDs. Accurate oxygen supply relies on three main factors: (i) membrane temperature, (ii) oxygen pressure, and (iii) liquid flow rate, which influences the residence time, so the oxygen uptake.[512] Controlling these three parameters, it was possible to calculate the O_2 concentration (50 mM) in CH_3OH at 110 °C and with a flow rate of 1 mL·min^{-1}. Homogeneous reaction conditions could be achieved at such high temperatures owing to the back-pressure regulator (BPR: 250 psi or ∼17 bar) and the high pressure of the oxygen supply. With this approach, more controllable conditions and thus more reproduceable outputs were obtained, compared to a biphasic system. The calculated productivity reached up to 2.75 mmol·h^{-1} with a STY of 1.4 mol·L^{-1}·h^{-3} and the product was isolated in 90% yield after further optimization (5 min residence time and 70 °C). Other substrates such as a sulfide, an amine, α-terpinene, and citronellol were easily oxidized in the system with some modifications (e.g., residence time, photosensitizer). Surprisingly, under heterogeneous gas−liquid conditions, conversion was generally lower.

De Souza et al. described the TPP-photocatalyzed oxidation of (*R*)-limonene in flow (Scheme 71).[513] The hydroperoxide

Scheme 71. (R)-Limonene Photooxidation in Flow Using a Tube-in-Tube Reactor in the Presence of TPP

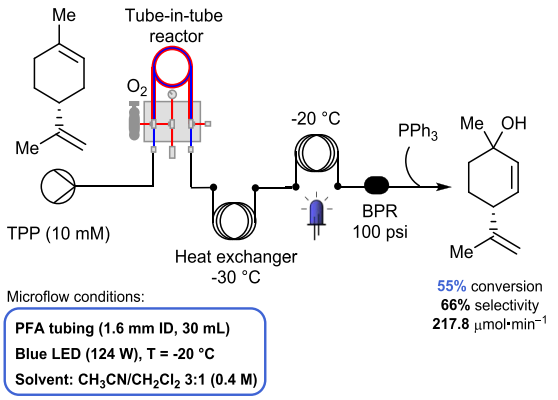

derived from the photooxidation is directly reduced with PPh_3 to afford a chiral alcohol which is an important cannabinoid precursor. A solvent mixture of acetonitrile and dichloromethane was used to maximize the solubility of oxygen and the lifetime of $^1O_2$. Initial optimization was performed in a small flow reactor (0.5 mm ID, 1 mL volume) irradiated with blue LEDs (124 W). In a larger reactor (1.6 mm ID, 30 mL volume), productivity was increased to 491.6 μmol·min^{-1} with 7.5 min residence time, compared to 14.6 μmol·min^{-1} in the smaller reactor, with constant selectivity (48%). Selectivity increased to 66% when performing the photooxidation at −20 °C but led to lower conversion (55%) and a decrease in productivity (217.8 μmol·min^{-1}).

Continuous-flow techniques also allowed for safe endoperoxidation of differently substituted dienes with successive Kornblum−DeLaMare (KDM)[514−516] rearrangement (Scheme 72).[517] The setup involved a gas−liquid flow reactor in a semipermeable Teflon AF-2400 membrane (tube-in-tube) and a homemade photochemical reactor (PFA capillary: 1.6 mm ID, 23 mL volume). The photooxidation and the KDM rearrangement were separated into two consecutive steps, because the base, which is necessary for the KDM rearrangement, quenched the photoexcitation state of the photosensitizer (TPP). Starting from cyclooctadiene, the endoperoxidation in flow resulted in 62% yield in 46 min residence time and a productivity of 8.2 g·day^{-1}. The KDM rearrangement was first performed in a 0.25 mL microchip at 140 °C (84% yield) and then in a 16 mL stainless-steel/PFA reactor at 60 °C (90% yield). When the photooxidation and rearrangement were telescoped, either DBU or Et_3N was used for the second step. With an in-line acid workup at 0 °C, the KDM keto-alcohol intermediate afforded furans, whereas at higher temperatures the more stable 1,4-dicarbonyl compounds could be obtained *via* an additional proton rearrangement.

Scheme 72. Photocatalytic Endoperoxidation of Dienes Followed by Kornblum−DeLaMare (KDM) Rearrangement in Flow

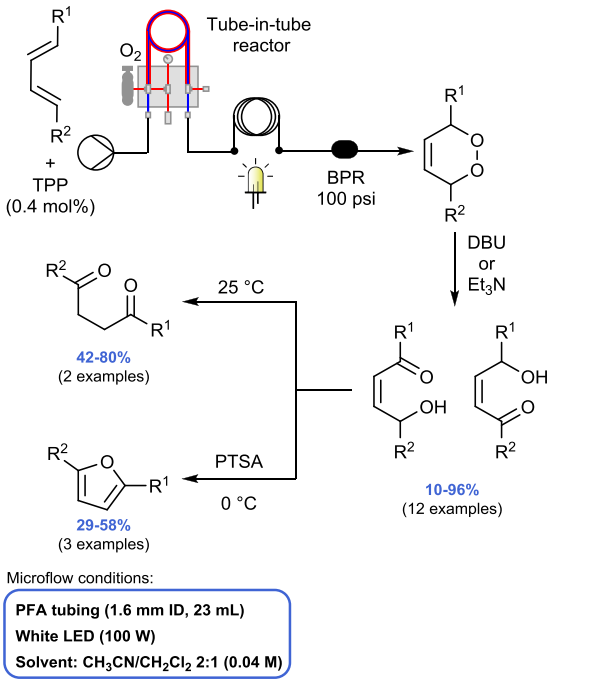

Von Wangelin et al. reported the photocatalytic oxidation of aryl cyclohexenes in flow (Scheme 73).[518] Aryl cyclohexenes constitute a very interesting class of substrates, as the benzylic position can be oxidized; although, the reaction is often plagued with selectivity issues. The FEP reactor (0.79 mm ID, 6.3 mL) was irradiated with 24 water-cooled high-power red LEDs (1.7 W) and equipped with a 12 bar BPR to increase oxygen solubility. The photooxidation works through a $^1O_2$-ene reaction and afforded allyl hydroperoxides. Mechanistic investigations including Hammett studies and DFT calculations corroborated the contribution of a zwitterionic intermediate in the mechanism. Other byproducts were observed and sometimes isolated, especially endoperoxides originating from [4 + 2] cycloaddition or 1,6-dicarbonyl compounds deriving from [2 + 2] cycloaddition. The allyl hydroperoxides could be reduced in more stable allylic alcohols or transformed into α,β-epoxy alcohols.

Singlet oxygen oxidation was also performed in flow to increase the productivity of artemisinin, a powerful antimalaria compound, derived from *Artemisia annua* plants.[519] In fact, because the plant contains only 1% of artemisinin and its total synthesis is not convenient, the authors suggested a semitotal synthesis starting from another compound present in the same

https://doi.org/10.1021/acs.chemrev.1c00332
Chem. Rev. 2022, 122, 2752−2906

Scheme 73. Photocatalytic $^1O_2$-ene Reaction of 1-Aryl-1-cyclohexenes in Flow

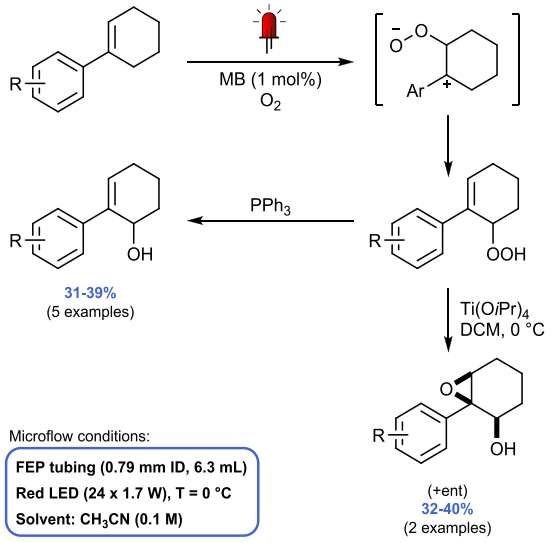

plant, that is, dihydroartemisinic acid (DHAA). In flow, DHAA reacts with $^1O_2$ to form a peroxide through a Schenck ene reaction to form artemisinin in the presence of a dye, either TPP or 9,10-dicyanoanthracene (DCA) (69% yield, 12 min).[488,519] More recently, the crude extract from the plant containing DHAA and chlorophyll was directly used as reaction mixture (Scheme 74).[520] The extraction was

Scheme 74. Artemisinin Synthesis in Flow Starting from *Artemisia annua* Crude Extract

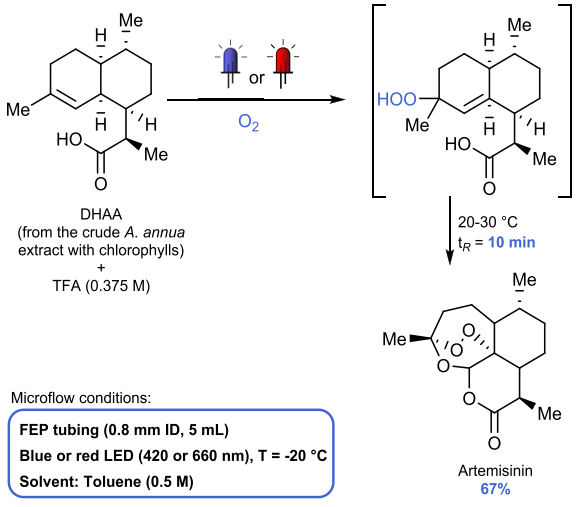

performed with toluene at 50 °C for 10 min. Photoirradiation took place in a 5 mL reactor, after preconditioning in a tube to cool down the reaction mixture to −20 °C. For comparison, the DHAA photooxidation was performed in the presence of isolated chlorophylls and DCA. Pure chlorophylls outperformed DCA in the photooxidation of pure DHAA (83% vs 20% of intermediate), but even better results were obtained with the crude extract. In fact, 90% of the hydroperoxide intermediate was formed in 7 min residence time. When starting from the extract of the chlorophyll sensitizers and DHAA, TFA was added for the intermediate to be transformed into artemisinin in the second reactor loop (residence time of 10 min). With blue LEDs at −20 °C artemisinin was obtained in 67% yield in 5 min (Scheme 74). Using more appropriate red LEDs allowed reduction of the reaction time to 3 min without a significant change in yield (64%), with an STY of 2.1 $kg \cdot L^{-1} \cdot day^{-1}$.

Wipf et al. described the photooxygenation of 4-aminothienopyridones (Scheme 75).[521] After preparation of the

Scheme 75. Photooxidation of Aminothienopyridinones with Singlet Oxygen in Continuous Flow

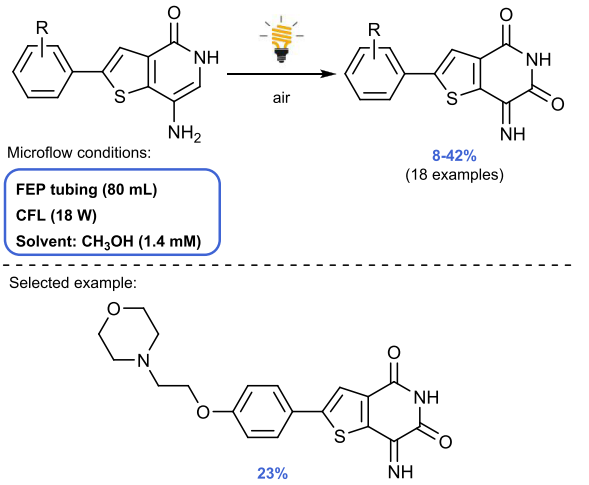

reaction mixture, the mixture was flown through a macroflow photoreactor (FEP tubing, 80 mL) irradiated with an 18 W CFL lamp. In flow, the residence time could significantly be reduced to 42 min residence time, compared to several days in batch. In most of the cases, it was possible to directly access the *N*−H-imines over the ketone. The proposed mechanism begins with an ene-type reaction between the starting material and singlet oxygen, followed by tautomerization and elimination of water. Later, the same group developed a 3D-printed polypropylene photoflow cell (ID 1.5 mm, 2.11 mL) which was successfully employed for the same reaction.[155] With 100 W blue LEDs, the residence time was decreased to 2 min.

In 2021, Wang et al. reported a continuous-flow synthesis of thiuram disulfides, which are functionalities with important industrial applications.[522] Their strategy was based on the eosin Y-mediated photooxidation of the adduct formed between CS_2 and an amine (Scheme 76). Although the authors proposed a mechanism involving the superoxide radical $(O_2)^{-\bullet}$, experiments with diphenylisobenzofuran, which is a singlet oxygen trapping agent, proved that singlet

Scheme 76. Synthesis of Thiuram Disulfides via Visible-Light Photocatalytic Aerobic Oxidation

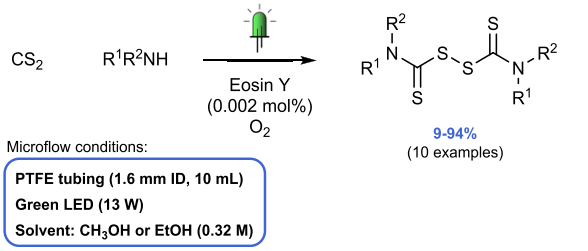

https://doi.org/10.1021/acs.chemrev.1c00332
Chem. Rev. 2022, 122, 2752−2906

Scheme 77. Tandem Photodeprotection and Decarboxylation in Flow, Followed by Azide−Alkyne Click Chemistry

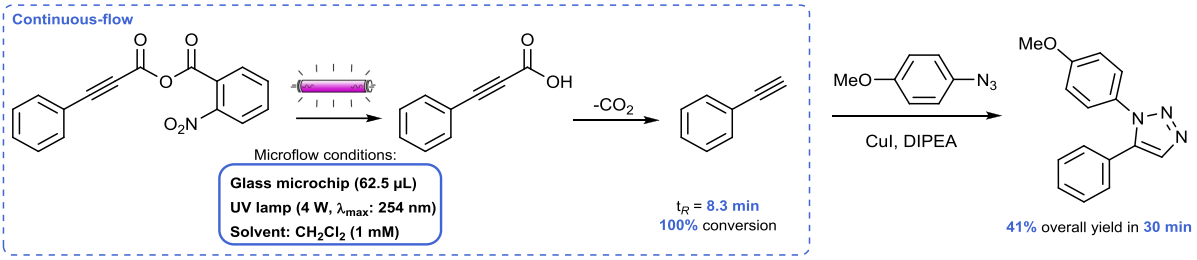

oxygen is involved in the mechanism, as claimed by the authors. However, it is important to note that even though eosin Y is known to be an excellent $^1O_2$ photosensitizer, the ability to generate singlet oxygen and superoxide radical is not mutually exclusive. Moreover, the conditions for the trapping experiment were different from those of the reaction itself, so it is possible that the starting amine is involved in an SET. The PTFE reactor (1.6 mm ID, 10 mL volume) was irradiated by 13 W green LEDs. The residence time was set at 25 min in ethanol and 20 min in methanol. However, in some cases, the low solubility of the product in both alcoholic media required faster flow rates to wash the precipitate away and avoid blockages, at expense of the yield.

The continuous-flow photooxygenation of phenols was described by Sparr et al. to afford benzoquinones in high yields.[523] Methylene blue was used as organic photocatalyst (0.9 mol %) to generate singlet oxygen. Reactions were performed in a PFA capillary coil (4.6 mL volume), irradiated with either 32 W white LEDs with an orange filter or with 9 W hyper red LEDs (660 nm) and were completed in 16−120 min residence time. The developed process was also applicable to naphthols and anilines (18 examples, 60−99% yield). Moreover, the process was employed to obtain *p*-quinols, by directly reducing the hydroperoxide intermediates with sodium thiosulfate.

5.5. Photocleavage and Photodeprotection

Protecting groups have been of invaluable importance in the field of synthetic organic chemistry and especially in the total synthesis of complex biologically active molecules.[524−526] An ideal protecting group should possess two characteristics: (1) to protect a sensitive functional group from undesired reactions during subsequent modifications of the parent molecule, and (2) it should be installed and removed in high yield and selectivity. Photocleavage is an ideal strategy for the deprotection of a functional group as it is often orthogonal to the more traditional thermal- or acid−base-type deprotection strategies.[527]

One example of the on-demand generation of a reactive compound using a photodeprotection strategy was given by Moth-Poulson et al.[528] The authors generated terminal alkynes by a tandem photodeprotection and decarboxylation in flow (Scheme 77). A solution of *ortho*-nitrobenzyl protected arylpropionic acid was subjected to UV-irradiation (4 W, 254 nm) in a quartz-based microchip (62.5 μL) and full conversion was achieved in 8.3 min residence time, to form phenylacetylene in one step. This reactive terminal alkyne was subsequently combined with CuI and azide in a batch reactor to initiate a copper catalyzed azide−alkyne cycloaddition, generating a 1,2,3-triazole in 41% overall yield.

The photochemical generation of thioaldehydes is another example of a reactive compound that was generated through photodeprotection in flow.[529] Phenacyl sulfides were irradiated with UV-light and the resulting highly reactive thioaldehydes were combined with various dienes to carry out a *thio*-Diels−Alder reaction yielding dihydro-thiopyrans in one step (Scheme 78). Using this approach, a wide variety of dihydro-

Scheme 78. *thio*-Diels−Alder Reactions of Photochemically Generated Thioaldehydes in Continuous Flow

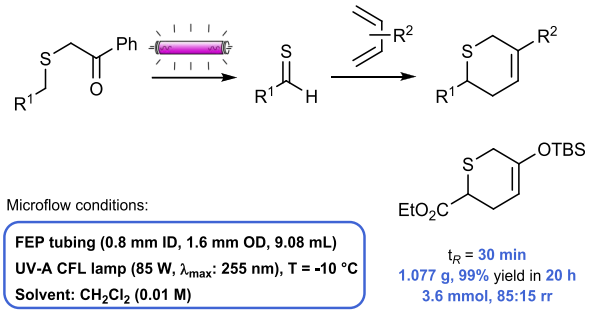

thiopyrans were prepared in generally high yields and good regioselectivities (64−99% for 19 examples). Additionally, a gram-scale reaction of the model substrate could easily be performed by scaling the reaction in flow (1.077 g, 99% yield, 84:16 regioisomeric ratio (rr) over 20 h reaction time). Compared to the batch method, the flow approach significantly improved the use of the highly reactive thioaldehydes, with a 22-fold improvement in productivity and a 60-fold improvement in space time yield (0.18 mmol·h^{-1}, 6.0 g·L^{-1}·h^{-1} in flow, versus 0.0083 mmol·h^{-1}, 0.1 g·L^{-1}·h^{-1} in batch).

A mild photocatalytic protocol was developed for the N-desulfonylation of N-heterocycles (Scheme 79).[530] The selective N−S bond cleavage of a benzene-sulfonyl protected indazole was first performed in batch in the presence of a copper photocatalyst, achieving 92% isolated yield in 24 h.

Scheme 79. Photocatalytic N-Desulfonylation of N-Heterocycles

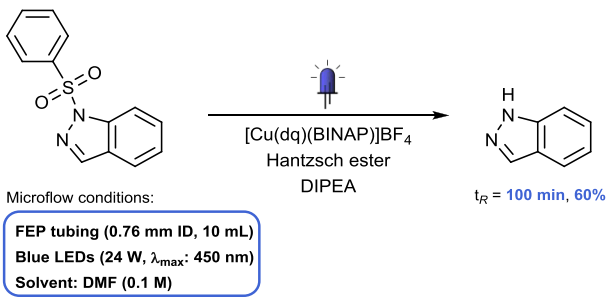

https://doi.org/10.1021/acs.chemrev.1c00332
Chem. Rev. 2022, 122, 2752−2906

Control experiments showed that both light and photocatalyst were required to perform the transformation. Additionally, improved results were obtained in the presence of Hantzsch ester and base. These optimized conditions were applied to a variety of indazoles, indoles, pyrazoles, and benzimidazoles with electron-donating and electron-withdrawing functional groups. Finally, the scale-up potential of the protocol was shown by performing the *N*-desulfonylation of the model indazole substrate in flow. A commercially available reactor (Vapourtec UV-150: 0.76 mm ID, 10 mL volume) was used and the reaction mixture was irradiated with 24 W blue LEDs (450 nm), achieving 60% yield in 100 min residence time.

The photochemical cleavage of C−O bonds in lignin systems could provide an easy route to benzylic alcohols and ketones as a biomass-valorization strategy from currently discarded plant materials. Within lignin systems, the β-O-4 linkage is one of the main connections and is thus an interesting target for cleavage in lignin depolymerization studies. Stephenson et al. developed a two-step procedure for the cleavage of β-O-4 linkages via catalytic oxidation and photocatalytic reduction in batch and in flow (Scheme 80).[531]

Scheme 80. Photocleavage of the β-O-4 Bond in Lignin Models under Blue LED or Solar Irradiation

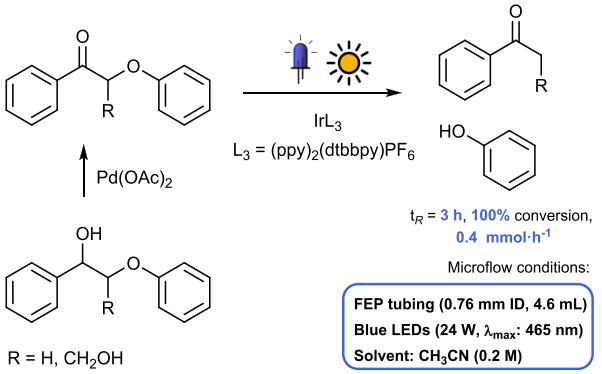

The palladium-catalyzed oxidation was first performed with various lignin model substrates, rendering the corresponding unsymmetrical ketones. After a workup procedure to enable a solvent switch, the crude mixture of the oxidation step was irradiated with blue LEDs in the presence of an iridium catalyst to achieve complete conversion for the β-O-4 cleavage in batch after 32 h. The photocleavage was subsequently translated to a flow protocol, resulting in a significant increase in productivity (0.4 mmol·h^{-1} in flow vs 0.013 mmol·h^{-1} in batch), exemplifying the practical utility of the flow procedure for large-scale operation. However, flow reactors generally require homogeneous reaction conditions and due to the low solubility of lignin polymers, the β-O-4 cleavage studies of these polymers were performed in batch. Different lignin polymers were subjected to the cleavage procedure under blue LED or solar irradiation and comparable yields were obtained for both, further adding to the potential greenness of the protocol.

After initial work of Seeberger et al. on the use of photolabile groups as linkers for solid phase synthesis of saccharides,[532] more publications appeared to either exploit this technology,[533−538] or to improve the photocleavage method.[539,540] Additionally, a commercially available instrument for the automated glycan assembly was developed.[541]

One approach for increasing the efficiency of the photocleavage method was proposed by Hurevich et al.,[539] who found that grinding of the porous polystyrene beads to expose more surface area to the irradiation significantly improved the photocleavage efficiency. The grinding was performed either by a magnetic stirrer or by using a shaker, prior to or while being subjected to UV-LED irradiation in a batch reactor. A higher degree of photocleavage was observed at higher stirring rates, with more than 80% of material cleaved at 1060 rpm after 6 h irradiation time.

Alternatively, a flow platform was created by Gilmour et al. for the photocleavage of glycans from their solid support (Scheme 81).[540] The platform contained a reaction unit with

Scheme 81. Photocleavage of a Polysaccharide from a Solid Support under Blue LED Irradiation in Continuous Flow

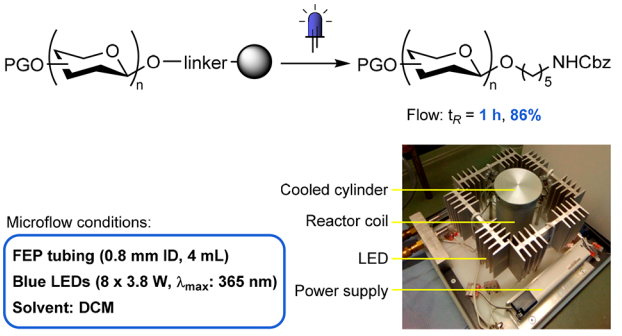

Reprinted with permission from ref 540. Copyright 2020 American Chemical Society.

FEP capillary (0.8 mm ID, 4 mL) coiled around a water-cooled cylinder, which was irradiated with eight LEDs (2−3.8 W at 750 mA, 365 nm). Using this setup, 79% photocleavage from the resin was obtained after 1 h irradiation time. A slight increase in photocleavage was observed when pregrinding the beads (86%). Importantly, the reproducibility of the flow protocol was shown by duplicating several experiments, with a maximum discrepancy of 5% between individual experiments with the same conditions.

Another important consideration in the synthesis of polysaccharides is the protection of hydroxyl groups. Potential protecting groups for these hydroxyl groups are benzyl ethers, which because of their inherent stability, can be applied to a wide range of different reaction conditions. However, harsh conditions are typically required for their removal. A mild photocatalytic method for the deprotection of benzyl ethers from saccharides was developed by Pieber, Seeberger, and coworkers (Scheme 82).[542] Reactions were first performed in batch and required 1−17 h to reach reaction completion for substrates carrying various other protecting groups. Most of these other protecting groups were compatible with the reaction conditions, including fluorenylmethoxycarbonyl, levulinic ester, allyl carbonate, and benzylidene, whereas benzyloxycarbonyl was partially cleaved leading to lower yields. In batch, switching from a green to a blue LED light source resulted in shorter reaction times, but significantly higher overoxidation and photodegradation was observed. In contrast, the precise control over the reaction time and more efficient irradiation in flow allowed for the intensification of the reaction conditions with blue LEDs, while maintaining high

https://doi.org/10.1021/acs.chemrev.1c00332
Chem. Rev. 2022, 122, 2752−2906

Scheme 82. Mild and Selective Photodeprotection of Benzyl Ethers from Saccharides in Batch and Flow

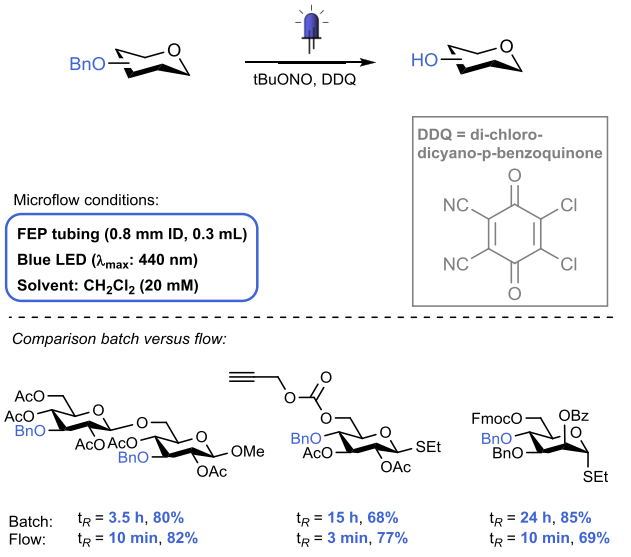

selectivities (batch = 68−85% yield in 3.5−24 h, flow = 69−82% in 3−10 min).

The continuous-flow photocleavage of a phthalimide group from a glucose derivative enabled the total synthesis of the polyhydroxy amino acid (+)-polyoxamic acid (Scheme 83).[543] The photocleavage generates an alkoxy radical, which, via β-scission, transforms into a more stable carbon radical. Finally, upon 1,5-hydrogen atom transfer and subsequent trapping of the benzyl cation with the unprotected OH-group, the desired benzylidene acetal is generated. The reaction was first optimized in batch to reach 63% yield after 24 h reaction time. In flow, the same yield was obtained in only 1 h residence time. In addition, the flow protocol enabled reduced catalyst loadings (5−2 mol %) and sufficient quantities of the benzylidene acetal could be generated to perform downstream reactions toward (+)-polyoxamic acid.

Scheme 83. Phthalimide Photocleavage Initiates a Radical Cascade to Benzylidene Acetal in the Total Synthesis of (+)-Polyoxamic Acid

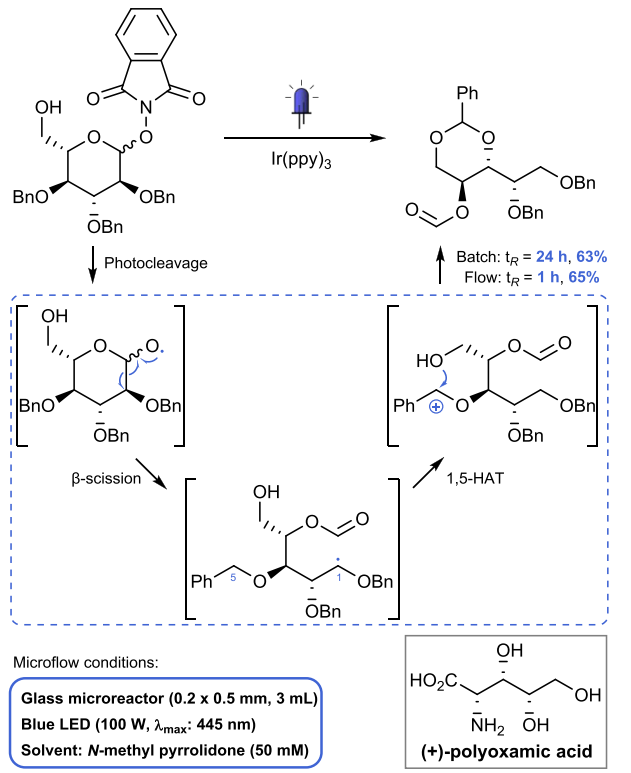

A multistep flow process for the synthesis of methylphenidate was developed by Monbaliu et al.,[544] based on either an intramolecular or an intermolecular mechanism. The intramolecular method with a tosyl deprotection and subsequent β-lactam ring formation step performed best under thermal conditions with 98% isolated yield in 5 min residence time at 180 °C, but was shown to also be feasible using a flow photochemical method (Scheme 84). In the photodeprotection, 97% conversion of tosyl hydrazone was obtained after 1 h under UV-A irradiation. An in-line workup was developed and direct methanolysis under acidic conditions provided methylphenidate hydrochloride in a telescoped process.

Scheme 84. Tosyl Hydrazone Deprotection and β-Lactam Ring Formation in the Synthesis of Methylphenidate Hydrochloride[a]

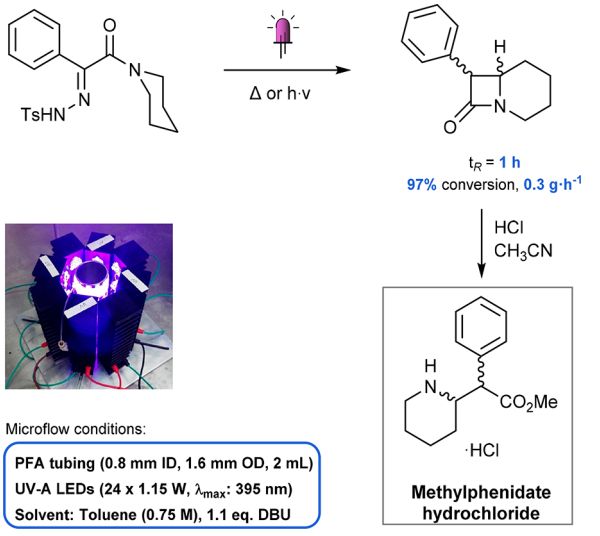

[a]Reprinted with permission from ref 544. Copyright 2017 Royal Society of Chemistry.

5.6. (De)Halogenation

5.6.1. Fluorination. Fluorine is characterized by the highest electronegativity of the periodic table. For this reason, material and medicinal chemists employ this element to modulate the lipophilicity and the bioavailability of new drugs[545] and tune the properties of polymers.[546,547] While keeping in mind the effects of fluorine on the environment and on human health,[548] it is important to develop newer and greener (de)fluorination methods, as well as fluoroalkylation procedures,[549] especially based on a late-stage functionalization approach.[550,551] Photochemistry can be considered to be a key strategy in this scenario.[552−554] Moreover, the combination of flow technology and fluorine chemistry opens up opportunities to easier and faster automation, as ^{19}F is ideal for rapid NMR analyses. This attribute was exploited by Rehm et al. to develop

https://doi.org/10.1021/acs.chemrev.1c00332
Chem. Rev. 2022, 122, 2752−2906

a continuous-flow synthesis lab plant and was combined with benchtop NMR spectroscopy for fluorinated molecules.[555]

Selectfluor is one of the most common reagents for electrophilic fluorination.[556−558] Lectka et al. used it to perform the selective photosensitized enone-directed β- and γ-fluorination of C(sp^3)−H bonds (Scheme 85).[559] Notably, in

Scheme 85. Terpenoidal-enone-Driven Sensitized Fluorination in Flow

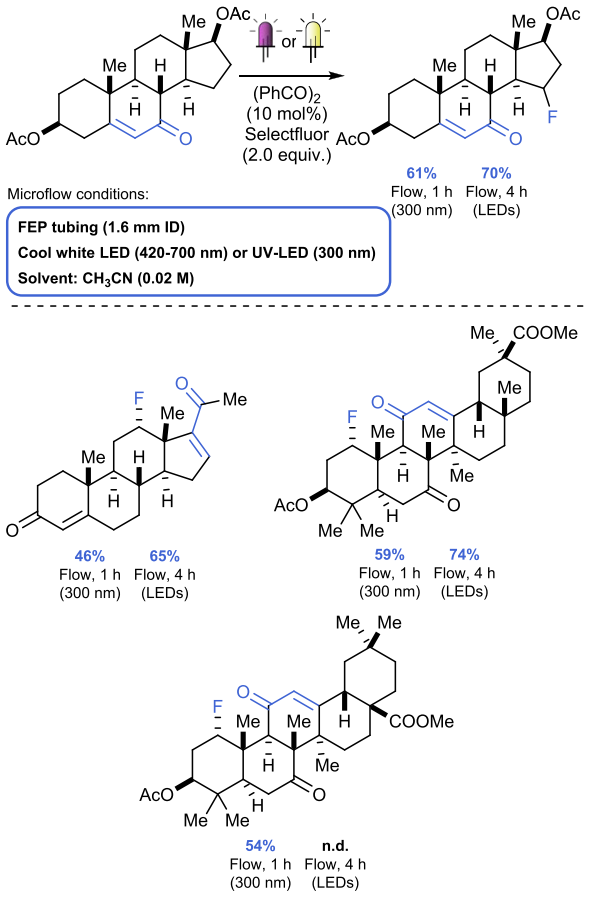

the set of steroidal substrates, the selectivity relied solely on the enone functionality, which guides the fluorination. The same group had already reported this reaction using a Rayonet reactor.[560] The addition of benzil as a photosensitizer improved yields to 94% and allowed the reaction to proceed with less energetic cool white LEDs (420−700 nm). However, the exact role of the benzil could not be established, and an electron-transfer mechanism could not be ruled out. When a continuous-flow reactor (FEP tubing, 1.6 mm ID, irradiated with six white LEDs) was employed, the residence time was reduced to 4 h, compared to that of batch, which required 14 h reaction time. When the FEP tubing was irradiated in a Rayonet reactor (300 nm), the residence time was further decreased to 1 h.

The decarboxylative fluorination of aryloxy acetic acids was performed by Seeberger, Gilmour, and co-workers by employing Selectfluor in a segmented flow regime (Scheme 86).[561] The segmented flow regime allows to handle solid materials, liquids, and even gases in a continuous-flow (photo)reactor, effectively avoiding issues with the settling and thus clogging of the heterogeneous catalyst (in this case, a modified carbon nitride: CMB-C_3N_4).[562] The use of segmented flow in a serial

Scheme 86. (A) Schematic Representation of the Use of Segmented Flow Regime to Avoid Clogging and (B) Photocatalytic Decarboxylative Fluorination in a Segmented Flow Regime

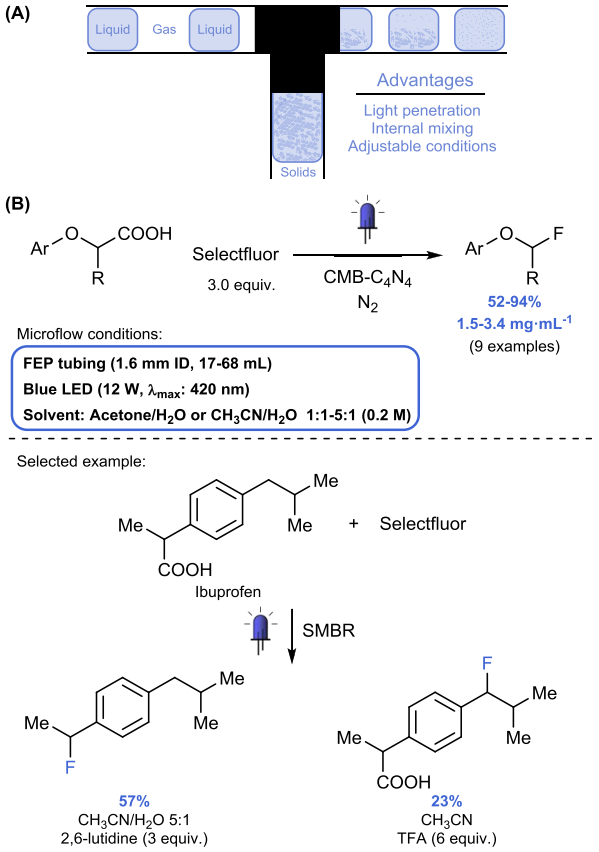

microbatch reactor (SMBR) represents an interesting alternative to (i) packed-bed reactors, which are not always suitable because of the impenetrability by light and (ii) pumping a suspension, which results in settling of the photocatalyst, clogging, and issues with reproducibility of results. In the segmented flow regime, the catalyst suspension is mixed using a T-connection with an inert gas which ensures the formation of different segments in which toroidal fluid currents are established which keep the heterogeneous photocatalysts in suspension (Scheme 86A). In their work, the CMB-C_3N_4 photocatalyst was suspended in 1-butyl-3-methylimidazolium tetrafluoroborate ([Bmim]BF_4·H_2O). The photoreactor consists of a PFA coil (1.6 mm ID, 17−68 mL volume) irradiated with blue LEDs (12 W, 420 nm). The fluorinated products were obtained in moderate to high yields (31−80%), with residence times varying between 14 and 24 min. No purification was necessary, and a three-step extraction allowed for the recovery of the ionic liquid and the catalyst. In a larger scale reaction, when starting from 16 mmol of phenoxyacetic acid, 90% of the fluorinated product was obtained within 6.5 h of total operational time (t_R = 16 min). The procedure was successfully applied to the fluorination of ibuprofen (Scheme 86B). Notably, besides the decarboxylative fluorination, it was possible to change the selectivity of the fluorination to the benzylic position by switching from basic to acid conditions.

Deoxyfluorinating agents, such as DAST (diethylaminosulfur trifluoride), are known for their drawbacks, such as toxicity and explosivity.[563] In contrast, SF_6 is a rather inert and cheap gas,

https://doi.org/10.1021/acs.chemrev.1c00332
Chem. Rev. 2022, 122, 2752−2906

and its application in organic synthesis is underexplored. Jamison et al. reported a photocatalytic activation of SF_6 and used it for the deoxyfluorination of allylic alcohols in flow (Scheme 87).[564] The continuous-flow system consisted of a

Scheme 87. Photocatalytic Deoxyfluorination of Allylic Alcohols with SF_6 in Flow

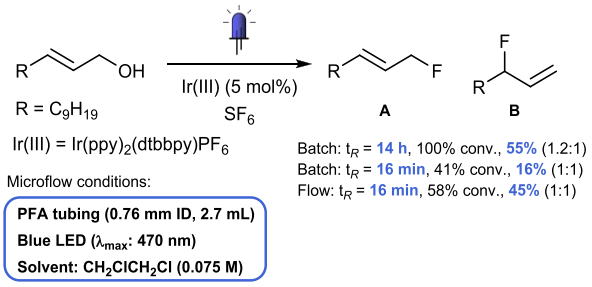

"pre-reactor" where the liquid and gas phase were mixed before entering the photoreactor. As a light source, blue LEDs (470 nm) were employed. The photoreactor, equipped with a back-pressure regulator, allowed to use high pressures (100 psi, 6.9 bar) in a safe way. This also enabled solubilizing the gas into the liquid phase. The productivity was increased, from 0.04 mmol·h^{-1} in batch (t = 4 h) to 0.19 mmol·h^{-1} in flow (t_R = 16 min). In flow, the starting material was transformed within 2 min into a mixture of the product and an intermediate (most likely $(RO)_2SF_4$) which is slowly converted back to the starting material. Consequently, the reaction in flow is more selective while affording both higher yields and conversion ratios.

Nagorny et al. used SF_6 to generate glycosyl fluorides through a photocatalytic deoxyfluorination.[565] The method was based on the use of 4,4′-dimethoxybenzophenone as the photocatalyst which is excited through irradiation with UV-A LED (λ_{max} = 365 nm). The scale-up of the reaction was performed in a PTFE flow reactor with pressurized SF_6 (100 psi, 6.9 bar). The residence time was 8.5 h, instead of 20 h in batch. The 0.033 M solution in dichloroethane was recirculated in the reactor for 120 h, to finally afford 7.2 g of the glycosyl fluoride product, resulting in a yield of 93%.

5.6.1.1. Fluoroalkylation. Photochemistry is an important alternative to classic transition metal catalysis to successfully realize trifluoromethylation and fluoroalkylation reactions.[566,567] Light-induced perfluoroalkyl radical (R_F = C_nF_{2n+1}, $n \geq 1$) generation can occur via either photocatalysis or photoexcitation of an electron donor−acceptor (EDA) complex formed in situ.[568] As amply demonstrated in this review, flow technology boosts the potential of photochemistry, especially in terms of reaction rate.

To elucidate the trifluoromethylation mechanism of trifluoromethylation in flow, Noël et al. investigated on the reaction between *N*-methyl pyrrole and gaseous CF_3I (Scheme 88).[72,569−571] The organic solution containing $Ru(bpy)_3Cl_2$, the heterocycle and a base (TMEDA) was pumped through a PFA capillary (0.75 mm ID, 0.93 mL volume) irradiated with blue LED light (3.12 W). The reaction resulted in a pseudo-zeroth-order for CF_3I and first order for the *N*-methyl pyrrole. Stern−Volmer kinetic analysis determined that TMEDA was the most effective quencher of the excited Ru(II) complex. This was an indication that the photocatalyst was more likely to undergo a reductive quenching rather than an oxidative one by CF_3I. Combining the photoreactor with an inline UV−vis

Scheme 88. Trifluoromethylation of *N*-Methyl Pyrrole and Mechanistic Elucidation

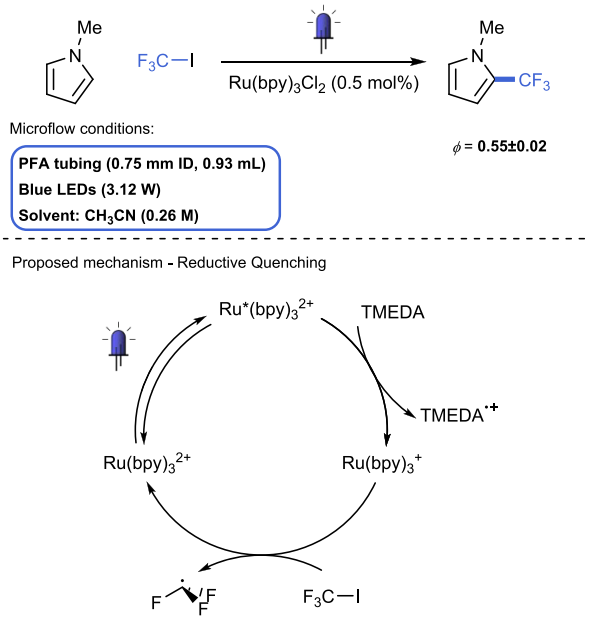

spectrophotometer, the photon flux could be measured (1.57 × 10^{-7} einstein·s^{-1}), while the calculated quantum yield was Φ = 0.55 ± 0.02 indicating that a chain reaction mechanism could be ruled out. The yield was strongly dependent on the photon flux, as demonstrated by changing the power input of the blue LEDs. The efficiency of the reaction also depended on the photocatalyst concentration, with a maximum yield afforded at 0.5 mol %. Higher catalyst loading can lead to self-quenching, low solubility, and higher attenuation effects (nonhomogeneous irradiation), leading to reduced yield.

The fluoroalkylation of heterocycles was also reported in another work by Carrillo, Noël et al., who described a series of bithiophene (BTP) derivatives as new organic photocatalysts (Scheme 89).[572] At first, a priori time-dependent density functional theory (TD-DFT) studies were performed to predict which derivatives would have the most interesting properties (absorption and emission maximum, redox potential). Finally, based on the obtained results, six of these BTP derivatives were synthesized and tested in C−H functionalization of heteroarenes with bromo malonate (Scheme 89A). Using a microcapillary flow reactor in PFA (0.76 mm ID, 2.5 mL volume) irradiated with 400 nm purple LEDs, the best result was obtained with BTP **A** (absorption maximum = 390 nm, $E_{1/2}^{ox}$ = 1.34 V vs SCE). The desired product was obtained in 70% yield after purification, in only 7 min residence time, compared to 5 h in batch. Similarly, the trifluoromethylation and difluoroalkylation were successfully accomplished (Scheme 89B) in a commercial reactor (FEP capillary, 1.33 mm ID, 5 mL volume) irradiated with 460 nm LEDs. Mechanistic studies demonstrated that this class of photocatalyst can be quenched both through an oxidative and a reductive pathway.

Gaseous CF_3I was also used by Noël et al. for the photocatalytic trifluoromethylation and hydrotrifluoromethylation of styrene derivatives (Scheme 90).[573] The microflow reactor consisted of a high purity PFA capillary (0.5 mm ID, 1.25 mL) irradiated with either blue LEDs (3.12 W) or a 24 W CFL, for the trifluoromethylation and hydrotrifluoromethyla-

https://doi.org/10.1021/acs.chemrev.1c00332
Chem. Rev. 2022, 122, 2752−2906

Scheme 89. (A) BTP Derivative Photocatalytic C−H Functionalization of Heteroarenes with Bromomalonate and (B) C−H Fluoroalkylation

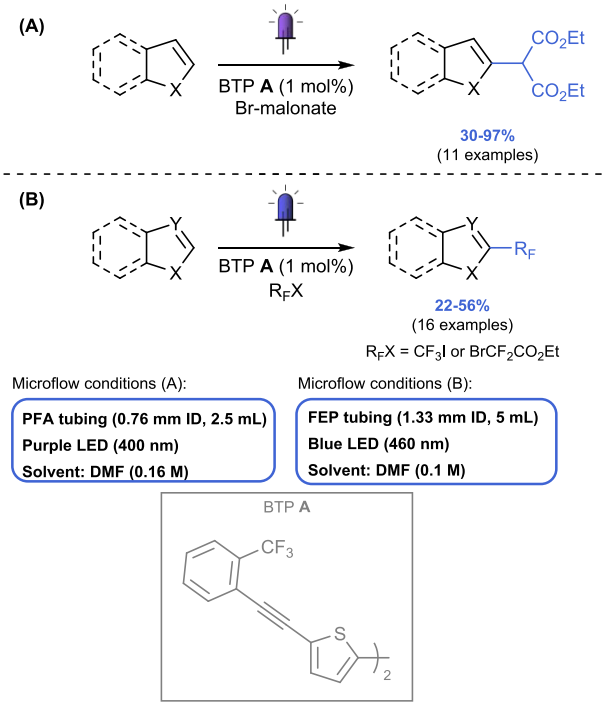

Scheme 90. (A) Photocatalytic Trifluoromethylation and (B) Hydrotrifluoromethylation of Styrene Derivatives in Batch and in Flow

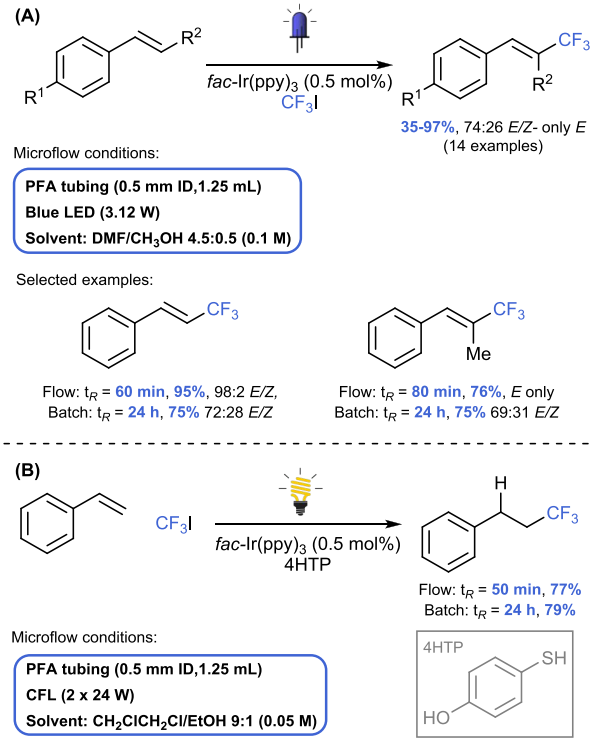

tion respectively. With translation to continuous-flow, the reaction time was reduced from 24 to 72 h to a maximum of 90 min and was accompanied by an increased *E*/*Z* selectivity (Scheme 90A). Notably, it was possible to minimize or completely avoid an unwanted energy transfer occurring during irradiation which caused the isomerization from the thermodynamically more stable *E*-diastereoisomer to the *Z* one. The hydrotrifluoromethylation was also achieved in the same system, just by the addition of 4-hydroxythiophenol (4HTP) as hydrogen atom donor (Scheme 90B).

R_FI compounds were employed by Kappe et al. to perform a light-induced atom-transfer radical addition (ATRA) reaction in flow (Scheme 91).[574] A commercial photoreactor (Corning

Scheme 91. Photoinduced Iodoperfluoroalkylation of Alkenes and Alkynes in Continuous Flow Resulting in an ATRA Reaction

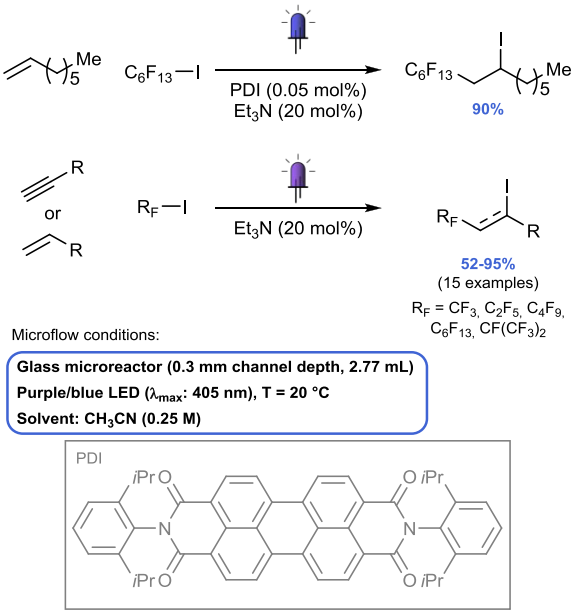

AFR, 2.8 mL volume) was used. Two procedures were employed based either on PDI photocatalysis via blue light irradiation (450 nm), or on the formation of a halogen-bonded electron donor−acceptor (EDA) complex between perfluoroalkyl iodide and Et_3N. In the latter case, the EDA complex requires higher energy for its photoactivation (405 nm). The residence time was generally set at 5 min, although some substrates required longer time to reach full conversion (up to 20 min). Notably, when compared to the 4 h required in batch, reactions went to completion in 5 min in continuous-flow.[575] The photocatalyst-free method afforded the product in a higher productivity (7.6 vs 6.1 $g \cdot h^{-1}$), so it was employed for the scope evaluation. However, the PDI-catalyzed procedure should be taken into consideration with those substrates which are more light-sensitive, as it is efficient even with a less energetic irradiation (up to 540 nm was allowed). Finally, the methodology was used for the fluoroalkylation of a synthetic intermediate of Fulvestrant, a breast cancer drug.[576]

The photocatalytic difluoroalkylation/1,2-heteroarene migration of allylic alcohols was reported by Noël et al. to obtain sp^3-rich heterocycles (Scheme 92).[577] This two-step procedure started from heteroaryl ketones, which underwent attack of vinylmagnesium bromide in flow. The flow reactor (PFA capillary, 1.65 mm ID, 0.7 mL volume) was kept a 0 °C in an ultrasonic bath to avoid clogging. The desired allylic alcohols were obtained in moderate to excellent yields (33−92%, 15

https://doi.org/10.1021/acs.chemrev.1c00332
Chem. Rev. 2022, 122, 2752−2906

Scheme 92. Photocatalytic Fluoroalkylation/1,2-Heteroarene Migration of Allylic Alcohols in Flow

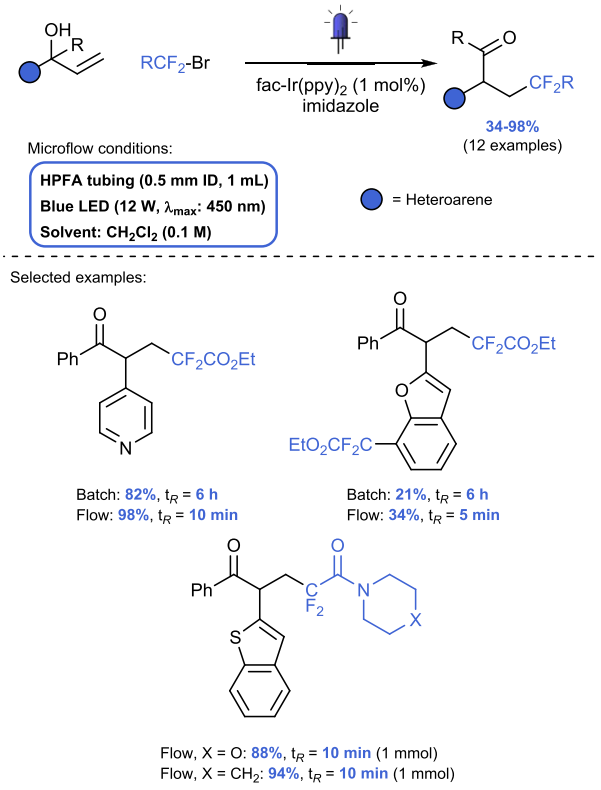

examples) in 5 min residence time and were then used as starting materials for the following photocatalytic transformation. The second step involved the photocatalytic generation of fluoroalkyl radicals under blue light irradiation (12 W, 450 nm). This transformation was performed either in batch, in a 7.5 mL reaction tube, or in flow, in a HPFA microcapillary (0.5 mm ID, 1 mL). The generated fluoroalkyl radicals reacted with the alkenes inducing a 1,2-heteroarene migration. In batch, the reaction time was 6 h, whereas the residence time in the photoreactor ranged from between 5 and 20 min. Moreover, yields were generally higher in flow. Electron-rich substrates, such as benzofuran, underwent a second functionalization on the aromatic ring.

Fluorinated alkyl iodides were employed by Noël et al. in the photocatalytic perfluoroalkylation of cysteine residues (Scheme 93).[98] In 1992, CF_3I was already reported to trifluoromethylate cysteine under UV light irradiation but under very harsh and unpractical conditions (−50 °C in liquid ammonia).[578] This

Scheme 93. Photocatalytic Perfluoroalkylation of Cysteine Residues in Flow

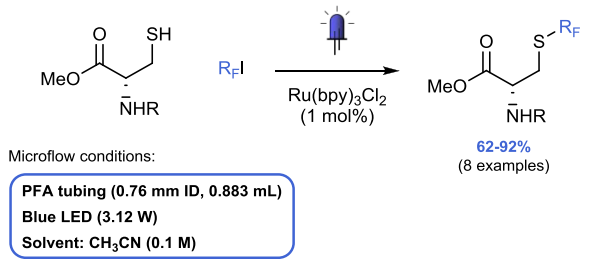

was avoided by employing a ruthenium(II) photocatalyst. Moreover, the implementation of a flow setup allowed for a great acceleration of the transformation, from 2 h in batch to 5 min in continuous-flow. The flow reactor was based on a PFA microcapillary (0.76 mm ID, 0.883 mL) coiled around a plastic holder and irradiated with blue LEDs (3.12 W). Notably, the afforded yields were on average 10% better in flow than in batch.

Further photomediated trifluoromethylations were described by Alcazar, Noël et al. for the trifluoromethylation of (hetero)arenes using the Langlois reagent (Scheme 94).[579]

Scheme 94. Photocatalytic Trifluoromethylation of (Hetero)Arenes in Continuous Flow

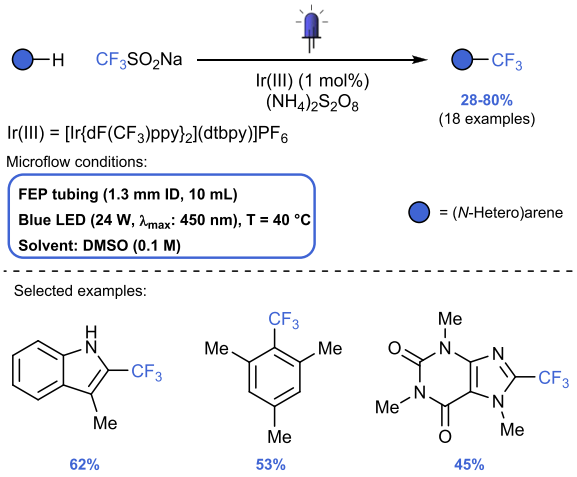

To select the best photocatalyst, luminescence quenching studies were first performed. The results showed higher quenching abilities of the Langlois reagent with $[Ir\{dF(CF_3)ppy\}_2](dtbpy)]PF_6$. Further optimization revealed that an oxidant, such as ammonium persulfate, was necessary for the final rearomatization which afforded the product. A residence time of 30 min was sufficient to achieve full conversion in the commercial photoreactor (10 mL FEP tubing irradiated with 24 W blue LEDs). Indole, benzimidazole, pyridine, pyrimidone, and pyrazole derivatives were trifluoromethylated, as well as unactivated arenes, which generally required longer reaction times in batch (up to 24 h).

In an effort to find cheap trifluoromethylation agents applicable to larger scales, Stephenson et al. described a photocatalytic method based on the use of trifluoroacetic anhydride (TFAA) and 4-phenyl-pyridine *N*-oxide (Scheme 95).[136] The pyridine *N*-oxide is acylated by the anhydride and can generate a trifluoromethyl radical via two possible pathways: either an interaction with the photocatalyst, or the formation of an EDA complex with the substrate or with another molecule of pyridine *N*-oxide. The transformation had a quantum yield of 0.87, indicating that a high photon flux was necessary to reach high conversions. For this reason, a microflow reactor (PFA capillary, 1.6 mm ID, ∼ 150 mL) irradiated with blue LEDs (4.4 W) was used to scale the reaction to kilogram-scale. The residence time was set at 30 min and was carried out at 45 °C. Under these conditions and starting from 1.2 kg of protected pyrrole, 0.95 kg of trifluoromethylated product was obtained over 48 h, corresponding to 50% yield with a productivity of 87.2 $mmol \cdot h^{-1}$.

https://doi.org/10.1021/acs.chemrev.1c00332
Chem. Rev. 2022, 122, 2752−2906

Scheme 95. Kilogram-Scale Photocatalytic Trifluoromethylation Mediated by Trifluoroacetic Anhydride and 4-Phenyl-pyridine *N*-Oxide in Flow

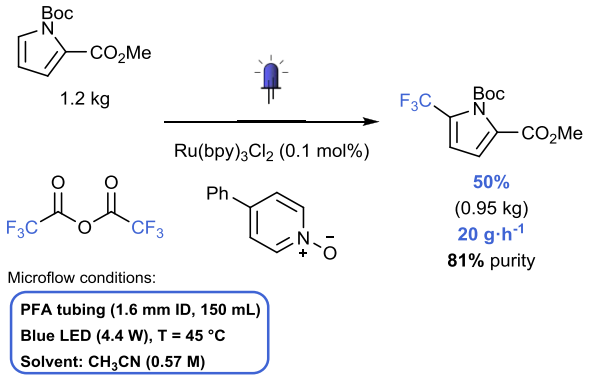

Trifluoroacetic acid was also used by Duan et al., who developed a reusable homogeneous photocatalyst, namely, ruthenium *tris*-[4,4′-bis(dinonylmethyl)-2,20-bipyridine] (Ru-[(DNM)$_2$bpy]$_3^{2+}$, Scheme 96).[580] This catalyst was prepared

Scheme 96. Recyclable Ru(II) Complex as a Visible-Light Photoredox Catalyst for Trifluoromethylation of Coumarin in Flow

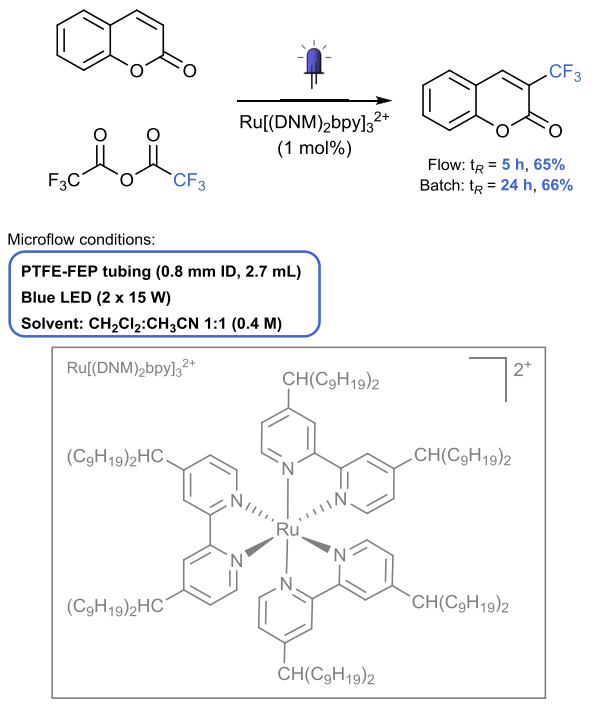

starting from commercially available 4,4′-dimethyl-2,2′-dipyridine and was applied to the trifluoromethylation of coumarin as benchmark reaction to test its photocatalytic activity. Notably, the recovery of the Ru(II) complex was made possible through an extraction in hexane. The photocatalyst was reused for 6 cycles, and the yield of the product remained relatively constant for 4 cycles (66 to 61%), decreasing slightly in the last two runs (57−51%). In the flow reactor (FEP capillary, 0.8 mm ID, 2.7 mL volume, irradiated with 2 blue 15 W LEDs), the reaction time was shortened from 24 to 5 h.

A sulfonium salt-based trifluoromethylating agent (Ph_2SCF_3OTf) was employed by Qiu, Guo et al. in the photocatalytic cyclization of 1,7-enynes in continuous flow (Scheme 97A).[581] The reaction was carried out in a PFA coil

Scheme 97. (A) Photocatalytic Trifluoromethylation/Cyclization of 1,7-Enynes and (B) Photocatalytic Tri- and Difluoromethylation/Cyclizations in Continuous Flow

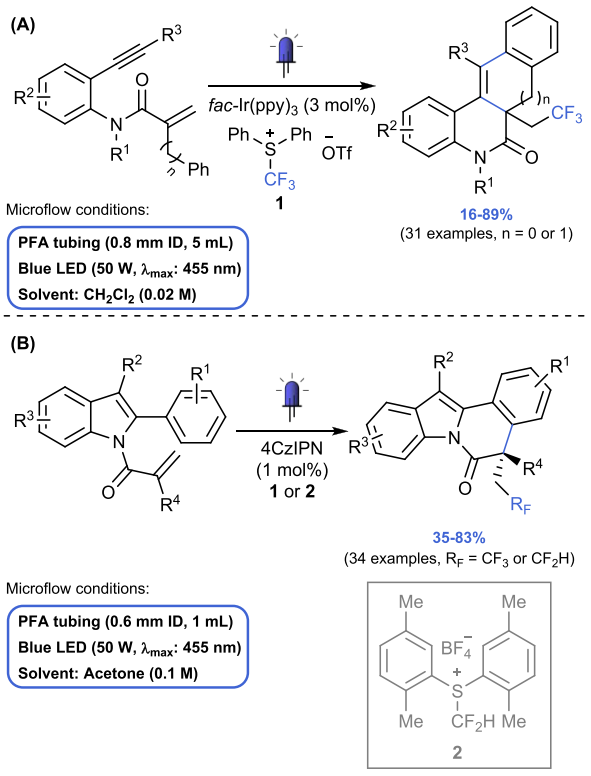

(0.8 mm ID, 5 mL volume) which was irradiated with 50 W blue LEDs (455 nm), with *fac*-Ir(ppy)$_3$ selected as the photocatalyst. The residence time was set at 5 min, whereas in batch 12 h were necessary to achieve comparable yields. In 2021, the photocatalytic trifluoromethylation/cyclization was performed by the same authors to obtain indole[2,1-*a*]isoquinolines (Scheme 97B).[582] In this case, 4CzIPN was a more efficient photocatalyst and the PFA reactor was smaller (0.6 mm ID, 1 mL volume). The Ph_2SCF_3OTf could be substituted with an analogous reagent ($Ar_2SCF_2HBF_4$) to perform difluoromethylation instead. The scaling of the reaction was performed (1 mmol) and the resulting product was afforded in 80% yield (0.29 g) with 10 min residence time.

Umemoto's reagent was used as a trifluoromethyl radical precursor in the light-induced hydrotrifluoromethylation of unsaturated *β*-keto esters (Scheme 98).[583] In the proposed mechanism, the key event was the formation of an EDA complex between the Umemoto's reagent and the tertiary amine DMPT, this was corroborated by DFT calculations. After a preliminary optimization in batch, the authors switched to a microflow photoreactor (PTFA capillary: 1.65 mm ID, 30 mL volume), which was subjected to irradiation with 120 W blue LEDs. In this way, only 2 equiv of DMPT were necessary, instead of three, and the residence time was reduced to 30 min, instead of 4.5 h required in batch. The reaction was scaled to 1 mmol, affording the trifluoromethylated product in comparable yield to the small-scale reaction (68% vs 74%).

The use of fluorinated sulfilimino iminiums in a photocatalytic transformation in flow was described by Dagousset,

https://doi.org/10.1021/acs.chemrev.1c00332
Chem. Rev. 2022, 122, 2752−2906

Scheme 98. Hydrotrifluoromethylation of Unsaturated β-Keto Esters Mediated by the Umemoto Reagent

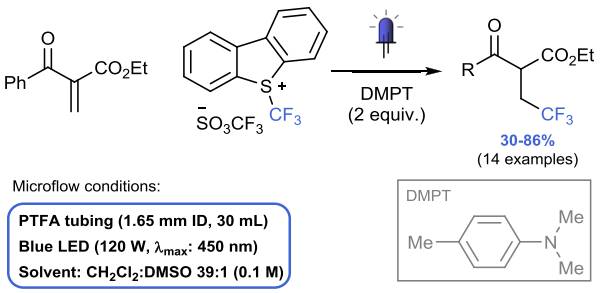

Magnier, and co-workers (Scheme 99).[584] In a previous report in batch, the authors reported this class of compounds which

Scheme 99. Photocatalytic Hydroperfluoroalkylation of Alkenes and Alkynes in Continuous Flow Mediated by Fluorinated Sulfilimino Iminium and Hantzsch Ester

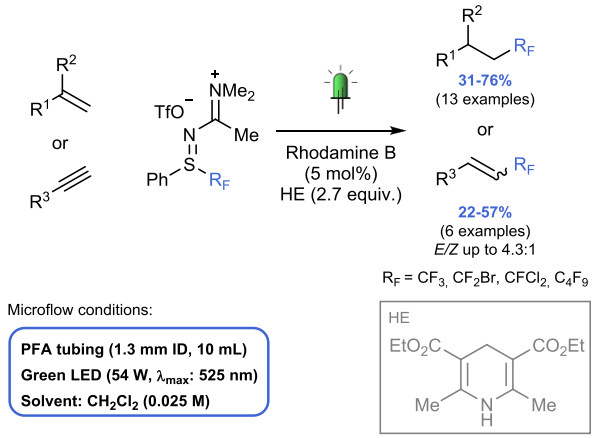

provide perfluoroalkyl radical under light irradiation in the presence of an iridium(III) catalyst for the first time.[585] In flow, fluorinated sulfilimino iminiums were used to hydroperfluoroalkylate alkynes and alkenes. Hantzsch ester (HE) was added as a H atom source, while rhodamine B was selected as the photocatalyst. The residence time was set at 10 min in a commercial reactor consisting of a PFA coil (1.3 mm ID, 10 mL) irradiated by green LEDs (525 nm, 54 W). The reaction was scaled up to 2 mmol, affording the product in comparable yields (70% vs 67%) with a throughput of 1.5 mmol·h^{-1}.

The preparation of labeled compounds is fundamental for PET (positron emission tomography), which is a diagnostic noninvasive imaging technique.[586] In 2017, the ^{18}F-fluorination of tertiary C−H bonds in branched aliphatic amino acids was proven to be feasible using TBADT as a HAT catalyst and [^{18}F]NFSI as the fluorinating reagent, in a flow reactor (PTFE capillary 0.7 mm ID, ∼2.5 mL volume) irradiated with a 15 W UV lamp.[587] In 2019, researchers at UCB Biopharma together with Luxen et al. described a photoinduced late-stage strategy to label N-heteroaromatics with a ^{18}F-difluoromethyl group in flow (Scheme 100).[588] The authors first proposed a 45 min-synthesis of the labeled benzothiazole **1** which was then used for the difluoromethylation of acyclovir, an antiherpetic drug.[589] The commercial flow reactor in use consisted of a FEP capillary (10 mL) irradiated by 470 nm LEDs (2 W). Under the optimized reaction conditions, a residence time of

Scheme 100. Photocatalytic ^{18}F-Difluoromethyl Labeling of N-Heteroaromatics in Flow

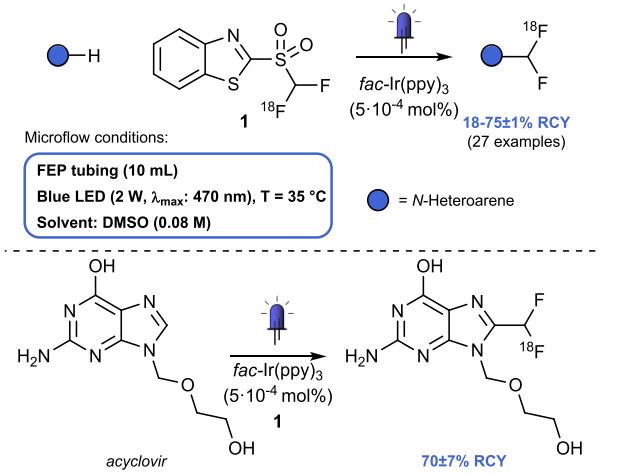

only 2 min was sufficient and the product was afforded with a radiochemical yield (RCY) of 70 ± 7% (n = 7). Moreover, the ^{18}F-labeled acyclovir showed a molar activity of 44.4 ± 11.1 GBq·μmol^{-1}, which represented a value sufficient for biological in vivo studies. The procedure was also effective with a set of *N*-heteroaromatics, caffeine derivatives, nucleosides, nucleic bases, and drugs. Later, the ^{18}F-difluoromethyl labeling of acyclovir was also automated with the help of a commercially available synthesizer, affording the radiolabeled product in 95 min and 35 GBq·μmol^{-1} molar activity.[294]

5.6.2. Chlorination. The continuous-flow photomediated chlorination of toluene derivatives was reported by Kappe et al. using in situ generated chlorine gas (Scheme 101).[590] First, optimal conditions for the in situ production of chlorine gas were investigated. For Cl_2 generation, aqueous solutions of

Scheme 101. Continuous-Flow Photomediated Chlorination of Benzylic Positions through in Situ Generation of Cl_2

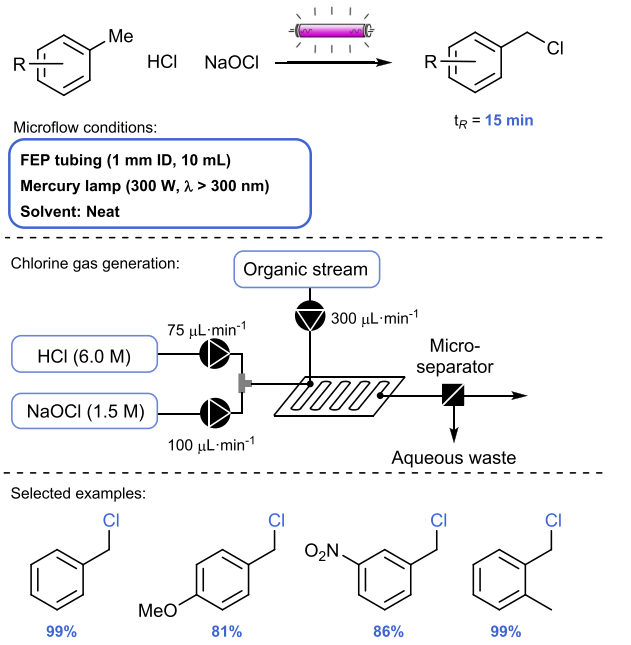

https://doi.org/10.1021/acs.chemrev.1c00332
Chem. Rev. 2022, 122, 2752−2906

HCl and NaOCl were mixed in a Y-mixer, which was then merged with a stream of an organic solvent via a second Y-mixer. Gas evolution was observed between the first and second Y-mixer and subsequently dissolved in the organic solvent after the second Y-mixer. The exiting solution was passed through an L−L separator (Zaiput) to separate the aqueous and the organic phase. The organic phase was then titrated against potassium iodide and the evolution of Cl_2 was ascertained. Optimal conditions for Cl_2 generation called for 3 equiv of aq. HCl. Next, the photomediated chlorination of toluene derivatives was investigated. The photoreactor consisted of a 300 W mercury lamp (>300 nm) wrapped with FEP capillary (1 mm ID, 10 mL volume). The same reactor design was indicated as for the optimization of the Cl_2 generation, but with a neat toluene derivative serving as substrate instead of the organic solvent. Very good yields between 81% and 99% were obtained for the 4 examples investigated with 15 min residence time. This compared favorably to similar batch setups which required hours of irradiation under reflux conditions.

Another example of continuous-flow C−H chlorination of cyclic alkanes was performed by Ryu, Fukuyama, and co-workers using in situ generated and on-site consumption of chlorine gas (Scheme 102).[591] For the flow reactions, aqueous

Scheme 102. Photochemical Chlorination of Alkanes through In Situ Formation of Chlorine in Flow

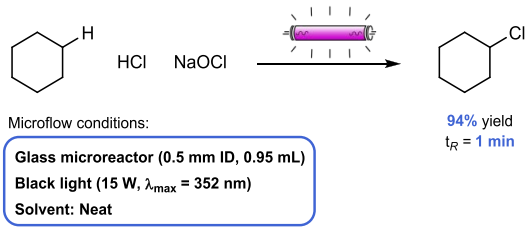

solutions of HCl and NaOCl were mixed in a T-mixer to in situ form chlorine gas, which created a segmented Taylor flow. This was, then, introduced to a stream of neat cyclic alkane using a T-mixer and was irradiated by either ambient lighting or a black light (15 W, 352 nm). Finally, the reaction mixture was quenched with an aq. Na_2CO_3 solution upon exit from the photoreactor. Under ambient light a residence time of 19 min was required to produce 74% yield. Upon reduction of the residence time to 1 min, the ambient lighting proved insufficient for high conversion. When a 15 W black light was used instead, yields of 94% were observed at 1 min residence time for the cyclohexyl derivative. A further scope of 6 examples was performed with cycloalkanes and toluene derivatives. Notably, this method, as well as the Kappe method explored before, enabled the chlorination of alkanes without the use of a chlorine gas cylinder as seen in other work with chlorinations.

A modular, continuous-flow platform was reported by Christmann, Heretsch, and co-workers for the photomediated late-stage functionalization of natural products (Scheme 103).[592] Sclareolide was chosen as the natural product on which to perform the TBADT-mediated transformation using the previously reported chlorinating agent Me_4-*N*-chlorosuccinimide (Me_4NCS). The reaction mixture flowed through FEP tubing (0.79 mm ID, 2.0 mL) and was then irradiated with

Scheme 103. TBADT-Photocatalyzed Late-Stage Functionalization in a Modular, Continuous-Flow Platform

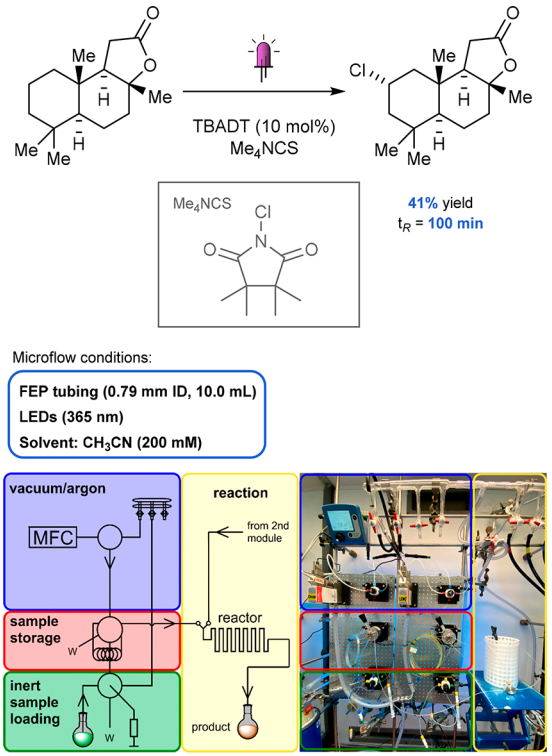

Reprinted with permission from ref 592. Copyright 2021 American Chemical Society.

LEDs (365 nm). An optimization was performed in flow to investigate the choice of chlorinating agent and loading, concentration, temperature, and residence time. Me_4NCS, TBADT (10 mol %), 0.2 M, 10 °C, and 100 min were found to be optimal for chlorinating source, concentration, temperature, and residence time respectively giving a yield of 41%. Additionally, a scale-up using the optimized conditions was performed (4 mmol) affording the chlorinated product in 38% yield.

The chlorination of silanes with dichloromethane was performed by Wu et al. with eosin Y as photocatalyst (Scheme 104).[593] Upon excitation, the photocatalyst activates the Si−H

Scheme 104. Photocatalytic Si−Cl Bond Formation in Flow Starting from Silanes and Dichloromethane

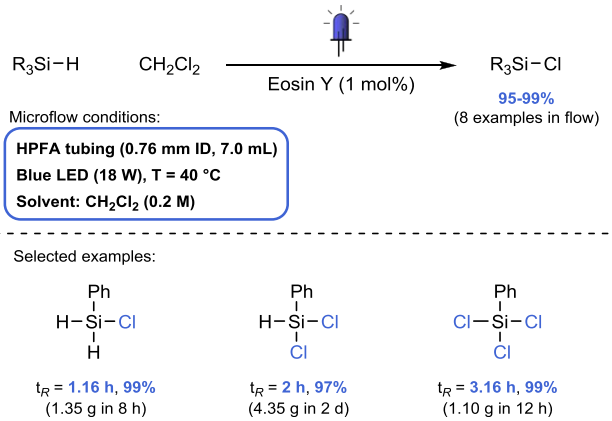

https://doi.org/10.1021/acs.chemrev.1c00332
Chem. Rev. 2022, 122, 2752−2906

bonds and the generated silicon radical subsequently interacts with the solvent (dichloromethane) to form a new Si−Cl bond. Performing the reaction in continuous-flow in an HPFA reactor (7 mL) irradiated with blue LEDs (18 W) did not only allow for the scale-up of the transformation but also for the selective, stepwise chlorination of di- and trihydrosilanes. Compared to the reaction time in batch (3−48 h), the residence time in the flow reactor is significantly reduced (no longer than 5 h).

5.6.3. Bromination. A number of photochemical brominations were performed under continuous-flow conditions, where *N*-bromosuccinimide (NBS), $BrCCl_3$, or molecular bromine were used as bromine source.

A first report by Kappe et al. on light-induced benzylic bromination was published in 2014.[594] A mixture of toluene derivatives and NBS was subjected to irradiation with a 25 W black-light CFL (compact fluorescent lamp) as light source (Scheme 105A). The protocol was readily scalable in a milli-

Scheme 105. Photochemical Benzylic Bromination in Flow with *N*-Bromosuccinimide

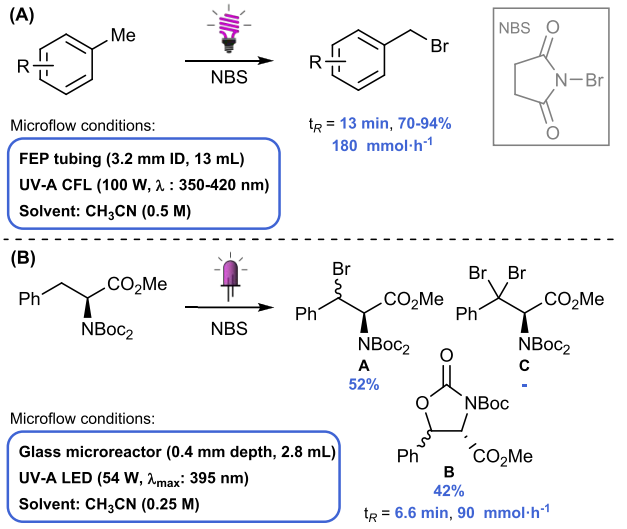

sized photoreactor (3.2 mm ID, 13 mL) with a 100 W light source, to achieve a productivity of 180 mmol·h^{-1}. An important consideration for benzylic brominations is the selectivity toward the monobrominated product over di- or polybrominated ones. Interestingly, the selectivity and conversion in this procedure could be tuned by increasing or lowering the reaction temperature, based on the reactivity of the substrate (0−60 °C), to obtain the monobrominated product in yields of 70−94% for 19 examples.

In a second report, the benzylic bromination of a di-*N*,*N*-Boc-protected methyl phenylalaninate was performed under UV irradiation with NBS in three different flow reactors (Scheme 105B).[595] Initial reaction optimization was performed in a self-fabricated PFA capillary reactor (0.8 mm ID, 2 mL volume) and the reaction mixture was irradiated with a low-pressure mercury lamp (8 W, λ_{max} = 365 nm). Surprisingly, by using an excess of NBS (2 equiv) instead of stoichiometric amounts (1.05 equiv), a higher selectivity was observed for the desired monobrominated product and the cyclized target compound over the undesired dibrominated product. This higher selectivity was attributed to faster generation of the monobrominated product under superstoichiometric conditions. Additionally, the cyclized product was formed from the monobrominated product under thermal conditions. To get better control over reaction temperature, reactions were subsequently performed in commercially available flow reactors (Vapourtec UV-150 0.8 mm ID, 2 mL; Corning Advanced-Flow 0.4 mm depth, 2.77 mL). This way, the protocol enabled the large-scale synthesis of a 2-oxazolidinone, with a productivity of 90 mmol·h^{-1}.

N-Bromosuccinimide (NBS) was also used by researchers at CSIRO Manufacturing for the photobromination of benzyl and phenyl rings in continuous-flow (Scheme 106).[596] First an

Scheme 106. Bromination of a Benzyl Ring Using *N*-Bromosuccinimide in a Corning G1 Photoreactor

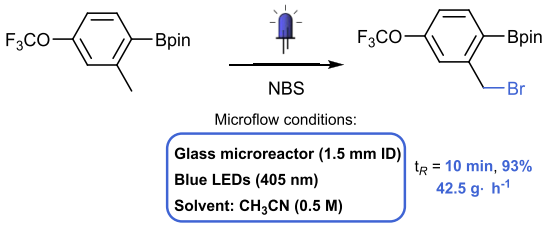

optimization was carried out in flow for light wavelength, temperature, solvent and NBS loading in a Corning G1 photoreactor. Notably, when reactions were run with 1.5 equiv of NBS, the competitive dibromination of the benzyl ring occurred. Next a continuous in-line separation was achieved by introducing a toluene stream and a water stream via a 4-way mixer after the photoreactor, followed by in-line separation using a Zaiput membrane separator. Finally, the reaction scope was expanded and scale-up was performed to demonstrate the generality of the transformation, with 8 examples at 10 mmol scale (79−99% yield, 0.32−2.35 kg·L^{-1}·h^{-1}STY).

A limitation to the use of NBS as Br-source, is the competitive electrophilic bromination for electron-rich aromatic substrates. Thus, an alternative method, with $BrCCl_3$ as bromine source was developed for the benzylic bromination of toluene derivatives (Scheme 107).[597] In this case, the C−Br bond was either directly cleaved under UV irradiation (8 W, 254 nm) or after triplet energy transfer from benzophenone, present as photosensitizer (8 W, 365 nm). As anticipated, electron-rich substrates were well tolerated, resulting in 84% isolated yield in 30 min residence time in the case of *p*-

Scheme 107. Photochemical Benzylic Bromination of Electron-Rich *p*-Methoxytoluene in Flow with $BrCCl_3$ and Its Use as a Protecting Group

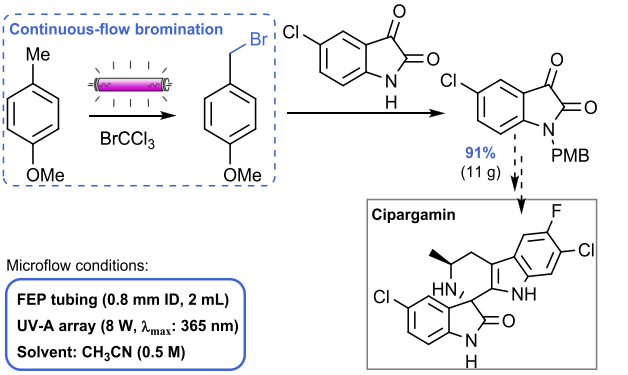

https://doi.org/10.1021/acs.chemrev.1c00332
Chem. Rev. 2022, 122, 2752−2906

methoxytoluene. Interestingly, this brominated *p*-methoxytoluene product is an alkylating agent that is used as a protecting group for reactive functional groups, such as alcohols and amines. To exemplify the potential of the developed protocol for the in situ generation and use of this labile compound as protecting group, the flow bromination was coupled with a protection step of an intermediate of cipargamin, an antimalarial drug candidate. The outlet of the bromination was continuously dosed over 4 h into a batch reaction flask, to generate 11 g of the protected intermediate in 91% yield.

Apart from NBS and $BrCCl_3$, molecular bromine represents another alternative bromine source for the photochemical bromination of organic substrates. In fact, due to its high atom efficiency and relatively low cost compared to stable bromine salts, molecular bromine remains one of the most attractive bromine sources for the chemical industry. However, the safe use and storage of molecular bromine is a challenging and infrastructure-intensive task. Therefore, the in situ formation and direct use of small amounts of molecular bromine, in combination with the inherent operational safety of continuous-flow protocols, represents a significant safety improvement.[598]

The concept of a Br_2 generator was applied in 2012 by Gao et al.,[599] who combined HBr and H_2O_2 to generate molecular bromine in flow for the photochemical bromination of toluene derivatives. The Br_2 generator concept was also applied and improved over three generations by Kappe et al.[223,600] In the first generation system, an aqueous solution of $NaBrO_3$ (0.66 M) and NaBr (3.34 M) was combined with aqueous HBr (4 M) generating a 1 M molecular bromine solution (Scheme 108A, B). With the generated Br_2, the bromination of *p*-fluorotoluene was successfully performed with a productivity of 35 $g{\cdot}h^{-1}$ (73% ^{19}F NMR yield, 15 min residence time). However, this first system was initially designed as a Br_2 feed for a BrCN generator, where a homogeneous aqueous Br_2 solution was required, and was not optimized for limiting waste generation.[600] The process mass index (PMI) is an indicator for the amount of waste generated in a process and is calculated as the total mass of materials used for the production of a specified mass of product (1 equiv). For the applied bromination process, the PMI amounted to 13.55 and could mainly be ascribed to the bromine generator (10.73). A second generation Br_2 generator was developed to optimize the PMI and to increase throughput (Scheme 108C). In this system, an aqueous solution of HBr (8.8 M) was first combined with the organic stream in a T-mixer before entering the reactor. The aqueous $NaBrO_3$ (2.2 M) solution was then added to the stream in a glass microreactor with an internal mixing structure. In this mixing structure, the exothermic formation of molecular bromine occurred, thus avoiding bromine accumulation and uncontrolled temperature rise before the reactor. Using this system, an increased productivity of 74 $g{\cdot}h^{-1}$ of brominated *p*-fluorotoluene was achieved, with a significantly reduced PMI of 6.93. For the third generation system, the stoichiometry of the bromination was re-evaluated, and it was observed that 1 equiv of HBr is formed for every successful bromination (Scheme 108D, E). Therefore, the relative amount of HBr added to the system could be reduced from 2 to 1 equiv, without a loss in performance. With the third-generation system the productivity was increased to 130 $g{\cdot}h^{-1}$. Remarkably, because of the recycling of the formed HBr, a better bromine atom economy was obtained than in case molecular bromine was used (75% of Br incorporated for third generation Br_2 generator, versus 50% for Br_2). Additionally, the substrate could be pumped without organic solvent, leading to a productivity of 228 $g{\cdot}h^{-1}$.

Scheme 108. Br_2 Generator over Three Generations and the Use of Molecular Bromine for Benzylic Bromination

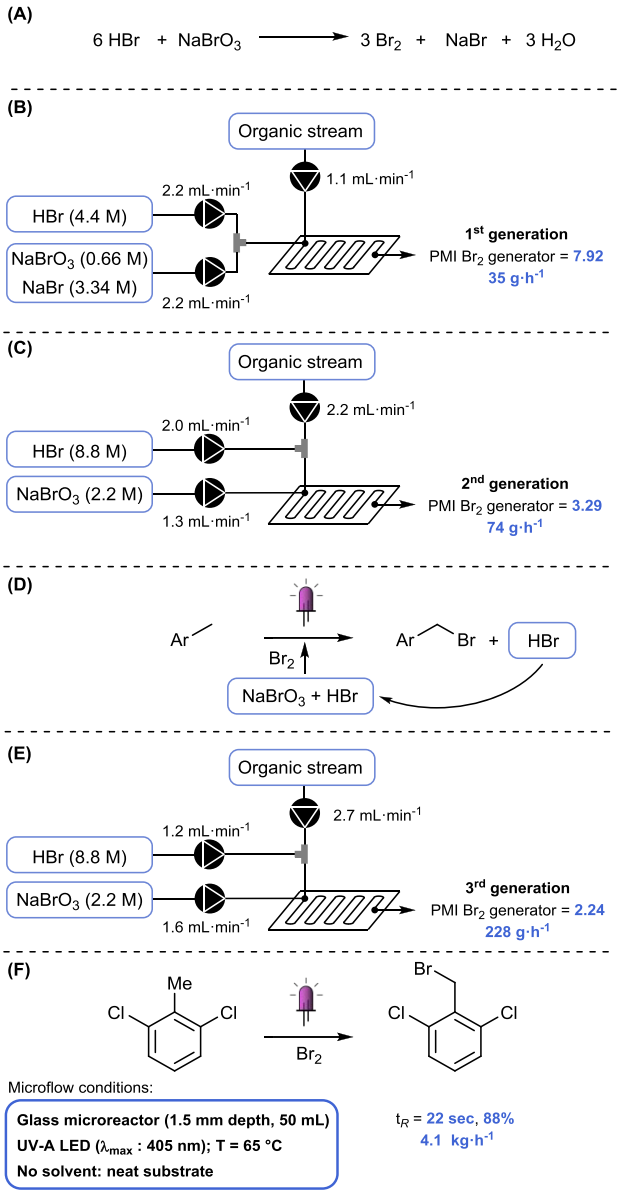

The optimized Br_2 generator was later applied in a smart dimensioning scale-up strategy to reach manufacturing-scale productivity (Scheme 108F).[224] 2,6-Dichlorotoluene was chosen as substrate because the steric hindrance, caused by the chlorine atoms, inhibits undesired dibromination and because the brominated product is a solid below 55 °C, enabling convenient isolation. With the previously used lab-scale photoreactor (Corning G1 LF: 0.4 mm depth, 2.8 mL volume), 1.17 kg of product was obtained in 4 h (97% yield, 300 $g{\cdot}h^{-1}$ productivity). For the scale-up, a 50 mL flow photoreactor was used (Corning G3 FM: 1.5 mm depth, 50 mL volume), which was designed to have the same heat- and mass transfer characteristics as the lab-scale reactor. The lab-scale protocol was applied in the 50 mL reactor, where the aqueous HBr and $NaBrO_3$ solutions were mixed inside the reactor plate to perform the exothermic Br_2 formation in a

https://doi.org/10.1021/acs.chemrev.1c00332
Chem. Rev. 2022, 122, 2752−2906

temperature-controlled environment. After the photochemical bromination reaction, excess Br_2 was quenched with an aqueous sodium thiosulfate stream in another temperature-controlled flow module. The reaction progress was monitored by benchtop ^1H NMR spectroscopy. Because of the safety risk associated with the protocol, a shutdown procedure was developed, which would be activated in case of equipment failure. Eventually, the benzylic bromination could be performed with a residence time of 22 s at 65 °C, resulting in a productivity of 4.1 kg·h^{-1}, 14 times higher than the lab-scale procedure.

Similar to the benzylic bromination with NBS, Li et al. performed the photochemical bromination of conjugated allylic compounds in continuous-flow (Scheme 109).[601] To

Scheme 109. Photochemical Bromination of Conjugated Allylic Compounds with NBS

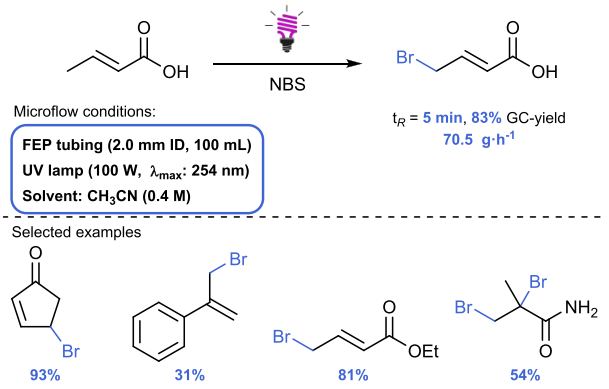

perform the reaction, a solution of crotonic acid (0.4 M) as model substrate and NBS as bromine source in acetonitrile was irradiated with a 10 W UV-lamp (λ_{max} = 254 nm) in a FEP capillary reactor (1 mm ID, 8.6 mL volume). Under optimal conditions, 81% GC-yield of the monobrominated product was obtained in 30 min residence time. The protocol was then scaled to a larger flow reactor (2 mm ID, 100 mL volume) and a higher power UV light source was used (100 W, λ_{max} = 254 nm). With the large-scale system, the desired monobrominated product could be formed in 83% GC-yield in just 5 min residence time, resulting in a productivity of 70.5 g·h^{-1}.

For a drug discovery program, the influence of a variable number of bromine atoms on the solubility and potency of a lead compound was investigate (Scheme 110).[602] Therefore,

Scheme 110. Photochemical Bromination of Pyrrole Ring with Variable Number of Bromine Atoms

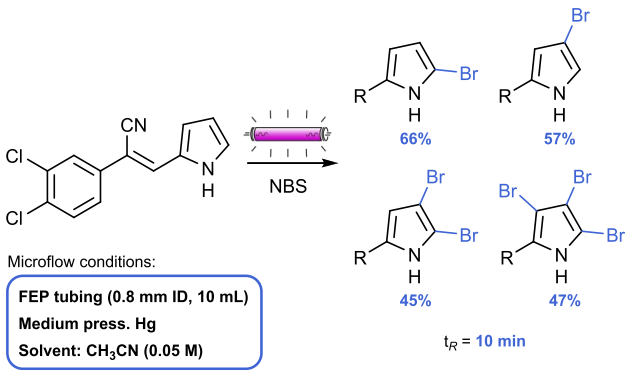

the photochemical bromination of the lead compound on its pyrrole ring was performed with NBS as bromine source in continuous-flow. The use of different UV filters resulted in a different regioselectivity for the bromination product. With the full spectrum of the UV light source, the 3-bromopyrrole was the main product, whereas the 2-bromopyrrole was mainly formed with a UV-light filter (cutoff λ > 340 nm). Additionally, di- and tribrominated products were obtained by increasing the equivalents of NBS added to the system. The four brominated products were easily separated via flash chromatography and their cytotoxicity was evaluated.

The incorporation of a bromine atom in organic substrates was also achieved through photocatalytic ATRA reactions (atom-transfer radical addition) of organobromides and olefins in the presence of a Bi_2O_3 catalyst and base (Scheme 111).[230]

Scheme 111. Solid Handling in Oscillatory Flow Reactor in a Bi_2O_3 Photocatalyzed ATRA Reaction for Bromine Incorporation

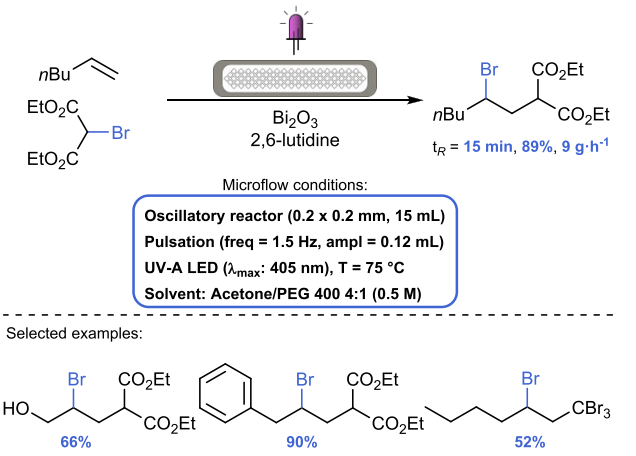

In batch, 95% GC-yield of the addition product between 1-hexene and diethyl bromomalonate was obtained after 5 h irradiation with a 400 nm LED. The bismuth oxide catalyst was added as a solid, which is often problematic in continuous-flow reactors, as settling of solids in narrow capillaries can easily lead to clogging of the reactor. Therefore, the flow reactions were performed in a commercially available flow reactor (HANU flow reactor = 2 mm × 2 mm), which is capable of handling suspensions by the combination of pulsatile flow and static mixing elements in the process channel. Using this oscillatory flow reactor and specific oscillatory parameter settings (frequency = 1.5 Hz, amplitude = 0.12 mL), a homogeneous suspension is maintained throughout the reactor and various organobromides were successfully added to olefins at 75 °C under 405 nm LED irradiation, leading to 52−97% isolated yield in 20 min residence time. Additionally, a scale-out of the model substrate was performed, producing 35.9 g in 4 h (t_R = 15 min, 89% yield, 9 g·h^{-1}). To investigate the nature of the bismuth oxide photocatalyst, a control experiment was performed, suggesting a homogeneous character. These observations were confirmed in a recent theoretical and experimental investigation by Riente, Noël, and co-worker, which revealed the homogeneous nature of the active species in bismuth oxide photocatalyzed transformations.[603]

5.6.4. Dehalogenation. The photocatalytic hydrodefluorination of electron-poor trifluoromethylarenes was described by

https://doi.org/10.1021/acs.chemrev.1c00332
Chem. Rev. 2022, 122, 2752−2906

Gouverneur et al. (Scheme 112).[279] The transformation was catalyzed by 4DPAIPN in the presence of 4-hydroxythiophenol

Scheme 112. 4DPAIPN-Photocatalyzed Hydrodefluorination of Trifluoromethylarenes[a]

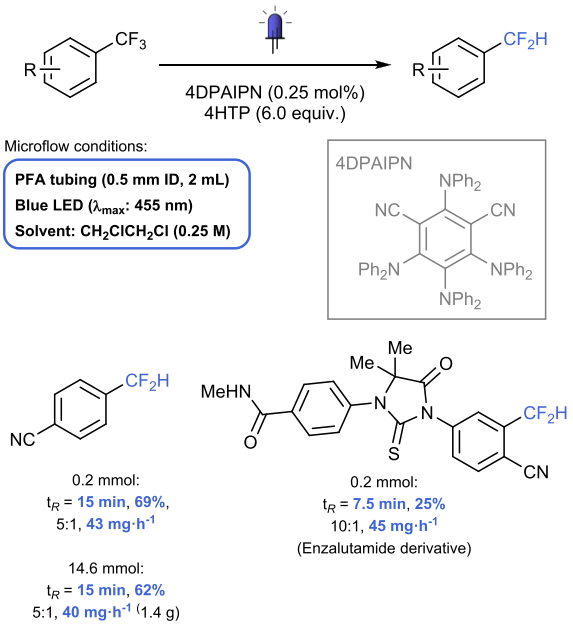

[a]4HTP = 4-hydroxythiophenol.

(4HTP) as a hydrogen atom donor. In a microflow photoreactor (PFA coil with 0.5 mm ID and 12 mL volume) irradiated with blue LEDs (455 nm), the reaction time was reduced from 12 h to 15 min. When the reaction was scaled up (14.6 mmol), comparable yields were obtained, and 1.4 g of product was obtained with a selectivity of CF_2H:CH_2F of 5:1. A number of APIs, such as enzalutamide, underwent the hydrodefluorination in flow, affording the defluorinated product in 25% yield and 10:1 selectivity.

The metal-free photomediated reductive dehalogenation of aryl halides was investigated by Kappe et al. by utilizing HAT catalysis in continuous-flow (Scheme 113).[604] First, an optimization was translated to flow from a previous reported batch reductive dehalogenation of 4-bromobenzonitrile and 4-chlorobenzonitrile yielding 97% and 96%, respectively.[605] Flow reactions took place in a Corning AFR module (0.4 mm ID, 2.8 mL volume) and irradiated by LEDs (365 nm, 44 W). Following this, a reaction scope of 15 examples was carried out affording yields of 83−99% for a diverse range of aryl halides.

5.7. Photodecarboxylations and -carboxylations

The photochemical extrusion of CO_2 from carboxylic acids is an effective strategy for chemo- and regioselective functionalization reactions.[606] This is partly due to the large driving force associated with the liberation of gaseous CO_2. On the other hand, the use of CO_2 as a C1-building block in the synthesis of useful chemicals provides exciting opportunities to install carboxylic acid functional groups.[607−611]

Decarboxylative reactions can be used to selectively install a functional group at the position where CO_2 is extruded. This concept was applied by Noël et al. in the photodecarboxylative difluoromethylation of α,β-unsaturated carboxylic acids to difluoroalkenes under batch and continuous-flow conditions (Scheme 114).[612] The protocol relied on a *fac*-Ir(ppy)$_3$ photocatalyst and EtO_2CF_2C−Br as an inexpensive CF_2-source and did not require strong oxidants or metal cocatalysts to facilitate CO_2 removal. The mild reaction conditions enabled

Scheme 113. Photocatalytic Metal-Free Dehalogenation of Aryl Halides in Continuous Flow

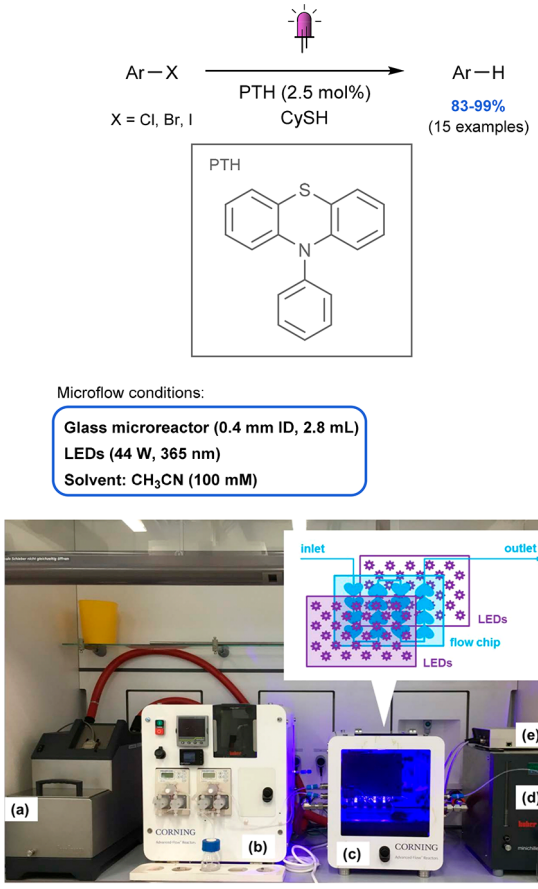

a temperature control for reaction plate
b contol module (pumps and MFC)
c fluidic module housing
d temperature control for LED panels
e wireless reciever for LED control

Reprinted with permission from ref 604. Copyright 2019 European Chemical Societies Publishing.

Scheme 114. Photodecarboxylative Difluoromethylation of Cinnamic Acids and Aryl Propiolic Acids

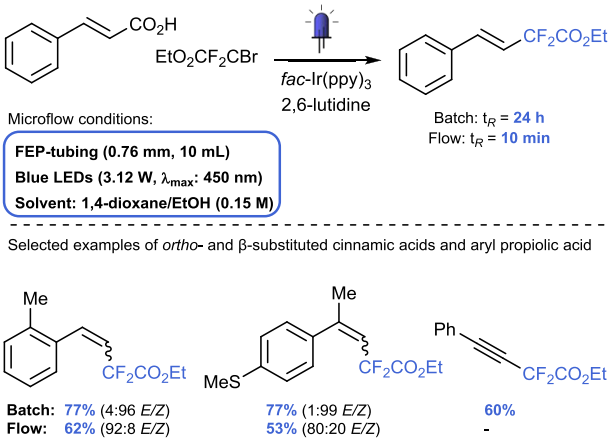

https://doi.org/10.1021/acs.chemrev.1c00332
Chem. Rev. 2022, 122, 2752−2906

the preparation of a broad substrate scope of difluoromethylated styrenes and phenylacetylenes. Interestingly, for *ortho*-substituted cinnamic acids a different stereoselectivity was observed when performing the reaction under batch (*E*-isomer) or under flow conditions (*Z*-isomer). This observation was explained by kinetic experiments, which showed that the thermodynamically more stable *Z*-isomer is initially formed and subsequently undergoes triplet−triplet energy transfer to form the *E*-isomer. In flow, the reaction could be stopped after formation of the *Z*-isomer, and thus before isomerization into the *E*-isomer. Hence, this unique strategy enables the possibility to access the desired isomer simply by changing the reactor type. Additionally, using a slightly modified protocol, the authors were able to carry out the decarboxylative functionalization of aryl propiolic acids as well.

Another example of a photodecarboxylative functionalization was performed by Gonzalez-Gomez et al., who selectively exchanged a carboxylic acid group for a cyano group to form aliphatic nitriles (Scheme 115A).[613] The reaction was

Scheme 115. Decarboxylative Functionalization of Aliphatic Carboxylic Acids with an Organic Photocatalyst: (A) Cyanation and (B) Trifluoromethylselenolation

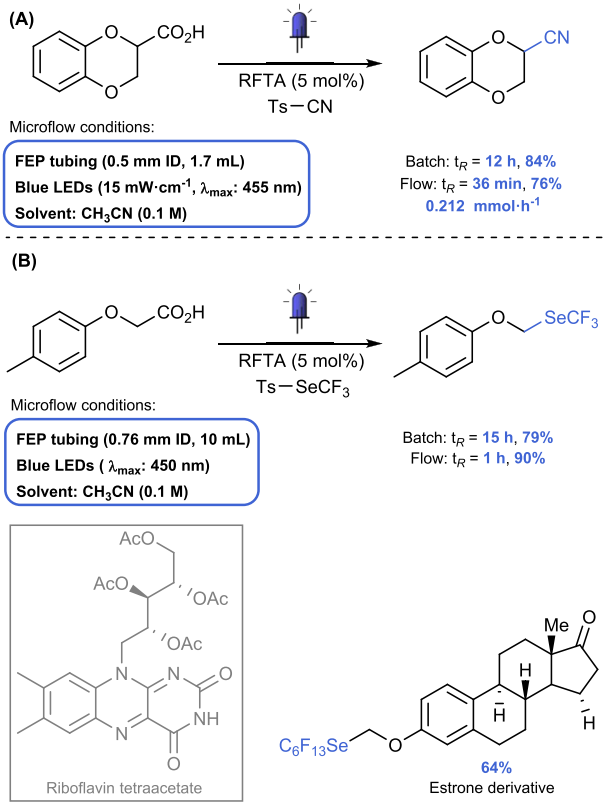

performed by irradiating a mixture of aliphatic carboxylic acid, tosyl cyanide and photocatalyst in acetonitrile with blue LEDs (15 mW·cm^{-2}, 455 nm). The photocatalyst, in this case, was the vitamin B_2 analogue riboflavin tetraacetate (RFTA), and no base, additives, or metals were required. In batch, yields of 40−84% were obtained for 28 examples in 12 h reaction time. However, the high absorption coefficient of the photocatalyst (~13 000 M^{-1}·cm^{-1}) limited the potential for scale-up in batch. Therefore, a flow protocol was developed and carried out in a PFA capillary microreactor (0.5 mm ID, 1.7 mL volume), which enabled the synthesis of 0.53 mmol of the model substrate in 150 min residence time, albeit in slightly lower yield than in batch (76% in flow vs 84% in batch).

Similarly, the RFTA photocatalyst was also used by Billard, Magnier, and co-worker for the incorporation of fluorine substituents through decarboxylative trifluoromethylselenolation (Scheme 115B).[614] Ts−$SeCF_3$ was selected as fluorinating agent and reactions were performed in batch and in flow and subjected to blue LED irradiation (450 nm). The reactions in flow required significantly lower reaction time (1 h versus 15 h in batch) and generally resulted in higher yields. A 3 mmol scale reaction was performed in flow resulting in 75% isolated yield. Additionally, other fluorinating agents, such as Ts−SeC_3F_7 and Ts−SeC_6F_{13} could be used, and the method was successfully applied to a number of bioactive compounds.

The incorporation of deuterium atoms into organic compounds is a field of increased interest, where methods providing high selectivity and high deuterium incorporation are especially valued.[615] The photocatalytic decarboxylative deuteration method, developed by Zhu et al.,[616] fulfills the requirements of high selectivity, high D-incorporation, broad functional group tolerance, and importantly, easy scalability in flow. A batch protocol was first developed, with D_2O as deuterium source and thiol as hydrogen atom transfer catalyst. This protocol was shown to be suitable for a variety of primary, secondary, and tertiary acids, as well as for complex carboxylic acids (Scheme 116). Importantly, high selectivity was observed

Scheme 116. Selective Decarboxylative Deuteration and Scale-up in a Glass Recirculation Reactor

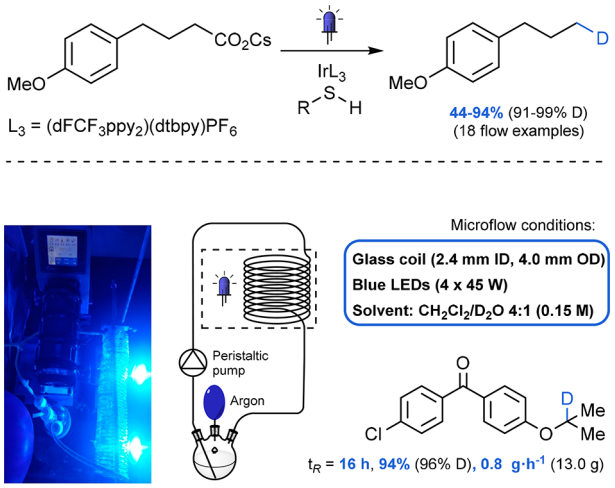

Reprinted from ref 616. Published by Royal Society of Chemistry.

for the decarboxylative deuteration, as reactive C−H bonds were generally unaffected. On the other hand, the deuteration of aromatic acids was unsuccessful, which was explained by the kinetically unfavorable radical decarboxylation for aromatics. After establishing the substrate scope, the reaction was proven to be easily scalable in a recirculating flow reactor (Scheme 116). In this flow reactor, 18 examples were readily deuterated on a 2 to 50 mmol scale with excellent D-incorporation (91−99%) in moderate to high yields (44−94%). For example, 13.0 g of a deuterated compound was obtained in the recirculating flow reactor in 16 h reaction time (94% yield, 96% D-incorporation, 0.8 g·h^{-1}).

https://doi.org/10.1021/acs.chemrev.1c00332
Chem. Rev. 2022, 122, 2752−2906

The formal total synthesis of the natural product L-ossamine was performed using a photodecarboxylative functionalization strategy in flow (Scheme 117).[617] A cyclic threonine derivative

Scheme 117. Formal Total Synthesis of L-Ossamine via Photodecarboxylative Functionalization

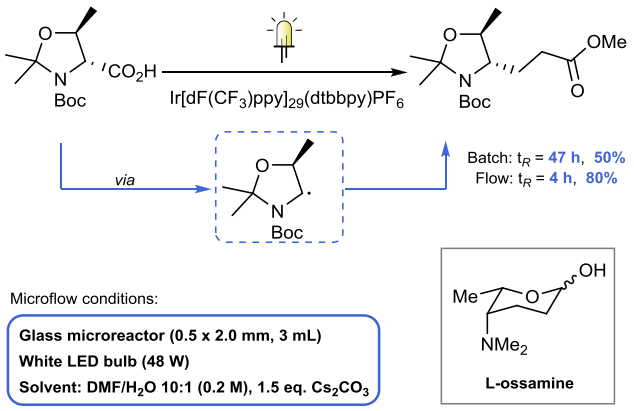

was coupled with methyl acrylate in the presence of an iridium catalyst and base. In batch, full conversion was observed after 47 h irradiation with a 48 W white LED lamp, leading to 50% yield of the desired compound. However, when performed in flow, 10 equiv of H_2O were added to homogenize the reaction mixture, and the yield was increased to 80%, in significantly shorter reaction time (4 h). The resulting compound could further be processed to a known precursor of L-ossamine,[618] thereby accomplishing the formal total synthesis of this natural product.

Similarly, L-proline was applied in photodecarboxylative annulation reactions with azides for the preparation of fused imidazoles (Scheme 118).[619] Upon visible-light irradiation in

Scheme 118. Decarboxylative Annulation of L-Proline to Fused Imidazoles

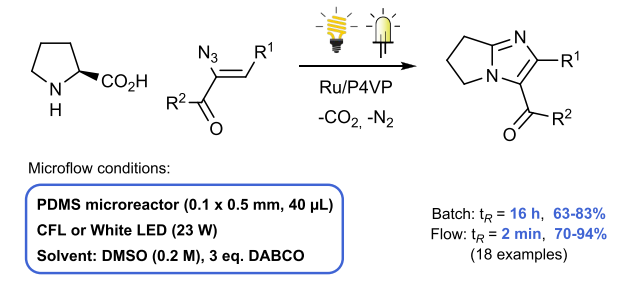

the presence of a ruthenium photocatalyst and base, CO_2 is excluded from L-proline and N_2 from the azide, after which the formation of two new C−N bonds generates the fused imidazole. Reactions were first performed in batch and required 16 h to reach 63−83% yield for 18 examples. For the flow experiments, a PDMS microreactor (0.1 × 0.5 mm, 40 μL) was fabricated through lithography, the channels were glass coated for chemical resistance and a Ru/P4VP catalyst was immobilized inside the channels. In this microreactor, increased yields (70−94%) were obtained for the same examples as the batch reactions and the reaction time could be reduced from 16 h to just 2 min.

Decarboxylative annulation reactions were also performed by Baumann et al. for the continuous-flow synthesis of benzyne (Scheme 119).[620] The benzyne was trapped with a number of azide-, diene-, or sydnone coupling partners to form 1,2,3-

Scheme 119. Photochemical Generation of Benzyne in Continuous-Flow and Quenching to Form 1,2,3-Benzotriazoles, Naphthalenes, and 2H-Indazoles

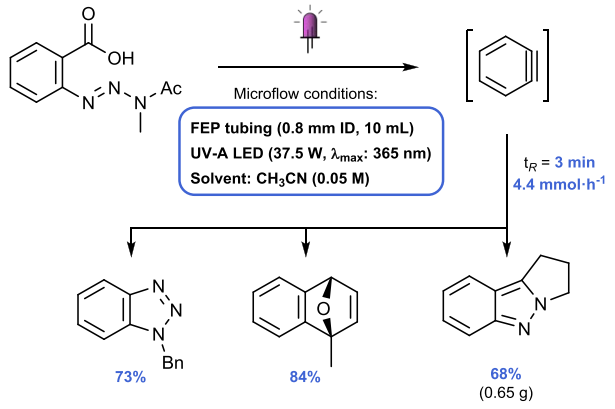

benzotriazoles, naphthalenes, and 2*H*-indazoles in one step. Reactions were performed in a FEP capillary reactor (0.8 mm ID, 10 mL volume) under UV-A LED irradiation (37.5 W, 365 nm). The scalability of the method was shown by a reaction using 760 mg of a proline derived sydnone, resulting in a productivity of 4.4 mmol·h^{-1} (68% yield).

A heterogeneous photocatalyst was developed by Cai, Tang, and co-workers and was applied in a decarboxylative alkyl/acyl radical addition with *p*-quinone methides in continuous-flow (Scheme 120).[621] Initial optimization of the reaction was

Scheme 120. Decarboxylative Alkyl/Acyl Radical Addition on *p*-Quinone Methides

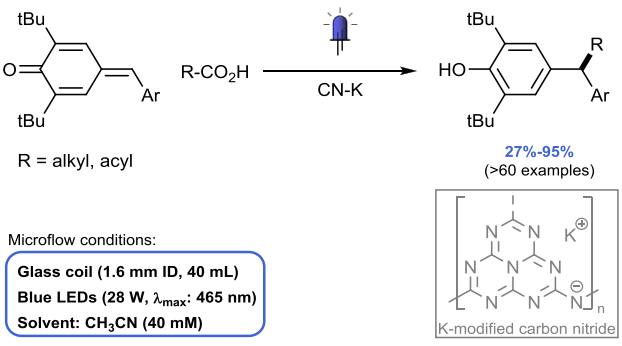

performed in batch, after which a broad substrate scope was established with a variety of carboxylic acids and *p*-quinone methides, achieving moderate to excellent yields in the decarboxylative radical addition (>60 examples, 27−95%). Thereafter, scale-up experiments were performed in a recirculating suspension flow reactor, consisting of a PTFE reactor coil (1.6 mm ID, 40 mL volume), using a peristaltic pump. Because of the high activity of the developed catalyst, only very low catalyst loading was required (0.25 mg·mL^{-1}) and the pump was able to recirculate the suspension without clogging. The methodology was applied to the synthesis of the natural product tamoxifen, which was obtained in 6 steps starting from the acyl addition product in 40% overall yield.

https://doi.org/10.1021/acs.chemrev.1c00332
Chem. Rev. 2022, 122, 2752−2906

The decarboxylative hydroformylation of styrenes was realized by Wang et al. with diethoxyacetic acid as formylating agent to generate terminal aldehydes in continuous-flow (Scheme 121A).[622] Traditional transition metal-catalyzed hydroformylation reactions of styrenes result in branched rather than linear aldehydes and often require complex ligands to control regio- and chemoselectivity. In contrast, the developed approach relied on a radical-based hydroformylation in the presence of a 4CzIPN photocatalyst and selectively produced the terminal aldehyde. A reaction mechanism was proposed with single electron transfer from the 2,2-ethoxyacetate to the singlet excited 4CzIPN photocatalyst and subsequent decarboxylation to generate the formyl radical equivalent. This formyl radical adds to the styrene derivative in an anti-Markovnikov fashion and the reduced photocatalyst donates an electron to the benzyl radical to form the carbanion. After protonation and hydrolysis of the ethoxy groups, the terminal aldehyde is formed. The hydroformylation reaction was performed under blue LED irradiation in batch and flow and was compatible with a range of substituted styrene derivatives, as well as heteroaromatics and complex structures to generate the terminal aldehyde in 50−90% yield. The reaction time was significantly reduced in flow (2.5 h in flow versus 36 h in batch) and was used to hydroformylate 3.44 g of 4-(trifluoromethyl)styrene in 87% yield. The authors later applied their decarboxylative approach to the formylation of aryl halides and vinyl bromides and to $C(sp^3)-C(sp^2)$ cross-coupling with β-aryl-vinyl halides (Scheme 121B).[623,624]

Scheme 121. (A) Decarboxylative Hydroformylation of Styrene Derivatives Towards Terminal Aldehydes in Continuous Flow and (B) Application of the Decarboxylative Method to Formylation and Cross-Coupling of Vinyl Bromides

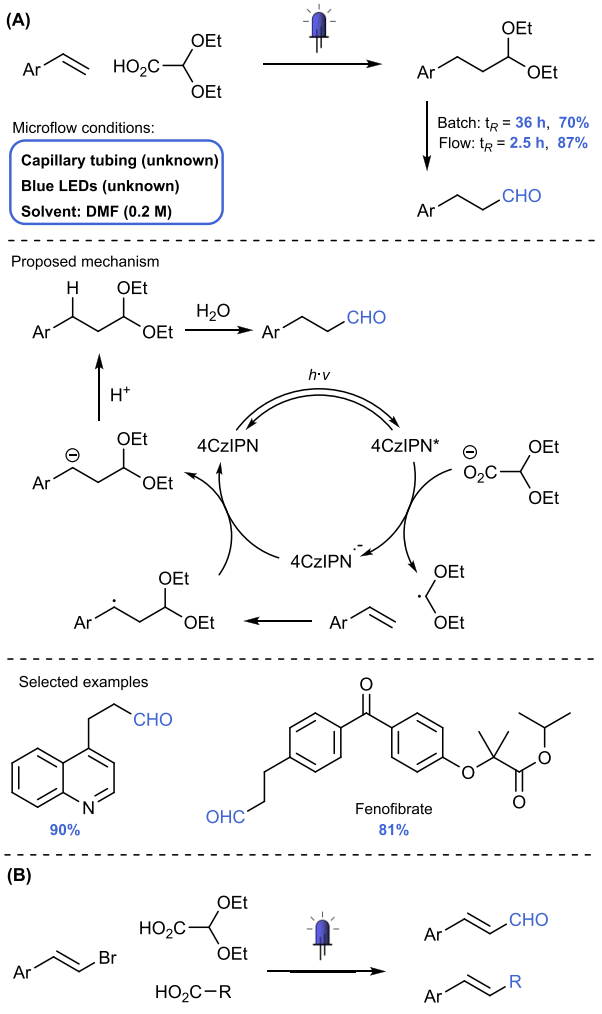

A number of photochemical decarboxylation reactions involving phthalimides were described using different reactor systems.[90,139,625−628] These decarboxylations were performed in a conventional chamber photoreactor, in an advanced falling-film reactor and in continuous-flow reactors. A performance comparison was carried out by Oelgemöller et al. between a commercially available batch and flow reactor (Scheme 122A).[625] The flow reactor generally allowed for shorter reaction times, higher isolated yields and easier scale-up for an α-photodecarboxylation, a photodecarboxylative addition, and a photodecarboxylative cyclization, where gram-scale preparations were easily performed in flow. Additionally, in the case of the cyclization, the flow decarboxylation could be telescoped with an acid-catalyzed thermal dehydration and amination in flow (Scheme 122B), affording 72−77% yield of bioactive compounds in a single step, which is a significant improvement compared to the multistep batch process (28−45% yield).[628]

The photodecarboxylative cyclization was also applied by George, Poliakoff, and co-workers in an annular continuous-flow reactor and by Booker-Milburn et al. in the "Firefly" reactor, achieving a productivity of 1.39 kg·day^{-1} in the latter case (Scheme 122C).[90,139] A final example of a photodecarboxylative reaction involving phthalimides involved a large-scale Minisci reaction.[134] These examples were discussed in more detail in the section 3.

Recently, a few examples were published on the photochemical incorporation of CO_2 into organic compounds under continuous-flow conditions.[629−631] Some protocols rely on the photocatalytic generation of the $CO_2^{\bullet-}$ radical anion via photocatalytic single electron reduction of CO_2 ($E^0 = -2.21$ V vs SCE in DMF), which requires a catalyst with a sufficiently high redox potential, such as *p*-terphenyl ($E^0 = -2.63$ V vs SCE in DMF). Such a transformation benefits from the large and well-defined interfacial area between the gas and the liquid phase leading to high mass transfer and reproducible reaction conditions.[459,463,508,632−634]

Jamison et al. developed a flow protocol for the photocatalytic activation of CO_2 to prepare racemic amino acids (Scheme 123).[629] In the flow reactor, a liquid stream containing the amine substrate, *p*-terphenyl photocatalyst and base was combined in a T-mixer with a gaseous CO_2 stream. The amount of CO_2 injected into the reactor coil was controlled with a mass flow controller (MFC) and the pressure was set and maintained using easily exchangeable back pressure regulators. The FEP capillary reactor coil was wrapped around a conical frame and was irradiated with a 500 W Hg (Xe) arc lamp.[635] A long wave UV-filter ($\lambda > 280$ nm) and an infrared mirror were placed between the light source and the reactor coil to avoid undesired side reactions associated with short wavelength irradiation and extensive heating. In this photochemical flow setup, 92% yield was obtained for the model reaction at 3.4 bar (3.6 equiv) of CO_2 in 5 min residence time. The improved gas−liquid contact and better control over reaction conditions was shown by comparing with a reaction performed in batch. By bubbling CO_2 in a glass flask only 30%

https://doi.org/10.1021/acs.chemrev.1c00332
Chem. Rev. 2022, 122, 2752−2906

Scheme 122. Photodecarboxylation Reactions with Phthalimides

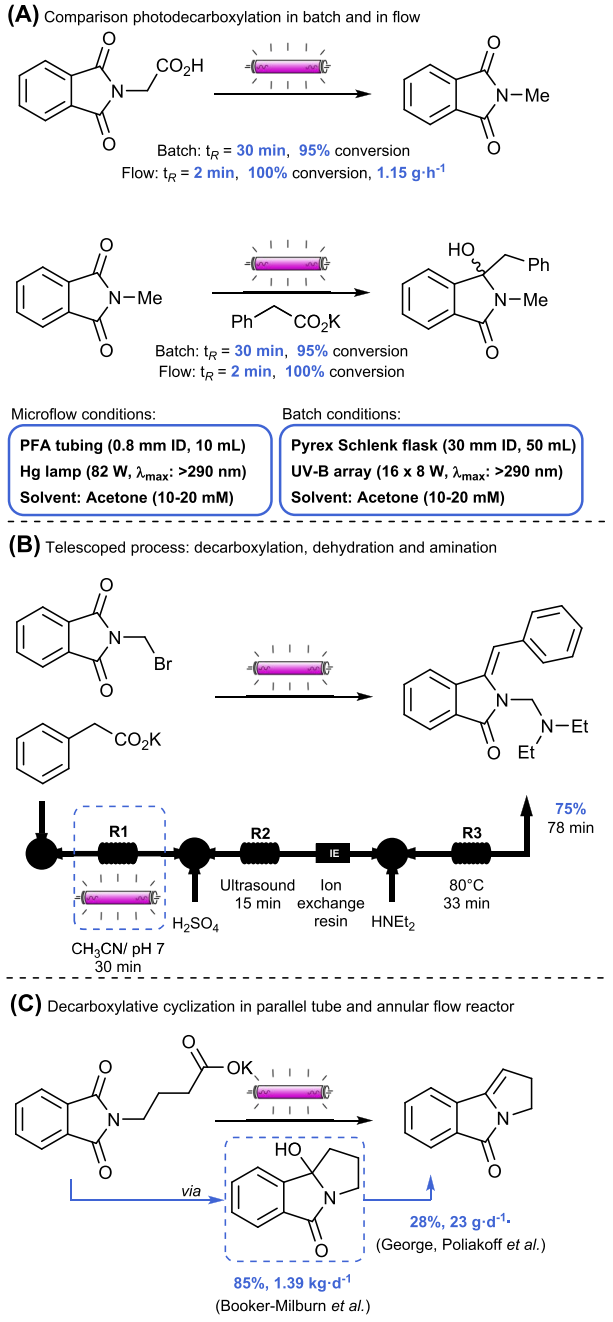

yield was obtained after 120 min irradiation time. A reaction mechanism was proposed by the authors (Scheme 123). The *p*-terphenyl photocatalyst is activated upon UV light irradiation and is quenched with the tertiary amine substrate, generating a tertiary amine radical cation and the strongly reducing *p*-terphenyl radical anion. This active species can subsequently reduce CO_2 via single electron transfer to $CO_2^{\bullet-}$, while the added base abstracts a proton from the tertiary amine radical cation. The $CO_2^{\bullet-}$ radical cation and α-amino radical then combine via radical−radical coupling to form the desired α-amino acid.

In the same setup as the amine carboxylation, a photochemical β-hydrocarboxylation of various styrenes was performed (Scheme 124).[630] In this case, a solution of styrene, *p*-terphenyl, 1,2,2,6,6-pentamethylpiperidine (PMP) as amine reductant, and water were combined with the gaseous CO_2 stream, leading to the β-selective formation of carboxylated product. With the developed flow method, a range of terminal-, α- and β-substituted styrenes were β-selectively carboxylated in moderate to excellent yields (37−87%, 23 examples) in 8 min residence time. Control experiments provided insight into the role of the different additives. Without PMP, almost no styrene conversion was observed (<5%), indicating its crucial role as external reductant of the excited *p*-terphenyl photocatalyst. In the absence of water, a significant amount of dicarboxylated product was observed. When replacing water with D_2O, the benzylic position was selectively deuterated, suggesting a reduction of the carbon radical to the anion and subsequent protonation.

Another example of a photocatalytic incorporation of CO_2 in continuous-flow is given by the work of Romo et al., where the hydrocarboxylation of α,β-substituted esters with CO_2 was applied as a versatile synthetic strategy toward β-lactones (Scheme 125).[631] The reaction sequence relied on a flow hydrocarboxylation, followed by an α-bromination and a β-lactonization in batch. In contrast to the examples given by Jamison et al.,[629,630] the flow setup contained a tube-in-tube reactor coil, with a semipermeable Teflon inner tube, which functions as a membrane through which CO_2 can be dosed into the reaction stream. The authors used a more bulky hydrogen atom donor $(TMS)_3SiH$ instead of water, which resulted in higher yields (73% in 20 min residence time). After validating the hydrocarboxylation method for a wide range of α,β-substituted esters, the subsequent α-halogenation-β-lactonization was optimized for the model substrate. Eventually, the synthesis of various β-lactones was performed without intermediate purification of the photodecarboxylation products in moderate to good overall yields (35−59%, 8 examples).

A tube-in-tube microfluidic solar reactor was also used by Abolhasani et al. for the continuous-flow desorption of CO_2 from aqueous amine sorbents under solar irradiation, and required minimal energy input for this traditionally energy-intensive process.[636] Notably, this strategy provided a better access to captured CO_2 for utilization as a C1 building block.

A third method for supplying CO_2 to a reaction mixture is to presaturate the solution by bubbling CO_2 gas in a vial before injecting the mixture in the flow reactor. This method was applied by Dell'Amico et al. for the direct carboxylation of the enol intermediate generated from photoexcitation of 2-methylbenzophenone in DMSO (Scheme 126).[361] In the flow reactor, excellent yield (98%) was obtained in 60 min residence time (0.039 mmol·h^{-1}), which is a significant improvement compared to the batch method (75% yield, 24 h, 0.003 mmol·h^{-1}).

The direct coupling of inactivated CO_2 to form value-added compounds was also achieved by Wu et al.[637] The difunctionalization of alkenes with CO_2 and silanes or C(sp^3)−H alkanes was performed through dual photoredox and hydrogen-atom-transfer catalysis (Scheme 127). The method relied on the use of 4CzIPN as photocatalyst and 3-acetoxyquinuclidine as HAT catalyst to generate value-added compounds, such as β-silacarboxylic acids and γ-heteroatom acids (N, O, S). A mechanism was proposed where the excited 4CzIPN is quenched by 3-acetoxyquinuclidine to form $4CzIPN^{\bullet-}$ and $HAT^{\bullet+}$ radical cation. The $HAT^{\bullet+}$ radical cation abstracts a H-atom from the silane or C(sp^3)−H alkane

https://doi.org/10.1021/acs.chemrev.1c00332
Chem. Rev. 2022, 122, 2752−2906

Scheme 123. Photocatalytic CO_2 Activation for Amino Acid Synthesis under Continuous-Flow Conditions

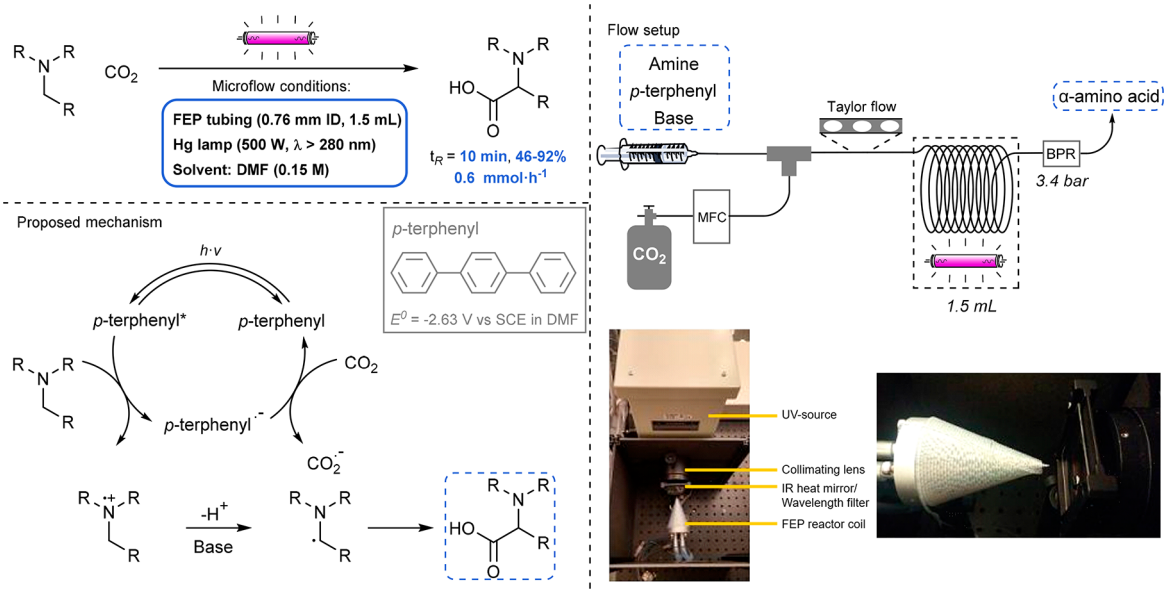

Reprinted with permission from ref 629. Copyright 2016 Nature Publishing Group.

Scheme 124. Photocatalytic β-Selective Hydrocarboxylation of Styrenes with CO_2 in Continuous Flow

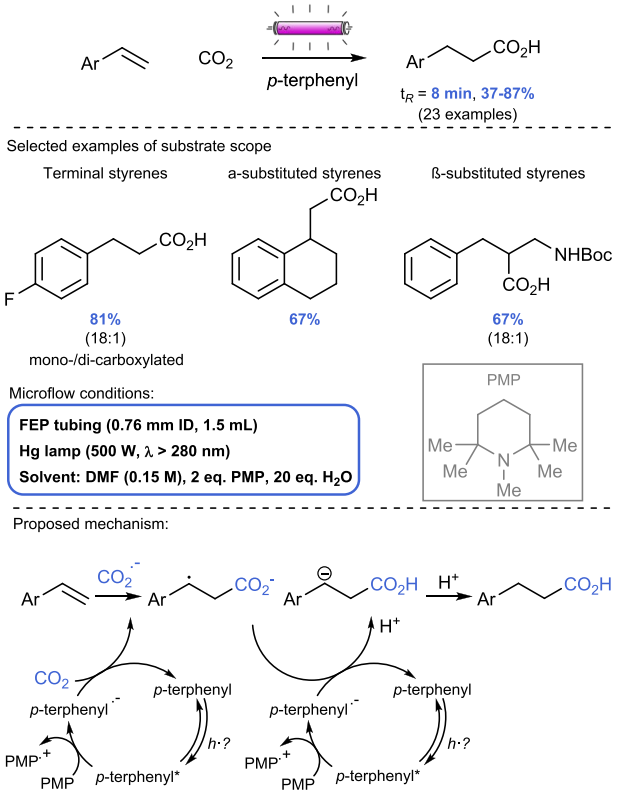

Scheme 125. Hydrocarboxylation of Electron-Deficient Alkenes in a Tube-in-Tube Reactor As a Versatile Synthetic Strategy Towards β-Lactones

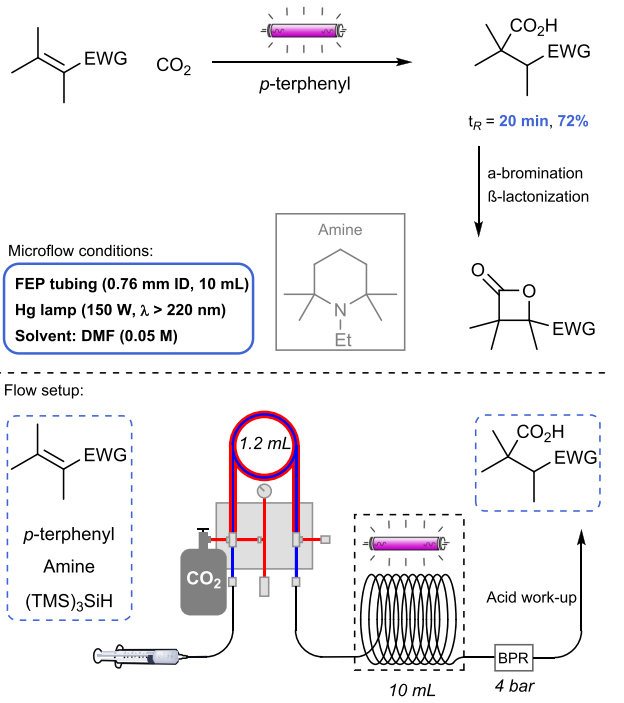

substrate, which subsequently adds to the alkene. The resulting carbon radical is then reduced by the 4CzIPN$^{\bullet-}$ photocatalyst to its carbanion, which performs a nucleophilic attack on CO_2 to deliver the desired silacarboxylated or carbocarboxylated product. A substrate scope was performed, showing compatibility with a broad range of silanes, C(sp^3)−H alkanes and alkenes. Additionally, a gram-scale reaction could be performed in a continuous-flow reactor, providing the difunctionalized products in slightly improved yields and reduced reaction times compared to the batch method (67−76% yield in 30 min in flow, versus 58−75% yield in 4 h in batch).

5.8. Photochemical C−C and C−X Bond Formation in Flow

The development of milder and more efficient synthetic processes to forge new C−C and C−X bonds (X = O, N, S, ...) under mild conditions remains a contemporary research subject.[638−641] Photocatalysis in flow represents an important

https://doi.org/10.1021/acs.chemrev.1c00332
Chem. Rev. 2022, 122, 2752−2906

Scheme 126. Direct Carboxylation by Photoinduced Enol Formation of 2-Methylbenzophenone in Continuous Flow

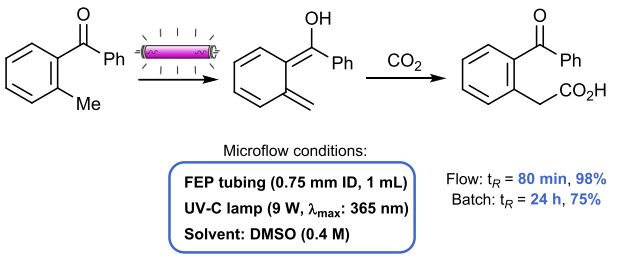

Scheme 127. Alkene Difunctionalization with CO_2 and Silanes or C(sp^3)−H Alkanes by Dual Photoredox and HAT Catalysis

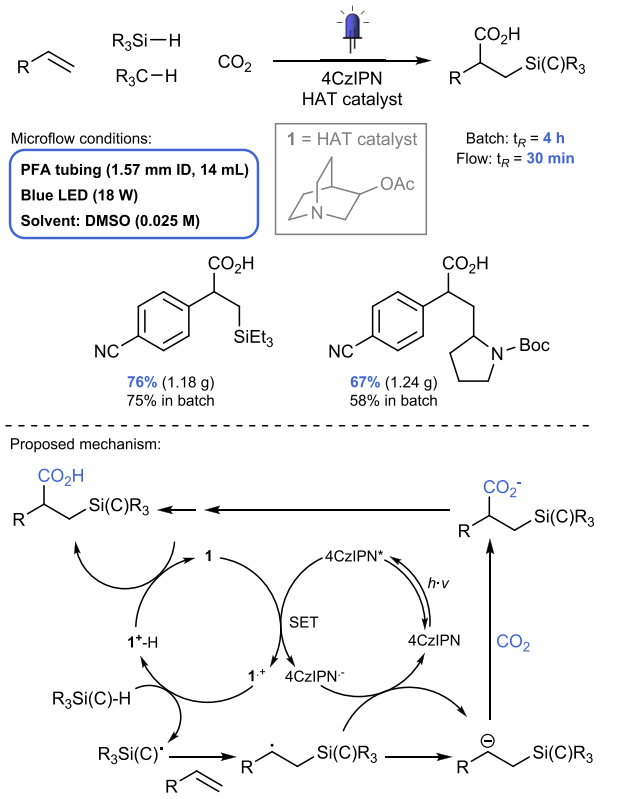

milestone in the pathway to fulfill that goal[6,642] because of its many advantages: milder conditions, higher selectivity, higher productivity, and easier scale-up.

5.8.1. Photocatalytic Cross-Coupling Reactions in Flow. The photomediated Fe-catalyzed C(sp^2)−C(sp^3) Kumada cross-coupling of aryl halides was reported by Noël, Alcázar et al. in continuous-flow (Scheme 128).[643] Iron(III) acetylacetonate ($Fe(acac)_3$) provided the best results in a 15 min residence time. Reactions were irradiated with blue LEDs (34 W, 450 nm) with reactions taking place in a commercially available Vapourtec UV-150 reactor module (2 mL volume). Notably, a variety of strongly electron-rich aryl chlorides, previously hardly reactive under dark Fe-catalyzed Kumada coupling conditions, could be efficiently coupled with aliphatic Grignard reagents at room temperature in high yields and within a few minutes residence time when subjected to light irradiation. It was suggested that the oxidative addition was accelerated by the absorption of photons. An extensive

Scheme 128. Photomediated C(sp^2)−C(sp^3) Kumada Cross-Coupling of Aryl Halides by Iron Catalysis in Continuous Flow

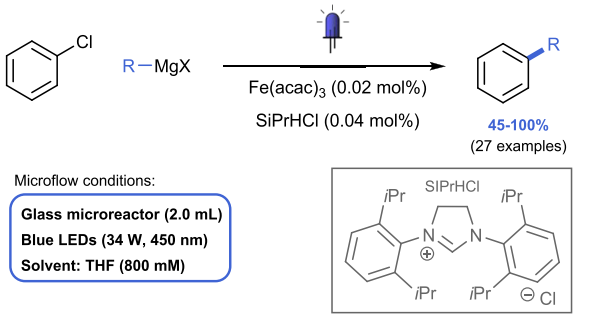

reaction scope was undertaken with different alkyl Grignard reagents and arylchloride coupling partners resulting in 27 examples which afforded yields of 45−100%.

A nickel-catalyzed Negishi-type cross-coupling between an organozinc bromide and a haloarene was performed in flow by researchers at Janssen Inc. and was shown to be accelerated by visible-light irradiation (Scheme 129).[644] To perform the

Scheme 129. Light-Accelerated Negishi Coupling of Organozinc Bromide with Aryl Halide and Scale-up

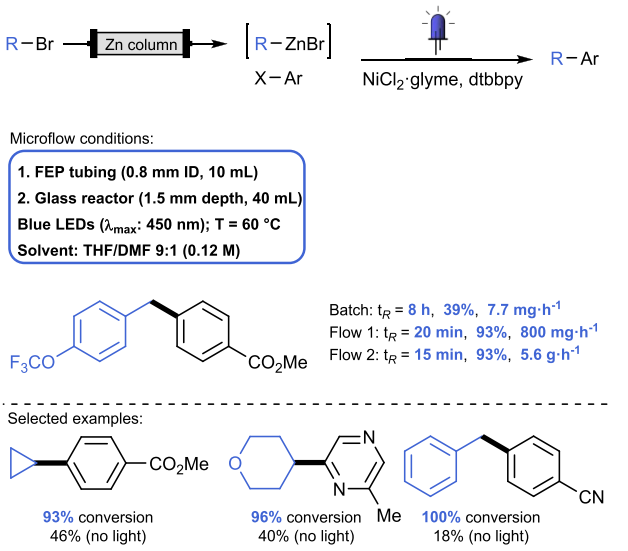

coupling reaction, an organozinc derivative was prepared by flowing the aryl- or alkyl- bromide substrate over an active zinc column, which was subsequently coupled with a bromo-, chloro-, or iodoarene under blue LED irradiation (450 nm) in the presence of a nickel(II) catalyst at 60 °C. In the absence of light, the reaction proceeds as well, albeit at lower conversion. Initial mechanistic investigations suggested that light accelerates the active catalyst formation, as well as the reductive elimination step of the catalytic cycle. The developed protocol is applicable to a wide range of coupling partners, performing remarkably well with a number of aryl chlorides in flow. Additionally, a scale-up was performed in batch and in flow with a significantly better performance in flow, providing 6.9 g of product in 8 h (93% yield, 800 mg·h^{-1} in flow, versus 39% yield, 7.7 mg·h^{-1} in batch).

https://doi.org/10.1021/acs.chemrev.1c00332
Chem. Rev. 2022, 122, 2752−2906

A further scale-up investigation of this transformation was later performed to generate sufficient material for preclinical studies.[645] The same method was employed, where one feed was run over an active Zn column to generate the organozinc derivative, which was subsequently combined with a coupling partner and nickel catalyst and irradiated with blue LEDs (405 nm) in a 40 mL glass microreactor (Corning G1 FM 1.5 mm depth, 40 mL volume). In this case, the organozinc formation was monitored with an in-line benchtop NMR and with an in-line density meter before and after the zinc column. The new setup was applied in a light-accelerated Negishi coupling, resulting in an increased productivity of 5.6 $g \cdot h^{-1}$ in the new setup compared to 0.8 $g \cdot h^{-1}$ in the previous 10 mL reactor setup.

The arylation of *N,N*-dialkylhydrazones in the presence of an iridium photocatalyst was performed by researchers at Janssen to enable the α-arylation of *N,N*-dialkylhydrazones in continuous-flow (Scheme 130).[646] The proposed mechanism

Scheme 130. Photocatalytic α-Arylation of *N,N*-Dialkylhydrazones in Continuous Flow

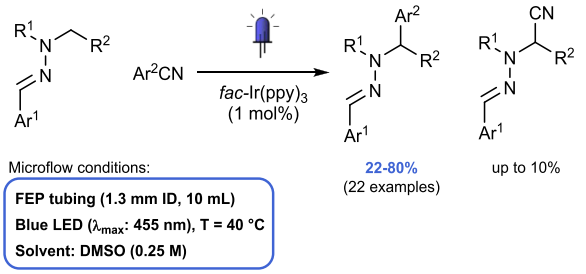

involves the photocatalytic oxidation of the trisubstituted nitrogen followed by deprotonation in the α-position, which is, then, functionalized. The arylation is performed with electron deficient aryl cyanides, minimizing the formation of unwanted nitrile products. Flow experiments were performed in a 10 mL reactor irradiated with 455 nm LEDs and resulted in better yields and selectivity than in batch. In fact, in batch 68% yield was obtained in 30 min, corresponding to 93.6 $mg \cdot h^{-1} \cdot mL^{-1}$. Using the flow photoreactor, the product was isolated in 64% yield in a 10 min residence time, corresponding to a STY of 264.3 $mg \cdot h^{-1} \cdot mL^{-1}$. When starting from 15.3 mmol, 75% yield was obtained in 10 min, which corresponds to a STY of 309.7 $mg \cdot h^{-1} \cdot mL^{-1}$.

Photocatalysis offers also novel methods to form C−C bonds, mainly based on generation of reactive intermediates.[647] One example is the metal-free C−C coupling of aryl halides in flow, which was investigated by Fagnoni, Protti, and co-workers (Scheme 131).[648] The mechanism of the transformation involved the heterolytic cleavage of the Ar−X bond in a protic solvent, followed by the generation of the triplet phenyl cation through UV-light irradiation. First, an optimization was undertaken in batch and in flow for the synthesis of 4-methoxybiphenyl as a model substrate and varying solvent, concentration, and reaction/residence time. Acetonitrile:water (5:1) with a concentration of 0.1 M proved to be the best conditions. Encouraged by these results the reaction scope was expanded in flow using the optimized reaction conditions for a broader range of mesitylenes (A). A total of 7 examples were investigated affording yields of 38−90%. Notably, shorter irradiation times were needed in flow (from 18 to 2 h 45 min). Next, the scope of the arylation

Scheme 131. Metal- and Catalyst-Free Arylation via Photogenerated Phenyl Cations under Flow Conditions

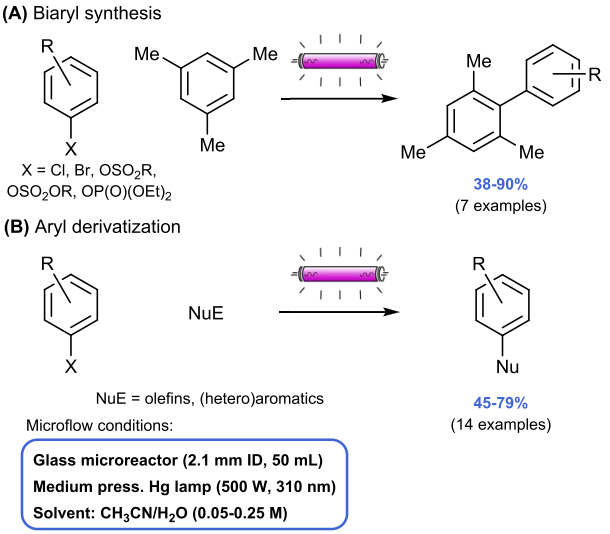

coupling partner (B) was further explored for a range of heteroaromatics (NuE), for a total of 14 examples yields of 45−79% were obtained.

Ley et al. generated carbon-centered radicals through acridinium-photocatalytic oxidation of activated boronic acids and esters, followed by a conjugate addition to a Michael acceptor (Scheme 132A).[214] After disclosing the importance of

Scheme 132. (A) Photocatalytic Radical Coupling of Boronic Acids in Flow in 30 mmol Scale and (B) Photocatalytic Coupling of Benzylboronic Esters and Aldehydes in Flow

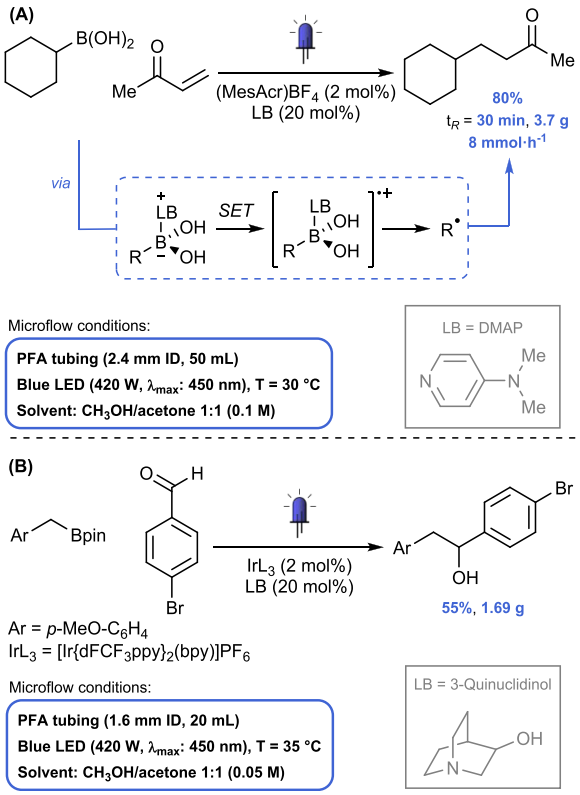

https://doi.org/10.1021/acs.chemrev.1c00332
Chem. Rev. 2022, 122, 2752−2906

a Lewis base (i.e., DMAP) to activate the trivalent boron in a photoredox process,[649] the protocol was translated to flow. Compared to a batch setup, the reaction in flow under blue LED irradiation (17 W) required significantly shorter reaction time to reach completion (70 min in flow vs 24 h in batch). The use of a commercial PFA reactor (PhotoSyn by Uniqsis, Ltd. 1 mm ID, 5 mL volume) equipped with a powerful light source (420 W) halved the residence time, thus motivating the authors to prepare a larger-scale experiment (30 mmol). For this, a 50 mL PFA coil (2.4 mm ID) was employed, and 3.7 g of product was obtained in 3 h (t_R = 30 min), corresponding to a throughput of 8 mmol·h^{-1}. This photocatalytic activation mode, starting from a boronic ester, was also exploited in a reaction with carbonyl compounds to synthesize alcohols (Scheme 132B).[215] Here, the acridinium photocatalyst was substituted by an Ir(III) complex and DMAP by 3-quinuclidinol. In this case, a 10 mL FEP coil (1.6 mm ID) was irradiated with violet LEDs (17 W, 420 nm), affording the alcohol in 70% yield and in 100 min residence time (compared to 8 h in batch). Once more, the scale-up with the 420 W lamp (450 nm) in the commercial PFA reactor (1.6 mm ID, 20 mL volume) allowed a faster reaction (t_R = 30 min, 10 h run) in comparable yield (55%, 1.69 g).

A different photocatalytic approach to obtain 1-phenyl ethanol was proposed by Zhang, Tang, and co-workers, who described the photooxidation of styrene in the presence of water, mediated by 9-mesityl-10-methylacridinium perchlorate.[650] This anti-Markovnikov hydration required phenyl disulfide as a HAT catalyst and was executed in a PFA capillary reactor (1 mm ID, 4 mL volume). The intensification in flow led to a 2.5 times higher productivity of 2-phenylethanol than the corresponding batch method (122 vs 3.6 mmol·h^{-1}·L^{-1}).[651]

A photochemical method to prepare alcohols from styrene derivatives and carbonyl compounds was disclosed by Jamison et al. The method proceeds through the generation of ketyl radicals from the corresponding carbonyl compound (Scheme 133).[652] Whereas ketyl radicals were previously obtained with

Scheme 133. Photocatalytic Coupling of Styrenes and Aldehydes with *p*-Terphenyl in Flow

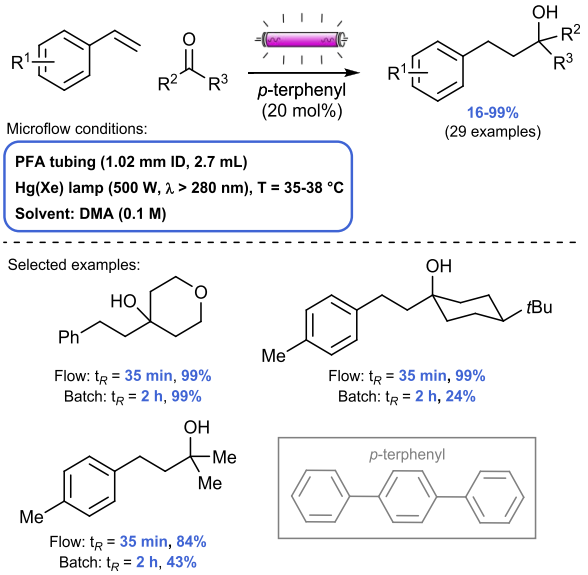

effective but very strong reducing agents (e.g., SmI_2 or alkali metals in ammonia),[653,654] a milder and metal-free procedure in flow was described using *p*-terphenyl as photocatalyst. Flow reactions were performed in a PFA capillary reactor (2.7 mL volume) equipped with a UV lamp and a long-pass filter. After ketyl radical formation and subsequent trapping with styrene, the corresponding alcohol was obtained in 99% yield in 35 min residence time. Although the model reaction also performed well in batch, the scope evaluation proved the superiority of the flow approach, as it provided higher yields for more challenging substrates.

For the synthesis of fluorinated tertiary alcohol derivatives, Polyzos et al. used fluorinated ketones as trapping reagents for visible-light-induced singlet nucleophilic carbenes (Scheme 134).[655] These carbenes were generated through irradiation of

Scheme 134. Visible-Light-Induced Generation of Singlet Nucleophilic Carbenes and Its Use for the Synthesis of Fluorinated Tertiary Alcohols

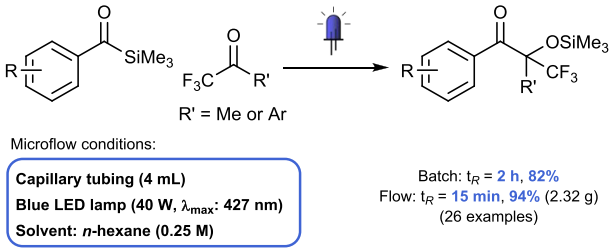

benzoyl trimethylsilane with blue LEDs (427 nm, 40 W) and were quenched with 2,2,2-trifluoroacetophenone derivatives or 1,1,1-trifluoroacetone. In batch, this resulted in 82% yield in 2 h for the model substrate. To improve the reaction efficiency and scalability, reactions were next performed in a capillary flow reactor (4 mL volume) using the same light source as in batch. In flow, a yield of 94% was obtained in 15 min residence time and 2.32 g of fluorinated tertiary alcohol was isolated.

The visible light photoredox-mediated catalysis of aryl cross-couplings was investigated by Chiba et al., who utilized continuous-flow for scale-up purposes (Scheme 135).[656] First a selection of polysulfide anions representing $S_3^{\bullet-}$, S_4^{2-}, and S_3^{2-} precatalysts were screened using the heterobiaryl coupling of *N*-methylpyrrole and 4′-bromoacetophenone as the model reaction. This indicated that K_2S_x gave the best results with 92% (86% isolated) yield, whereas neutral triisopropylsilylthiol (iPr$_3$SiSH) also gave promising results affording the product in 82% yield. This was followed with an extensive substrate scope using either of the precatalysts. Further, a scale-up was carried out in continuous-flow using a photoreactor (HPFA capillary 1.55 mm ID, 56 mL) irradiated by 6 Kessil lamps (40 W, 440 nm) and cooled with fans to achieve a stable temperature (27−33 °C). The heterobiaryl cross-coupling was first scaled up in flow (22 mmol, Scheme 135A) using iPr$_3$SiSH as a precatalyst and tetramethylguanidine (TMG) as a base. The desired product was obtained in 78% yield corresponding to a productivity of 1.75 g·h^{-1}. The same catalyst/base system was used for the scale-up of the borylation of 4′-bromoacetophenone with B_2pin_2 affording the product in 83% yield (6.9 g·h^{-1}, Scheme 135B).

5.8.2. Metallaphotoredox Catalysis in Flow. The combination of photoredox catalysis and transition metal catalysis paves the pathway to new reactivities and thus novel

https://doi.org/10.1021/acs.chemrev.1c00332
Chem. Rev. 2022, 122, 2752−2906

Scheme 135. Scale-up of (A) the Heterobiaryl Coupling and (B) the Borylatation of an Aryl Bromide Using iPr_3SiSH as Precatalyst in Flow

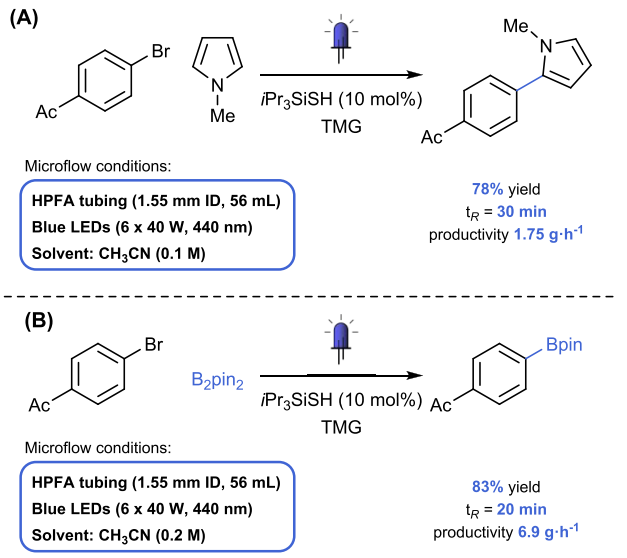

synthetic opportunities.[657] This includes the ability (i) to perform cross couplings with nontraditional nucleophiles and (ii) to modify the oxidation state of the transition metal through photocatalytic SET.[14,658] In particular, the use of photoredox/nickel dual catalysis has emerged as a powerful new tool to enable the formation of C−C and C−X (X = N, B, S, Si, ...) bonds under mild conditions.[659] The work by Molander et al.,[660] where trifluoroborates were coupled with aryl bromides, and by Macmillan et al.,[661] where amino acids were decarboxylatively coupled with aryl halides, inspired other groups to apply this dual catalysis method to new transformations, often using continuous-flow technology to benefit from the improved light irradiation and better reaction control compared to batch conditions.

Ley et al. translated the $C(sp^2)-C(sp^3)$ cross-coupling method by Molander et al. to a flow protocol (Scheme 136).[662] However, initial experiments with trifluoroborates immediately led to clogging issues. To achieve homogeneous reaction conditions, boronic esters were employed as an alternative to trifluoroborates and DMAP (4-(dimethylamino)-pyridine) was identified as a suitable base. The reaction mixture was irradiated with blue LEDs (17 W, 420 nm) in an FEP capillary (1.3 mm ID, 10 mL volume), resulting in yields lower than those in the reported batch method, but in significantly reduced reaction time (82% in 50 min, STY of 100 $mmol \cdot h^{-1} \cdot L^{-1}$ in flow, versus 94% in 24 h, STY of 2 $mmol \cdot h^{-1} \cdot L^{-1}$ in batch). In terms of practicality, the protocol suffered from two disadvantages: the use of large amounts of additives and the glovebox solution preparation of the air-sensitive nickel catalyst. The use of an external base additive could be circumvented by using cyanopyridines instead of aryl bromides as electrophilic coupling partner. These cyanopyridines serve as a Lewis base, accepting an electron from the boronic ester partner, providing a net neutral photoredox process.

A nickel/photoredox dual catalysis approach was developed by researchers at Vertex Pharmaceuticals for the $C(sp^2)-C(sp^3)$ cross-coupling of (hetero)aryl bromides with potassium alkyl trifluoroborates in continuous-flow (Scheme 137).[663] At the outset of the investigation, the following requirements were

Scheme 136. Activation of boronic esters for $C(sp^2)-C(sp^3)$ Cross-Coupling via Dual Photoredox/Nickel Catalysis in Flow

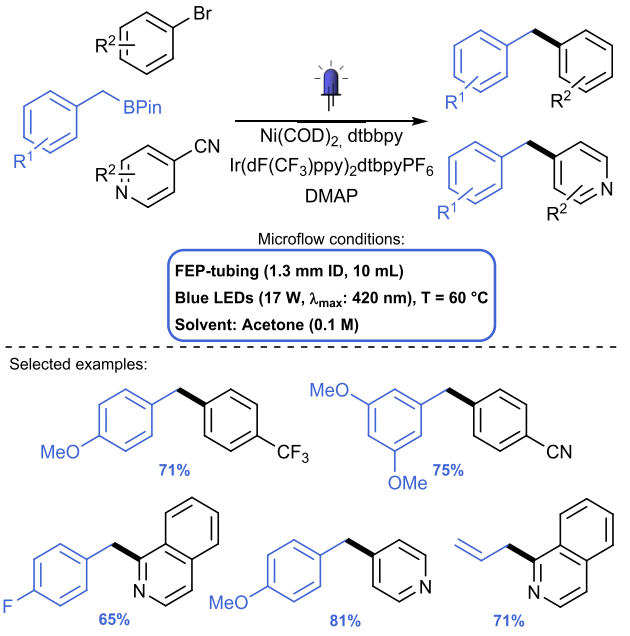

Scheme 137. Universal Flow Protocol for Dual Catalytic $C(sp^2)-C(sp^3)$ Cross-Coupling of Aryl Bromides with Primary and Secondary Alkyls

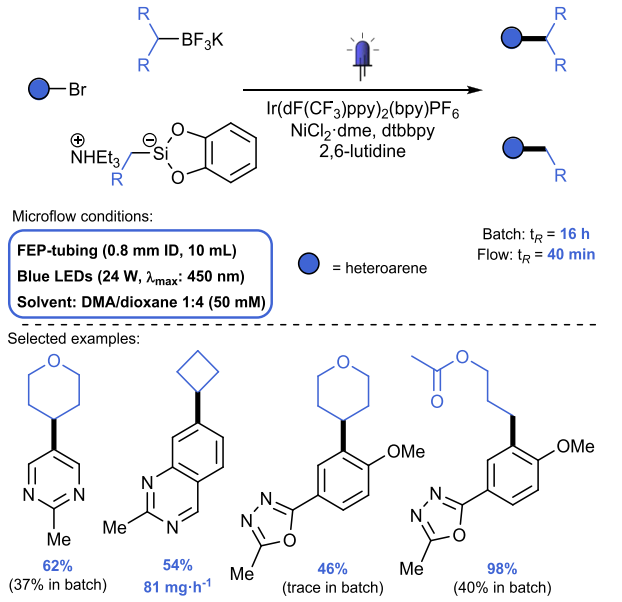

defined for the cross-coupling protocol: (1) to allow for rapid, parallel synthesis with minimal O_2 exclusion, (2) to generate sufficient material for screening and pharmacokinetic studies, (3) to allow for a broad substrate scope, and (4) to achieve sufficiently high yields. Initial experiments in batch provided 37% yield of the cross-coupled product in 16 h but were heterogeneous in nature. For the flow reactions, a homogeneous reaction mixture was required, which was achieved by using 2,6-lutidine as base instead of Cs_2CO_3 and by using a 1:4 DMA/dioxane solvent mixture. The new reaction conditions were applied in flow, resulting in 62% yield in a significantly shorter reaction time (40 min). After setting the optimal

https://doi.org/10.1021/acs.chemrev.1c00332
Chem. Rev. 2022, 122, 2752−2906

reaction conditions, a substrate scope was carried out. To create a library of cross-coupled products, a stock solution was prepared of aryl bromide, nickel precatalyst, ligand, photocatalyst and base, which was added to a number of potassium trifluoroborates and diluted with dioxane. The cross-coupling reaction in flow under blue LED irradiation (24 W, 450 nm) provided the desired products in sufficiently high yields for further investigation, with the limitation that primary alkyl trifluoroborates were not reactive. Additionally, the cross-coupling of a challenging compound with a 1,3,4-oxadiazole moiety provided 46% isolated yield with the flow protocol, whereas only trace amounts of product were obtained in batch.

The limitation of unreactive primary alkyl trifluoroborates was later addressed by using catechol silicates as primary alkyl coupling partner (Scheme 137).[664] As these catechol silicates are generally not commercially available or easily accessible, a protocol compatible with both alkyl donors was desirable. Additionally, to enable the preparation of a convenient stock solution, an air-stable nickel and photocatalyst were used ($NiCl_2$·dme and $[Ir(dF(CF_3)ppy)_2(bpy)]PF_6$), which are compatible with both coupling partners. Hence, a universal protocol was developed for both alkyl trifluoroborates and alkyl silicates, providing a wide range of products with high sp^3 character.

By using the same catalytic system and flow setup, the method was also applied to the $C(sp^2)-C(sp^3)$ cross-coupling of bromo azaindoles and cycloalkyl boronic acids (Scheme 138).[665] An extensive scope was performed with 2-, 3-, 4-, 5-,

Scheme 138. $C(sp^2)-C(sp^3)$ Cross-Coupling of Bromo Azaindoles and Cycloalkyl Boronic Acids to Prepare a Library of Monosubstituted 7-Azaindoles

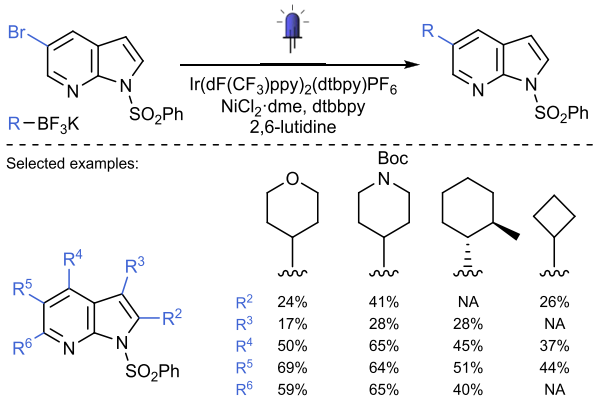

or 6-bromo-substituted 7-azaindoles, creating a range of regioisomers when coupled with various carbo- and heterocycles. As in the case of the (hetero)aryl bromides, the reaction time could be significantly reduced by going from batch (24 h) to flow (40 min).

A reductive coupling between benzyl chlorides and (hetero)aryl bromides was performed by researchers at Merck, providing access to a library of di(hetero)arylmethanes in continuous-flow (Scheme 139).[666] A reported batch protocol[667] was first adjusted to enable the coupling with benzylic bromides under homogeneous reaction conditions with DIPEA as base and DMA as solvent. In the flow reactor, comparable results were obtained under blue LED irradiation (24 W, 450 nm) in 30 min residence time, which enabled the screening of 20−24 reaction conditions per day by using an

Scheme 139. Reductive Coupling between Benzyl Chlorides and Aryl Bromides by Dual Photoredox/Nickel Catalysis

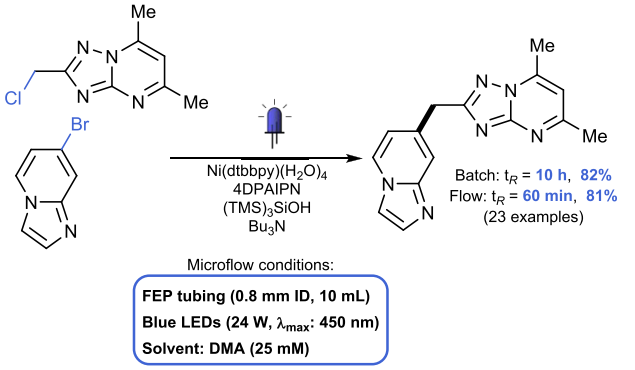

autosampler. After these screening tests, an alternative organophotocatalyst (4DPAIPN), reducing agent ($(TMS)_3SiOH$) and base (tributyl amine) were selected. The inability of $(TMS)_3SiOH$ to serve as a hydrogen atom donor resulted in less dechlorination side product, compared to reactions performed with $(TMS)_3SiH$. Higher yields were also observed with extended residence times (81% in 60 min, versus 61% in 30 min), but short residence times were preferred to enable rapid library synthesis. Two libraries were generated, the first containing variations of aryl bromide, the second containing variations of benzyl chloride. In general, complex coupling partners, relevant for medicinal chemistry studies were used and in 23 out of 34 cases, sufficient material was formed for in vitro pharmacological assays.

N-Boc-protected proline was used by researchers at Janssen Pharmaceuticals in $C(sp^2)-C(sp^3)$ cross-coupling reactions with various aryl halides using dual photoredox and nickel catalysis (Scheme 140).[668] Reactions were first carried out in

Scheme 140. Dual Catalytic $C(sp^2)-C(sp^3)$ Cross-Coupling of N-Boc-Protected Proline with Aryl Halides

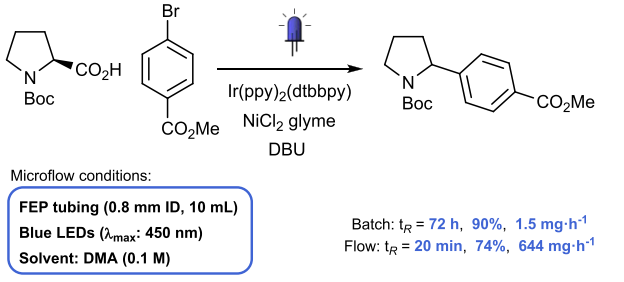

batch in a parallel screening photoreactor. The different vials were irradiated with a CFL lamp (9 W, 450 nm) to evaluate different solvents and bases. After DMA and DBU were identified as best performing solvent and base, respectively, the protocol was subsequently translated to flow. For the flow reactions, a solution of photocatalyst and carboxylic acid was mixed in a T-mixer with a solution of aromatic halide, nickel catalyst and base and introduced in a FEP capillary reactor (0.8 mm ID, 10 mL volume), equipped with a blue LED light source (450 nm). This resulted in modest to good isolated yields of 30−74% for a wide range of aromatic halides, including aryl bromides bearing ester, nitrile and trifluoromethyl functional groups and monocyclic or bicyclic heterocycles. Importantly, the reaction time could be

https://doi.org/10.1021/acs.chemrev.1c00332
Chem. Rev. 2022, 122, 2752−2906

significantly reduced in flow (20−40 min) compared to batch (3 days).

The cross-coupling of alkylsilicates with aryl chlorides was investigated by Fensterbank, Olivier, and co-workers utilizing photoredox/nickel catalysis in flow (Scheme 141).[669] An

Scheme 141. Metal-Free Borylation of Electron-Rich Aryl Halides under Continuous Flow

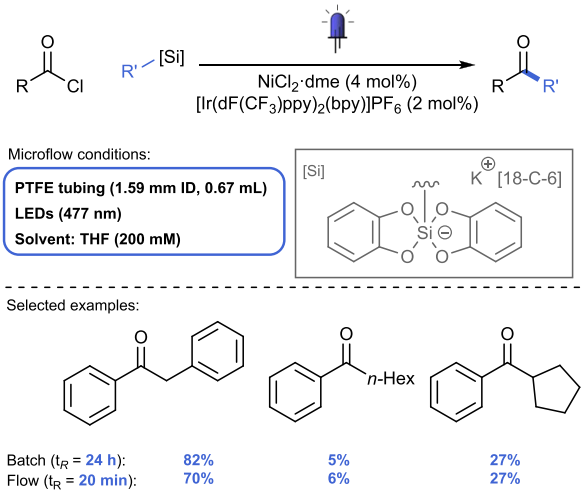

optimization of the solvent, photocatalyst and leaving group was first carried out in batch for the coupling of cyclohexyl silicate ([Si]) and a selection of benzoyl halides. The best conditions were found to involve THF, an iridium photocatalyst ($[Ir(dF(CF_3)ppy)_2(bpy)]PF_6$) and acyl chlorides. Next, a substrate scope of 24 examples was completed in batch with irradiation for 24 h, yields of 8−88% were obtained for a range of silicates and benzoyl chlorides. Finally, 3 examples were performed in continuous-flow in a PTFE capillary (1.59 mm ID, 0.67 mL volume) and irradiated with blue LEDs (477 nm). Comparable yields were obtained in flow with the reaction time being reduced from 24 h in batch to just 20 min in flow.

5.8.3. C−H Activation. An increasing amount of research has been devoted to the development of novel C−H bond activation methods to form carbon−carbon bond linkages.[670,671] Notably, this is also an important strategy to enable late-stage functionalizations.[672,673] However, this approach is often limited by the relative inertness of the C−H bond, resulting in harsh reaction conditions, with high catalyst loadings and long reaction times. However, flow technology has the potential to boost C−H functionalization.[314,639,640] Interestingly, Hydrogen atom transfer (HAT) photocatalysis represents a powerful tool in this sense, as it allows a homolytic C−H bond cleavage.[65,674]

The use of eosin Y[675] as a HAT photocatalyst for C−H activation was reported by Wu et al. (Scheme 142).[676] The neutral form of this cheap photocatalyst activates different $C(sp^3)$−H bonds using visible light irradiation.[677] Ethers, thioethers, alcohols, aldehydes, benzylic positions, and cycloalkanes can all efficiently undergo the hydrogen atom abstraction forming a radical, which is subsequently trapped by electron-deficient olefins. To prove the scalability of this reaction, three examples were performed in a flow reactor, consisting of a HPFA capillary (0.76 mm ID, 15 m length, 7 mL volume) that was heated to around 50 °C in a water bath.

Scheme 142. Eosin Y-Photocatalytic HAT Activation of C−H Bonds

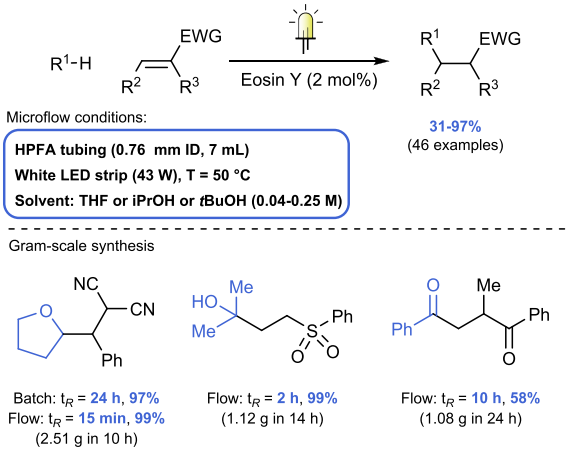

The irradiation was performed with a 43.2 W white LED strip. This resulted in high yields and productivities, in much shorter reaction time compared to batch. For example, the reaction with THF resulted in 99% yield in 15 min residence time in flow (0.25 $g \cdot h^{-1}$), compared to 97% yield in 24 h in batch.

Light alkanes are very challenging toward activation, because of the high BDE of the C−H bonds (up to 105 $kcal \cdot mol^{-1}$ for methane). A method to activate these inert alkanes was suggested by Zuo et al., who applied LMCT-enabled HAT catalysis with a cheap cerium(IV) chloride salt (Scheme 143).[678] The authors suggested that Ce(IV)-alkoxy complex,

Scheme 143. Chlorine Radical-Photocatalyzed C−H Activation of Alkanes in Flow

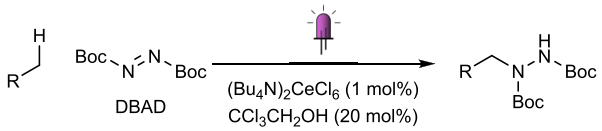

Microflow conditions:
PFA tubing (3.17 mm ID, 4.5 mL)
UV LED (400 nm)
Solvent: CH_3CN (0.05 M)

Alkane	t_R	Yield	Productivity
CH_4 (1800 kPa)	15 min	15%	0.6 $mmol \cdot d^{-1}$
C_2H_6 (1500 kPa)	6 min	90%	2.0 $mmol \cdot h^{-1}$
C_3H_8 (800 kPa)	6 min	76%	1.7 $mmol \cdot h^{-1}$
C_4H_{10} (800 kPa)	6 min	56%	1.3 $mmol \cdot h^{-1}$
C_6H_{12} (22 mL)	9 min	70%	4.2 $mmol \cdot h^{-1}$

formed in situ from an alcohol and a Ce(IV) salt, would undergo photoinduced LMCT. This would generate a reduced Ce(III) and an alkoxy radical, which abstracts a hydrogen from the light alkane. The so-formed radical rapidly reacts with a suitable radical acceptor, for example, di-*tert*-butyl azodicarboxylate (DBAD). However, more recently, it became apparent that not the alkoxy radical but the chlorine radical is the HAT-inducing species.[679] The implementation of a continuous-flow system involved 10 parallel microreactors for a total volume of 4.5 mL (PFA tubing, 3.17 mm ID). When

https://doi.org/10.1021/acs.chemrev.1c00332
Chem. Rev. 2022, 122, 2752−2906

ethane and higher alkanes were employed, the amination products were obtained in good to excellent yields, with good productivities (up to 2 mmol·h^{-1} for ethane and 4.2 mmol·h^{-1} for cyclohexane). However, methane was not easily functionalized in flow. In batch, it was possible to use a higher pressure (5000 kPa), which was prohibitive in flow because of the physical limitations of the photoreactor. However, with 1800 kPa of methane, 15% of product was obtained.

A different photocatalytic approach was developed by Noël et al. to activate light alkanes (Scheme 144).[680] In this case,

Scheme 144. TBADT-Photocatalyzed C−H Activation of Gaseous Feedstocks in Continuous Flow

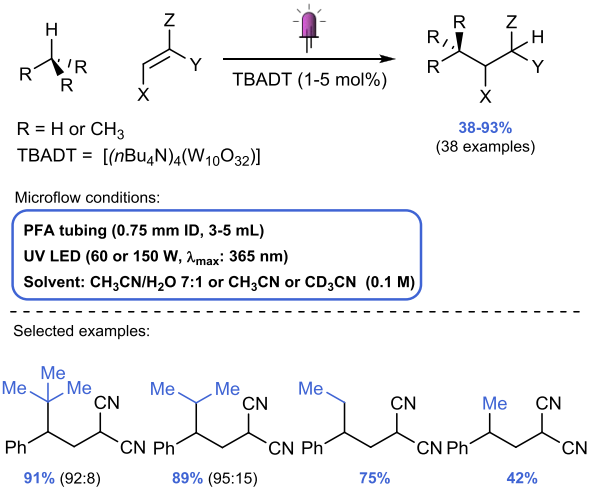

tetrabutylammonium decatungstate ($[(n\mathrm{Bu}_4\mathrm{N})_4(\mathrm{W}_{10}\mathrm{O}_{32})]$, TBADT) was employed in flow to activate the C−H bonds of various gaseous alkanes, namely isobutane, propane, ethane and methane. Using a Vapourtec UV-150 photochemical flow reactor (3−5 mL PFA tubing irradiated with 60 W UV-LEDs) and a back-pressure regulator to ensure the complete solubilization of the gaseous substrate. The feasibility of the reaction was tested with a few TEMPO trapping experiments and showed the high selectivity of the generation of the most stable radical in the case of isobutane and propane. Encouraged by the positive results obtained, the reaction with electron-poor olefins was evaluated, with complete conversion obtained in only 4 h residence time. The solvent of choice was either acetonitrile/water or neat acetonitrile, depending on the solubility of the starting materials. To activate methane, a higher pressure and catalyst loading (5 mol %) were required and a more powerful UV-LED (150 W) was used. Under these intensified conditions, deuterated acetonitrile was used instead of acetonitrile to avoid activation of the solvent. Flow technology was essential to obtain the desired results, as it facilitated the two-phase process.

TBADT is also known to activate aldehydes.[681] An interesting example is reported by Fagnoni, Ravelli, and co-workers, who described the multistep synthesis of β/γ-substituted ketones starting from the addition of aldehydes onto vinyl sulfones in continuous-flow (Scheme 145A).[682] After the first TBADT-photocatalytic step (PTFE tubing, 12 mL), the subsequent desulfonylation was performed in basic conditions by adding tetramethyl guanidine to the reaction stream through a T-mixer. The obtained α,β-unsaturated carbonyl compound could undergo Michael addition of a

Scheme 145. (A) Continuous-Flow Multistep Alkylation of Indoles Starting from the Photocatalytic Acylation of Electron-Poor Olefins and (B) TBADT-Photocatalyzed Synthesis of Aminopropylsulfone in Flow

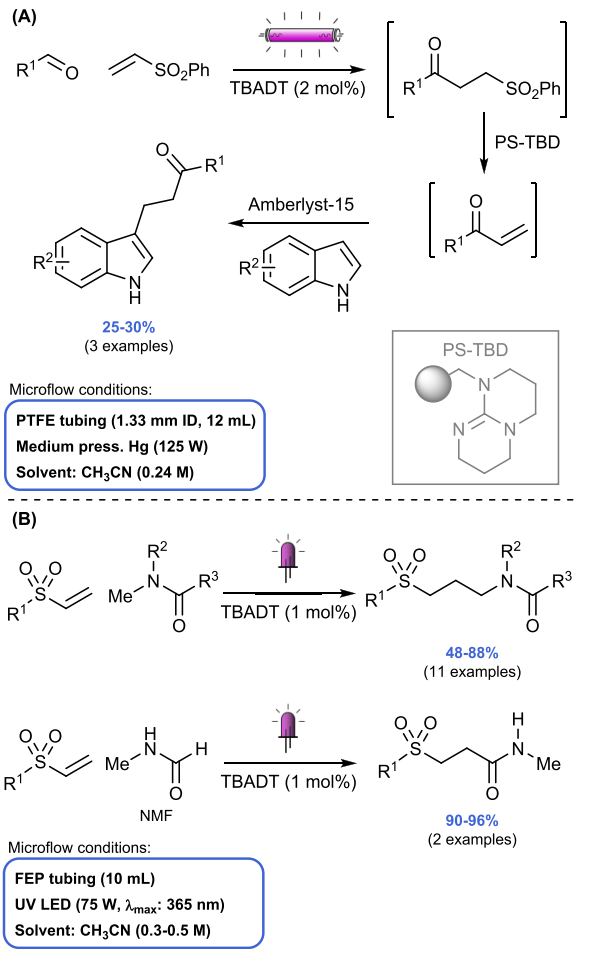

nitroalkane affording a γ-nitro carbonyl compound (3 examples, 52−67%). Alternatively, the desulfonylation took place in a column containing PS-supported TBD (polystyrene supported-triazabicyclodecene), after which an indole was introduced in flow to perform a Friedel−Crafts reaction with the α,β-unsaturated carbonyl. The resulting β-(3-indolyl) ketone was obtained in 25−30% overall yield (3 examples). The application of a flow system was particularly advantageous in this case, because it allowed the combination of orthogonal reaction conditions with the presence of supported reagents/catalysts. For aldehyde substrates that possess other labile C−H bonds or which are too volatile, Fagnoni et al. reported an alternative method.[683] In this method, the acyl radical was formed starting from acylsilanes in the presence of TBADT or acridinium salt as the photocatalysts. The reaction between the so-formed acyl radical and the electron-poor olefin was repeated in flow, in a 12 mL PTFE reactor irradiated with a 125 W medium-pressure mercury lamp. The product was isolated in slightly better yield than in batch (72% vs 69%), requiring 4 h reaction time instead of 8 h to reach full conversion.

In another work on vinyl sulfones, TBADT was used to activate alkyl amides whose radical would perform a Michael addition, thus forming γ-aminopropylsulfones (Scheme

https://doi.org/10.1021/acs.chemrev.1c00332
Chem. Rev. 2022, 122, 2752−2906

145B).[684] To this end, a Vapourtec E-series reactor was chosen (10 mL FEP coil). The nature of the light source proved to affect the reaction outcome. In fact, high-power 365 nm LED outperformed a medium-pressure mercury lamp (110 W), especially at higher concentrations and in shorter residence times (15 min). This was most likely due to the higher photon flux at the desired wavelength. Interestingly, when using *N*-monomethylformamide (NMF), the formyl C−H bond was activated instead of the *N*-methyl group. The reliability of the process was confirmed in a scale-up reaction, which afforded the product in 95% yields with a productivity of 20 mmol·h^{-1}.

Wu et al. combined iridium photocatalysis and nickel catalysis to activate ethers and amides, which can then be alkenylated (Scheme 146).[685] The authors employed con-

Scheme 146. Chemo- and Regioselective Functionalization of Internal Alkynes Photocatalyzed by Ir(III)/Ni(II) in Flow[a]

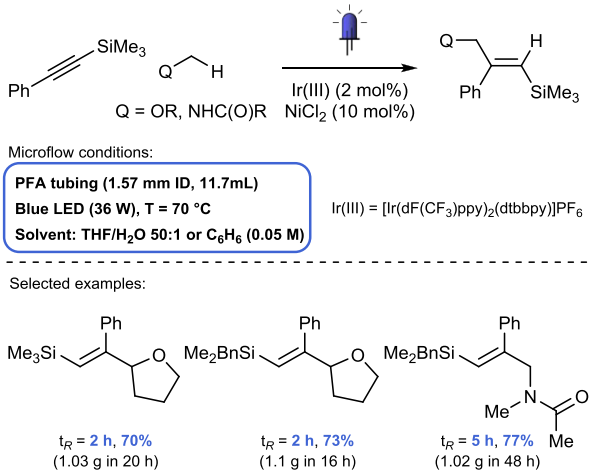

[a]Regioselectivity and *E*/*Z* ratio are >20:1 for the three compounds.

tinuous-flow technology to carry out a gram-scale experiment of the proposed method. To this end, a PFA coil (11.7 mL) was placed in a water bath at 70 °C equipped with 18 W blue LEDs. The yields were comparable to those in batch, but the reaction time was dramatically decreased, from up to 48 h in batch to 2−5 h in flow.

The development of homogeneous palladium catalysis in flow is a fast-growing research area.[641] An example of a dual photoredox/transition-metal catalysis in flow is the C−H acylation of indoles reported by Noël, Van der Eycken, and co-workers (Scheme 147).[686] Both aromatic and aliphatic aldehydes were employed as acyl surrogates. Even though batch conditions were effective, reactions in flow (PFA capillary 0.76 mm ID, 1.3 mL volume irradiated with 3.12 W blue LED) performed better, reaching higher yields in shorter reaction times (20 h in batch vs 2 h in flow) with lower photocatalyst loading (from 2 to 0.5 mol %). This difference was explained by poorer light absorption in batch, especially in the larger-scale reaction. In the proposed mechanism, the Pd(II)-catalyst is responsible for C−H activation of the indole, whereas the excited Ir(III)-photocatalyst is needed to produce the *t*BuO$^{\bullet}$ radical from TBHP, which subsequently reacts with the aldehyde to give an acyl radical. Moreover, the photocatalytic cycle allows the oxidation of the Pd(II)-complex to Pd(IV), before the reductive elimination takes place.

Scheme 147. Combination of Photo- and Transition Metal Catalysis to Acylate Indoles in Continuous Flow

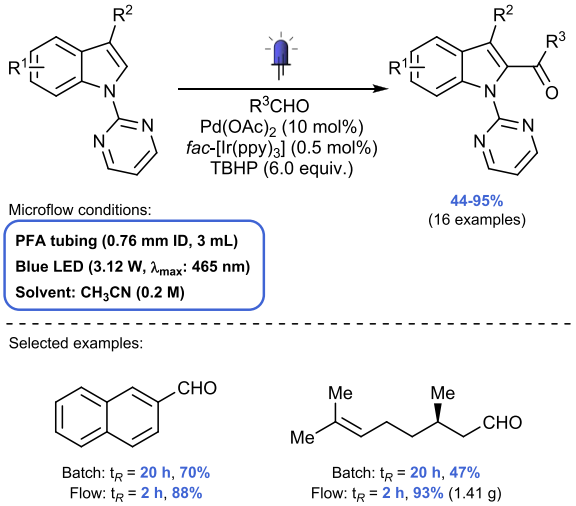

TBADT was also used as a photocatalyst for the alkylation of vinylpyridines, affording the corresponding alkylpyridines.[687] To this end, various C−H bonds were activated (ethers, acetals, amide, nitriles, silane, aldehyde, and cyclohexane). In two cases, the reaction was performed in a flow PTFE reactor (1.3 mm ID, 12 mL volume) irradiated with a 125 W medium-pressure mercury lamp. The reported yields were comparable (64% vs 67%) or higher (86% vs 68%) in flow compared to batch, although the reaction time was much shorter (5 vs 16−24 h).

Wu et al. described the use of a "stop-flow" microtubing (SFMT) parallel reactor system for C−H functionalization.[688] The aim was to address some issues related to conventional flow systems, such as the inefficient parallel screening of parameters and the difficulty of performing reactions at longer residence times. The SFMT reactor provides a suitable platform for parallel reaction screening of continuous-flow parameters. In the SFMT reactor, the flow of reagents can be stopped when the tubing has been filled with the desired volume and pressure. After both shut-off valves at either end of the tubing have been closed, the reactors are irradiated for the required time. However, it should be noted that due to the stop flow procedure, mixing is solely driven by diffusion processes and thus a complete comparison with continuous-flow cannot be made.

SFMT reactors were employed in the [Acr-Mes]ClO_4-photocatalytic oxidation of unactivated benzylic and allylic C−H bonds (Scheme 148).[689] This transformation was notable because it represents the first oxidation of this kind performed with an organo-photocatalyst. Under light irradiation, the excited state of [Acr$^+$-Mes]ClO_4 performs an SET and the formed benzylic/allylic radical cation was then deprotonated, which proceeds to attack the Michael acceptor. SFMT reactors are used both to considerably shorten reaction times in some cases (from 20 to 5 h), as well as to afford better results when conversions were low. To scale up the reaction, a continuous-flow reactor (HPFA coil, 1.6 mm ID) was used to obtain 1.1 g of product after 25 h of collection.

Acridinium perchlorate was also used to produce chlorine radicals from HCl under visible light irradiation in continuous-flow by Wu et al. (Scheme 149A).[690] Acridinium ions can oxidize chloride ions forming chlorine radicals, these radicals

https://doi.org/10.1021/acs.chemrev.1c00332
Chem. Rev. 2022, 122, 2752−2906

Scheme 148. Photocatalytic Allylic Alkylation with Acridinium Ion Performed in a SFMT Reactor with [Acr-Mes]ClO_4

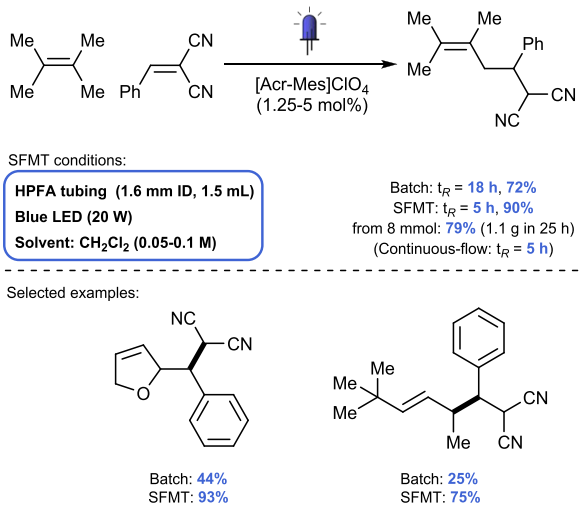

Scheme 149. (A) Photocatalytic Alkylation of Unactivated C−H Bonds Mediated by Chlorine Radical in a SFMT Reactor and (B) Photocatalytic Alkylation and Amination of Unactivated C−H Bonds Mediated by Bromine Radical in a SFMT Reactor

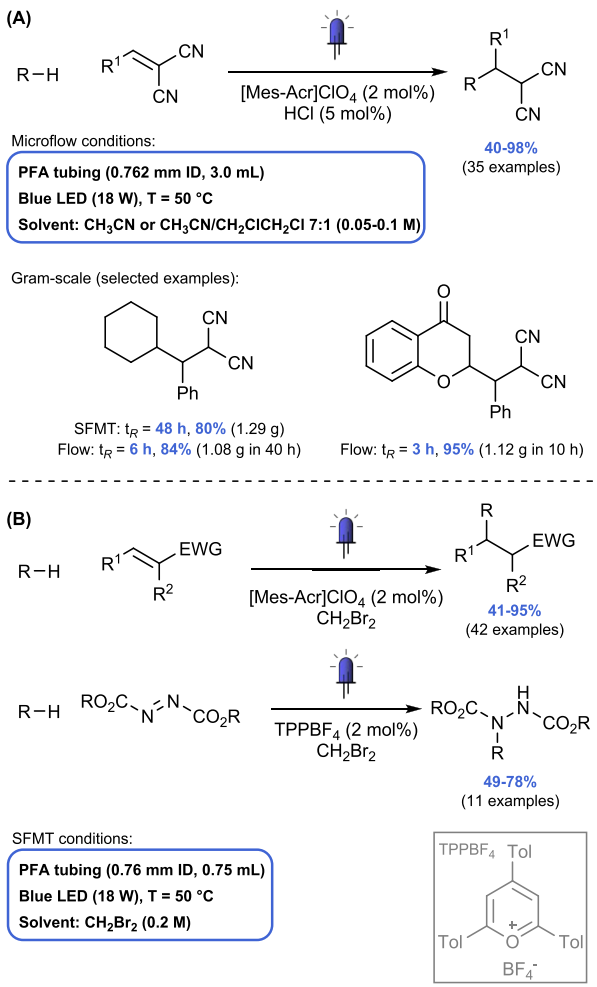

are known to abstract hydrogen atoms from unactivated alkanes (even primary ones, such as ethane). SFMT reactors (0.76 mm ID, 3.0 mL volume at 50 °C) ensure better conversions and excellent reproducibility since HCl cannot escape from the reaction mixture. The scale-up of the reaction was performed both in a larger SFMT reactor (27.2 mL) and in a continuous-flow microreactor. Similar yields were obtained for both methods (~80%, but in 48 h for SFMT and in 6 h in continuous-flow).

In a more recent report from Wu et al., acridinium photocatalysis was used to generate bromine radicals from CH_2Br_2 (Scheme 149B).[691] The generated C-centered radical was capable of alkylating electron-poor olefins and dialkylazodicarboxylates, when switching to a pyrylium salt ($TPPBF_4$) as photocatalyst. A PFA capillary (0.76 mm ID, 0.75 mL volume) was placed in a water bath at 50 °C and irradiated with 18 W LEDs. Compared to previous work from the same authors,[690] bromine radicals were more selective than chlorine radicals. An SFMT reactor (1.58 mm ID, 27.2 or 59.3 mL volume) was used to provide scale-up to gram-scale and proved to be a very efficient method for avoiding loss of the in situ generated HBr, which acted as a more reactive bromine radical source.

Recently, an SFMT reactor was used by Zhang, Wang, and co-workers for the gram-scale reaction between a tertiary amine and benzoyl cyanide.[692] Their system exploited the formation of an electron donor−acceptor (EDA) complex, which then undergoes SET followed by a HAT process to finally yield α-amino nitriles. The SFMT reactor led to high yield (81%) in shorter reaction time compared to batch (4 h in SFMT vs 24 h in batch).

5.8.4. C−H Arylation Processes Using Diazonium Salts. Among different photochemical approaches to establish C−C bonds,[693] diazonium salts play an important role, being widely studied as aryl radical precursors.[694−696] The use of these unstable salts (due to the release of nitrogen) benefits from a higher safety degree associated with flow technology. For instance, the C−H arylation of 2*H*-indazole was previously only possible through transition metal catalysis, with expensive ligands and additives.[697,698] Recently, however, a photocatalytic procedure was developed starting from an aryl diazonium tetrafluoroborate using inexpensive eosin Y as the photocatalyst (Scheme 150).[699] The batch transformation,

Scheme 150. Continuous-Flow Photocatalytic C−H Arylation of 2*H*-Indazole

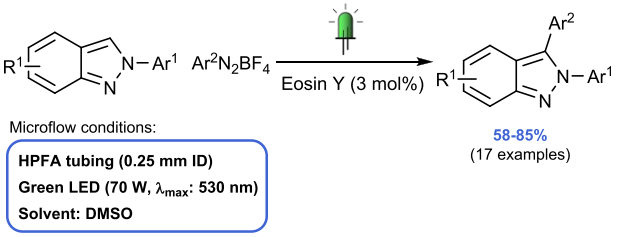

which provided 60% yield in 18 h, was greatly improved in flow (HPFA capillary coil = 0.25 mm ID). In fact, the arylated product was obtained in 76% requiring only 4 min residence time. This improvement was attributed to the high surface/volume ratio of the microfluidic reactor, resulting in more homogeneous irradiation of the reaction mixture and improved mixing.

https://doi.org/10.1021/acs.chemrev.1c00332
Chem. Rev. 2022, 122, 2752−2906

The photocatalytic arylation of heteroarenes with aryl diazonium salts was investigated by Rueping, Rehm, and co-workers in a microstructured falling film reactor (FFMR, Scheme 151).[172] The working principle of a FFMR relies on

Scheme 151. (A) FFMR Design and (B) Arylation of Heteroarenes with TiO_2 as an Immobilized Photocatalyst in FFMR

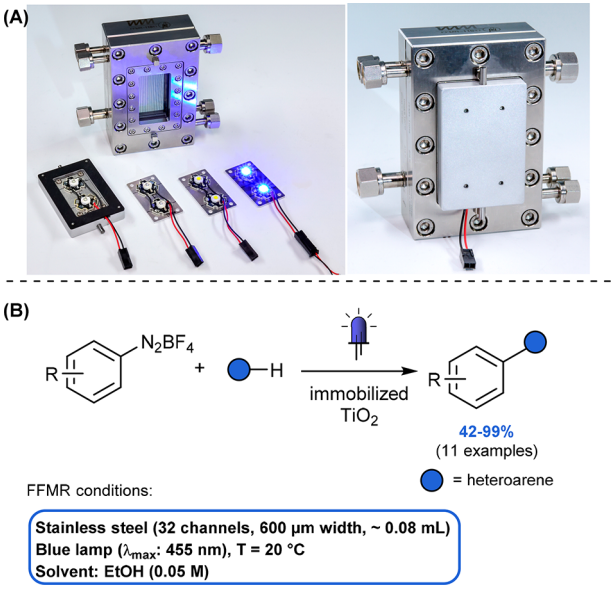

Panel A: Reprinted from ref 172. Published by Royal Society of Chemistry. Copyright Fraunhofer IMM.

the formation of a liquid thin film in the microchannels with a film thickness below 100 μm. After a previous report in batch,[700] the development of a flow system was difficult due to the heterogeneity of the reaction mixture.[483] Therefore, the heterogeneous semiconductor catalyst was immobilized on the microchannels of the reactor. Interestingly, only blue light (and not UV light) was required for the transformation, as a TiO_2-diazo ether is formed which absorbs light around 450 nm. The reusability of the immobilized catalyst was demonstrated with a 180 min run and was successfully applied in batch and in the FFMR. The specific reactor performance in the FFMR was around 6000 times better than in batch (0.32 vs 5.4 × 10^{-5} · mol·L^{-1} min^{-1}, respectively). This was explained by the significantly improved irradiation of the photocatalyst in the microchannels.

The arylation of (hetero)arenes with aryl diazonium salts was done by Ackermann et al. using a Mn(I)-catalyzed strategy (Scheme 152).[701] The mechanism involves the coordination of the two coupling partners at the metal center and subsequent photoexcitation of the complex, which generates subsequently radical intermediates. After radical combination, the aryl-heteroarene product is formed. Reactions were performed in a capillary coil (1.3 mm ID, 10 mL volume) irradiated with blue LEDs (450 nm). The method enabled a broad scope with excellent yields and high regioselectivity. Additionally, results in flow outperformed those obtained in batch, especially at gram-scale. In fact, when starting from 10 mmol of diazonium salt, 64% yield was observed in flow in 60 min residence time, whereas only 25% was obtained in batch.

A continuous-flow method for the synthesis of benzofuran was developed by Polyzos et al. through annulative carbon-

Scheme 152. Mn(I)-Photocatalytic Arylation of (Hetero)Arenes with Diazonium Salts

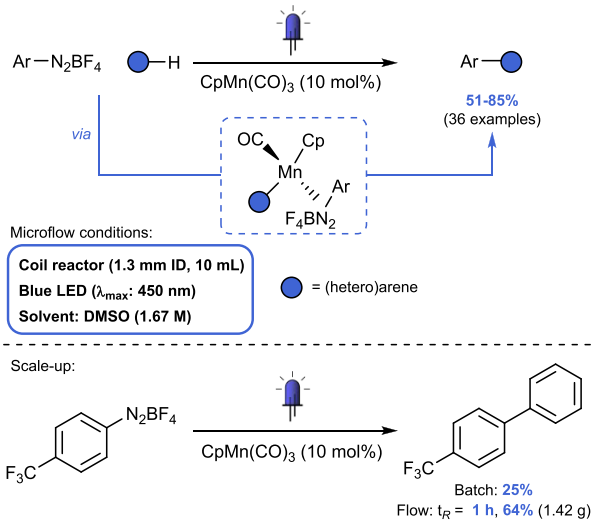

ylation of alkenyl-tethered arenediazonium salts (Scheme 153).[702] Subjected to blue LED irradiation (14 W), the

Scheme 153. Benzofuran Synthesis through Ir(III)-Photocatalyzed Carbonylation

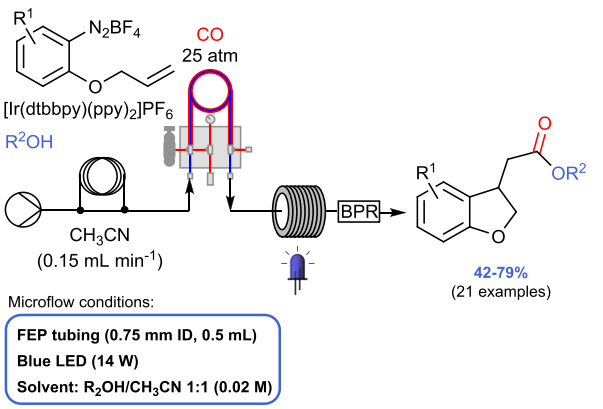

photocatalyst induces the homolytic cleavage of the C–N bond, which is followed by intramolecular radical alkene addition. The resulting carbon-centered radical reacts with CO and is subsequently quenched with the alcohol. For this purpose, a commercially available Teflon AF-2400 tube-in-tube reactor was used to facilitate the handling of CO gas. Compared to batch, the flow setup (FEP capillary: 0.75 mm ID, 0.5 mL volume) facilitates process intensification and easy scale-up. By changing to a reactor volume of 1.5 mL, the scale of the reaction could be increased 20 times (to 4 mmol), affording the dihydrobenzofuran in 72% yield.

Basso et al. proposed an intermolecular synthesis of benzofuranones and benzopyranones starting from benzene-diazonium salts and alkenes (ethyl 2-vinylbenzoate and methyl methacrylate, respectively).[703] $Ru(bpy)_3Cl_2$ was selected as the photocatalyst. The presence of an ester functionality either in the benzenediazonium salt or in the styrene counterpart determines the selectivity toward the benzo-fused six- or five-membered ring. The flow reactor consisted of a FEP capillary (0.8 mm ID, 1 mL volume) irradiated with blue LEDs (440 nm). With a residence time of 10 h, the obtained yield for the

https://doi.org/10.1021/acs.chemrev.1c00332
Chem. Rev. 2022, 122, 2752–2906

benzopyranone scope were generally higher than in batch (up to 20% better).

Diazonium salts were also used in the coupling with arylate enol acetates, as reported by de Oliveira et al. using a porphyrin-catalyzed flow process (Scheme 154).[704] Compared

Scheme 154. Porphyrin-Photocatalyzed Arylation of Enol Acetate in Flow with Porphyrin Photocatalyst

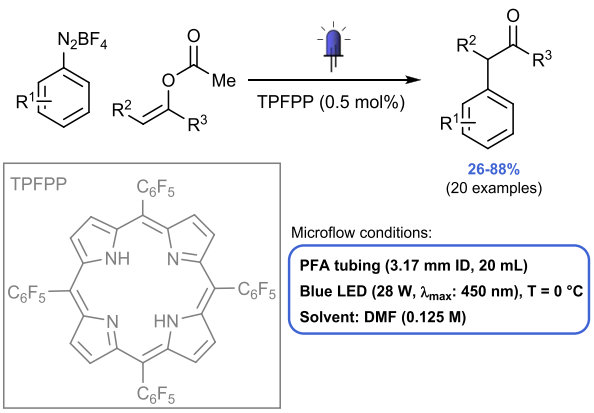

to previous results in batch where a ruthenium(II) photocatalyst was used,[705] the flow setup showed several advantages: (i) no transition metal is needed, (ii) improved safety regarding diazonium salts, (iii) higher yields, and (iv) shorter reaction times, which altogether led to (v) a broader scope. The reactor consisted of PFA tubing (3.17 mm ID, 20 mL volume) irradiated with blue LEDs (28 W, 450 nm). In this setup, the activation of diazonium salt was achieved with only 0.5 mol % of porphyrin photocatalyst, providing generally high yields of the arylated product (26−88%) in 25 min residence time (vs 2 h in batch).

A new reactivity of diazonium salts was disclosed by Basso, Ravelli, and co-workers, as they reported the photocatalyzed generation of acetonyl radicals in flow (Scheme 155).[706] Irradiation of the diazonium salt and ethyl 2-vinylbenzoate in acetone in the presence of $[Ru(bpy)_3]Cl_2$ (1 mol %) afforded

Scheme 155. (A) Continuous-Flow Photocatalytic Generation of Acetonyl Radical from a Diazionium Salt and (B) Photocatalytic Reaction between Acetonyl Radical and Silyl Enol Ethers in Flow

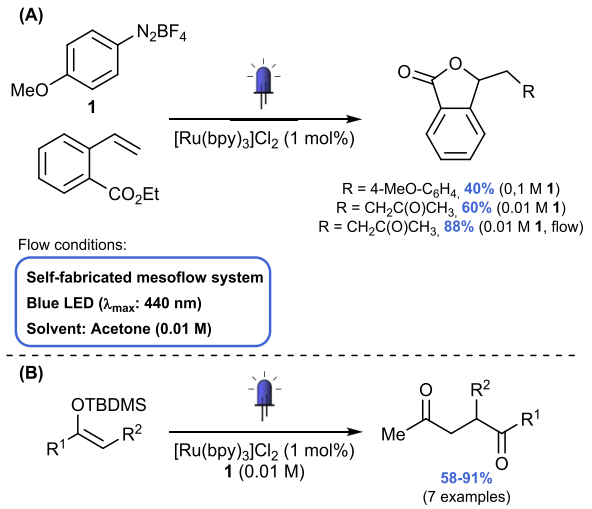

the arylated lactone. However, when diluting the reaction mixture 10 times, the acylated lactone was obtained (Scheme 155A). These results were explained by the formation of an acetonyl radical through HAT from the diazonium salt derived aryl radical. Computational studies and deuterium labeling experiments confirmed this hypothesis. When acetonitrile was used instead of acetone, the corresponding nitrile was observed in traces with GC-MS, because the cyanomethyl radical does not add to the double bond. However, the described conditions worked efficiently also for other radical cyclizations initiated by diazonium salts, and with electron-rich olefins, such as silyl enol ethers (Scheme 155B) because of the electrophilic nature of the acetonyl radical. Reactions in flow generally resulted in higher yields and provided improved safety of operation.

5.8.5. C−H Arylation Processes Using Arylazo Sulfones. Diazonium salts are also suitable precursors for the preparation of a different class of arylating compounds, namely arylazo sulfones. These compounds absorb directly visible light irradiation without the need of a photocatalyst (Scheme 156A).[707] In fact, these reactive compounds either

Scheme 156. (A) Azosulfone-Mediated Arylation in a Sunflow Reactor and (B) Selective Arylation of Xanthene with Aryl Azo Sulfones in a Sunflow Reactor

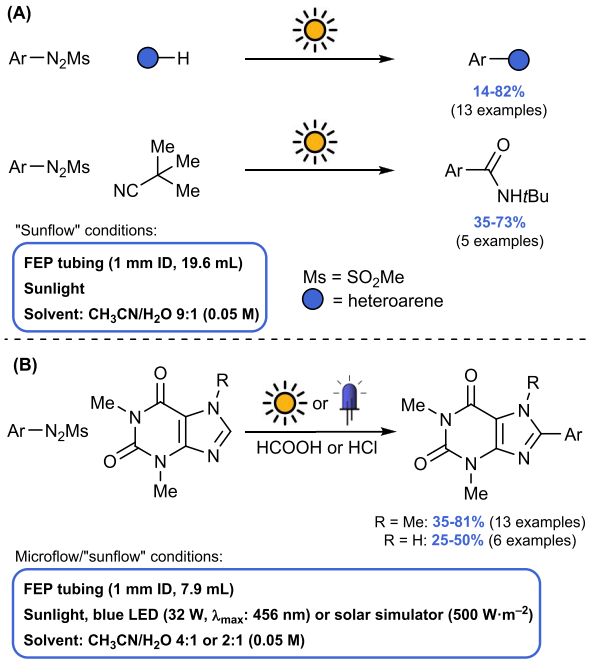

generate an aryl radical through N−S homolysis when irradiated by visible light, or instead generate a triplet aryl cation through N−S heterolysis when UV light is used. Starting from arylazo sulfones, the arylation of heteroarenes was described by Da Silva Emery, Protti, Opatz, and co-workers for the synthesis of benzamide in a "sunflow" reactor.[707] This reactor consists of a FEP capillary (1 mm ID, 25 m length, 19.6 mL volume) which is exposed to sunlight and is moved every hour for better irradiation conditions. The reactor has already proven its efficiency in a number of cross coupling reactions.[708] The reaction between arylazo sulfones and furan or thiophene was completed within 1 h in the sunflow reactor. The sunflow reactor was 8 times faster than batch and irradiation with a 500 W solar simulator in batch provided only a very low yield

https://doi.org/10.1021/acs.chemrev.1c00332
Chem. Rev. 2022, 122, 2752−2906

Scheme 157. Continuous-Flow Reactions with Oxadiazolines As Precursors of Unstable Diazo Compounds: (A) Application to Reactions with Boronic Acids, (B) Synthesis of Ketones from Aldehydes and Oxadiazolines, (C) Three-Component Synthesis of Homoallylic Alcohols and Amines, and (D) Photochemical Homologation of Nonstabilized Diazo Compounds in Flow

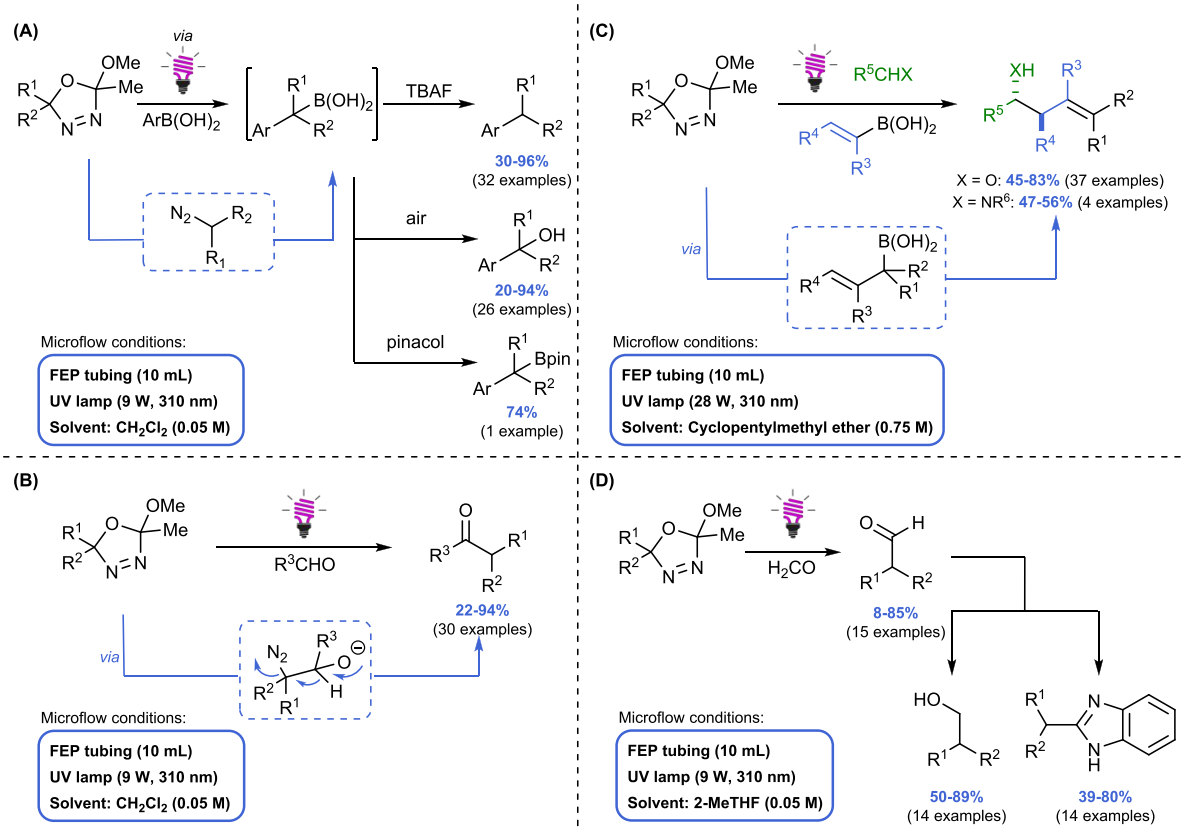

(7%). These results encouraged further investigation on the topic, leading to the development of a metal-free selective 8-arylation of xanthines, compounds with an important biological profile (Scheme 156B).[709] The arylation was mediated by the arylazo sulfones without any catalyst in a stopped "sunflow" reactor (1 mm ID, 10 m length, 7.9 mL volume) irradiated with sunlight for 4 h. Alternatively, a 32 W blue LED could be used as well.

5.8.6. C−H Alkylation Processes Using Oxadiazolines. Oxadiazolines are an interesting alternative to diazo compounds. They are bench-stable heterocycles synthesized from the corresponding ketone.[710] However, under UV light irradiation, they decompose into the corresponding diazo compounds.[711] Ley et al. described how microflow setups allow a safe handling of these intermediates, even the most unstable ones.[456] For instance, the alkyl−aryl cross-coupling of oxadiazolines with boronic acids was reported in a FEP flow reactor (10 mL) irradiated by a UV lamp (9 W, 310 nm) (Scheme 157A).[712] The tertiary boronic acid intermediate is obtained in 80 min residence time and can be reduced with TBAF or oxidized to the corresponding tertiary alcohol. Moreover, treatment with pinacol yields the *B*-pinacolate (Bpin) product, which is used in cross-coupling in flow. In another case, oxadiazolines were employed to react with aldehydes (Scheme 157B).[713] After addition to the carbonyl group, a ketone is formed through 1,2-hydride shift in only 40 min residence time in a FEP capillary reactor (10 mL volume). The transformation has a wide scope, showing good tolerance of various functionalities. Also, a multicomponent reaction was developed, involving an oxadiazoline, a vinylboronic acid, and an aldehyde (Scheme 157C).[714] Through UV irradiation, an allylic boronic acid intermediate is formed which attacks the carbonyl group of the aldehyde, generating its corresponding homoallylic alcohol. For aldehydes with strong absorption at 310 nm, the system could be modified to perform the addition of a carbonyl-bearing compound in a second step. Interestingly, the aldehyde could be substituted with imines and indoles, to afford homoallylic amines instead. To make the process greener, cyclopentylmethyl ether was used as a solvent instead of THF. Finally, a homologation reaction was performed starting from formaldehyde and nonstabilized diazo compounds (Scheme 157D).[715] Once more, a 10 mL FEP reactor was chosen and irradiated with a UV lamp (9 W, 310 nm) without photocatalyst. Despite the excellent conversion, aldehydes were sometimes difficult to isolate in high yields, because of the presence of a large amount of water in the reaction medium and because of their volatility. For this reason, the authors decided to either reduce the crude product with $NaBH_4$ to get the corresponding alcohol, or to perform an oxidative condensation with *o*-phenylenediamine leading to 2-substituted benzimidazole.

5.8.7. C−O Bond Formation. Styrene derivatives were used by Dagousset et al. as traps for alkoxyl radicals which were photogenerated from *N*-alkoxypyridinium salts (Scheme 158).[716] Alkoxy radical addition and subsequent oxidation generates a carbocation, which reacts with a nucleophile in the reaction mixture (e.g., water present in the solvent). Using a capillary reactor (10 mL volume) irradiated with blue LEDs, the products were obtained in comparable yields, but in only 67 min residence time, compared to 24−36 h in batch. The

https://doi.org/10.1021/acs.chemrev.1c00332
Chem. Rev. 2022, 122, 2752−2906

Scheme 158. Photocatalytic Anti-Markovnikov Alkoxylation of Styrene Derivatives in Flow

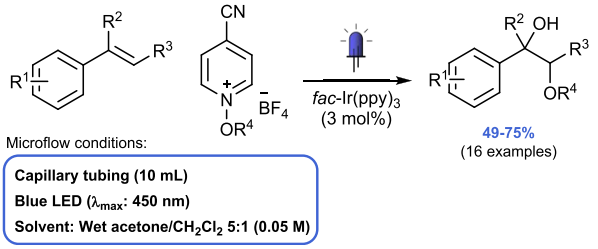

scalability of the transformation proved feasible (4 mmol) in similar yields.

Another example in which oxygen was used as terminal oxidant was provided by Kappe, Cantillo, and co-workers for the *N*-demethylation of oxycodone (Scheme 159).[717] This

Scheme 159. Photocatalytic N-Demethylation of Oxycodone in Flow with Oxygen and RB

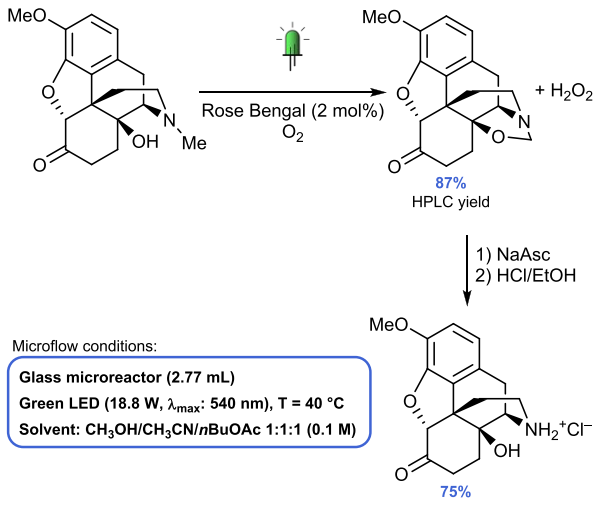

process affords noroxycodone, an important intermediate in the synthesis of naloxone and other medicinally relevant compounds.[718,719] In this study, the demethylation was performed using Rose Bengal (RB) as the photocatalyst, which was excited to its singlet state by green LED irradiation. After intersystem crossing, the RB triplet state was responsible for the oxidation of oxycodone, which subsequently undergoes an HAT from the reduced oxygen. This oxygen species was finally reduced to H_2O_2. The photocatalytic step takes place in a glass microreactor (2.77 mL volume) and was irradiated with green LEDs (18.8 W) to photoexcite RB. The optimal residence time at 40 °C was 3.5 min, as degradation products were observed at longer residence times. After the photocatalytic step, the reaction mixture underwent a workup with sodium ascorbate (NaAsc) to quench the hydrogen peroxide. With a final acidic hydrolysis, the hydrochloric salt of noroxycodone was obtained in 75% yield. At larger scale (6.2 mmol), 1.4 g of the product was collected over 124 min, corresponding to a 68% yield.

Benzylic C−H oxidations are transformations with great potential for the late-stage functionalization of drug-like molecules and thus have extensive benefits for medicinal chemistry. Researchers at UCB Biopharma reported a continuous-flow benzylic C−H oxidation photocatalyzed by riboflavin tetraacetate (RFTA) with iron perchlorate as an additive to allow catalyst regeneration (Scheme 160A).[720] In

Scheme 160. (A) RFTA-Photocatalytic Flow C(sp^3)−H Benzylic Oxidation, (B) Photocatalytic Oxidation of the Remote C−H Bonds of Aliphatic Amines, and (C) TBADT-Photocatalytic Oxidation of C(sp^3)−H Bonds in Flow Using Oxygen

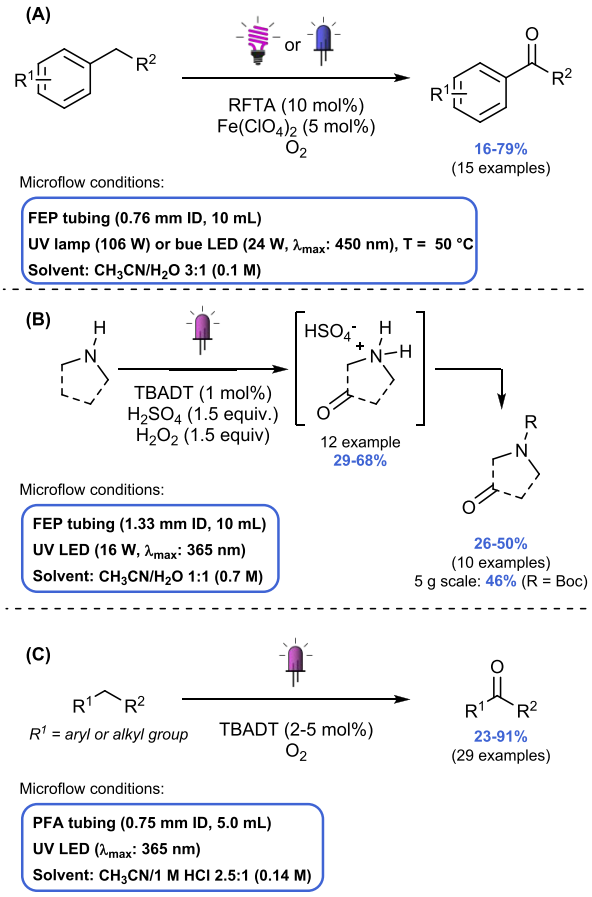

the proposed mechanism, the authors describe the formation of a benzylic radical which interacts with singlet oxygen to generate a peroxo-radical intermediate. The flow system consisted of a capillary coil (1.3 mm ID, 10 mL volume) irradiated by a UV lamp at 50 °C. The transformation works efficiently in 25 min residence time. A different approach for C−H oxidations was proposed by Schultz et al., who employed tetrabutylammonium decatungstate (TBADT) as the photocatalyst (Scheme 160B).[721] Unbiased aliphatic amines were oxidized at remote C−H bonds using oxygen as the terminal oxidant (or with hydrogen peroxide in batch). Using a Vapourtec UV-150 photoreactor (10 mL) irradiated with 16 W UV-LEDs (365 nm), the corresponding ammonium salt was obtained in 29−68% yield and after further derivatization, the protected amine could be isolated. A scale-up was performed by recirculating an acidic solution of pyrrolidine (70 mmol) for 22 h under UV light irradiation. After basic workup and protection with Boc_2O, the oxidized product was obtained in 46% yield (5.98 g). In a more general study on C−H oxidations, Noël et al. reported the continuous-flow photooxidation of alkanes (Scheme 160C).[722] A microflow photoreactor (0.75 mm ID, 5 mL volume) was employed to increase the access to oxygen. In fact, in flow the oxygen delivered by a

https://doi.org/10.1021/acs.chemrev.1c00332
Chem. Rev. 2022, 122, 2752−2906

mass flow controller (MFC) established a segmented flow pattern, thus resulting in improved mixing due to the presence of Taylor recirculation. In this way, both benzylic positions and unactivated C(sp^3)−H were oxidized efficiently, including some biologically active molecules, such as artemisinin, (−)-ambroxide, pregnenolone, and sclareolide. Moreover, a 5 mmol scale reaction was performed, with comparable yields obtained (59% vs 55% yield).

The activation of benzylic C(sp^3)−H bonds and subsequent oxidation to aldehydes without overoxidation to carboxylic acids was optimized in flow by Singh et al. (Scheme 161).[723]

Scheme 161. Photoinduced Synthesis of Phthalides in Flow Mediated by the Oxidation of Aryl Ketones

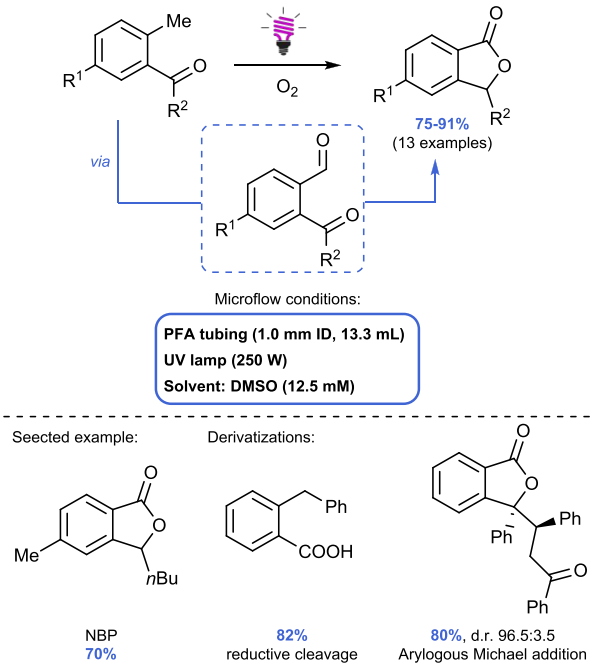

The starting aryl ketone was pumped into a 13.3 mL PFA coil and irradiated with UV light (250 W). Oxygen, introduced to the solution with an MFC, was used to oxidize the excited starting material, transforming it into the corresponding benzaldehyde. After isomerization, phthalide derivatives were formed over a 12.1 min residence time. The flow setup was integrated with an in-line liquid−liquid extraction and a phase microseparator, which allowed for the removal of aqueous DMSO from the reaction mixture and to collect a stream of the product, facilitating further workup steps. Notably, one of the obtained products was an ischemic-stroke relevant natural product (3-*n*-butylphthalide, NBP). This process was further used in two telescoped syntheses, showing its adaptability to multistep synthesis. Notably, the phthalide could undergo (i) a reductive cleavage in a ThalesNano H-Cube (t_R = 2.1 min), affording a benzoic acid, and (ii) an arylogous Michael addition with chalcone in flow (PFA capillary 1 mm ID, 0 °C, t_R = 51 min).

In 2020, Noël et al. reported the first photocatalytic trifluoromethoxylation in flow (Scheme 162).[724] The authors used the Ngai CF_3O-agent, known to generate a trifluoromethoxy radical in the presence of a ruthenium(II) catalyst under light irradiation.[725] The flow setup consists of a PFA coil (0.75 mm ID, 2.3 mL volume) irradiated with 400 nm LEDs (10 W). The reaction was much faster in flow than in batch (1

Scheme 162. Photocatalytic Trifluoromethoxylation of (Hetero)Arenes Systems in Flow

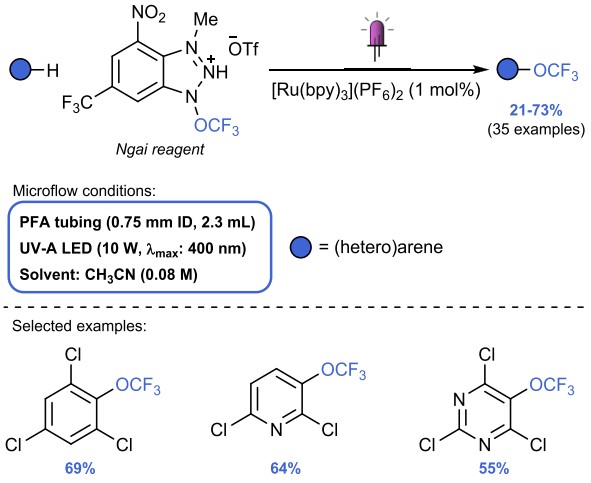

vs 18 h). Notably, the addition of a base (KH_2PO_4, 1.0 equiv) was key to reach higher yields in batch but did not improve results in flow.

5.8.8. C−N Bond Formation. Aromatic amines are important moieties present in many drugs and materials. The classic synthetic strategy to access this functionality is the electrophilic aromatic substitution, based on either (i) nitration and reduction or (ii) halogenation followed by nucleophilic substitution or Buchwald−Hartwig, Ullmann, or Chan-Lam cross-coupling.[726] Marden et al. reported a photochemical intramolecular C−H amination which does not require prefunctionalization of the arene partner (Scheme 163A).[727] The idea was to start from *N*-chloroamines, which have been known since the 1960s to generate aminium radicals under light irradiation.[728] After describing the homogeneous amination in batch,[729] the development of a flow strategy was reported (FEP capillary: 5 mL volume) to overcome limitations of the batch setup; that is, (i) the limited scale-up and (ii) the safe handling of the hazardous *N*-chloroamines.

Scheme 163. (A) *N*-Chloroamines as Intermediates to Form New C−N Bonds in Flow and (B) Photocatalytic Amination Process Scaled up in Flow

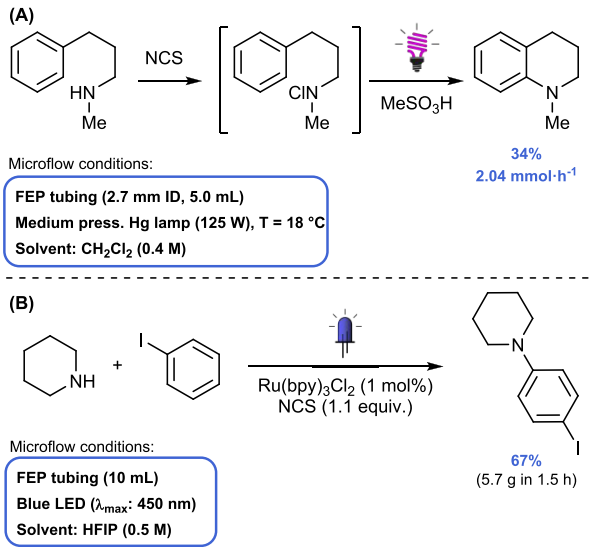

https://doi.org/10.1021/acs.chemrev.1c00332
Chem. Rev. 2022, 122, 2752−2906

The authors optimized the *N*-chloroamine synthesis and amination as two separated flow steps, and finally show the results of the combination of the two reactions. Interestingly, the overall yield was inferior to the ones in batch (34% vs 60%), probably because of the nonoptimal conditions for the photochemical step. In fact, optimal conditions in the photochemical step required higher concentrations which was not compatible with the previous synthesis, as the maximum solubility of *N*-chlorosuccinimide (NCS) in dichloromethane was limited to 0.41 M. However, the flow process surpassed the batch setup in terms of productivity (2.04 mmol·h^{-1} in flow vs 1.0 mmol·h^{-1} in batch), proving its superiority for larger-scale reactions.

Similarly, Leonori et al. developed a photocatalytic amination process in batch and in continuous-flow (Scheme 163B).[271] The core event was the SET between the excited Ru(II) complex and the in situ generated *N*-chloroamine. The reaction, which proved to be very versatile, was scaled in flow in one case. Using a Vapourtec E-series reactor (10 mL) and starting from 29.4 mmol of piperidine, the desired product was afforded in 5.65 g, corresponding to a 67% yield and a productivity of 13.1 mmol·h^{-1}, with a lower catalyst loading than in batch (1 vs 5 mol %) and shorter time (10 min vs 30 min).

A different approach was proposed by Sen et al. in 2021.[730] In this case, aryldiazoesters were employed as carbene precursors in flow to perform a N−H insertion to indoles. With a PFA microreactor (2 mm ID, 6.3 mL volume) irradiated with blue LEDs (3−4 W), the reaction time was reduced from 22 h in batch to only 3 h in flow affording the products in slightly higher yields than in batch (75% vs 70% for the model compound).

Traditionally, HAT-mediated C−N bond formation was limited to the use of an electrophilic N═N double bond, such DIAD.[359] However, Noël et al. demonstrated that the combination of HAT catalysis (TBADT) and oxidative radical-polar crossover strategy (RPC) triggers a new mechanism for C−N bond formation (Scheme 164).[731] In fact, the HAT-generated alkyl radical can be oxidized with TBHP to form a carbocation which is trapped by a suitable nitrogen nucleophile, for example, azoles. To ensure the carbocation is sufficiently stable, oxocarbenium ions were selected. The transformation, which is also suitable for late-stage functionalization, was translated into flow. To this end, a Vapourtec UV-150 reactor (PFA tubing, 1.3 mm ID, 10 mL) was irradiated with 60 W 365 nm LEDs. In flow, the reaction required 1 h residence time, compared to 16 h in batch, without any decrease in yield, and was also performed in a 10 mmol scale.

A dual photoredox/nickel catalyzed (hetero)aryl amination method in batch was translated to a flow protocol by Buchwald et al. (Scheme 165).[264,732] The flow reactions were performed in a PFA capillary (0.8 mm, 10 mL volume) subjected to blue LED irradiation (450 nm). Applying the batch conditions in flow lead to clogging issues but were avoided by using DMSO as solvent. The relatively short residence time in flow (1 vs 19 h in batch) enabled quick reaction optimization. Notably, optimization revealed that a lower photocatalyst loading resulted in less dehalogenation as side reaction and increased yields. Optimal results were obtained at 80 °C with a Ru(bpy)$_3$ photocatalyst, NiBr$_2$·dme catalyst and DABCO (1,4-diazabicyclo[2.2.2]octane) as base. Next, the substrate scope of the developed flow protocol was investigated. For the C−N cross-coupling with pyrrolidine, electron-poor, electron-neutral, and electron-rich aryl bromides were well tolerated as aryl electrophile (67−98% yield). Additionally, electron-poor aryl chlorides were also found to be suitable coupling partners (71−93% yield), whereas coupling with electron-neutral and electron-poor aryl chlorides resulted in low yields. Also, a number of primary and cyclic, secondary amine substrates were successfully coupled with aryl halides. To make a comparison with batch conditions and to exemplify the scale-up potential of the method, a number of reactions were performed on a 10 and 50 mmol scale in batch and in flow. As expected, in flow the high yield was maintained at larger scale, while yield dropped for the larger scale batch reaction.

Scheme 164. C−N Bond Formation Mediated by HAT Catalysis and RPC in Flow

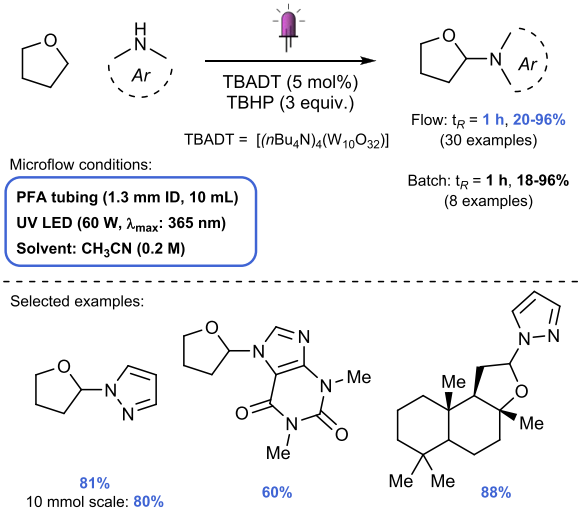

Scheme 165. (Hetero)Aryl Amination in Continuous Flow by Dual Photoredox/Nickel Catalysis

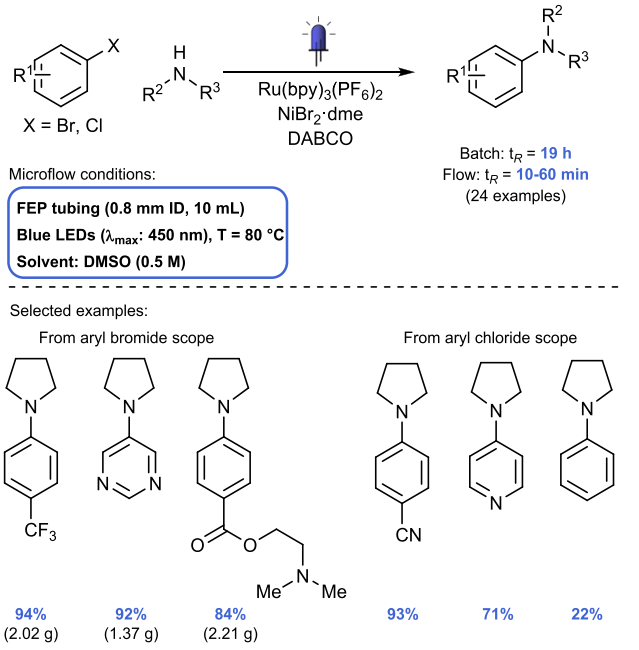

https://doi.org/10.1021/acs.chemrev.1c00332
Chem. Rev. 2022, 122, 2752−2906

A nickel/photoredox catalyzed C−N coupling was also proposed by Kappe, Williams et al. for the continuous-flow synthesis of arylhydrazine derivatives (Scheme 166).[733] A

Scheme 166. Nickel/Photoredox Catalyzed Synthesis of Arylhydrazine Derivatives in Flow

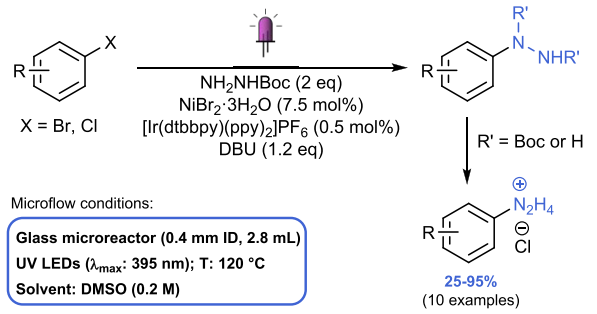

mixture of aryl halide and *tert*-butyl carbazate (NH_2NHBoc) in DMSO was irradiated with UV-LEDs (395 nm) in a glass microreactor (Corning AFR 0.4 mm ID, 2.8 mL volume) in the presence of an iridium photocatalyst ($[Ir(dtbbpy)(ppy)_2]PF_6$), nickel catalyst ($NiBr_2·3H_2O$), and base (DBU). A rapid reaction optimization was performed in a Design of Experiments study, which showed the strong dependency of the reaction rate on photocatalyst loading and reaction temperature. Under optimal conditions, 86% yield of the HCl salt was isolated after Boc deprotection for the model substrate (4-(trifluoromethyl)benzyl bromide). A substrate scope was performed for a number of aryl halides, including N-heterocycles and aryl chlorides, resulting in yields of 25−95%.

5.8.9. C−S and C−Se Bond Formation. Modifications of amino acids are fundamental transformations as they provide drugs, biotechnological tools, and catalysts.[2,734] A photocatalytic example in flow is the arylation of cysteine by Noël et al. (Scheme 167).[735,736] In this case, a diazonium salt was formed in situ starting from an aniline and *t*BuONO. By irradiating the reaction mixture in the presence of eosin Y, the

Scheme 167. Photocatalytic Arylation of Cysteine and Cysteine-Containing Dipeptides in Flow

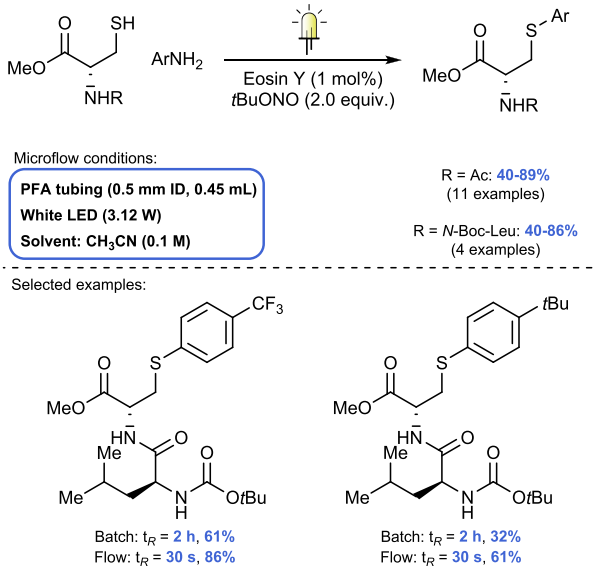

aryl radical was promptly formed, which reacted with the free thiol moiety of cysteine. Using a microflow reactor (PFA coil: 0.5 mm ID, 0.45 mL volume), irradiated with 3.12 W white LEDs, it was possible to reduce the reaction time to 30 s, with the ability to scale up the reaction to 1 g. Moreover, a number of dipeptides bearing a cysteine moiety were successfully modified.

More recently, a different approach to modify thiols, cysteine derivatives, and cysteine-containing dipeptides in flow was reported.[737] In this case, diazoalkanes were used under visible light irradiation to perform a S−H bond insertion. In the flow setup (PFA coil 0.5 mm ID, 0.98 mL) irradiated with 50 W blue LEDs, a 110-fold increase in productivity was observed compared to batch, as the reaction time was reduced from 12 h in batch to 6.5 min in continuous-flow.

Baumann et al. prepared [1.1.1]propellane in flow and subsequently coupled it with diphenyl disulfide without intermediate purification (Scheme 168).[738] The PFA reactor

Scheme 168. Photoinduced S−H and C−C Bond Insertion Using [1.1.1]Propellane in Flow

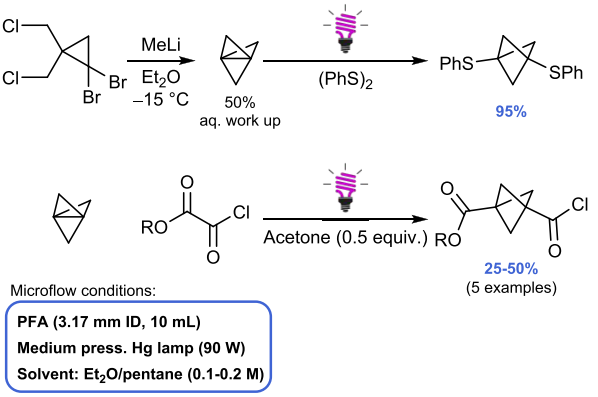

(3.17 mm ID, 10 mL volume) was irradiated with a medium-pressure Hg lamp (90 W) and the desired product was obtained in 95% yield in 10 min residence time. Considering these interesting results, the procedure was also applied to 2-chloro-2-oxoacetates, to form new C−C bonds. The obtained acyl chlorides could be further functionalized with an aniline, to afford the corresponding amide in 18−48% overall yield (5 min residence time).

A continuous-flow method based on dual photoredox/nickel catalysis was developed by Collins et al. to form alkynyl sulfides through C(sp)−S bond formation (Scheme 169).[739] To perform the C(sp)−S cross-coupling, a solution of bromo alkyne and terminal sulfide was irradiated with blue LEDs (465 nm) in a PFA capillary reactor (1.0 mm ID, 13 mL volume), in the presence of 4CzIPN as organophotocatalyst and a nickel catalyst. In the flow setup, this resulted in 96% yield for the model substrates in 30 min residence time. With optimized conditions in hand, a substrate scope was performed, which showed that electronic and steric variations in both coupling partners are well tolerated. One notable example of the scope was provided by the synthesis of a phenylalanine-substituted thioalkyne in 94% yield. This encouraging result shows the potential of the method to incorporate alkyne moieties into peptide chains. Also, a photochemical macrocyclization was performed through the C(sp)−S coupling of an alkyne and a

https://doi.org/10.1021/acs.chemrev.1c00332
Chem. Rev. 2022, 122, 2752−2906

Scheme 169. Thioalkyne Formation via C(sp)−S Coupling of Bromoalkyne and Terminal Thiols via Dual Photoredox/Nickel Catalysis

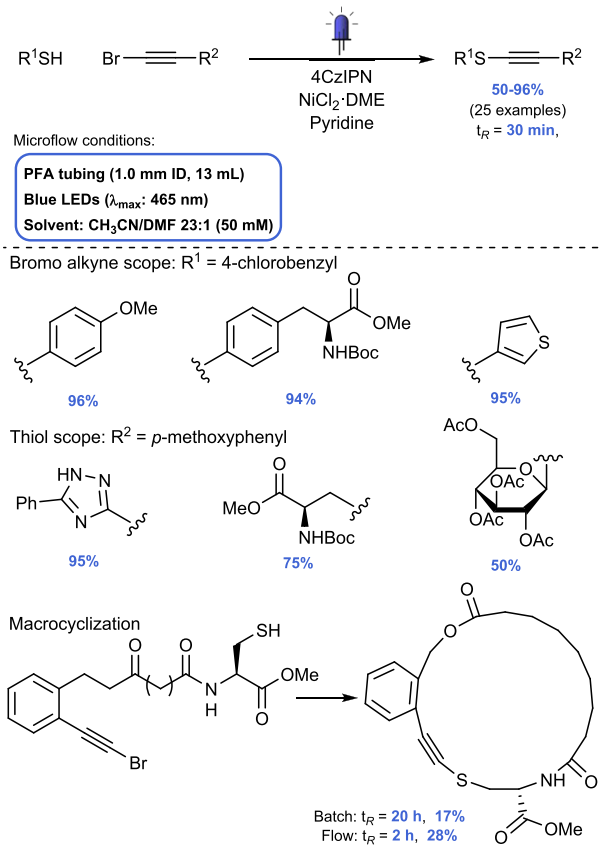

cysteine moiety, which is the first example of a thioalkyne incorporation in a macrocyclic structure.

The dehalogenative C−S coupling of thiosugars in flow was investigated by Messaoudi et al. by utilizing nickel/photoredox dual photocatalysis (Scheme 170).[740] First, optimization was

Scheme 170. Arylation of 1-Thiosugar through Ni(II)/Ru(II)-Photocatalyzed in Flow

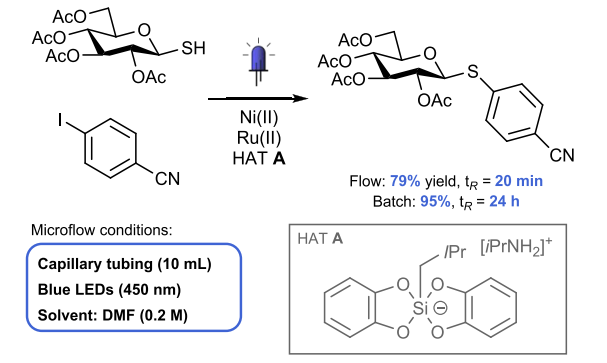

carried out in batch confirming that aryl-iodides and dimethylformamide (DMF) gave the best results. The presence of the HAT reagent **A** was necessary to abstract the hydrogen atom from the S−H bond. The selected (pre)-catalysts were $Ni(dtbbpy)(H_2O)_4]Cl_2$ (5 mol %), $[Ru(bpy)_3]$-$(PF_6)_2$ (2 mol %). Next, an extensive scope was carried out with 29 examples consisting of various aryl halides and heterocycles with yields of 30−96%. Finally, the reaction was translated to flow for the coupling of thioglucose with 4-iodobenzonitrile at a 0.8 mmol scale in a capillary reactor (10 mL volume) irradiated with blue LEDs (450 nm) with a residence time of 20 min affording the product in 79% yield.

Considering the growing importance of fluoroalkylsulfanyl and fluoroalkylselenolyl functionalities in medicinal and agrochemistry, new photochemical transformations in flow were developed to allow late-stage derivatization of organic compounds in this direction.[567] One example is the 4CzIPN-enabled trifluoromethylthiolation of benzylic bonds of various alkyl (hetero)arenes (Scheme 171).[741] The regioselectivity of

Scheme 171. 4CzIPN-Photocatalytic Trifluoromethylthiolation of Benzylic Bonds in Continuous Flow

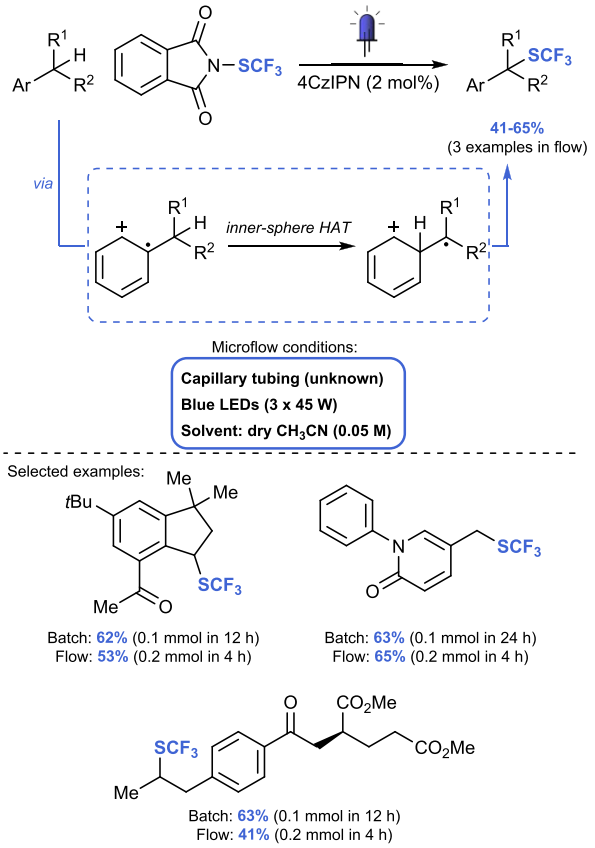

the transformation relies on the inner-sphere HAT process that always results with the generation of a radical at the benzylic position. The procedure allows for the modification of structurally diverse benzylic positions in moderate to good yields. The scope is broad and shows an excellent functional group compatibility. Flow technology was applied for the late-stage trifluoromethylthiolation of three compounds. The reaction was scaled up to 1 mmol and the productivity was increased from 0.1 mmol in 12−24 h in batch to 0.2 mmol in 4 h in flow.

Regarding the light-induced C−Se bond formation in flow, the selenolation of indoles reported by Argüello, Oksdath-Mansilla, and co-workers is an interesting example because the flow techniques allow for coupling under both reductive and oxidative conditions and, therefore, to perform multistep syntheses without the need for intermediate purification

https://doi.org/10.1021/acs.chemrev.1c00332
Chem. Rev. 2022, 122, 2752−2906

(Scheme 172A).[742] The process starts with the formation of diselenide intermediates derived from the chemical reduction

Scheme 172. (A) Organic Selenides Multistep Preparation under Visible Light Irradiation and (B) Photocatalytic Trifluoromethylselenolation of Indoles in Flow

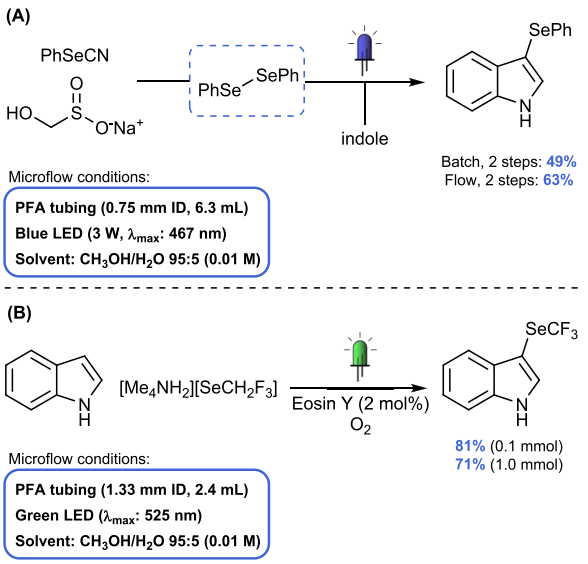

of selenocyanates, which took place in 1 min residence time. The following light-induced oxidative C(sp^2)−H activation of indoles in flow occurred in a PFA reactor (0.75 mm ID, 6.3 mL volume) subjected to blue LED irradiation (3 W, 467 nm) and led to the selenolated product in 64% yield in 2 h residence time. One of the main challenges of this multistep transformation, was the choice of a solvent mixture which is suitable for both steps. After a first optimization in batch, it was found that a 10−30 mM solution in CH_3OH/H_2O (95:5 mixture afforded the best results without any precipitation. The C(sp^2)−H activation required blue LEDs and 2 equiv of indole, while no oxidant was needed as ambient oxygen proved sufficient. When the two steps were combined, the final product was obtained in 63% overall yield, compared to 49% in batch.

Similarly, Dagousset, Pégot, Magnier, and co-workers described the metal-free trifluoromethylselenolation of indoles and pyrroles using the nucleophilic $[Me_4N][SeCF_3]$ (Scheme 172B).[743] This reagent interacts with the excited eosin Y, affording a radical which reacts with the electron-rich aromatic heterocycle. In contrast to their batch setup, which only necessitates air, the continuous-flow reactor required oxygen to be supplied to the reactor (PFA coil: 2.35 mL volume, irradiated with green LEDs) to reach higher conversions. Optimizing the continuous flow protocol, it was possible to reach comparable yields as in batch but in much shorter reaction time (50 min in flow vs 18 h in batch). Moreover, the scale-up of the reaction to 1 mmol worked very efficiently.

5.8.10. C−B Bond Formation. The photochemical synthesis of 1,2- and 1,3-diborylarenes was carried out by Larionov et al. through a dual C−H/C−X borylation of haloarenes with B_2Pin_2 in flow (Scheme 173).[744] The metal- and additive-free method occurs under UV-C irradiation and was performed in batch and in flow. Interestingly, the regioselectivity of the reaction could be tuned by changing the solvent and the electronic properties of the arene

Scheme 173. Photochemical C−H/C−X Diborylation of Haloarenes with B_2Pin_2 in Continuous-Flow

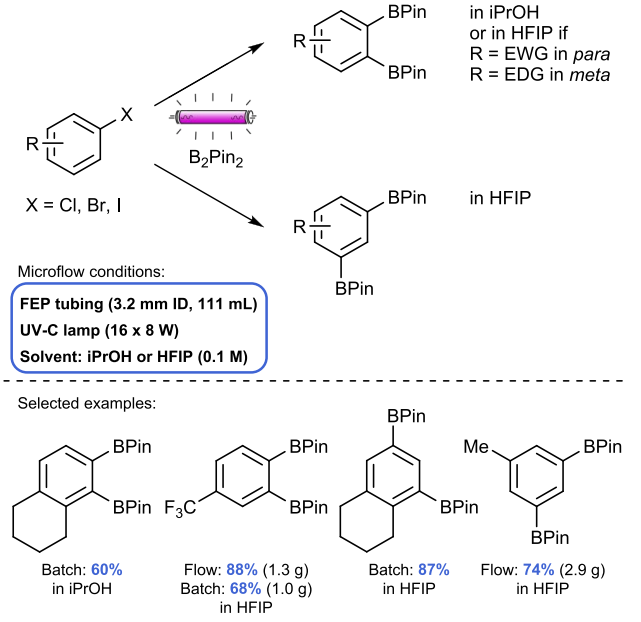

functional groups. The synthesis of 1,2-diborylated arenes was performed with excellent selectivity in isopropanol. In HFIP (hexafluoroisopropanol), 1,2-selectivity could also be obtained with substrates bearing electron-withdrawing groups at the para position or with electron-donating groups at the meta position. A reaction scope for the synthesis of 1,3-diborylated arenes was performed in HFIP with good selectivity for 2-, 4-, and 2,3-alkyl-substituted haloarenes. Apart from the electronic effects of the substituents, the difference in regioselectivity in isopropanol and HFIP was explained by their polarity and by the formation of a solvent cage trapping of the radical intermediates. The gram-scale diborylation of a number of arenes was performed in batch and in flow. The flow reactor consisted of a FEP capillary (3.2 mm ID, 111 mL) placed in a photochemical chamber reactor with 16 × 8 W UV-C lamps. Comparable results were obtained in batch and in flow, but the reaction time could be reduced from 16 h in batch to 3.7 h in flow.

Similarly, the photoinduced borylation of haloarenes and arylammonium salts was performed to synthesize arene boronic acids and esters (Scheme 174).[745] Initial experiments between bromobenzene and tetrahydroxydiboron as boron source provided the desired phenylboronic acid in 92% yield after 3 h irradiation with a UV-C lamp (254 nm) at 15 °C. The reaction scope with bromoarenes showed broad functional group tolerance, with high yields obtained for the borylation of electron-rich and electron-poor arenes and with N-, O-, and S-containing heterocycles. Additionally, the method was successfully applied to iodo- and chloroarenes and even to fluoroarenes containing electron-donating substituents. A number of alternative borylating agents were used as well, such as esters derived from pinacol, neopentyl glycol, and 1,1,3-trimethylethylene glycol, providing the corresponding boronic esters in 75−90% yield. For two examples with $B_2(OH)_4$, the borylation was carried out in a FEP flow reactor, resulting in 60% and 90% yield.

The metal-free borylation of various electron-rich aryl halides in flow was achieved by Li, Lin, and co-workers

https://doi.org/10.1021/acs.chemrev.1c00332
Chem. Rev. 2022, 122, 2752−2906

Scheme 174. Photoinduced Synthesis of Aromatic Boronic Acids and Esters from Haloarenes and Arylammonium Salts

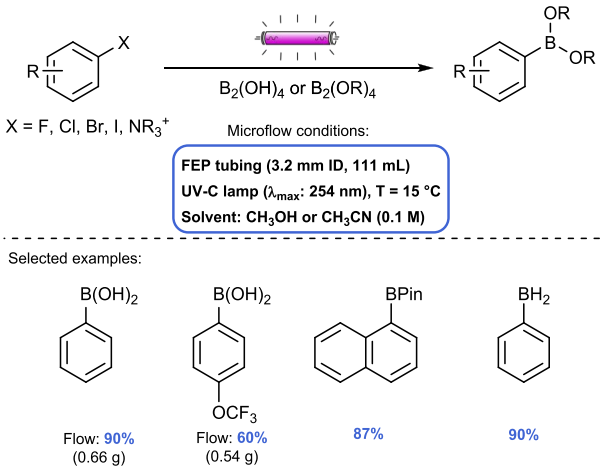

using photocatalytic conditions (Scheme 175).[746] Reactions were first carried out in batch under irradiation with a 300 W high-pressure mercury lamp. Acetonitrile with both water and acetone as cosolvents were identified as the best solvent system, whereas tetramethylethylenediamine (TMEDA) was selected as base. Finally, it was found that yields could be increased to 40% in batch when 2 equiv of B_2pin_2 were employed. However, 10 h of irradiation was necessary to reach those results. To improve the performance of the protocol, flow technology was implemented. To this end, a FEP capillary (1.0 mm ID, 0.78 mL volume) was wrapped around a cooled quartz immersion well which held the mercury lamp previously used in the batch reactions. A stock solution containing all reactants and reagents was infused using a syringe pump, resulting in 77% yield in only 26 min residence time. When 0.1 equiv of tetrabutylammonium fluoride (TBAF) was used as an additive the yield was further increased to 87% (85% isolated yield). Lastly, an extensive scope was carried out in flow with optimized conditions using both B_2pin_2 and the neopentyl glycolato-derivative B_2neop_2 as borylating agents resulting in 22−85% yield for 34 examples (t_R = 26−52 min).

Scheme 175. Metal-Free Borylation of Electron-Rich Aryl Halides under Continuous Flow Conditions

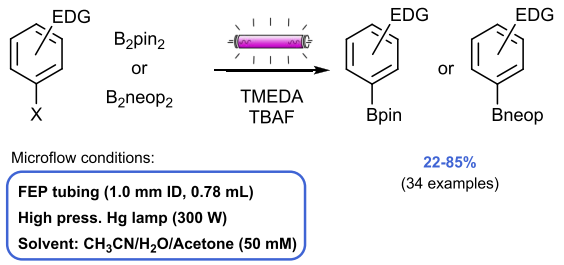

Another example of a photomediated borylation of organic halides in continuous-flow is given by Poisson et al. A heteroleptic copper complex was used to enable the photocatalytic borylation of aryl, heteroaryl, vinyl, and alkyl halides, affording the corresponding boronic-acid esters (Scheme 176A).[747] Reactions were screened for base (DIPEA) loading, heteroleptic copper catalyst choice and loading, and acetonitrile and water cosolvent loading. Under optimal conditions, yields of 80% were obtained with a newly designed copper(I) catalyst. An extensive scope with 42 examples was performed in batch. Four of these examples were subsequently translated to flow to enable scale-up to 2.2 mmol, affording yields of 68−81%. Similar yields were obtained for the scale-up experiments as in batch. As an example, the borylation of *para*-iodoanisole was isolated in 73% yield at a 21.3 mmol scale.

Scheme 176. Light-Induced Cu(I)-Photocatalyzed Borylation of Aryl Iodides in Continuous Flow

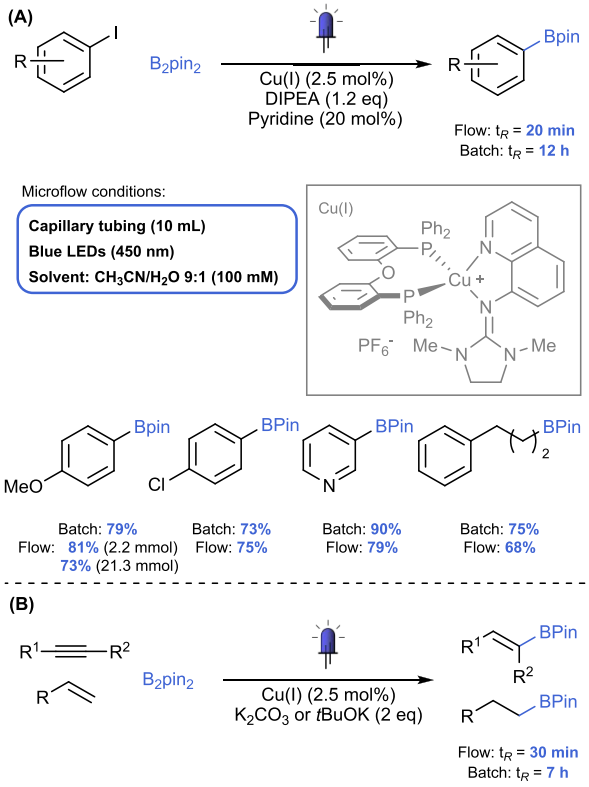

The same group also developed copper catalysts for the photochemical hydroboration of alkynes and alkenes in continuous-flow (Scheme 176B).[748] Reactions in batch and in flow were performed under similar conditions as for the borylation of aryl iodides using B_2Pin_2 as reagent. With the developed method, a total of 54 terminal and internal alkynes and alkenes were hydroborated in 43−97% yield. A scale-up to 20 mmol for phenylacetylene resulted in similar high yields (78%). Interestingly, by changing the reagent from B_2Pin_2 to $PhMe_2Si$−BPin an anti-Markovnikov hydrosilylation of alkynes and alkenes was achieved.[749] As in the previous cases, the Cu-photocatalyzed hydrosilylation method was applied to a wide range of substrates resulting in generally excellent yields in continuous-flow (>90% yield for 34 examples).

Another example of a metal-free borylation in continuous-flow is given by Li et al., who performed a photomediated borylation of aryl halides with tetrahydroxydiboron (Scheme 177).[750] Reactions were first carried out in batch with B_2pin_2 as the borylating reagent. After identifying acetonitrile/water with acetone as cosolvent and *N,N,N′,N′*-tetramethyldiaminomethane (TMDAM) as the best solvent system and base additive respectively, the system was translated to a flow system (FEP capillary 1.0 mm ID, 0.78 mL volume). The photochemical borylation in flow afforded the desired products

https://doi.org/10.1021/acs.chemrev.1c00332
Chem. Rev. 2022, 122, 2752−2906

Scheme 177. Light-Induce Metal-Free Borylation of Aryl Halides under Continuous Flow Conditions

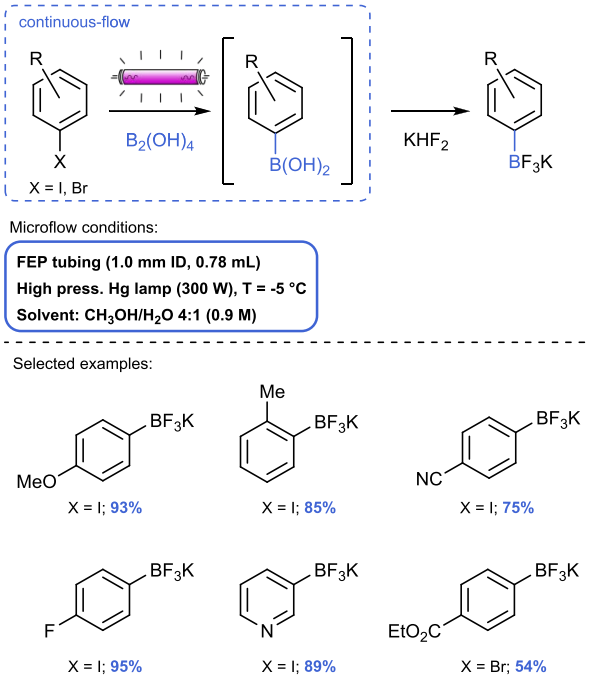

in 37−93% yield and in shorter times than in batch (up to 30 min vs 4 h). Encouraged by these results, the use of a more atom-economical borylating agent (tetrahydroxydiboron) was investigated. With a small variation to the previous conditions (methanol/water 4:1 as solvent system), the 4-iodoanisole derivative was afforded in quantitative yields by ^{1}H NMR in only 10 min residence time. Because of the difficulties associated with isolating the pure aryl boronic acid, aqueous KHF_2 was added to the product after irradiation to afford the potassium aryltrifluoroborate in yields up to 93%.

A scalable method for the generation of bicyclo[1.1.1]-pentane (BCP) trifluoroborate salts starting from their corresponding acids was developed by researchers at Merck (Scheme 178).[751] A solution of BCP and catechol diboron was irradiated with blue LEDs (100 W, 460−465 nm) in five flow reactors placed in series (30 mL total volume). The outlet stream was collected in a reaction flask and combined with Et_3N and pinacol to form BCP BPin in 65% isolated yield and was then treated with KHF_2 to form BCP BF_3K. A scale-up

Scheme 178. Scalable Generation of Bicyclo[1.1.1]pentane Trifluoroborate Salts

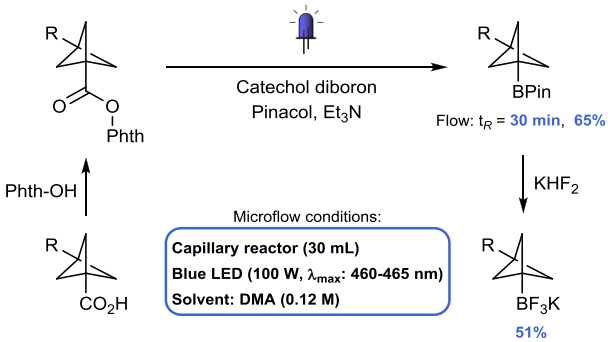

borylation reaction was performed, converting 200 g of BCP in 51% yield over two steps.

5.9. Miscellaneous

5.9.1. O_2 Oxidation. The visible-light mediated synthesis of disulfides was investigated by Noël et al. via a mild method involving aerobic oxidation and heterogeneous titanium(IV) oxide photocatalysis (Scheme 179).[752] Reactions first took

Scheme 179. TiO_2-Photocatalyzed Thiol Dimerization in Flow with a Glass Packed-Bed Reactor

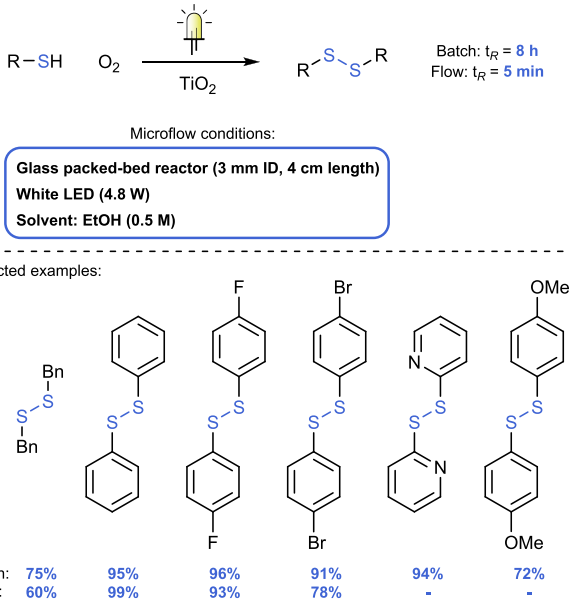

place in batch and were later performed in continuous-flow to accelerate the transformation. A reaction optimization was carried out in batch to screen solvent, base, and light source (CFL or white LED). The optimal conditions in batch were provided by the use of ethanol, tetramethylethylenediamine (TMEDA) and white LEDs, which afforded 75% yield for the symmetrical disulfide cross-coupling of benzyl mercaptan in 8 h. To both reduce the risk in handling molecular oxygen and to accelerate the reaction, the transformation was translated to continuous-flow via a packed bed reactor (PBR) strategy. The PBR (3 mm ID, 4 cm length) consisted of a glass reactor which was packed with TiO_2 (60 mg), glass beads (310 mg) and void space (200 μL). To avoid leaching of TiO_2 particles and clogging, the PBR was first flushed with a 1 M solution of TMEDA in ethanol, which allowed the TiO_2 to form larger aggregates and effectively avoided leaching during the reaction. Again, the system was irradiated with white LEDs (4.8 W), but a substantial rate acceleration was achieved in continuous-flow. Full conversion was observed in 5 min residence time with comparable isolated yields as in batch for 4 symmetrical disulfides and 1 asymmetrical disulfide. Of note was that the photocatalyst system remained stable over the course of 28 h of run-time in continuous-flow, attesting to the TiO_2 aggregation method employed in the PBR.

Another packed bed reactor is described by Reisner et al., who used a packed column photoreactor (PCP) filled with a mesoporous graphitic carbon nitride material (mpg-CN_x) to perform triphasic reactions, such as the photocatalytic oxidation of benzylic alcohols and amines (Scheme 180).[753] This heterogeneous catalyst is responsible for the oxidation of

https://doi.org/10.1021/acs.chemrev.1c00332
Chem. Rev. 2022, 122, 2752−2906

Scheme 180. Photocatalytic Triphasic Oxidation of Benzylic Alcohols and Amines Performed in a Packed Column Photoreactor

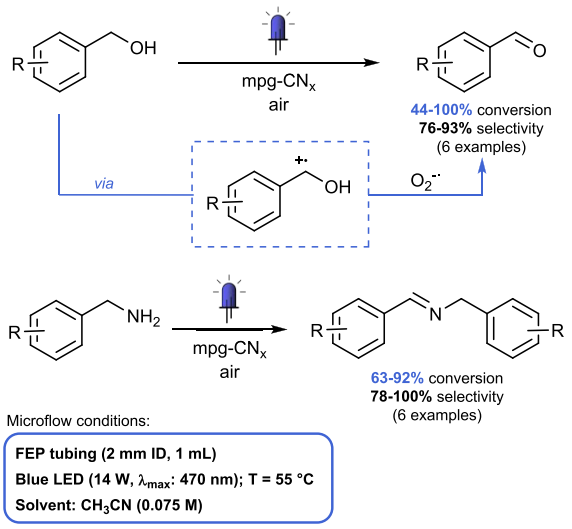

Scheme 181. Pt(II)-Photocatalyzed Oxidation of Sulfides to Sulfoxides in Continuous Flow

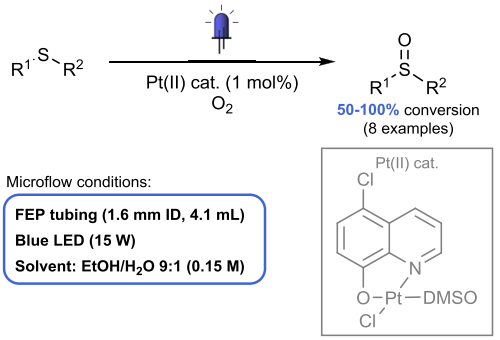

the benzylic position under irradiation, while aerobic oxygen gets reduced and finally acts as the terminal oxidant. The reactor consisted of an FEP coil (2 mm ID, ~1 mL volume) where mpg-CN_x was packed (3.5 wt % in a glass bead mixture). The air flow is controlled by an MFC. Blue LEDs (14.4 W, 470 nm) were used to irradiate the PCP. When switching to a biphasic (liquid−solid) system, the solvent and substrate were presaturated with air. However, the conversion dropped from 80% to 11%. The morphology of the photocatalyst was also important, as nonporous, bulk CN_x tends to provoke high back-pressures leading to the hampering of the biphasic flow. Furthermore, bulk CN_x suffers from a poor charge separation. With mpg-CN_x, the residence time to reach full conversion was 90 min, although after 75 min overoxidation products were observed. In batch, the conversion was only 39% after the same time. To test the reusability of the photocatalyst, the reactor was used for 25 cycles consisting of 2.5 mL of benzyl alcohol in acetonitrile (100 mM), followed by 2.5 mL of neat acetonitrile. The final conversion was almost constant, dropping only 10%.

The visible-light-mediated oxidation of sulfides to sulfoxides was investigated by Alemán, Cabrera, and co-workers using Pt(II) complexes as photocatalyst in continuous-flow (Scheme 181).[754] Reactions were first carried out in batch to evaluate the optimal solvent and platinum catalyst to run the reaction with EtOH/water (9:1) provided quantitative yields after 10 h irradiation (CFL, 23 W) using the Pt(II) complex outlined in Scheme 181. This was followed by a small substrate scope in batch of 10 examples affording yields of 62−98%. Following this, the reaction was translated to continuous-flow. The reaction solution was pumped with an HPLC pump and was combined in a T-mixer with oxygen before it was introduced in a FEP photoreactor (1.6 mm ID, 4.1 mL) irradiated with blue LEDs (15 W). In flow, a considerable increase in reaction rate was achieved compared to batch, with full conversion for the oxidation of methyl-*p*-tolylsulfide in 11 min residence time (10 h in batch). Additionally, for the 8 sulfoxides investigated comparable yields were obtained as in batch. Concerning the catalyst, this class of platinum complex is known to absorb light in the visible spectrum region owing to a metal-to-ligand charge transfer (MLCT) and can work as a homogeneous photocatalyst. In the studied transformation, its photocatalytic ability outperformed those of $Ru(bpy)_3Cl_2$ and $Ir(ppy)_3$ and it was more selective than both Rose Bengal and tetra-*O*-acetylriboflavine. The authors suggest a radical mechanism involving the formation of oxygen radical anion instead of an energy transfer generating singlet oxygen. In fact, the reaction is not accelerated in deuterated solvents and was shut off by the addition of benzoquinone, a scavenger of superoxide radicals.

Another oxidation-mediated by oxygen radical anion is reported by Chen et al. using Rose Bengal for the photocatalyzed *N*-demethylation of *N*,*N*-dimethylphenyl amines (Scheme 182).[755] Aiming to provide a practical route to *N*-demethylate compounds, continuous-flow was used. The flow reactor consisted of a FEP capillary (0.8 mm ID, 20 mL volume) coiled around a quartz tube, which was irradiated with 34 W LED corn-shaped light bulb. The addition of an excess of acetic acid (25 equiv) accelerated the transformation from 24 to 3 h. In order to fully convert the intermediate hyperoxide into the product, either an acidic work up was performed, or vitamin C was used as a hydrolytic reagent as a milder alternative. The scale-up of the reaction was performed with a steroid (mifepristone), which underwent demethylation in 65% yield and 1.5 h residence time. Without acetic acid, the reaction took more than 48 h in flow, whereas it took 6 h under standard conditions in batch. Notably, during the reaction *N*-formyl byproduct was formed, but this could be converted into the desired product when treated with acid, thus increasing the yield to 83%.

Horváth, Škoric, and co-workers reported the photocatalytic oxidation of heterostilbenes.[756] Manganese(III) porphyrins worked as the photocatalyst. Differently from metal-free porphyrins, these catalysts perform an electron transfer after light irradiation, affording Mn(IV) and Mn(V) complexes which are then involved in follow-up reactions. The photooxidation of the less aromatic furostilbene afforded a mixture of up to five products. On the other hand, when starting from the more aromatic and stable thienostilbene, the reaction was more selective (up to two oxidized products were obtained). Different glass microflow reactors were tested (0.376−0.498 mm ID, 4−32 μL volume), resulting in the acceleration of the photooxidation. The complete conversion was obtained in less than 4 min for the thienyl derivative (vs almost 16 h in batch) and in less than 2 min for the furyl derivative (vs more than 2 h in batch). As expected, with a residence time of 12 s, higher

https://doi.org/10.1021/acs.chemrev.1c00332
Chem. Rev. 2022, 122, 2752−2906

Scheme 182. Acetic Acid Accelerated Photocatalytic *N*-Demethylation of *N,N*-Dimethylphenyl Amines

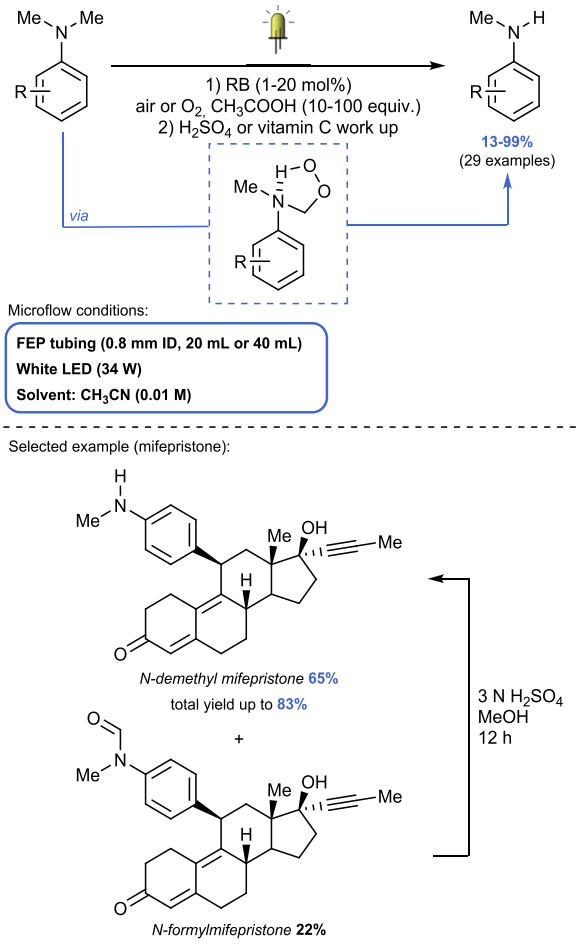

conversions were obtained with a smaller channel architecture (86% vs 81%).

The selective photooxidation of benzene into phenol was reported by Su et al. using DDQ as photocatalyst.[757] This is a challenging transformation, especially because the product is more prone to oxidation than the starting material. The authors screened several parameters, such as residence time, benzene concentration, molar ratio, and solvents. Optimal results were obtained for a 30 mM benzene solution in acetonitrile with 12:1:1.5 molar ratio of H_2O:benzene:DDQ, affording 94% phenol yield with >99% selectivity in 1 h residence time. The implementation of a microreactor (PFA tubing, 1 mm ID) irradiated with a 450 nm blue LED strip proved to be beneficial for the transformation, outperforming all the reported batch processes.

The oxygen-mediated photooxidation of benzylic organotrifluoroborates in flow was reported by Wang et al. (Scheme 183).[758] In a batch setup equipped with an oxygen balloon, the corresponding aldehyde was obtained in only 12% yield over 180 min. In contrast, when switching to a flow setup (FEP capillary 1.58 mm ID, 0.875 mL), irradiated with high-power UV-LED, the aldehyde was obtained in 82% NMR yield. Increasing the residence time to 7 min, while keeping the oxygen flow constant, resulted in quantitative yields of benzaldehyde. This result proved the importance of the stoichiometry of the reaction, requiring at least 5 equiv of oxygen. The excited Ir(III) complex catalyzes the SET that

Scheme 183. Photocatalytic Oxidation of Benzylic Trifluoroborates in Flow

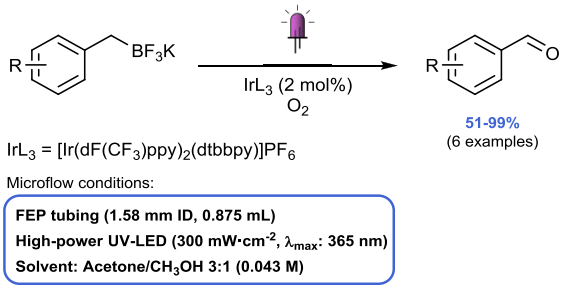

oxidizes the trifluoroborates with generation of a benzyl radical.

5.9.2. Multistep Synthesis. En route to the completion of a four-step synthesis to pyocyanin, Baxendale et al. utilized continuous-flow photocatalysis for the key final step of the synthesis, allowing them to easily produce pyocyanin in gram quantities (Scheme 184).[759] The final step consisted of the

Scheme 184. Flow Preparation of Pyocyanin in a Continuous Mode through a Photooxidation

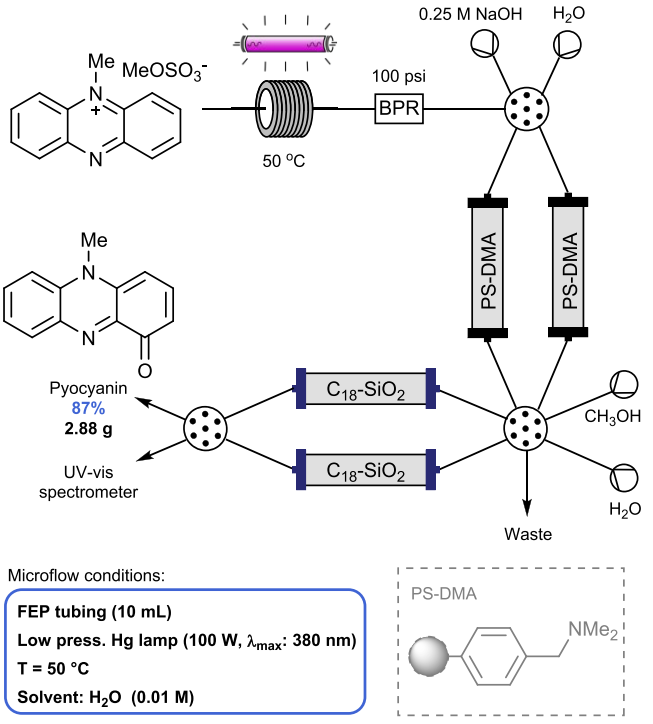

photooxidation of a methylated salt to give pyocyanin and was performed in a FEP capillary reactor (10 mL volume) irradiated with a 100 W low-pressure mercury lamp equipped with a blue wavelength filter (λ_{max} = 380 nm). The system was kept at 50 °C and 100 psi (6.9 bar), and required a residence time of 30 min. Notably, as proven by experiments with deuterated water, phenazine methosulfate is excited by UV light irradiation and reacts with water, to finally afford the product by deprotonation and oxidation. To avoid a long extraction of the pyocyanin, which tends to stay in water because of its zwitterionic nature, an in-line work up was performed with a polymer-supported base (PS-DMA) as a

https://doi.org/10.1021/acs.chemrev.1c00332
Chem. Rev. 2022, 122, 2752−2906

quencher. Then, a reusable C18 functionalized silica packed bed was employed to retain the pyocyanin, whereas the unreacted salt was eluted. Finally, methanol was used to wash away the product. To ensure the process could run continuously, two quenching columns were used in parallel, followed by two parallel purification columns. Using a set of automated switching valves, it was possible to run the process in one side, while the other was washed with water. An in-line UV detector was integrated at the end to indicate when it was necessary to switch to the parallel column. Using this method, 87% of pyocyanin was obtained starting from 1080 mL of stock solution, corresponding to 2.88 g over 18 h run.

The synthesis of isoxazoles through a modular flow strategy was reported by Oh et al. via a telescoped process.[760] A Friedel−Crafts acylation of alkynes is followed by the azide conjugate addition to the corresponding β-chlorovinyl ketones, which undergo a photochemical-thermal reaction sequence to afford the isoxazole (Scheme 185). The authors described how

Scheme 185. Continuous-Flow Synthesis of Isoxazoles through a Modular Flow Strategy

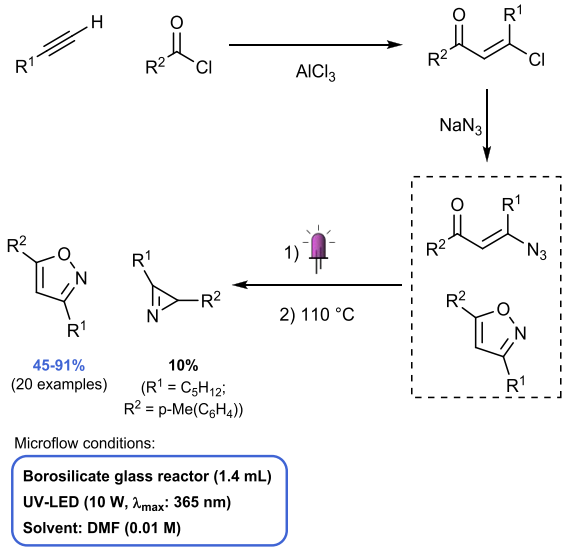

the β-chlorovinyl ketones also underwent cyclization with $NH_2OH{\cdot}HCl$ in the presence of potassium hydroxide. However, the strongly basic conditions represented a limitation in the scope evaluation. The reaction with sodium azide was a valid alternative, especially when UV-LED (10 W, 365 nm) was used to irradiate the reaction. The desired isoxazole was obtained in 69% yield in batch; however, also 31% of 2*H*-azirine was formed. To improve the chemoselectivity toward isoxazole, a thermal treatment of the mixture after the photochemical step was investigated in continuous-flow, to avoid working with remaining unreacted azide species at high temperature. NaN_3 (0.9 g) was placed in a stainless-steel column (4.6 mm ID) with both ends closed with sea sand. After addition of the azide to the β-chlorovinyl ketone, the reaction mixture was injected in an in-line photoreactor (borosilicate glass reactor, 1.4 mL volume) to afford the isoxazole and the 2*H*-azirine, in a 67:33 ratio (t_R = 9 min), followed by an in-line heating module (PTFE tubing, 3 mL volume) at 110 °C (t_R = 20 min). The azide was completely consumed, thus avoiding safety issues. After the thermal treatment, the isoxazole was obtained in 90% yield, with only 10% 2*H*-azirine side-product. With these positive results in hand, the continuous-flow synthesis was applied to a total of 20 substrates in 45−91% yield.

5.9.3. Flow-Selective Transformations. The selective synthesis of azoxybenzenes from nitrobenzenes was reported by Nishiyama et al. by visible light irradiation under continuous-flow conditions (Scheme 186).[761] Interestingly,

Scheme 186. Reactor-Dependent Photocatalytic Azoxybenzene Synthesis

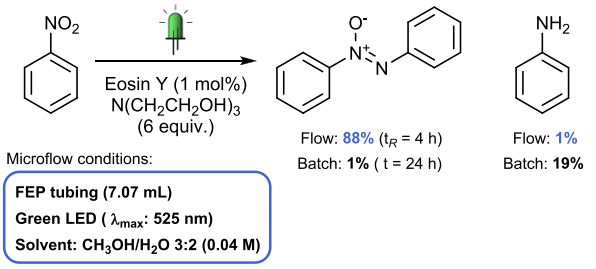

when the reaction was performed in batch, the photoreduction of nitrobenzene with eosin Y and triethanolamine with a green LED (525 nm) resulted mostly in the formation of aniline (19% yield) and other reduction intermediates (nitrosobenzenes and phenyl hydroxylamines) after 24 h irradiation. However, when the same reaction was translated to continuous-flow by using PTFE capillary tubing (1 mm ID, 2.36 mL volume), 71% of azoxybenzene was obtained and only 7% of aniline with 4 h of residence time. Further investigation demonstrated that the material of the tubing (clouded PTFE or transparent FEP) did not have much effect on the reaction outcome. The elongation of the photoreactor, while keeping the residence time constant by increasing the flow rate (>2 $mL{\cdot}h^{-1}$), led to a higher selectivity, most likely because of the better mixing at higher flow rates. Notably, it was found that the residence time can be shortened by increasing the equivalents of the reducing agent (triethanolamine). In another work, the photosynthesis of azo compounds from nitrobenzene was performed with graphitic carbon nitride ($g\text{-}C_3N_4$) as heterogeneous catalyst in flow.[762] To avoid clogging, a gas−liquid−solid segmented flow was established, by pumping nitrogen gas into the photoreactor (PFA capillary, 1.6 mm ID, 30 mL volume), which was irradiated with purple LED (405 nm). The best productivity of the process (26.1 $mmol{\cdot}h^{-1}{\cdot}L^{-1}$ with 7.5 min of residence time) was 5.6 times better compared to the one obtained in batch (4.7 $mmol{\cdot}h^{-1}{\cdot}L^{-1}$).

The photomediated reduction of *ortho*-methyl phenyl ketones to secondary alcohols was reported by Singh, Pabbaraja, and co-workers utilizing water as a hydrogen source to perform a phototransfer hydrogenation reaction (PTHR) (Scheme 187).[763] For the optimization, 2-methylbenzophenone was introduced to a stream of water via a T-mixer, which then entered a HPFA reactor (1 mm ID, 3 mL volume) irradiated with a medium pressure 250 W lamp. The flow rate of both inputs was varied with the optimal condition affording a yield of 89% in 29 min residence time. For the scope, an in-line work up system was implemented, which consisted of an inlet stream of diethyl ether being introduced to the reaction stream after the photoreactor followed by in-line liquid−liquid separation with a hydrophobic PTFE membrane microseparator. Using this procedure, 25 ketones were successfully reduced in yields of 37−88%.

https://doi.org/10.1021/acs.chemrev.1c00332
Chem. Rev. 2022, 122, 2752−2906

Scheme 187. Photochemical Reduction of Diaryl Ketones in Flow with Water

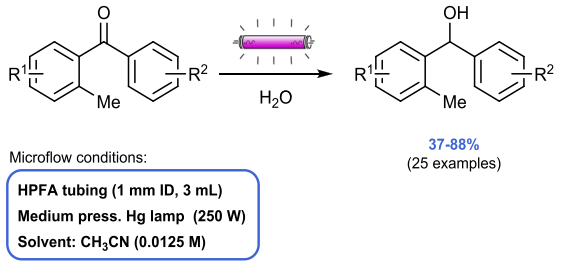

Similarly, Polyzos et al. reported the photocatalytic reduction of imines in flow in the presence of triethylamine as a cheap reducing agent (Scheme 188).[764] This work

Scheme 188. Photocatalytic Reduction of Diphenylimines in Flow with Triethylamine

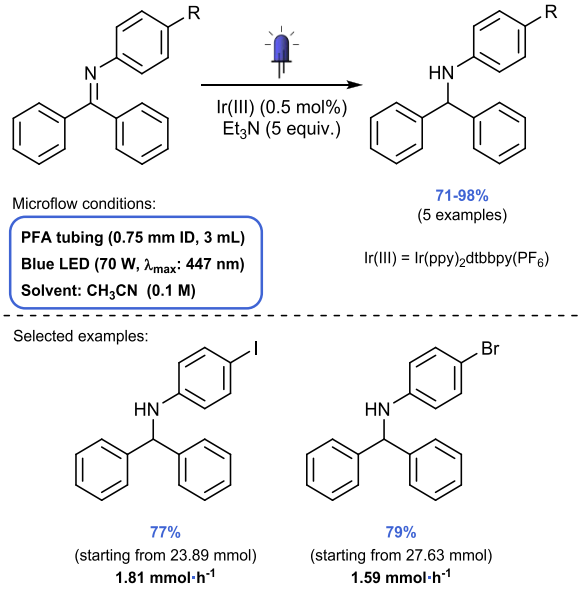

followed a previous report in batch where the main limitation was the competitive dehalogenation of iodoarene substituents.[765] The flow photoreactor consisted of coiled PFA capillary (0.75 mm ID, 3 mL volume) irradiated by two blue LED arrays (7 W, 447 nm) and pressurized to 40 psi (2.8 bar). The system was combined with an in-line FlowIR (FTIR) spectrometer which monitored the output over 9 h reaction time. Starting from 23.89 mmol, with 7 min of residence time, the desired amine was obtained in 77% (7.68 g), whereas the deiodination process was almost completely suppressed. For the *N*-(4-bromo-phenyl)-imine (27.63 mmol), the residence time was extended to 9 min, resulting in 79% yield. On a smaller scale (0.4 mmol), 5 different imines successfully underwent photoreduction. Under the same conditions in batch, significantly lower selectivity was observed, with 64% of the dehalogenated amine obtained after 3 h of irradiation.

5.9.4. Si−H Activation. Organosilanes are useful functionalities in medicinal chemistry and material science. Silicon-centered radicals can be generated by hydrogen atom transfer (HAT) in a straightforward strategy to activate silicon hydride (Si−H), through either: (i) a direct HAT catalysis, (ii) an indirect HAT event, or (iii) a proton-coupled electron transfer (PCET).[766]

In one example, Si−H bonds were activated in an SFMT reactor through the combination of the organophotoredox catalyst 4CzIPN with an HAT catalyst (Scheme 189A).[767] The

Scheme 189. (A) Photocatalytic Hydrosylilation of Alkenes through an HAT Process in STFM and in Continuous Flow and (B) Scale-up of the Photocatalytic Deuteration of Triethylsilane in Continuous Flow with HAT Catalyst

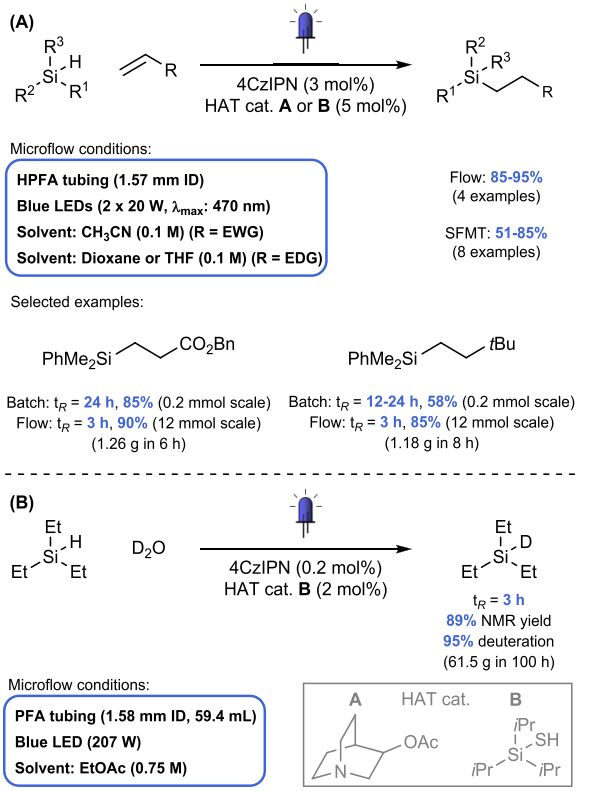

so-formed silyl radical reacted with both electron-poor and electron-rich alkenes. In the latter case, the polarity-reversal catalyst **B** for hydrogen atom abstraction was necessary. The reaction was developed in batch, however, SFMT reactors (HPFA capillary 0.762 mm ID, 1.5 mL volume) were employed in case of low conversions to improve the results. Larger-scale experiments (12 mmol) required a continuous-flow reactor (HPFA capillary 1.57 mm ID). In this way, high yields were obtained in only 3 h of residence time.

The photocatalytic deuteration of Si−H bonds in flow was described by Wu et al. (Scheme 189B).[768] 4CzIPN activates the HAT catalyst **B**, while **B**$^{\bullet}$ abstracts the hydrogen from the Si−H bond. The feasibility of a large-scale synthesis was evaluated using continuous-flow technology. The deuteration of 100 g of starting material (Et_3SiH) afforded 89% NMR yield of the desired product. Moreover, flow conditions were much more appealing than batch conditions, requiring (i) lower HAT catalyst loading (2 mol % vs 10 mol %), (ii) lower photocatalyst loading (0.2 mol % vs 2 mol %), (iii) fewer D_2O equivalents (30 vs 50), and (iv) shorter reaction time (3 h vs 12 h).

https://doi.org/10.1021/acs.chemrev.1c00332
Chem. Rev. 2022, 122, 2752−2906

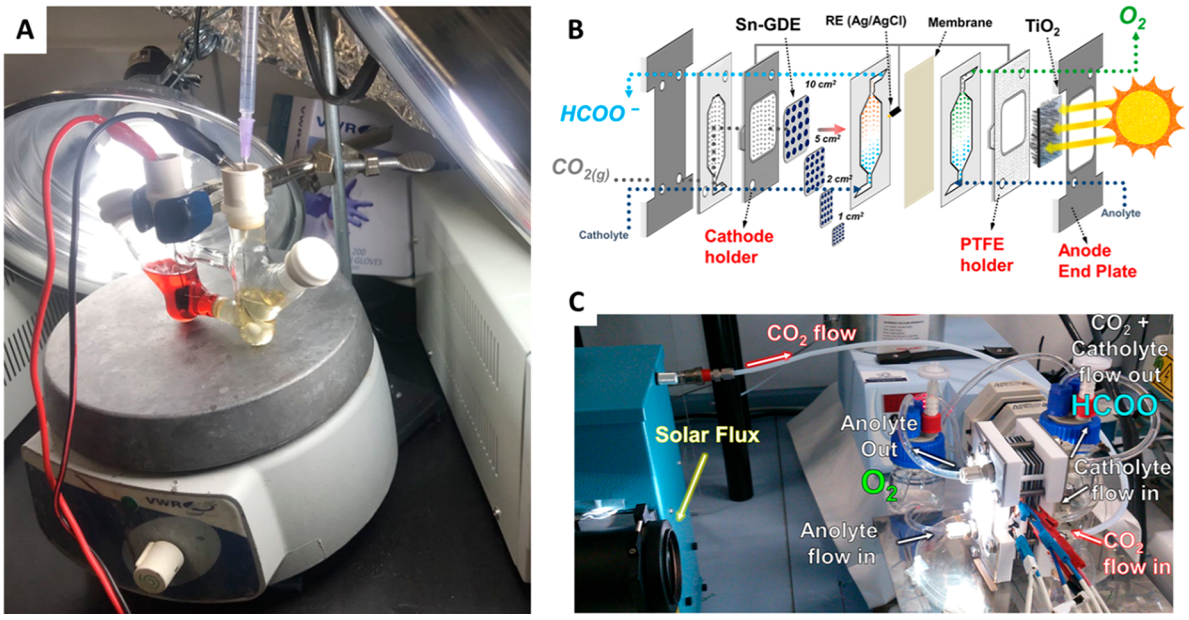

Figure 63. Examples of photoelectrochemical setups: (A) Homemade photoelectrochemical batch setup based on an H-type divided cell with an "F" glass filter as membrane. Schematic representation (B) and picture (C) of a photoelectrochemical flow cell using TiO_2 deposited on FTO as photoanode. Panel A: Reprinted from ref 780. Reprinted with permission from AAAS. Panels B and C: Reprinted with permission from ref 781. Copyright 2017, with permission from Elsevier.

6. PHOTOELECTROCATALYSIS: MERGING PHOTOREDOX CATALYSIS WITH ELECTROCHEMISTRY

Synthetic organic electrochemistry and photoredox catalysis have almost simultaneously witnessed a remarkable renaissance in the past decade and are often compared to each other.[31] In most cases,[769] single-electron transfer (SET) is the key step in both techniques, leading to the generation of radical intermediates.[770] However, the main difference between the two activation modes is the way the electron transfer occurs. In electrochemistry, SET occurs at an electrode surface and the applied voltage is tuned via an external potentiostat.[771] In contrast, photocatalysis uses photons as energy carrier leading to an excited state photocatalyst which can engage in SETs with other organic molecules. In photocatalysis, the redox properties are dependent on the molecular structure of the photocatalyst. Because of the difference in energy supply, it is immediately clear that both scenarios pose different technological challenges and, thus, require disparate reactor designs to carry out and scale these reactions.[772]

The merger of electrochemistry and photocatalysis has recently led to some new exciting opportunities for synthetic organic chemists.[29,30,773] While it is technologically quite complex as both electrode-processes and photon transport phenomena need to be harmonized, their combination is often used to solve a specific synthetic problem associated with either photocatalysis or electrochemistry. As we will show in this specific section, photoelectrochemistry allows to remove certain oxidants and reductants, to close the catalytic cycle, or to generate very powerful oxidants or reductants. It further facilitates the lowering of the applied potentials in electrochemistry leading to milder reaction conditions and, thus, to more selective transformations.

6.1. General Considerations for Design of Photoelectrochemical Batch and Flow Reactors

Combining electrochemistry and photocatalysis can be quite challenging from the vantage point of reactor design. In a single reactor, electrodes need to be installed, and simultaneously, a proper illumination of the reaction medium has to be ensured. This means that technological hurdles in both electrochemistry and photochemistry need to be overcome at the same time. Notably, when highly reactive species are involved, it is important that both the delivery of electrons and photons are on par with each other. Hence, a proper design of the reactor setup is crucial to ensure highly efficient and reproducible reactions. However, as the field is relatively new, the reported reactor designs are often exploratory and homemade, and thus suboptimal with regard to the optimization of electron, photon, mass, and heat transport. Nevertheless, these designs provide some useful insights, and as the field grows, it can be anticipated that commercially available and standardized systems will become available in the near future.

In batch, homemade reactors are the most common in the current literature. The simplest arrangement consists of a small-sized glass reactor equipped with two electrodes which is subjected to light irradiation originating from LED or CFL light sources. If the two electrochemical half-reactions are incompatible, a divided cell can be used where the two half-cells are separated by a suitable membrane (Figure 63A) (i.e., cation-exchange or anion-exchange membrane). It can easily be understood that such devices might lead to interlaboratory reproducibility issues.

The challenges associated with photochemistry (e.g., attenuation of light) and electrochemistry (i.e., ohmic drop) can often be overcome when the reaction is miniaturized using for example microreactor technology. It is reasonable to state that all relevant processes will occur in the proximity of electrodes due to short living nature of the generated reactive

https://doi.org/10.1021/acs.chemrev.1c00332
Chem. Rev. 2022, 122, 2752−2906

species. Hence, it is important that photons are delivered efficiently proximal to the electrode surface. So far, the reports on flow photoelectrochemistry have been limited to the conversion of relatively simple molecules, such as CO_2 or formic acid (see section 0 for more information). In these examples, a suitable photocatalyst, such as TiO_2,[774] Cu_2O,[775] CuO,[776] and $BiVO_4/WO_3$,[777] is deposited on fluorine-doped tin oxide glass (FTO). FTO is an electrically conductive, chemically inert and transparent material and is often used as a less expensive alternative to indium tin oxide (ITO) electrodes in the development organic solar cells (Figure 63B and C).[778] The reagents can subsequently be directed over the photoelectrode using a suitable pump. While these photoelectrochemical flow cells could find use in synthetic organic chemistry, it is our belief that this design, due to the nontransparent nature of the heterogeneous photocatalyst, is not going to be generally applicable (e.g., for homogeneous photocatalysis). A suitable strategy would be to fill the narrow interelectrode gap with electrolyte while the reaction solution is flowing on the opposite side of the nontransparent, porous electrodes (Figure 64).[779] This side is subsequently covered with a transparent plate, through which the reaction solution can be irradiated.

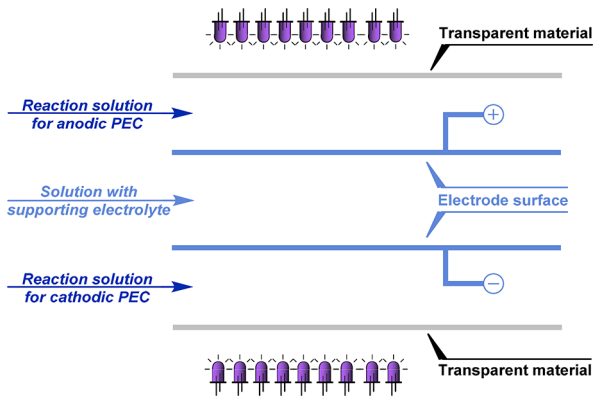

Figure 64. Schematic representation of generally applicable photoelectrochemical flow reactor (PEC = photoelectrochemical cell).

6.2. Generation of Highly Oxidizing/Reducing Species Using Photoelectrochemistry

One of the most relevant applications of photoelectrochemistry is the generation of extremely powerful oxidizing or reducing species, stemming from the excitation of an oxidized/reduced photocatalyst. As shown in Scheme 190, the photocatalyst (PC) interacts first with an electrode. Then, the oxidized/reduced PC is excited by light irradiation to a highly oxidizing/reducing species, which reacts subsequently with the organic substrates (Sub). This allows to engage previously unreactive substrates in useful synthetic transformations, effectively expanding the substrate scope of a transformation. The requirements to be met are (i) the photocatalyst has to be reduced/oxidized at low voltages; (ii) after electron transfer, the intermediates must be able to absorb light and (iii) the resulting reactive species must live sufficiently long to enable interaction with the substrate.

In one of the earliest synthetically useful examples (in 1979), Moutet and Reverdy described the anodic oxidation of phenothiazine (PTZ, $E_{1/2}$ = 0.79 V)[782] which generates a radical cation (Scheme 191).[783] After irradiation using a

Scheme 190. Photoelectrogeneration of Highly Oxidizing (A) or Reducing (B) Species[a]

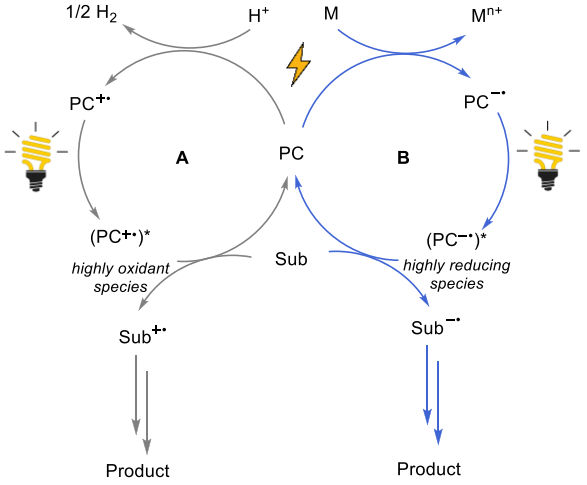

[a]PC = photocatalyst; Sub = substrate.

Scheme 191. Oxidation of Diphenylethylene Using Phenothiazine (PTZ) as a Photoelectrochemical Catalyst

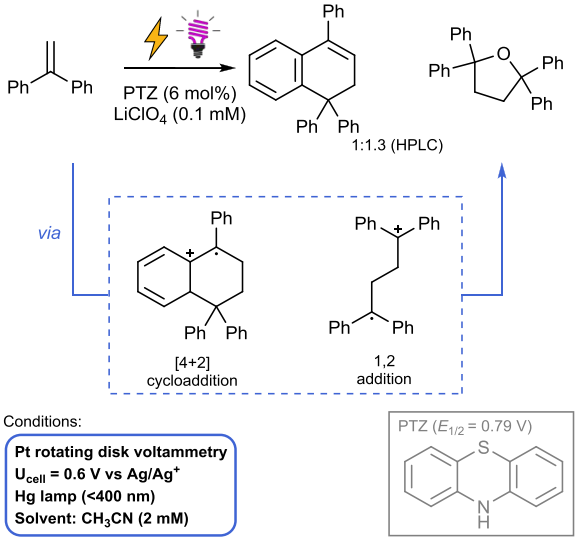

mercury lamp (<400 nm), a highly oxidizing species is obtained, which can subsequently oxidize diphenylethylene (DPE). The so-formed radical cation of DPE reacts with another DPE molecule undergoing either a [4 + 2] cycloaddition or a 1,2-addition.

Successively, the same authors reported the oxidation of benzylic alcohols to the corresponding aldehyde using *N,N,N′,N′*-tetraphenyl-p-phenylenediamine (TPPD) as the photoelectrocatalyst (Scheme 192).[784] After being anodically oxidized ($E_{1/2}$ = +0.68 V), TPPD generates a radical cation which, under UV irradiation, reaches an excited state able to oxidize the alcohol. Unfortunately, no yield was reported.

About four decades after these pioneering examples, Lambert et al. reported an oxidative coupling of arenes using trisaminocyclopropenium (TAC) ion as an photoelectrocatalyst.[785] The electrochemical behavior of such an ion had already been described in the 1970s,[786−788] while in 2017 it was used as an electrolyte.[789] Lambert et al. described how TAC ions can be easily oxidized by a graphite anode ($E_{1/2}$ =

https://doi.org/10.1021/acs.chemrev.1c00332
Chem. Rev. 2022, 122, 2752−2906

Scheme 192. Photoelectrochemical Oxidation of Benzyl Alcohol with TPPD

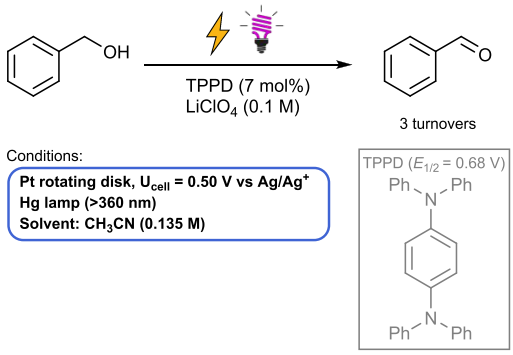

+1.26 V vs SCE) generating the corresponding air-stable radical dication, which forms an extremely oxidizing species after irradiation with white light. The radical TAC dication, generated by the oxidation of TAC^+, represents an open-shell doublet photocatalyst which undergoes an electron transition from HOMO to SOMO when irradiated by visible light (23 W CFL) (Scheme 193C). The SOMO−HOMO level inversion explains its extremely high oxidation potential (E^*_{ox} = 3.33 V vs SCE). Depending on the substrate, the reactor is either a divided or an undivided cell equipped with graphite and Pt electrodes, where the reaction mixture is exposed to irradiation from a 23 W CFL. Notably, easy-to-oxidize substrates do not need a divided cell configuration. The generated excited dication $(TAC^{2+\bullet})^*$ can oxidize even benzene, whose radical cation can be trapped by pyrazole (Scheme 193A). In this case, TAC works as an SET catalyst (Scheme 193C).[785] As an SET photoelectrocatalyst, TAC^+ was also employed for the syn-stereoselective acetoxyhydroxylation of olefins, affording the corresponding glycol monoesters (36 examples, 31−82% yield).[790] It was also possible to translate the batch process into a recirculating flow one for the scale-up (12−50 mmol). The flow setup consisted of two separated reactors, namely, the electrochemical cell and a PTFE-capillary photoreactor irradiated with a 23 W CFL.

Calculations demonstrated that the strongly oxidizing $(TAC^{2+\bullet})^*$ species has an aminyl radical cation character, and for this reason, it can also act as a hydrogen atom transfer (HAT) acceptor (Scheme 193B).[791] Compared to other known HAT acceptors, such as selectfluor,[792] *N*-hydroxy succinimide,[793] and $K_2S_2O_8$,[794] TAC offers several advantages, including that it can be used in catalytic amounts (8 mol %), it is regioselective, and no external oxidants are required. In this

Scheme 193. Use of TAC^+ as a Photoelectrocatalyst: (A) SET and (B) HAT Photoelectrocatalysis with TAC^+, (C) Proposed Mechanism for the Photoelectrolyzed Transformations with the Orbital Configuration of the Oxidized and Photoexcited $TAC^{2+\bullet}$ Species, and (D) Photoelectrocatalytic Diamination of Vicinal C−H Bonds

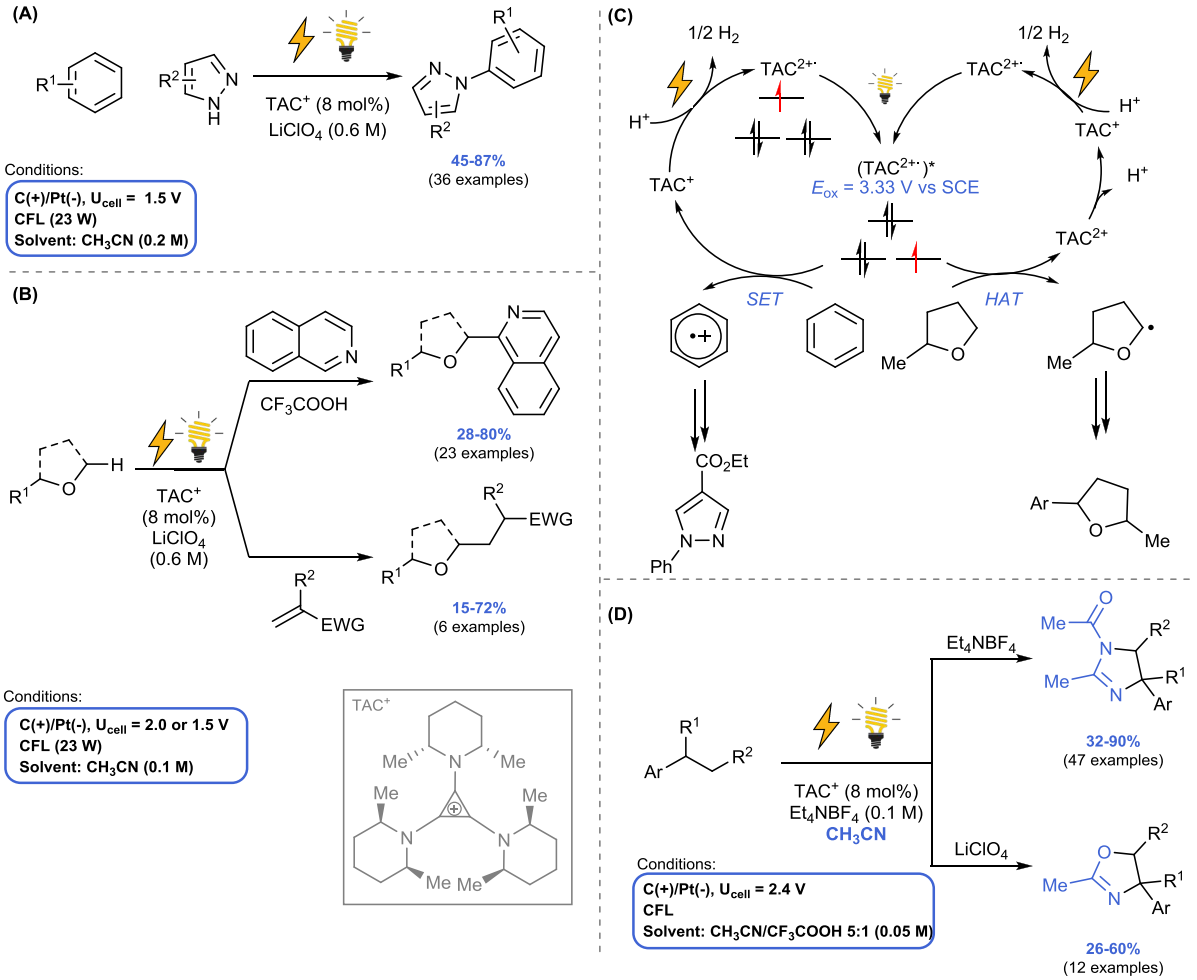

https://doi.org/10.1021/acs.chemrev.1c00332
Chem. Rev. 2022, 122, 2752−2906

way, activated C−H bonds, that is, located at the α-position from ethers, can be functionalized with isoquinolines, azoles, alkenes and alkynes. In 2021, the same group reported the TAC^+-photoelectrocatalytic diamination of vicinal C−H bonds (Scheme 193D).[780] In this case, the excited dication $(TAC^{2+\bullet})^*$ oxidizes the alkylated arene substrate twice, thus producing a cationic species, which undergoes multiple Ritter-type C−H functionalization reactions with acetonitrile. The reaction was performed in a H-type electrolytic cell equipped with carbon felt anode and platinum cathode, irradiated with a CFL. Interestingly, the choice of the supporting electrolyte determined the selectivity to either the 3,4-dihydroimidazole or the 2-oxazoline. The transformation proved to be generally applicable and was used to functionalize nine bioactive molecules and synthesize four, in good yields (31−72%). When starting from benzylic-unbranched substrates, the monoamination product is obtained instead.[795] In fact, in the case of branched substrates, an acid-catalyzed elimination step takes place after the first amination, leading to a styrene intermediate, which undergoes further oxidation and Ritter-type functionalization. On the other hand, for unbranched substrates the elimination would require a stronger acid than TFA, and thus generates a benzylic amide.

To trigger photoelectrochemical reductions, a different set of catalysts has to be taken into consideration. For instance, 9,10-dicyanoanthracene (DCA) behaves as an electron-primed photocatalyst, which is able to reduce various aryl halides to their corresponding radical anions (Scheme 194A).[796] These species undergo mesolytic cleavage, forming the corresponding aryl radical by losing the halide. Then, the aryl radical reacts with other reagents (namely, boron pinacolate, hexamethylditin, *N*-methyl pyrrole). The setup consists of an H-type divided electrochemical cell equipped with a carbon felt cathode and a zinc plate in the anodic half-cell. The entire electrochemical cell is irradiated with blue LEDs. DCA can be cathodically reduced to form an anion radical which is subsequently excited by blue light irradiation, leading to a highly reducing species (estimated at −3.2 V vs SCE) owing to a SOMO-HOMO level inversion (Scheme 194B). Such a low reduction potential can be compared to those of alkali metals. The use of alkali metals has provided many synthetic opportunities to organic chemists, yet these methods are plague with issues related to safety and poor chemoselectivity.[797] Mechanistic studies revealed that an alternative pathway for DCA to first get photoexcited and then reduced is less probable, as DCA does not absorb in the blue region of the UV−vis spectrum.

DCA is not the only option to enable photoelectrocatalytic reductions. A naphthalene-based analogue of perylene monoimide (NpMI) can be reduced at a reticulated vitreous carbon (RVC) cathode in a H-type electrochemical cell when an adequate potential is applied (Scheme 195A).[798] As the other−synthetically less important− half reaction, the oxidation of Et_3N was selected. The electrochemical reduction of NpMI results in the formation of a mild reductant, which is subsequently transformed into a highly potent one (E_{red}< −3.3 V) upon absorption of blue light. NpMI proved efficient in the reduction of aryl bromides and chlorides, which display a low

Scheme 194. (A) Photoelectrochemical Reductions with DCA Allow the Activation of Aryl Halides and (B) Molecular Orbitals of DCA and of Its Reduced and Excited Derivatives

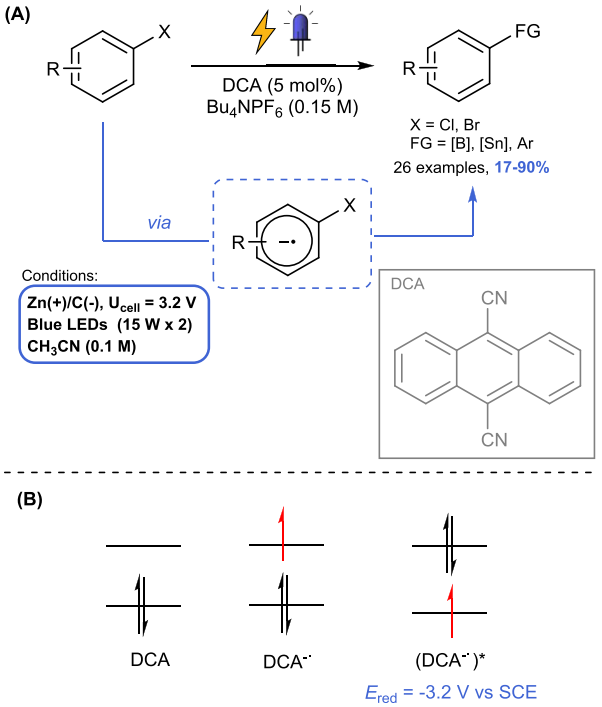

Scheme 195. Electron-Primed Photoredox Catalysis with NpMI: (A) Photoelectrocatalyzed Arbuzov Reaction and Coupling with *N*-Methyl Pyrrole and (B) Comparison among Photoelectrochemical, Electrochemical, and Photochemical Aryl Cross-Coupling versus Reduction

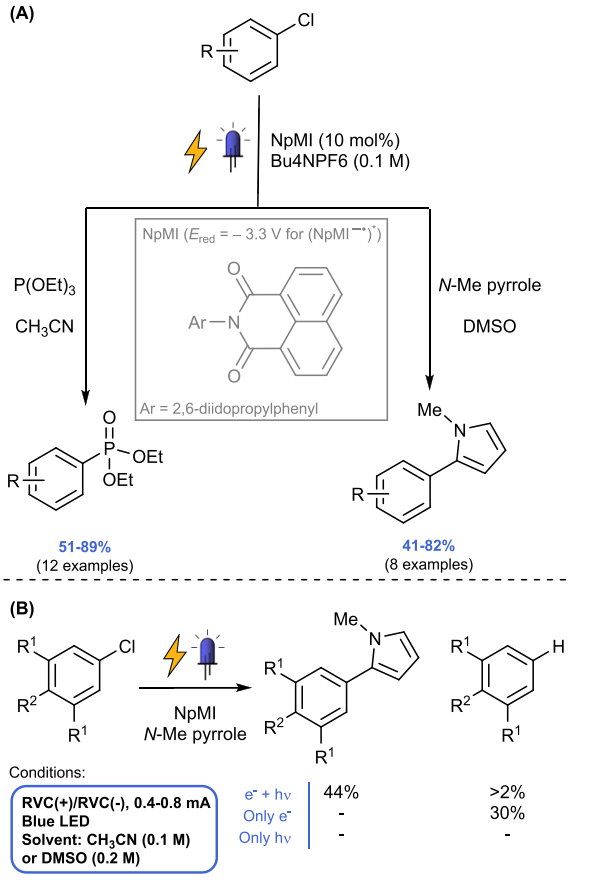

https://doi.org/10.1021/acs.chemrev.1c00332
Chem. Rev. 2022, 122, 2752−2906

Scheme 196. (A) Example of a Photocatalytic Cycle Where Electricity Is Used to Restore the Photocatalyst in the Last Step, (B) Photoelectrochemical Alkylation of Heteroarenes Using Organotrifluoroborates, (C) Photoelectrochemical Trifluoromethylation of Arenes with the Langlois Reagent, and (D) Trifluoromethylation of Mesitylene in Flow, with Spatial and Temporal Separation of the Electro- and Photocatalytic Steps

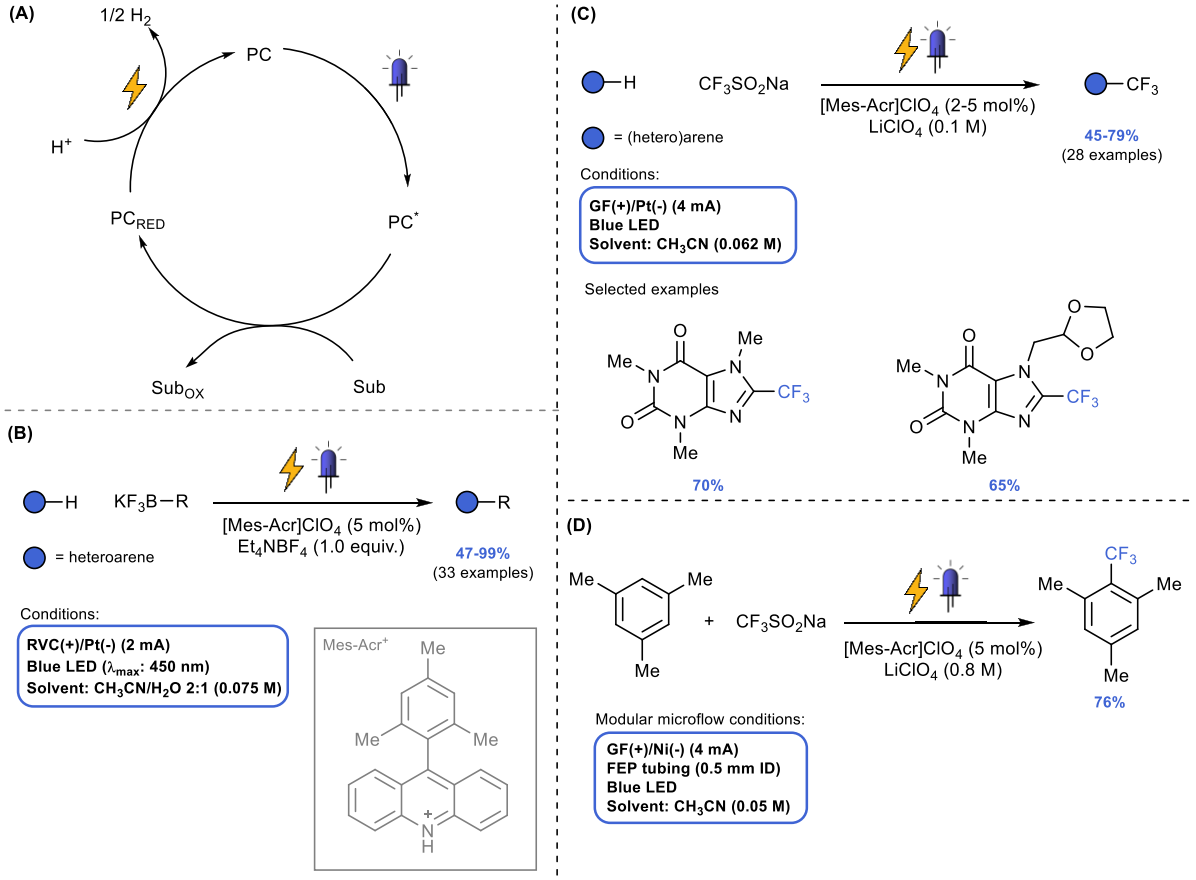

redox potential (∼−2.4 V). In this way, the photoelectrocatalyzed Arbuzov reaction was made possible using electron-rich aryl chlorides as substrates. The radical coupling of (electron-rich) aryl chlorides with *N*-methyl pyrrole was also feasible. The direct comparison between the photoelectro activation and the individual photon or electron activation modes showed a clear benefit of photoelectrocatalysis. Neither photocatalysis nor electrolysis alone afforded the cross-coupling product (Scheme 195B).

6.3. Closing the Photocatalytic Cycle with an Electrochemical SET

Understanding the underlying mechanism of a photocatalytic transformation is a crucial research aspect within synthetic organic chemistry.[603] Fundamental insight into the photocatalytic cycle allows researchers to devise new synthetic pathways as well as to overcome present limitations.[34,73,799,800] Particularly, closing of the catalytic cycle and regeneration of the photocatalyst is of fundamental importance to increase TON and TOF values, although this is often overlooked. Photocatalyst regeneration does not involve light and can take place in several ways, involving either a cocatalyst, an external stoichiometric agent or by quenching of a reactive intermediate.[801] However, the use of electrochemistry to close the cycle provides a more atom-economical solution as it does not require any additional sacrificial agent (Scheme 196A). One important example is presented by the work of Xu et al., where photocatalysis and electrochemistry were merged to develop an oxidant-free C−H alkylation of heteroarenes with organotrifluoroborates as coupling partners (Scheme 196B).[802] Mes-Acr$^+$ was selected as a suitable photocatalyst, which is excited by blue LED irradiation in an undivided electrolytic cell. The excited species Mes-Acr^{+}* (2.06 V vs SCE) can undergo an SET with organotrifluoroborate, yielding the corresponding alkyl radical and Mes-Acr. Whereas the alkyl radical further reacts with the heteroarene yielding the target compound, Mes-Acr is oxidized at the RVC anode back to Mes-Acr$^+$.

Mes-Acr$^+$ can also enable the trifluoromethylation of (hetero)arenes using the Langlois reagent as CF_3-source (Scheme 196C).[803] The transformation is carried out in an undivided electrolytic cell with a graphite felt (GF) anode and a Pt cathode, subjected to blue LED irradiation. Importantly, a continuous-flow version of this transformation proved to be efficient, showing that the photoexcitation and electrooxidation can occur sequentially in two different reactors (Scheme 196D). The flow system consists of a modular electro-flow cell based on a commercial flow reactor by IKA[804] connected to a transparent FEP capillary subjected to blue LEDs.

Based on their previous work,[785] Lambert et al. have proposed an photoelectrocatalytic approach to trigger the nucleophilic aromatic substitution (S_NAr) of fluorinated arenes using 2,3-dichloro-5,6-dicyanoquinone (DDQ) as the photocatalyst (Scheme 197).[805] Although S_NAr is widespread in

https://doi.org/10.1021/acs.chemrev.1c00332
Chem. Rev. 2022, 122, 2752−2906

Scheme 197. Photoelectrocatalytic S_NAr Starting from Unactivated Aryl Fluorides and DDQ as Photocatalyst

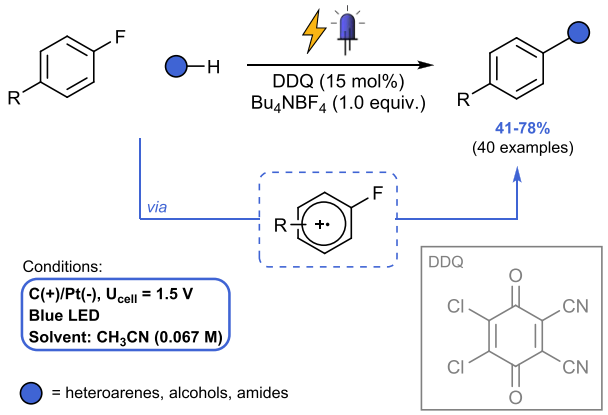

Scheme 198. Flavin-Photocatalytic Oxidation of Alcohols Using Electrochemistry to Close the Photocatalytic Cycle

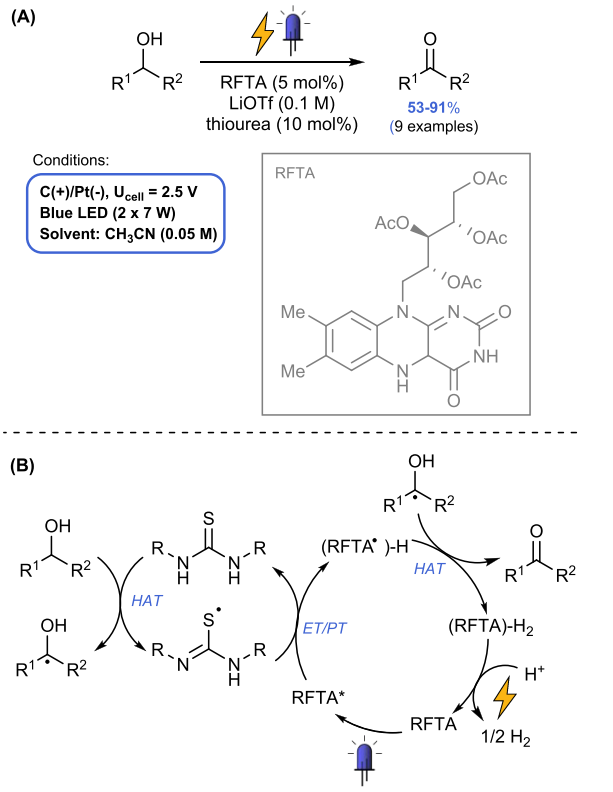

organic chemistry, unactivated substrates are challenging unless very harsh reaction conditions (e.g., high temperatures, strong bases) are employed. However, when irradiated with blue LEDs, DDQ gets into an excited state (3.18 V vs SCE) which is sufficiently high in energy to oxidize fluorinated arenes. The generated aryl radical cation subsequently reacts with a nucleophile to afford a radical which is most likely reduced by the Pt cathode. The anion can then remove fluoride after which the targeted substitution product is formed. At the anode, $DDQ^{\bullet-}$ is oxidized to complete the catalytic cycle. When N-containing heteroarenes, alcohols and amides are used as nucleophiles, the obtained yields are moderate to good (41−78%). The same photocatalyst (DDQ) was used by Lambert et al. to oxidize arenes and form phenols in the presence of water.[806] Moreover, the radical cation obtained by oxidation with DDQ can also react with alcohols, acids, and nitrogen nucleophiles. For the batch reactions, a three-neck flask was equipped with a carbon felt anode and a platinum wire cathode and was irradiated with blue LEDs. To prove the scalability of the transformation, the light-induced step was performed in continuous-flow. The flow reactor consisted of an electrochemical cell coupled with one or three PFA coils placed in series, irradiated with blue LEDs. In these setups, 4 mmol of benzene was processed in 48 and 22 h, respectively, resulting in comparable yields of phenol (55% and 60%). The reaction was further scaled up to 15 mmol, affording the 56% yield over 60 h.

Another interesting example where the use of electrochemistry allowed to close the photocatalytic cycle is the oxidation of alcohols using flavin. Photocatalytic methods for this reaction were limited to the oxidation of benzylic alcohols,[807−809] due to the limited redox potential of the photocatalyst.[810] One method to improve results for the alcohol oxidation was reported by König et al., who reported that the addition of catalytic amounts of thiourea, serving as an electron-transfer mediator, improved yields.[811] However, the applicability of the transformation remained limited. On the basis of this insight, Lin et al. expanded the scope to secondary alcohols by using electricity as the final oxidant of the photocatalyst (Scheme 198A).[812] All reactions were performed in a glass tube containing a carbon foam anode and a platinum coil cathode which was irradiated with blue LEDs. Detailed mechanistic studies revealed that thiourea is oxidized by the excited state of riboflavin tetraacetate (RFTA*) and the resulting radical abstracts a hydrogen atom from the alcohol, forming a ketyl radical. This ketyl radical reacts further with (RFTA$^{\bullet}$)-H affording the desired ketone together with (RFTA)-H_2, which is subsequently oxidized at the anodic surface, closing the photocatalytic cycle (Scheme 198B). The use of electrochemistry is key to success, as the previously used final oxidant (O_2) provoked thiourea degradation.

An photoelectrocatalytic oxidative azidation was developed by Lei et al., which involves the use of a HAT photocatalyst (DDQ, 9-fluorenone or bis(4-methoxyphenyl)methanone) and a Mn(II) complex in an electrochemical cell (Scheme 199A).[813] The transformation performs well with secondary benzyl and tertiary C(sp^3)−H bonds. In addition, the late-stage azidation of several biologically active molecules was realized as well. The core events in the proposed mechanism are (i) the coordination of the azide by Mn(II), which is subsequently oxidized to Mn(III) and (ii) the excitation of the photocatalyst, which induces the HAT on the substrate, generating a carbon-centered radical (Scheme 199B).

HAT photocatalysis was also employed by Ravelli et al. in the photoelectrocatalytic cross-dehydrogenative coupling between unactivated alkanes and benzothiazoles (Scheme 200A).[814] In this transformation, TBADT fulfills three roles: (i) HAT photocatalyst, (ii) photoredox catalyst, and (iii) electrocatalyst. In fact, the authors proposed the following mechanism (Scheme 200B): the reactive excited state of TBADT (^{1}O) abstracts a hydrogen from the unactivated alkane, affording a carbon-centered radical which interacts with the benzothiazole. The so-formed N-centered radical can undergo two possible pathways, either a spin-center shift (SCS) or a back-HAT (b-HAT). Both processes lead to the formation of a carbon-centered radical intermediate which gets

https://doi.org/10.1021/acs.chemrev.1c00332
Chem. Rev. 2022, 122, 2752−2906

Scheme 199. (A) Photoelectrochemical Azidation of Secondary Benzylic and Tertiary C−H Bonds and (B) Proposed Mechanism

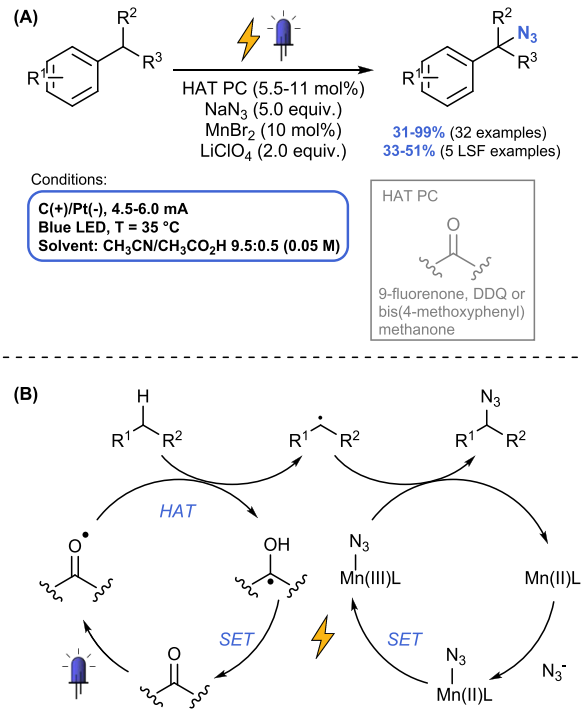

Scheme 200. (A) Photoelectrocatalytic Cross-Dehydrogenative Coupling between Alkanes and Benzothiazoles with TBADT and (B) the Proposed Mechanism

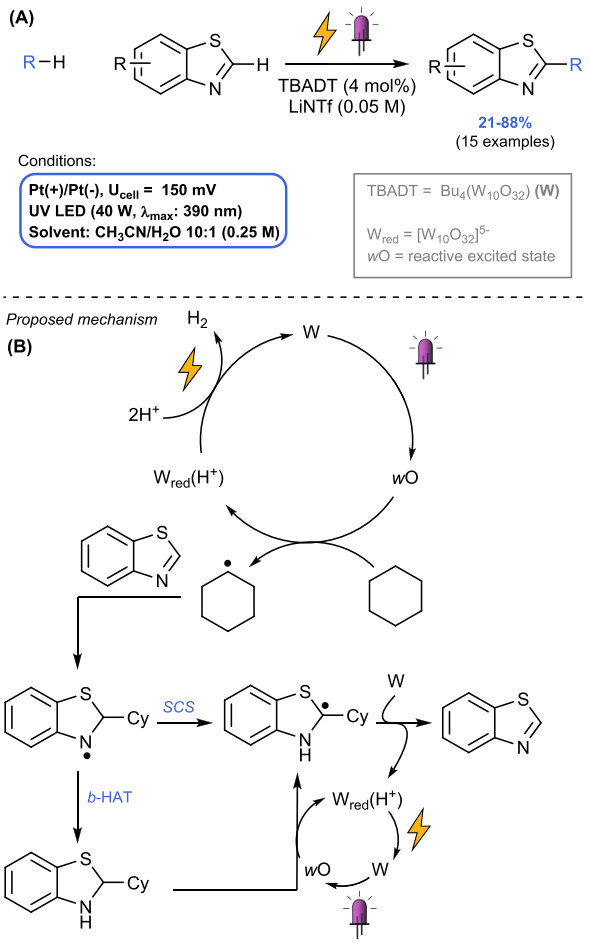

oxidized by TBADT (Scheme 200B). The reaction was performed in a H-type electrochemical cell irradiated by UV-LED and modest to good yields of the coupled products were obtained (21−88% yield, 15 examples).

6.4. Decoupled Light-Induced and Electricity-Driven Processes

In some cases, the photon-induced and the electron-induced processes do not interact in the same catalytic cycle. In this Review, we refer to such processes as decoupled. One example of a decoupled process is reported by Thiyagarajan et al. in the synthesis of maleic acid from furfural, where the photocatalytic and electrochemical step occur in two separated steps.[815] First, the photochemical oxidation of furfural with MB as photosensitizer takes place affording the 5-hydroxy-2(5*H*)-furanone. This is, then, transformed into maleic acid through an electrochemical or even biochemical step, involving the Laccase−TEMPO system.

This two-step approach was also adopted by Xu et al. to selectively alkylate acridinium dyes.[816] A photochemical microflow reactor (PFA, 0.9 mm ID, 2 mL) was combined with an electrochemical flow reactor (graphite(+), Pt(−), 0.25 mm distance between electrodes, 0.25 mL volume, 85 mA) to first perform a cross-coupling with an organotrifluoroborate and then (after pumping TEMPO into the mixture) an electrocatalytic dehydrogenation to restore the aromaticity of the acridinium dye (12 examples, 48−98% yield). The procedure could be repeated twice to obtain 3,6-disubstituted compounds.

In another example, Stephenson et al. described a one-pot transformation for the depolymerization of lignin in which the two activation modes take place in two different moments.[817] First, an *N*-hydroxyphthalimide (NHPI)/2,6-lutidine-electrocatalyzed benzylic oxidation of several lignin model compounds was performed. Then, without any work up or isolation, $[Ir(ppy)_2(dtbbpy)]PF_6$ photocatalyst and other additives were added, and the corresponding reaction mixture was irradiated with blue LEDs. This resulted in the cleavage of the C−O bond. Notably, the reaction works efficiently with native lignin as well. The second step was also performed in a flow reactor (4.6 mL, 0.76 mm ID, 0.1 mL·min^{-1}) affording the cleavage products in good to excellent yields in 46 min residence time (Scheme 201).

In other cases, the electro- and photochemical process occur in the same reactor, as reported by Scheffold et al. in 1983.[818] Vitamin B_{12a} was used to catalyze the nucleophilic acylation of electron-poor alkenes with anhydrides at a stirred Hg-pool cathode in an H-type cell under argon. The reaction mixture was irradiated with two 500 W incandescent bulbs at 30 cm distance for 10−15 h. The Co(III)- and Co(II)-complexes present in the vitamin core can be easily reduced at the cathode to form Co(I), which reacts with the anhydride yielding Co(II)-acyl complexes. These intermediates fragment under light irradiation. The formed acyl radicals subsequently attack the olefin resulting in the formation of the corresponding 1,4-dicarbonyl product (Scheme 202).

More recently, Stahl et al. reported a decoupled photochemical/electrochemical method enabling C(sp^3)−H amina-

https://doi.org/10.1021/acs.chemrev.1c00332
Chem. Rev. 2022, 122, 2752−2906

Scheme 201. One-Pot Electrocatalytic Oxidation−Photocatalytic Reductive Cleavage of Lignin Model Compounds

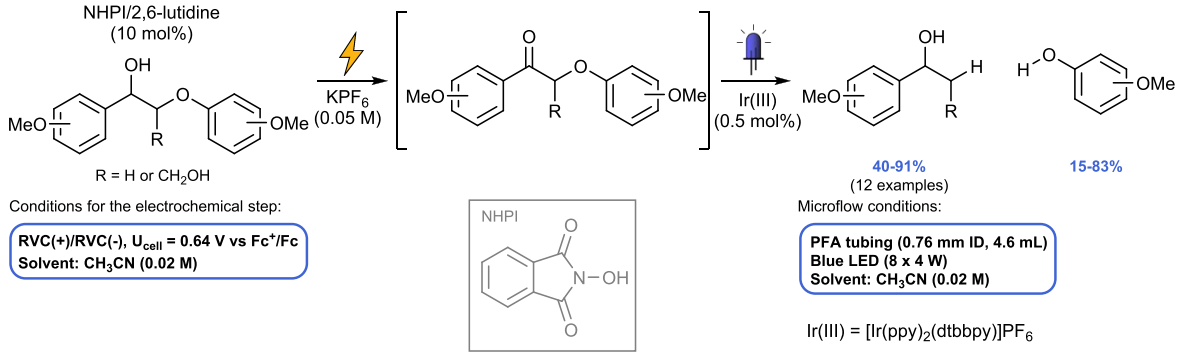

Scheme 202. Photoelectrocatalytic Acylation of Electron-Poor Alkenes with Vitamin B_{12a} Starting from Anhydrides

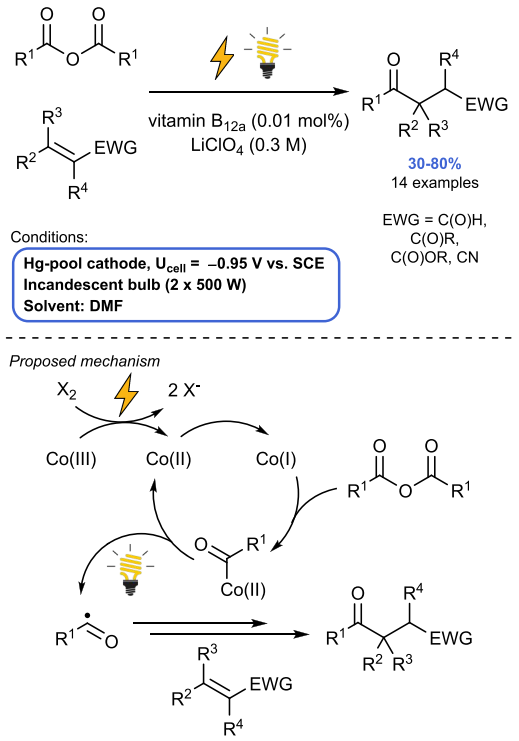

Scheme 203. Photoelectrochemical C(sp^3)−H Amination Mediated by Iodide Trifluoroethoxide As Base for the Synthesis of (A) Pyrrolidines, (B) Oxazolines, and (C) Amino Alcohols

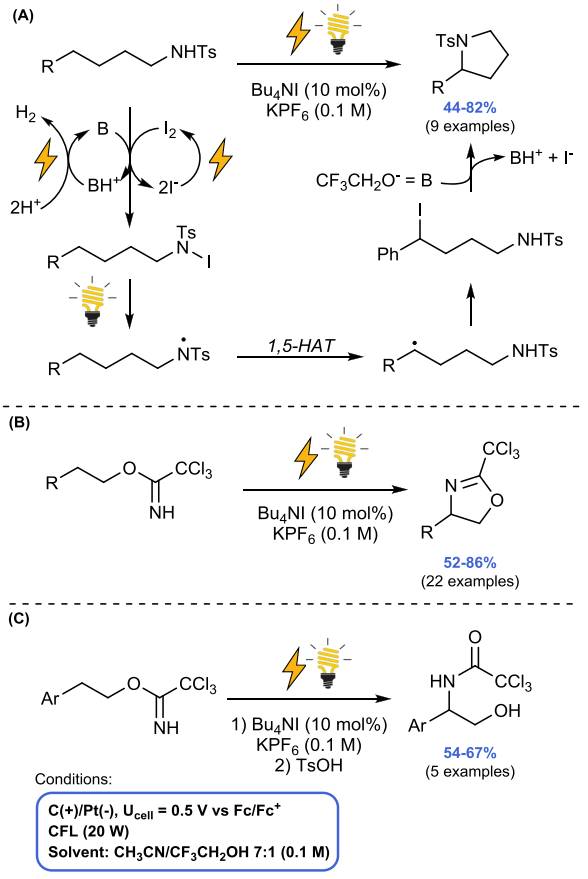

tions under mild conditions (i.e., lower cell voltage) (Scheme 203).[819] Because of the lower voltage, a higher functional group tolerance was achieved compared to strategies, which rely solely on electrochemistry.[820−823] To improve the versatility of the electrochemical reaction, a low-potential electron-mediator ($2I^- \rightarrow I_2$) was employed. The Brønsted base ($CF_3CH_2O^-$) deprotonates the substrate, promoting the iodination. Next, light induces the homolytic cleavage of the N−I bond, yielding an N-centered radical (Scheme 203A).[819] Reactions were carried out using an undivided cell equipped with a graphite anode, a platinum wire cathode, and a Ag/Ag^+ reference electrode. The reactor was irradiated with a CFL light source. This transformation could be applied to the synthesis of pyrrolidines, oxazolines, and amino alcohols (Scheme 203A−C, respectively).

Inspired by the photoelectrochemical C−H alkylation using alkyl trifluoroborates as coupling partners,[802] Song, Xu et al. developed a Minisci-type reaction where ubiquitous carboxylic acids were used as precursors for the generation of carbon-centered radicals.[824] The reaction is performed in an undivided cell equipped with RVC and a platinum plate, irradiated by blue LEDs. The authors managed to perform the alkylation of a diverse set of heteroarenes using cerium(III) chloride in the presence of HCl (Scheme 204A). However, when oxamic acids were used as starting materials, 4CzIPN instead of $CeCl_3$ was employed (Scheme 204B). Although these two transformations present similarities, the authors proposed that light and electricity are necessary in different steps. Concerning the reaction with carboxylic acids, cerium trichloride is oxidized at the anode and forms Ce(IV), a species able to coordinate the starting material. Subjected to irradiation, this transient species undergoes a ligand-to-metal charge transfer (LMCT) leading

https://doi.org/10.1021/acs.chemrev.1c00332
Chem. Rev. 2022, 122, 2752−2906

Scheme 204. (A) Photoelectrocatalytic Minisci-Type Alkylation Using $CeCl_3$, (B) Decarboxylative Cross-Coupling of Heteroarenes with Oxamic Acids Using 4CzIPN as a Photocatalyst, and Proposed Mechanisms (C) and (D) of the Two Transformations

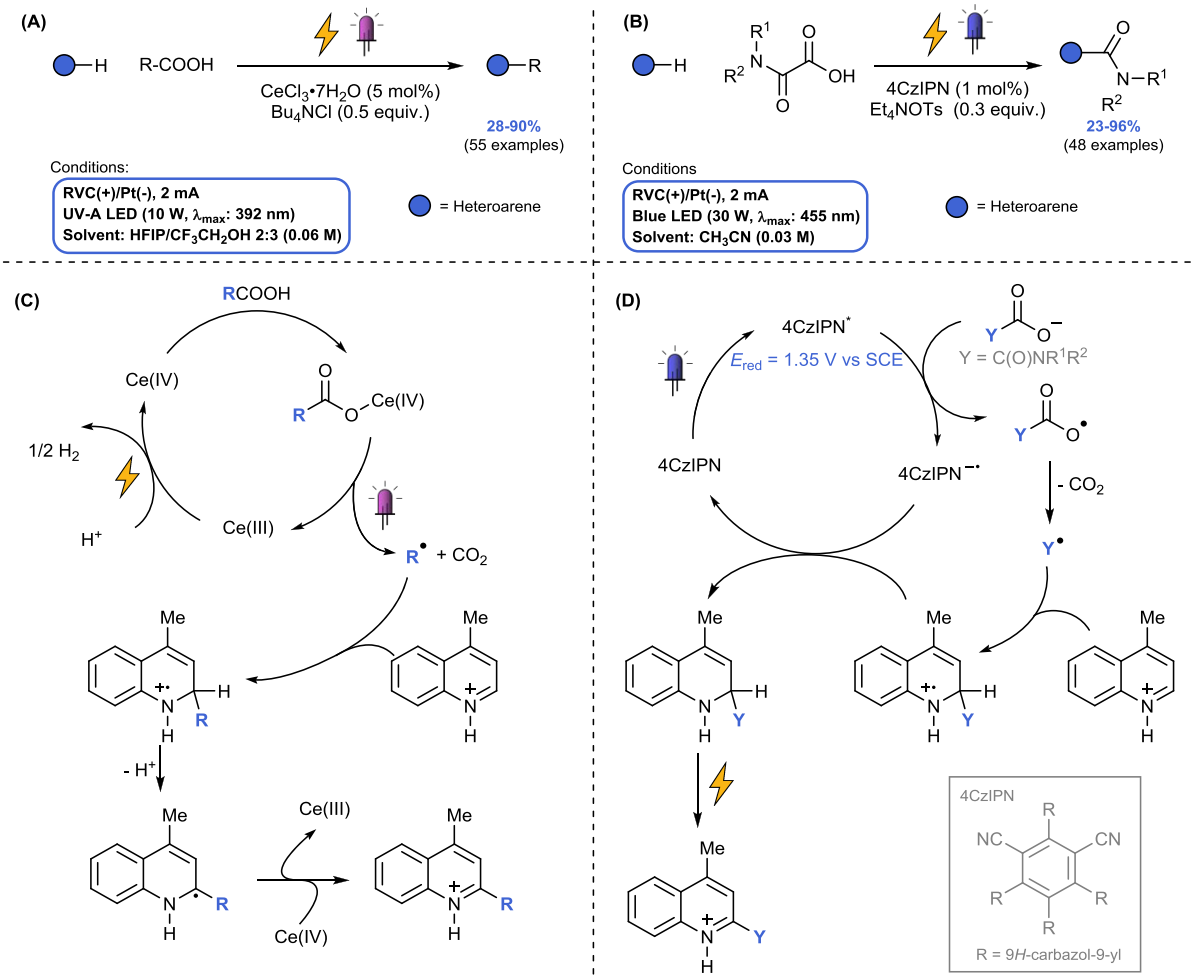

to decarboxylation and formation of the alkyl radical (Scheme 204C). In this case, electricity is used to close the photocatalytic cycle. In contrast, when starting from the oxamic acids, the excited photo-organocatalyst mediates an SET transforming the carboxylate into a radical that extrudes CO_2. The photocatalytic cycle is closed by the radical cation intermediate, while at the anode the final oxidation takes place yielding the desired product (Scheme 204D).

A photoelectrochemical dehydrogenative cross-coupling was developed by Xu et al. using chlorine radicals as HAT agents (Scheme 205A).[825] Chloride was anodically oxidized generating chlorine which is subsequently homolytically cleaved by UV light. These chlorine radicals induce a HAT process, thus forming carbon-centered radicals, which subsequently react with a suitable heterocyclic acceptor (Scheme 205B). The transformation proved to be very general and scalable; 122 mmol of starting material could be efficiently converted yielding 67% of the target product with a reaction time of 86 h. This was achieved using a 1 L beaker-type cell equipped with two pieces of RVC (anode) sandwiching a Pt plate cathode. This cell, which was irradiated with four 398 nm LEDs (20 W each), was connected with a 5 L reservoir containing the reaction mixture. A peristaltic pump would maintain the flow

Scheme 205. (A) Photoelectrochemical Dehydrogenative Cross-Coupling Using Chloride as HAT Agent and (B) Proposed Mechanism

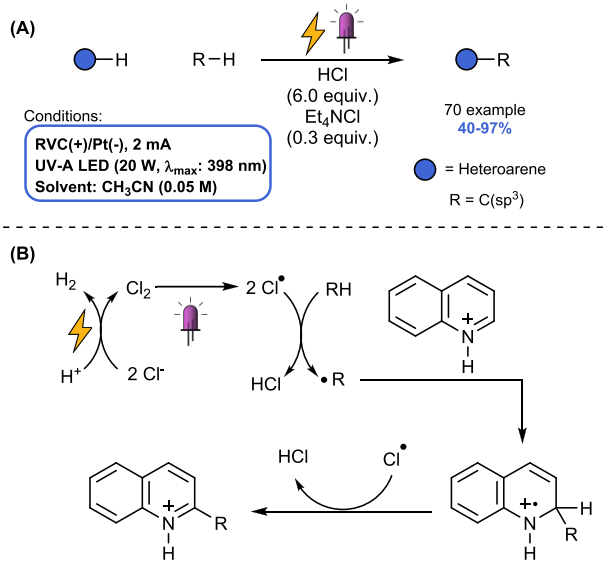

https://doi.org/10.1021/acs.chemrev.1c00332
Chem. Rev. 2022, 122, 2752−2906

between the cell and the reservoir with a flow rate 13.5 mL·min^{-1}.

6.5. Photoelectrochemical CO_2 Reduction

The energy needs of our society result in the generation of large quantities of greenhouse gases, especially CO_2, impacting severely our climate.[826] To minimize the emission of these gases in the atmosphere, it is necessary to promote a shift from a fossil-based economy to a circular carbon-neutral one. Up to date, one of the most promising energy alternatives would be sunlight, which is the most abundantly available energy source and could be stored into the chemical bonds of the so-called "solar fuels", most commonly hydrogen derived from water splitting.[827−830] Another possibility is represented by the reduction of CO_2,[831] which can be converted into high-energy containing molecules, such as carbon monoxide, formic acid, methanol, and methane. However, it is a very complicated reaction due to the potential generation of various reduction products (Scheme 206A-H). To tackle this grand challenge,

Scheme 206. Possible Half Reactions of Electrochemical CO_2 Redcutions and Water Oxidation (E^0 vs RHE)[855]

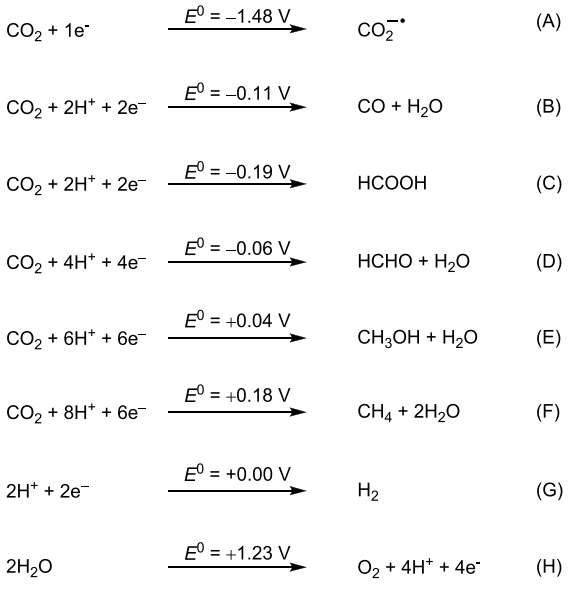

several approaches have been described, including solar thermo-catalytic,[832] biological,[833] photothermal,[834,835] solar-driven,[836,837] electrochemical[838−842] (in some cases the electric energy is supplied by a photovoltaic system),[843,844] photochemical,[845−850] and photoelectrochemical (PEC)[850−852] methods.

Unfortunately, all these technologies share several important challenges. First, the poor selectivity remains one of the main issues, and is caused by the similar redox potentials of carbon dioxide to different reduction products. Moreover, the derived products of CO_2 reduction are generally more reactive than the starting material itself. Also, undesired, parallel hydrogen evolution reactions subtract the required protons from the reaction medium (see Scheme 206A-H). To address this issue, the conversion of CO_2 and H_2O into syngas (a mixture of CO and H_2) often represents a good compromise and is a useful product for the Fischer−Tropsch synthesis.[838,853] Second, the generation of products, such as methane, methanol, and formic acid, is generally kinetically unfavored due to multiple proton-coupled electron transfer (PCET) steps associated with the process. Last but not least, although the amount of this gas has increased in the atmosphere, CO_2 is not easily available and thus any strategy for CO_2 valorization implies also CO_2 production.[854]

Compared to other techniques, photochemical methods do not require high temperatures or pressures. Photochemical approaches can be divided into: (i) photocatalysis,[856−858] (ii) electrochemical reduction coupled with a photovoltaic system (PV-EC),[859,860] and (iii) photoelectrochemical reduction with one (or two) photoelectrodes. The first strategy implies the use of a catalyst and eventually a photosensitizer; its efficiency can be measured by the photochemical quantum yield.[850] In the PV-EC approach, the two involved technologies can be optimized separately, but the need for current−voltage matching as well as the high associated cost constitute drawbacks of this strategy.

In the next sections, we will detail some of the fundamental concepts about PEC technology,[861] which presents several advantages, such as lower operative cost, the possibility to apply a bias potential to reduce overpotentials and induce selectivity (especially together with a cocatalyst), and good stability.[855] Later on, we will focus our attention on the development of continuous-flow systems for PEC reductions.

6.5.1. PEC Cells: Main Components. As any other electrochemical cell, PEC devices consist of three electrodes (working, counter, and reference electrode), of which at least one is photosensitive, immersed in a solution containing an electrolyte (Figure 65). The modular approach (PV−PEC)

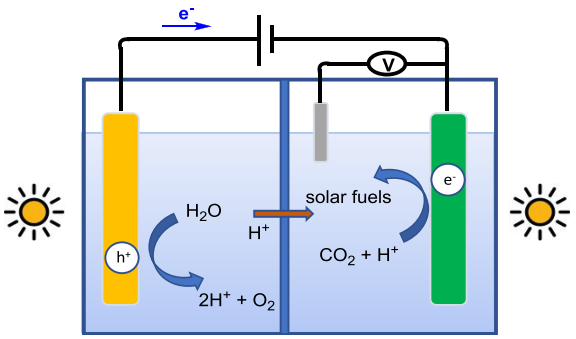

Figure 65. Schematic representation of a PEC cell: in yellow the (photo)anode, in green the (photo)cathode, and in gray the reference electrode. Blue line in the middle: proton-transfer membrane.

refers to the case when the applied potential has a photovoltaic origin.[860] Considering the equations in Scheme 206, the conduction band of the (photo)cathode should match the required CO_2 reduction potential, whereas the valence band should be more positive than the oxidation potential of water (Figure 65). In fact, when irradiated by light of a suitable wavelength, one electron in the semiconductor is promoted from the valence band (VB) to the conduction band (CB), leaving a hole behind. These electron−hole pairs can trigger reductions and oxidations. In fact, from this excited state, the SET takes place initiating the reaction in solution and the recirculation of current in the reactor.

Different electrodes have been developed in the past decades and are based on the combination of a semiconductor material and a metal, or on the use of two different semiconductors (Table 2). In this case, the use of external bias is often necessary.[862] Since the first report on photoassisted water splitting in 1972,[863] TiO_2 has been the preferred choice for

https://doi.org/10.1021/acs.chemrev.1c00332
Chem. Rev. 2022, 122, 2752−2906

Table 2. Selected Examples of PEC Electrode Materials[a]

PEC system	Anode	Cathode	Electrolyte
Photoanode	n-type semiconductor: TiO_2,[872−874] $BiVO_4$,[875] WO_3[876]	Pt, Cu_2O, Sn/SnO_x, biocathode[877]	0.5 M NaCl, 0.5 M $NaHCO_3$
			0.5 M H_2SO_4
Photocathode	Metal or metal alloy (Pt)	p-type semiconductor: Cu_2O|[Re complex],[870] $Cu_3Nb_2O_8$,[878] Au/p-GaN,[879] Si NW@CoN/CN[880]	0.5 M $NaHCO_3$
			0.05 M K_2CO_3
Photoanode and photocathode	n-$SrTiO_3$[869,881]	InP|[Ru complex],[881] TiO_2|N,Zn−Fe_2O_3| Cr_2O_3[869]	0.1 M $KHCO_3$
			0.1 M $NaHCO_3$

[a]For more examples, see refs 851, 854, 855, and 871.

catalyzing photoelectrochemical reactions, despite the need for UV light. Other materials such as WO_3, α-Fe_2O_3 and $BiVO_4$ have been studied as well[864−866] to exploit a larger share of the solar light spectrum. Hybrid photoelectrodes have also been reported, consisting of a semiconductor with molecular catalyst anchored on it.[867−870]

p-Type semiconductors are doped with impurities which are accepting electrons from the valence band and are used as material for the photocathode. Subjected to irradiation, holes will be generated in the p-type semiconductors. These holes can accept electrons when in contact with a proper electrolyte, whose redox potential is within the semiconductor band gap but with a different Fermi level (E_F). The phenomenon continues until the two E_F are equal (Figure 66A).[882,883] At the interface between the electrode and the solution, a space-charge region is formed due to the movement of electrons. This is called a depletion layer on the electrode side or Helmholtz layer at the electrolyte site. The in-built electric field in this region provokes an upward bending of both valence and conductive bands. This bending band effect is essential to break the electron−hole pairs and consequently to transfer the electrons to carbon dioxide more efficiently. Photocathodes are made of a conductive material coated with a p-type semiconductor with the following properties: (i) it can absorb light in the visible region, (ii) it is chemically resistant in the reaction medium, and (iii) its CB energy level is more negative than the redox potential of CO_2.

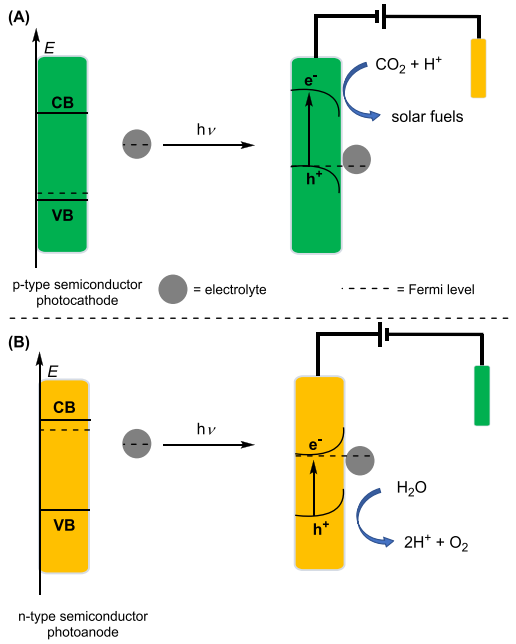

Figure 66. p-Type (A) and n-type (B) semiconductors in PEC cells (CB = conduction band, VB = valence band, h^+ = hole).

n-Type semiconductors, which are employed as material for photoanodes, consist of semiconductors doped with impurities donating an excess of electrons to the conduction band. Therefore, when they are immersed in a solution with a suitable electrolyte, they can transfer electrons to the electrolyte with a consequent decrease of their E_F and downward valence and conduction band bending (Figure 66B). The VB holes are pushed toward the electrolyte solution and for this reason n-type semiconductors are used for oxidations.[871,884] In a photoanode−photocathode PEC device, a p-type and an n-type semiconductor are connected through an ohmic contact.

The nature of the electrolytic solution is equally important as the choice of the electrodes. In fact, pH plays a key role in the reduction of CO_2.[855] For instance, if the proton source is missing in the media, the major reduction product is CO. A sacrificial proton-donor can be used to overcome this issue (e.g., amines). The reactor design is another crucial factor for the success of the process. In fact, it should minimize resistive losses between the electrodes, avoid optical losses and limit mass-transfer issues. Proton-exchange membranes are often used to separate the anodic and cathodic chambers and it is fundamental to prevent undesired reactivity which would lower the overall productivity of the PEC cell.

The performance of a PEC cell can be described by calculating various parameters, such as the solar-to-fuel (STF) efficiency,[885] current density, faradaic efficiency,[886] stability of the electrodes,[870,873,887,888] turnover number (TON), turnover frequency (TOF),[889] and the overall production rate (Table 3).

6.5.2. PEC CO_2 Reduction and Continuous-Flow Techniques. Carrying out PEC reductions in continuous-flow would be crucial to develop industrial applications. The reactor design requires careful evaluation to minimize issues related to mass-, heat-, photon- and charge-transport phenomena.[890] The main requirements are (i) the homogeneity of the light irradiation (xenon arc lamps are the most used, while the window in the reactor is generally Pyrex or quartz); (ii) the dissipation of the generated heat; and (iii) the separation of the anode and cathode into two compartments, often with proton exchange membranes (PEMs), anion exchange membranes (AEMs) or alternatively bipolar membranes (BPMs).[891] Moreover, theoretical studies based on a validated multiphysics and multiphase (gas, solid and liquid phases) model confirmed the importance of CO_2 flow rate on the current density and on CO_2 conversion efficiency.[892]

One of the earlier reports dates back from 2015.[893] On the basis of the results obtained in batch,[894,895] the authors

https://doi.org/10.1021/acs.chemrev.1c00332
Chem. Rev. 2022, 122, 2752−2906

Table 3. Overview of the Main Parameters to Evaluate the Efficiency of a PEC[852] Cell[a]

parameter	definition	formula
solar-to-fuel efficiency (STF)	total chemical energy produced by the solar energy which reached the electrode area (with no external voltage applied)	$\mathrm{STF} = \frac{r_{\mathrm{fuel}}\left(\frac{\mathrm{mmol}}{\mathrm{s}}\right)\cdot \Delta G^{\circ}\left(\frac{\mathrm{kJ}}{\mathrm{mol}}\right)}{P_{\mathrm{sol}}\left(\frac{\mathrm{mW}}{\mathrm{cm}^2}\right)\cdot \mathrm{area}\ (\mathrm{cm}^2)}$
current density (CD)	charge flow produced at the electrode	$\mathrm{CD} = \frac{I\ (\mathrm{A})}{\mathrm{area}\ (\mathrm{cm}^2)}$
faradaic efficiency (FE)	ratio between the current contributing to CO_2 reduction and the observed current.	$\mathrm{FE} = \frac{n_{\mathrm{product}}\ (\mathrm{mol})\cdot Y\cdot F\left(\frac{\mathrm{C}}{\mathrm{mol}}\right)}{Q\ (\mathrm{C})} \times 100$
energy efficiency (EE)	amount of the applied electrical energy used to make the product	$\mathrm{EE} = \mathrm{FE}\cdot\frac{E_{\mathrm{therm}}\ (\mathrm{V})}{E_{\mathrm{cell}}\ (\mathrm{V})}$
electrode stability	the photocurrent should be stable in time	time (h)
turnover number (TON)	molar formation of product per unit of catalyst.	$\mathrm{TON} = n_{\mathrm{product}}\ (\mathrm{mol})/n_{\mathrm{catalyst}}\ (\mathrm{mol})$
turnover frequency (TOF)	it is the TON divided by time	$\mathrm{TOF} = n_{\mathrm{product}}\ (\mathrm{mol})/(n_{\mathrm{catalyst}}\ (\mathrm{mol})\cdot t\ (\mathrm{s}))$
production rate (PR)	production of a selective product per time and per electrode area	$\mathrm{PR} = \frac{n_{\mathrm{product}}\ (\mathrm{mmol})}{\mathrm{time}\ (\mathrm{h}) \times \mathrm{area}\ (\mathrm{cm}^2)}$

[a] r_{fuel} = generated chemical fuel per time unit; ΔG^0 = change in Gibbs energy for that particular fuel; P_{sol} = power density of the light source; I = current; n = number of moles; Y = number of electrons required to reduce CO_2 to that particular product; F = Faraday constant; Q = measured charge; E_{therm} = thermodynamic potential.

selected copper(I) and copper(II) oxides as photoelectrodes, having suitable band gap of about 2.0−2.2 and 1.3−1.6 eV, respectively. The main parts of the designed reactor are (i) a reference electrode (Ag/AgCl/saturated KCl), (ii) an optical window (transparent slab), (iii) a gasket with the microchannel, placed on top of the cathode, (iv) a photocathode (6 cm^2, in CuO/Cu_2O hybrid nanorod arrays supported on copper foil), (v) a gasket with microchannel arrays, positioned under the cathode, (vi) an ion exchange membrane (Nafion NER-212), (vii) a microchannel arrays over the anode, (viii) a stainless steel anode, and (ix) the various in- and outlets, for the anolyte and the catholyte (Figure 67A). The reactor was illuminated with a solar simulator and the reaction mixture was pumped through the reactor assembly with a flow rate of 5 mL·h^{-1}. The major reduction products in flow were longer-chain alcohols such as ethanol and isopropanol (FE = 75−96%, Figure 67B), whereas the batch setup with no microchannels was selectively affording methanol. The production rate was 0.22 mL·m^{-2}·h^{-1}, which is 6 times higher than in batch.

Differential electrochemical mass spectrometry (DEMS) is an analytical technique that can be used as an online quantitative analytical tool to detect the evolution of O_2 and CO_2.[896−898] Recently, it has been used in combination with a photoelectrochemical thin-layer flow cell in the simultaneous photoelectrocatalytic oxidation of water and formic acid under well-defined mass-transfer controlled conditions.[774] The thin-layer photoelectrochemical flow cell has a rectangular shape.[899] The quartz cylinder (thickness 4 mm, diameter 10−12 mm) is positioned in front of the TiO_2/FTO working electrode. These two parts form a thin-layer channel with a volume of about 8 μL. The counter electrode consists of a platinum foil which is in a separate compartment connected to the electrolyte inlet port. The reactor is illuminated by a 200 W Hg(Xe) arc light source (LOT-QD). DEMS is used to monitor the overall photocurrent and the mass spectrometric ion currents of the water and formic acid oxidation products, that is, O_2 and CO_2, respectively (Figure 68). Although the addition of formic acid causes an increase in the overall photocurrent, it also inhibits the oxygen evolution as formic acid is competitive with water absorbed and oxidized at the anode.

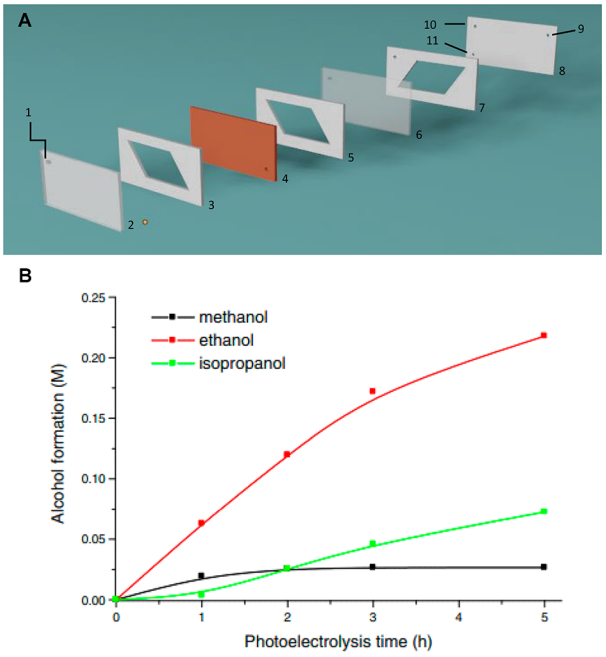

Figure 67. (A) Photoelectrochemical reactor in flow and its main parts: (1) catholyte inlet and location of the reference electrode, (2) optical window (transparent slab), (3, 5, and 7) microchannel arrays, (4 and 8) electrodes, (6) ion exchange membrane, (9) outlet of anolyte, (10) outlet of catholyte, and (11) inlet of anolyte. (B) CO_2 reduction products (flow rate = 5 mL·h^{-1}). Panel B: Reprinted with permission from ref 893. Copyright The Electrochemical Society. Reproduced by permission of IOP Publishing, Ltd. All rights reserved.

Andreu et al. developed a PEC flow cell to convert CO_2 into formate.[781] TiO_2 was used as the photoanode, while the cathode consisted of electrodeposited tin on a gas diffusion electrode (GDE), which was placed next to the reference electrode (Ag/AgCl 3.4 M KCl). GDEs are porous electrodes

https://doi.org/10.1021/acs.chemrev.1c00332
Chem. Rev. 2022, 122, 2752−2906

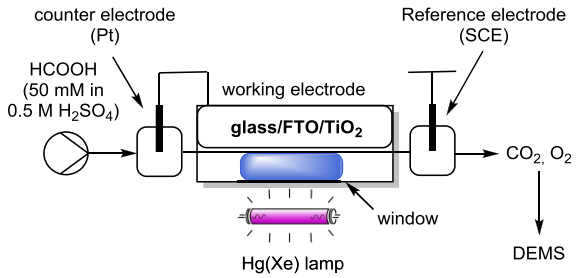

Figure 68. Photoelectrochemical oxidation of formic acid in flow using DEMS to detect the evolution of oxygen and CO_2 (SCE = standard calomel electrode).

which enable the electrochemical reaction between a liquid and a gaseous phase.[900] The anodic and cathodic compartments were divided by an ion exchange membrane (Nafion 117). A solution of 0.5 M NaOH and one of 0.5 M $NaHCO_3$ served as the anolyte and catholyte, respectively. A mass flow controller delivered the required amount of CO_2 (10 mL·min^{-1}) to the reactor and the photoanode was irradiated with light emitted by a solar simulator (Solar Light 16S equipped with a 300 W Xe-lamp and AM 1.5G filter, Figure 63B). The PEC flow cell, which requires an external bias, can reach up to 64% FE, 70% EE, and 0.24% STF.

Kalamaras, Xuan, Andresen, and co-workers designed a sandwich-type microfluidic photoreactor with a 100 mm PMMA sheet placed between the working and the counter electrode in Pt.[776] Two gaskets of a thermoplastic film (Surlyn 30 mm, Dyesol) were positioned between the PMMA layer and the electrodes, resulting in a total reactor volume of ∼50 μL (Figure 69A). This reactor was compared to a 15 mL batch reactor. As a light source, a solar simulator (AM 1.5G, 100 mW·cm^{-2}) was chosen. For the working electrode, different semiconductors (α-Fe_2O_3/CuO, CuO/Cu_2O, Cu_2O, CuO) were deposited on the FTO support and were evaluated in terms of their activity in a 0.2 M $NaHCO_3$ solution (Figure 69C). The authors found that 0.08 mL·min^{-1} was the optimal flow rate for CO_2; longer residence times resulted in the reoxidation of the products and the formation of oxygen bubbles which decreased the overall efficiency, whereas at higher flow rates the reaction time was too short to observe sufficient product formation. The best STF (0.48% after 1 h) was obtained with α-Fe_2O_3/CuO. This constitutes a very good result considering the low solubility of CO_2 in aqueous media, and compared to the batch reactor (best STF 0.2% after 12 h, Figure 69B). It is also worth noticing that the continuous-flow microfluidic PEC reactor displays an enhanced formation of methanol with the α-Fe_2O_3/CuO.

Urbain et al. reported on the production of syngas (a mixture of H_2 and CO) in a PEC cell combined with silicon photovoltaics, which requires no external bias.[901] The cell,[902] separated by a bipolar ionic exchange membrane, operates with 1 M KOH as anolyte and 0.5 M $KHCO_3$ as catholyte. The cell is equipped with a leak-free Ag/AgCl 3.4 M KCl reference electrode. The cathode is made of copper foam coated with nanosized zinc flakes, whereas the photoanode consists of a silicon heterojunction solar cell structure with nickel foam. Such a system was thought to improve the efficiency of water oxidation, which represents the anodic transformation. The photoanode is irradiated by a 150 W xenon lamp (Figure 70). The use of Si heterojunction technology and other cheap and abundant metals is an important economic factor for

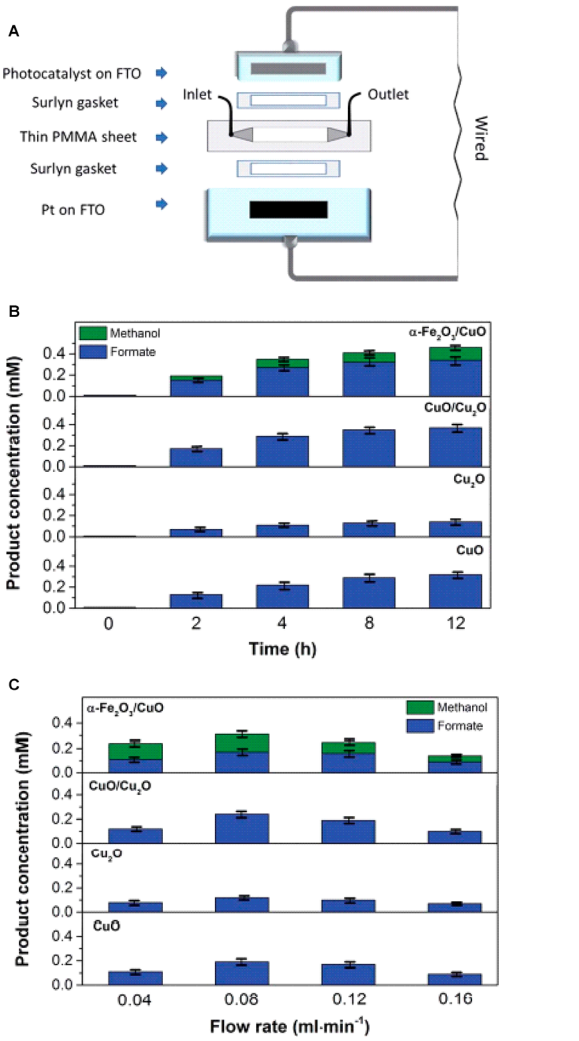

Figure 69. (A) Microfluidic reactor for CO_2 reduction into formate and methanol. (B) Product concentration in a batch setup after different times. (C) Product concentration at different flow rates after 1 h PEC reduction. Reprinted with permission from ref 776. Copyright 2019 Royal Society of Chemistry.

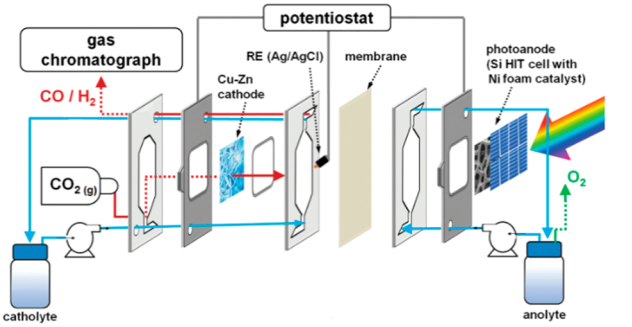

Figure 70. Photoelectrochemical flow reactor for syngas production based on the use of silicon photovoltaics as photoanode. Reprinted with permission from ref 901. Copyright 2017 Royal Society of Chemistry.

scalability. With a flow rate of 20 mL·min^{-1}, the FE for CO production reached up to 85% and displayed an STF of 4.3%.

6.5.3. PEC Cells Applied in Organic Synthesis. *6.5.3.1. Alcohol Oxidation.* As said, PEC cells are mostly studied for solar fuel production, reducing either water to

https://doi.org/10.1021/acs.chemrev.1c00332
Chem. Rev. 2022, 122, 2752−2906

hydrogen or CO_2 to alcohols and other organic compounds, whereas oxygen is produced at the anode. However, the oxygen evolution reaction (OER) is kinetically not favored. A potential solution could be to replace the water oxidation reaction with another one which is more favored, hereby affording more valuable compounds. Alcohol oxidation represents a classic transformation and is often used to test the efficacy of photoanodic materials. As a concrete example, the synthesis of 2,5-furandicarboxylic acid (FDCA) from 5-hydroxymethylfurfural (HMF) is highly relevant from an industrial standpoint.[903] Choi et al. evaluated a PEC cell with a $BiVO_4$ photoanode under solar illumination to oxidize HMF to FDCA (Scheme 207).[904] Using a reactor equipped with a fritted glass to separate the anodic and cathodic chamber, the product was obtained in high yields (FE > 93%) owing to the use of TEMPO as a mediator. In an electrochemical cell, TEMPO enables the use of non-precious-metal electrode, such as carbon felt electrode, although with higher applied potential (1.54 V vs RHE). The proposed oxidation could potentially work as a counter-reaction for hydrogen production, possibly without overpotential if the photoanode material is modified.

Scheme 207. HMF Oxidation to FDCA in a PEC Cell with a n-Type $BiVO_4$ Photoanode

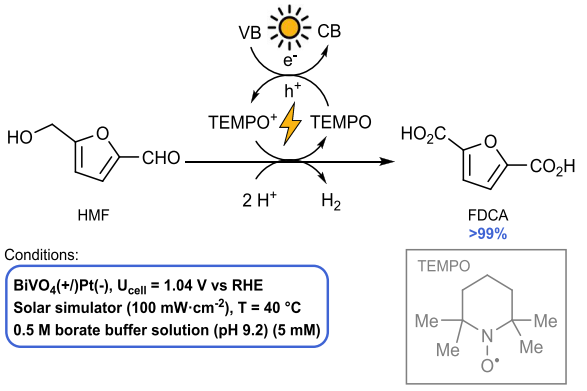

$BiVO_4/WO_3$ composite photoelectrodes are known to provide higher performances in water splitting due to the capacity of WO_3 to transport the photoexcited electron from the conduction band of $BiVO_4$ to the F-doped SnO_2 (FTO) conductive glass substrate.[777] This n-doped semiconductor proved its utility also in the photoelectrochemical oxidation of benzylic alcohols (Table 4, entry 1).[905] The photoelectrode proved to be stable and a TON of around 1200 was reported.

The use of an aqueous medium often limits the scope of application because of the limited solubility of organic molecules and accelerates photoanode corrosion. An alternative is presented for both alcohol oxidation and even more challenging C−H functionalizations (e.g., oxidation of cyclohexene and tetralin), which can be performed in acetonitrile with a $BiVO_4$-based photoanode subjected to simulated sunlight (Table 4, entry 2).[906] Although these reactions have been already widely studied,[907−915] this procedure reduces the electrical energy use by 60% and suppresses the photocorrosion of the photoanode. *N*-Hydroxysuccinimide (NHS) serves as a useful hole-transporter, whereas pyridine is important to deprotonate NHS. In the case of cyclohexene and tetralin, *t*BuOOH is also necessary as an external oxygen source (Figure 71).

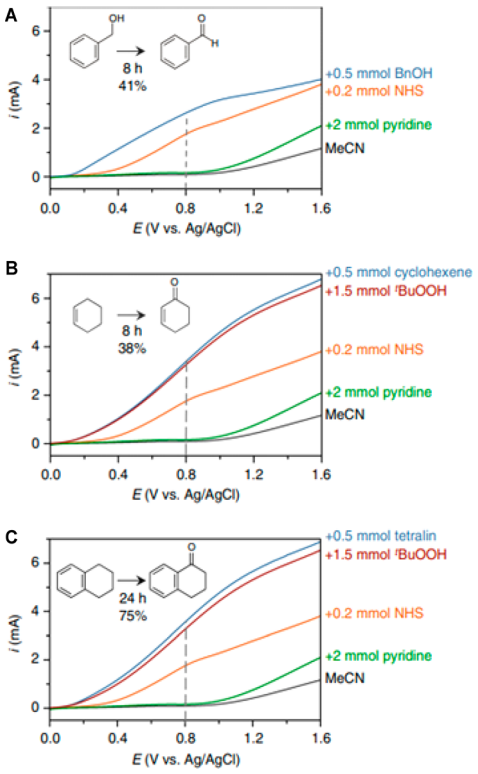

Figure 71. Linear sweep voltammetry curves of the NHS-mediated oxidation of benzylic alcohol (A), cyclohexene (B), and tetraline (C) in a PEC cell equipped with $BiVO_4$ photoanode (scan rate = 10 mV·s^{-1}). Reprinted from ref 906. Published by Nature Publishing Group.

Dye-sensitized photoelectrosynthesis cells (DSPEC),[916−921] employed in water splitting, constitute a special example of PEC cells, in which light absorption by organic molecules and catalysis are merged with wide band gap n-type semiconductors.[907] Light is absorbed by a molecular compound, while an electron injection occurs into the conduction band of the semiconductor. Subsequently, there is a catalytic single electron transfer initiating the water oxidation.

Table 4. Oxidation of Benzylic Alcohols to Carbonylic Compounds in PEC Cells

	photoanode	cathode	solution	irradiation	results	ref
1	$BiVO_4/WO_3$	Pt wire	0.1 M Bu_4NBF_4 MeCN	visible light irradiation (100 mW·cm^{-2})	5 examples, (63−97%)	905
2	$BiVO_4$	glassy carbon	0.1 M $LiClO_4$, NHS, pyridine MeCN	solar simulator integrated with a xenon arc lamp (100 W)	3 examples (38−75%)	906
3	nanoITO/TiO_2 coderivatized with $Ru^{II}P^{2+}$ and $Ru^{II}OH_2^{2+}$	Pt wire	20 mM acetate buffer, 0.1 M $LiClO_4$	Lumencor spectral light engine (λ_{max} = 445 nm)	injection efficiency = 27% current efficiency = 3.7%	907

https://doi.org/10.1021/acs.chemrev.1c00332
Chem. Rev. 2022, 122, 2752−2906

Meyer et al. used a photoanode made of mesoporous films of TiO_2 nanoparticles or of core/shell nanoparticles with tin-doped In_2O_3 nanoparticle cores (nanoITO) and thin layers of TiO_2 deposited by atomic layer deposition (nanoITO/TiO_2).[907] Next, the metal oxide was functionalized with an oxidation catalyst ($Ru(II)OH_2^{2+}$) and a chromophore ($Ru(II)P^{2+}$, Scheme 208A). The oxidation was performed in a customized three-neck cell (Table 4, entry 3). After excitation of the chromophore and electron injection into the CB of the semiconductor, the catalyst oxidizes benzylic alcohol affording the corresponding aldehyde (Scheme 208B). At the counter-electrode, hydrogen is produced. The current efficiency based on benzyl alcohol dehydrogenation reached 3.7%, which is 10 times better than the values obtained with TiO_2.

Scheme 208. (A) Structure of the Modified Photoanode Material nanoITO/TiO_2 and (B) Anodic and Cathodic Reactions in a DSPEC

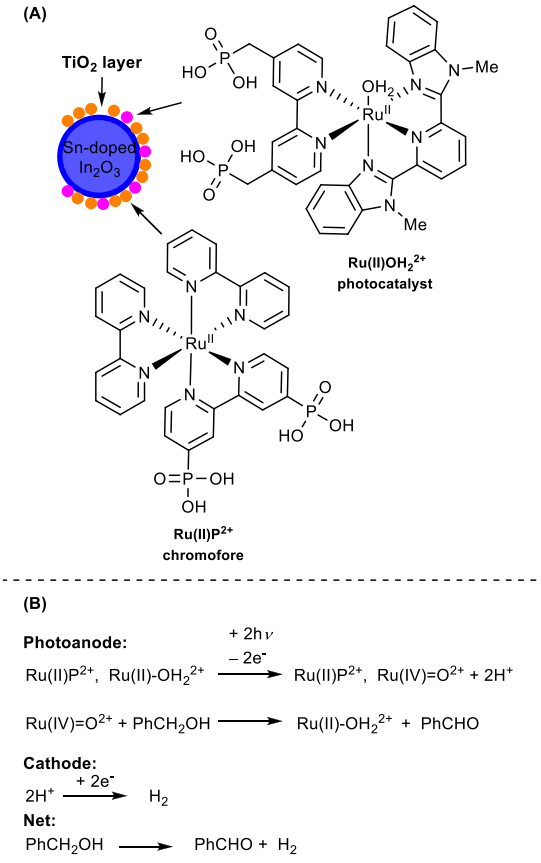

In the examples discussed so far, hydrogen is the sole product produced at the cathode. A notable exception was described in 2020, describing a PEC platform configured with a molybdenum (Mo)-doped bismuth vanadate (Mo:$BiVO_4$) photoanode and an inverse opal ITO (IO-ITO) used for cathodic reactions.[922] The setup consists of two compartments connected by a salt bridge. The ene-reductase of the Old Yellow Enzyme family from *Thermus scotoductus* (*Ts*OYE) is hosted in the cathodic compartment. *Ts*OYEs are known to catalyze the asymmetric *trans*-hydrogenation of conjugated C=C double bonds.[923] Flavin mononucleotide (FMN) is used to regenerate the enzyme. N-type $BiVO_4$ was selected as the photoanode material, because of its ability to oxidize water into hydrogen peroxide. However, to improve its electrical properties, hexavalent molybdenum has been used as a metallic dopant to form Mo:$BiVO_4$. The use of molybdenum allowed to reduce the resistance at the electrode interface. The production of hydrogen peroxide was exploited to perform an enantioselective hydroxylation of ethylbenzene to (*R*)-1-phenyl-1-hydroxyethane in the presence of unspecific peroxygenase from *Agrocybe aegerita* (*Aae*UPO) as a biocatalyst. Ethylbenzene was converted into the corresponding alcohol with high enantioselectivity (99% ee) independently from the applied voltage. The production reached its maximum at 0.8 V (0.51 $mM \cdot h^{-1}$). In contrast, the reduction is less selective due to nonenzymatic racemization of the product, which reaches the highest production at 1.0 V (0.5 $mM \cdot h^{-1}$ with 82% ee, Scheme 209). The photocurrent response was studied using linear sweep voltammetry and showed a great increase in photocurrent when the system was irradiated.

Scheme 209. Use of Biocatalysts in a PEC Cell to Enantioselectively Combine Oxyfunctionalization and Hydrogenation Reactions

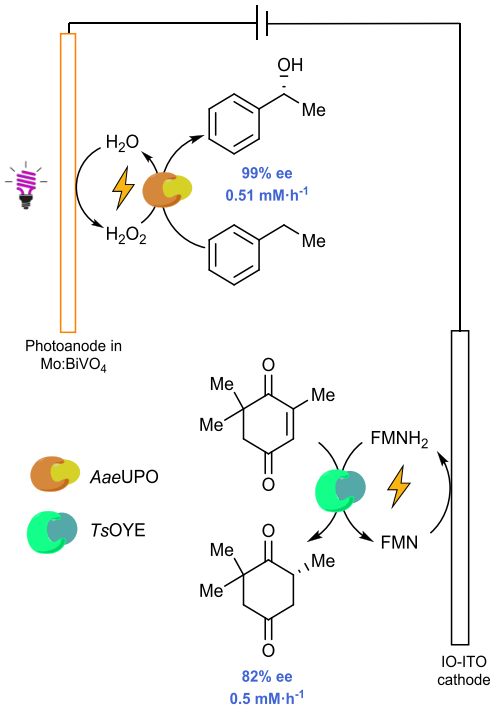

6.5.3.2. C−H Functionalization in PEC Cells. Since PEC cells combine the selectivity of electrochemistry with the ability to modulate the photoelectrode material, they are anticipated to be very interesting for C−H functionalization chemistry. A specific example is the dehydrogenative C−P cross-coupling between N-substituted tetrahydroisoquinolines and diphenylphosphine oxide. The PEC cell consists of a photoanode in $BiVO_4$, which was subjected to irradiation from blue LEDs.[924] The addition of *N*-hydroxyphthalimide (NHPI) as a mediator in the system was key to reach higher yields (Scheme 210). The pure electrochemical version of the transformation proved to be also effective (21 examples, 43−99% yield), but required much higher voltages (0.1 V vs 1.5 V).

The modified $BiVO_4/WO_3$ photoelectrode presents advantages with respect to the pristine material due to the position of the conduction band of WO_3 (+0.42 eV), which facilitates electron injection from the conduction band on $BiVO_4$ (0 eV).

https://doi.org/10.1021/acs.chemrev.1c00332
Chem. Rev. 2022, 122, 2752−2906

Scheme 210. C−P Cross-Coupling in a PEC Cell

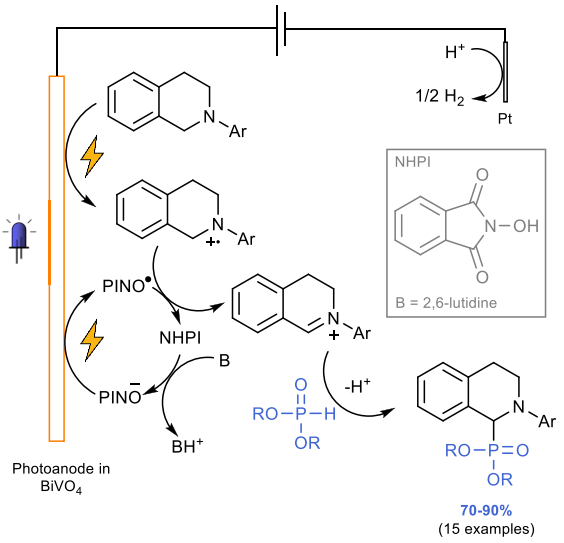

As a consequence, lower applied voltages are needed to enable the dimethoxylation of furan.[925] In addition, excellent faradaic efficiencies were obtained (up to 99%).[925] Notably, the oxidation is mediated by bromide which is oxidized to a Br^+ species, with a TON of 122 (Scheme 211A). The use of a mediator reduces the formation of byproducts, which were reported in dark conditions.[926,927] These byproducts are derived from the oxidation of methanol.

Another relevant characteristic of the valence band of WO_3 is that it has almost identical potential as that of titanium dioxide, while the conduction band can reduce oxygen. However, differently from TiO_2, WO_3 absorbs in the visible light region. Sayama et al. took advantage of these properties, performing the oxidation of cyclohexane into a mixture of cyclohexanol C-ol and cyclohexanone C-one (KA oil).[928] Earlier, the oxidation of cyclohexane to KA oil was reported with molecular oxygen using WO_3 loaded with Pt particles (Pt/WO_3) under visible light irradiation.[929] However, the quantum efficiency was relatively low because of the poor charge separation of the photocatalyst, that implies a fast charge recombination of the photogenerated electron−hole pair. This limitation can be overcome using porous WO_3 as the photoanode. The system also involves a mixture of *t*BuOH and HNO_3 and a platinum cathode, where oxygen is reduced to water (Scheme 211B). The longer the reaction time, the higher the ratio of C-one:C-ol was. The production rate can be increased by applying a smaller voltage. CO_2 is also detected, stemming from the total oxidation of cyclohexane. However, the selectivity calculated as the partial oxidation is excellent (99%) with an apparent faradaic efficiency of 76%.[928]

Another material often employed as photoanode is hematite (α-Fe_2O_3).[930,931] As an example, a PEC cell equipped with hematite was used to aminate C−H bonds (Scheme 211C).[932] The addition of HFIP to the reaction mixture leads to a high ortho-selectivity probably due to the hydrogen-bond network.[933] Hematite is characterized by a valence band with a potential comparable to the oxidation potential of mesityl acridinium and can, therefore, have similar reactivity. The hole produced in hematite by blue light irradiation is transferred to the arene which gets oxidized, while the photoexcited electron is transferred to the cathode where hydrogen is produced. Although the transformation was already known, this process is

Scheme 211. (A) Bromide as a Mediator in the Methoxylation of Furan, (B) Use of WO_3 Photoanode in the Oxidation of Cyclohexane, and (C) Hematite Photoanode Used for C−H Amination

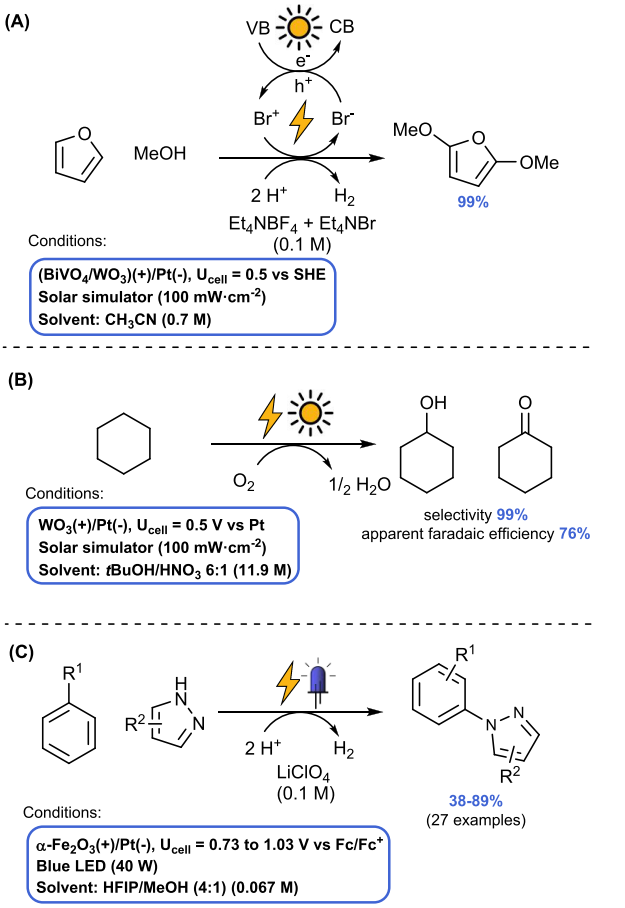

conceptually different from previous strategies, which were either photochemical[934,935] or electrochemical.[936−939] First, the light is absorbed by a solid-state semiconductor, while in photoredox catalysis the process is homogeneous. Second, in an electrochemical process, the applied voltage is used to match the Fermi level of the metal electrode with the redox potential of the substrate. In PEC, the energy level of the valence band transferring the hole is independent from the applied potential.

7. OUTLOOK

The impact technology makes is directly correlated with how deep it is embedded in a certain field. It is fair to say that the use of flow reactors for photochemical transformations is one of the most successful examples in flow chemistry. Capillary reactors have delivered many advantages over classical batch vessels, including a more homogeneous irradiation of the reaction mixture, ease of scale-up and the potential of handling challenging reaction conditions. Arguably, these advantages propelled transparent capillaries to the forefront as the best and most suitable reactor technology for photochemistry.

High-throughput experimentation (HTE) platforms have enabled researchers in industry to accelerate the drug discovery process. Recent trends in HTE include the miniaturization of the experiments (e.g., droplet microfluidics or well plates) to limit the consumption of precious scaffolds. Key in successful

https://doi.org/10.1021/acs.chemrev.1c00332
Chem. Rev. 2022, 122, 2752−2906

HTE is the possibility to analyze the individual experiments quickly and accurately. Owing to rapid developments in on- and in-line analytical tools (so-called process analytical technology, PAT), a large variety of sensors (e.g., NMR, MS, IR, UV−vis, Raman, pressure, and temperature sensors) have been developed in the past decade which allow to analyze reaction samples in real time.[940]

These HTE techniques allow experimentalists to execute a large number of experiments in an automated and parallel version. It should be further noted that microreactors and other miniaturized experiments provide a high degree of control over transport phenomena, thus allowing the collection of reliable data which is not affected by mass, heat and photon transport limitations. Furthermore, the impact of human error on the data is minimized when the entire system is automated. In other words, HTE platforms allow to gather reproducible, standardized kinetic data, which are generated under identical experimental conditions. The collected data includes both positive and negative results which is otherwise rarely reported in the literature. It is therefore highly attractive to use this data to feed different machine learning algorithms and accelerate the pace of future reaction optimization. Notable examples have illustrated the intriguing synergy between HTE and AI in other disciplines.[246,249] However, it can be anticipated that it is only a matter of time before the first examples are reported in synthetic photochemistry and photocatalysis.

Another area where technology can make an impact is the field of photoelectrocatalysis. This innovative activation mode is still at its infancy and, hence, unoptimized homemade setups have been used so far. It can be anticipated that in the near future more studies on the key chemical engineering aspects of photoelectrocatalysis will be carried out, leading to improved reactor designs. Because of the important scale effects of both electrochemistry and photochemistry, microreactors should provide decisive benefits for the reproducibility and scalability of photoelectrocatalysis.

Despite the clear advantages of using technology for photochemical transformations, there is still a lot of techno-skepticism in synthetic organic chemistry. One potential reason is the lack of knowledge due to the classical compartmentalization of the different disciplines. Chemistry, chemical engineering, and computer sciences have all their individual course programs, and there is little to no communication between these disciplines. Implementation of technology in synthesis is often only done out of sheer desperation, even in industry. To avoid such scenarios, students should be brought into contact with different technological courses as early as possible, including flow chemistry,[941] artificial intelligence, and basic programming. Integrated courses should be developed linking chemistry with other disciplines, which show clear-cut advantages of technology for, for example, organic synthesis, and these courses should also explain how these fields are interrelated. In that way, at later stages of their career, chemists will recognize technological opportunities faster and will have the courage to implement technology with less hesitation.[942] Another reason for the aversion to technology is its often-perceived complexity. This is a clear message to the engineers who develop new technology: diminish the complexity to make products as simple and as easy to use as possible. It is not needed that a single product should solve all potential problems, which would increase the complexity significantly. In contrast, it is often said that "*simplification is the ultimate sophistication*".[943] Indeed, the creation of user-friendly technology will ensure a rapid uptake by the widest possible audience. Engineers and technology developers must realize that most chemists essentially do not care about the technology behind a reactor, as long as it works and solves the issues they are facing. As a final reason for avoiding technology, the high investment costs can be quoted. This is especially the case in academia, where investments are often avoided due to limited funds. However, advances in DIY-assembled flow setups,[569,944] 3D-printing technology,[148] and cheap electronic toolkits[945] (e.g., Arduino) have democratized technology in recent years.

AUTHOR INFORMATION

Corresponding Author

Timothy Noël − *Flow Chemistry Group, van 't Hoff Institute for Molecular Sciences (HIMS), Universiteit van Amsterdam (UvA), 1098 XH Amsterdam, The Netherlands;* orcid.org/0000-0002-3107-6927; Email: t.noel@uva.nl

Authors

Laura Buglioni − *Micro Flow Chemistry and Synthetic Methodology, Department of Chemical Engineering and Chemistry, Eindhoven University of Technology, 5600 MB Eindhoven, The Netherlands; Flow Chemistry Group, van 't Hoff Institute for Molecular Sciences (HIMS), Universiteit van Amsterdam (UvA), 1098 XH Amsterdam, The Netherlands*

Fabian Raymenants − *Flow Chemistry Group, van 't Hoff Institute for Molecular Sciences (HIMS), Universiteit van Amsterdam (UvA), 1098 XH Amsterdam, The Netherlands*

Aidan Slattery − *Flow Chemistry Group, van 't Hoff Institute for Molecular Sciences (HIMS), Universiteit van Amsterdam (UvA), 1098 XH Amsterdam, The Netherlands*

Stefan D. A. Zondag − *Flow Chemistry Group, van 't Hoff Institute for Molecular Sciences (HIMS), Universiteit van Amsterdam (UvA), 1098 XH Amsterdam, The Netherlands;* orcid.org/0000-0003-1463-4867

Complete contact information is available at: https://pubs.acs.org/10.1021/acs.chemrev.1c00332

Author Contributions

[§]L.B. and F.R. contributed equally to this work.

Notes

The authors declare no competing financial interest.

Biographies

Laura Buglioni studied chemistry at the University of Camerino (Italy). Next, she moved to RWTH Aachen (Germany) to carry out her PhD in the group of Prof. Dr. Carsten Bolm. After getting a COFUND (MSCA-Severo Ochoa) fellowship, she joined the group of Prof. Miquel A. Pericàs at ICIQ (Tarragona, Spain) where she worked on photocatalysis. After a period as project manager at ICIQ, she received an MSCA-IF fellowship which allowed her to join the Flow Chemistry group of Prof. Timothy Noël. Her current research focus involves organic electrochemistry in flow.

Fabian Raymenants studied Bioscience engineering at the KU Leuven in Belgium, where he obtained his masters in 2017. After gaining industrial experience with Janssen Pharmaceuticals, Inc., he returned to academia in 2020 to start his PhD in flow chemistry in the Noël Research Group. He is currently working at the University of

https://doi.org/10.1021/acs.chemrev.1c00332
Chem. Rev. 2022, 122, 2752−2906

Amsterdam on the Horizon 2020 project FLIX, applying flow technology to isotopic exchange in organic molecules.

Aidan Slattery studied Chemistry of Pharmaceutical Compounds in University College Cork, Ireland where he graduated with First Class Honors in 2019. Following his undergraduate, he joined Snapdragon Chemistry, Inc., Boston, MA, USA, where he worked on flow photochemistry. He is currently pursuing a PhD at the University of Amsterdam under the supervision of Prof. Timothy Noël, where he is developing a high-throughput experimentation platform for the photocatalytic functionalization of organic molecules.

Stefan Zondag worked on the use of ultrasound applications for emulsification (at Queen's University Belfast) and for solids-handling in micro flow during his MSc studies. In 2020, he graduated *Cum Laude* as a Chemical Engineer from Eindhoven University of Technology. He is currently pursuing a PhD at the University of Amsterdam under the supervision of Prof. Dr. Timothy Noël. His current research aims at design, modeling, and optimization of photochemical flow reactors.

Timothy Noël currently holds a position as Full Professor at the University of Amsterdam and he is the chair of Flow Chemistry. His research interest ranges from organic chemistry to chemical engineering and encompass more specifically flow chemistry, organic synthesis and synthetic catalytic methodology development. His work received several awards, including most recently the VIDI award (2015), the Thieme Chemistry Journal Award (2016), the DECHEMA prize (2017), the Hoogewerff Jongerenprijs (2019), and the IUPAC-ThalesNano prize in flow chemistry and microfluidics (2020). He also serves as editor-in-chief of Journal of Flow Chemistry.

ACKNOWLEDGMENTS

The authors would like to acknowledge kind financial support from the European Union: MSCA Individual Fellowship program (ELECTROSULF, No. 840724, L.B.), FETopen (FLIX, No. 862179, F.R. and T.N.), and RIA-NMBP (FlowPhotoChem, No. 862453, S.D.A.Z. and T.N.). We also would like to thank the Dutch Research Council (NWO) for the funding of the Open Technology Program project (MultiModalPhotochemistry, No. 18433, A.S. and T.N.). Finally, we express our appreciation to ir. Remy Broersma and Dr. Grigory Onushkin (both Signify) for questions related to light sources.

ABBREVIATIONS

4CzIPN	1,2,3,5-tetrakis(carbazol-9-yl)-4,6-dicyanobenzene
4DPAIPN	2,4,5,6-tetrakis(diphenylamino)-isophthalonitrile
4HTP	4-hydroxythiophenol
*Aae*UPO	*Agrocybe aegerita* unspecific peroxygenase
Acac	acetylacetonate
AEM	anion exchange membrane
AFR	advanced-flow reactor
AI	artificial intelligence
AIBN	azobis(isobutyronitrile)
aq.	aqueous
ATRA	atom-transfer radical addition
BCP	bicyclo[1.1.1]pentane
BDE	bond-dissociation energy
BINAP	2,2′-bis(diphenylphosphino)-1,1′-binaphthyl
BODIPY	4,4-difluoro-4-bora-3a,4a-diaza-s-indacene
BPM	bipolar membrane
BPO	benzoyl peroxide
bpy	2,2′-bipyridine
BPR	back pressure regulator
BTP	bithiophene
BTZ	2,1,3-benzothiadiazole
CB	conduction band
CCF	central composite face-centered
CD	current density
CFL	compact fluorescent lamp
CMP	conjugated microporous polymer
CMY	cyan−magenta−yellow
CNS	central nervous system
CoN/CN	N-doped carbon-wrapped CoN
CSTR	continuous stirred-tank reactor
CTAB	cetyltrimethylammonium bromide
CTF	covalent triazine-based framework material
DABCO	1,4-diazabicyclo[2.2.2]octane
DAST	diethylaminosulfur trifluoride
DBAD	di-*tert*-butyl azodicarboxylate
DBU	1,8-diazabicyclo[5.4.0]undec-7-ene
DCA	9,10-dicyanoanthracene
DDQ	2,3-dichloro-5,6-dicyanoquinone
DEMS	differential electrochemical mass spectrometry
DFT	density functional theory
DHAA	dihydroartemisinic acid
DHN	dihydroxynaphthalene
DIPA	diisopropylamine
DIPEA	*N,N*-diisopropylethylamine
DIY	do-it-yourself
DLP	digital light processing
DMA	dimethylacetamide
DMAP	4-(dimethylamino)pyridine
DMBP	4,4′-dimethoxybenzophenone
dme	dimethoxyethane
DMF	dimethylformamide
DMPT	*N,N*-dimethyl-*p*-toluidine
DMSO	dimethyl sulfoxide
DoE	design of experiments
DPA	9,10-diphenylanthracene
DPE	diphenylethylene
dq	2,2′-biquinoline
dr (d.r.)	diastereomeric ratio
DSPEC	dye-sensitized photoelectrosynthesis cell
dtbbpy	4,4′-di-*tert*-butyl-2,2′-bipyridine
DVA	divinyl adipate
DVB	divinylbenzene
EDA	electron donor−acceptor
EDG	electron-donating group
ee (e.e.)	enantiomeric excess
EE	energy efficiency
ESI	electrospray ionization
ESIPT	excited-state intramolecular proton transfer
ET	energy transfer
EWG	Electron-withdrawing group
FDCA	2,5-furandicarboxylic acid
FDM	fused deposition modeling
FE	Faradaic efficiency
FEP	fluorinated ethylene propylene
FFMR	falling film microreactor
FFPM	fluorescent fluid photochemical microreactor
FMN	flavin mononucleotide
FTIR	Fourier-transform infrared spectroscopy
FTO	fluorine-doped tin oxide glass

https://doi.org/10.1021/acs.chemrev.1c00332
Chem. Rev. 2022, 122, 2752−2906

GC	gas chromatography
GDE	gas diffusion electrode
GF	graphite felt
HAT	hydrogen atom transfer
HE	Hantzsch ester
HER	hydrogen evolution rate
HFIP	hexafluoroisopropanol
HMF	5-hydroxymethylfurfural
HOMO	highest occupied molecular orbital
HPFA	high purity perfluoro alkoxy alkane
HPLC	high-performance liquid chromatography
HPMC	hydroxypropyl methylcellulose
HTE	high-throughput experimentation
ID	inner diameter
IJP	inkjet printing
IL	ionic liquid
IEDDA	inverse electron-demand Diels−Alder
IR	infrared
ISC	intersystem crossing
ITO	indium tin oxide
KDM	Kornblum−DeLaMare
LA	Lewis acid
LB	Lewis base
LC	liquid chromatography
LED	light-emitting diode
LMCT	ligand-to-metal charge transfer
LR305	Lumogen F Red 305
LSC-PM	luminescent solar concentrator photomicroreactor
MALDI-TOF	matrix-assisted laser desorption/ionization-time-of-flight
MB	methylene blue
MFC	mass flow controller
MHC	multiple heart-cutting
MLCT	metal-to-ligand charge transfer
Mpg	mesoporous graphitic
MS	mass spectrometry
MSA	mesylate
MSIM	modified Simplex algorithm
MSNs	mesoporous silica nanoparticles
MTP	microtiter plate
NaAsc	sodium ascorbate
NaFl	sodium fluorescein
NBA	*o*-nitrobenzaldehyde
NBP	3-*n*-butylphthalide
NBS	*N*-bromosuccinimide
NCS	*N*-chlorosuccinimide
NDSA	2,6-naphthalenedisulfonic acid disodium salt
neop	neopentanediolate
NHPI	*N*-hydroxyphtalimide
NHS	*N*-hydroxysuccinimide
NIR	near-infrared
NMF	*N*-monomethylformamide
NMP	*N*-methyl-2-pyrrolidone
NMR	nuclear magnetic resonance
NpMI	naphthalene-based analogue of perylene monoimide
NW	nanowires
OD	outer diameter
OER	oxygen evolution reaction
PAT	process analytical technology
PBR	packed bed reactor
PC	photocatalyst
PCBM	[6,6]-phenyl-C61-butyric acid methyl ester
PCET	proton-coupled electron transfer
PCP	packed column photoreactor
PDDA	photoinitiated dehydro-Diels−Alder
PDI	perylenediimide
PDMS	polydimethylsiloxane
PEEK	polyether ether ketone
PEC	photoelectrochemical
PEM	proton exchange membrane
PET	Positron emission tomography
PFA	perfluoro alkoxy alkane
PFR	plug flow reactor
phen	1,10-phenanthroline
pin	pinacolate
PINO	Phthalimide-*N*-oxyl
PMB	*p*-methoxybenzyl
PMI	process mass index
PMMA	poly(methyl methacrylate)
PMP	1,2,2,6,6-pentamethylpiperidine
PP	polypropylene
ppy	2-phenylpyridine
PQT	parallel quartz tubes
PR	production rate
pRS-SDR	photo rotor-stator spinning disk reactor
PrTPP	propyl-TPP
PS	polystyrene
PTC	phase-transfer catalyst
PTFE	polytetrafluoroethylene
PTFR	parallel tube flow reactor
PTH	10-phenylphenothiazine
PTHR	phototransfer hydrogenation reaction
PTSA	*p*-toluenesulfonic acid
PTZ	phenothiazine
PV-EC	photovoltaic-electrochemical
quintri	2-(1-(*p*-tolyl)-1H-1,2,3-triazol-4-yl)quinoline
RB	rose bengal
RCY	radiochemical yield
RFTA	riboflavin tetraacetate
RHE	reversible hydrogen electrode
RPC	radical-polar crossover
rpm	Revolutions per minute
rr	regioisomeric ratio
RVC	reticulated vitreous carbon
SCE	saturated calomel electrode
SCS	spin-center shift
SEC	size exclusion chromatography
SET	single-electron transfer
SFMT	stop-flow microtubing
SHE	standard hydrogen electrode
SLA	stereolithography
SLAP	silicone amine protocol
SMBR	serial microbatch reactor
SnAP	tin amine protocol
SNOBFIT	stable noisy optimization by branch and fit
SOMO	singly occupied molecular orbital
STF	solar-to-fuel efficiency
STY	space-time yield
TAC	trisaminocyclopropenium
TBADT	tetrabutylammonium decatungstate
TBAF	tetrabutylammonium fluoride
TBD	triazabicyclodecene
TBDMS	*tert*-butyldimethylsilyl
TBEC	*tert*-butylperoxy 2-ethylhexyl carbonate

https://doi.org/10.1021/acs.chemrev.1c00332
Chem. Rev. 2022, 122, 2752−2906

TBHP	*tert*-butyl hydroperoxide
TBPA	*tert*-butyl peracetate
TBPB	*tert*-butyl perbenzoate
TCO	*trans*-cyclooctene
TcPP	*meso*-tetracarboxyphenylporphyrin
TD	time-dependent
TEA	triethylamine
TEMPO	(2,2,6,6-tetramethylpiperidin-1-yl)oxyl
TFA	trifluoroacetic acid
TFAA	trifluoroacetic acid anhydride
TFE	2,2,2-trifluoroethanol
THF	tetrahydrofuran
TMDAM	*N*,*N*,*N*′,*N*′-tetramethyldiaminomethane
TMEDA	tetramethylethylenediamine
TMG	tetramethylguanidine
tmp	trimethoxy-2−2′-bipyridine
TMS	trimethylsilyl
TOF	turnover frequency
TON	turnover number
TPFPP	5,10,15,20-tetrakis(pentafluorophenyl)-porphyrin
TPP	tetraphenylporphyrin
$TPPBF_4$	2,4,6-triphenylpyrylium tetrafluoroborate
TPPD	*N*,*N*,*N*′,*N*′-tetraphenyl-p-phenylenediamine
*Ts*OYE	*Thermus scotoductus* old yellow enzyme
UPLC	ultraperformance liquid chromatography
UV	ultraviolet
VB	valence band
VBRB	vinylbenzyl rose bengal
Vis	visible
VTO	volume−time output
WPE	wall-plug efficiency
Xantphos	4,5-bis(diphenylphosphino)-9,9-dimethylxanthene

REFERENCES

(1) Reischauer, S.; Pieber, B. Emerging Concepts in Photocatalytic Organic Synthesis. *iScience* **2021**, *24*, 102209.
(2) Bottecchia, C.; Noël, T. Photocatalytic Modification of Amino Acids, Peptides, and Proteins. *Chem. - Eur. J.* **2019**, *25*, 26−42.
(3) Michelin, C.; Hoffmann, N. Photocatalysis Applied to Organic Synthesis - A Green Chemistry Approach. *Curr. Opin. Green Sustain. Chem.* **2018**, *10*, 40−45.
(4) König, B. Photocatalysis in Organic Synthesis - Past, Present, and Future. *Eur. J. Org. Chem.* **2017**, *2017*, 1979−1981.
(5) Staveness, D.; Bosque, I.; Stephenson, C. R. J. Free Radical Chemistry Enabled by Visible Light-Induced Electron Transfer. *Acc. Chem. Res.* **2016**, *49*, 2295−2306.
(6) Douglas, J. J.; Sevrin, M. J.; Stephenson, C. R. J. J. Visible Light Photocatalysis: Applications and New Disconnections in the Synthesis of Pharmaceutical Agents. *Org. Process Res. Dev.* **2016**, *20*, 1134−1147.
(7) Corrigan, N.; Shanmugam, S.; Xu, J.; Boyer, C. Photocatalysis in Organic and Polymer Synthesis. *Chem. Soc. Rev.* **2016**, *45*, 6165−6212.
(8) Narayanam, J. M. R.; Stephenson, C. R. J. Visible Light Photoredox Catalysis: Applications in Organic Synthesis. *Chem. Soc. Rev.* **2011**, *40*, 102−113.
(9) Balzani, V.; Bergamini, G.; Ceroni, P. Light: A Very Peculiar Reactant and Product. *Angew. Chem., Int. Ed.* **2015**, *54*, 11320−11337.
(10) Skubi, K. L.; Blum, T. R.; Yoon, T. P. Dual Catalysis Strategies in Photochemical Synthesis. *Chem. Rev.* **2016**, *116*, 10035−10074.
(11) Shee, M.; Singh, N. D. P. Cooperative Photoredox and Palladium Catalysis: Recent Advances in Various Functionalization Reactions. *Catal. Sci. Technol.* **2021**, *11*, 742.
(12) Kojima, M.; Matsunaga, S. The Merger of Photoredox and Cobalt Catalysis. *Trends Chem.* **2020**, *2*, 410−426.
(13) De Abreu, M.; Belmont, P.; Brachet, E. Synergistic Photoredox/Transition-Metal Catalysis for Carbon-Carbon Bond Formation Reactions. *Eur. J. Org. Chem.* **2020**, *2020*, 1327−1378.
(14) Twilton, J.; Le, C. C.; Zhang, P.; Shaw, M. H.; Evans, R. W.; MacMillan, D. W. C. C. The Merger of Transition Metal and Photocatalysis. *Nat. Rev. Chem.* **2017**, *1*, 0052.
(15) Hopkinson, M. N.; Tlahuext-Aca, A.; Glorius, F. Merging Visible Light Photoredox and Gold Catalysis. *Acc. Chem. Res.* **2016**, *49*, 2261−2272.
(16) Fabry, D. C.; Rueping, M. Merging Visible Light Photoredox Catalysis with Metal Catalyzed C-H Activations: On the Role of Oxygen and Superoxide Ions as Oxidants. *Acc. Chem. Res.* **2016**, *49*, 1969−1979.
(17) Özgen, F. F.; Runda, M. E.; Schmidt, S. Photo-Biocatalytic Cascades: Combining Chemical and Enzymatic Transformations Fueled by Light. *ChemBioChem* **2021**, *22*, 790.
(18) Edwards, E. H.; Bren, K. L. Light-driven Catalysis with Engineered Enzymes and Biomimetic Systems. *Biotechnol. Appl. Biochem.* **2020**, *67*, 463−483.
(19) Seel, C. J.; Gulder, T. Biocatalysis Fueled by Light: On the Versatile Combination of Photocatalysis and Enzymes. *ChemBioChem* **2019**, *20*, 1871−1897.
(20) Prentice, C.; Morrisson, J.; Smith, A. D.; Zysman-Colman, E. Recent Developments in Enantioselective Photocatalysis. *Beilstein J. Org. Chem.* **2020**, *16*, 2363−2441.
(21) Rigotti, T.; Alemán, J. Visible Light Photocatalysis - From Racemic to Asymmetric Activation Strategies. *Chem. Commun.* **2020**, *56*, 11169−11190.
(22) Saha, D. Catalytic Enantioselective Radical Transformations Enabled by Visible Light. *Chem. - Asian J.* **2020**, *15*, 2129−2152.
(23) Hong, B. C. Enantioselective Synthesis Enabled by Visible Light Photocatalysis. *Org. Biomol. Chem.* **2020**, *18*, 4298−4353.
(24) Zhang, H. H.; Chen, H.; Zhu, C.; Yu, S. A Review of Enantioselective Dual Transition Metal/Photoredox Catalysis. *Sci. China: Chem.* **2020**, *63*, 637−647.
(25) Jiang, C.; Chen, W.; Zheng, W. H.; Lu, H. Advances in Asymmetric Visible-Light Photocatalysis, 2015−2019. *Org. Biomol. Chem.* **2019**, *17*, 8673−8689.
(26) Silvi, M.; Melchiorre, P. Enhancing the Potential of Enantioselective Organocatalysis with Light. *Nature* **2018**, *554*, 41−49.
(27) Wang, C.; Lu, Z. Catalytic Enantioselective Organic Transformations via Visible Light Photocatalysis. *Org. Chem. Front.* **2015**, *2*, 179−190.
(28) Meyer, T. H.; Choi, I.; Tian, C.; Ackermann, L. Powering the Future: How Can Electrochemistry Make a Difference in Organic Synthesis? *Chem.* **2020**, *6*, 2484−2496.
(29) Liu, J.; Lu, L.; Wood, D.; Lin, S. New Redox Strategies in Organic Synthesis by Means of Electrochemistry and Photochemistry. *ACS Cent. Sci.* **2020**, *6*, 1317−1340.
(30) Barham, J. P.; König, B. Synthetic Photoelectrochemistry. *Angew. Chem., Int. Ed.* **2020**, *59*, 11732−11747.
(31) Verschueren, R. H.; De Borggraeve, W. M. Electrochemistry and Photoredox Catalysis: A Comparative Evaluation in Organic Synthesis. *Molecules* **2019**, *24*, 2122.
(32) Allmand, A. J. Photochemistry, 1914−1925. *Annu. Rep. Prog. Chem.* **1925**, *22*, 333−373.
(33) Noyes, W. A.; Kassel, L. S. A Review of Photochemistry. *Chem. Rev.* **1926**, *3*, 199−225.
(34) Buzzetti, L.; Crisenza, G. E. M.; Melchiorre, P. Mechanistic Studies in Photocatalysis. *Angew. Chem., Int. Ed.* **2019**, *58*, 3730−3747.
(35) Marchini, M.; Bergamini, G.; Cozzi, P. G.; Ceroni, P.; Balzani, V. Photoredox Catalysis: The Need to Elucidate the Photochemical Mechanism. *Angew. Chem., Int. Ed.* **2017**, *56*, 12820−12821.

https://doi.org/10.1021/acs.chemrev.1c00332
Chem. Rev. 2022, 122, 2752−2906

(36) Pitre, S. P.; McTiernan, C. D.; Scaiano, J. C. Understanding the Kinetics and Spectroscopy of Photoredox Catalysis and Transition-Metal-Free Alternatives. *Acc. Chem. Res.* **2016**, *49*, 1320−1330.
(37) Sender, M.; Ziegenbalg, D. Light Sources for Photochemical Processes - Estimation of Technological Potentials. *Chem. Ing. Tech.* **2017**, *89*, 1159−1173.
(38) Visan, A.; Van Ommen, J. R.; Kreutzer, M. T.; Lammertink, R. G. H. Photocatalytic Reactor Design: Guidelines for Kinetic Investigation. *Ind. Eng. Chem. Res.* **2019**, *58*, 5349−5357.
(39) Noël, T.; Escriba Gelonch, M.; Huvaere, K. Industrial Photochemistry: From Laboratory Scale to Industrial Scale. In *Photochemical Processes in Continuous-Flow Reactors*; World Scientific (Europe), 2017; pp 245−267.
(40) Merck. The brilliant history of photoredox catalysis. *Nature Research Custom Media*. https://www.nature.com/articles/d42473-019-00033-7.
(41) DiRocco, D. A.; Schultz, D. M. 20 Photocatalysis in the Pharmaceutical Industry. In *Photocatalysis in Organic Synthesis*; König, Ed.; Georg Thieme Verlag: Stuttgart, 2019; Vol. *6*, pp 611−635.
(42) Khanh, T. Q.; Bodrogi, P.; Vinh, Q. T.; Winkler, H. *LED Lighting: Technology and Perception*; Khanh, T. Q., Bodrogi, P., Vinh, Q. T., Winkler, H., Eds.; Wiley-VCH Verlag GmbH & Co. KGaA: Weinheim, Germany, 2014.
(43) Rehm, T. H. Reactor Technology Concepts for Flow Photochemistry. *ChemPhotoChem.* **2020**, *4*, 235−254.
(44) Noël, T. A Personal Perspective on the Future of Flow Photochemistry. *J. Flow Chem.* **2017**, *7*, 87−93.
(45) Schroll, P. 1. Early Pioneers of Organic Photochemistry. In *Chemical Photocatalysis*; De Gruyter, 2020; pp 1−16.
(46) Dzebo, A.; Janetschek, H.; Brandi, C.; Iacobuta, G. *Connections between the Paris Agreement and the 2030 Agenda The Case for Policy Coherence*; Stockholm Environment Institute, 2019.
(47) Crisenza, G. E. M.; Melchiorre, P. Chemistry Glows Green with Photoredox Catalysis. *Nat. Commun.* **2020**, *11*, 803.
(48) Ravelli, D.; Dondi, D.; Fagnoni, M.; Albini, A. Photocatalysis. A Multi-Faceted Concept for Green Chemistry. *Chem. Soc. Rev.* **2009**, *38*, 1999−2011.
(49) Albini, A.; Fagnoni, M. Green Chemistry and Photochemistry Were Born at the Same Time. *Green Chem.* **2004**, *6*, 1−6.
(50) Anastas, P. T.; Warner, J. C. *Green Chemistry: Theory and Practice*; Oxford University Press: New York, 1998.
(51) Cambié, D.; Bottecchia, C.; Straathof, N. J. W.; Hessel, V.; Noël, T. Applications of Continuous-Flow Photochemistry in Organic Synthesis, Material Science, and Water Treatment. *Chem. Rev.* **2016**, *116*, 10276−10341.
(52) Van Gerven, T.; Stankiewicz, A. Structure, Energy, Synergy, Time: The Fundamentals of Process Intensification. *Ind. Eng. Chem. Res.* **2009**, *48*, 2465−2474.
(53) Hessel, V.; Kralisch, D.; Kockmann, N.; Noël, T.; Wang, Q. Novel Process Windows for Enabling, Accelerating, and Uplifting Flow Chemistry. *ChemSusChem* **2013**, *6*, 746−789.
(54) Kappe, C. O.; Pieber, B.; Dallinger, D. Microwave Effects in Organic Synthesis: Myth or Reality? *Angew. Chem., Int. Ed.* **2013**, *52*, 1088−1094.
(55) Avery, H. E. *Basic Reaction Kinetics and Mechanisms*; Macmillan Education UK: London, 1974.
(56) Bloh, J. Z. A Holistic Approach to Model the Kinetics of Photocatalytic Reactions. *Front. Chem.* **2019**, DOI: 10.3389/fchem.2019.00128.
(57) Bonfield, H. E.; Knauber, T.; Lévesque, F.; Moschetta, E. G.; Susanne, F.; Edwards, L. J. Photons as a 21st Century Reagent. *Nat. Commun.* **2020**, *11*, 804.
(58) McAtee, R. C.; McClain, E. J.; Stephenson, C. R. J. Illuminating Photoredox Catalysis. *Trends Chem.* **2019**, *1*, 111−125.
(59) Goddard, J. P.; Ollivier, C.; Fensterbank, L. Photoredox Catalysis for the Generation of Carbon Centered Radicals. *Acc. Chem. Res.* **2016**, *49*, 1924−1936.
(60) Shaw, M. H.; Twilton, J.; MacMillan, D. W. C. Photoredox Catalysis in Organic Chemistry. *J. Org. Chem.* **2016**, *81*, 6898−6926.
(61) Nicholls, T. P.; Leonori, D.; Bissember, A. C. Applications of Visible Light Photoredox Catalysis to the Synthesis of Natural Products and Related Compounds. *Nat. Prod. Rep.* **2016**, *33*, 1248−1254.
(62) Romero, N. A.; Nicewicz, D. A. Organic Photoredox Catalysis. *Chem. Rev.* **2016**, *116*, 10075−10166.
(63) Prier, C. K.; Rankic, D. A.; MacMillan, D. W. C. Visible Light Photoredox Catalysis with Transition Metal Complexes: Applications in Organic Synthesis. *Chem. Rev.* **2013**, *113*, 5322−5363.
(64) Capaldo, L.; Ravelli, D. Hydrogen Atom Transfer (HAT): A Versatile Strategy for Substrate Activation in Photocatalyzed Organic Synthesis. *Eur. J. Org. Chem.* **2017**, *2017*, 2056−2071.
(65) Protti, S.; Fagnoni, M.; Ravelli, D. Photocatalytic C-H Activation by Hydrogen-Atom Transfer in Synthesis. *ChemCatChem* **2015**, *7*, 1516−1523.
(66) Gentry, E. C.; Knowles, R. R. Synthetic Applications of Proton-Coupled Electron Transfer. *Acc. Chem. Res.* **2016**, *49*, 1546−1556.
(67) Strieth-Kalthoff, F.; Glorius, F. Triplet Energy Transfer Photocatalysis: Unlocking the Next Level. *Chem.* **2020**, *6*, 1888−1903.
(68) Strieth-Kalthoff, F.; James, M. J.; Teders, M.; Pitzer, L.; Glorius, F. Energy Transfer Catalysis Mediated by Visible Light: Principles, Applications, Directions. *Chem. Soc. Rev.* **2018**, *47*, 7190−7202.
(69) Metternich, J. B.; Gilmour, R. Photocatalytic E → Z Isomerization of Alkenes. *Synlett* **2016**, *27*, 2541−2552.
(70) Tastan, U.; Seeber, P.; Kupfer, S.; Ziegenbalg, D. Photochlorination of Toluene-the Thin Line between Intensification and Selectivity. Part 2: Selectivity. *React. Chem. Eng.* **2021**, *6*, 90−99.
(71) Roibu, A.; Morthala, R. B.; Leblebici, M. E.; Koziej, D.; Van Gerven, T.; Kuhn, S. Design and Characterization of Visible-Light LED Sources for Microstructured Photoreactors. *React. Chem. Eng.* **2018**, *3*, 849−865.
(72) Su, Y.; Kuijpers, K. P. L. L.; König, N.; Shang, M.; Hessel, V.; Noël, T. A Mechanistic Investigation of the Visible-Light Photocatalytic Trifluoromethylation of Heterocycles Using CF_3I in Flow. *Chem. - Eur. J.* **2016**, *22*, 12295−12300.
(73) Cismesia, M. A.; Yoon, T. P. Characterizing Chain Processes in Visible Light Photoredox Catalysis. *Chem. Sci.* **2015**, *6*, 5426−5434.
(74) Corcoran, E. B.; McMullen, J. P.; Lévesque, F.; Wismer, M. K.; Naber, J. R. Photon Equivalents as a Parameter for Scaling Photoredox Reactions in Flow: Translation of Photocatalytic C-N Cross-Coupling from Lab Scale to Multikilogram Scale. *Angew. Chem., Int. Ed.* **2020**, *59*, 11964−11968.
(75) Leigh, W. J. Techniques and Applications of Far-UV Photochemistry in Solution. The Photochemistry of the C_3H_4 and C_4H_6 Hydrocarbons. *Chem. Rev.* **1993**, *93*, 487−505.
(76) Poplata, S.; Tröster, A.; Zou, Y.-Q.; Bach, T. Recent Advances in the Synthesis of Cyclobutanes by Olefin [2 + 2] Photocycloaddition Reactions. *Chem. Rev.* **2016**, *116*, 9748−9815.
(77) Kärkäs, M. D.; Porco, J. A.; Stephenson, C. R. J. J. Photochemical Approaches to Complex Chemotypes: Applications in Natural Product Synthesis. *Chem. Rev.* **2016**, *116*, 9683−9747.
(78) Bach, T.; Hehn, J. P. Photochemical Reactions as Key Steps in Natural Product Synthesis. *Angew. Chem., Int. Ed.* **2011**, *50*, 1000−1045.
(79) Reintjens, R.; Puhl, A. Photochemical Process for the Preparation of a Previtamin D. WO2008128782, 2008.
(80) Shelby, J. E. Optical Materials: Color Filter and Absorption Glasses. In *Encyclopedia of Modern Optics*; Elsevier, 2004; pp 440−446.
(81) Madsen, C. K.; Zhao, J. H. Optical Filter Design and Analysis: A Signal Processing Approach; *Wiley Series in Microwave and Optical Engineering*; John Wiley & Sons, Inc.: New York, USA, 1999.
(82) Haas, C. P.; Roider, T.; Hoffmann, R. W.; Tallarek, U. Light as a Reaction Parameter-Systematic Wavelength Screening in Photochemical Synthesis. *React. Chem. Eng.* **2019**, *4*, 1912−1916.
(83) Song, K.; Mohseni, M.; Taghipour, F. Application of Ultraviolet Light-Emitting Diodes (UV-LEDs) for Water Disinfection: A Review. *Water Res.* **2016**, *94*, 341−349.

(84) Muramoto, Y.; Kimura, M.; Nouda, S. Development and Future of Ultraviolet Light-Emitting Diodes: UV-LED Will Replace the UV Lamp. *Semicond. Sci. Technol.* **2014**, *29*, 084004.
(85) Khan, A.; Balakrishnan, K.; Katona, T. Ultraviolet Light-Emitting Diodes Based on Group Three Nitrides. *Nat. Photonics* **2008**, *2*, 77−84.
(86) Kneissl, M.; Seong, T. Y.; Han, J.; Amano, H. The Emergence and Prospects of Deep-Ultraviolet Light-Emitting Diode Technologies. *Nat. Photonics* **2019**, *13*, 233−244.
(87) Yole Développement. UV LEDs—Market and Technology Trends. *i-Micronews Media*, 2020. https://www.i-micronews.com/products/uv-leds-market-and-technology-trends-2020/ (accessed 2021-02-01).
(88) Anyaogu, K. C.; Ermoshkin, A. A.; Neckers, D. C.; Mejiritski, A.; Grinevich, O.; Fedorov, A. V. Performance of the Light Emitting Diodes Versus Conventional Light Sources in the UV Light Cured Formulations. *J. Appl. Polym. Sci.* **2007**, *105*, 803−808.
(89) Decker, C. The Use of UV Irradiation in Polymerization. *Polym. Int.* **1998**, *45*, 133−141.
(90) DeLaney, E. N.; Lee, D. S.; Elliott, L. D.; Jin, J.; Booker-Milburn, K. I.; Poliakoff, M.; George, M. W. A Laboratory-Scale Annular Continuous Flow Reactor for UV Photochemistry Using Excimer Lamps for Discrete Wavelength Excitation and Its Use in a Wavelength Study of a Photodecarboxlyative Cyclisation. *Green Chem.* **2017**, *19*, 1431−1438.
(91) Gellert, B.; Kogelschatz, U. Generation of Excimer Emission in Dielectric Barrier Discharges. *Appl. Phys. B: Photophys. Laser Chem.* **1991**, *52*, 14−21.
(92) Dalapati, P.; Manik, N. B.; Basu, A. N. Effect of Temperature on the Intensity and Carrier Lifetime of an AlGaAs Based Red Light Emitting Diode. *J. Semicond.* **2013**, *34*, 092001.
(93) Guo, W.; Jia, X.; Yin, F.; Cui, B.; Gao, W.; Liu, Y.; Yan, W. Characteristics of High Power LEDs at High and Low Temperature. *J. Semicond.* **2011**, *32*, 044007.
(94) Auf Der Maur, M.; Pecchia, A.; Penazzi, G.; Rodrigues, W.; Di Carlo, A. Efficiency Drop in Green InGaN/GaN Light Emitting Diodes: The Role of Random Alloy Fluctuations. *Phys. Rev. Lett.* **2016**, *116*, 027401.
(95) Bulashevich, K. A.; Kulik, A. V.; Karpov, S. Y. Optimal Ways of Colour Mixing for High-Quality White-Light LED Sources. *Phys. Status Solidi A* **2015**, *212*, 914−919.
(96) Hoelen, C. G. A.; Benoy, D. A.; Cornelissen, H. J.; Vdovin, A. V.; Bruls, D. High Brightness Light Sources Based on LD-Pumped Luminescent Converters and LED-Pumped Luminescent Concentrators. *Light-Emitting Devices, Materials, and Applications* **2019**, *1094015*, 41.
(97) de Boer, D. K. G.; Bruls, D.; Hoelen, C.; Jagt, H. High Lumen Density Sources Based on LED-Pumped Phosphor Rods: Opportunities for Performance Improvement. *Sixteenth International Conference on Solid State Lighting and LED-based Illumination Systems* **2017**, 22.
(98) Bottecchia, C.; Wei, X.-J.; Kuijpers, K. P. L.; Hessel, V.; Noël, T. Visible Light-Induced Trifluoromethylation and Perfluoroalkylation of Cysteine Residues in Batch and Continuous Flow. *J. Org. Chem.* **2016**, *81*, 7301−7307.
(99) Wang, L.; Xu, X.; Cheng, Q.; Dou, S. X.; Du, Y. Near-Infrared-Driven Photocatalysts: Design, Construction, and Applications. *Small* **2021**, *17*, 1904107.
(100) Ravetz, B. D.; Pun, A. B.; Churchill, E. M.; Congreve, D. N.; Rovis, T.; Campos, L. M. Photoredox Catalysis Using Infrared Light via Triplet Fusion Upconversion. *Nature* **2019**, *565*, 343−346.
(101) Majek, M.; Faltermeier, U.; Dick, B.; Pérez-Ruiz, R.; JacobivonWangelin, A. Application of Visible-to-UV Photon Upconversion to Photoredox Catalysis: The Activation of Aryl Bromides. *Chem. - Eur. J.* **2015**, *21*, 15496−15501.
(102) Bharmoria, P.; Bildirir, H.; Moth-Poulsen, K. Triplet-Triplet Annihilation Based near Infrared to Visible Molecular Photon Upconversion. *Chem. Soc. Rev.* **2020**, *49*, 6529−6554.
(103) Ciamician, G. The Photochemistry of the Future. *Science* **1912**, *36*, 385−394.
(104) Cambié, D.; Noël, T. Solar Photochemistry in Flow. *Top. Curr. Chem.* **2018**, *376*, 45.
(105) Oelgemöller, M. Solar Photochemical Synthesis: From the Beginnings of Organic Photochemistry to the Solar Manufacturing of Commodity Chemicals. *Chem. Rev.* **2016**, *116*, 9664−9682.
(106) Noël, T. *Photochemical Processes in Continuous-Flow Reactors: From Engineering Principles to Chemical Applications*; World Scientific (Europe), 2017.
(107) Donnelly, K.; Baumann, M. Scalability of Photochemical Reactions in Continuous Flow Mode. *J. Flow Chem.* **2021**, DOI: 10.1007/s41981-021-00168-z.
(108) Su, Y.; Straathof, N. J. W.; Hessel, V.; Noël, T. Photochemical Transformations Accelerated in Continuous-Flow Reactors: Basic Concepts and Applications. *Chem. - Eur. J.* **2014**, *20*, 10562−10589.
(109) Dong, Z.; Wen, Z.; Zhao, F.; Kuhn, S.; Noël, T. Scale-up of Micro- and Milli-Reactors: An Overview of Strategies, Design Principles and Applications. *Chem. Eng. Sci. X* **2021**, *10*, 100097.
(110) Berton, M.; de Souza, J. M.; Abdiaj, I.; McQuade, D. T.; Snead, D. R. Scaling Continuous API Synthesis from Milligram to Kilogram: Extending the Enabling Benefits of Micro to the Plant. *J. Flow Chem.* **2020**, *10*, 73−92.
(111) Zhang, J.; Wang, K.; Teixeira, A. R.; Jensen, K. F.; Luo, G. Design and Scaling up of Microchemical Systems: A Review. *Annu. Rev. Chem. Biomol. Eng.* **2017**, *8*, 285−305.
(112) Su, Y.; Kuijpers, K.; Hessel, V.; Noël, T. A Convenient Numbering-up Strategy for the Scale-up of Gas-Liquid Photoredox Catalysis in Flow. *React. Chem. Eng.* **2016**, *1*, 73−81.
(113) Kuijpers, K. P. L.; Van Dijk, M. A. H.; Rumeur, Q. G.; Hessel, V.; Su, Y.; Noël, T. A Sensitivity Analysis of a Numbered-up Photomicroreactor System. *React. Chem. Eng.* **2017**, *2*, 109−115.
(114) Friedland, J.; Güttel, R. Challenges in Transfer of Gas-Liquid Reactions from Batch to Continuous Operation: Dimensional Analysis and Simulations for Aerobic Oxidation. *J. Flow Chem.* **2021**, DOI: 10.1007/s41981-021-00176-z.
(115) Moschetta, E. G.; Richter, S. M.; Wittenberger, S. J. Heuristics, Protocol, and Considerations for Flow Chemistry in Photoredox Catalysis. *ChemPhotoChem.* **2017**, *1*, 539−543.
(116) Sambiagio, C.; Noël, T. Flow Photochemistry: Shine Some Light on Those Tubes! *Trends Chem.* **2020**, *2*, 92−106.
(117) Oliveira de Brito Lira, J.; Riella, H. G.; Padoin, N.; Soares, C. An Overview of Photoreactors and Computational Modeling for the Intensification of Photocatalytic Processes in the Gas-Phase: State-of-Art. *J. Environ. Chem. Eng.* **2021**, *9*, 105068.
(118) Di Filippo, M.; Bracken, C.; Baumann, M. Continuous Flow Photochemistry for the Preparation of Bioactive Molecules. *Molecules* **2020**, *25*, 356.
(119) Claes, T.; Gerven, T. V.; Leblebici, M.E. Design Considerations for Photocatalytic Structured Packed Bed Reactors. *Chem. Eng. J.* **2021**, *403*, 126355.
(120) Kayahan, E.; Jacobs, M.; Braeken, L.; Thomassen, L. C. J.; Kuhn, S.; Van Gerven, T.; Leblebici, M. E. Dawn of a New Era in Industrial Photochemistry: The Scale-up of Micro: The Mesostructured Photoreactors. *Beilstein J. Org. Chem.* **2020**, *16*, 2484−2504.
(121) Sezen-Edmonds, M.; Tabora, J. E.; Cohen, B. M.; Zaretsky, S.; Simmons, E. M.; Sherwood, T. C.; Ramirez, A. Predicting Performance of Photochemical Transformations for Scaling Up in Different Platforms by Combining High-Throughput Experimentation with Computational Modeling. *Org. Process Res. Dev.* **2020**, *24*, 2128−2138.
(122) Fernandez Rivas, D.; Boffito, D. C.; Faria-Albanese, J.; Glassey, J.; Cantin, J.; Afraz, N.; Akse, H.; Boodhoo, K. V. K.; Bos, R.; Chiang, Y. W.; et al. Process Intensification Education Contributes to Sustainable Development Goals. Part 2. *Educ. Chem. Eng.* **2020**, *32*, 15−24.
(123) Fernandez Rivas, D.; Boffito, D. C.; Faria-Albanese, J.; Glassey, J.; Afraz, N.; Akse, H.; Boodhoo, K. V. K.; Bos, R.; Cantin, J.; Chiang, Y. W.; et al. Process Intensification Education Contributes to

Sustainable Development Goals. Part 1. *Educ. Chem. Eng.* **2020**, *32*, 1−14.
(124) Williams, J. D.; Kappe, C. O. Recent Advances toward Sustainable Flow Photochemistry. *Curr. Opin. Green Sustain. Chem.* **2020**, *25*, 100351.
(125) Stankiewicz, A.; Van Gerven, T.; Georgios, S. *The Fundamentals of Process Intensification*; Wiley-VCH Verlag: Weinheim, Germany, 2019.
(126) Jensen, K. F. Flow Chemistry-Microreaction Technology Comes of Age. *AIChE J.* **2017**, *63*, 858−869.
(127) Loubière, K.; Oelgemöller, M.; Aillet, T.; Dechy-Cabaret, O.; Prat, L. Continuous-Flow Photochemistry: A Need for Chemical Engineering. *Chem. Eng. Process.* **2016**, *104*, 120−132.
(128) Lutze, P.; Gani, R.; Woodley, J. M. Process Intensification: A Perspective on Process Synthesis. *Chem. Eng. Process.* **2010**, *49*, 547−558.
(129) Stankiewicz, A.; Moulijn, J. A. Process Intensification. *Ind. Eng. Chem. Res.* **2002**, *41*, 1920−1924.
(130) Van Gerven, T.; Mul, G.; Moulijn, J.; Stankiewicz, A. A Review of Intensification of Photocatalytic Processes. *Chem. Eng. Process.* **2007**, *46*, 781−789.
(131) Hook, B. D. A.; Dohle, W.; Hirst, P. R.; Pickworth, M.; Berry, M. B.; Booker-Milburn, K. I. A Practical Flow Reactor for Continuous Organic Photochemistry. *J. Org. Chem.* **2005**, *70*, 7558−7564.
(132) Elliott, L. D.; Knowles, J. P.; Stacey, C. S.; Klauber, D. J.; Booker-Milburn, K. I. Using Batch Reactor Results to Calculate Optimal Flow Rates for the Scale-up of UV Photochemical Reactions. *React. Chem. Eng.* **2018**, *3*, 86−93.
(133) Maskill, K. G.; Knowles, J. P.; Elliott, L. D.; Alder, R. W.; Booker-Milburn, K. I. Complexity from Simplicity: Tricyclic Aziridines from the Rearrangement of Pyrroles by Batch and Flow Photochemistry. *Angew. Chem., Int. Ed.* **2013**, *52*, 1499−1502.
(134) Graham, M. A.; Noonan, G.; Cherryman, J. H.; Douglas, J. J.; Gonzalez, M.; Jackson, L. V.; Leslie, K.; Liu, Z.; McKinney, D.; Munday, R. H.; et al. Development and Proof of Concept for a Large-Scale Photoredox Additive-Free Minisci Reaction. *Org. Process Res. Dev.* **2021**, *25*, 57−67.
(135) Chen, Y.; Sabio, J. C.; Hartman, R. L. When Solids Stop Flow Chemistry in Commercial Tubing. *J. Flow Chem.* **2015**, *5*, 166−171.
(136) Beatty, J. W.; Douglas, J. J.; Miller, R.; McAtee, R. C.; Cole, K. P.; Stephenson, C. R. J. J. Photochemical Perfluoroalkylation with Pyridine N-Oxides: Mechanistic Insights and Performance on a Kilogram Scale. *Chem.* **2016**, *1*, 456−472.
(137) Lévesque, F.; Di Maso, M. J.; Narsimhan, K.; Wismer, M. K.; Naber, J. R. Design of a Kilogram Scale, Plug Flow Photoreactor Enabled by High Power LEDs. *Org. Process Res. Dev.* **2020**, *24*, 2935−2940.
(138) Beaver, M. G.; Zhang, E. X.; Liu, Z. Q.; Zheng, S. Y.; Wang, B.; Lu, J. P.; Tao, J.; Gonzalez, M.; Jones, S.; Tedrow, J. S. Development and Execution of a Production-Scale Continuous [2 + 2] Photocycloaddition. *Org. Process Res. Dev.* **2020**, *24*, 2139−2146.
(139) Elliott, L. D.; Berry, M.; Harji, B.; Klauber, D.; Leonard, J.; Booker-Milburn, K. I. A Small-Footprint, High-Capacity Flow Reactor for UV Photochemical Synthesis on the Kilogram Scale. *Org. Process Res. Dev.* **2016**, *20*, 1806−1811.
(140) Siopa, F.; António, J. P. M. J. P. M.; Afonso, C. A. M. M. Flow-Assisted Synthesis of Bicyclic Aziridines via Photochemical Transformation of Pyridinium Salts. *Org. Process Res. Dev.* **2018**, *22*, 551−556.
(141) Fortunato, M. A. G.; Ly, C.; Siopa, F.; Afonso, C. A. M. Process Intensification for the Synthesis of 6-Allyl-6-Azabicyclo[3.1.0]Hex-3-En-2-Ol from 1-Allylpyridinium Salt Using a Continuous UV-Light Photoflow Approach. *Methods Protoc.* **2019**, *2*, 67.
(142) Escribà-Gelonch, M.; Halpin, A.; Noël, T.; Hessel, V. Laser-Mediated Photo-High-p,T Intensification of Vitamin D_3 Synthesis in Continuous Flow. *ChemPhotoChem.* **2018**, *2*, 922−930.
(143) Escribà-Gelonch, M.; Noël, T.; Hessel, V. Microflow High-p,T Intensification of Vitamin D3 Synthesis Using an Ultraviolet Lamp. *Org. Process Res. Dev.* **2018**, *22*, 147−155.
(144) Price, A. J. N.; Capel, A. J.; Lee, R. J.; Pradel, P.; Christie, S. D. R. An Open Source Toolkit for 3D Printed Fluidics. *J. Flow Chem.* **2021**, *11*, 37−51.
(145) Sans, V. Emerging Trends in Flow Chemistry Enabled by 3D Printing: Robust Reactors, Biocatalysis and Electrochemistry. *Curr. Opin. Green Sustain. Chem.* **2020**, *25*, 100367.
(146) Harding, M. J.; Brady, S.; O'Connor, H.; Lopez-Rodriguez, R.; Edwards, M. D.; Tracy, S.; Dowling, D.; Gibson, G.; Girard, K. P.; Ferguson, S. 3D Printing of PEEK Reactors for Flow Chemistry and Continuous Chemical Processing. *React. Chem. Eng.* **2020**, *5*, 728−735.
(147) Hartings, M. R.; Ahmed, Z. Chemistry from 3D Printed Objects. *Nat. Rev. Chem.* **2019**, *3*, 305−314.
(148) Capel, A. J.; Rimington, R. P.; Lewis, M. P.; Christie, S. D. R. 3D Printing for Chemical, Pharmaceutical and Biological Applications. *Nat. Rev. Chem.* **2018**, *2*, 422−436.
(149) Neumaier, J. M.; Madani, A.; Klein, T.; Ziegler, T. Low-Budget 3D-Printed Equipment for Continuous Flow Reactions. *Beilstein J. Org. Chem.* **2019**, *15*, 558−566.
(150) Parra-Cabrera, C.; Achille, C.; Kuhn, S.; Ameloot, R. 3D Printing in Chemical Engineering and Catalytic Technology: Structured Catalysts, Mixers and Reactors. *Chem. Soc. Rev.* **2018**, *47*, 209−230.
(151) Au, A. K.; Huynh, W.; Horowitz, L. F.; Folch, A. 3D-Printed Microfluidics. *Angew. Chem., Int. Ed.* **2016**, *55*, 3862−3881.
(152) Capel, A. J.; Edmondson, S.; Christie, S. D. R.; Goodridge, R. D.; Bibb, R. J.; Thurstans, M. Design and Additive Manufacture for Flow Chemistry. *Lab Chip* **2013**, *13*, 4583−4590.
(153) Dragone, V.; Sans, V.; Rosnes, M. H.; Kitson, P. J.; Cronin, L. 3D-Printed Devices for Continuous-Flow Organic Chemistry. *Beilstein J. Org. Chem.* **2013**, *9*, 951−959.
(154) Guba, F.; Tastan, Ü.; Gugeler, K.; Buntrock, M.; Rommel, T.; Ziegenbalg, D. Rapid Prototyping for Photochemical Reaction Engineering. *Chem. Ing. Tech.* **2018**, *91*, 17−29.
(155) Rastelli, E. J.; Yue, D.; Millard, C.; Wipf, P. 3D-Printed Cartridge System for in-Flow Photo-Oxygenation of 7-Amino-thienopyridinones. *Tetrahedron* **2021**, *79*, 131875.
(156) Zhao, F.; Cambié, D.; Janse, J.; Wieland, E. W.; Kuijpers, K. P. L.; Hessel, V.; Debije, M. G.; Noël, T. Scale-up of a Luminescent Solar Concentrator-Based Photomicroreactor via Numbering-Up. *ACS Sustainable Chem. Eng.* **2018**, *6*, 422−429.
(157) Cambié, D.; Zhao, F.; Hessel, V.; Debije, M. G.; Noël, T. A Leaf-Inspired Luminescent Solar Concentrator for Energy-Efficient Continuous-Flow Photochemistry. *Angew. Chem., Int. Ed.* **2017**, *56*, 1050−1054.
(158) Cambié, D.; Zhao, F.; Hessel, V.; Debije, M. G.; Noël, T. Every Photon Counts: Understanding and Optimizing Photon Paths in Luminescent Solar Concentrator-Based Photomicroreactors (LSC-PMs). *React. Chem. Eng.* **2017**, *2*, 561−566.
(159) Niu, W.; Zheng, Y.; Li, Y.; Du, L.; Liu, W. Photochemical Microfluidic Synthesis of Vitamin D_3 by Improved Light Sources with Photoluminescent Substrates. *Chin. J. Chem. Eng.* **2021**, *29*, 204−211.
(160) Cambié, D.; Dobbelaar, J.; Riente, P.; Vanderspikken, J.; Shen, C.; Seeberger, P. H.; Gilmore, K.; Debije, M. G.; Noël, T. Energy-Efficient Solar Photochemistry with Luminescent Solar Concentrator Based Photomicroreactors. *Angew. Chem., Int. Ed.* **2019**, *58*, 14374−14378.
(161) Zhao, F.; Cambié, D.; Hessel, V.; Debije, M. G.; Noël, T. Real-Time Reaction Control for Solar Production of Chemicals under Fluctuating Irradiance. *Green Chem.* **2018**, *20*, 2459−2464.
(162) de Oliveira, G. X.; Lira, J. O. B.; Cambié, D.; Noël, T.; Riella, H. G.; Padoin, N.; Soares, C. CFD Analysis of a Luminescent Solar Concentrator-Based Photomicroreactor (LSC-PM) with Feedforward Control Applied to the Synthesis of Chemicals under Fluctuating Light Intensity. *Chem. Eng. Res. Des.* **2020**, *153*, 626−634.

https://doi.org/10.1021/acs.chemrev.1c00332
Chem. Rev. 2022, 122, 2752−2906

(163) Zhang, L.; Zhu, Z.; Liu, B.; Li, C.; Yu, Y.; Tao, S.; Li, T. Fluorescent Fluid in 3D-Printed Microreactors for the Acceleration of Photocatalytic Reactions. *Adv. Sci.* **2019**, *6*, 1900583.
(164) Zhu, Z.; Yang, L.; Yu, Y.; Zhang, L.; Tao, S. Scale-up Design of a Fluorescent Fluid Photochemical Microreactor by 3D Printing. *ACS Omega* **2020**, *5*, 7666−7674.
(165) Ioannou, G. I.; Montagnon, T.; Kalaitzakis, D.; Pergantis, S. A.; Vassilikogiannakis, G. A Novel Nebulizer-Based Continuous Flow Reactor: Introducing the Use of Pneumatically Generated Aerosols for Highly Productive Photooxidations. *ChemPhotoChem.* **2017**, *1*, 173−177.
(166) Zheng, L.; Xue, H.; Wong, W. K.; Cao, H.; Wu, J.; Khan, S. A. Cloud-Inspired Multiple Scattering for Light Intensified Photochemical Flow Reactors. *React. Chem. Eng.* **2020**, *5*, 1058−1063.
(167) Ioannou, G. I.; Montagnon, T.; Kalaitzakis, D.; Pergantis, S. A.; Vassilikogiannakis, G. Synthesis of Cyclopent-2-Enones from Furans Using a Nebulizer-Based Continuous Flow Photoreactor. *Org. Biomol. Chem.* **2017**, *15*, 10151−10155.
(168) Ioannou, G. I.; Montagnon, T.; Kalaitzakis, D.; Pergantis, S. A.; Vassilikogiannakis, G. One-Pot Synthesis of Diverse γ-Lactam Scaffolds Facilitated by a Nebulizer-Based Continuous Flow Photoreactor. *ChemPhotoChem.* **2018**, *2*, 860−864.
(169) Kalaitzakis, D.; Sofiadis, M.; Tsopanakis, V.; Montagnon, T.; Vassilikogiannakis, G. Merging Singlet-Oxygen Induced Furan Oxidations with Organocatalysis: Synthesis of Enantiopure Cyclopentanones and Hydrindanes. *Org. Biomol. Chem.* **2020**, *18*, 2817−2822.
(170) Kayahan, E.; Urbani, D.; Dambruoso, P.; Massi, A.; Braeken, L.; Van Gerven, T.; Leblebici, M. E. Overcoming Mass and Photon Transfer Limitations in a Scalable Reactor: Oxidation in an Aerosol Photoreactor. *Chem. Eng. J.* **2021**, *408*, 127357.
(171) Kong, C. J.; Fisher, D.; Desai, B. K.; Yang, Y.; Ahmad, S.; Belecki, K.; Gupton, B. F. High Throughput Photo-Oxidations in a Packed Bed Reactor System. *Bioorg. Med. Chem.* **2017**, *25*, 6203−6208.
(172) Fabry, D. C.; Ho, Y. A.; Zapf, R.; Tremel, W.; Panthöfer, M.; Rueping, M.; Rehm, T. H. Blue Light Mediated C-H Arylation of Heteroarenes Using TiO_2 as an Immobilized Photocatalyst in a Continuous-Flow Microreactor. *Green Chem.* **2017**, *19*, 1911−1918.
(173) Yeong, K. K.; Gavriilidis, A.; Zapf, R.; Hessel, V. Catalyst Preparation and Deactivation Issues for Nitrobenzene Hydrogenation in a Microstructured Falling Film Reactor. *Catal. Today* **2003**, *81*, 641−651.
(174) Rehm, T. H.; Gros, S.; Löb, P.; Renken, A. Photonic Contacting of Gas-Liquid Phases in a Falling Film Microreactor for Continuous-Flow Photochemical Catalysis with Visible Light. *React. Chem. Eng.* **2016**, *1*, 636−648.
(175) Renner, M.; Griesbeck, A. Think and Print: 3D Printing of Chemical Experiments. *J. Chem. Educ.* **2020**, *97*, 3683−3689.
(176) Hansen, A.; Renner, M.; Griesbeck, A. G.; Büsgen, T. From 3D to 4D Printing: A Reactor for Photochemical Experiments Using Hybrid Polyurethane Acrylates for Vat-Based Polymerization and Surface Functionalization. *Chem. Commun.* **2020**, *56*, 15161−15164.
(177) Zhakeyev, A.; Jones, M. C.; Thomson, C. G.; Tobin, J. M.; Wang, H.; Vilela, F.; Xuan, J. Additive Manufacturing of Intricate and Inherently Photocatalytic Flow Reactor Components. *Addit. Manuf.* **2021**, *38*, 101828.
(178) Britton, J.; Stubbs, K. A.; Weiss, G. A.; Raston, C. L. Vortex Fluidic Chemical Transformations. *Chem. - Eur. J.* **2017**, *23*, 13270−1327.
(179) Tibbetts, J. D.; Carbery, D. R.; Emanuelsson, E. A. C. An In-Depth Study of the Use of Eosin Y for the Solar Photocatalytic Oxidative Coupling of Benzylic Amines. *ACS Sustainable Chem. Eng.* **2017**, *5*, 9826−9835.
(180) Chaudhuri, A.; Kuijpers, K. P. L. L.; Hendrix, R. B. J. J.; Shivaprasad, P.; Hacking, J. A.; Emanuelsson, E. A. C. C.; Noël, T.; van der Schaaf, J. Process Intensification of a Photochemical Oxidation Reaction Using a Rotor-Stator Spinning Disk Reactor: A Strategy for Scale Up. *Chem. Eng. J.* **2020**, *400*, 125875.
(181) van der Schaaf, J.; Schouten, J. High-Gravity and High-Shear Gas-Liquid Contactors for the Chemical Process Industry. *Curr. Opin. Chem. Eng.* **2011**, *1*, 84−88.
(182) Meeuwse, M.; van der Schaaf, J.; Kuster, B. F. M.; Schouten, J. C. Gas-Liquid Mass Transfer in a Rotor-Stator Spinning Disc Reactor. *Chem. Eng. Sci.* **2010**, *65*, 466−471.
(183) Lee, D. S.; Amara, Z.; Clark, C. A.; Xu, Z.; Kakimpa, B.; Morvan, H. P.; Pickering, S. J.; Poliakoff, M.; George, M. W. Continuous Photo-Oxidation in a Vortex Reactor: Efficient Operations Using Air Drawn from the Laboratory. *Org. Process Res. Dev.* **2017**, *21*, 1042−1050.
(184) Lee, D. S.; Sharabi, M.; Jefferson-Loveday, R.; Pickering, S. J.; Poliakoff, M.; George, M. W. Scalable Continuous Vortex Reactor for Gram to Kilo Scale for UV and Visible Photochemistry. *Org. Process Res. Dev.* **2020**, *24*, 201−206.
(185) Clark, C. A.; Lee, D. S.; Pickering, S. J.; Poliakoff, M.; George, M. W. A Simple and Versatile Reactor for Photochemistry. *Org. Process Res. Dev.* **2016**, *20*, 1792−1798.
(186) Hermens, J. G. H.; Freese, T.; Van den Berg, K. J.; Van Gemert, R.; Feringa, B. L. A Coating from Nature. *Sci. Adv.* **2020**, *6*, eabe0026.
(187) Obst, M.; Shaikh, R. S.; König, B. Solvent-Free Coupling of Aryl Halides with Pyrroles Applying Visible-Light Photocatalysis. *React. Chem. Eng.* **2017**, *2*, 472−478.
(188) Clark, C. A.; Lee, D. S.; Pickering, S. J.; Poliakoff, M.; George, M. W. UV PhotoVap: Demonstrating How a Simple and Versatile Reactor Based on a Conventional Rotary Evaporator Can Be Used for UV Photochemistry. *Org. Process Res. Dev.* **2018**, *22*, 595−599.
(189) Obst, M.; König, B. Solvent-Free, Visible-Light Photocatalytic Alcohol Oxidations Applying an Organic Photocatalyst. *Beilstein J. Org. Chem.* **2016**, *12*, 2358−2363.
(190) O'Neill, R. T.; Boulatov, R. The Many Flavours of Mechanochemistry and Its Plausible Conceptual Underpinnings. *Nat. Rev. Chem.* **2021**, *5*, 148−167.
(191) Friščić, T.; Mottillo, C.; Titi, H. M. Mechanochemistry for Synthesis. *Angew. Chem., Int. Ed.* **2020**, *59*, 1018−1029.
(192) Do, J.-L.; Friščić, T. Mechanochemistry: A Force of Synthesis. *ACS Cent. Sci.* **2017**, *3*, 13−19.
(193) Hernández, J. G. Mechanochemical Borylation of Aryldiazonium Salts; Merging Light and Ball Milling. *Beilstein J. Org. Chem.* **2017**, *13*, 1463−1469.
(194) Tan, D.; Friščić, T. Mechanochemistry for Organic Chemists: An Update. *Eur. J. Org. Chem.* **2018**, *2018*, 18−33.
(195) Hartman, R. L. Managing Solids in Microreactors for the Upstream Continuous Processing of Fine Chemicals. *Org. Process Res. Dev.* **2012**, *16*, 870−887.
(196) Hu, C. Reactor Design and Selection for Effective Continuous Manufacturing of Pharmaceuticals. *J. Flow Chem.* **2021**, DOI: 10.1007/s41981-021-00164-3.
(197) Harper, K. C.; Moschetta, E. G.; Bordawekar, S. V.; Wittenberger, S. J. A Laser Driven Flow Chemistry Platform for Scaling Photochemical Reactions with Visible Light. *ACS Cent. Sci.* **2019**, *5*, 109−115.
(198) Pomberger, A.; Mo, Y.; Nandiwale, K. Y.; Schultz, V. L.; Duvadie, R.; Robinson, R. I.; Altinoglu, E. I.; Jensen, K. F. A Continuous Stirred-Tank Reactor (CSTR) Cascade for Handling Solid-Containing Photochemical Reactions. *Org. Process Res. Dev.* **2019**, *23*, 2699−2706.
(199) Dong, Z.; Zondag, S. D. A.; Schmid, M.; Wen, Z.; Noël, T. A Meso-Scale Ultrasonic Milli-Reactor Enables Gas-Liquid-Solid Photocatalytic Reactions in Flow. *Chem. Eng. J.* **2022**, *428*, 130968.
(200) Noël, T.; Naber, J. R.; Hartman, R. L.; Mcmullen, J. P.; Jensen, K. F.; Buchwald, S. L. Palladium-Catalyzed Amination Reactions in Flow: Overcoming the Challenges of Clogging via Acoustic Irradiation. *Chem. Sci.* **2011**, *2*, 287−290.
(201) Hartman, R. L.; Naber, J. R.; Zaborenko, N.; Buchwald, S. L.; Jensen, K. F. Overcoming the Challenges of Solid Bridging and Constriction during Pd-Catalyzed C-N Bond Formation in Microreactors. *Org. Process Res. Dev.* **2010**, *14*, 1347−1357.

(202) Horie, T.; Sumino, M.; Tanaka, T.; Matsushita, Y.; Ichimura, T.; Yoshida, J. I. Photodimerization of Maleic Anhydride in a Microreactor without Clogging. *Org. Process Res. Dev.* **2010**, *14*, 405−410.
(203) Kuhn, S.; Noël, T.; Gu, L.; Heider, P. L.; Jensen, K. F. A Teflon Microreactor with Integrated Piezoelectric Actuator to Handle Solid Forming Reactions. *Lab Chip* **2011**, *11*, 2488−2492.
(204) Le, C. C.; Wismer, M. K.; Shi, Z. C.; Zhang, R.; Conway, D. V.; Li, G.; Vachal, P.; Davies, I. W.; MacMillan, D. W. C. A General Small-Scale Reactor to Enable Standardization and Acceleration of Photocatalytic Reactions. *ACS Cent. Sci.* **2017**, *3*, 647−653.
(205) Schiel, F.; Peinsipp, C.; Kornigg, S.; Böse, D. A 3D-Printed Open Access Photoreactor Designed for Versatile Applications in Photoredox- and Photoelectrochemical Synthesis. *ChemPhotoChem.* **2021**, *5*, 431.
(206) Photoreactors LEDs Accessories. *HepatoChem*. https://www.hepatochem.com/photoreactors-leds-accessories/#photoreactors (accessed 2021-03-22).
(207) PhotoreactorM2. *Penn PhD*. https://www.pennphd.com/product/5 (accessed 2021-03-24).
(208) Photochemistry LED Illuminator. *Pacer*. https://www.pacer.co.uk/case-studies/medical-case-studies/led-illuminator.html (accessed 2021-03-24).
(209) Bonfield, H. E.; Mercer, K.; Diaz-Rodriguez, A.; Cook, G. C.; McKay, B. S. J. J.; Slade, P.; Taylor, G. M.; Ooi, W. X.; Williams, J. D.; Roberts, J. P. M. M.; et al. The Right Light: De Novo Design of a Robust Modular Photochemical Reactor for Optimum Batch and Flow Chemistry. *ChemPhotoChem.* **2020**, *4*, 45−51.
(210) PhotoCube. *ThalesNano*. https://thalesnano.com/products-and-services/photocube/ (accessed 2021-03-24).
(211) Vapourtec, Ltd. *International Flow Chemistry Equipment*. https://www.vapourtec.com/ (accessed 2021-03-22).
(212) Vapourtec, Ltd. *Photochemical Reactions UV-150 Reactor*. https://www.vapourtec.com/flow-chemistry-resource-centre/applications-photolytic-reactions/ (accessed 2021-03-25).
(213) Uniqsis, Ltd. *PhotoSyn*. https://www.uniqsis.com/paProductsDetail.aspx?ID=PhotoSyn (accessed 2021-03-24).
(214) Lima, F.; Grunenberg, L.; Rahman, H. B. A.; Labes, R.; Sedelmeier, J.; Ley, S. V. Organic Photocatalysis for the Radical Couplings of Boronic Acid Derivatives in Batch and Flow. *Chem. Commun.* **2018**, *54*, 5606−5609.
(215) Chen, Y.; May, O.; Blakemore, D. C.; Ley, S. V. A Photoredox Coupling Reaction of Benzylboronic Esters and Carbonyl Compounds in Batch and Flow. *Org. Lett.* **2019**, *21*, 6140−6144.
(216) Future Chemistry. FlowStart Evo. *Photochemistry Module*. https://futurechemistry.com/product/photochemistry-module/ (accessed 2021-03-24).
(217) YMC Co., Ltd. KeyChem Series. *Flow Reactor Systems*. https://www.ymc.co.jp/en/nanotech/keychem/ (accessed Mar 24, 2021-03-24).
(218) Snapdragon Chemistry, Inc. https://www.snapdragonchemistry.com/ (accessed 2021-03-24).
(219) Corning. Corning Advanced-Flow Reactors. *Advanced-Flow Reactor Technology*. https://www.corning.com/emea/en/innovation/corning-emerging-innovations/advanced-flow-reactors/achema-2018.html (accessed 2021-03-22).
(220) Creaflow. *Scalable Flow Reactors*. https://www.creaflow.be/ (accessed 2021-03-24).
(221) Roibu, A.; Horn, C. R.; Van Gerven, T.; Kuhn, S. Photon Transport and Hydrodynamics in Gas-Liquid Flow Part 2: Characterization of Bubbly Flow in an Advanced-Flow Reactor. *ChemPhotoChem.* **2020**, *4*, 5193−5200.
(222) Williams, J. D.; Nakano, M.; Gérardy, R.; Rincón, J. A.; de Frutos, Ó.; Mateos, C.; Monbaliu, J.-C. M.; Kappe, C. O. Finding the Perfect Match: A Combined Computational and Experimental Study toward Efficient and Scalable Photosensitized [2 + 2] Cycloadditions in Flow. *Org. Process Res. Dev.* **2019**, *23*, 78−87.
(223) Steiner, A.; Williams, J. D.; de Frutos, O.; Rincón, J. A.; Mateos, C.; Kappe, C. O. Continuous Photochemical Benzylic Bromination Using: In Situ Generated Br_2: Process Intensification towards Optimal PMI and Throughput. *Green Chem.* **2020**, *22*, 448−454.
(224) Steiner, A.; Roth, P. M. C.; Strauss, F. J.; Gauron, G.; Tekautz, G.; Winter, M.; Williams, J. D.; Kappe, C. O. Multikilogram per Hour Continuous Photochemical Benzylic Brominations Applying a Smart Dimensioning Scale-up Strategy. *Org. Process Res. Dev.* **2020**, *24*, 2208−2216.
(225) Bianchi, P.; Williams, J. D.; Kappe, C. O. Oscillatory Flow Reactors for Synthetic Chemistry Applications. *J. Flow Chem.* **2020**, *10*, 475−490.
(226) Creaflow. *COSTA Technology*. https://www.creaflow.be/costatm-technology (accessed 2021-03-25).
(227) Wen, Z.; Maheshwari, A.; Sambiagio, C.; Deng, Y.; Laudadio, G.; Van Aken, K.; Sun, Y.; Gemoets, H. P. L. L.; Noël, T. Optimization of a Decatungstate-Catalyzed $C(Sp^3)$-H Alkylation Using a Continuous Oscillatory Millistructured Photoreactor. *Org. Process Res. Dev.* **2020**, *24*, 2356−2361.
(228) Rosso, C.; Gisbertz, S.; Williams, J. D.; Gemoets, H. P. L.; Debrouwer, W.; Pieber, B.; Kappe, C. O. An Oscillatory Plug Flow Photoreactor Facilitates Semi-Heterogeneous Dual Nickel/Carbon Nitride Photocatalytic C−N Couplings. *React. Chem. Eng.* **2020**, *5*, 597−604.
(229) Debrouwer, W.; Kimpe, W.; Dangreau, R.; Huvaere, K.; Gemoets, H. P. L.; Mottaghi, M.; Kuhn, S.; Van Aken, K. Ir/Ni Photoredox Dual Catalysis with Heterogeneous Base Enabled by an Oscillatory Plug Flow Photoreactor. *Org. Process Res. Dev.* **2020**, *24*, 2319−2325.
(230) Bianchi, P.; Williams, J. D.; Kappe, C. O. Continuous Flow Processing of Bismuth-Photocatalyzed Atom Transfer Radical Addition Reactions Using an Oscillatory Flow Reactor. *Green Chem.* **2021**, *23*, 2685.
(231) Creaflow. *MPDS EVO*. https://www.creaflow.be/mpdsrevo (accessed 2021-03-26).
(232) Grainger, R.; Whibley, S. A Perspective on the Analytical Challenges Encountered in High-Throughput Experimentation. *Org. Process Res. Dev.* **2021**, *25*, 354−364.
(233) Welch, C. J. High Throughput Analysis Enables High Throughput Experimentation in Pharmaceutical Process Research. *React. Chem. Eng.* **2019**, *4*, 1895−1911.
(234) Mennen, S. M.; Alhambra, C.; Allen, C. L.; Barberis, M.; Berritt, S.; Brandt, T. A.; Campbell, A. D.; Castañón, J.; Cherney, A. H.; Christensen, M.; et al. The Evolution of High-Throughput Experimentation in Pharmaceutical Development and Perspectives on the Future. *Org. Process Res. Dev.* **2019**, *23*, 1213−1242.
(235) Campos, K. R.; Coleman, P. J.; Alvarez, J. C.; Dreher, S. D.; Garbaccio, R. M.; Terrett, N. K.; Tillyer, R. D.; Truppo, M. D.; Parmee, E. R. The Importance of Synthetic Chemistry in the Pharmaceutical Industry. *Science* **2019**, *363*, No. eaat0805.
(236) Krska, S. W.; DiRocco, D. A.; Dreher, S. D.; Shevlin, M. The Evolution of Chemical High-Throughput Experimentation To Address Challenging Problems in Pharmaceutical Synthesis. *Acc. Chem. Res.* **2017**, *50*, 2976−2985.
(237) Maier, W. F. Early Years of High-Throughput Experimentation and Combinatorial Approaches in Catalysis and Materials Science. *ACS Comb. Sci.* **2019**, *21*, 437−444.
(238) Lipinski, C. A.; Lombardo, F.; Dominy, B. W.; Feeney, P. J. Experimental and Computational Approaches to Estimate Solubility and Permeability in Drug Discovery and Development Settings PII of Original Article: S0169−409X(96)00423−1. The Article Was Originally Published in Advanced Drug Delivery Reviews 23 (1997). *Adv. Drug Delivery Rev.* **2001**, *46*, 3−26.
(239) de Vries, J. G.; de Vries, A. H. M. The Power of High-Throughput Experimentation in Homogeneous Catalysis Research for Fine Chemicals. *Eur. J. Org. Chem.* **2003**, *2003*, 799−811.
(240) Troshin, K.; Hartwig, J. F. Snap Deconvolution: An Informatics Approach to High-Throughput Discovery of Catalytic Reactions. *Science* **2017**, *357*, 175−181.

https://doi.org/10.1021/acs.chemrev.1c00332
Chem. Rev. 2022, 122, 2752−2906

(241) Allen, C. L.; Leitch, D. C.; Anson, M. S.; Zajac, M. A. The Power and Accessibility of High-Throughput Methods for Catalysis Research. *Nat. Catal.* **2019**, *2*, 2−4.
(242) Perera, D.; Tucker, J. W.; Brahmbhatt, S.; Helal, C. J.; Chong, A.; Farrell, W.; Richardson, P.; Sach, N. W. A Platform for Automated Nanomole-Scale Reaction Screening and Micromole-Scale Synthesis in Flow. *Science* **2018**, *359*, 429−434.
(243) Schneider, G. Automating Drug Discovery. *Nat. Rev. Drug Discovery* **2018**, *17*, 97−113.
(244) Buitrago Santanilla, A.; Regalado, E. L.; Pereira, T.; Shevlin, M.; Bateman, K.; Campeau, L.-C.; Schneeweis, J.; Berritt, S.; Shi, Z.-C.; Nantermet, P.; et al. Nanomole-Scale High-Throughput Chemistry for the Synthesis of Complex Molecules. *Science* **2015**, *347*, 49−53.
(245) Li, X.; Maffettone, P. M.; Che, Y.; Liu, T.; Chen, L.; Cooper, A. I. Combining Machine Learning and High-Throughput Experimentation to Discover Photocatalytically Active Organic Molecules. *Chem. Sci.* **2021**, DOI: 10.1039/D1SC02150H.
(246) Eyke, N. S.; Koscher, B. A.; Jensen, K. F. Toward Machine Learning-Enhanced High-Throughput Experimentation. *Trends Chem.* **2021**, *3*, 120−132.
(247) Struble, T. J.; Alvarez, J. C.; Brown, S. P.; Chytil, M.; Cisar, J.; DesJarlais, R. L.; Engkvist, O.; Frank, S. A.; Greve, D. R.; Griffin, D. J.; et al. Current and Future Roles of Artificial Intelligence in Medicinal Chemistry Synthesis. *J. Med. Chem.* **2020**, *63*, 8667−8682.
(248) Gromski, P. S.; Granda, J. M.; Cronin, L. Universal Chemical Synthesis and Discovery with "The Chemputer". *Trends Chem.* **2020**, *2*, 4−12.
(249) Häse, F.; Roch, L. M.; Aspuru-Guzik, A. Next-Generation Experimentation with Self-Driving Laboratories. *Trends Chem.* **2019**, *1*, 282−291.
(250) Lindsey, J. S. A Retrospective on the Automation of Laboratory Synthetic Chemistry. *Chemom. Intell. Lab. Syst.* **1992**, *17*, 15−45.
(251) Fitzpatrick, D. E.; Battilocchio, C.; Ley, S. V. Enabling Technologies for the Future of Chemical Synthesis. *ACS Cent. Sci.* **2016**, *2*, 131−138.
(252) Breen, C. P.; Nambiar, A. M. K.; Jamison, T. F.; Jensen, K. F. Ready, Set, Flow! Automated Continuous Synthesis and Optimization. *Trends Chem.* **2021**, *3*, 373.
(253) Cawse, J. N. Experimental Strategies for Combinatorial and High-Throughput Materials Development. *Acc. Chem. Res.* **2001**, *34*, 213−221.
(254) Upadhya, R.; Kosuri, S.; Tamasi, M.; Meyer, T. A.; Atta, S.; Webb, M. A.; Gormley, A. J. Automation and Data-Driven Design of Polymer Therapeutics. *Adv. Drug Delivery Rev.* **2021**, *171*, 1−28.
(255) Williams, T.; McCullough, K.; Lauterbach, J. A. Enabling Catalyst Discovery through Machine Learning and High-Throughput Experimentation. *Chem. Mater.* **2020**, *32*, 157−165.
(256) McNally, A.; Prier, C. K.; MacMillan, D. W. C. Discovery of an α-Amino C-H Arylation Reaction Using the Strategy of Accelerated Serendipity. *Science* **2011**, *334*, 1114−1117.
(257) Lin, S.; Dikler, S.; Blincoe, W. D.; Ferguson, R. D.; Sheridan, R. P.; Peng, Z.; Conway, D. V.; Zawatzky, K.; Wang, H.; Cernak, T.; et al. Mapping the Dark Space of Chemical Reactions with Extended Nanomole Synthesis and MALDI-TOF MS. *Science* **2018**, *361*, No. eaar6236.
(258) Huff, C. A.; Cohen, R. D.; Dykstra, K. D.; Streckfuss, E.; DiRocco, D. A.; Krska, S. W. Photoredox-Catalyzed Hydroxymethylation of Heteroaromatic Bases. *J. Org. Chem.* **2016**, *81*, 6980−6987.
(259) Nicastri, M. C.; Lehnherr, D.; Lam, Y.; DiRocco, D. A.; Rovis, T. Synthesis of Sterically Hindered Primary Amines by Concurrent Tandem Photoredox Catalysis. *J. Am. Chem. Soc.* **2020**, *142*, 987−998.
(260) DiRocco, D. A.; Dykstra, K.; Krska, S.; Vachal, P.; Conway, D. V.; Tudge, M. Late-Stage Functionalization of Biologically Active Heterocycles Through Photoredox Catalysis. *Angew. Chem., Int. Ed.* **2014**, *53*, 4802−4806.
(261) Yayla, H. G.; Peng, F.; Mangion, I. K.; McLaughlin, M.; Campeau, L.-C.; Davies, I. W.; DiRocco, D. A.; Knowles, R. R. Discovery and Mechanistic Study of a Photocatalytic Indoline Dehydrogenation for the Synthesis of Elbasvir. *Chem. Sci.* **2016**, *7*, 2066−2073.
(262) Lee, H.; Boyer, N. C.; Deng, Q.; Kim, H.-Y.; Sawyer, T. K.; Sciammetta, N. Photoredox Ni-Catalyzed Peptide C(Sp^2)-O Cross-Coupling: From Intermolecular Reactions to Side Chain-to-Tail Macrocyclization. *Chem. Sci.* **2019**, *10*, 5073−5078.
(263) Halperin, S. D.; Kwon, D.; Holmes, M.; Regalado, E. L.; Campeau, L.-C.; DiRocco, D. A.; Britton, R. Development of a Direct Photocatalytic C-H Fluorination for the Preparative Synthesis of Odanacatib. *Org. Lett.* **2015**, *17*, 5200−5203.
(264) Corcoran, E. B.; Pirnot, M. T.; Lin, S.; Dreher, S. D.; DiRocco, D. A.; Davies, I. W.; Buchwald, S. L.; MacMillan, D. W. C. Aryl Amination Using Ligand-Free Ni(II) Salts and Photoredox Catalysis. *Science* **2016**, *353*, 279−283.
(265) González-Esguevillas, M.; Fernández, D. F.; Rincón, J. A.; Barberis, M.; de Frutos, O.; Mateos, C.; García-Cerrada, S.; Agejas, J.; MacMillan, D. W. C. Rapid Optimization of Photoredox Reactions for Continuous-Flow Systems Using Microscale Batch Technology. *ACS Cent. Sci.* **2021**, *7* (7), 1126−1134.
(266) Sherwood, T. C.; Xiao, H.-Y.; Bhaskar, R. G.; Simmons, E. M.; Zaretsky, S.; Rauch, M. P.; Knowles, R. R.; Dhar, T. G. M. Decarboxylative Intramolecular Arene Alkylation Using N-(Acyloxy)-Phthalimides, an Organic Photocatalyst, and Visible Light. *J. Org. Chem.* **2019**, *84*, 8360−8379.
(267) Minozzi, C.; Caron, A.; Grenier-Petel, J.-C.; Santandrea, J.; Collins, S. K. Heteroleptic Copper(I)-Based Complexes for Photocatalysis: Combinatorial Assembly, Discovery, and Optimization. *Angew. Chem., Int. Ed.* **2018**, *57*, 5477−5481.
(268) Betori, R. C.; Scheidt, K. A. Reductive Arylation of Arylidene Malonates Using Photoredox Catalysis. *ACS Catal.* **2019**, *9*, 10350−10357.
(269) Kölmel, D. K.; Meng, J.; Tsai, M.-H.; Que, J.; Loach, R. P.; Knauber, T.; Wan, J.; Flanagan, M. E. On-DNA Decarboxylative Arylation: Merging Photoredox with Nickel Catalysis in Water. *ACS Comb. Sci.* **2019**, *21*, 588−597.
(270) Grainger, R.; Heightman, T. D.; Ley, S. V.; Lima, F.; Johnson, C. N. Enabling Synthesis in Fragment-Based Drug Discovery by Reactivity Mapping: Photoredox-Mediated Cross-Dehydrogenative Heteroarylation of Cyclic Amines. *Chem. Sci.* **2019**, *10*, 2264−2271.
(271) Ruffoni, A.; Juliá, F.; Svejstrup, T. D.; McMillan, A. J.; Douglas, J. J.; Leonori, D. Practical and Regioselective Amination of Arenes Using Alkyl Amines. *Nat. Chem.* **2019**, *11*, 426−433.
(272) Hopkinson, M. N.; Gómez-Suárez, A.; Teders, M.; Sahoo, B.; Glorius, F. Accelerated Discovery in Photocatalysis Using a Mechanism-Based Screening Method. *Angew. Chem., Int. Ed.* **2016**, *55*, 4361−4366.
(273) Teders, M.; Pitzer, L.; Buss, S.; Glorius, F. Regioselective Synthesis of 2-Substituted Indoles from Benzotriazoles and Alkynes by Photoinitiated Denitrogenation. *ACS Catal.* **2017**, *7*, 4053−4056.
(274) Gensch, T.; Teders, M.; Glorius, F. Approach to Comparing the Functional Group Tolerance of Reactions. *J. Org. Chem.* **2017**, *82*, 9154−9159.
(275) Candish, L.; Pitzer, L.; Gómez-Suárez, A.; Glorius, F. Visible Light-Promoted Decarboxylative Di- and Trifluoromethylthiolation of Alkyl Carboxylic Acids. *Chem. - Eur. J.* **2016**, *22*, 4753−4756.
(276) Teders, M.; Gómez-Suárez, A.; Pitzer, L.; Hopkinson, M. N.; Glorius, F. Diverse Visible-Light-Promoted Functionalizations of Benzotriazoles Inspired by Mechanism-Based Luminescence Screening. *Angew. Chem., Int. Ed.* **2017**, *56*, 902−906.
(277) Teders, M.; Henkel, C.; Anhäuser, L.; Strieth-Kalthoff, F.; Gómez-Suárez, A.; Kleinmans, R.; Kahnt, A.; Rentmeister, A.; Guldi, D.; Glorius, F. The Energy-Transfer-Enabled Biocompatible Disulfide-Ene Reaction. *Nat. Chem.* **2018**, *10*, 981−988.
(278) Teders, M.; Bernard, S.; Gottschalk, K.; Schwarz, J. L.; Standley, E. A.; Decuypere, E.; Daniliuc, C. G.; Audisio, D.; Taran, F.; Glorius, F. Accelerated Discovery in Photocatalysis by a Combined Screening Approach Involving MS Tags. *Org. Lett.* **2019**, *21*, 9747−9752.

(279) Sap, J. B. I.; Straathof, N. J. W.; Knauber, T.; Meyer, C. F.; Médebielle, M.; Buglioni, L.; Genicot, C.; Trabanco, A. A.; Noël, T.; Am Ende, C. W.; et al. Organophotoredox Hydrodefluorination of Trifluoromethylarenes with Translational Applicability to Drug Discovery. *J. Am. Chem. Soc.* **2020**, *142*, 9181−9187.
(280) Rein, J.; Annand, J. R.; Wismer, M. K.; Fu, J.; Siu, J. C.; Klapars, A.; Strotman, N. A.; Kalyani, D.; Lehnherr, D.; Lin, S. Unlocking the Potential of High-Throughput Experimentation for Electrochemistry with a Standardized Microscale Reactor. *ChemRxiv*, 14173538, ver. 2, 2021. DOI: 10.26434/chemrxiv.14173538.v2.
(281) Motz, R. N.; Lopato, E. M.; Connell, T. U.; Bernhard, S. High-Throughput Screening of Earth-Abundant Water Reduction Catalysts toward Photocatalytic Hydrogen Evolution. *Inorg. Chem.* **2021**, *60*, 774−781.
(282) Lopato, E. M.; Eikey, E. A.; Simon, Z. C.; Back, S.; Tran, K.; Lewis, J.; Kowalewski, J. F.; Yazdi, S.; Kitchin, J. R.; Ulissi, Z. W.; et al. Parallelized Screening of Characterized and DFT-Modeled Bimetallic Colloidal Cocatalysts for Photocatalytic Hydrogen Evolution. *ACS Catal.* **2020**, *10*, 4244−4252.
(283) Song, W.; Lopato, E. M.; Bernhard, S.; Salvador, P. A.; Rohrer, G. S. High-Throughput Measurement of the Influence of PH on Hydrogen Production from $BaTiO_3/TiO_2$ Core/Shell Photocatalysts. *Appl. Catal., B* **2020**, *269*, 118750.
(284) Poznik, M.; König, B. Fast Colorimetric Screening for Visible Light Photocatalytic Oxidation and Reduction Reactions. *React. Chem. Eng.* **2016**, *1*, 494−500.
(285) Bai, Y.; Wilbraham, L.; Slater, B. J.; Zwijnenburg, M. A.; Sprick, R. S.; Cooper, A. I. Accelerated Discovery of Organic Polymer Photocatalysts for Hydrogen Evolution from Water through the Integration of Experiment and Theory. *J. Am. Chem. Soc.* **2019**, *141*, 9063−9071.
(286) Meier, C. B.; Clowes, R.; Berardo, E.; Jelfs, K. E.; Zwijnenburg, M. A.; Sprick, R. S.; Cooper, A. I. Structurally Diverse Covalent Triazine-Based Framework Materials for Photocatalytic Hydrogen Evolution from Water. *Chem. Mater.* **2019**, *31*, 8830−8838.
(287) Manson, J. A.; Clayton, A. D.; Niño, C. G.; Labes, R.; Chamberlain, T. W.; Blacker, A. J.; Kapur, N.; Bourne, R. A. A Hybridised Optimisation of an Automated Photochemical Continuous Flow Reactor. *Chimia* **2019**, *73*, 817−822.
(288) Aillet, T.; Loubiere, K.; Dechy-Cabaret, O.; Prat, L. Accurate Measurement of the Photon Flux Received Inside Two Continuous Flow Microphotoreactors by Actinometry. *Int. J. Chem. React. Eng.* **2014**, *12*, 257−269.
(289) Kuijpers, K. P. L.; Bottecchia, C.; Cambié, D.; Drummen, K.; König, N. J.; Noël, T. A Fully Automated Continuous-Flow Platform for Fluorescence Quenching Studies and Stern-Volmer Analysis. *Angew. Chem., Int. Ed.* **2018**, *57*, 11278−11282.
(290) Hsieh, H.-W.; Coley, C. W.; Baumgartner, L. M.; Jensen, K. F.; Robinson, R. I. Photoredox Iridium-Nickel Dual-Catalyzed Decarboxylative Arylation Cross-Coupling: From Batch to Continuous Flow via Self-Optimizing Segmented Flow Reactor. *Org. Process Res. Dev.* **2018**, *22*, 542−550.
(291) Coley, C. W.; Abolhasani, M.; Lin, H.; Jensen, K. F. Material-Efficient Microfluidic Platform for Exploratory Studies of Visible-Light Photoredox Catalysis. *Angew. Chem., Int. Ed.* **2017**, *56*, 9847−9850.
(292) Rubens, M.; Vrijsen, J. H.; Laun, J.; Junkers, T. Precise Polymer Synthesis by Autonomous Self-Optimizing Flow Reactors. *Angew. Chem., Int. Ed.* **2019**, *58*, 3183−3187.
(293) Sun, A. C.; Steyer, D. J.; Allen, A. R.; Payne, E. M.; Kennedy, R. T.; Stephenson, C. R. J. A Droplet Microfluidic Platform for High-Throughput Photochemical Reaction Discovery. *Nat. Commun.* **2020**, *11*, 6202.
(294) Trump, L.; Lemos, A.; Jacq, J.; Pasau, P.; Lallemand, B.; Mercier, J.; Genicot, C.; Luxen, A.; Lemaire, C. Development of a General Automated Flow Photoredox ^{18}F-Difluoromethylation of N-Heteroaromatics in an AllinOne Synthesizer. *Org. Process Res. Dev.* **2020**, *24*, 734−744.
(295) Poscharny, K.; Fabry, D. C.; Heddrich, S.; Sugiono, E.; Liauw, M. A.; Rueping, M. Machine Assisted Reaction Optimization: A Self-Optimizing Reactor System for Continuous-Flow Photochemical Reactions. *Tetrahedron* **2018**, *74*, 3171−3175.
(296) Chatterjee, S.; Guidi, M.; Seeberger, P. H.; Gilmore, K. Automated Radial Synthesis of Organic Molecules. *Nature* **2020**, *579*, 379−384.
(297) Bédard, A.-C.; Adamo, A.; Aroh, K. C.; Russell, M. G.; Bedermann, A. A.; Torosian, J.; Yue, B.; Jensen, K. F.; Jamison, T. F. Reconfigurable System for Automated Optimization of Diverse Chemical Reactions. *Science* **2018**, *361*, 1220−1225.
(298) Huyer, W.; Neumaier, A. SNOBFIT – Stable Noisy Optimization by Branch and Fit. *ACM Trans. Math. Softw.* **2008**, *35*, 1−25.
(299) Freeman, D. B.; Furst, L.; Condie, A. G.; Stephenson, C. R. J. Functionally Diverse Nucleophilic Trapping of Iminium Intermediates Generated Utilizing Visible Light. *Org. Lett.* **2012**, *14*, 94−97.
(300) Haas, C. P.; Biesenroth, S.; Buckenmaier, S.; van de Goor, T.; Tallarek, U. Automated Generation of Photochemical Reaction Data by Transient Flow Experiments Coupled with Online HPLC Analysis. *React. Chem. Eng.* **2020**, *5*, 912−920.
(301) Borlinghaus, N.; Kaschel, J.; Klee, J.; Haller, V.; Schetterl, J.; Heitz, S.; Lindner, T.; Dietrich, J. D.; Braje, W. M.; Jolit, A. Reagent and Catalyst Capsules: A Chemical Delivery System for Reaction Screening and Parallel Synthesis. *J. Org. Chem.* **2021**, *86*, 1357−1370.
(302) Zhang, M.; Lee, J.; Wang, L.; Duan, Q.; Zhang, J.; Qi, H. A Novel High-Throughput Screening of Multicomponent Photocatalysts for Decomposition of Organic Pollutants Based on Fluorescence Imaging. *ChemCatChem* **2015**, *7*, 3978−3984.
(303) Bi, S.; Liu, F.; Wang, W.; Duan, Q.; Chen, J.; Luo, R.; Feng, Y.; Lee, J. High-Throughput Screening of Multimetal Sulfides-Modified g-C_3N_4 for Degradation of Organic Contaminations Based on Ink-Jet Printing (IJP) Technology. *Catal. Lett.* **2020**, *150*, 1650−1658.
(304) Akwi, F. M.; Watts, P. Continuous Flow Chemistry: Where Are We Now? Recent Applications, Challenges and Limitations. *Chem. Commun.* **2018**, *54*, 13894−13928.
(305) Guidi, M.; Seeberger, P. H.; Gilmore, K. How to Approach Flow Chemistry. *Chem. Soc. Rev.* **2020**, *49*, 8910−8932.
(306) Ramanjaneyulu, B. T.; Vishwakarma, N. K.; Vidyacharan, S.; Adiyala, P. R.; Kim, D.-P. Towards Versatile Continuous-Flow Chemistry and Process Technology Via New Conceptual Microreactor Systems. *Bull. Korean Chem. Soc.* **2018**, *39*, 757−772.
(307) Noël, T.; Su, Y.; Hessel, V. Beyond Organometallic Flow Chemistry: The Principles behind the Use of Continuous-Flow Reactors for Synthesis. *Top. Organomet. Chem.* **2015**, *57*, 1−41.
(308) Gérardy, R.; Emmanuel, N.; Toupy, T.; Kassin, V.-E.; Tshibalonza, N. N.; Schmitz, M.; Monbaliu, J.-C. M. Continuous Flow Organic Chemistry: Successes and Pitfalls at the Interface with Current Societal Challenges. *Eur. J. Org. Chem.* **2018**, *2018*, 2301−2351.
(309) Gutmann, B.; Cantillo, D.; Kappe, C. O. Continuous-Flow Technology-A Tool for the Safe Manufacturing of Active Pharmaceutical Ingredients. *Angew. Chem., Int. Ed.* **2015**, *54*, 6688−6728.
(310) Bogdan, A. R.; Dombrowski, A. W. Emerging Trends in Flow Chemistry and Applications to the Pharmaceutical Industry. *J. Med. Chem.* **2019**, *62*, 6422−6468.
(311) Baumann, M.; Moody, T. S.; Smyth, M.; Wharry, S. A Perspective on Continuous Flow Chemistry in the Pharmaceutical Industry. *Org. Process Res. Dev.* **2020**, *24*, 1802−1813.
(312) Ferlin, F.; Lanari, D.; Vaccaro, L. Sustainable Flow Approaches to Active Pharmaceutical Ingredients. *Green Chem.* **2020**, *22*, 5937−5955.
(313) Domokos, A.; Nagy, B.; Szilágyi, B.; Marosi, G.; Nagy, Z. K. Integrated Continuous Pharmaceutical Technologies—A Review. *Org. Process Res. Dev.* **2021**, *25*, 721−739.
(314) Sivo, A.; Galaverna, R. de S.; Gomes, G. R.; Pastre, J. C.; Vilé, G. From Circular Synthesis to Material Manufacturing: Advances,

Challenges, and Future Steps for Using Flow Chemistry in Novel Application Area. *React. Chem. Eng.* **2021**, *6*, 756.
(315) Noël, T.; Wang, X.; Hessel, V. Accelerating Photoredox Catalysis in Continuous Microflow. *Chim. Oggi* **2013**, *31*, 10−14.
(316) Mizuno, K.; Nishiyama, Y.; Ogaki, T.; Terao, K.; Ikeda, H.; Kakiuchi, K. Utilization of Microflow Reactors to Carry out Synthetically Useful Organic Photochemical Reactions. *J. Photochem. Photobiol., C* **2016**, *29*, 107−147.
(317) Xie, J.; Zhao, D. Continuous-Flow Photochemistry: An Expanding Horizon of Sustainable Technology. *Chin. Chem. Lett.* **2020**, *31*, 2395−2400.
(318) Politano, F.; Oksdath-Mansilla, G. Light on the Horizon: Current Research and Future Perspectives in Flow Photochemistry. *Org. Process Res. Dev.* **2018**, *22*, 1045−1062.
(319) Rehm, T. H. Flow Photochemistry as a Tool in Organic Synthesis. *Chem. - Eur. J.* **2020**, *26*, 16952−16974.
(320) Lam, H.; Abel-Snape, X.; Köllen, M. F.; Lautens, M. Recent Advances in Transition-Metal-Free (4 + 3)-Annulations. *Synthesis* **2021**, DOI: 10.1055/s-0040-1706023.
(321) Zhang, Z.; Zhou, Y.; Liang, X.-W. Total Synthesis of Natural Products Using Photocycloaddition Reactions of Arenes. *Org. Biomol. Chem.* **2020**, *18*, 5558−5566.
(322) Sarkar, D.; Bera, N.; Ghosh, S. [2 + 2] Photochemical Cycloaddition in Organic Synthesis. *Eur. J. Org. Chem.* **2020**, *2020*, 1310−1326.
(323) García-Lacuna, J.; Domínguez, G.; Pérez-Castells, J. Flow Chemistry for Cycloaddition Reactions. *ChemSusChem* **2020**, *13*, 5138−5163.
(324) Alcaide, B.; Almendros, P.; Aragoncillo, C. Exploiting [2 + 2] Cycloaddition Chemistry: Achievements with Allenes. *Chem. Soc. Rev.* **2010**, *39*, 783−816.
(325) Ramamurthy, V.; Sivaguru, J. Supramolecular Photochemistry as a Potential Synthetic Tool: Photocycloaddition. *Chem. Rev.* **2016**, *116*, 9914−9993.
(326) Cox, B.; Booker-Milburn, K. I.; Elliott, L. D.; Robertson-Ralph, M.; Zdorichenko, V. Escaping from Flatland: [2 + 2] Photocycloaddition; Conformationally Constrained Sp^3-Rich Scaffolds for Lead Generation. *ACS Med. Chem. Lett.* **2019**, *10*, 1512−1517.
(327) El Achi, N.; Gelat, F.; Cheval, N. P.; Mazzah, A.; Bakkour, Y.; Penhoat, M.; Chausset-Boissarie, L.; Rolando, C. Sensitized [2 + 2] Intramolecular Photocycloaddition of Unsaturated Enones Using UV LEDs in a Continuous Flow Reactor: Kinetic and Preparative Aspects. *React. Chem. Eng.* **2019**, *4*, 828−837.
(328) Blanco-Ania, D.; Gawade, S. A.; Zwinkels, L. J. L.; Maartense, L.; Bolster, M. G.; Benningshof, J. C. J.; Rutjes, F. P. J. T. Rapid and Scalable Access into Strained Scaffolds through Continuous Flow Photochemistry. *Org. Process Res. Dev.* **2016**, *20*, 409−413.
(329) Ratković, A.; Marinić, Š.; Škorić, I. Flow-Photochemical Synthesis of the Functionalized Benzobicyclo[3.2.1]Octadiene Skeleton. *J. Mol. Struct.* **2018**, *1168*, 165−174.
(330) Meltzer, P. C.; Blundell, P.; Yong, Y. F.; Chen, Z.; George, C.; Gonzalez, M. D.; Madras, B. K. 2-Carbomethoxy-3-Aryl-8-Bicyclo-[3.2.1]Octanes: Potent Non-Nitrogen Inhibitors of Monoamine Transporters. *J. Med. Chem.* **2000**, *43*, 2982−2991.
(331) Elliott, L. D.; Booker-Milburn, K. I. Photochemically Produced Aminocyclobutanes as Masked Dienes in Thermal Electrocyclic Cascade Reactions. *Org. Lett.* **2019**, *21*, 1463−1466.
(332) Levterov, V. V.; Michurin, O.; Borysko, P. O.; Zozulya, S.; Sadkova, I. V.; Tolmachev, A. A.; Mykhailiuk, P. K. Photochemical In-Flow Synthesis of 2,4-Methanopyrrolidines: Pyrrolidine Analogues with Improved Water Solubility and Reduced Lipophilicity. *J. Org. Chem.* **2018**, *83*, 14350−14361.
(333) Tanino, K.; Takahashi, M.; Tomata, Y.; Tokura, H.; Uehara, T.; Narabu, T.; Miyashita, M. Total Synthesis of Solanoeclepin A. *Nat. Chem.* **2011**, *3*, 484−488.
(334) Kleinnijenhuis, R. A.; Timmer, B. J. J.; Lutteke, G.; Smits, J. M. M.; de Gelder, R.; van Maarseveen, J. H.; Hiemstra, H. Formal Synthesis of Solanoeclepin A: Enantioselective Allene Diboration and Intramolecular [2 + 2] Photocycloaddition for the Construction of the Tricyclic Core. *Chem. - Eur. J.* **2016**, *22*, 1266−1269.
(335) Collin, D. E.; Jackman, E. H.; Jouandon, N.; Sun, W.; Light, M. E.; Harrowven, D. C.; Linclau, B. Decagram Synthesis of Dimethyl 1,4-Cubanedicarboxylate Using Continuous-Flow Photochemistry. *Synthesis* **2021**, *53*, 1307−1314.
(336) Falkiner, M. J.; Littler, S. W.; McRae, K. J.; Savage, G. P.; Tsanaktsidis, J. Pilot-Scale Production of Dimethyl 1,4-Cubanedicarboxylate. *Org. Process Res. Dev.* **2013**, *17*, 1503−1509.
(337) Staveness, D.; Sodano, T. M.; Li, K.; Burnham, E. A.; Jackson, K. D.; Stephenson, C. R. J. Providing a New Aniline Bioisostere through the Photochemical Production of 1-Aminonorbornanes. *Chem.* **2019**, *5*, 215−226.
(338) Corcoran, E. B.; Lévesque, F.; McMullen, J. P.; Naber, J. R. Studies Toward the Scaling of Gas-Liquid Photocycloadditions. *ChemPhotoChem.* **2018**, *2*, 931−937.
(339) Xu, W.; Su, Y.; Song, Y.; Shang, M.; Zha, L.; Lu, Q. Process Analysis on Preparation of Cyclobutanetetracarboxylic Dianhydride in a Photomicroreactor within Gas-Liquid Taylor Flow. *Ind. Eng. Chem. Res.* **2018**, *57*, 2476−2485.
(340) Serrano, E.; Juan, A.; García-Montero, A.; Soler, T.; Jiménez-Márquez, F.; Cativiela, C.; Gomez, M. V.; Urriolabeitia, E. P. Stereoselective Synthesis of 1,3-Diaminotruxillic Acid Derivatives: An Advantageous Combination of C-H-Ortho-Palladation and On-Flow [2 + 2]-Photocycloaddition in Microreactors. *Chem. - Eur. J.* **2016**, *22*, 144−152.
(341) García-Montero, A.; Rodriguez, A. M.; Juan, A.; Velders, A. H.; Denisi, A.; Jiménez-Osés, G.; Gómez-Bengoa, E.; Cativiela, C.; Gómez, M. V.; Urriolabeitia, E. P. Metal-Free [2 + 2]-Photocycloaddition of (Z)-4-Aryliden-5(4H)-Oxazolones as Straightforward Synthesis of 1,3-Diaminotruxillic Acid Precursors: Synthetic Scope and Mechanistic Studies. *ACS Sustainable Chem. Eng.* **2017**, *5*, 8370−8381.
(342) Telmesani, R.; White, J. A. H.; Beeler, A. B. Liquid-Liquid Slug-Flow-Accelerated [2 + 2] Photocycloaddition of Cinnamates. *ChemPhotoChem.* **2018**, *2*, 865−869.
(343) Roiban, D.; Serrano, E.; Soler, T.; Grosu, I.; Cativiela, C.; Urriolabeitia, E. P. Unexpected [2 + 2] C-C Bond Coupling Due to Photocycloaddition on Orthopalladated (Z)-2-Aryl-4-Arylidene-5(4H)-Oxazolones. *Chem. Commun.* **2009**, No. 31, 4681−4683.
(344) Liu, Q.; Li, N.; Yuan, Y.; Lu, H.; Wu, X.; Zhou, C.; He, M.; Su, H.; Zhang, M.; Wang, J.; et al. Cyclobutane Derivatives As Novel Nonpeptidic Small Molecule Agonists of Glucagon-Like Peptide-1 Receptor. *J. Med. Chem.* **2012**, *55*, 250−267.
(345) Lawrenz, D.; Mohr, S.; Wendländer, B. Formation of 1,3-Diazetidines via C-N Dimerization of 4-Cycloalkylidene-Oxazol-5(4H)-Ones in the Solid State. *J. Chem. Soc., Chem. Commun.* **1984**, No. 13, 863−865.
(346) Blanco-Lomas, M.; Funes-Ardoiz, I.; Campos, P. J.; Sampedro, D. Oxazolone-Based Photoswitches: Synthesis and Properties. *Eur. J. Org. Chem.* **2013**, *2013*, 6611−6618.
(347) Runčevski, T.; Blanco-Lomas, M.; Marazzi, M.; Cejuela, M.; Sampedro, D.; Dinnebier, R. E. Following a Photoinduced Reconstructive Phase Transformation and Its Influence on the Crystal Integrity: Powder Diffraction and Theoretical Study. *Angew. Chem., Int. Ed.* **2014**, *53*, 6738−6742.
(348) Yang, C.; Li, R.; Zhang, K. A. I.; Lin, W.; Landfester, K.; Wang, X. Heterogeneous Photoredox Flow Chemistry for the Scalable Organosynthesis of Fine Chemicals. *Nat. Commun.* **2020**, *11*, 1239.
(349) Blackham, E. E.; Knowles, J. P.; Burgess, J.; Booker-Milburn, K. I. Combining Photochemistry and Catalysis: Rapid Access to Sp^3-Rich Polyheterocycles from Simple Pyrroles. *Chem. Sci.* **2016**, *7*, 2302−2307.
(350) Blackham, E. E.; Booker-Milburn, K. I. A Short Synthesis of (±)-3-Demethoxyerythratidinone by Ligand-Controlled Selective Heck Cyclization of Equilibrating Enamines. *Angew. Chem., Int. Ed.* **2017**, *56*, 6613−6616.

(351) Sayes, M.; Benoit, G.; Charette, A. B. Borocyclopropanation of Styrenes Mediated by UV-Light Under Continuous Flow Conditions. *Angew. Chem., Int. Ed.* **2018**, *57*, 13514−13518.
(352) Hommelsheim, R.; Guo, Y.; Yang, Z.; Empel, C.; Koenigs, R. M. Blue-Light-Induced Carbene-Transfer Reactions of Diazoalkanes. *Angew. Chem., Int. Ed.* **2019**, *58*, 1203−1207.
(353) Empel, C.; Koenigs, R. M. Continuous-Flow Photochemical Carbene Transfer Reactions. *J. Flow Chem.* **2020**, *10*, 157−160.
(354) Wang, W.; Cencic, R.; Whitesell, L.; Pelletier, J.; Porco, J. A., Jr Synthesis of Aza-Rocaglates via ESIPT-Mediated (3 + 2) Photocycloaddition. *Chem. - Eur. J.* **2016**, *22*, 12006−12010.
(355) Yueh, H.; Gao, Q.; Porco, J. A.; Beeler, A. B. A Photochemical Flow Reactor for Large Scale Syntheses of Aglain and Rocaglate Natural Product Analogues. *Bioorg. Med. Chem.* **2017**, *25*, 6197−6202.
(356) Wang, W.; Clay, A.; Krishnan, R.; Lajkiewicz, N. J.; Brown, L. E.; Sivaguru, J.; Porco, J. A., Jr Total Syntheses of the Isomeric Aglain Natural Products Foveoglin A and Perviridisin B: Selective Excited-State Intramolecular Proton-Transfer Photocycloaddition. *Angew. Chem., Int. Ed.* **2017**, *56*, 14479−14482.
(357) Czarnecki, M.; Wessig, P. Scaling Up UV-Mediated Intramolecular Photodehydro-Diels-Alder Reactions Using a Home-made High-Performance Annular Continuous-Flow Reactor. *Org. Process Res. Dev.* **2018**, *22*, 1823−1827.
(358) Ge, X.; Jiang, H.; Li, J. Rapid Continuous Photoflow Synthesis of Naturally Occurring Arylnaphthalene Lignans and Their Analogs. *Nat. Prod. Res.* **2021**, 1−5.
(359) Hu, A.; Chen, Y.; Guo, J.-J.; Yu, N.; An, Q.; Zuo, Z. Cerium-Catalyzed Formal Cycloaddition of Cycloalkanols with Alkenes through Dual Photoexcitation. *J. Am. Chem. Soc.* **2018**, *140*, 13580−13585.
(360) Mateos, J.; Meneghini, N.; Bonchio, M.; Marino, N.; Carofiglio, T.; Companyó, X.; Dell'Amico, L. Microfluidic Light-Driven Synthesis of Tetracyclic Molecular Architectures. *Beilstein J. Org. Chem.* **2018**, *14*, 2418−2424.
(361) Mateos, J.; Cherubini-Celli, A.; Carofiglio, T.; Bonchio, M.; Marino, N.; Companyó, X.; Dell'Amico, L. A Microfluidic Photoreactor Enables 2-Methylbenzophenone Light-Driven Reactions with Superior Performance. *Chem. Commun.* **2018**, *54*, 6820−6823.
(362) Mateos, J.; Cuadros, S.; Vega-Peñaloza, A.; Dell'Amico, L. Unlocking the Synthetic Potential of Light-Excited Aryl Ketones: Applications in Direct Photochemistry and Photoredox Catalysis. *Synlett* **2021**, DOI: 10.1055/a-1403-4613.
(363) Gomtsyan, A. Heterocycles in Drugs and Drug Discovery. *Chem. Heterocycl. Compd.* **2012**, *48*, 7−10.
(364) Nakano, M.; Morimoto, T.; Noguchi, J.; Tanimoto, H.; Mori, H.; Tokumoto, S.; Koishi, H.; Nishiyama, Y.; Kakiuchi, K. Accelerated Organic Photoreactions in Flow Microreactors under Gas-Liquid Slug Flow Conditions Using N_2 Gas as an Unreactive Substance. *Bull. Chem. Soc. Jpn.* **2019**, *92*, 1467−1473.
(365) Nakano, M.; Nishiyama, Y.; Tanimoto, H.; Morimoto, T.; Kakiuchi, K. Remarkable Improvement of Organic Photoreaction Efficiency in the Flow Microreactor by the Slug Flow Condition Using Water. *Org. Process Res. Dev.* **2016**, *20*, 1626−1632.
(366) Ralph, M.; Ng, S.; Booker-Milburn, K. I. Short Flow-Photochemistry Enabled Synthesis of the Cytotoxic Lactone (+)-Goniofufurone. *Org. Lett.* **2016**, *18*, 968−971.
(367) Green, L.; Livingstone, K.; Bertrand, S.; Peace, S.; Jamieson, C. UV-Induced 1,3,4-Oxadiazole Formation from 5-Substituted Tetrazoles and Carboxylic Acids in Flow. *Chem. - Eur. J.* **2020**, *26*, 14866−14870.
(368) Figueroa, F. N.; Heredia, A. A.; Peñéñory, A. B.; Sampedro, D.; Argüello, J. E.; Oksdath-Mansilla, G. Regioselective Photocycloaddition of Saccharin Anion to π-Systems: Continuous-Flow Synthesis of Benzosultams. *J. Org. Chem.* **2019**, *84*, 3871−3880.
(369) Ganguly, A. K.; Alluri, S. S.; Caroccia, D.; Biswas, D.; Wang, C.-H.; Kang, E.; Zhang, Y.; McPhail, A. T.; Carroll, S. S.; Burlein, C.; et al. Design, Synthesis, and X-Ray Crystallographic Analysis of a Novel Class of HIV-1 Protease Inhibitors. *J. Med. Chem.* **2011**, *54*, 7176−7183.
(370) Rayabarapu, D. K.; Zhou, A.; Jeon, K. O.; Samarakoon, T.; Rolfe, A.; Siddiqui, H.; Hanson, P. R. α-Haloarylsulfonamides: Multiple Cyclization Pathways to Skeletally Diverse Benzofused Sultams. *Tetrahedron* **2009**, *65*, 3180−3188.
(371) Chandrasekhar, D.; Borra, S.; Nanubolu, J. B.; Maurya, R. A. Visible Light Driven Photocascade Catalysis: $Ru(Bpy)_3(PF_6)_2$/TBHP-Mediated Synthesis of Fused β-Carbolines in Batch and Flow Microreactors. *Org. Lett.* **2016**, *18*, 2974−2977.
(372) Borra, S.; Chandrasekhar, D.; Adhikary, S.; Rasala, S.; Gokulnath, S.; Maurya, R. A. Visible-Light Driven Photocascade Catalysis: Union of N,N-Dimethylanilines and α-Azidochalcones in Flow Microreactors. *J. Org. Chem.* **2017**, *82*, 2249−2256.
(373) Lefebvre, C.; Fortier, L.; Hoffmann, N. Photochemical Rearrangements in Heterocyclic Chemistry. *Eur. J. Org. Chem.* **2020**, *2020*, 1393−1404.
(374) Molloy, J. J.; Morack, T.; Gilmour, R. Positional and Geometrical Isomerisation of Alkenes: The Pinnacle of Atom Economy. *Angew. Chem., Int. Ed.* **2019**, *58*, 13654−13664.
(375) Shen, C.; Shang, M.; Zhang, H.; Su, Y. A UV-LEDs Based Photomicroreactor for Mechanistic Insights and Kinetic Studies in the Norbornadiene Photoisomerization. *AIChE J.* **2020**, *66*, No. e16841.
(376) El Achi, N.; Bakkour, Y.; Chausset-Boissarie, L.; Penhoat, M.; Rolando, C. Rapid and Facile Chemical Actinometric Protocol for Photo-Microfluidic Systems Using Azobenzene and NMR Spectroscopy. *RSC Adv.* **2017**, *7*, 29815−29820.
(377) Roibu, A.; Fransen, S.; Leblebici, M. E.; Meir, G.; Van Gerven, T.; Kuhn, S. An Accessible Visible-Light Actinometer for the Determination of Photon Flux and Optical Pathlength in Flow Photo Microreactors. *Sci. Rep.* **2018**, *8*, 5421.
(378) Reiner, T.; Zeglis, B. M. The Inverse Electron Demand Diels-Alder Click Reaction in Radiochemistry. *J. Labelled Compd. Radiopharm.* **2014**, *57*, 285−290.
(379) Inoue, Y.; Takamuku, S.; Kunitomi, Y.; Sakurai, H. Singlet Photosensitization of Simple Alkenes. Part 1. Cis-Trans-Photoisomerization of Cyclo-Octene Sensitized by Aromatic Esters. *J. Chem. Soc., Perkin Trans. 2* **1980**, No. 11, 1672−1677.
(380) Tsuneishi, H.; Hakushi, T.; Inoue, Y. Singlet-versus Triplet-Sensitized Enantiodifferentiating Photoisomerization of Cyclooctene: Remarkable Effects of Spin Multiplicity upon Optical Yield. *J. Chem. Soc., Perkin Trans. 2* **1996**, No. 8, 1601−1605.
(381) Royzen, M.; Yap, G. P. A.; Fox, J. M. A Photochemical Synthesis of Functionalized Trans-Cyclooctenes Driven by Metal Complexation. *J. Am. Chem. Soc.* **2008**, *130*, 3760−3761.
(382) Pigga, J. E.; Fox, J. M. Flow Photochemical Syntheses of Trans-Cyclooctenes and Trans-Cycloheptenes Driven by Metal Complexation. *Isr. J. Chem.* **2020**, *60*, 207−218.
(383) Billaud, E. M. F.; Shahbazali, E.; Ahamed, M.; Cleeren, F.; Noël, T.; Koole, M.; Verbruggen, A.; Hessel, V.; Bormans, G. Micro-Flow Photosynthesis of New Dienophiles for Inverse-Electron-Demand Diels-Alder Reactions. Potential Applications for Pretargeted in Vivo PET Imaging. *Chem. Sci.* **2017**, *8*, 1251−1258.
(384) Shahbazali, E.; Billaud, E. M. F.; Fard, A. S.; Meuldijk, J.; Bormans, G.; Noël, T.; Hessel, V. Photo Isomerization of Cis-Cyclooctene to Trans-Cyclooctene: Integration of a Micro-Flow Reactor and Separation by Specific Adsorption. *AIChE J.* **2021**, *67*, No. e17067.
(385) Svatunek, D.; Denk, C.; Rosecker, V.; Sohr, B.; Hametner, C.; Allmaier, G.; Fröhlich, J.; Mikula, H. Efficient Low-Cost Preparation of Trans-Cyclooctenes Using a Simplified Flow Setup for Photoisomerization. *Monatsh. Chem.* **2016**, *147*, 579−585.
(386) Blanco-Ania, D.; Maartense, L.; Rutjes, F. P. J. T. Rapid Production of Trans-Cyclooctenes in Continuous Flow. *ChemPhotoChem.* **2018**, *2*, 898−905.
(387) Fang, Y.; Zhang, H.; Huang, Z.; Scinto, S. L.; Yang, J. C.; am Ende, C. W.; Dmitrenko, O.; Johnson, D. S.; Fox, J. M. Photochemical Syntheses, Transformations, and Bioorthogonal Chemistry of Trans-Cycloheptene and Sila Trans-Cycloheptene Ag(I) Complexes. *Chem. Sci.* **2018**, *9*, 1953−1963.

(388) Di Filippo, M.; Baumann, M. Continuous Flow Synthesis of Quinolines via a Scalable Tandem Photoisomerization-Cyclization Process. *Eur. J. Org. Chem.* **2020**, *2020*, 6199−6211.
(389) Chen, X.; Qiu, S.; Wang, S.; Wang, H.; Zhai, H. Blue-Light-Promoted Carbon-Carbon Double Bond Isomerization and Its Application in the Syntheses of Quinolines. *Org. Biomol. Chem.* **2017**, *15*, 6349−6352.
(390) Raji Reddy, C.; Ganesh, V.; Singh, A. K. *E*−*Z* Isomerization of 3-Benzylidene-Indolin-2-Ones Using a Microfluidic Photo-Reactor. *RSC Adv.* **2020**, *10*, 28630−28634.
(391) Prüfert, C.; Urban, R. D.; Fischer, T. G.; Villatoro, J.; Riebe, D.; Beitz, T.; Belder, D.; Zeitler, K.; Löhmannsröben, H.-G. In Situ Monitoring of Photocatalyzed Isomerization Reactions on a Microchip Flow Reactor by IR-MALDI Ion Mobility Spectrometry. *Anal. Bioanal. Chem.* **2020**, *412*, 7899−7911.
(392) Gonzalez-Gomez, J. C.; Ramirez, N. P.; Lana-Villarreal, T.; Bonete, P. A Photoredox-Neutral Smiles Rearrangement of 2-Aryloxybenzoic Acids. *Org. Biomol. Chem.* **2017**, *15*, 9680−9684.
(393) Karjule, N.; Sharma, M. K.; Nithyanandhan, J.; Kulkarni, A. A. Modulation of Reactivity of Singlet Radical Pair in Continuous Flow: Photo-Fries Rearrangement. *J. Photochem. Photobiol., A* **2018**, *364*, 316−321.
(394) Chien, C.-C.; Kao, S.-C.; Chen, C.-J.; Wu, Y.-K. Photo-Fries Rearrangement in Flow under Aqueous Micellar Conditions. *Chem. Commun.* **2020**, *56*, 15470−15472.
(395) Gao, B.; Yao, F.; Zhang, Z.; Ding, H. Total Synthesis of (+)-Alsmaphorazine C and Formal Synthesis of (+)-Strictamine: A Photo-Fries Approach. *Angew. Chem., Int. Ed.* **2021**, *60*, 10603−10607.
(396) Frébault, F.; Luparia, M.; Oliveira, M. T.; Goddard, R.; Maulide, N. A Versatile and Stereoselective Synthesis of Functionalized Cyclobutenes. *Angew. Chem., Int. Ed.* **2010**, *49*, 5672−5676.
(397) Williams, J. D.; Otake, Y.; Coussanes, G.; Saridakis, I.; Maulide, N.; Kappe, C. O. Towards a Scalable Synthesis of 2-Oxabicyclo[2.2.0]Hex-5-En-3-One Using Flow Photochemistry. *ChemPhotoChem.* **2019**, *3*, 229−232.
(398) Yamashita, T.; Nishikawa, H.; Kawamoto, T. Scale-up Synthesis of a Deuterium-Labeled Cis-Cyclobutane-1,3-Dicarboxylic Acid Derivative Using Continuous Photo Flow Chemistry. *Tetrahedron* **2019**, *75*, 617−623.
(399) Javaheripour, H.; Neckers, D. C. Solid Phase and Solution Photochemistry of Coumalate Esters. *J. Org. Chem.* **1977**, *42*, 1844−1850.
(400) Gant, T. G. Using Deuterium in Drug Discovery: Leaving the Label in the Drug. *J. Med. Chem.* **2014**, *57*, 3595−3611.
(401) Edel, K.; Yang, X.; Ishibashi, J. S. A.; Lamm, A. N.; Maichle-Mössmer, C.; Giustra, Z. X.; Liu, S.-Y.; Bettinger, H. F. The Dewar Isomer of 1,2-Dihydro-1,2-Azaborinines: Isolation, Fragmentation, and Energy Storage. *Angew. Chem., Int. Ed.* **2018**, *57*, 5296−5300.
(402) Giustra, Z. X.; Yang, X.; Chen, M.; Bettinger, H. F.; Liu, S.-Y. Accessing 1,2-Substituted Cyclobutanes through 1,2-Azaborine Photoisomerization. *Angew. Chem., Int. Ed.* **2019**, *58*, 18918−18922.
(403) Chen, Y.; Cantillo, D.; Kappe, C. O. Visible Light-Promoted Beckmann Rearrangements: Separating Sequential Photochemical and Thermal Phenomena in a Continuous Flow Reactor. *Eur. J. Org. Chem.* **2019**, *2019*, 2163−2171.
(404) Lattes, A.; Oliveros, E.; Riviere, M.; Belzeck, C.; Mostowicz, D.; Abramskj, W.; Piccinni-Leopardi, C.; Germain, G.; Van Meerssche, M. Photochemical and Thermal Rearrangement of Oxaziridines. Experimental Evidence in Support of the Stereoelectronic Control Theory. *J. Am. Chem. Soc.* **1982**, *104*, 3929−3934.
(405) Aube, J.; Wang, Y.; Hammond, M.; Tanol, M.; Takusagawa, F.; Vander Velde, D. Synthetic Aspects of an Asymmetric Nitrogen-Insertion Process: Preparation of Chiral, Non-Racemic Caprolactams and Valerolactams. Total Synthesis of (−)-Alloyohimbane. *J. Am. Chem. Soc.* **1990**, *112*, 4879−4891.
(406) Cochran, J. E.; Waal, N. Photochemical Rearrangement of Chiral Oxaziridines in Continuous Flow: Application Toward the Scale-Up of a Chiral Bicyclic Lactam. *Org. Process Res. Dev.* **2016**, *20*, 1533−1539.
(407) Brown, M.; Aljarah, M.; Asiki, H.; Leung, L. M. H.; Smithen, D. A.; Miller, N.; Nemeth, G.; Davies, L.; Niculescu-Duvaz, D.; Zambon, A.; Springer, C. Toward the Scale-Up of a Bicyclic Homopiperazine via Schmidt Rearrangement and Photochemical Oxaziridine Rearrangement in Continuous-Flow. *Org. Process Res. Dev.* **2021**, *25*, 148−156.
(408) Jones, R. C. F.; Chatterley, A.; Marty, R.; Owton, W. M.; Elsegood, M. R. J. Isoxazole to Oxazole: A Mild and Unexpected Transformation. *Chem. Commun.* **2015**, *51*, 1112−1115.
(409) Ullman, E. F.; Singh, B. Photochemical Transposition of Ring Atoms in Five-Membered Heterocycles. The Photorearrangement of 3,5-Diphenylisoxazole. *J. Am. Chem. Soc.* **1966**, *88*, 1844−1845.
(410) Singh, B.; Ullman, E. F. Photochemical Transposition of Ring Atoms in 3,5-Diarylisoxazoles. Unusual Example of Wavelength Control in a Photochemical Reaction of Azirines. *J. Am. Chem. Soc.* **1967**, *89*, 6911−6916.
(411) Bracken, C.; Baumann, M. Development of a Continuous Flow Photoisomerization Reaction Converting Isoxazoles into Diverse Oxazole Products. *J. Org. Chem.* **2020**, *85*, 2607−2617.
(412) Babra, J. S.; Russell, A. T.; Smith, C. D.; Zhang, Y. Combining C-H Functionalisation and Flow Photochemical Heterocyclic Metamorphosis (FP-HM) for the Synthesis of Benzo[1,3]Oxazepines. *Tetrahedron* **2018**, *74*, 5351−5357.
(413) Mailloux, M. J.; Fleming, G. S.; Kumta, S. S.; Beeler, A. B. Unified Synthesis of Azepines by Visible-Light-Mediated Dearomative Ring Expansion of Aromatic N-Ylides. *Org. Lett.* **2021**, *23*, 525−529.
(414) Manning, M. A.; Sun, W.; Light, M. E.; Harrowven, D. C. A Photochemical Ring Expansion of 6- to 8-Membered Nitrogen Heterocycles by [1,3]-Sigmatropic Rearrangement. *Chem. Commun.* **2021**, *57*, 4556−4559.
(415) Zhang, Z.; Ratnikov, M.; Spraggon, G.; Alper, P. B. Photoinduced Rearrangement of Dienones and Santonin Rerouted by Amines. *Angew. Chem., Int. Ed.* **2018**, *57*, 904−908.
(416) Seyler, H.; Wong, W. W. H.; Jones, D. J.; Holmes, A. B. Continuous Flow Synthesis of Fullerene Derivatives. *J. Org. Chem.* **2011**, *76*, 3551−3556.
(417) Rossi, E.; Carofiglio, T.; Venturi, A.; Ndobe, A.; Muccini, M.; Maggini, M. Continuous-Flow Synthesis of an Efficient Methanofullerene Acceptor for Bulk-Heterojunction Solar Cells. *Energy Environ. Sci.* **2011**, *4*, 725−727.
(418) Ueda, M.; Imai, N.; Yoshida, S.; Yasuda, H.; Fukuyama, T.; Ryu, I. Scalable Flow Synthesis of [6,6]-Phenyl-C_{61}-Butyric Acid Methyl Ester (PCBM) Using a Flow Photoreactor with a Sodium Lamp. *Eur. J. Org. Chem.* **2017**, *2017*, 6483−6485.
(419) Moustakim, M.; Ledford, B.; Garwin, J. A.; Boyd, M. J. Photocyclization of Enamines to Access Spiroindolines and Spirooxindoles in Continuous Flow. *Tetrahedron Lett.* **2020**, *61*, 152111.
(420) Takeuchi, H.; Inuki, S.; Nakagawa, K.; Kawabe, T.; Ichimura, A.; Oishi, S.; Ohno, H. Total Synthesis of Zephycarinatines via Photocatalytic Reductive Radical Ipso-Cyclization. *Angew. Chem., Int. Ed.* **2020**, *59*, 21210−21215.
(421) Wen, S.; Boyce, J. H.; Kandappa, S. K.; Sivaguru, J.; Porco, J. A. Regiodivergent Photocyclization of Dearomatized Acylphloroglucinols: Asymmetric Syntheses of (−)-Nemorosone and (−)-6-Epi-Garcimultiflorone A. *J. Am. Chem. Soc.* **2019**, *141*, 11315−11321.
(422) Lisiecki, K.; Krawczyk, K. K.; Roszkowski, P.; Maurin, J. K.; Czarnocki, Z. Formal Synthesis of (−)-Podophyllotoxin through the Photocyclization of an Axially Chiral 3,4-Bisbenzylidene Succinate Amide Ester - a Flow Photochemistry Approach. *Org. Biomol. Chem.* **2016**, *14*, 460−469.
(423) Lisiecki, K.; Roszkowski, P.; Krawczyk, K. K.; Maurin, J. K.; Czarnocki, Z. Unexpected Regioselectivity in the Photocyclization of a Chiral 2,3-Bisbenzylidenesuccinate, Leading to a Podophyllotoxin Related Cyclolignan. *J. Photochem. Photobiol., A* **2018**, *364*, 297−302.
(424) Fang, Y.; Tranmer, G. K. Continuous Flow Photochemistry as an Enabling Synthetic Technology: Synthesis of Substituted-6(5H)-

https://doi.org/10.1021/acs.chemrev.1c00332
Chem. Rev. 2022, 122, 2752−2906

Phenanthridinones for Use as Poly(ADP-Ribose) Polymerase Inhibitors. *MedChemComm* **2016**, *7*, 720−724.
(425) Fang, Y.; Tranmer, G. K. Expedited Access to Thieno[3,2-c]Quinolin-4(5H)-Ones and Benzo[h]-1,6-Naphthyridin-5(6H)-Ones via a Continuous Flow Photocyclization Method. *Org. Biomol. Chem.* **2016**, *14*, 10799−10803.
(426) Bhakuni, B. S.; Kumar, A.; Balkrishna, S. J.; Sheikh, J. A.; Konar, S.; Kumar, S. KOtBu Mediated Synthesis of Phenanthridinones and Dibenzoazepinones. *Org. Lett.* **2012**, *14*, 2838−2841.
(427) Pierre, F.; Regan, C. F.; Chevrel, M.-C.; Siddiqui-Jain, A.; Macalino, D.; Streiner, N.; Drygin, D.; Haddach, M.; O'Brien, S. E.; Rice, W. G.; et al. Novel Potent Dual Inhibitors of CK2 and Pim Kinases with Antiproliferative Activity against Cancer Cells. *Bioorg. Med. Chem. Lett.* **2012**, *22*, 3327−3331.
(428) Poduval, M. K.; Burrezo, P. M.; Casado, J.; López Navarrete, J. T.; Ortiz, R. P.; Kim, T.-H. Novel Thiophene-Phenylene-Thiophene Fused Bislactam-Based Donor-Acceptor Type Conjugate Polymers: Synthesis by Direct Arylation and Properties. *Macromolecules* **2013**, *46*, 9220−9230.
(429) Chatterjee, A.; Cutler, S. J.; Doerksen, R. J.; Khan, I. A.; Williamson, J. S. Discovery of Thienoquinolone Derivatives as Selective and ATP Non-Competitive CDK5/P25 Inhibitors by Structure-Based Virtual Screening. *Bioorg. Med. Chem.* **2014**, *22*, 6409−6421.
(430) Fukuyama, T.; Fujita, Y.; Rashid, M. A.; Ryu, I. Flow Update for a Cossy Photocyclization. *Org. Lett.* **2016**, *18*, 5444−5446.
(431) Cossy, J.; Ranaivosata, J.-L.; Bellosta, V. Formation of Radicals by Irradiation of Alkyl Halides in the Presence of Triethylamine. *Tetrahedron Lett.* **1994**, *35*, 8161−8162.
(432) Parisien-Collette, S.; Cruché, C.; Abel-Snape, X.; Collins, S. K. Photochemical Intramolecular Amination for the Synthesis of Heterocycles. *Green Chem.* **2017**, *19*, 4798−4803.
(433) Hernandez-Perez, A. C.; Collins, S. K. A Visible-Light-Mediated Synthesis of Carbazoles. *Angew. Chem., Int. Ed.* **2013**, *52*, 12696−12700.
(434) Parisien-Collette, S.; Collins, S. K. Exploiting Photochemical Processes in Multi-Step Continuous Flow: Derivatization of the Natural Product Clausine C. *ChemPhotoChem.* **2018**, *2*, 855−859.
(435) Ruggeri, M.; Dombrowski, A. W.; Djuric, S. W.; Baxendale, I. R. Photochemical Flow Synthesis of 3-Hydroxyazetidines. *ChemPhotoChem.* **2019**, *3*, 1212−1218.
(436) Renata, H.; Zhou, Q.; Baran, P. S. Strategic Redox Relay Enables A Scalable Synthesis of Ouabagenin, A Bioactive Cardenolide. *Science* **2013**, *339*, 59−63.
(437) Secci, F.; Porcu, S.; Luridiana, A.; Frongia, A.; Ricci, P. C. Visible Light Promoted Continuous Flow Photocyclization of 1,2-Diketones. *Org. Biomol. Chem.* **2020**, *18*, 3684−3689.
(438) Kawamata, T.; Nagatomo, M.; Inoue, M. Total Synthesis of Zaragozic Acid C: Implementation of Photochemical C(Sp^3)-H Acylation. *J. Am. Chem. Soc.* **2017**, *139*, 1814−1817.
(439) Jindakun, C.; Hsieh, S.-Y.; Bode, J. W. Iridium-Catalyzed Synthesis of Saturated N-Heterocycles from Aldehydes and SnAP Reagents with Continuous Flow Photochemistry. *Org. Lett.* **2018**, *20*, 2071−2075.
(440) Jackl, M. K.; Legnani, L.; Morandi, B.; Bode, J. W. Continuous Flow Synthesis of Morpholines and Oxazepanes with Silicon Amine Protocol (SLAP) Reagents and Lewis Acid Facilitated Photoredox Catalysis. *Org. Lett.* **2017**, *19*, 4696−4699.
(441) Sambiagio, C.; Ferrari, M.; van Beurden, K.; della Ca', N.; van Schijndel, J.; Noël, T. Continuous-Flow Synthesis of Pyrylium Tetrafluoroborates: Application to Synthesis of Katritzky Salts and Photoinduced Cationic RAFT Polymerization. *Org. Lett.* **2021**, *23*, 2042−2047.
(442) Hsieh, S.-Y.; Bode, J. W. Silicon Amine Reagents for the Photocatalytic Synthesis of Piperazines from Aldehydes and Ketones. *Org. Lett.* **2016**, *18*, 2098−2101.
(443) Gérardy, R.; Winter, M.; Horn, C. R.; Vizza, A.; Van Hecke, K.; Monbaliu, J.-C. M. Continuous-Flow Preparation of γ-Butyrolactone Scaffolds from Renewable Fumaric and Itaconic Acids under Photosensitized Conditions. *Org. Process Res. Dev.* **2017**, *21*, 2012−2017.
(444) Lakshmaiah, G.; Kawabata, T.; Shang, M.; Fuji, K. Total Synthesis of (−)-Horsfiline via Asymmetric Nitroolefination. *J. Org. Chem.* **1999**, *64*, 1699−1704.
(445) Lisiecki, K.; Czarnocki, Z. Flow Photochemistry as a Tool for the Total Synthesis of (+)-Epigalcatin. *Org. Lett.* **2018**, *20*, 605−607.
(446) Lisiecki, K.; Czarnocki, Z. Advances in the Synthesis of Aryltetralin and Arylnaphthalene Lignans Using Photocyclization. *Org. Prep. Proced. Int.* **2018**, *50*, 527−543.
(447) Okamoto, H.; Takane, T.; Gohda, S.; Kubozono, Y.; Sato, K.; Yamaji, M.; Satake, K. Efficient Synthetic Photocyclization for Phenacenes Using a Continuous Flow Reactor. *Chem. Lett.* **2014**, *43*, 994−996.
(448) Okamoto, H.; Takahashi, H.; Takane, T.; Nishiyama, Y.; Kakiuchi, K.; Gohda, S.; Yamaji, M. Convenient Phenacene Synthesis by Sequentially Performed Wittig Reaction and Mallory Photocyclization Using Continuous-Flow Techniques. *Synthesis* **2017**, *49*, 2949−2957.
(449) Yuan, F.; Yan, D.-M.; Gao, P.-P.; Shi, D.-Q.; Xiao, W.-J.; Chen, J.-R. Photoredox-Catalyzed Multicomponent Cyclization of 2-Vinyl Phenols, N-Alkoxypyridinium Salts, and Sulfur Ylides for Synthesis of Dihydrobenzofurans. *ChemCatChem* **2021**, *13*, 543−547.
(450) Hone, C. A.; Kappe, C. O. The Use of Molecular Oxygen for Liquid Phase Aerobic Oxidations in Continuous Flow. *Top. Curr. Chem.* **2019**, *377*, 2.
(451) Pibiri, I.; Buscemi, S.; Palumbo Piccionello, A.; Pace, A. Photochemically Produced Singlet Oxygen: Applications and Perspectives. *ChemPhotoChem.* **2018**, *2*, 535−547.
(452) Ghogare, A. A.; Greer, A. Using Singlet Oxygen to Synthesize Natural Products and Drugs. *Chem. Rev.* **2016**, *116*, 9994−10034.
(453) Elsherbini, M.; Allemann, R. K.; Wirth, T. Dark" Singlet Oxygen Made Easy. *Chem. - Eur. J.* **2019**, *25*, 12486−12490.
(454) Zhao, Y.; Sun, M.; Wang, X.; Wang, C.; Lu, D.; Ma, W.; Kube, S. A.; Ma, J.; Elimelech, M. Janus Electrocatalytic Flow-through Membrane Enables Highly Selective Singlet Oxygen Production. *Nat. Commun.* **2020**, *11*, 6228.
(455) Gavriilidis, A.; Constantinou, A.; Hellgardt, K.; Hii, K. K.; Hutchings, G. J.; Brett, G. L.; Kuhn, S.; Marsden, S. P. Aerobic Oxidations in Flow: Opportunities for the Fine Chemicals and Pharmaceuticals Industries. *React. Chem. Eng.* **2016**, *1*, 595−612.
(456) Movsisyan, M.; Delbeke, E. I. P.; Berton, J. K. E. T.; Battilocchio, C.; Ley, V. S.; Stevens, V. C. Taming Hazardous Chemistry by Continuous Flow Technology. *Chem. Soc. Rev.* **2016**, *45*, 4892−4928.
(457) Gemoets, H. P. L.; Su, Y.; Shang, M.; Hessel, V.; Luque, R.; Noël, T. Liquid Phase Oxidation Chemistry in Continuous-Flow Microreactors. *Chem. Soc. Rev.* **2016**, *45*, 83−117.
(458) Kockmann, N.; Thenée, P.; Fleischer-Trebes, C.; Laudadio, G.; Noël, T. Safety Assessment in Development and Operation of Modular Continuous-Flow Processes. *React. Chem. Eng.* **2017**, *2*, 258−280.
(459) Han, S.; Kashfipour, M. A.; Ramezani, M.; Abolhasani, M. Accelerating Gas-Liquid Chemical Reactions in Flow. *Chem. Commun.* **2020**, *56*, 10593−10606.
(460) Schachtner, J.; Bayer, P.; Jacobi von Wangelin, A. A Flow Reactor Setup for Photochemistry of Biphasic Gas/Liquid Reactions. *Beilstein J. Org. Chem.* **2016**, *12*, 1798−1811.
(461) Peng, Z.; Gai, S.; Barma, M.; Rahman, M. M.; Moghtaderi, B.; Doroodchi, E. Experimental Study of Gas-Liquid-Solid Flow Characteristics in Slurry Taylor Flow-Based Multiphase Microreactors. *Chem. Eng. J.* **2021**, *405*, 126646.
(462) Yue, J. Multiphase Flow Processing in Microreactors Combined with Heterogeneous Catalysis for Efficient and Sustainable Chemical Synthesis. *Catal. Today* **2018**, *308*, 3−19.
(463) Liu, Y.; Chen, G.; Yue, J. Manipulation of Gas-Liquid-Liquid Systems in Continuous Flow Microreactors for Efficient Reaction Processes. *J. Flow Chem.* **2020**, *10*, 103−121.

https://doi.org/10.1021/acs.chemrev.1c00332
Chem. Rev. 2022, 122, 2752−2906

(464) Günther, A.; Jensen, K. F. Multiphase Microfluidics: From Flow Characteristics to Chemical and Materials Synthesis. *Lab Chip* **2006**, *6*, 1487−1503.
(465) Horn, C. R.; Gremetz, S. A Method to Determine the Correct Photocatalyst Concentration for Photooxidation Reactions Conducted in Continuous Flow Reactors. *Beilstein J. Org. Chem.* **2020**, *16*, 871−879.
(466) Heugebaert, T. S. A.; Stevens, V. C.; Kappe, C. O. Singlet-Oxygen Oxidation of 5-Hydroxymethylfurfural in Continuous Flow. *ChemSusChem* **2015**, *8*, 1648−1651.
(467) Maurya, R. A.; Park, C. P.; Kim, D.-P. Triple-Channel Microreactor for Biphasic Gas-Liquid Reactions: Photosensitized Oxygenations. *Beilstein J. Org. Chem.* **2011**, *7*, 1158−1163.
(468) Wootton, R. C. R.; Fortt, R.; de Mello, A. J. A Microfabricated Nanoreactor for Safe, Continuous Generation and Use of Singlet Oxygen. *Org. Process Res. Dev.* **2002**, *6*, 187−189.
(469) Loponov, K. N.; Lopes, J.; Barlog, M.; Astrova, V. E.; Malkov, V. A.; Lapkin, A. A. Optimization of a Scalable Photochemical Reactor for Reactions with Singlet Oxygen. *Org. Process Res. Dev.* **2014**, *18*, 1443−1454.
(470) Gu, X.; Li, X.; Chai, Y.; Yang, Q.; Li, P.; Yao, Y. A Simple Metal-Free Catalytic Sulfoxidation under Visible Light and Air. *Green Chem.* **2013**, *15*, 357−361.
(471) Colomer, J. P.; Traverssi, M.; Oksdath-Mansilla, G. Oxidation of Organosulfur Compounds Promoted by Continuous-Flow Chemistry. *J. Flow Chem.* **2020**, *10*, 123−138.
(472) Bühler, S.; Goettert, M.; Schollmeyer, D.; Albrecht, W.; Laufer, S. A. Chiral Sulfoxides as Metabolites of 2-Thioimidazole-Based P38α Mitogen-Activated Protein Kinase Inhibitors: Enantioselective Synthesis and Biological Evaluation. *J. Med. Chem.* **2011**, *54*, 3283−3297.
(473) Mendoza, C.; Emmanuel, N.; Páez, C. A.; Dreesen, L.; Monbaliu, J.-C. M.; Heinrichs, B. Transitioning from Conventional Batch to Microfluidic Processes for the Efficient Singlet Oxygen Photooxygenation of Methionine. *J. Photochem. Photobiol., A* **2018**, *356*, 193−200.
(474) Emmanuel, N.; Mendoza, C.; Winter, M.; Horn, C. R.; Vizza, A.; Dreesen, L.; Heinrichs, B.; Monbaliu, J.-C. M. Scalable Photocatalytic Oxidation of Methionine under Continuous-Flow Conditions. *Org. Process Res. Dev.* **2017**, *21*, 1435−1438.
(475) Mendoza, C.; Désert, A.; Chateau, D.; Monnereau, C.; Khrouz, L.; Lerouge, F.; Andraud, C.; Monbaliu, J.-C. M.; Parola, S.; Heinrichs, B. Au Nanobipyramids@mSiO_2 Core-Shell Nanoparticles for Plasmon-Enhanced Singlet Oxygen Photooxygenations in Segmented Flow Microreactors. *Nanoscale Adv.* **2020**, *2*, 5280−5287.
(476) Emmanuel, N.; Bianchi, P.; Legros, J.; Monbaliu, J.-C. M. A Safe and Compact Flow Platform for the Neutralization of a Mustard Gas Simulant with Air and Light. *Green Chem.* **2020**, *22*, 4105−4115.
(477) Radjagobalou, R.; Blanco, J.-F.; Dechy-Cabaret, O.; Oelgemöller, M.; Loubière, K. Photooxygenation in an Advanced Led-Driven Flow Reactor Module: Experimental Investigations and Modelling. *Chem. Eng. Process.* **2018**, *130*, 214−228.
(478) Shvydkiv, O.; Jähnisch, K.; Steinfeldt, N.; Yavorskyy, A.; Oelgemöller, M. Visible-Light Photooxygenation of α-Terpinene in a Falling Film Microreactor. *Catal. Today* **2018**, *308*, 102−118.
(479) Zanfir, M.; Gavriilidis, A.; Wille, C.; Hessel, V. Carbon Dioxide Absorption in a Falling Film Microstructured Reactor: Experiments and Modeling. *Ind. Eng. Chem. Res.* **2005**, *44*, 1742−1751.
(480) Behm, K.; Fazekas, E.; Paterson, M. J.; Vilela, F.; McIntosh, R. D. Discrete Ti-O-Ti Complexes: Visible-Light-Activated, Homogeneous Alternative to TiO_2 Photosensitisers. *Chem. - Eur. J.* **2020**, *26*, 9486−9494.
(481) Masuda, K.; Ichitsuka, T.; Koumura, N.; Sato, K.; Kobayashi, S. Flow Fine Synthesis with Heterogeneous Catalysts. *Tetrahedron* **2018**, *74*, 1705−1730.
(482) Franchi, D.; Amara, Z. Applications of Sensitized Semiconductors as Heterogeneous Visible-Light Photocatalysts in Organic Synthesis. *ACS Sustainable Chem. Eng.* **2020**, *8*, 15405−15429.
(483) Thomson, C. G.; Lee, A.-L.; Vilela, F. Heterogeneous Photocatalysis in Flow Chemical Reactors. *Beilstein J. Org. Chem.* **2020**, *16*, 1495−1549.
(484) Riente, P.; Noël, T. Application of Metal Oxide Semiconductors in Light-Driven Organic Transformations. *Catal. Sci. Technol.* **2019**, *9*, 5186−5232.
(485) Radjagobalou, R.; Blanco, J.-F.; Petrizza, L.; Le Bechec, M.; Dechy-Cabaret, O.; Lacombe, S.; Save, M.; Loubiere, K. Efficient Photooxygenation Process of Biosourced α-Terpinene by Combining Controlled LED-Driven Flow Photochemistry and Rose Bengal-Anchored Polymer Colloids. *ACS Sustainable Chem. Eng.* **2020**, *8*, 18568−18576.
(486) Mendoza, C.; Emmanuel, N.; Páez, C. A.; Dreesen, L.; Monbaliu, J.-C. M.; Heinrichs, B. Improving Continuous Flow Singlet Oxygen Photooxygenation Reactions with Functionalized Mesoporous Silica Nanoparticles. *ChemPhotoChem.* **2018**, *2*, 890−897.
(487) Masuda, K.; Wang, Y.; Onozawa, S.; Shimada, S.; Koumura, N.; Sato, K.; Kobayashi, S. Robust Organic Photosensitizers Immobilized on a Vinylimidazolium Functionalized Support for Singlet Oxygen Generation under Continuous-Flow Conditions. *Synlett* **2020**, *31*, 497−501.
(488) Lévesque, F.; Seeberger, P. H. Continuous-Flow Synthesis of the Anti-Malaria Drug Artemisinin. *Angew. Chem., Int. Ed.* **2012**, *51*, 1706−1709.
(489) Tobin, J. M.; Liu, J.; Hayes, H.; Demleitner, M.; Ellis, D.; Arrighi, V.; Xu, Z.; Vilela, F. BODIPY-Based Conjugated Microporous Polymers as Reusable Heterogeneous Photosensitisers in a Photochemical Flow Reactor. *Polym. Chem.* **2016**, *7*, 6662−6670.
(490) Thomson, C. G.; Jones, C. M. S.; Rosair, G.; Ellis, D.; Marques-Hueso, J.; Lee, A.-L.; Vilela, F. Continuous-Flow Synthesis and Application of Polymer-Supported BODIPY Photosensitisers for the Generation of Singlet Oxygen; Process Optimised by in-Line NMR Spectroscopy. *J. Flow Chem.* **2020**, *10*, 327−345.
(491) Tobin, J. M.; McCabe, T. J. D.; Prentice, A. W.; Holzer, S.; Lloyd, G. O.; Paterson, M. J.; Arrighi, V.; Cormack, P. A. G.; Vilela, F. Polymer-Supported Photosensitizers for Oxidative Organic Transformations in Flow and under Visible Light Irradiation. *ACS Catal.* **2017**, *7*, 4602−4612.
(492) Valverde, D.; Porcar, R.; Izquierdo, D.; Burguete, M. I.; Garcia-Verdugo, E.; Luis, V. S. Rose Bengal Immobilized on Supported Ionic-Liquid-like Phases: An Efficient Photocatalyst for Batch and Flow Processes. *ChemSusChem* **2019**, *12*, 3996−4004.
(493) Rybicka-Jasińska, K.; Shan, W.; Zawada, K.; Kadish, K. M.; Gryko, D. Porphyrins as Photoredox Catalysts: Experimental and Theoretical Studies. *J. Am. Chem. Soc.* **2016**, *138*, 15451−15458.
(494) Costa e Silva, R.; Oliveira da Silva, L.; de Andrade Bartolomeu, A.; Brocksom, T. J.; de Oliveira, K. T. Recent Applications of Porphyrins as Photocatalysts in Organic Synthesis: Batch and Continuous Flow Approaches. *Beilstein J. Org. Chem.* **2020**, *16*, 917−955.
(495) de Oliveira, K. T.; Miller, L. Z.; McQuade, D. T. Exploiting Photooxygenations Mediated by Porphyrinoid Photocatalysts under Continuous Flow Conditions. *RSC Adv.* **2016**, *6*, 12717−12725.
(496) Blanchard, V.; Asbai, Z.; Cottet, K.; Boissonnat, G.; Port, M.; Amara, Z. Continuous Flow Photo-Oxidations Using Supported Photocatalysts on Silica. *Org. Process Res. Dev.* **2020**, *24*, 822−826.
(497) Hamami, Z. E.; Vanoye, L.; Fongarland, P.; de Bellefon, C.; Favre-Réguillon, A. Improved Reactor Productivity for the Safe Photo-Oxidation of Citronellol Under Visible Light LED Irradiation. *ChemPhotoChem.* **2019**, *3*, 122−128.
(498) Bayer, P.; Jacobi von Wangelin, A. An Entirely Solvent-Free Photooxygenation of Olefins under Continuous Flow Conditions. *Green Chem.* **2020**, *22*, 2359−2364.
(499) Worrall, D. R.; Abdel-Shafi, A. A.; Wilkinson, F. Factors Affecting the Rate of Decay of the First Excited Singlet State of Molecular Oxygen $O_2(a^1\Delta_g)$ in Supercritical Fluid Carbon Dioxide. *J. Phys. Chem. A* **2001**, *105*, 1270−1276.
(500) Wu, L.; Abada, Z.; Lee, D. S.; Poliakoff, M.; George, M. W. Combining Engineering and Chemistry for the Selective Continuous

https://doi.org/10.1021/acs.chemrev.1c00332
Chem. Rev. 2022, 122, 2752−2906

Production of Four Different Oxygenated Compounds by Photo-Oxidation of Cyclopentadiene Using Liquid and Supercritical CO_2 as Solvents. *Tetrahedron* **2018**, *74*, 3107−3112.
(501) Wu, L.; Lee, D. S.; Boufroura, H.; Poliakoff, M.; George, M. W. Photooxidation of Fulvenes in a Continuous Flow Photoreactor Using Carbon Dioxide as a Solvent. *ChemPhotoChem.* **2018**, *2*, 509.
(502) Herrero-Gomez, E.; van der Loo, C. H. M.; Huck, L.; Rioz-Martínez, A.; Keene, N. F.; Li, B.; Pouwer, K.; Allais, C. Photo-Oxidation of Cyclopentadiene Using Continuous Processing: Application to the Synthesis of (1R,4S)-4-Hydroxycyclopent-2-En-1-Yl Acetate. *Org. Process Res. Dev.* **2020**, *24*, 2304−2310.
(503) Das, S.; Chandrasekhar, S.; Yadav, J. S.; Grée, R. Recent Developments in the Synthesis of Prostaglandins and Analogues. *Chem. Rev.* **2007**, *107*, 3286−3337.
(504) Tang, X.-F.; Zhao, J.-N.; Wu, Y.-F.; Zheng, Z.-H.; Feng, S.-H.; Yu, Z.-Y.; Liu, G.-Z.; Meng, Q.-W. Enantioselective Photooxygenation of β-Dicarbonyl Compounds in Batch and Flow Photomicroreactors. *Org. Biomol. Chem.* **2019**, *17*, 7938−7942.
(505) Yu, T.; Ding, Z.; Nie, W.; Jiao, J.; Zhang, H.; Zhang, Q.; Xue, C.; Duan, X.; Yamada, Y. M. A.; Li, P. Recent Advances in Continuous-Flow Enantioselective Catalysis. *Chem. - Eur. J.* **2020**, *26*, 5729−5747.
(506) Tang, X.-F.; Zhao, J.-N.; Wu, Y.-F.; Feng, S.-H.; Yang, F.; Yu, Z.-Y.; Meng, Q.-W. Visible-Light-Driven Enantioselective Aerobic Oxidation of β-Dicarbonyl Compounds Catalyzed by Cinchona-Derived Phase Transfer Catalysts in Batch and Semi-Flow. *Adv. Synth. Catal.* **2019**, *361*, 5245−5252.
(507) Polyzos, A.; O'Brien, M.; Petersen, T. P.; Baxendale, I. R.; Ley, V. S. The Continuous-Flow Synthesis of Carboxylic Acids Using CO2 in a Tube-In-Tube Gas Permeable Membrane Reactor. *Angew. Chem.* **2011**, *123*, 1222−1225.
(508) Noël, T.; Hessel, V. Membrane Microreactors: Gas-Liquid Reactions Made Easy. *ChemSusChem* **2013**, *6*, 405−407.
(509) Kouridaki, A.; Huvaere, K. Singlet Oxygen Oxidations in Homogeneous Continuous Flow Using a Gas-Liquid Membrane Reactor. *React. Chem. Eng.* **2017**, *2*, 590−597.
(510) Elvira, K. S.; Wootton, R. C. R.; Reis, N. M.; Mackley, M. R.; deMello, A. J. Through-Wall Mass Transport as a Modality for Safe Generation of Singlet Oxygen in Continuous Flows. *ACS Sustainable Chem. Eng.* **2013**, *1*, 209−213.
(511) Park, C. P.; Maurya, R. A.; Lee, J. H.; Kim, D.-P. Efficient Photosensitized Oxygenations in Phase Contact Enhanced Micro-reactors. *Lab Chip* **2011**, *11*, 1941−1945.
(512) Yang, L.; Jensen, K. F. Mass Transport and Reactions in the Tube-in-Tube Reactor. *Org. Process Res. Dev.* **2013**, *17*, 927−933.
(513) Aguillón, A. R.; Leão, R. A. C.; de Oliveira, K. T.; Brocksom, T. J.; Miranda, L. S. M.; de Souza, R. O. M. A. Process Intensification for Obtaining a Cannabidiol Intermediate by Photo-Oxygenation of Limonene under Continuous-Flow Conditions. *Org. Process Res. Dev.* **2020**, *24*, 2017−2024.
(514) Kornblum, N.; DeLaMare, H. E. THE BASE CATALYZED DECOMPOSITION OF A DIALKYL PEROXIDE. *J. Am. Chem. Soc.* **1951**, *73*, 880−881.
(515) Seebach, D. Methods of Reactivity Umpolung. *Angew. Chem., Int. Ed. Engl.* **1979**, *18*, 239−258.
(516) Kelly, D. R.; Bansal, H.; Morgan, J. J. G. The Mechanism of the Tertiary Amine Catalysed Isomerisation of Endoperoxides to Hydroxyketones: Synthesis and Chemistry of the Intermediate Postulated in the Peroxide Attack Mechanism. *Tetrahedron Lett.* **2002**, *43*, 9331−9333.
(517) de Souza, J. M.; Brocksom, T. J.; McQuade, D. T.; de Oliveira, K. T. Continuous Endoperoxidation of Conjugated Dienes and Subsequent Rearrangements Leading to C-H Oxidized Synthons. *J. Org. Chem.* **2018**, *83*, 7574−7585.
(518) Bayer, P.; Schachtner, J.; Májek, M.; Jacobi von Wangelin, A. Visible Light-Mediated Photo-Oxygenation of Arylcyclohexenes. *Org. Chem. Front.* **2019**, *6*, 2877−2883.
(519) Kopetzki, D.; Lévesque, F.; Seeberger, P. H. A Continuous-Flow Process for the Synthesis of Artemisinin. *Chem. - Eur. J.* **2013**, *19*, 5450−5456.
(520) Triemer, S.; Gilmore, K.; Vu, G. T.; Seeberger, P. H.; Seidel-Morgenstern, A. Literally Green Chemical Synthesis of Artemisinin from Plant Extracts. *Angew. Chem., Int. Ed.* **2018**, *57*, 5525−5528.
(521) Tasker, N. R.; Rastelli, E. J.; Blanco, I. K.; Burnett, J. C.; Sharlow, E. R.; Lazo, J. S.; Wipf, P. In-Flow Photooxygenation of Aminothienopyridinones Generates Iminopyridinedione PTP4A3 Phosphatase Inhibitors. *Org. Biomol. Chem.* **2019**, *17*, 2448−2466.
(522) Xu, H.-X.; Zhao, Z.-R.; Patehebieke, Y.; Chen, Q.-Q.; Fu, S.-G.; Chang, S.-J.; Zhang, X.-X.; Zhang, Z.-L.; Wang, X. Continuous-Flow Step-Economical Synthesis of Thiuram Disulfides via Visible-Light Photocatalytic Aerobic Oxidation. *Green Chem.* **2021**, *23*, 1280−1285.
(523) Wellauer, J.; Miladinov, D.; Buchholz, T.; Schütz, J.; Stemmler, R. T.; Medlock, J. A.; Bonrath, W.; Sparr, C. Organo-photocatalytic Aerobic Oxygenation of Phenols in a Visible-Light Continuous-Flow Photoreactor. *Chem. - Eur. J.* **2021**, *27*, 9748.
(524) Wuts, P. G. M.; Greene, T. W. *Greene's Protective Groups in Organic Synthesis*; John Wiley & Sons, Inc.: Hoboken, NJ, USA, 2006.
(525) Sartori, G.; Ballini, R.; Bigi, F.; Bosica, G.; Maggi, R.; Righi, P. Protection (and Deprotection) of Functional Groups in Organic Synthesis by Heterogeneous Catalysis. *Chem. Rev.* **2004**, *104*, 199−250.
(526) Schelhaas, M.; Waldmann, H. Protecting Group Strategies in Organic Synthesis. *Angew. Chem., Int. Ed. Engl.* **1996**, *35*, 2056−2083.
(527) Klán, P.; Šolomek, T.; Bochet, C. G.; Blanc, A.; Givens, R.; Rubina, M.; Popik, V.; Kostikov, A.; Wirz, J. Photoremovable Protecting Groups in Chemistry and Biology: Reaction Mechanisms and Efficacy. *Chem. Rev.* **2013**, *113*, 119−191.
(528) Tebikachew, B. E.; Borjesson, K.; Kann, N.; Moth-Poulsen, K.; et al. Release of Terminal Alkynes via Tandem Photodeprotection and Decarboxylation of O-Nitrobenzyl Arylpropiolates in a Flow Micro-channel Reactor. *Bioconjugate Chem.* **2018**, *29*, 1178.
(529) Sachse, F.; Gebauer, K.; Schneider, C. Continuous Flow Synthesis of 2H-Thiopyrans via Thia-Diels-Alder Reactions of Photochemically Generated Thioaldehydes. *Eur. J. Org. Chem.* **2021**, *2021*, 2.
(530) Hunter, C. J.; Boyd, M. J.; May, G. D.; Fimognari, R. Visible-Light-Mediated N-Desulfonylation of N-Heterocycles Using a Heteroleptic Copper(I) Complex as a Photocatalyst. *J. Org. Chem.* **2020**, *85*, 8732−8739.
(531) Magallanes, G.; Kärkäs, M. D.; Bosque, I.; Lee, S.; Maldonado, S.; Stephenson, C. R. J. Selective C-O Bond Cleavage of Lignin Systems and Polymers Enabled by Sequential Palladium-Catalyzed Aerobic Oxidation and Visible-Light Photoredox Catalysis. *ACS Catal.* **2019**, *9*, 2252−2260.
(532) Eller, S.; Collot, M.; Yin, J.; Hahm, H. S.; Seeberger, P. H. Automated Solid-Phase Synthesis of Chondroitin Sulfate Glycosaminoglycans. *Angew. Chem., Int. Ed.* **2013**, *52*, 5858−5861.
(533) Kandasamy, J.; Schuhmacher, F.; Hahm, H. S.; Klein, J. C.; Seeberger, P. H. Modular Automated Solid Phase Synthesis of Dermatan Sulfate Oligosaccharides. *Chem. Commun.* **2014**, *50*, 1875−1877.
(534) Fair, R. J.; Hahm, H. S.; Seeberger, P. H. Combination of Automated Solid-Phase and Enzymatic Oligosaccharide Synthesis Provides Access to α(2,3)-Sialylated Glycans. *Chem. Commun.* **2015**, *51*, 6183−6185.
(535) Wilsdorf, M.; Schmidt, D.; Bartetzko, M. P.; Dallabernardina, P.; Schuhmacher, F.; Seeberger, P. H.; Pfrengle, F. A Traceless Photocleavable Linker for the Automated Glycan Assembly of Carbohydrates with Free Reducing Ends. *Chem. Commun.* **2016**, *52*, 10187−10189.
(536) Naresh, K.; Schumacher, F.; Hahm, H. S.; Seeberger, P. H. Pushing the Limits of Automated Glycan Assembly: Synthesis of a 50mer Polymannoside. *Chem. Commun.* **2017**, *53*, 9085−9088.
(537) Budhadev, D.; Saxby, K.; Walton, J.; Davies, G.; Tyler, P. C.; Schwörer, R.; Fascione, M. A. Using Automated Glycan Assembly

https://doi.org/10.1021/acs.chemrev.1c00332
Chem. Rev. 2022, 122, 2752−2906

(AGA) for the Practical Synthesis of Heparan Sulfate Oligosaccharide Precursors. *Org. Biomol. Chem.* **2019**, *17*, 1817−1821.
(538) Le Mai Hoang, K.; Pardo-Vargas, A.; Zhu, Y.; Yu, Y.; Loria, M.; Delbianco, M.; Seeberger, P. H. Traceless Photolabile Linker Expedites the Chemical Synthesis of Complex Oligosaccharides by Automated Glycan Assembly. *J. Am. Chem. Soc.* **2019**, *141*, 9079.
(539) Bakhatan, Y.; Alshanski, I.; Grunhaus, D.; Hurevich, M. The Breaking Beads Approach for Photocleavage from Solid Support. *Org. Biomol. Chem.* **2020**, *18*, 4183−4188.
(540) Teschers, C. S.; Gilmour, R. Flow Photocleavage for Automated Glycan Assembly (AGA). *Org. Process Res. Dev.* **2020**, *24*, 2234−2239.
(541) Hahm, H. S.; Schlegel, M. K.; Hurevich, M.; Eller, S.; Schuhmacher, F.; Hofmann, J.; Pagel, K.; Seeberger, P. H. Automated Glycan Assembly Using the Glyconeer 2.1 Synthesizer. *Proc. Natl. Acad. Sci. U. S. A.* **2017**, *114*, E3385−E3389.
(542) Cavedon, C.; Sletten, E. T.; Madani, A.; Niemeyer, O.; Seeberger, P. H.; Pieber, B. Visible-Light-Mediated Oxidative Debenzylation Enables the Use of Benzyl Ethers as Temporary Protecting Groups. *Org. Lett.* **2021**, *23*, 514−518.
(543) Matsuoka, T.; Inuki, S.; Miyagawa, T.; Oishi, S.; Ohno, H. Total Synthesis of (+)-Polyoxamic Acid via Visible-Light-Mediated Photocatalytic β-Scission and 1,5-Hydrogen Atom Transfer of Glucose Derivative. *J. Org. Chem.* **2020**, *85*, 8271−8278.
(544) Gérardy, R.; Winter, M.; Vizza, A.; Monbaliu, J.-C. M. Assessing Inter- and Intramolecular Continuous-Flow Strategies towards Methylphenidate (Ritalin) Hydrochloride. *React. Chem. Eng.* **2017**, *2*, 149−158.
(545) Zhou, Y.; Wang, J.; Gu, Z.; Wang, S.; Zhu, W.; Aceña, J. L.; Soloshonok, V. A.; Izawa, K.; Liu, H. Next Generation of Fluorine-Containing Pharmaceuticals, Compounds Currently in Phase II-III Clinical Trials of Major Pharmaceutical Companies: New Structural Trends and Therapeutic Areas. *Chem. Rev.* **2016**, *116*, 422−518.
(546) Ameduri, B.; Sawada, H. *Fluorinated Polymers*, Polymer Chemistry Series; The Royal Society of Chemistry, 2017.
(547) Améduri, B. The Promising Future of Fluoropolymers. *Macromol. Chem. Phys.* **2020**, *221*, 1900573.
(548) Han, J.; Kiss, L.; Mei, H.; Remete, A. M.; Ponikvar-Svet, M.; Sedgwick, D. M.; Roman, R.; Fustero, S.; Moriwaki, H.; Soloshonok, V. A. Chemical Aspects of Human and Environmental Overload with Fluorine. *Chem. Rev.* **2021**, *121*, 4678.
(549) Wang, X.; Lei, J.; Liu, Y.; Ye, Y.; Li, J.; Sun, K. Fluorination and Fluoroalkylation of Alkenes/Alkynes to Construct Fluoro-Containing Heterocycles. *Org. Chem. Front.* **2021**, *8*, 2079.
(550) Cannalire, R.; Pelliccia, S.; Sancineto, L.; Novellino, E.; Tron, G. C.; Giustiniano, M. Visible Light Photocatalysis in the Late-Stage Functionalization of Pharmaceutically Relevant Compounds. *Chem. Soc. Rev.* **2021**, *50*, 766−897.
(551) Nobile, E.; Castanheiro, T.; Besset, T. Radical-Promoted Distal C-H Functionalization of C(sp^3) Centers with Fluorinated Moieties. *Angew. Chem., Int. Ed.* **2021**, *60*, 12170.
(552) Carvalho, D. R.; Christian, A. H. Modern Approaches towards the Synthesis of Geminal Difluoroalkyl Groups. *Org. Biomol. Chem.* **2021**, *19*, 947−964.
(553) Rehm, T. H. Photochemical Fluorination Reactions - A Promising Research Field for Continuous-Flow Synthesis. *Chem. Eng. Technol.* **2016**, *39*, 66−80.
(554) Yakubov, S.; Barham, J. P. Photosensitized Direct C-H Fluorination and Trifluoromethylation in Organic Synthesis. *Beilstein J. Org. Chem.* **2020**, *16*, 2151−2192.
(555) Rehm, T. H.; Hofmann, C.; Reinhard, D.; Kost, H.-J.; Löb, P.; Besold, M.; Welzel, K.; Barten, J.; Didenko, A.; Sevenard, V. D.; et al. Continuous-Flow Synthesis of Fluorine-Containing Fine Chemicals with Integrated Benchtop NMR Analysis. *React. Chem. Eng.* **2017**, *2*, 315−323.
(556) Nyffeler, P. T.; Durón, S. G.; Burkart, M. D.; Vincent, S. P.; Wong, C.-H. Selectfluor: Mechanistic Insight and Applications. *Angew. Chem., Int. Ed.* **2005**, *44*, 192−212.
(557) Stavber, S. Recent Advances in the Application of SelectfluorTM F-TEDA-BF4 as a Versatile Mediator or Catalyst in Organic Synthesis. *Molecules* **2011**, *16*, 6432.
(558) Guyon, H.; Cahard, D. Selectfluor and Its Analogs Electrophilic Fluorination for Preparing Alkyl Fluorides. In *Fluorination*; Hu, J., Umemoto, T., Eds.; Springer: Singapore, 2018; pp 1−24.
(559) Bume, D. D.; Harry, S. A.; Pitts, C. R.; Lectka, T. Sensitized Aliphatic Fluorination Directed by Terpenoidal Enones: A "Visible Light" Approach. *J. Org. Chem.* **2018**, *83*, 1565−1575.
(560) Pitts, C. R.; Bume, D. D.; Harry, S. A.; Siegler, M. A.; Lectka, T. Multiple Enone-Directed Reactivity Modes Lead to the Selective Photochemical Fluorination of Polycyclic Terpenoid Derivatives. *J. Am. Chem. Soc.* **2017**, *139*, 2208−2211.
(561) Pieber, B.; Shalom, M.; Antonietti, M.; Seeberger, P. H.; Gilmore, K. Continuous Heterogeneous Photocatalysis in Serial Micro-Batch Reactors. *Angew. Chem., Int. Ed.* **2018**, *57*, 9976−9979.
(562) Shalom, M.; Guttentag, M.; Fettkenhauer, C.; Inal, S.; Neher, D.; Llobet, A.; Antonietti, M. In Situ Formation of Heterojunctions in Modified Graphitic Carbon Nitride: Synthesis and Noble Metal Free Photocatalysis. *Chem. Mater.* **2014**, *26*, 5812−5818.
(563) Ni, C.; Hu, M.; Hu, J. Good Partnership between Sulfur and Fluorine: Sulfur-Based Fluorination and Fluoroalkylation Reagents for Organic Synthesis. *Chem. Rev.* **2015**, *115*, 765−825.
(564) McTeague, T. A.; Jamison, T. F. Photoredox Activation of SF_6 for Fluorination. *Angew. Chem., Int. Ed.* **2016**, *55*, 15072−15075.
(565) Kim, S.; Khomutnyk, Y.; Bannykh, A.; Nagorny, P. Synthesis of Glycosyl Fluorides by Photochemical Fluorination with Sulfur(VI) Hexafluoride. *Org. Lett.* **2021**, *23*, 190−194.
(566) Barata-Vallejo, S.; Bonesi, S. M.; Postigo, A. Photocatalytic Fluoroalkylation Reactions of Organic Compounds. *Org. Biomol. Chem.* **2015**, *13*, 11153−11183.
(567) Yerien, D. E.; Barata-Vallejo, S.; Postigo, A. New Visible Light Organo(Metal)-Photocatalyzed Fluoroalkylsulfanylation (R_FS-) and Fluoroalkylselenolation (R_FSe-) Reactions of Organic Substrates. *J. Fluorine Chem.* **2020**, *240*, 109652.
(568) Barata-Vallejo, S.; Cooke, M. V.; Postigo, A. Radical Fluoroalkylation Reactions. *ACS Catal.* **2018**, *8*, 7287−7307.
(569) Straathof, N. J. W. W.; Su, Y.; Hessel, V.; Noël, T. Accelerated Gas-Liquid Visible Light Photoredox Catalysis with Continuous-Flow Photochemical Microreactors. *Nat. Protoc.* **2016**, *11*, 10−21.
(570) Straathof, N. J. W.; Gemoets, H. P. L.; Wang, X.; Schouten, J. C.; Hessel, V.; Noël, T. Rapid Trifluoromethylation and Perfluoroalkylation of Five-Membered Heterocycles by Photoredox Catalysis in Continuous Flow. *ChemSusChem* **2014**, *7*, 1612−1617.
(571) Straathof, N.; Osch, D.; Schouten, A.; Wang, X.; Schouten, J.; Hessel, V.; Noël, T. Visible Light Photocatalytic Metal-Free Perfluoroalkylation of Heteroarenes in Continuous Flow. *J. Flow Chem.* **2015**, *4*, 12−17.
(572) Bottecchia, C.; Martín, R.; Abdiaj, I.; Crovini, E.; Alcazar, J.; Orduna, J.; Blesa, M. J.; Carrillo, J. R.; Prieto, P.; Noël, T. De Novo Design of Organic Photocatalysts: Bithiophene Derivatives for the Visible-Light Induced C-H Functionalization of Heteroarenes. *Adv. Synth. Catal.* **2019**, *361*, 945−950.
(573) Straathof, N. J. W.; Cramer, S. E.; Hessel, V.; Noël, T. Practical Photocatalytic Trifluoromethylation and Hydrotrifluoromethylation of Styrenes in Batch and Flow. *Angew. Chem., Int. Ed.* **2016**, *55*, 15549−15553.
(574) Rosso, C.; Williams, J. D.; Filippini, G.; Prato, M.; Kappe, C. O. Visible-Light-Mediated Iodoperfluoroalkylation of Alkenes in Flow and Its Application to the Synthesis of a Key Fulvestrant Intermediate. *Org. Lett.* **2019**, *21*, 5341−5345.
(575) Rosso, C.; Filippini, G.; Cozzi, P. G.; Gualandi, A.; Prato, M. Highly Performing Iodoperfluoroalkylation of Alkenes Triggered by the Photochemical Activity of Perylene Diimides. *ChemPhotoChem.* **2019**, *3*, 193−197.
(576) Bundred, N.; Howell, A. Fulvestrant (Faslodex™): Current Status in the Therapy of Breast Cancer. *Expert Rev. Anticancer Ther.* **2002**, *2*, 151−160.

https://doi.org/10.1021/acs.chemrev.1c00332
Chem. Rev. 2022, 122, 2752−2906

(577) Wei, X.-J.; Noël, T. Visible-Light Photocatalytic Difluoroalkylation-Induced 1, 2-Heteroarene Migration of Allylic Alcohols in Batch and Flow. *J. Org. Chem.* **2018**, *83*, 11377−11384.
(578) Soloshonok, V.; Kukhar, V.; Pustovit, Y.; Nazaretian, V. A New and Convenient Synthesis of S-Trifluoromethyl-Containing Amino Acids. *Synlett* **1992**, *1992*, 657−658.
(579) Abdiaj, I.; Bottecchia, C.; Alcazar, J.; Noël, T. Visible-Light-Induced Trifluoromethylation of Highly Functionalized Arenes and Heteroarenes in Continuous Flow. *Synthesis* **2017**, *49*, 4978−4985.
(580) Zhang, X.; Li, Y.; Hao, X.; Jin, K.; Zhang, R.; Duan, C. Recyclable Alkylated $Ru(Bpy)_3^{2+}$ Complex as a Visible-Light Photoredox Catalyst for Perfluoroalkylation. *Tetrahedron* **2018**, *74*, 1742−1748.
(581) Zhuang, K.; Cui, Y.; Yuan, X.; Qin, L.; Sun, Q.; Duan, X.; Chen, L.; Zhang, X.; Qiu, J.; Guo, K. Visible-Light-Induced Trifluoromethylation/Cyclization of 1,7-Enynes in Continuous Flow. *ACS Sustainable Chem. Eng.* **2020**, *8*, 11729−11736.
(582) Yuan, X.; Duan, X.; Cui, Y.-S.; Sun, Q.; Qin, L.-Z.; Zhang, X.-P.; Liu, J.; Wu, M.-Y.; Qiu, J.-K.; Guo, K. Visible-Light Photocatalytic Tri- and Difluoroalkylation Cyclizations: Access to a Series of Indole[2,1-a]Isoquinoline Derivatives in Continuous Flow. *Org. Lett.* **2021**, *23*, 1950−1954.
(583) Batista, G. M. F.; de Castro, P. P.; Dos Santos, H. F.; de Oliveira, K. T.; Amarante, G. W. Electron-Donor-Acceptor Complex-Enabled Flow Methodology for the Hydrotrifluoromethylation of Unsaturated β-Keto Esters. *Org. Lett.* **2020**, *22*, 8598−8602.
(584) Barthelemy, A.-L.; Dagousset, G.; Magnier, E. Metal-Free Visible-Light-Mediated Hydrotrifluoromethylation of Unactivated Alkenes and Alkynes in Continuous Flow. *Eur. J. Org. Chem.* **2020**, *2020*, 1429−1432.
(585) Daniel, M.; Dagousset, G.; Diter, P.; Klein, P.-A.; Tuccio, B.; Goncalves, A.-M.; Masson, G.; Magnier, E. Fluorinated Sulfilimino Iminiums: Efficient and Versatile Sources of Perfluoroalkyl Radicals under Photoredox Catalysis. *Angew. Chem., Int. Ed.* **2017**, *56*, 3997−4001.
(586) Deng, X.; Rong, J.; Wang, L.; Vasdev, N.; Zhang, L.; Josephson, L.; Liang, S. H. Chemistry for Positron Emission Tomography: Recent Advances in ^{11}C-, ^{18}F-, ^{13}N-, and ^{15}O-Labeling Reactions. *Angew. Chem., Int. Ed.* **2019**, *58*, 2580−2605.
(587) Nodwell, M. B.; Yang, H.; Čolović, M.; Yuan, Z.; Merkens, H.; Martin, R. E.; Bénard, F.; Schaffer, P.; Britton, R. ^{18}F-Fluorination of Unactivated C-H Bonds in Branched Aliphatic Amino Acids: Direct Synthesis of Oncological Positron Emission Tomography Imaging Agents. *J. Am. Chem. Soc.* **2017**, *139*, 3595−3598.
(588) Trump, L.; Lemos, A.; Lallemand, B.; Pasau, P.; Mercier, J.; Lemaire, C.; Luxen, A.; Genicot, C. Late-Stage ^{18}F-Difluoromethyl Labeling of N-Heteroaromatics with High Molar Activity for PET Imaging. *Angew. Chem., Int. Ed.* **2019**, *58*, 13149−13154.
(589) Dobson, A. T.; Little, B. B.; Scott, L. L. Prevention of Herpes Simplex Virus Infection and Latency by Prophylactic Treatment with Acyclovir in a Weanling Mouse Model. *Am. J. Obstet. Gynecol.* **1998**, *179*, 527−532.
(590) Strauss, F. J.; Cantillo, D.; Guerra, J.; Kappe, C. O. A Laboratory-Scale Continuous Flow Chlorine Generator for Organic Synthesis. *React. Chem. Eng.* **2016**, *1*, 472−476.
(591) Fukuyama, T.; Tokizane, M.; Matsui, A.; Ryu, I. A Greener Process for Flow C-H Chlorination of Cyclic Alkanes Using in Situ Generation and on-Site Consumption of Chlorine Gas. *React. Chem. Eng.* **2016**, *1*, 613−615.
(592) Kleoff, M.; Schwan, J.; Christmann, M.; Heretsch, P. A Modular, Argon-Driven Flow Platform for Natural Product Synthesis and Late-Stage Transformations. *Org. Lett.* **2021**, *23*, 2370−2374.
(593) Fan, X.; Xiao, P.; Jiao, Z.; Yang, T.; Dai, X.; Xu, W.; Tan, D. J.; Cui, G.; Su, H.; Fang, W.; et al. Neutral-Eosin-Y-Photocatalyzed Silane Chlorination Using Dichloromethane. *Angew. Chem., Int. Ed.* **2019**, *58*, 12580−12584.
(594) Cantillo, D.; de Frutos, O.; Rincon, J. A.; Mateos, C.; Kappe, C. O. A Scalable Procedure for Light-Induced Benzylic Brominations in Continuous Flow. *J. Org. Chem.* **2014**, *79*, 223−229.
(595) Chen, Y.; de Frutos, O.; Mateos, C.; Rincon, J. A.; Cantillo, D.; Kappe, C. O. Continuous Flow Photochemical Benzylic Bromination of a Key Intermediate in the Synthesis of a 2-Oxazolidinone. *ChemPhotoChem.* **2018**, *2*, 906−912.
(596) Waterford, M.; Saubern, S.; Hornung, C. H. Evaluation of a Continuous-Flow Photo-Bromination Using N-Bromosuccinimide for Use in Chemical Manufacture. *Aust. J. Chem.* **2021**, DOI: 10.1071/CH20372.
(597) Otake, Y.; Williams, J. D.; Rincón, J. A.; de Frutos, O.; Mateos, C.; Kappe, C. O. Photochemical Benzylic Bromination in Continuous Flow Using $BrCCl_3$ and Its Application to Telescoped *p*-Methoxybenzyl Protection. *Org. Biomol. Chem.* **2019**, *17*, 1384−1388.
(598) Dallinger, D.; Gutmann, B.; Kappe, C. O. The Concept of Chemical Generators: On-Site On-Demand Production of Hazardous Reagents in Continuous Flow. *Acc. Chem. Res.* **2020**, *53*, 1330−1341.
(599) Yu, W.; Yu, D.; Zheng, M.; Shan, S.; Li, Y.; Gao, J. Catalyst and Solvent-Free Bromination of Toluene Derivatives by $HBr-H_2O_2$ with Visible-Light Photocatalysis Using a Continuous-Flow Micro Reactor. *J. Chem. Res.* **2012**, *36*, 258−260.
(600) Glotz, G.; Lebl, R.; Dallinger, D.; Kappe, C. O. Integration of Bromine and Cyanogen Bromide Generators for the Continuous-Flow Synthesis of Cyclic Guanidines. *Angew. Chem., Int. Ed.* **2017**, *56*, 13786−13789.
(601) Zhou, J.; Chen, Z.; He, Y.; Lin, Z.; Wang, C.; Li, Z.; Li, J. Efficient Scale up of Photochemical Bromination of Conjugated Allylic Compounds in Continuous-Flow. *J. Flow Chem.* **2021**, *11*, 127.
(602) Baker, J. R.; Gilbert, J.; Paula, S.; Zhu, X.; Sakoff, J. A.; McCluskey, A. Dichlorophenylacrylonitriles as AhR Ligands That Display Selective Breast Cancer Cytotoxicity in Vitro. *ChemMedChem* **2018**, *13*, 1447−1458.
(603) Riente, P.; Fianchini, M.; Llanes, P.; Pericàs, M. A.; Noël, T. Shedding Light on the Nature of the Catalytically Active Species in Photocatalytic Reactions Using Bi_2O_3 Semiconductor. *Nat. Commun.* **2021**, *12*, 625.
(604) Steiner, A.; Williams, J. D.; Rincón, J. A.; de Frutos, O.; Mateos, C.; Kappe, C. O. Implementing Hydrogen Atom Transfer (HAT) Catalysis for Rapid and Selective Reductive Photoredox Transformations in Continuous Flow. *Eur. J. Org. Chem.* **2019**, *2019*, 5807−5811.
(605) Treat, N. J.; Sprafke, H.; Kramer, J. W.; Clark, P. G.; Barton, B. E.; Read de Alaniz, J.; Fors, B. P.; Hawker, C. J. Metal-Free Atom Transfer Radical Polymerization. *J. Am. Chem. Soc.* **2014**, *136*, 16096−16101.
(606) Schwarz, J.; König, B. Decarboxylative Reactions with and without Light - a Comparison. *Green Chem.* **2018**, *20*, 323−361.
(607) Hepburn, C.; Adlen, E.; Beddington, J.; Carter, E. A.; Fuss, S.; Mac Dowell, N.; Minx, J. C.; Smith, P.; Williams, C. K. The Technological and Economic Prospects for CO_2 Utilization and Removal. *Nature* **2019**, *575*, 87−97.
(608) Seo, H.; Nguyen, V. L.; Jamison, T. F. Using Carbon Dioxide as a Building Block in Continuous Flow Synthesis. *Adv. Synth. Catal.* **2019**, *361*, 247−264.
(609) Yeung, C. S. Photoredox Catalysis as a Strategy for CO_2 Incorporation: Direct Access to Carboxylic Acids from a Renewable Feedstock. *Angew. Chem., Int. Ed.* **2019**, *58*, 5492−5502.
(610) Tortajada, A.; Juliá-Hernández, F.; Börjesson, M.; Moragas, T.; Martin, R. Transition-Metal-Catalyzed Carboxylation Reactions with Carbon Dioxide. *Angew. Chem., Int. Ed.* **2018**, *57*, 15948−15982.
(611) Cao, Y.; He, X.; Wang, N.; Li, H.-R.; He, L.-N. Photochemical and Electrochemical Carbon Dioxide Utilization with Organic Compounds. *Chin. J. Chem.* **2018**, *36*, 644−659.
(612) Wei, X.-J.; Boon, W.; Hessel, V.; Noël, T. Visible-Light Photocatalytic Decarboxylation of α,β-Unsaturated Carboxylic Acids: Facile Access to Stereoselective Difluoromethylated Styrenes in Batch and Flow. *ACS Catal.* **2017**, *7*, 7136−7140.
(613) Ramirez, N. P.; König, B.; Gonzalez-Gomez, J. C. Decarboxylative Cyanation of Aliphatic Carboxylic Acids via Visible-Light Flavin Photocatalysis. *Org. Lett.* **2019**, *21*, 1368−1373.

(614) Grollier, K.; De Zordo-Banliat, A.; Bourdreux, F.; Pegot, B.; Dagousset, G.; Magnier, E.; Billard, T. (Trifluoromethylselenyl)-Methylchalcogenyl as Emerging Fluorinated Groups: Synthesis under Photoredox Catalysis and Determination of the Lipophilicity. *Chem. - Eur. J.* **2021**, *27*, No. 6028.
(615) Atzrodt, J.; Derdau, V.; Kerr, W. J.; Reid, M. Deuterium- and Tritium-Labelled Compounds: Applications in the Life Sciences. *Angew. Chem., Int. Ed.* **2018**, *57*, 1758−1784.
(616) Li, N.; Ning, Y.; Wu, X.; Xie, J.; Li, W.; Zhu, C. A Highly Selective Decarboxylative Deuteration of Carboxylic Acids. *Chem. Sci.* **2021**, *12*, 5505−5510.
(617) Inuki, S.; Sato, K.; Fukuyama, T.; Ryu, I.; Fujimoto, Y. Formal Total Synthesis of L-Ossamine via Decarboxylative Functionalization Using Visible-Light-Mediated Photoredox Catalysis in a Flow System. *J. Org. Chem.* **2017**, *82*, 1248−1253.
(618) Malik, A.; Afza, N.; Voelter, W. Stereospecific Syntheses of D-Ossamine and D-Tolyposamine. *Liebigs Ann. der Chemie* **1984**, *1984*, 636−640.
(619) Adiyala, P. R.; Jang, S.; Vishwakarma, N. K.; Hwang, Y.-H.; Kim, D.-P. Continuous-Flow Photo-Induced Decarboxylative Annulative Access to Fused Imidazole Derivatives via a Microreactor Containing Immobilized Ruthenium. *Green Chem.* **2020**, *22*, 1565−1571.
(620) Bracken, C.; Batsanov, A. S.; Baumann, M. Development of a Continuous Photochemical Benzyne-Forming Process. *SynOpen* **2021**, *5*, 29−35.
(621) Yang, Q.; Pan, G.; Wei, J.; Wang, W.; Tang, Y.; Cai, Y. Remarkable Activity of Potassium-Modified Carbon Nitride for Heterogeneous Photocatalytic Decarboxylative Alkyl/Acyl Radical Addition and Reductive Dimerization of Para-Quinone Methides. *ACS Sustainable Chem. Eng.* **2021**, *9*, 2367−2377.
(622) Huang, H.; Yu, C.; Zhang, Y.; Zhang, Y.; Mariano, P. S.; Wang, W. Chemo- and Regioselective Organo-Photoredox Catalyzed Hydroformylation of Styrenes via a Radical Pathway. *J. Am. Chem. Soc.* **2017**, *139*, 9799−9802.
(623) Huang, H.; Li, X.; Yu, C.; Zhang, Y.; Mariano, P. S.; Wang, W. Visible-Light-Promoted Nickel- and Organic-Dye-Cocatalyzed Formylation Reaction of Aryl Halides and Triflates and Vinyl Bromides with Diethoxyacetic Acid as a Formyl Equivalent. *Angew. Chem., Int. Ed.* **2017**, *56*, 1500−1505.
(624) Huang, H.; Zhang, Y.; Ji, P.; Mariano, P. S.; Wang, W. Organophotocatalyzed E and Z Stereoselective $C(Sp^3)$-$C(Sp^2)$ Bond Forming Cross Coupling Reactions of Carboxylic Acids with β-Aryl-Vinyl Halides. *Green Synth. Catal.* **2021**, *2*, 27−31.
(625) Josland, S.; Mumtaz, S.; Oelgemöller, M. Photodecarboxylations in an Advanced Meso-Scale Continuous-Flow Photoreactor. *Chem. Eng. Technol.* **2016**, *39*, 81−87.
(626) Anamimoghadam, O.; Mumtaz, S.; Nietsch, A.; Saya, G.; Motti, C. A.; Wang, J.; Junk, P. C.; Qureshi, A. M.; Oelgemöller, M. The Photodecarboxylative Addition of Carboxylates to Phthalimides as a Key-Step in the Synthesis of Biologically Active 3-Arylmethylene-2,3-Dihydro-1H-Isoindolin-1-Ones. *Beilstein J. Org. Chem.* **2017**, *13*, 2833−2841.
(627) Mumtaz, S.; Robertson, M. J.; Oelgemöller, M. Recent Advances in Photodecarboxylations Involving Phthalimides. *Aust. J. Chem.* **2018**, *71*, 634−648.
(628) Mumtaz, S.; Robertson, M. J.; Oelgemöller, M. Continuous Flow Photochemical and Thermal Multi-Step Synthesis of Bioactive 3-Arylmethylene-2,3-Dihydro-1H-Isoindolin-1-Ones. *Molecules* **2019**, *24*, 4527.
(629) Seo, H.; Katcher, M. H.; Jamison, T. F. Photoredox Activation of Carbon Dioxide for Amino Acid Synthesis in Continuous Flow. *Nat. Chem.* **2017**, *9*, 453−456.
(630) Seo, H.; Liu, A.; Jamison, T. F. Direct β-Selective Hydrocarboxylation of Styrenes with CO_2 Enabled by Continuous Flow Photoredox Catalysis. *J. Am. Chem. Soc.* **2017**, *139*, 13969−13972.
(631) Kang, G.; Romo, D. Photocatalyzed, β-Selective Hydrocarboxylation of α,β-Unsaturated Esters with CO_2 under Flow for β-Lactone Synthesis. *ACS Catal.* **2021**, *11*, 1309−1315.
(632) Mallia, C. J.; Baxendale, I. R. The Use of Gases in Flow Synthesis. *Org. Process Res. Dev.* **2016**, *20*, 327−360.
(633) Chen, G.; Yue, J.; Yuan, Q. Gas-Liquid Microreaction Technology: Recent Developments and Future Challenges. *Chin. J. Chem. Eng.* **2008**, *16*, 663−669.
(634) Zhang, Z.; Ye, J.-H.; Ju, T.; Liao, L.-L.; Huang, H.; Gui, Y.-Y.; Zhou, W.-J.; Yu, D.-G. Visible-Light-Driven Catalytic Reductive Carboxylation with CO 2. *ACS Catal.* **2020**, *10*, 10871−10885.
(635) Telmesani, R.; Park, S. H.; Lynch-Colameta, T.; Beeler, A. B. [2 + 2] Photocycloaddition of Cinnamates in Flow and Development of a Thiourea Catalyst. *Angew. Chem., Int. Ed.* **2015**, *54*, 11521−11525.
(636) Campbell, Z. S.; Han, S.; Marre, S.; Abolhasani, M. Continuous Flow Solar Desorption of CO_2 from Aqueous Amines. *ACS Sustainable Chem. Eng.* **2021**, *9*, 2570−2579.
(637) Hou, J.; Ee, A.; Cao, H.; Ong, H. W.; Xu, J. H.; Wu, J. Visible-Light-Mediated Metal-Free Difunctionalization of Alkenes with CO_2 and Silanes or $C(Sp^3)$-H Alkanes. *Angew. Chem., Int. Ed.* **2018**, *57*, 17220−17224.
(638) Noël, T.; Buchwald, S. L. Cross-Coupling in Flow. *Chem. Soc. Rev.* **2011**, *40*, 5010.
(639) Santoro, S.; Ferlin, F.; Ackermann, L.; Vaccaro, L. C-H Functionalization Reactions under Flow Conditions. *Chem. Soc. Rev.* **2019**, *48*, 2767−2782.
(640) Govaerts, S.; Nyuchev, A.; Noël, T. Pushing the Boundaries of C-H Bond Functionalization Chemistry Using Flow Technology. *J. Flow Chem.* **2020**, *10*, 13−71.
(641) Markovič, M.; Lopatka, P.; Gracza, T.; Koóš, P. Recent Applications of Continuous Flow in Homogeneous Palladium Catalysis. *Synthesis* **2020**, *52*, 3511−3529.
(642) Wang, H.; Gao, X.; Lv, Z.; Abdelilah, T.; Lei, A. Recent Advances in Oxidative R^1-H/R^2-H Cross-Coupling with Hydrogen Evolution via Photo-/Electrochemistry. *Chem. Rev.* **2019**, *119*, 6769−6787.
(643) Wei, X. J.; Abdiaj, I.; Sambiagio, C.; Li, C.; Zysman-Colman, E.; Alcázar, J.; Noël, T. Visible-Light-Promoted Iron-Catalyzed $C(Sp^2)$-$C(Sp^3)$ Kumada Cross-Coupling in Flow. *Angew. Chem., Int. Ed.* **2019**, *58*, 13030−13034.
(644) Abdiaj, I.; Fontana, A.; Gomez, M. V.; de la Hoz, A.; Alcázar, J. Visible-Light-Induced Nickel-Catalyzed Negishi Cross-Couplings by Exogenous-Photosensitizer-Free Photocatalysis. *Angew. Chem., Int. Ed.* **2018**, *57*, 8473−8477.
(645) Abdiaj, I.; Horn, C. R.; Alcazar, J. Scalability of Visible-Light-Induced Nickel Negishi Reactions: A Combination of Flow Photochemistry, Use of Solid Reagents, and In-Line NMR Monitoring. *J. Org. Chem.* **2019**, *84*, 4748−4753.
(646) Vega, J. A.; Alonso, J. M.; Méndez, G.; Ciordia, M.; Delgado, F.; Trabanco, A. A. Continuous Flow α-Arylation of N,N-Dialkylhydrazones under Visible-Light Photoredox Catalysis. *Org. Lett.* **2017**, *19*, 938−941.
(647) Ravelli, D.; Protti, S.; Fagnoni, M. Carbon-Carbon Bond Forming Reactions via Photogenerated Intermediates. *Chem. Rev.* **2016**, *116*, 9850−9913.
(648) Bergami, M.; Protti, S.; Ravelli, D.; Fagnoni, M. Flow Metal-Free Ar-C Bond Formation via Photogenerated Phenyl Cations. *Adv. Synth. Catal.* **2016**, *358*, 1164−1172.
(649) Lima, F.; Sharma, U. K.; Grunenberg, L.; Saha, D.; Johannsen, S.; Sedelmeier, J.; Van der Eycken, E. V.; Ley, S. V. A Lewis Base Catalysis Approach for the Photoredox Activation of Boronic Acids and Esters. *Angew. Chem., Int. Ed.* **2017**, *56*, 15136−15140.
(650) Chen, Y.; Zhang, J.; Tang, Z.; Sun, Y. Visible Light Catalyzed Anti-Markovnikov Hydration of Styrene to 2-Phenylethanol: From Batch to Continuous. *J. Photochem. Photobiol., A* **2020**, *392*, 112340.
(651) Hu, X.; Zhang, G.; Bu, F.; Lei, A. Visible-Light-Mediated Anti-Markovnikov Hydration of Olefins. *ACS Catal.* **2017**, *7*, 1432−1437.

https://doi.org/10.1021/acs.chemrev.1c00332
Chem. Rev. 2022, 122, 2752−2906

(652) Seo, H.; Jamison, T. F. Catalytic Generation and Use of Ketyl Radical from Unactivated Aliphatic Carbonyl Compounds. *Org. Lett.* **2019**, *21*, 10159−10163.
(653) Kahn, B. E.; Rieke, R. D. Carbonyl Coupling Reactions Using Transition Metals, Lanthanides, and Actinides. *Chem. Rev.* **1988**, *88*, 733−745.
(654) Szostak, M.; Fazakerley, N. J.; Parmar, D.; Procter, D. J. Cross-Coupling Reactions Using Samarium(II) Iodide. *Chem. Rev.* **2014**, *114*, 5959−6039.
(655) Priebbenow, D. L.; Pilkington, R. L.; Hearn, K. N.; Polyzos, A. Fluorinated Ketones as Trapping Reagents for Visible-Light-Induced Singlet Nucleophilic Carbenes. *Org. Lett.* **2021**, *23*, 2783−2789.
(656) Li, H.; Tang, X.; Pang, J. H.; Wu, X.; Yeow, E. K. L.; Wu, J.; Chiba, S. Polysulfide Anions as Visible Light Photoredox Catalysts for Aryl Cross-Couplings. *J. Am. Chem. Soc.* **2021**, *143*, 481−487.
(657) Kim, S. D.; Lee, J.; Kim, N.-J.; Park, B. Y. Visible-Light-Mediated Cross-Couplings and C-H Activation via Dual Photoredox/Transition-Metal Catalysis in Continuous-Flow Processes. *Asian J. Org. Chem.* **2019**, *8*, 1578−1587.
(658) Zhou, W.-J.; Zhang, Y.-H.; Gui, Y.-Y.; Sun, L.; Yu, D.-G. Merging Transition-Metal Catalysis with Photoredox Catalysis: An Environmentally Friendly Strategy for C-H Functionalization. *Synthesis* **2018**, *50*, 3359−3378.
(659) Gui, Y.-Y.; Sun, L.; Lu, Z.-P.; Yu, D.-G. Photoredox Sheds New Light on Nickel Catalysis: From Carbon-Carbon to Carbon-Heteroatom Bond Formation. *Org. Chem. Front.* **2016**, *3*, 522−526.
(660) Tellis, J. C.; Primer, D. N.; Molander, G. A. Single-Electron Transmetalation in Organoboron Cross-Coupling by Photoredox/Nickel Dual Catalysis. *Science* **2014**, *345*, 433−436.
(661) Zuo, Z.; Ahneman, D. T.; Chu, L.; Terrett, J. A.; Doyle, A. G.; MacMillan, D. W. C. Merging Photoredox with Nickel Catalysis: Coupling of α-Carboxyl Sp^3-Carbons with Aryl Halides. *Science* **2014**, *345*, 437−440.
(662) Lima, F.; Kabeshov, M. A.; Tran, D. N.; Battilocchio, C.; Sedelmeier, J.; Sedelmeier, G.; Schenkel, B.; Ley, S. V. Visible Light Activation of Boronic Esters Enables Efficient Photoredox $C(Sp^2)$-$C(Sp^3)$ Cross-Couplings in Flow. *Angew. Chem., Int. Ed.* **2016**, *55*, 14085−14089.
(663) DeLano, T. J.; Bandarage, U. K.; Palaychuk, N.; Green, J.; Boyd, M. J. Application of the Photoredox Coupling of Trifluoroborates and Aryl Bromides to Analog Generation Using Continuous Flow. *J. Org. Chem.* **2016**, *81*, 12525−12531.
(664) Raynor, K. D.; May, G. D.; Bandarage, U. K.; Boyd, M. J. Generation of Diversity Sets with High Sp^3 Fraction Using the Photoredox Coupling of Organotrifluoroborates and Organosilicates with Heteroaryl/Aryl Bromides in Continuous Flow. *J. Org. Chem.* **2018**, *83*, 1551−1557.
(665) Palaychuk, N.; DeLano, T. J.; Boyd, M. J.; Green, J.; Bandarage, U. K. Synthesis of Cycloalkyl Substituted 7-Azaindoles via Photoredox Nickel Dual Catalytic Cross-Coupling in Batch and Continuous Flow. *Org. Lett.* **2016**, *18*, 6180−6183.
(666) Brill, Z. G.; Ritts, C. B.; Mansoor, U. F.; Sciammetta, N. Continuous Flow Enables Metallaphotoredox Catalysis in a Medicinal Chemistry Setting: Accelerated Optimization and Library Execution of a Reductive Coupling between Benzylic Chlorides and Aryl Bromides. *Org. Lett.* **2020**, *22*, 410−416.
(667) Zhang, P.; Le, C.; MacMillan, D. W. C. Chip"; MacMillan, D. W. C. Silyl Radical Activation of Alkyl Halides in Metallaphotoredox Catalysis: A Unique Pathway for Cross-Electrophile Coupling. *J. Am. Chem. Soc.* **2016**, *138*, 8084−8087.
(668) Abdiaj, I.; Alcázar, J. Improving the Throughput of Batch Photochemical Reactions Using Flow: Dual Photoredox and Nickel Catalysis in Flow for C(Sp2)-C(Sp3) Cross-Coupling. *Bioorg. Med. Chem.* **2017**, *25*, 6190−6196.
(669) Levernier, E.; Corcé, V.; Rakotoarison, L.-M.; Smith, A.; Zhang, M.; Ognier, S.; Tatoulian, M.; Ollivier, C.; Fensterbank, L. Cross Coupling of Alkylsilicates with Acyl Chlorides via Photoredox/Nickel Dual Catalysis: A New Synthesis Method for Ketones. *Org. Chem. Front.* **2019**, *6*, 1378−1382.
(670) Hartwig, J. F.; Larsen, M. A. Undirected, Homogeneous C-H Bond Functionalization: Challenges and Opportunities. *ACS Cent. Sci.* **2016**, *2*, 281−292.
(671) Sambiagio, C.; Schönbauer, D.; Blieck, R.; Dao-Huy, T.; Pototschnig, G.; Schaaf, P.; Wiesinger, T.; Zia, M. F.; Wencel-Delord, J.; Besset, T.; et al. A Comprehensive Overview of Directing Groups Applied in Metal-Catalysed C-H Functionalisation Chemistry. *Chem. Soc. Rev.* **2018**, *47*, 6603−6743.
(672) Yamaguchi, J.; Yamaguchi, A. D.; Itami, K. C-H Bond Functionalization: Emerging Synthetic Tools for Natural Products and Pharmaceuticals. *Angew. Chem., Int. Ed.* **2012**, *51*, 8960−9009.
(673) Cernak, T.; Dykstra, K. D.; Tyagarajan, S.; Vachal, P.; Krska, S. W. The Medicinal Chemist's Toolbox for Late Stage Functionalization of Drug-like Molecules. *Chem. Soc. Rev.* **2016**, *45*, 546−576.
(674) Capaldo, L.; Quadri, L. L.; Ravelli, D. Photocatalytic Hydrogen Atom Transfer: The Philosopher's Stone for Late-Stage Functionalization? *Green Chem.* **2020**, *22*, 3376−3396.
(675) Amos, S. G. E.; Garreau, M.; Buzzetti, L.; Waser, J. Photocatalysis with Organic Dyes: Facile Access to Reactive Intermediates for Synthesis. *Beilstein J. Org. Chem.* **2020**, *16*, 1163−1187.
(676) Yan, D.-M.; Chen, J.-R.; Xiao, W.-J. New Roles for Photoexcited Eosin Y in Photochemical Reactions. *Angew. Chem., Int. Ed.* **2019**, *58*, 378−380.
(677) Fan, X.-Z.; Rong, J.-W.; Wu, H.-L.; Zhou, Q.; Deng, H.-P.; Tan, D. J.; Xue, C.-W.; Wu, L.-Z.; Tao, H.-R.; Wu, J. Eosin Y as a Direct Hydrogen-Atom Transfer Photocatalyst for the Functionalization of C-H Bonds. *Angew. Chem., Int. Ed.* **2018**, *57*, 8514−8518.
(678) Hu, A.; Guo, J.-J.; Pan, H.; Zuo, Z. Selective Functionalization of Methane, Ethane, and Higher Alkanes by Cerium Photocatalysis. *Science* **2018**, *361*, 668−672.
(679) Yang, Q.; Wang, Y.-H.; Qiao, Y.; Gau, M.; Carroll, P. J.; Walsh, P. J.; Schelter, E. J. Photocatalytic C-H Activation and the Subtle Role of Chlorine Radical Complexation in Reactivity. *Science* **2021**, *372*, 847−852.
(680) Laudadio, G.; Deng, Y.; van der Wal, K.; Ravelli, D.; Nuño, M.; Fagnoni, M.; Guthrie, D.; Sun, Y.; Noël, T. $C(Sp^3)$-H Functionalizations of Light Hydrocarbons Using Decatungstate Photocatalysis in Flow. *Science* **2020**, *369*, 92−96.
(681) Fagnoni, M.; Bonassi, F.; Palmieri, A.; Protti, S.; Ravelli, D.; Ballini, R. Flow Synthesis of Substituted γ-Lactones by Consecutive Photocatalytic/Reductive Reactions. *Adv. Synth. Catal.* **2014**, *356*, 753−758.
(682) Garbarino, S.; Protti, S.; Gabrielli, S.; Fagnoni, M.; Palmieri, A.; Ravelli, D. Multi-Step Continuous Flow Synthesis of β/γ-Substituted Ketones. *ChemPhotoChem.* **2018**, *2*, 847−850.
(683) Capaldo, L.; Riccardi, R.; Ravelli, D.; Fagnoni, M. Acyl Radicals from Acylsilanes: Photoredox-Catalyzed Synthesis of Unsymmetrical Ketones. *ACS Catal.* **2018**, *8*, 304−309.
(684) Bonciolini, S.; Di Filippo, M.; Baumann, M. A Scalable Continuous Photochemical Process for the Generation of Aminopropylsulfones. *Org. Biomol. Chem.* **2020**, *18*, 9428−9432.
(685) Deng, H.-P.; Fan, X.-Z.; Chen, Z.-H.; Xu, Q.-H.; Wu, J. Photoinduced Nickel-Catalyzed Chemo- and Regioselective Hydroalkylation of Internal Alkynes with Ether and Amide α-Hetero $C(Sp^3)$-H Bonds. *J. Am. Chem. Soc.* **2017**, *139*, 13579−13584.
(686) Sharma, U. K.; Gemoets, H. P. L.; Schröder, F.; Noël, T.; Van der Eycken, E. V. Merger of Visible-Light Photoredox Catalysis and C-H Activation for the Room-Temperature C-2 Acylation of Indoles in Batch and Flow. *ACS Catal.* **2017**, *7*, 3818−3823.
(687) Capaldo, L.; Fagnoni, M.; Ravelli, D. Vinylpyridines as Building Blocks for the Photocatalyzed Synthesis of Alkylpyridines. *Chem. - Eur. J.* **2017**, *23*, 6527−6530.
(688) Xue, F.; Deng, H.; Xue, C.; Mohamed, D. K. B.; Tang, K. Y.; Wu, J. Reaction Discovery Using Acetylene Gas as the Chemical Feedstock Accelerated by the "Stop-Flow" Micro-Tubing Reactor System. *Chem. Sci.* **2017**, *8*, 3623−3627.
(689) Zhou, R.; Liu, H.; Tao, H.; Yu, X.; Wu, J. Metal-Free Direct Alkylation of Unfunctionalized Allylic/Benzylic Sp^3 C-H Bonds via

https://doi.org/10.1021/acs.chemrev.1c00332
Chem. Rev. 2022, 122, 2752−2906

Photoredox Induced Radical Cation Deprotonation. *Chem. Sci.* **2017**, *8*, 4654−4659.
(690) Deng, H.-P.; Zhou, Q.; Wu, J. Microtubing-Reactor-Assisted Aliphatic C-H Functionalization with HCl as a Hydrogen-Atom-Transfer Catalyst Precursor in Conjunction with an Organic Photoredox Catalyst. *Angew. Chem., Int. Ed.* **2018**, *57*, 12661−12665.
(691) Jia, P.; Li, Q.; Poh, W. C.; Jiang, H.; Liu, H.; Deng, H.; Wu, J. Light-Promoted Bromine-Radical-Mediated Selective Alkylation and Amination of Unactivated C(Sp^3)-H Bonds. *Chem.* **2020**, *6*, 1766−1776.
(692) Xia, Q.; Li, Y.; Cheng, L.; Liang, X.; Cao, C.; Dai, P.; Deng, H.; Zhang, W.; Wang, Q. Electron Donor-Acceptor Complex-Initiated Photochemical Cyanation for the Preparation of α-Amino Nitriles. *Org. Lett.* **2020**, *22*, 9638−9643.
(693) Fagnoni, M.; Dondi, D.; Ravelli, D.; Albini, A. Photocatalysis for the Formation of the C-C Bond. *Chem. Rev.* **2007**, *107*, 2725−2756.
(694) Mo, F.; Qiu, D.; Zhang, L.; Wang, J. Recent Development of Aryl Diazonium Chemistry for the Derivatization of Aromatic Compounds. *Chem. Rev.* **2021**, *121*, 5741.
(695) Mo, F.; Dong, G.; Zhang, Y.; Wang, J. Recent Applications of Arene Diazonium Salts in Organic Synthesis. *Org. Biomol. Chem.* **2013**, *11*, 1582−1593.
(696) Ghosh, I.; Marzo, L.; Das, A.; Shaikh, R.; König, B. Visible Light Mediated Photoredox Catalytic Arylation Reactions. *Acc. Chem. Res.* **2016**, *49*, 1566−1577.
(697) Hattori, K.; Yamaguchi, K.; Yamaguchi, J.; Itami, K. Pd- and Cu-Catalyzed C-H Arylation of Indazoles. *Tetrahedron* **2012**, *68*, 7605−7612.
(698) Basu, K.; Poirier, M.; Ruck, R. T. Solution to the C_3-Arylation of Indazoles: Development of a Scalable Method. *Org. Lett.* **2016**, *18*, 3218−3221.
(699) Vidyacharan, S.; Ramanjaneyulu, B. T.; Jang, S.; Kim, D.-P. Continuous-Flow Visible Light Organophotocatalysis for Direct Arylation of 2H-Indazoles: Fast Access to Drug Molecules. *ChemSusChem* **2019**, *12*, 2581−2586.
(700) Zoller, J.; Fabry, D. C.; Rueping, M. Unexpected Dual Role of Titanium Dioxide in the Visible Light Heterogeneous Catalyzed C-H Arylation of Heteroarenes. *ACS Catal.* **2015**, *5*, 3900−3904.
(701) Liang, Y.-F.; Steinbock, R.; Yang, L.; Ackermann, L. Continuous Visible-Light Photoflow Approach for a Manganese-Catalyzed (Het)Arene C-H Arylation. *Angew. Chem., Int. Ed.* **2018**, *57*, 10625−10629.
(702) Micic, N.; Polyzos, A. Radical Carbonylation Mediated by Continuous-Flow Visible-Light Photocatalysis: Access to 2,3-Dihydrobenzofurans. *Org. Lett.* **2018**, *20*, 4663−4666.
(703) Anselmo, M.; Moni, L.; Ismail, H.; Comoretto, D.; Riva, R.; Basso, A. Photocatalyzed Synthesis of Isochromanones and Isobenzofuranones under Batch and Flow Conditions. *Beilstein J. Org. Chem.* **2017**, *13*, 1456−1462.
(704) de Souza, A. A. N.; Silva, N. S.; Müller, V. A.; Polo, A. S.; Brocksom, T. J.; de Oliveira, K. T. Porphyrins as Photoredox Catalysts in Csp^2-H Arylations: Batch and Continuous Flow Approaches. *J. Org. Chem.* **2018**, *83*, 15077−15086.
(705) Hering, T.; Hari, D. P.; König, B. Visible-Light-Mediated α-Arylation of Enol Acetates Using Aryl Diazonium Salts. *J. Org. Chem.* **2012**, *77*, 10347−10352.
(706) Anselmo, M.; Basso, A.; Protti, S.; Ravelli, D. Photoredox-Catalyzed Generation of Acetonyl Radical in Flow: Theoretical Investigation and Synthetic Applications. *ACS Catal.* **2019**, *9*, 2493−2500.
(707) Crespi, S.; Protti, S.; Fagnoni, M. Wavelength Selective Generation of Aryl Radicals and Aryl Cations for Metal-Free Photoarylations. *J. Org. Chem.* **2016**, *81*, 9612−9619.
(708) Nauth, A. M.; Lipp, A.; Lipp, B.; Opatz, T. Sunflow: Sunlight Drives Fast and Green Photochemical Flow Reactions in Simple Microcapillary Reactors - Application to Photoredox and H-Atom-Transfer Chemistry. *Eur. J. Org. Chem.* **2017**, *2017*, 2099−2103.
(709) Abdulla, H. O.; Amin, A. A.; Raviola, C.; Opatz, T.; Protti, S.; Fagnoni, M. Smooth Metal-Free Photoinduced Preparation of Valuable 8-Arylxanthines. *Eur. J. Org. Chem.* **2020**, *2020*, 1448−1452.
(710) Majchrzak, M. W.; Bekhazi, M.; Tse-Sheepy, I.; Warkentin, J. Photolysis of 2-Alkoxy-.DELTA.3−1,3,4-Oxadiazolines. A New Route to Diazoalkanes. *J. Org. Chem.* **1989**, *54*, 1842−1845.
(711) Hock, K. J.; Koenigs, R. M. The Generation of Diazo Compounds in Continuous-Flow. *Chem. - Eur. J.* **2018**, *24*, 10571−10583.
(712) Greb, A.; Poh, J.-S.; Greed, S.; Battilocchio, C.; Pasau, P.; Blakemore, D. C.; Ley, V. S. A Versatile Route to Unstable Diazo Compounds via Oxadiazolines and Their Use in Aryl-Alkyl Cross-Coupling Reactions. *Angew. Chem., Int. Ed.* **2017**, *56*, 16602−16605.
(713) Dingwall, P.; Greb, A.; Crespin, L. N. S.; Labes, R.; Musio, B.; Poh, J.-S.; Pasau, P.; Blakemore, D. C.; Ley, V. S. C-H Functionalisation of Aldehydes Using Light Generated, Non-Stabilised Diazo Compounds in Flow. *Chem. Commun.* **2018**, *54*, 11685−11688.
(714) Chen, Y.; Blakemore, D. C.; Pasau, P.; Ley, V. S. Three-Component Assembly of Multiply Substituted Homoallylic Alcohols and Amines Using a Flow Chemistry Photoreactor. *Org. Lett.* **2018**, *20*, 6569−6572.
(715) Chen, Y.; Leonardi, M.; Dingwall, P.; Labes, R.; Pasau, P.; Blakemore, D. C.; Ley, V. S. Photochemical Homologation for the Preparation of Aliphatic Aldehydes in Flow. *J. Org. Chem.* **2018**, *83*, 15558−15568.
(716) Barthelemy, A.-L.; Tuccio, B.; Magnier, E.; Dagousset, G. Alkoxyl Radicals Generated under Photoredox Catalysis: A Strategy for Anti-Markovnikov Alkoxylation Reactions. *Angew. Chem., Int. Ed.* **2018**, *57*, 13790−13794.
(717) Chen, Y.; Glotz, G.; Cantillo, D.; Kappe, C. O. Organo-photocatalytic N-Demethylation of Oxycodone Using Molecular Oxygen. *Chem. - Eur. J.* **2020**, *26*, 2973−2979.
(718) Sadove, M. S.; Balagot, R. C.; Hatano, S.; Jobgen, E. A. Study of a Narcotic Antagonist— N-Allyl-Noroxymorphone. *JAMA* **1963**, *183*, 666−668.
(719) Werner, L.; Wernerova, M.; Machara, A.; Endoma-Arias, M. A.; Duchek, J.; Adams, D. R.; Cox, D. P.; Hudlicky, T. Unexpected N-Demethylation of Oxymorphone and Oxycodone N-Oxides Mediated by the Burgess Reagent: Direct Synthesis of Naltrexone, Naloxone, and Other Antagonists from Oxymorphone. *Adv. Synth. Catal.* **2012**, *354*, 2706−2712.
(720) Lesieur, M.; Genicot, C.; Pasau, P. Development of a Flow Photochemical Aerobic Oxidation of Benzylic C-H Bonds. *Org. Lett.* **2018**, *20*, 1987−1990.
(721) Schultz, D. M.; Lévesque, F.; DiRocco, D. A.; Reibarkh, M.; Ji, Y.; Joyce, L. A.; Dropinski, J. F.; Sheng, H.; Sherry, B. D.; Davies, I. W. Oxyfunctionalization of the Remote C-H Bonds of Aliphatic Amines by Decatungstate Photocatalysis. *Angew. Chem., Int. Ed.* **2017**, *56*, 15274−15278.
(722) Laudadio, G.; Govaerts, S.; Wang, Y.; Ravelli, D.; Koolman, H. F.; Fagnoni, M.; Djuric, S. W.; Noël, T. Selective C(Sp^3)-H Aerobic Oxidation Enabled by Decatungstate Photocatalysis in Flow. *Angew. Chem., Int. Ed.* **2018**, *57*, 4078−4082.
(723) Aand, D.; Karekar, S.; Mahajan, B.; Pawar, A. B.; Singh, A. K. Controlled Photo-Flow Oxidative Reaction (UV-FOR) Platform for Ultra-Fast Phthalide and API Synthesis. *Green Chem.* **2018**, *20*, 4584−4590.
(724) Nyuchev, V. A.; Wan, T.; Cendón, B.; Sambiagio, C.; Struijs, J. J. C.; Ho, M.; Gulías, M.; Wang, Y.; Noël, T. Photocatalytic Trifluoromethoxylation of Arenes and Heteroarenes in Continuous-Flow. *Beilstein J. Org. Chem.* **2020**, *16*, 1305−1312.
(725) Zheng, W.; Lee, J. W.; Morales-Rivera, C. A.; Liu, P.; Ngai, M.-Y. Redox-Active Reagents for Photocatalytic Generation of the OCF_3 Radical and (Hetero)Aryl C-H Trifluoromethoxylation. *Angew. Chem., Int. Ed.* **2018**, *57*, 13795−13799.
(726) Ruiz-Castillo, P.; Buchwald, S. L. Applications of Palladium-Catalyzed C-N Cross-Coupling Reactions. *Chem. Rev.* **2016**, *116*, 12564−12649.

https://doi.org/10.1021/acs.chemrev.1c00332
Chem. Rev. 2022, 122, 2752−2906

(727) Cosgrove, S. C.; Douglas, G. E.; Raw, S. A.; Marsden, S. P. Continuous Flow for the Photochemical C-H Amination of Arenes. *ChemPhotoChem.* **2018**, *2*, 851−854.
(728) Minisci, F.; Galli, R. A New, Highly Selective, Type of Aromatic Substitution. Homolytic Amination of Phenolic Ethers. *Tetrahedron Lett.* **1965**, *6*, 433−436.
(729) Cosgrove, S. C.; Plane, J. M. C.; Marsden, S. P. Radical-Mediated Direct C-H Amination of Arenes with Secondary Amines. *Chem. Sci.* **2018**, *9*, 6647−6652.
(730) Maiti, D.; Das, R.; Sen, S. Blue LED-Mediated N-H Insertion of Indoles into Aryldiazoesters at Room Temperature in Batch and Flow: Reaction Kinetics, Density Functional Theory, and Mechanistic Study. *J. Org. Chem.* **2021**, *86*, 2522−2533.
(731) Wan, T.; Capaldo, L.; Laudadio, G.; Nyuchev, A.; Rincon, J.; Garcia-Losada, P.; Mateos, C.; Frederick, M. O.; Nuno, M.; Noel, T. Decatungstate-mediated C(Sp^3)-H Heteroarylation via Radical-Polar Crossover in Batch and Flow. *Angew. Chem.* **2021**, DOI: 10.1002/ange.202104682.
(732) Park, B. Y.; Pirnot, M. T.; Buchwald, S. L. Visible Light-Mediated (Hetero)Aryl Amination Using Ni(II) Salts and Photoredox Catalysis in Flow: A Synthesis of Tetracaine. *J. Org. Chem.* **2020**, *85*, 3234−3244.
(733) Mata, A.; Tran, D. N.; Weigl, U.; Williams, J. D.; Kappe, C. O. Continuous Flow Synthesis of Arylhydrazines via Nickel/Photoredox Coupling of Tert -Butyl Carbazate with Aryl Halides. *Chem. Commun.* **2020**, *56*, 14621−14624.
(734) Yuan, Z.; Liu, X.; Liu, C.; Zhang, Y.; Rao, Y. Recent Advances in Rapid Synthesis of Non-Proteinogenic Amino Acids from Proteinogenic Amino Acids Derivatives via Direct Photo-Mediated C-H Functionalization. *Molecules* **2020**, *25*, 5270.
(735) Wang, X.; Cuny, G. D.; Noël, T. A Mild, One-Pot Stadler-Ziegler Synthesis of Arylsulfides Facilitated by Photoredox Catalysis in Batch and Continuous-Flow. *Angew. Chem., Int. Ed.* **2013**, *52*, 7860−7864.
(736) Bottecchia, C.; Rubens, M.; Gunnoo, S. B.; Hessel, V.; Madder, A.; Noël, T. Visible-Light-Mediated Selective Arylation of Cysteine in Batch and Flow. *Angew. Chem., Int. Ed.* **2017**, *56*, 12702−12707.
(737) Qin, L.-Z.; Yuan, X.; Cui, Y.-S.; Sun, Q.; Duan, X.; Zhuang, K.-Q.; Chen, L.; Qiu, J.-K.; Guo, K. Visible-Light-Mediated S-H Bond Insertion Reactions of Diazoalkanes with Cysteine Residues in Batch and Flow. *Adv. Synth. Catal.* **2020**, *362*, 5093−5104.
(738) Donnelly, K.; Baumann, M. A Continuous Flow Synthesis of [1.1.1]Propellane and Bicyclo[1.1.1]Pentane Derivatives. *Chem. Commun.* **2021**, *57*, 2871.
(739) Santandrea, J.; Minozzi, C.; Cruché, C.; Collins, S. K. Photochemical Dual-Catalytic Synthesis of Alkynyl Sulfides. *Angew. Chem., Int. Ed.* **2017**, *56*, 12255−12259.
(740) Zhu, M.; Dagousset, G.; Alami, M.; Magnier, E.; Messaoudi, S. Ni/Photoredox-Dual-Catalyzed Functionalization of 1-Thiosugars. *Org. Lett.* **2019**, *21*, 5132−5137.
(741) Xu, W.; Wang, W.; Liu, T.; Xie, J.; Zhu, C. Late-Stage Trifluoromethylthiolation of Benzylic C-H Bonds. *Nat. Commun.* **2019**, *10*, 4867.
(742) Heredia, A. A.; Soria-Castro, S. M.; Castro-Godoy, W. D.; Lemir, I. D.; López-Vidal, M.; Bisogno, F. R.; Argüello, J. E.; Oksdath-Mansilla, G. Multistep Synthesis of Organic Selenides under Visible Light Irradiation: A Continuous-Flow Approach. *Org. Process Res. Dev.* **2020**, *24*, 540−545.
(743) De Zordo-Banliat, A.; Barthélémy, L.; Bourdreux, F.; Tuccio, B.; Dagousset, G.; Pégot, B.; Magnier, E. Visible-Light-Induced Metal-Free Trifluoromethylselenolation of Electron-Rich Heteroarenes Using the Nucleophilic [Me_4N][$SeCF_3$] Reagent. *Eur. J. Org. Chem.* **2020**, *2020*, 506−509.
(744) Mfuh, A. M.; Nguyen, V. T.; Chhetri, B.; Burch, J. E.; Doyle, J. D.; Nesterov, V. N.; Arman, H. D.; Larionov, O. V. Additive- and Metal-Free, Predictably 1,2- and 1,3-Regioselective, Photoinduced Dual C-H/C-X Borylation of Haloarenes. *J. Am. Chem. Soc.* **2016**, *138*, 8408−8411.
(745) Mfuh, A. M.; Doyle, J. D.; Chhetri, B.; Arman, H. D.; Larionov, O. V. Scalable, Metal- and Additive-Free, Photoinduced Borylation of Haloarenes and Quaternary Arylammonium Salts. *J. Am. Chem. Soc.* **2016**, *138*, 2985−2988.
(746) Chen, K.; Cheung, M. S.; Lin, Z.; Li, P. Metal-Free Borylation of Electron-Rich Aryl (Pseudo)Halides under Continuous-Flow Photolytic Conditions. *Org. Chem. Front.* **2016**, *3*, 875−879.
(747) Nitelet, A.; Thevenet, D.; Schiavi, B.; Hardouin, C.; Fournier, J.; Tamion, R.; Pannecoucke, X.; Jubault, P.; Poisson, T. Copper-Photocatalyzed Borylation of Organic Halides under Batch and Continuous-Flow Conditions. *Chem. - Eur. J.* **2019**, *25*, 3262−3266.
(748) Zhong, M.; Gagné, Y.; Hope, T. O.; Pannecoucke, X.; Frenette, M.; Jubault, P.; Poisson, T. Copper-Photocatalyzed Hydroboration of Alkynes and Alkenes. *Angew. Chem., Int. Ed.* **2021**, *60*, 14498−14503.
(749) Zhong, M.; Pannecoucke, X.; Jubault, P.; Poisson, T. Copper Photocatalyzed Hydrosilylation of Alkynes and Alkenes under Continuous Flow. *Chem. - Eur. J.* **2021**, xx DOI: 10.1002/chem.202101753.
(750) Chen, K.; Zhang, S.; He, P.; Li, P. Efficient Metal-Free Photochemical Borylation of Aryl Halides under Batch and Continuous-Flow Conditions. *Chem. Sci.* **2016**, *7*, 3676−3680.
(751) Vanheyst, M. D.; Qi, J.; Roecker, A. J.; Hughes, J. M. E.; Cheng, L.; Zhao, Z.; Yin, J. Continuous Flow-Enabled Synthesis of Bench-Stable Bicyclo[1.1.1]Pentane Trifluoroborate Salts and Their Utilization in Metallaphotoredox Cross-Couplings. *Org. Lett.* **2020**, *22*, 1648−1654.
(752) Bottecchia, C.; Erdmann, N.; Tijssen, P. M. A.; Milroy, L.-G.; Brunsveld, L.; Hessel, V.; Noël, T. Batch and Flow Synthesis of Disulfides by Visible-Light-Induced TiO_2 Photocatalysis. *ChemSusChem* **2016**, *9*, 1781−1785.
(753) Bajada, M. A.; Vijeta, A.; Savateev, A.; Zhang, G.; Howe, D.; Reisner, E. Visible-Light Flow Reactor Packed with Porous Carbon Nitride for Aerobic Substrate Oxidations. *ACS Appl. Mater. Interfaces* **2020**, *12*, 8176−8182.
(754) Casado-Sánchez, A.; Gómez-Ballesteros, R.; Tato, F.; Soriano, F. J.; Pascual-Coca, G.; Cabrera, S.; Alemán, J. Pt(II) Coordination Complexes as Visible Light Photocatalysts for the Oxidation of Sulfides Using Batch and Flow Processes. *Chem. Commun.* **2016**, *52*, 9137−9140.
(755) Wu, G.; Li, Y.; Yu, X.; Gao, Y.; Chen, H. Acetic Acid Accelerated Visible-Light Photoredox Catalyzed N-Demethylation of N,N-Dimethylaminophenyl Derivatives. *Adv. Synth. Catal.* **2017**, *359*, 687−692.
(756) Mlakić, M.; Šalić, A.; Bačić, M.; Zelić, B.; Šagud, I.; Horváth, O.; Škorić, I. Photocatalytic Oxygenation of Heterostilbenes—Batch versus Microflow Reactor. *Catalysts* **2021**, *11*, 395.
(757) Shi, X.; Liu, S.; Duanmu, C.; Shang, M.; Qiu, M.; Shen, C.; Yang, Y.; Su, Y. Visible-Light Photooxidation of Benzene to Phenol in Continuous-Flow Microreactors. *Chem. Eng. J.* **2021**, *420*, 129976.
(758) Roseau, M.; Dhaouadi, N.; Rolando, C.; Chausset-Boissarie, L.; Penhoat, M. Continuous Photocatalyzed Aerobic Oxidation of Benzylic Organotrifluoroborates to Benzaldehydes under Taylor Flow Conditions. *J. Flow Chem.* **2020**, *10*, 347−352.
(759) Mortzfeld, F. B.; Pietruszka, J.; Baxendale, I. R. A Simple and Efficient Flow Preparation of Pyocyanin a Virulence Factor of Pseudomonas Aeruginosa. *Eur. J. Org. Chem.* **2019**, *2019*, 5424−5433.
(760) Koo, H.; Kim, H. Y.; Oh, K. Continuous Flow Synthesis of Isoxazoles via Vinyl Azides from Friedel-Crafts Acylation of Alkynes: A Modulated Troubleshooting Optimization Approach. *Org. Lett.* **2019**, *21*, 10063−10068.
(761) Nishiyama, Y.; Fujii, A.; Mori, H. Selective Synthesis of Azoxybenzenes from Nitrobenzenes by Visible Light Irradiation under Continuous Flow Conditions. *React. Chem. Eng.* **2019**, *4*, 2055−2059.
(762) Chen, Y.; Zhang, Y.; Zou, H.; Li, M.; Wang, G.; Peng, M.; Zhang, J.; Tang, Z. Tuning the Gas-Liquid-Solid Segmented Flow for Enhanced Heterogeneous Photosynthesis of Azo- Compounds. *Chem. Eng. J.* **2021**, *423*, 130226.

(763) Aand, D.; Mahajan, B.; Pabbaraja, S.; Singh, A. K. Integrated Continuous Flow/Batch Protocol for the Photoreduction of Ortho-Methyl Phenyl Ketones Using Water as the Hydrogen Source. *React. Chem. Eng.* **2019**, *4*, 812−817.
(764) Pilkington, R. L.; Rossouw, N. P.; van As, D. J.; Polyzos, A. A Chemoselective and Scalable Transfer Hydrogenation of Aryl Imines by Rapid Continuous Flow Photoredox Catalysis. *Chimia* **2019**, *73*, 823−827.
(765) van As, D. J.; Connell, T. U.; Brzozowski, M.; Scully, A. D.; Polyzos, A. Photocatalytic and Chemoselective Transfer Hydrogenation of Diarylimines in Batch and Continuous Flow. *Org. Lett.* **2018**, *20*, 905−908.
(766) Li, J.-S.; Wu, J. Recent Developments in the Photo-Mediated Generation of Silyl Radicals and Their Application in Organic Synthesis. *ChemPhotoChem.* **2018**, *2*, 839−846.
(767) Zhou, R.; Goh, Y. Y.; Liu, H.; Tao, H.; Li, L.; Wu, J. Visible-Light-Mediated Metal-Free Hydrosilylation of Alkenes through Selective Hydrogen Atom Transfer for Si-H Activation. *Angew. Chem., Int. Ed.* **2017**, *56*, 16621−16625.
(768) Zhou, R.; Li, J.; Cheo, H. W.; Chua, R.; Zhan, G.; Hou, Z.; Wu, J. Visible-Light-Mediated Deuteration of Silanes with Deuterium Oxide. *Chem. Sci.* **2019**, *10*, 7340−7344.
(769) Zhou, Q.-Q.; Zou, Y.-Q.; Lu, L.-Q.; Xiao, W.-J. Visible-Light-Induced Organic Photochemical Reactions through Energy-Transfer Pathways. *Angew. Chem., Int. Ed.* **2019**, *58*, 1586−1604.
(770) Yu, Y.; Guo, P.; Zhong, J.-S.; Yuan, Y.; Ye, K.-Y. Merging Photochemistry with Electrochemistry in Organic Synthesis. *Org. Chem. Front.* **2020**, *7*, 131−135.
(771) Kingston, C.; Palkowitz, M. D.; Takahira, Y.; Vantourout, J. C.; Peters, B. K.; Kawamata, Y.; Baran, P. S. A Survival Guide for the "Electro-Curious. *Acc. Chem. Res.* **2020**, *53*, 72−83.
(772) Noël, T.; Cao, Y.; Laudadio, G. The Fundamentals behind the Use of Flow Reactors in Electrochemistry. *Acc. Chem. Res.* **2019**, *52*, 2858−2869.
(773) Capaldo, L.; Quadri, L. L.; Ravelli, D. Merging Photocatalysis with Electrochemistry: The Dawn of a New Alliance in Organic Synthesis. *Angew. Chem., Int. Ed.* **2019**, *58*, 17508−17510.
(774) Reichert, R.; Jusys, Z.; Behm, R. J. A Novel Photo-electrochemical Flow Cell with Online Mass Spectrometric Detection: Oxidation of Formic Acid on a Nanocrystalline TiO2 Electrode. *Phys. Chem. Chem. Phys.* **2014**, *16*, 25076−25080.
(775) de Brito, J. F.; Araujo, A. R.; Rajeshwar, K.; Zanoni, M. V. B. Photoelectrochemical Reduction of CO_2 on Cu/Cu_2O Films: Product Distribution and PH Effects. *Chem. Eng. J.* **2015**, *264*, 302−309.
(776) Kalamaras, E.; Belekoukia, M.; Tan, J. Z. Y.; Xuan, J.; Maroto-Valer, M. M.; Andresen, J. M. A Microfluidic Photoelectrochemical Cell for Solar-Driven CO_2 Conversion into Liquid Fuels with CuO-Based Photocathodes. *Faraday Discuss.* **2019**, *215*, 329−344.
(777) Saito, R.; Miseki, Y.; Sayama, K. Highly Efficient Photo-electrochemical Water Splitting Using a Thin Film Photoanode of $BiVO_4/SnO_2/WO_3$ Multi-Composite in a Carbonate Electrolyte. *Chem. Commun.* **2012**, *48*, 3833−3835.
(778) Way, A.; Luke, J.; Evans, A. D.; Li, Z.; Kim, J.-S.; Durrant, J. R.; Hin Lee, H. K.; Tsoi, W. C. Fluorine Doped Tin Oxide as an Alternative of Indium Tin Oxide for Bottom Electrode of Semi-Transparent Organic Photovoltaic Devices. *AIP Adv.* **2019**, *9*, 085220.
(779) Cao, Y.; Soares, C.; Padoin, N.; Noël, T. Gas Bubbles Have Controversial Effects on Taylor Flow Electrochemistry. *Chem. Eng. J.* **2021**, *406*, 126811.
(780) Shen, T.; Lambert, T. H. Electrophotocatalytic Diamination of Vicinal C-H Bonds. *Science* **2021**, *371*, 620−626.
(781) Irtem, E.; Hernández-Alonso, M. D. D.; Parra, A.; Fàbrega, C.; Penelas-Pérez, G.; Morante, J. R. R.; Andreu, T. A Photo-electrochemical Flow Cell Design for the Efficient CO_2 Conversion to Fuels. *Electrochim. Acta* **2017**, *240*, 225−230.
(782) Zhao, Y.; Zhang, Q.; Chen, K.; Gao, H.; Qi, H.; Shi, X.; Han, Y.; Wei, J.; Zhang, C. Triphenothiazinyl Triazacoronenes: Donor-Acceptor Molecular Graphene Exhibiting Multiple Fluorescence and Electrogenerated Chemiluminescence Emissions. *J. Mater. Chem. C* **2017**, *5*, 4293−4301.
(783) Moutet, J.-C.; Reverdy, G. Photochemistry of Cation Radicals in Solution: Photoinduced Oxidation by the Phenothiazine Cation Radical. *Tetrahedron Lett.* **1979**, *20*, 2389−2392.
(784) Moutet, J.-C.; Reverdy, G. Phototochemistry of Cation Radicals in Solution; Photoinduced Electron-Transfer Reactions between Alcholos and the N,N,N′,N′,-Tetraphenyl-p-Phenylenediamine Cation Radical. *J. Chem. Soc., Chem. Commun.* **1982**, *0* (12), 654−655.
(785) Huang, H.; Strater, Z. M.; Rauch, M.; Shee, J.; Sisto, T. J.; Nuckolls, C.; Lambert, T. H. Electrophotocatalysis with a Trisaminocyclopropenium Radical Dication. *Angew. Chem., Int. Ed.* **2019**, *58*, 13318−13322.
(786) Gerson, F.; Plattner, G.; Yoshida, Z. Tris(Dimethylamino)-Cyclopropenium Radical Dication. *Mol. Phys.* **1971**, *21*, 1027−1032.
(787) Johnson, R. W. Electrochemistry of Heterosubstituted Cyclopropenyl Cations. *Tetrahedron Lett.* **1976**, *17*, 589−592.
(788) Weiss, R.; Schloter, K. Stable Radical Dications. *Tetrahedron Lett.* **1975**, *16*, 3491−3494.
(789) Sevov, C. S.; Samaroo, S. K.; Sanford, M. S. Cyclopropenium Salts as Cyclable, High-Potential Catholytes in Nonaqueous Media. *Adv. Energy Mater.* **2017**, *7*, 1602027.
(790) Huang, H.; Lambert, T. H. Electrophotocatalytic Acetoxyhydroxylation of Aryl Olefins. *J. Am. Chem. Soc.* **2021**, *143*, 7247−7252.
(791) Huang, H.; Strater, Z. M.; Lambert, T. H. Electrophotocatalytic C-H Functionalization of Ethers with High Regioselectivity. *J. Am. Chem. Soc.* **2020**, *142*, 1698−1703.
(792) Zhou, J.; Zou, Y.; Zhou, P.; Chen, Z.; Li, J. Copper-Catalyzed Versatile C(Sp^3)-H Arylation: Synthetic Scope and Regioselectivity Investigations. *Org. Chem. Front.* **2019**, *6*, 1594−1598.
(793) Liu, S.; Liu, A.; Zhang, Y.; Wang, W. Direct Cα-Heteroarylation of Structurally Diverse Ethers via a Mild N-Hydroxysuccinimide Mediated Cross-Dehydrogenative Coupling Reaction. *Chem. Sci.* **2017**, *8*, 4044−4050.
(794) Jin, J.; MacMillan, D. W. C. Direct α-Arylation of Ethers through the Combination of Photoredox-Mediated C-H Functionalization and the Minisci Reaction. *Angew. Chem., Int. Ed.* **2015**, *54*, 1565−1569.
(795) Shen, T.; Lambert, T. H. C-H Amination via Electrophotocatalytic Ritter-Type Reaction. *J. Am. Chem. Soc.* **2021**, *143*, 8597−8602.
(796) Kim, H.; Kim, H.; Lambert, T. H.; Lin, S. Reductive Electrophotocatalysis: Merging Electricity and Light To Achieve Extreme Reduction Potentials. *J. Am. Chem. Soc.* **2020**, *142*, 2087−2092.
(797) Joshi, D. K.; Sutton, J. W.; Carver, S.; Blanchard, J. P. Experiences with Commercial Production Scale Operation of Dissolving Metal Reduction Using Lithium Metal and Liquid Ammonia. *Org. Process Res. Dev.* **2005**, *9*, 997−1002.
(798) Cowper, N. G. W.; Chernowsky, C. P.; Williams, O. P.; Wickens, Z. K. Potent Reductants via Electron-Primed Photoredox Catalysis: Unlocking Aryl Chlorides for Radical Coupling. *J. Am. Chem. Soc.* **2020**, *142*, 2093−2099.
(799) Majek, M.; Jacobi von Wangelin, A. Mechanistic Perspectives on Organic Photoredox Catalysis for Aromatic Substitutions. *Acc. Chem. Res.* **2016**, *49*, 2316−2327.
(800) Arias-Rotondo, D. M.; McCusker, J. K. The Photophysics of Photoredox Catalysis: A Roadmap for Catalyst Design. *Chem. Soc. Rev.* **2016**, *45*, 5803−5820.
(801) Capaldo, L.; Ravelli, D. The Dark Side of Photocatalysis: One Thousand Ways to Close the Cycle. *Eur. J. Org. Chem.* **2020**, No. 2783.
(802) Yan, H.; Hou, Z.-W.; Xu, H.-C. Photoelectrochemical C-H Alkylation of Heteroarenes with Organotrifluoroborates. *Angew. Chem., Int. Ed.* **2019**, *58*, 4592−4595.
(803) Qiu, Y.; Scheremetjew, A.; Finger, L. H.; Ackermann, L. Electrophotocatalytic Undirected C-H Trifluoromethylations of (Het)Arenes. *Chem. - Eur. J.* **2020**, *26*, 3241−3246.

https://doi.org/10.1021/acs.chemrev.1c00332
Chem. Rev. 2022, 122, 2752−2906

(804) Kong, W.-J.; Finger, L. H.; Messinis, A. M.; Kuniyil, R.; Oliveira, J. C. A.; Ackermann, L. Flow Rhodaelectro-Catalyzed Alkyne Annulations by Versatile C-H Activation: Mechanistic Support for Rhodium(III/IV). *J. Am. Chem. Soc.* **2019**, *141*, 17198−17206.
(805) Huang, H.; Lambert, T. H. Electrophotocatalytic SNAr Reactions of Unactivated Aryl Fluorides at Ambient Temperature and Without Base. *Angew. Chem., Int. Ed.* **2020**, *59*, 658−662.
(806) Huang, H.; Lambert, T. H. Electrophotocatalytic C-H Heterofunctionalization of Arenes. *Angew. Chem., Int. Ed.* **2021**, *60*, No. 11163.
(807) Korvinson, K. A.; Hargenrader, G. N.; Stevanovic, J.; Xie, Y.; Joseph, J.; Maslak, V.; Hadad, C. M.; Glusac, K. D. Improved Flavin-Based Catalytic Photooxidation of Alcohols through Intersystem Crossing Rate Enhancement. *J. Phys. Chem. A* **2016**, *120*, 7294−7300.
(808) Hering, T.; Mühldorf, B.; Wolf, R.; König, B. Halogenase-Inspired Oxidative Chlorination Using Flavin Photocatalysis. *Angew. Chem., Int. Ed.* **2016**, *55*, 5342−5345.
(809) Kurfiřt, M.; Špačková, J.; Svobodová, E.; Cibulka, R. Flavin Derivatives Immobilized on Mesoporous Silica: A Versatile Tool in Visible-Light Photooxidation Reactions. *Monatsh. Chem.* **2018**, *149*, 863−869.
(810) König, B.; Pelka, M.; Reichenbach-Klinke, R.; Schelter, J.; Daub, J. A Model System for Flavoenzyme Activity - Binding of Flavin and Modulation of Its Redox Potentials through Coordination to a Lewis-Acidic Azamacrocyclic Zinc(II) Complex. *Eur. J. Org. Chem.* **2001**, *2001*, 2297−2303.
(811) Svoboda, J.; Schmaderer, H.; König, B. Thiourea-Enhanced Flavin Photooxidation of Benzyl Alcohol. *Chem. - Eur. J.* **2008**, *14*, 1854−1865.
(812) Zhang, W.; Carpenter, K. L.; Lin, S. Electrochemistry Broadens the Scope of Flavin Photocatalysis: Photoelectrocatalytic Oxidation of Unactivated Alcohols. *Angew. Chem., Int. Ed.* **2020**, *59*, 409−417.
(813) Niu, L.; Jiang, C.; Liang, Y.; Liu, D.; Bu, F.; Shi, R.; Chen, H.; Chowdhury, A. D.; Lei, A. Manganese-Catalyzed Oxidative Azidation of C(Sp^3)-H Bonds under Electrophotocatalytic Conditions. *J. Am. Chem. Soc.* **2020**, *142*, 17693−17702.
(814) Capaldo, L.; Quadri, L. L.; Merli, D.; Ravelli, D. Photoelectrochemical Cross-Dehydrogenative Coupling of Benzothiazoles with Strong Aliphatic C-H Bonds. *Chem. Commun.* **2021**, *57*, 4424−4427.
(815) Thiyagarajan, S.; Franciolus, D.; Bisselink, R. J. M.; Ewing, T. A.; Boeriu, C. G.; van Haveren, J. Selective Production of Maleic Acid from Furfural via a Cascade Approach Combining Photochemistry and Electro- or Biochemistry. *ACS Sustainable Chem. Eng.* **2020**, *29*, 10626−10632.
(816) Yan, H.; Zhu, S.; Xu, H.-C. Integrating Continuous-Flow Electrochemistry and Photochemistry for the Synthesis of Acridinium Photocatalysts Via Site-Selective C-H Alkylation. *Org. Process Res. Dev.* **2021**, DOI: 10.1021/acs.oprd.1c00038.
(817) Bosque, I.; Magallanes, G.; Rigoulet, M.; Kärkäs, M. D.; Stephenson, C. R. J. Redox Catalysis Facilitates Lignin Depolymerization. *ACS Cent. Sci.* **2017**, *3*, 621−628.
(818) Scheffold, R.; Orlinski, R. Synthesis and Reactions of Porphine-Type Metal Complexes. 15. Carbon-Carbon Bond Formation by Light Assisted B_{12}-Catalysis. Nucleophilic Acylation of Michael Olefins. *J. Am. Chem. Soc.* **1983**, *105*, 7200−7202.
(819) Wang, F.; Stahl, S. S. Merging Photochemistry with Electrochemistry: Functional-Group Tolerant Electrochemical Amination of C(Sp^3)-H Bonds. *Angew. Chem., Int. Ed.* **2019**, *58*, 6385−6390.
(820) Shono, T.; Matsumura, Y.; Katoh, S.; Takeuchi, K.; Sasaki, K.; Kamada, T.; Shimizu, R. Electroorganic Chemistry. 120. New Patterns of Anodic Oxidation of Amides. Synthesis of α-Amino Aldehyde Acetals and Pyrrolidines from Amines. *J. Am. Chem. Soc.* **1990**, *112*, 2368−2372.
(821) Hu, X.; Zhang, G.; Bu, F.; Nie, L.; Lei, A. Electrochemical-Oxidation-Induced Site-Selective Intramolecular C(Sp^3)-H Amination. *ACS Catal.* **2018**, *8*, 9370−9375.
(822) Zhang, S.; Li, L.; Xue, M.; Zhang, R.; Xu, K.; Zeng, C. Electrochemical Formation of N-Acyloxy Amidyl Radicals and Their Application: Regioselective Intramolecular Amination of Sp^2 and Sp^3 C-H Bonds. *Org. Lett.* **2018**, *20*, 3443−3446.
(823) Herold, S.; Bafaluy, D.; Muñiz, K. Anodic Benzylic C(Sp^3)-H Amination: Unified Access to Pyrrolidines and Piperidines. *Green Chem.* **2018**, *20*, 3191−3196.
(824) Lai, X.-L.; Shu, X.-M.; Song, J.; Xu, H.-C. Electrophotocatalytic Decarboxylative C-H Functionalization of Heteroarenes. *Angew. Chem., Int. Ed.* **2020**, *59*, 10626−10632.
(825) Xu, P.; Chen, P.-Y.; Xu, H.-C. Scalable Photoelectrochemical Dehydrogenative Cross-Coupling of Heteroarenes with Aliphatic C-H Bonds. *Angew. Chem., Int. Ed.* **2020**, *59*, 14275−14280.
(826) Lacis, A. A.; Schmidt, G. A.; Rind, D.; Ruedy, R. A. Atmospheric CO_2: Principal Control Knob Governing Earth's Temperature. *Science* **2010**, *330*, 356−359.
(827) Walter, M. G.; Warren, E. L.; McKone, J. R.; Boettcher, S. W.; Mi, Q.; Santori, E. A.; Lewis, N. S. Solar Water Splitting Cells. *Chem. Rev.* **2010**, *110*, 6446−6473.
(828) Ager, J. W.; Shaner, M. R.; Walczak, K. A.; Sharp, I. D.; Ardo, S. Experimental Demonstrations of Spontaneous, Solar-Driven Photoelectrochemical Water Splitting. *Energy Environ. Sci.* **2015**, *8*, 2811−2824.
(829) Hankin, A.; Bedoya-Lora, F. E.; Ong, C. K.; Alexander, J. C.; Petter, F.; Kelsall, G. H. From Millimetres to Metres: The Critical Role of Current Density Distributions in Photo-Electrochemical Reactor Design. *Energy Environ. Sci.* **2017**, *10*, 346−360.
(830) Chiu, Y.-H.; Lai, T.-H.; Kuo, M.-Y.; Hsieh, P.-Y.; Hsu, Y.-J. Photoelectrochemical Cells for Solar Hydrogen Production: Challenges and Opportunities. *APL Mater.* **2019**, *7*, 080901.
(831) Batrice, R. J.; Gordon, J. C. Powering the next Industrial Revolution: Transitioning from Nonrenewable Energy to Solar Fuels via CO_2 Reduction. *RSC Adv.* **2021**, *11*, 87−113.
(832) Steinfeld, A.; Weimer, A. Thermochemical Production of Fuels with Concentrated Solar Energy. *Opt. Express* **2010**, *18*, A100−11.
(833) Sultana, S.; Chandra Sahoo, P.; Martha, S.; Parida, K. A Review of Harvesting Clean Fuels from Enzymatic CO_2 Reduction. *RSC Adv.* **2016**, *6*, 44170−44194.
(834) Ren, J.; Ouyang, S.; Xu, H.; Meng, X.; Wang, T.; Wang, D.; Ye, J. Targeting Activation of CO_2 and H_2 over Ru-Loaded Ultrathin Layered Double Hydroxides to Achieve Efficient Photothermal CO_2 Methanation in Flow-Type System. *Adv. Energy Mater.* **2017**, *7*, 1601657.
(835) Chen, G.; Gao, R.; Zhao, Y.; Li, Z.; Waterhouse, G. I. N.; Shi, R.; Zhao, J.; Zhang, M.; Shang, L.; Sheng, G.; et al. Alumina-Supported CoFe Alloy Catalysts Derived from Layered-Double-Hydroxide Nanosheets for Efficient Photothermal CO_2 Hydrogenation to Hydrocarbons. *Adv. Mater.* **2018**, *30*, 1704663.
(836) Zhao, Y.; Waterhouse, G. I. N.; Chen, G.; Xiong, X.; Wu, L.-Z.; Tung, C.-H.; Zhang, T. Two-Dimensional-Related Catalytic Materials for Solar-Driven Conversion of CO_x into Valuable Chemical Feedstocks. *Chem. Soc. Rev.* **2019**, *48*, 1972−2010.
(837) He, J.; Janáky, C. Recent Advances in Solar-Driven Carbon Dioxide Conversion: Expectations versus Reality. *ACS Energy Lett.* **2020**, *5*, 1996−2014.
(838) Hernández, S.; Amin Farkhondehfal, M.; Sastre, F.; Makkee, M.; Saracco, G.; Russo, N. Syngas Production from Electrochemical Reduction of CO_2: Current Status and Prospective Implementation. *Green Chem.* **2017**, *19*, 2326−2346.
(839) Zhang, W.; Hu, Y.; Ma, L.; Zhu, G.; Wang, Y.; Xue, X.; Chen, R.; Yang, S.; Jin, Z. Progress and Perspective of Electrocatalytic CO_2 Reduction for Renewable Carbonaceous Fuels and Chemicals. *Adv. Sci.* **2018**, *5*, 1700275.
(840) Salvatore, D. A.; Weekes, D. M.; He, J.; Dettelbach, K. E.; Li, Y. C.; Mallouk, T. E.; Berlinguette, C. P. Electrolysis of Gaseous CO_2 to CO in a Flow Cell with a Bipolar Membrane. *ACS Energy Lett.* **2018**, *3*, 149−154.

(841) Endrődi, B.; Bencsik, G.; Darvas, F.; Jones, R.; Rajeshwar, K.; Janáky, C. Continuous-Flow Electroreduction of Carbon Dioxide. *Prog. Energy Combust. Sci.* **2017**, *62*, 133−154.
(842) Endrődi, B.; Kecsenovity, E.; Samu, A.; Darvas, F.; Jones, V. R.; Török, V.; Danyi, A.; Janáky, C. Multilayer Electrolyzer Stack Converts Carbon Dioxide to Gas Products at High Pressure with High Efficiency. *ACS Energy Lett.* **2019**, *4*, 1770−1777.
(843) Sriramagiri, G. M.; Ahmed, N.; Luc, W.; Dobson, K. D.; Hegedus, S. S.; Jiao, F. Toward a Practical Solar-Driven CO_2 Flow Cell Electrolyzer: Design and Optimization. *ACS Sustainable Chem. Eng.* **2017**, *5*, 10959−10966.
(844) Cheng, W.-H.; Richter, M. H.; Sullivan, I.; Larson, D. M.; Xiang, C.; Brunschwig, B. S.; Atwater, H. A. CO_2 Reduction to CO with 19% Efficiency in a Solar-Driven Gas Diffusion Electrode Flow Cell under Outdoor Solar Illumination. *ACS Energy Lett.* **2020**, *5*, 470−476.
(845) Inoue, T.; Fujishima, A.; Konishi, S.; Honda, K. Photoelectrocatalytic Reduction of Carbon Dioxide in Aqueous Suspensions of Semiconductor Powders. *Nature* **1979**, *277*, 637−638.
(846) Tu, W.; Zhou, Y.; Zou, Z. Photocatalytic Conversion of CO_2 into Renewable Hydrocarbon Fuels: State-of-the-Art Accomplishment, Challenges, and Prospects. *Adv. Mater.* **2014**, *26*, 4607−4626.
(847) Indrakanti, V. P.; Kubicki, J. D.; Schobert, H. H. Photoinduced Activation of CO_2 on Ti-Based Heterogeneous Catalysts: Current State, Chemical Physics-Based Insights and Outlook. *Energy Environ. Sci.* **2009**, *2*, 745−758.
(848) Zeng, S.; Kar, P.; Thakur, U. K.; Shankar, K. A Review on Photocatalytic CO_2 Reduction Using Perovskite Oxide Nanomaterials. *Nanotechnology* **2018**, *29*, 052001.
(849) Shi, R.; Waterhouse, G. I. N.; Zhang, T. Recent Progress in Photocatalytic CO_2 Reduction Over Perovskite Oxides. *Sol. RRL* **2017**, *1*, 1700126.
(850) Kumar, B.; Llorente, M.; Froehlich, J.; Dang, T.; Sathrum, A.; Kubiak, C. P. Photochemical and Photoelectrochemical Reduction of CO_2. *Annu. Rev. Phys. Chem.* **2012**, *63*, 541−569.
(851) Sivula, K.; van de Krol, R. Semiconducting Materials for Photoelectrochemical Energy Conversion. *Nat. Rev. Mater.* **2016**, *1*, 15010.
(852) Kalamaras, E.; Maroto-Valer, M. M.; Shao, M.; Xuan, J.; Wang, H. Solar Carbon Fuel via Photoelectrochemistry. *Catal. Today* **2018**, *317*, 56−75.
(853) Graves, C.; Ebbesen, S. D.; Mogensen, M.; Lackner, K. S. Sustainable Hydrocarbon Fuels by Recycling CO_2 and H_2O with Renewable or Nuclear Energy. *Renewable Sustainable Energy Rev.* **2011**, *15*, 1−23.
(854) Galan-Mascaros, J. R. Photoelectrochemical Solar Fuels from Carbon Dioxide, Water and Sunlight. *Catal. Sci. Technol.* **2020**, *10*, 1967−1974.
(855) Pawar, A. U.; Kim, C. W.; Nguyen-Le, M.-T.; Kang, Y. S. General Review on the Components and Parameters of Photoelectrochemical System for CO_2 Reduction with in Situ Analysis. *ACS Sustainable Chem. Eng.* **2019**, *7*, 7431−7455.
(856) Tahir, M. Photocatalytic Carbon Dioxide Reduction to Fuels in Continuous Flow Monolith Photoreactor Using Montmorillonite Dispersed Fe/TiO_2 Nanocatalyst. *J. Cleaner Prod.* **2018**, *170*, 242−250.
(857) Sorcar, S.; Hwang, Y.; Lee, J.; Kim, H.; Grimes, K. M.; Grimes, C. A.; Jung, J.-W.; Cho, C.-H.; Majima, T.; Hoffmann, M. R.; et al. CO_2, Water, and Sunlight to Hydrocarbon Fuels: A Sustained Sunlight to Fuel (Joule-to-Joule) Photoconversion Efficiency of 1%. *Energy Environ. Sci.* **2019**, *12*, 2685−2696.
(858) Ješić, D.; LašičJurković, D.; Pohar, A.; Suhadolnik, L.; Likozar, B. Engineering Photocatalytic and Photoelectrocatalytic CO_2 Reduction Reactions: Mechanisms, Intrinsic Kinetics, Mass Transfer Resistances, Reactors and Multi-Scale Modelling Simulations. *Chem. Eng. J.* **2021**, *407*, 126799.
(859) Sacco, A.; Speranza, R.; Savino, U.; Zeng, J.; Farkhondehfal, M. A.; Lamberti, A.; Chiodoni, A.; Pirri, C. F. An Integrated Device for the Solar-Driven Electrochemical Conversion of CO_2 to CO. *ACS Sustainable Chem. Eng.* **2020**, *8*, 7563−7568.
(860) Creissen, C. E.; Fontecave, M. Solar-Driven Electrochemical CO_2 Reduction with Heterogeneous Catalysts. *Adv. Energy Mater.* **2020**, 2002652.
(861) Grätzel, M. Photoelectrochemical Cells. *Nature* **2001**, *414*, 338−344.
(862) Liu, Y.; Guo, L. On Factors Limiting the Performance of Photoelectrochemical CO_2 Reduction. *J. Chem. Phys.* **2020**, *152*, 100901.
(863) Fujishima, A.; Honda, K. Electrochemical Photolysis of Water at a Semiconductor Electrode. *Nature* **1972**, *238*, 37−38.
(864) Chen, X.; Shen, S.; Guo, L.; Mao, S. S. Semiconductor-Based Photocatalytic Hydrogen Generation. *Chem. Rev.* **2010**, *110*, 6503−6570.
(865) Hisatomi, T.; Kubota, J.; Domen, K. Recent Advances in Semiconductors for Photocatalytic and Photoelectrochemical Water Splitting. *Chem. Soc. Rev.* **2014**, *43*, 7520−7535.
(866) Moniz, S. J. A.; Shevlin, S. A.; Martin, D. J.; Guo, Z.-X.; Tang, J. Visible-Light Driven Heterojunction Photocatalysts for Water Splitting - a Critical Review. *Energy Environ. Sci.* **2015**, *8*, 731−759.
(867) Roy, S.; Miller, M.; Warnan, J.; Leung, J. J.; Sahm, C. D.; Reisner, E. Electrocatalytic and Solar-Driven Reduction of Aqueous CO_2 with Molecular Cobalt Phthalocyanine-Metal Oxide Hybrid Materials. *ACS Catal.* **2021**, *11*, 1868−1876.
(868) Shan, B.; Vanka, S.; Li, T.-T.; Troian-Gautier, L.; Brennaman, M. K.; Mi, Z.; Meyer, T. J. Binary Molecular-Semiconductor p-n Junctions for Photoelectrocatalytic CO_2 Reduction. *Nat. Energy* **2019**, *4*, 290−299.
(869) Sekizawa, K.; Sato, S.; Arai, T.; Morikawa, T. Solar-Driven Photocatalytic CO_2 Reduction in Water Utilizing a Ruthenium Complex Catalyst on p-Type Fe_2O_3 with a Multiheterojunction. *ACS Catal.* **2018**, *8*, 1405−1416.
(870) Schreier, M.; Gao, P.; Mayer, M. T.; Luo, J.; Moehl, T.; Nazeeruddin, M. K.; Tilley, S. D.; Grätzel, M. Efficient and Selective Carbon Dioxide Reduction on Low Cost Protected Cu_2O Photocathodes Using a Molecular Catalyst. *Energy Environ. Sci.* **2015**, *8*, 855−861.
(871) Pang, H.; Masuda, T.; Ye, J. Semiconductor-Based Photoelectrochemical Conversion of Carbon Dioxide: Stepping Towards Artificial Photosynthesis. *Chem. - Asian J.* **2018**, *13*, 127−142.
(872) Cheng, J.; Zhang, M.; Liu, J.; Zhou, J.; Cen, K. A Cu Foam Cathode Used as a Pt-RGO Catalyst Matrix to Improve CO_2 Reduction in a Photoelectrocatalytic Cell with a TiO_2 Photoanode. *J. Mater. Chem. A* **2015**, *3*, 12947−12957.
(873) Chang, X.; Wang, T.; Zhang, P.; Wei, Y.; Zhao, J.; Gong, J. Stable Aqueous Photoelectrochemical CO_2 Reduction by a Cu_2O Dark Cathode with Improved Selectivity for Carbonaceous Products. *Angew. Chem., Int. Ed.* **2016**, *55*, 8840−8845.
(874) Wang, D.; He, Y.; Zhong, N.; He, Z.; Shen, Y.; Zeng, T.; Lu, X.; Ma, J.; Song, S. In Situ Chloride-Mediated Synthesis of TiO_2 Thin Film Photoanode with Enhanced Photoelectrochemical Activity for Carbamazepine Oxidation Coupled with Simultaneous Cathodic H2 Production and CO_2 Conversion to Fuels. *J. Hazard. Mater.* **2021**, *410*, 124563.
(875) Kim, C. W.; Kang, M. J.; Ji, S.; Kang, Y. S. Artificial Photosynthesis for Formaldehyde Production with 85% of Faradaic Efficiency by Tuning the Reduction Potential. *ACS Catal.* **2018**, *8*, 968−974.
(876) Magesh, G.; Kim, E. S.; Kang, H. J.; Banu, M.; Kim, J. Y.; Kim, J. H.; Lee, J. S. A Versatile Photoanode-Driven Photoelectrochemical System for Conversion of CO_2 to Fuels with High Faradaic Efficiencies at Low Bias Potentials. *J. Mater. Chem. A* **2014**, *2*, 2044−2049.
(877) Xiao, S.; Li, Z.; Fu, Q.; Li, Y.; Li, J.; Zhang, L.; Liao, Q.; Zhu, X. Hybrid Microbial Photoelectrochemical System Reduces CO_2 to CH_4 with 1.28% Solar Energy Conversion Efficiency. *Chem. Eng. J.* **2020**, *390*, 124530.

https://doi.org/10.1021/acs.chemrev.1c00332
Chem. Rev. 2022, 122, 2752−2906

(878) Kamimura, S.; Murakami, N.; Tsubota, T.; Ohno, T. Fabrication and Characterization of a P-Type $Cu_3Nb_2O_8$ Photocathode toward Photoelectrochemical Reduction of Carbon Dioxide. *Appl. Catal., B* **2015**, *174*−*175*, 471−476.
(879) DuChene, J. S.; Tagliabue, G.; Welch, A. J.; Cheng, W.-H.; Atwater, H. A. Hot Hole Collection and Photoelectrochemical CO_2 Reduction with Plasmonic Au/p-GaN Photocathodes. *Nano Lett.* **2018**, *18*, 2545−2550.
(880) Weng, B.; Wei, W.; Yiliguma, Y.; Wu, H.; Alenizi, A. M.; Zheng, G. Bifunctional CoP and CoN Porous Nanocatalysts Derived from ZIF-67 in Situ Grown on Nanowire Photoelectrodes for Efficient Photoelectrochemical Water Splitting and CO_2 Reduction. *J. Mater. Chem. A* **2016**, *4*, 15353−15360.
(881) Arai, T.; Sato, S.; Kajino, T.; Morikawa, T. Solar CO_2 Reduction Using H_2O by a Semiconductor/Metal-Complex Hybrid Photocatalyst: Enhanced Efficiency and Demonstration of a Wireless System Using $SrTiO_3$ Photoanodes. *Energy Environ. Sci.* **2013**, *6*, 1274−1282.
(882) Rajeshwar, K. Fundamentals of Semiconductor Electrochemistry and Photoelectrochemistry. *J. Appl. Electrochem.* **2007**, *37*, 765.
(883) van de Krol, R., Grätzel, M., Eds. Photoelectrochemical Hydrogen Production. *Electronic Materials: Science & Technology*; Springer US: Boston, MA, 2012; Vol. *102*.
(884) Kumaravel, V.; Bartlett, J.; Pillai, S. C. Photoelectrochemical Conversion of Carbon Dioxide (CO_2) into Fuels and Value-Added Products. *ACS Energy Lett.* **2020**, *5*, 486−519.
(885) Chen, Z.; Jaramillo, T. F.; Deutsch, T. G.; Kleiman-Shwarsctein, A.; Forman, A. J.; Gaillard, N.; Garland, R.; Takanabe, K.; Heske, C.; Sunkara, M.; et al. Accelerating Materials Development for Photoelectrochemical Hydrogen Production: Standards for Methods, Definitions, and Reporting Protocols. *J. Mater. Res.* **2010**, *25*, 3−16.
(886) Kang, U.; Choi, S. K.; Ham, D. J.; Ji, S. M.; Choi, W.; Han, D. S.; Abdel-Wahab, A.; Park, H. Photosynthesis of Formate from CO_2 and Water at 1% Energy Efficiency via Copper Iron Oxide Catalysis. *Energy Environ. Sci.* **2015**, *8*, 2638−2643.
(887) Zeng, G.; Qiu, J.; Li, Z.; Pavaskar, P.; Cronin, S. B. CO_2 Reduction to Methanol on TiO_2-Passivated GaP Photocatalysts. *ACS Catal.* **2014**, *4*, 3512−3516.
(888) Lee, D. K.; Choi, K.-S. Enhancing Long-Term Photostability of $BiVO_4$ Photoanodes for Solar Water Splitting by Tuning Electrolyte Composition. *Nat. Energy* **2018**, *3*, 53−60.
(889) Zhang, N.; Long, R.; Gao, C.; Xiong, Y. Recent Progress on Advanced Design for Photoelectrochemical Reduction of CO_2 to Fuels. *Sci. China Mater.* **2018**, *61*, 771−805.
(890) Castro, S.; Albo, J.; Irabien, A. Photoelectrochemical Reactors for CO_2 Utilization. *ACS Sustainable Chem. Eng.* **2018**, *6*, 15877−15894.
(891) Giesbrecht, P. K.; Freund, M. S. Recent Advances in Bipolar Membrane Design and Applications. *Chem. Mater.* **2020**, *32*, 8060−8090.
(892) Luo, X.; Xuan, J.; Fernandez, E. S.; Maroto-Valer, M. M. Modeling and Simulation for Photoelectrochemical CO_2 Utilization. *Energy Procedia* **2019**, *158*, 809−815.
(893) Homayoni, H.; Chanmanee, W.; de Tacconi, N.; Dennis, B.; Rajeshwar, K. Continuous Flow Photoelectrochemical Reactor for Solar Conversion of Carbon Dioxide to Alcohols. *J. Electrochem. Soc.* **2015**, *162*, E115−E122.
(894) Ghadimkhani, G.; de Tacconi, N. R.; Chanmanee, W.; Janaky, C.; Rajeshwar, K. Efficient Solar Photoelectrosynthesis of Methanol from Carbon Dioxide Using Hybrid CuO-Cu_2O Semiconductor Nanorod Arrays. *Chem. Commun.* **2013**, *49*, 1297.
(895) Rajeshwar, K.; de Tacconi, N. R.; Ghadimkhani, G.; Chanmanee, W.; Janáky, C. Tailoring Copper Oxide Semiconductor Nanorod Arrays for Photoelectrochemical Reduction of Carbon Dioxide to Methanol. *ChemPhysChem* **2013**, *14*, 2251−2259.
(896) Bogdanoff, P.; Alonso-Vante, N. On-Line Determination via Differential Electrochemical Mass Spectroscopy (DEMS) of Chemical Products Formed in Photoelectrocatalytical Systems. *Berichte der Bunsengesellschaft für Phys. Chemie* **1993**, *97*, 940−943.
(897) Bogdanoff, P.; Alonso-Vante, N. A Kinetic Approach of Competitive Photoelectrooxidation of HCOOH and H_2O on TiO_2 Anatase Thin Layers via on-Line Mass Detection. *J. Electroanal. Chem.* **1994**, *379*, 415−421.
(898) Neumann, B.; Bogdanoff, P.; Tributsch, H.; Sakthivel, S.; Kisch, H. Electrochemical Mass Spectroscopic and Surface Photovoltage Studies of Catalytic Water Photooxidation by Undoped and Carbon-Doped Titania. *J. Phys. Chem. B* **2005**, *109*, 16579−16586.
(899) Fuhrmann, J.; Zhao, H.; Holzbecher, E.; Langmach, H.; Chojak, M.; Halseid, R.; Jusys, Z.; Behm, J. Experimental and Numerical Model Study of the Limiting Current in a Channel Flow Cell with a Circular Electrode. *Phys. Chem. Chem. Phys.* **2008**, *10*, 3784−3795.
(900) Higgins, D.; Hahn, C.; Xiang, C.; Jaramillo, T. F.; Weber, A. Z. Gas-Diffusion Electrodes for Carbon Dioxide Reduction: A New Paradigm. *ACS Energy Lett.* **2019**, *4*, 317−324.
(901) Urbain, F.; Tang, P.; Carretero, N. M.; Andreu, T.; Gerling, L. G.; Voz, C.; Arbiol, J.; Morante, J. R. A Prototype Reactor for Highly Selective Solar-Driven CO_2 Reduction to Synthesis Gas Using Nanosized Earth-Abundant Catalysts and Silicon Photovoltaics. *Energy Environ. Sci.* **2017**, *10*, 2256−2266.
(902) Hernández-Alonso, M. D.; Penelas-Pérez, G.; Andreu, T.; Irtem, E.; Parra, A.; Fábrega, C.; Morante, J. R. Filter-Press Photoelectrochemical Water Oxidation and CO_2 Reduction Cell. WO2016097247, 2016.
(903) Bozell, J. J.; Petersen, G. R. Technology Development for the Production of Biobased Products from Biorefinery Carbohydrates—the US Department of Energy's "Top 10" Revisited. *Green Chem.* **2010**, *12*, 539−554.
(904) Cha, H. G.; Choi, K.-S. Combined Biomass Valorization and Hydrogen Production in a Photoelectrochemical Cell. *Nat. Chem.* **2015**, *7*, 328−333.
(905) Tateno, H.; Miseki, Y.; Sayama, K. Photoelectrochemical Oxidation of Benzylic Alcohol Derivatives on $BiVO_4/WO_3$ under Visible Light Irradiation. *ChemElectroChem* **2017**, *4*, 3283−3287.
(906) Li, T.; Kasahara, T.; He, J.; Dettelbach, K. E.; Sammis, G. M.; Berlinguette, C. P. Photoelectrochemical Oxidation of Organic Substrates in Organic Media. *Nat. Commun.* **2017**, *8*, 390.
(907) Song, W.; Vannucci, A. K.; Farnum, B. H.; Lapides, A. M.; Brennaman, M. K.; Kalanyan, B.; Alibabaei, L.; Concepcion, J. J.; Losego, M. D.; Parsons, G. N.; et al. Visible Light Driven Benzyl Alcohol Dehydrogenation in a Dye-Sensitized Photoelectrosynthesis Cell. *J. Am. Chem. Soc.* **2014**, *136*, 9773−9779.
(908) Tojo, G.; Fernandez, M. I. *Oxidation of Alcohols to Aldehydes and Ketones*; Springer Science & Business Media, 2006.
(909) Bäckvall, J.-E. *Modern Oxidation Methods* **2011**.
(910) Weidmann, V.; Maison, W. Allylic Oxidations of Olefins to Enones. *Synthesis* **2013**, *45*, 2201−2221.
(911) You, B.; Liu, X.; Jiang, N.; Sun, Y. A General Strategy for Decoupled Hydrogen Production from Water Splitting by Integrating Oxidative Biomass Valorization. *J. Am. Chem. Soc.* **2016**, *138*, 13639−13646.
(912) Badalyan, A.; Stahl, S. S. Cooperative Electrocatalytic Alcohol Oxidation with Electron-Proton-Transfer Mediators. *Nature* **2016**, *535*, 406−410.
(913) Hickey, D. P.; Schiedler, D. A.; Matanovic, I.; Doan, P. V.; Atanassov, P.; Minteer, S. D.; Sigman, M. S. Predicting Electrocatalytic Properties: Modeling Structure-Activity Relationships of Nitroxyl Radicals. *J. Am. Chem. Soc.* **2015**, *137*, 16179−16186.
(914) Shono, T.; Ikeda, A. Electroorganic Chemistry. X. Anodic Allylic Substitution. *J. Am. Chem. Soc.* **1972**, *94*, 7892−7898.
(915) Horn, E. J.; Rosen, B. R.; Chen, Y.; Tang, J.; Chen, K.; Eastgate, M. D.; Baran, P. S. Scalable and Sustainable Electrochemical Allylic C-H Oxidation. *Nature* **2016**, *533*, 77−81.
(916) Youngblood, W. J.; Lee, S.-H. A.; Kobayashi, Y.; Hernandez-Pagan, E. A.; Hoertz, P. G.; Moore, T. A.; Moore, A. L.; Gust, D.; Mallouk, T. E. Photoassisted Overall Water Splitting in a Visible

https://doi.org/10.1021/acs.chemrev.1c00332
Chem. Rev. 2022, 122, 2752−2906

Light-Absorbing Dye-Sensitized Photoelectrochemical Cell. *J. Am. Chem. Soc.* **2009**, *131*, 926−927.
(917) Moore, G. F.; Blakemore, J. D.; Milot, R. L.; Hull, J. F.; Song, H.; Cai, L.; Schmuttenmaer, C. A.; Crabtree, R. H.; Brudvig, G. W. A Visible Light Water-Splitting Cell with a Photoanode Formed by Codeposition of a High-Potential Porphyrin and an Iridium Water-Oxidation Catalyst. *Energy Environ. Sci.* **2011**, *4*, 2389−2392.
(918) Brimblecombe, R.; Koo, A.; Dismukes, G. C.; Swiegers, G. F.; Spiccia, L. Solar Driven Water Oxidation by a Bioinspired Manganese Molecular Catalyst. *J. Am. Chem. Soc.* **2010**, *132*, 2892−2894.
(919) Gao, Y.; Ding, X.; Liu, J.; Wang, L.; Lu, Z.; Li, L.; Sun, L. Visible Light Driven Water Splitting in a Molecular Device with Unprecedentedly High Photocurrent Density. *J. Am. Chem. Soc.* **2013**, *135*, 4219−4222.
(920) Alibabaei, L.; Brennaman, M. K.; Norris, M. R.; Kalanyan, B.; Song, W.; Losego, M. D.; Concepcion, J. J.; Binstead, R. A.; Parsons, G. N.; Meyer, T. J. Solar Water Splitting in a Molecular Photoelectrochemical Cell. *Proc. Natl. Acad. Sci. U. S. A.* **2013**, *110*, 20008−20013.
(921) Lv, H.; Geletii, V. Y.; Zhao, C.; Vickers, J. W.; Zhu, G.; Luo, Z.; Song, J.; Lian, T.; Musaev, D. G.; Hill, C. L. Polyoxometalate Water Oxidation Catalysts and the Production of Green Fuel. *Chem. Soc. Rev.* **2012**, *41*, 7572−7589.
(922) Choi, D. S.; Kim, J.; Hollmann, F.; Park, C. B. Solar-Assisted EBiorefinery: Photoelectrochemical Pairing of Oxyfunctionalization and Hydrogenation Reactions. *Angew. Chem., Int. Ed.* **2020**, *59*, 15886−15890.
(923) Toogood, H. S.; Scrutton, N. S. Discovery, Characterization, Engineering, and Applications of Ene-Reductases for Industrial Biocatalysis. *ACS Catal.* **2018**, *8*, 3532−3549.
(924) Wang, J.-H.; Li, X.-B.; Li, J.; Lei, T.; Wu, H.-L.; Nan, X.-L.; Tung, C.-H.; Wu, L.-Z. Photoelectrochemical Cell for P-H/C-H Cross-Coupling with Hydrogen Evolution. *Chem. Commun.* **2019**, *55*, 10376−10379.
(925) Tateno, H.; Miseki, Y.; Sayama, K. Photoelectrochemical Dimethoxylation of Furan via a Bromide Redox Mediator Using a $BiVO_4/WO_3$ Photoanode. *Chem. Commun.* **2017**, *53*, 4378−4381.
(926) Becker, J. Y.; Zemach, D. The Effect of Electrochemically Generated Positive Bromine Species in Acetonitrile on the Cleavage of C-Br and C-Cl Bonds. *J. Chem. Soc., Perkin Trans. 2* **1981**, No. 2, 336−340.
(927) Nad, S.; Breinbauer, R. Electroorganic Synthesis on the Solid Phase Using Polymer Beads as Supports. *Angew. Chem., Int. Ed.* **2004**, *43*, 2297−2299.
(928) Tateno, H.; Iguchi, S.; Miseki, Y.; Sayama, K. Photo-Electrochemical C-H Bond Activation of Cyclohexane Using a WO_3 Photoanode and Visible Light. *Angew. Chem., Int. Ed.* **2018**, *57*, 11238−11241.
(929) Shiraishi, Y.; Sugano, Y.; Ichikawa, S.; Hirai, T. Visible Light-Induced Partial Oxidation of Cyclohexane on WO_3 Loaded with Pt Nanoparticles. *Catal. Sci. Technol.* **2012**, *2*, 400−405.
(930) Tamirat, A. G.; Rick, J.; Dubale, A. A.; Su, W.-N.; Hwang, B.-J. Using Hematite for Photoelectrochemical Water Splitting: A Review of Current Progress and Challenges. *Nanoscale Horizons* **2016**, *1*, 243−267.
(931) Sivula, K.; Le Formal, F.; Grätzel, M. Solar Water Splitting: Progress Using Hematite (α-Fe_2O_3) Photoelectrodes. *ChemSusChem* **2011**, *4*, 432−449.
(932) Zhang, L.; Liardet, L.; Luo, J.; Ren, D.; Grätzel, M.; Hu, X. Photoelectrocatalytic Arene C-H Amination. *Nat. Catal.* **2019**, *2*, 366−373.
(933) Bhattacharya, T.; Ghosh, A.; Maiti, D. Hexafluoroisopropanol: The Magical Solvent for Pd-Catalyzed C-H Activation. *Chem. Sci.* **2021**, *12*, 3857−3870.
(934) Romero, N. A.; Margrey, K. A.; Tay, N. E.; Nicewicz, D. A. Site-Selective Arene C-H Amination via Photoredox Catalysis. *Science* **2015**, *349*, 1326−1330.
(935) Margrey, K. A.; McManus, J. B.; Bonazzi, S.; Zecri, F.; Nicewicz, D. A. Predictive Model for Site-Selective Aryl and Heteroaryl C-H Functionalization via Organic Photoredox Catalysis. *J. Am. Chem. Soc.* **2017**, *139*, 11288−11299.
(936) Morofuji, T.; Shimizu, A.; Yoshida, J. Electrochemical C-H Amination: Synthesis of Aromatic Primary Amines via N-Arylpyridinium Ions. *J. Am. Chem. Soc.* **2013**, *135*, 5000−5003.
(937) Morofuji, T.; Shimizu, A.; Yoshida, J. Direct C-N Coupling of Imidazoles with Aromatic and Benzylic Compounds via Electrooxidative C-H Functionalization. *J. Am. Chem. Soc.* **2014**, *136*, 4496−4499.
(938) Morofuji, T.; Shimizu, A.; Yoshida, J. Heterocyclization Approach for Electrooxidative Coupling of Functional Primary Alkylamines with Aromatics. *J. Am. Chem. Soc.* **2015**, *137*, 9816−9819.
(939) Morofuji, T.; Shimizu, A.; Yoshida, J. Electrochemical Intramolecular C-H Amination: Synthesis of Benzoxazoles and Benzothiazoles. *Chem. - Eur. J.* **2015**, *21*, 3211−3214.
(940) Baumann, M. Integrating Continuous Flow Synthesis with In-Line Analysis and Data Generation. *Org. Biomol. Chem.* **2018**, *16*, 5946−5954.
(941) Kuijpers, K. P. L.; Weggemans, W. M. A.; Verwijlen, C. J. A.; Noël, T. Flow Chemistry Experiments in the Undergraduate Teaching Laboratory: Synthesis of Diazo Dyes and Disulfides. *J. Flow Chem.* **2021**, *11*, 7−12.
(942) Noël, T. Flow into the chemistry curriculum. *Chemistry World*. https://www.chemistryworld.com/opinion/flow-into-the-chemistry-curriculum/4010382.article?adredir=1.
(943) Note: This quote is often attributed to Leonardo Da Vinci, however, up to now no published occurrence of such an attribution has yet been located in Da Vinci's work.
(944) Britton, J.; Jamison, T. F. The Assembly and Use of Continuous Flow Systems for Chemical Synthesis. *Nat. Protoc.* **2017**, *12*, 2423−2446.
(945) Prabhu, G. R. D.; Urban, P. L. Elevating Chemistry Research with a Modern Electronics Toolkit. *Chem. Rev.* **2020**, *120*, 9482−9553.

https://doi.org/10.1021/acs.chemrev.1c00332
Chem. Rev. 2022, 122, 2752−2906